frontiers | Research Topics

Extracellular vesicles: From characterization to treatment

Edited by
Xinlei Li, Jeffrey David Galley and Ming Dong

Published in
Frontiers in Cell and Developmental Biology

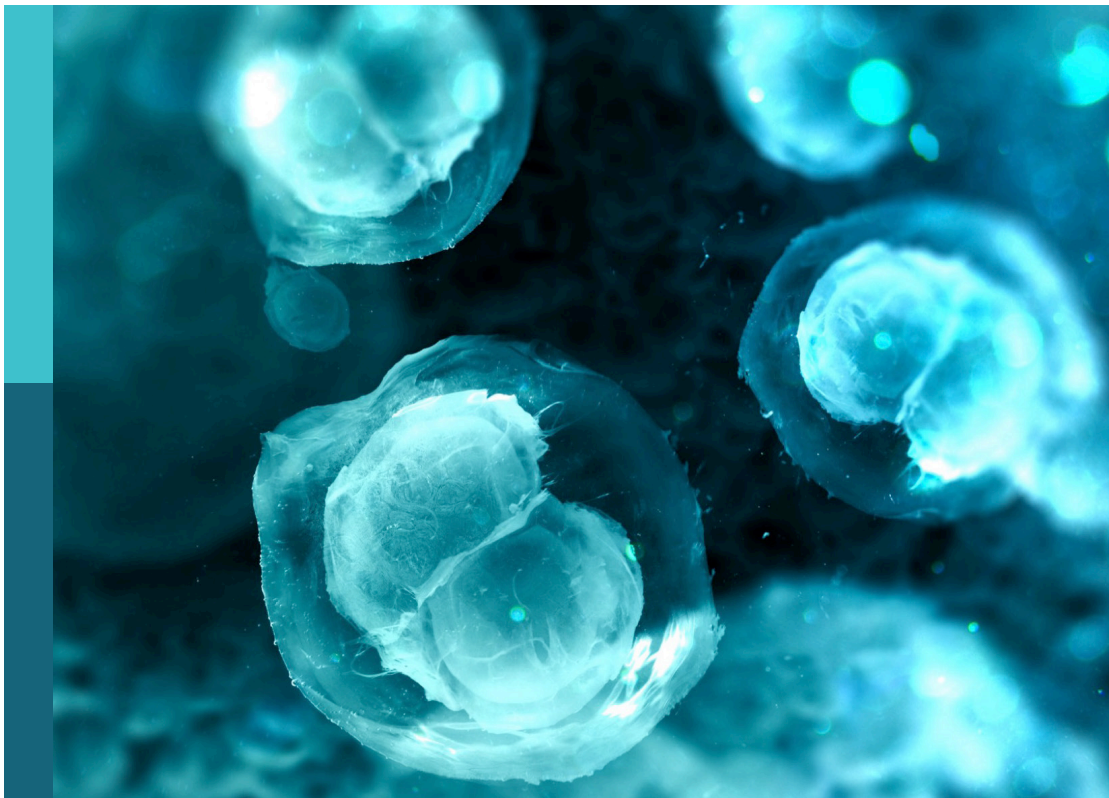

ISSN 1664-8714
ISBN 978-2-88976-550-8
DOI 10.3389/978-2-88976-550-8

About Frontiers

Frontiers is more than just an open access publisher of scholarly articles: it is a pioneering approach to the world of academia, radically improving the way scholarly research is managed. The grand vision of Frontiers is a world where all people have an equal opportunity to seek, share and generate knowledge. Frontiers provides immediate and permanent online open access to all its publications, but this alone is not enough to realize our grand goals.

Frontiers journal series

The Frontiers journal series is a multi-tier and interdisciplinary set of open-access, online journals, promising a paradigm shift from the current review, selection and dissemination processes in academic publishing. All Frontiers journals are driven by researchers for researchers; therefore, they constitute a service to the scholarly community. At the same time, the *Frontiers journal series* operates on a revolutionary invention, the tiered publishing system, initially addressing specific communities of scholars, and gradually climbing up to broader public understanding, thus serving the interests of the lay society, too.

Dedication to quality

Each Frontiers article is a landmark of the highest quality, thanks to genuinely collaborative interactions between authors and review editors, who include some of the world's best academicians. Research must be certified by peers before entering a stream of knowledge that may eventually reach the public - and shape society; therefore, Frontiers only applies the most rigorous and unbiased reviews. Frontiers revolutionizes research publishing by freely delivering the most outstanding research, evaluated with no bias from both the academic and social point of view. By applying the most advanced information technologies, Frontiers is catapulting scholarly publishing into a new generation.

What are Frontiers Research Topics?

Frontiers Research Topics are very popular trademarks of the *Frontiers journals series*: they are collections of at least ten articles, all centered on a particular subject. With their unique mix of varied contributions from Original Research to Review Articles, Frontiers Research Topics unify the most influential researchers, the latest key findings and historical advances in a hot research area.

Find out more on how to host your own Frontiers Research Topic or contribute to one as an author by contacting the Frontiers editorial office: frontiersin.org/about/contact

Extracellular vesicles: From characterization to treatment

Topic editors

Xinlei Li — Nationwide Children's Hospital, United States
Jeffrey David Galley — The Ohio State University, United States
Ming Dong — Guangzhou Institutes of Biomedicine and Health, Chinese Academy of Sciences (CAS), China

Citation

Li, X., Galley, J. D., Dong, M., eds. (2023). *Extracellular vesicles: From characterization to treatment*. Lausanne: Frontiers Media SA.
doi: 10.3389/978-2-88976-550-8

Table of contents

frontiers | Frontiers in Cell and Developmental Biology

EDITORIAL
published: 17 June 2022
doi: 10.3389/fcell.2022.945529

Editorial: Extracellular Vesicles: From Characterization to Treatment

Xinlei Li[1*†] *and Jeffrey David Galley*[2*†]

[1]Center for Clinical and Translational Research, The Abigail Wexner Research Institute at Nationwide Children's Hospital, Columbus, OH, United States, [2]Institute for Behavioral Medicine Research, The Ohio State University Wexner Medical Center, Columbus, OH, United States

Keywords: extracellular vesicles, diagnostics, treatment target, disease progression, therapeutics

Editorial on the Research Topic

Extracellular Vesicles: From Characterization to Treatment

Extracellular vesicles (EVs) are nanoparticles released from virtually all types of cells, ranging from 50–500 nm in diameter. Some EVs are assembled at and bud from the plasma membrane; these EVs are typically large and called large EVs or ectosomes. Alternatively, some EVs originate from intracellular multivesicular bodies (MVB) and are secreted in bulk through membrane fusion between the MVB and cell membrane. These EVs are relatively small in size and are named small EVs or exosomes. Both EV types have been proven to mediate intercellular communication through the delivery of payloads including proteins, lipids, and nucleic acids, in both physiological and pathological conditions. EV biogenesis represents a snapshot of the status of the producer cells; the yield and composition of EVs can be regulated by different stimuli. Therefore, the EVs circulating in the bloodstream or urine can be used as liquid biopsy tools for the diagnosis or prognosis of different diseases. In addition, upon cargo delivery, EVs released from diseased cells or tissues may lead to the initiation or progression of pathogenesis in target cells or tissues. Thus, EVs under pathophysiological conditions represent potential targets for disease treatment. Additionally, natural or engineered EVs derived from normal differentiated cells or stem cells can serve as potent therapeutics against fibrogenic disorders, inflammatory diseases, congenital syndromes, or cancers (Murphy et al., 2019; Claridge et al., 2021). Collectively, because of these properties, the translational potential of EVs as diagnostics, treatment targets, or therapeutics has attracted considerable attention.

In this Research Topic, there were 12 submissions in total: specifically, three review articles (including one mini review), two brief research reports, one method article, and six original research articles. One major aim of the Research Topic involves new advances in EV biogenesis/characterization, and five reports have contributed new findings to it. Alcohol consumption induces liver injury and elevated EV secretion in alcoholic hepatitis patients (Szabo and Momen-Heravi, 2017). Bala et al. reported in their research article that alcohol promotes exosome biogenesis and release from hepatocytes through modulating Rabs, vesicle-associated membrane proteins, and miR-192. It suggests alcohol imposes a systemic impact on a variety of genes to promote EV biogenesis and secretion. -Omics (proteomics, transcriptomics, or lipidomics) tools are a powerful strategy to characterize EVs payloads and reports herein associate proteome profiling of EVs derived from either physiological or pathological conditions. Lim et al. isolated small and large EVs through differential centrifugation and compared the proteome difference in terms of well-known EV markers, evolutionary conservation, and biological functions. In the nervous system, Torres et al. identified hippocampal neuronal-secreted EVs that carry Wnt, specifically Wnt3a, Wnt5a, and Wnt7a on the EV surface membrane, and then detailed how EVs and Wnt become associated. Differential ultracentrifugation is the most common approach to isolate EVs. However,

Edited and reviewed by:
Ramani Ramchandran, Medical College of Wisconsin, United States

***Correspondence:**
Xinlei Li
Xinlei.li@nationwidechildrens.org
Jeffrey David Galley
jeffrey.galley@osumc.edu

†These authors have contributed equally to this work

Specialty section:
This article was submitted to Molecular and Cellular Pathology, a section of the journal Frontiers in Cell and Developmental Biology

Received: *16 May 2022*
Accepted: *02 June 2022*
Published: *17 June 2022*

Citation:
Li X and Galley JD (2022) Editorial: Extracellular Vesicles: From Characterization to Treatment. Front. Cell Dev. Biol. 10:945529. doi: 10.3389/fcell.2022.945529

not all laboratories have access to it. Zoia et al. established two protocols for EV isolation from normal or malaria-infected cells, without requiring ultracentrifugation. The high yield and purity of EVs isolated justify that the two methods could have potential use in resource strapped countries. Within the tumor microenvironment, tumor cells release EVs that have emerged as a vital means of cell communication and immune modulation (Xu et al., 2018). In their mini review, Reed et al. discussed how macrophages and tumor-derived EVs interact, in both pro- and anti-tumor ways.

The capacity of EVs to act as cargo carriers and to have unique surface protein signatures has led to them being utilized as sources of biomarkers, particularly for cancer (Bernard et al., 2019; Logozzi et al., 2019) or studied for their involvement in cancer progression (Liu et al., 2019). Advances herein could completely remodel early-stage disease detection and treatment options. This Research Topic provides such a focus, with two novel and important reports that closely associated EV cargoes with cancers, in many cases employing cutting edge methodologies. Verel-Yilmaz et al. identified ADAM8, a metalloprotease-integrin that is expressed on the EV surface, as well as multiple cargo miRNAs as potential biomarkers for pancreatic ductal adenocarcinoma (PDAC), providing a two-pronged approach that exhibits how EV-based diagnostics can utilize both the surface and the cargo of these nanoparticles. Liquid biopsies for biospecimen collection have become attractive alternatives to more invasive procedures and attempts to combine this with economical and rapid EV collection and characterization is a major research question. Purcell et al. utilized liquid biopsies from patients to identify EV biomarkers for non-small cell lung cancer in both protein and RNA collections, focusing on epidermal growth factor receptor mutations that were detected with Western blot and digital droplet PCR.

EVs can be used in non-cancer diseases as well, and in this Research Topic Wang et al. identified EV-associated miRNA-193a as a urinary biomarker for focal segmental glomerulosclerosis, a nephrotic syndrome. Further, the authors here identified how podocytes were capable of transporting miRNAs, suggesting a method by which the disease could be spread through EV communication. Atherosclerosis is another disease covered in this Research Topic by Hildebrandt et al., wherein the authors were able to identify unique miRNA signatures for multiple types of atherosclerotic types, some of which provided further corroboration based on previous studies. Lastly, Nakao et al. demonstrated how EVs that are involved in lipotoxicity during nonalcoholic steatohepatitis carry damage-associated molecular patterns that may spur disease progression and could potentially be used in diagnostics.

In addition to being used as diagnostic biomarkers, EVs are also being studied in potential treatment applications. Much of the excitement regarding these developments stems from paracrinal activity of EVs, as well as the ability to load EVs with specific cargoes that could then be trafficked to distant sites. Here, two manuscripts look at therapeutic effects that could be leveraged from EVs. Wu et al. present a review on the involvement of EVs in mediating cell death, with a focus on dysfunction due to myocardial infarction. The review covers multiple mechanisms that may be future avenues of EV-based therapeutics, including EVs ability to reduce pyroptosis and abrogate cell death. Amini et al. put forward a review of the relationship between melatonin and EV production/efflux. Melatonin is a pleiotropic molecule produced in the pineal gland that could potentially improve the therapeutic effect of stem cell-derived EVs when used in combination (Sun et al., 2017; Alzahrani, 2019; Chang et al., 2019). They detail how melatonin may work with EVs to reduce inflammation and alter the miRNA cargo of EVs, amongst numerous other interactions.

This Research Topic of EVs, focusing on their characterization and potential uses in diagnostics and therapeutics, represent some of the most exciting work presently being performed in this field. Notably, novel scientific reports on focusing on advances in EVs as therapeutic targets, particularly for anti-tumor treatment, were not covered in this Research Topic and should be a point of emphasis in the future. Going forward, studies focusing on the precise characterization of EV payloads would facilitate the diagnostic application of EVs in liquid biopsy and could potentially lead to the translational use of natural or engineered EVs for disease treatment. In general, we are excited for further development in the EV sub-field of treatment and look forward to these studies reported here reaching new readers as well as for the future analyses that will sprout from results and findings published herein.

AUTHOR CONTRIBUTIONS

XL and JDG have made a substantial, direct, and intellectual contribution to the work and approved it for publication.

ACKNOWLEDGMENTS

We are deeply thankful for all authors who have contributed to this Research Topic as well as the dedicated reviewers for their thorough and timely comments. We also express our thanks to the Frontiers in Cell and Developmental Biology Editorial Office for the cooperation that we have received from the initiation to the completion of this Research Topic.

REFERENCES

Alzahrani, F. A. (2019). Melatonin Improves Therapeutic Potential of Mesenchymal Stem Cells-Derived Exosomes against Renal Ischemia-Reperfusion Injury in Rats. *Am. J. Transl. Res.* 11 (5), 2887–2907.

Bernard, V., Kim, D. U., Anthony San Lucas, F., Castillo, J., Allenson, K., Mulu, F. C., et al. (2019). Circulating Nucleic Acids are Associated with Outcomes of Patients with Pancreatic Cancer. *Gastroenterology* 156, 108–118. doi:10.1053/j.gastro.2018.09.022

Chang, C. L., Chen, C. H., Chiang, J. Y., Sun, C. K., Chen, Y. L., Chen, K. H., et al. (2019). Synergistic Effect of Combined Melatonin and Adipose-Derived Mesenchymal Stem

Cell (ADMSC)-derived Exosomes on Amelioration of Dextran Sulfate Sodium (DSS)-induced Acute Colitis. *Am. J. Transl. Res.* 11 (5), 2706–2724.

Claridge, B., Lozano, J., Poh, Q. H., and Greening, D. W. (2021). Development of Extracellular Vesicle Therapeutics: Challenges, Considerations, and Opportunities. *Front. Cell Dev. Biol.* 9, 734720. doi:10.3389/fcell.2021.734720

Liu, X., Cheng, D., Cui, M., Qu, F., Yu, J., Tang, Z., et al. (2022). Exosome Marker Proteins of Tumor-Associated Fibroblasts and Exosome-Derived miR-92a-3p Act as Potential Biomarkers for Liver Cancer. *Crit. Rev. Eukaryot. Gene. Expr.* 32, 49–57. doi:10.1615/CritRevEukaryotGeneExpr.2021039570

Logozzi, M., Angelini, D. F., Giuliani, A., Mizzoni, D., Di Raimo, R., Maggi, M., et al. (2019). Increased Plasmatic Levels of PSA-Expressing Exosomes Distinguish Prostate Cancer Patients from Benign Prostatic Hyperplasia: A Prospective Study. *Cancers (Basel)* 11, 1449. doi:10.3390/cancers11101449

Murphy, D. E., de Jong, O. G., Brouwer, M., Wood, M. J., Lavieu, G., Schiffelers, R. M., et al. (2019). Extracellular Vesicle-Based Therapeutics: Natural versus Engineered Targeting and Trafficking. *Exp. Mol. Med.* 51 (3), 1–12. doi:10.1038/s12276-019-0223-5

Sun, C. K., Chen, C. H., Chang, C. L., Chiang, H. J., Sung, P. H., Chen, K. H., et al. (2017). Melatonin Treatment Enhances Therapeutic Effects of Exosomes against Acute Liver Ischemia-Reperfusion Injury. *Am. J. Transl. Res.* 9 (4), 1543–1560.

Szabo, G., and Momen-Heravi, F. (2017). Extracellular Vesicles in Liver Disease and Potential as Biomarkers and Therapeutic Targets. *Nat. Rev. Gastroenterol. Hepatol.* 14 (8), 455–466. doi:10.1038/nrgastro.2017.71

Xu, R., Rai, A., Chen, M., Suwakulsiri, W., Greening, D. W., and Simpson, R. J. (2018). Extracellular Vesicles in Cancer - Implications for Future Improvements in Cancer Care. *Nat. Rev. Clin. Oncol.* 15 (10), 617–638. doi:10.1038/s41571-018-0036-9

Conflict of Interest: The authors declare that the research was conducted in the absence of any commercial or financial relationships that could be construed as a potential conflict of interest.

Publisher's Note: All claims expressed in this article are solely those of the authors and do not necessarily represent those of their affiliated organizations, or those of the publisher, the editors and the reviewers. Any product that may be evaluated in this article, or claim that may be made by its manufacturer, is not guaranteed or endorsed by the publisher.

frontiers in Cell and Developmental Biology

REVIEW
published: 08 June 2021
doi: 10.3389/fcell.2021.686551

An Examination of the Putative Role of Melatonin in Exosome Biogenesis

Hassan Amini[1], Aysa Rezabakhsh[2], Morteza Heidarzadeh[3], Mehdi Hassanpour[4], Shahriar Hashemzadeh[5], Shahrouz Ghaderi[6], Emel Sokullu[3], Reza Rahbarghazi[4,7†] and Russel J. Reiter[8*†]*

[1] Student Research Committee, Tabriz University of Medical Sciences, Tabriz, Iran, [2] Cardiovascular Research Center, Tabriz University of Medical Sciences, Tabriz, Iran, [3] Koç University Translational Medicine Research Center (KUTTAM), Istanbul, Turkey, [4] Stem Cell Research Center, Tabriz University of Medical Sciences, Tabriz, Iran, [5] Tuberculosis and Lung Disease Research Center, Tabriz University of Medical Sciences, Tabriz, Iran, [6] Medical Faculty, Institute of Molecular Medicine III, Heinrich Heine University Düsseldorf, Düsseldorf, Germany, [7] Department of Applied Cell Sciences, Faculty of Advanced Medical Sciences, Tabriz University of Medical Sciences, Tabriz, Iran, [8] Department of Cell Systems and Anatomy, University of Texas Health Science Center at San Antonio, San Antonio, TX, United States

OPEN ACCESS

Edited by:
Ming Dong,
Guangzhou Institutes of Biomedicine and Health, Chinese Academy of Sciences (CAS), China

Reviewed by:
Youliang Wang,
Beijing Institute of Technology, China
Shasha Zhang,
Southeast University, China

***Correspondence:**
Reza Rahbarghazi
rahbarghazir@tbzmed.ac.ir;
Rezarahbardvm@gmail.com
Russel J. Reiter
reiter@uthscsa.edu

† These authors have contributed equally to this work

Specialty section:
This article was submitted to Molecular Medicine, a section of the journal Frontiers in Cell and Developmental Biology

Received: *27 March 2021*
Accepted: *07 May 2021*
Published: *08 June 2021*

Citation:
Amini H, Rezabakhsh A, Heidarzadeh M, Hassanpour M, Hashemzadeh S, Ghaderi S, Sokullu E, Rahbarghazi R and Reiter RJ (2021) An Examination of the Putative Role of Melatonin in Exosome Biogenesis. Front. Cell Dev. Biol. 9:686551. doi: 10.3389/fcell.2021.686551

During the last two decades, melatonin has been found to have pleiotropic effects via different mechanisms on its target cells. Data are abundant for some aspects of the signaling pathways within cells while other casual mechanisms have not been adequately addressed. From an evolutionary perspective, eukaryotic cells are equipped with a set of interrelated endomembrane systems consisting of intracellular organelles and secretory vesicles. Of these, exosomes are touted as cargo-laden secretory vesicles that originate from the endosomal multivesicular machinery which participate in a mutual cross-talk at different cellular interfaces. It has been documented that cells transfer various biomolecules and genetic elements through exosomes to sites remote from the original cell in a paracrine manner. Findings related to the molecular mechanisms between melatonin and exosomal biogenesis and cargo sorting are the subject of the current review. The clarification of the interplay between melatonin and exosome biogenesis and cargo sorting at the molecular level will help to define a cell's secretion capacity. This review precisely addresses the role and potential significance of melatonin in determining the efflux capacity of cells via the exosomal pathway. Certain cells, for example, stem cells actively increase exosome efflux in response to melatonin treatment which accelerates tissue regeneration after transplantation into the injured sites.

Keywords: melatonin, exosome biogenesis, interplay signaling pathways, cross talk, paracrine activity

INTRODUCTION

Numerous bioactivities and therapeutic effects of melatonin have been reported, especially within the last two decades. This hydrophobic molecule is produced by the pineal gland, specifically during the night, and in perhaps the mitochondria of all other cells (Tan et al., 2013; Reiter et al., 2020; **Figure 1**). Melatonin functions via well-described signaling pathways in host cells (Wei et al., 2020). When used by humans, melatonin is typically taken in the evening to improve sleep and, under some clinical conditions, also throughout the day (Castillo et al., 2020; Matar et al., 2021). By means of juxtacrine interactions, cells can transfer soluble biomolecules and factors to other cells at near and remote distances in a paracrine manner using nano-sized vesicles identified as exosomes (Whitham et al., 2018). Exosomes, which range from 40 to 200 μm, develop a suitable

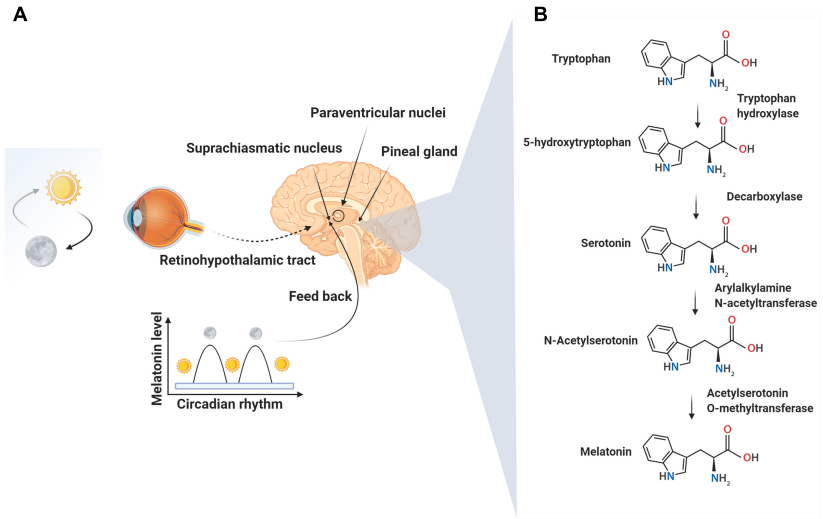

FIGURE 1 | Neural control of melatonin synthesis in the pineal gland **(A)**. Melatonin, a well-known sleep-promoting molecule, is produced in the pineal gland as summarized in this figure. The secretion of melatonin is tightly controlled by suprachiasmatic and paraventricular nuclei in response to the light: dark cycle and the circadian clock mechanisms of the suprachiasmatic nuclei. The peak secretion of melatonin occurs at night time and reaches minimum levels at day. The synthesis of melatonin is a result of the enzymatic conversion of tryptophan to melatonin via the intermediate, molecule, serotonin **(B)**.

biological platform of biomolecule exchange and mutual crosstalk. Distinct intracellular mechanisms for sorting, trafficking, and abscission have been described, all of which are relevant to exosome biogenesis (Soekmadji et al., 2017). The presence of various genomic and proteomic factors inside exosomes makes them important agents that promote/inhibit certain signaling pathways once they reach their target cells (Minciacchi et al., 2015). Cells release the exosomes under physiological and pathological conditions in response to different factors. Whether the quantity and quality of exosomal cargo differ in different states is the subject of debate (Hooper et al., 2020). Research progress has led to a partial understanding of the intracellular mechanisms involved in exosome biogenesis. Several factors involving the regulation, synthesis, and abscission of exosomes require further studies. Various signaling cascades with multiple effectors are differentially regulated by endogenous or exogenous molecules which in turn influence exosome homeostasis (Bagheri et al., 2018). Within a cell, reciprocal crosstalk between the exosome-contained molecules and other signaling pathways regulate the paracrine capacity via the modulation of exosome biogenesis and abscission (Hassanpour et al., 2018a; Xu et al., 2018). Recent work has focused on the regulatory impact of melatonin on exosome biogenesis (Yoon et al., 2020). This review provides information related to the association of exosomes with melatonin signaling pathways. These pathways have been shown to determine and/or enhance the paracrine actions of melatonin.

EXOSOME BIOGENESIS AND FUNCTION

Exosomes are small microvesicles of endosomal origin. Exosomes are functionally linked to multivesicular bodies (MVBs) and released after the fusion of MVBs with the cell membrane (**Figure 2**; Théry et al., 2009). Exosomes originate from terminal endosomes that are formed by the inward budding of the MVB membrane. In large MVBs, numerous intraluminal vesicles (ILVs) harboring exosomes are obvious (Minciacchi et al., 2015). Of note, ILVs are enriched in various cytosolic components such as soluble proteins, DNA, RNA, or microRNA. The receptor-mediated fusing of MVBs with the cell membrane releases the ILVs, now known as exosomes, into the extracellular matrix (ECM) (Valadi et al., 2007; Sahu et al., 2011). The complex protein machinery consists of four separate proteins including ESCRT-0, -I, -II, and -III and constitute the endosomal sorting complex required for transport (ESCRT) which accounts for MVB formation, vesicle budding, and cytosolic component cargo sorting (**Figure 2**; Record, 2014). The integrity of ESCRTs and complementary proteins is central to exosome biogenesis (Hurley, 2015). All the ESCRT subunits act via an ubiquitin-dependent pathway. The ubiquitin-binding subunits of ESCRT-0 sequester the ubiquitinated proteins at specialized domains of the endosomal membrane. Following the sequestration of target molecules, ESCRT-I and -II join the complex to develop a high-affinity recognition domain for the ubiquitinated proteins. The addition of the final subunit, ESCRT-III, causes the invagination of the lipid membrane and isolation of ILVs inside the MVB. Vps4 protein provides the energy required to separate buds from the MVB to form ILVs after the addition of ESCRT-III to the ESCRT-0, -I, and -II complexes (**Figure 2**; Ageta and Tsuchida, 2019). It is postulated that ESCRT machinery may influence exosomal quantity, size, and major cargo protein (Colombo et al., 2013).

The apparent specificity and function of exosomes have been determined. They are known to not only harbor exhausted biomolecules but also may contain specific therapeutic molecules

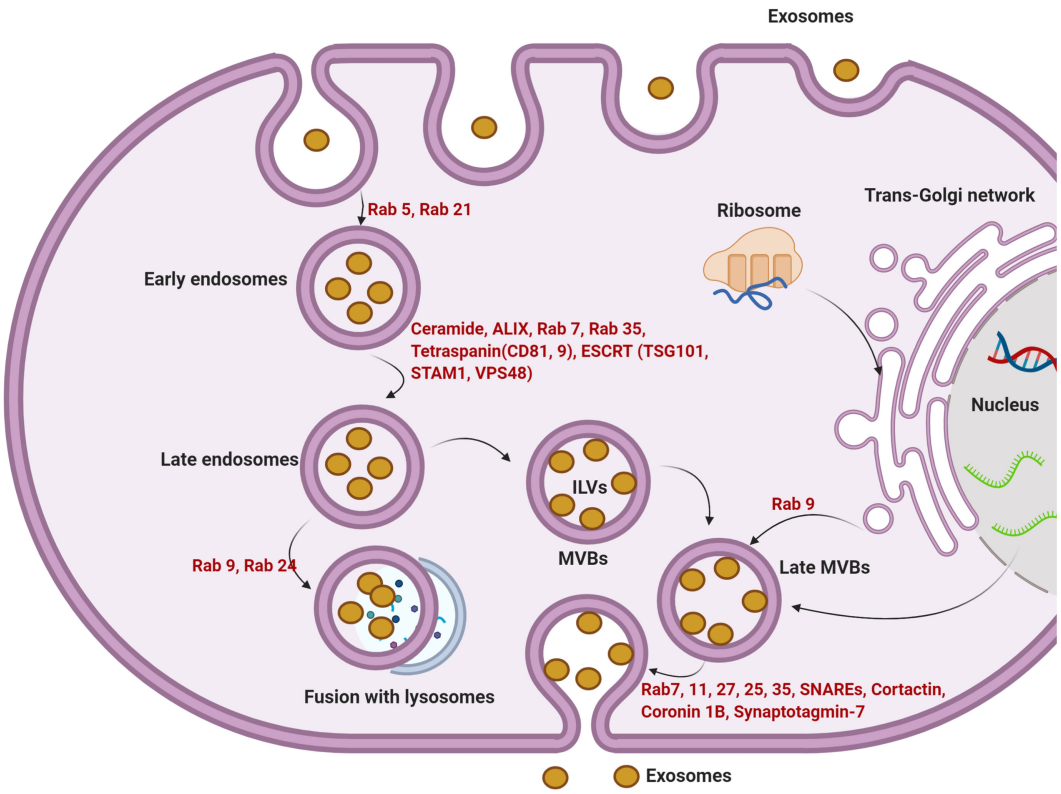

FIGURE 2 | The multi-step intracellular maturation of exosomes is illustrated. For the initial internalization via endocytosis, GTPases including Rab5 and Rab21 play a significant role in the formation of early endosomes. The formation of late endosomes is done via engaging other important factors such as ceramide, ALIX, Rab7, 35, tetraspanins, and ESCRT complex. Due to the activity of other Rab types (Rab9 and 24), later endosomes are directed to lysosomes. Alternatively, late endosomes become MVBs. The invagination of the MVBs membrane forms numerous ILVs. Upon the release of ILVs to the ECM, they are thereafter referred to as exosomes. *Trans*-Golgi apparatus further supports an alternative way to form MVBs by the activity of certain GTPases such as Rab9. The fusion of later MVBs to the cell membrane is mediated by different effectors including Rab7, 11, 27, 25, 37, SNAREs, and other elements. ILVs, intraluminal vesicles; MVBs, multivesicular bodies; ESCRT, endosomal sorting complex required for transport; SNARE, soluble N-ethylmaleimide-sensitive factor attachment protein receptors.

with the ability to alter the function of target cells in relation to the immune response, antigen presentation, multiple signaling transduction actions in distant cells far from the original host cell (Huang-Doran et al., 2017; Hessvik and Llorente, 2018). The critical roles of exosomes have been implicated in multiple biological phenomena including important functions in tissue growth and development (Yáñez-Mó et al., 2015). However, direct evidence for the exact mechanism of action of exosomes on target cells is lacking. Using an N-ethyl maleimide-sensitive agent, an attachment protein receptor (SNARE) and membrane-bound Rab-GTPase, mainly Rab27, 11, and 35, were identified. Via these elements, MVBs are directed to the plasma membrane for the release of ILVs, exosomes, into the extracellular matrix (ECM) (**Figure 2**; Rezaie et al., 2018).

Evidence points to the paracrine and autocrine activity of released exosomes (Fitzner et al., 2011; Colombo et al., 2014). How released exosome contents act on specific distant cells in an autocrine manner rather than interacting with neighboring cells requires further investigation. The autocrine activity likely occurs in response to conditions when the host cells require stimulation or to recycle cargo protein (Xu et al., 2018). Numerous studies have explored the exosome cellular uptake and intracellular trafficking in acceptor cells. Several lines of evidence show that exosome influx is achieved through different pathways including direct fusion with the host cell membrane, receptor/ligand interaction, and internalization. Macropinocytosis, phagocytosis, and endocytosis are non-specific internalization mean for the transfer of exosomes into the cytosol (Mulcahy et al., 2014).

The rate of endocytosis increases when the generation of filopodia and lamellipodia is initiated. The distribution of cell membrane via cytoskeletal remodeling provides a platform to determine their uptake by different cells (Kamerkar et al., 2017). The existence of CD47 on the exosome surface mediates the "do not eat me" signal and helps them to evade internalization into the target cells (Kamerkar et al., 2017). CD47 also has an essential function to increase exosome transit time in the biofluids and blood (Zheng et al., 2020). Unlike the internalization pathway, the receptor/ligand interaction relies on the specific binding of ICAM-1 at the exosome surface with the LFA-1 receptor on the target cell plasma membrane (Segura et al., 2005). Data suggest the existence of specific molecules on the exosome's surface that determine exosome

internalization (Huang-Doran et al., 2017; Hessvik and Llorente, 2018). Whether receptor/ligand interaction, fusion, and the internalization pathway are dominant in exosome uptake under certain conditions remain undefined.

MELATONIN BIOGENESIS AND MECHANISM OF ACTION

N-acetyl-5-methoxytryptamine, known as melatonin, is produced in the pineal gland and likely in the mitochondria of all other tissues; this ubiquitous molecule has highly pleiotropic effects (Claustrat and Leston, 2015). Pineal melatonin secretion into the blood and cerebrospinal fluid is linked to the light/dark cycle (**Figure 1**; Reiter et al., 2014). Other cells that synthesize melatonin may release the product into the extracellular space but not into the blood. While the pineal gland is touted as the main site of melatonin synthesis, the total amount of melatonin originating from the pineal is small compared to that produced in other cells (Acuña-Castroviejo et al., 2014; Touitou et al., 2017). In the pineal gland, the endogenous rhythm of secretion is regulated by the activity of suprachiasmatic nuclei, the activity of which, in turn, is influenced by the light perception by the retina (**Figure 1**; Pfeffer et al., 2018). Significant roles of melatonin include conveying circadian information related to the daily cycle of light and darkness and the regulation of immune system function, antioxidant defenses, glucose metabolism, angiogenesis, etc (Manchester et al., 2015; Tordjman et al., 2017; Zhou et al., 2018). The binding of norepinephrine to adrenergic receptors on the pinealocytes is the accepted mechanism leading to the nocturnal synthesis of melatonin by the pineal gland. Following norepinephrine-adrenergic receptor engagement, the activation of adenylate cyclase increases cAMP and *de novo* synthesis of serotonin-N-acetyl transferase, the rate-limiting enzyme in melatonin production (González et al., 2012). In addition to the ligand-receptor pathway, the melatonin synthesis rate may be influenced by intracellular tryptophan and substrate (serotonin) availability and by folic acid and pyridoxine (Zhao D. et al., 2019). Two membrane-bound melatonin receptors (MT1 and MT2) have been identified on pinealocyte membranes which trigger the changes in cAMP through inhibitory G proteins. The increase of cAMP activates downstream effectors like phospholipase-C and protein kinase-C through the MAPK/PI3K/Akt axis. It has been suggested that melatonin, because of its high lipophilicity, directly crosses the cell membrane to enter the blood and cerebrospinal fluid. This capacity facilitates melatonin's bio-distribution and access to all cells in the organism (Tan et al., 2018).

MELATONIN SIGNALING PATHWAY

The melatonin membrane receptors, MT1 and MT2, belong to G-protein coupled receptor (GPCR) subfamily and are widely distributed, accounting for many of melatonin's pleiotropic functions (**Figure 3**; Dupré et al., 2018). Besides its receptor-mediated actions, melatonin also enters cells where it has receptor-independent functions (Hardeland, 2009). Once melatonin crosses the plasma membrane, it may also bind to a cytosolic receptor, MT3. The underlying mechanisms supporting the exact role of intracellular MT3 need further investigation.

MT1 and MT2 have seven transmembrane domains and they have several different signaling pathways within cells (Salon et al., 2011). Studies targeting MTs and GPCR indicate that the binding of melatonin to these receptors leads to increased cAMP production, phosphorylation, calcium movements, and morphological adaptation (Ellisdon and Halls, 2016). Results show that MT1 inhibits forskolin-stimulated cAMP formation, phosphorylation of cAMP-responsive element-binding protein (CREB), and PKA activity after melatonin binding (**Figure 3**; Emet et al., 2016). The activation of MT1 by melatonin is thought to trigger ERK1/2 responsible for cytoskeleton filament remodeling in neuronal cells (Moreno et al., 2020). MT1 and MT2 have glycosylation sites in the extracellular N-terminal region while the cytoplasmic tail consists of fourth intracellular loops and cysteine residues with palmitoylation capability (Dubocovich and Markowska, 2005). The binding of melatonin to MT2 is in accord with phase-shifting and circadian rhythms while MT1 blunts neural firing and phase-shifting (Hunt et al., 2001; Hardeland, 2009). Both MT1 and MT2 are heterodimers and attached to G proteins like α_{i2}, α_{i3}, α_i, and β and γ. The function of melatonin inside the cells is associated with the activation of diverse subunits of G-proteins connected to MTs and the pattern of downstream interactions.

The activation of MT2 by melatonin is responsible for the reduction of intracellular cAMP ratio and activation of protein kinase C and phospholipase C (**Figure 3**; Hunt et al., 2001; Rivera-Bermúdez et al., 2004; Birnbaumer, 2007). Activation of G-proteins mediates membrane permeability, allowing ion channels to be opened (Hardeland, 2009). Because of cGMP elevation, it is postulated that this secondary messenger enhances calcium uptake via the cyclic nucleotide-gated channels (Rimler et al., 2007). Melatonin is involved in several transcription processes and gene expression via the regulation of CREB and ERK (Cecon et al., 2018). Binding to multiple intracellular effectors is an additional mechanism-specific to melatonin which is associated with its lipophilic properties (Emet et al., 2016). This is based on the results showing the existence of several putative cytosolic melatonin receptors including enzyme quinone reductase 2 (the MT3 receptor), RORα/RZR nuclear receptors, and calmodulin (**Figure 3**; Jockers et al., 2008). Evidence points to immune cells as the main sites of RORα1 and RORα2 responsible for mediating melatonin effects while RZRβ is abundant in the pineal gland (Pandi-Perumal et al., 2006). RORα was shown to be an active receptor in the regulation of antioxidant enzymes (Hardeland, 2009). The function of RORα in rat cardiomyocytes after myocardial ischemic reperfusion injury shows its basic role in the control of inflammation and oxidative stress (**Figure 3**; He et al., 2016). It is similarly observed that melatonin reaches different cellular constituents through its lipophilic property and via receptor-independent pathways (Venegas et al., 2012).

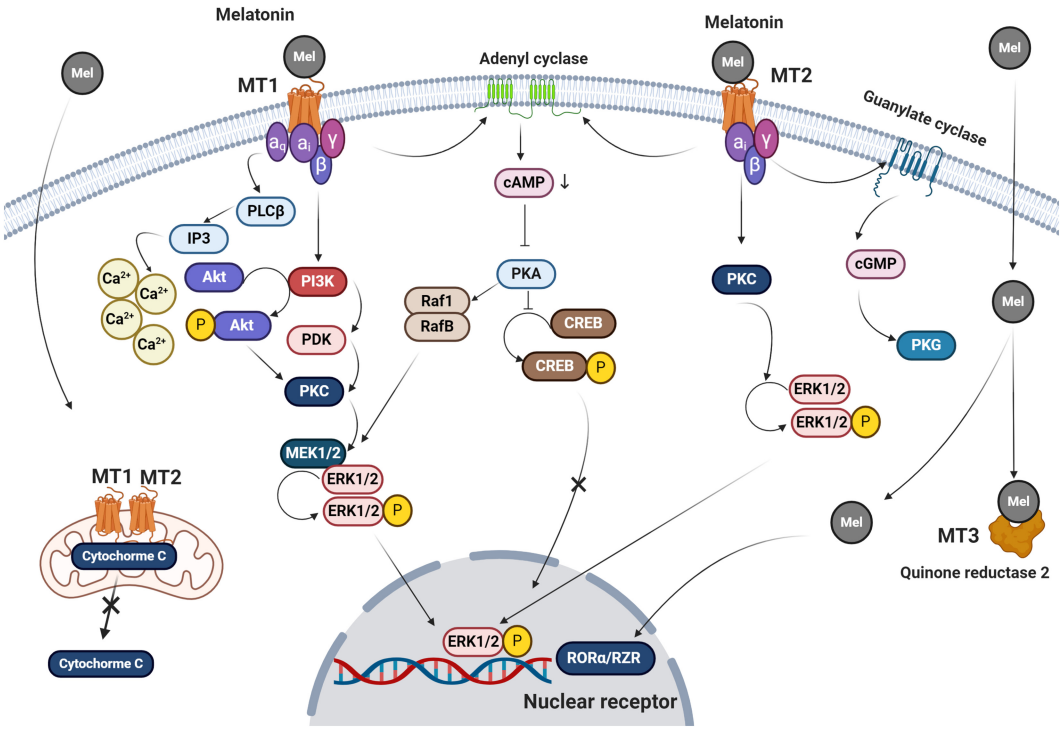

FIGURE 3 | Melatonin signaling pathways are summarized in this figure. Both MT1 and MT2 belong to the GPCRs family of receptors. Melatonin also crosses the plasma membrane via passive diffusion. Upon the attachment of melatonin to MT1 and MT2, different effectors including PKC, PLCβ, and PKA are recruited as second messengers to trigger downstream signaling pathways. For subsequent events, the melatonin-MT1 complex linked α_q, α_i, β, and γ subunits to activate IP3 and intracellular accumulation of Ca^{+2} after its release from the endoplasmic reticulum. Ca^{+2} phosphorylates both PKC and ERK1/2. MT1 receptor also acts through membrane adenyl cyclase, which blocks the phosphorylation of CREB by activation of cAMP and PKC. Melatonin binding to MT2 activates the adenyl cyclase and leads to CREB inactivation. Melatonin promotes conformational changes in MT2 and activation of α_i subunit leads to stimulation of PKG via guanylate cyclase. Also, MT2 engages PKC and ErK1/2 complexes. Melatonin crosses the plasma membrane via passive diffusion and transporters and activates both mitochondrial MT1 and 2 thereby reducing the escape of cytochrome C into the cytosol. Other possible melatonin receptors include cytosolic quinone reductase 2 which activates nuclear RORα/RZR. Mel, melatonin; cAMP, cyclic adenosine monophosphate; cGMP, cyclic guanosine monophosphate; MT, melatonin receptor; PKC, protein kinase C; PKA, protein kinase A; CREB, cAMP response element-binding protein; IP3, inositol trisphosphate; and PDK, pyruvate dehydrogenase kinase.

EFFECT OF MELATONIN ON EXOSOME BIOGENESIS AND RELEASE

Due to the unique diverse functions of melatonin, it is considered a possible modulator of exosome biogenesis and function (Yoon et al., 2020). How melatonin modulates the function of exosomes under physiological and pathological conditions is under investigation (**Figure 4**). By identifying the mechanism of action of melatonin as it relates to exosome function, will allow researchers and clinicians to take advantage of the known functions of these important microvesicles. As an example, this may allow for the control of stem cell therapeutic effects in the context of regeneration and other pathological conditions. Using a variety of experimental models in stem cell research, knowledge related to the possible role of exosomes in the alleviation of pathological changes has accumulated (Bang and Kim, 2019; Park et al., 2019; Zhao L. et al., 2019). Recent investigations have established the synergistic effect of melatonin and adipose-derived mesenchymal stem cell (MSC) exosomes in suppressing inflammation, oxidative stress, and apoptosis in a rat model of hepatic ischemia/reperfusion (I/R) (Sun et al., 2017; Chang et al., 2019).

These data are also consistent with other observations showing that exosomes of bone marrow MSCs pre-conditioned with melatonin have benefits in MSCs via paracrine which improved therapeutic efficacy on I/R induced acute renal failure (Alzahrani, 2019; Zahran et al., 2020). However, the exact relevance of melatonin as to its activities, such as those conveyed by exosomes, remains unknown (He et al., 2016). Based on our recent findings melatonin alters exosome size and production in bovine granulosa cells in a dose-dependent manner in which higher melatonin concentrations contribute to the elevated release of small-sized exosomes (Pournaghi et al., 2021). This may be due to the promotion of ILVs formation and/or alterations of exosome physicochemical properties.

Whether melatonin is also transferred via exosomes between the cells needs further investigation. The direct passive diffusion of melatonin through cell membranes is accepted. Also, oligopeptide and glucose transporters are alternate routes to deliver melatonin into the cytosol (Venegas et al., 2012; Mayo et al., 2017). Given its lipophilicity and rapid passive diffusion,

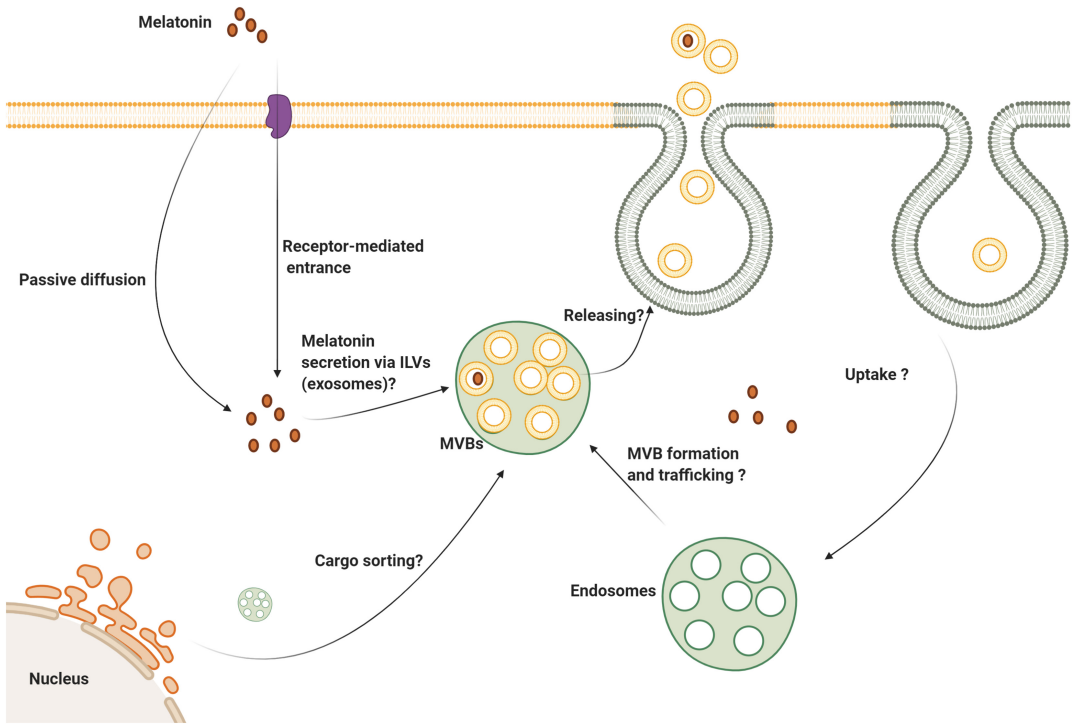

FIGURE 4 | Several aspects of melatonin's effect on exosome biogenesis and secretion are still unknown. Melatonin can enter the cells via membrane-bound receptors and passive diffusion. It is logical to state that melatonin can be secret via the exosomes to the extracellular niche. Whether melatonin directly or indirectly influences exosome biogenesis, trafficking and abscission need further investigation.

it is speculated that melatonin transfers horizontally between cells independent of membrane transporters. Interestingly, the transfer of MT1 via internalization, endocytic transport has been explored directly (Abd-Elhafeez et al., 2017). Once melatonin binds MT1, vacuolar sorting machinery transfers the internalized MT1 to the early endosomes using Rab5. Due to the activity of other GTPases like Rab11 and 7, endosomes carrying MT1 can be recycled to the plasma membrane. Alternatively, late endosomes with surface Rab7 activity fuse with the lysosomes (Abd-Elhafeez et al., 2017). The inhibition of β-arrestin-2 by Valproic acid reduces basal endocytic transport of MT1 (Abd-Elhafeez et al., 2017). These data show the potential capacity of exosome transport in intracellular localization of the downstream effectors of the MT signaling pathway (**Figure 5**).

Although investigated to a lesser extent, the modulation of exosome biogenesis and changes in cargo composition in host cells has been studied. Using an *in vitro* model of Alzheimer's disease, Ozansoy et al. (2020) showed a reduction of tau carried by exosomes in human neuroblastoma cell line SHSY-5Y incubated with melatonin. They also observed that melatonin pre-treatment of cells before amyloid-β incubation did not affect exosomal tau levels or the intracellular hyperphosphorylated tau content (Ozansoy et al., 2020). A recent histological analysis of sheep testes showed enhanced exosome secretion from cytoplasmic extensions of telocytes located in seminal vesicles after administration of melatonin (Abd-Elhafeez et al., 2017). Following the application of melatonin, the morphology of telocytes was changed and the number and diameter of releasable exosomes increased (Abd-Elhafeez et al., 2017). This issue contrasts with some other results and the difference regarding melatonin's effect on exosome secretion may be associated with the final concentration of melatonin (either physiological or pharmacological dose). On the basis of the published data, and despite its unique functions in different cell types, it is proposed that melatonin has the potential to regulate exocytosis and exosome delivery.

It is unclear why and how melatonin increases or decreases exosome secretion under different metabolic circumstances. Whether the dose of melatonin or the physiological state of a cell is influential in the exocytosis rate should be further examined. Moreover, the precise signaling pathways involved in exosome biogenesis and secretion upon treatment with melatonin remain unclear. Attempts to identify a correlation between melatonin receptors and exocytosis yielded evidence of relevant signaling cascades (Liu et al., 2015). This group found that the Akt/GSK-3β/CRMP-2 axis is an intermediate molecular process between MT2 and exocytosis in rat hippocampal neurons (**Figure 5**; Liu et al., 2015). Upon treatment of neurons with melatonin and activation of MT2, the PI3K/Akt axis suppressed GSK-3β activity and reduced phosphorylation of CRMP-2 allowing axonogenesis, exocytosis, and synaptic transmission (Liu et al., 2015). This pathway may be relevant to the regulation of exosome secretion and other extracellular vesicle types.

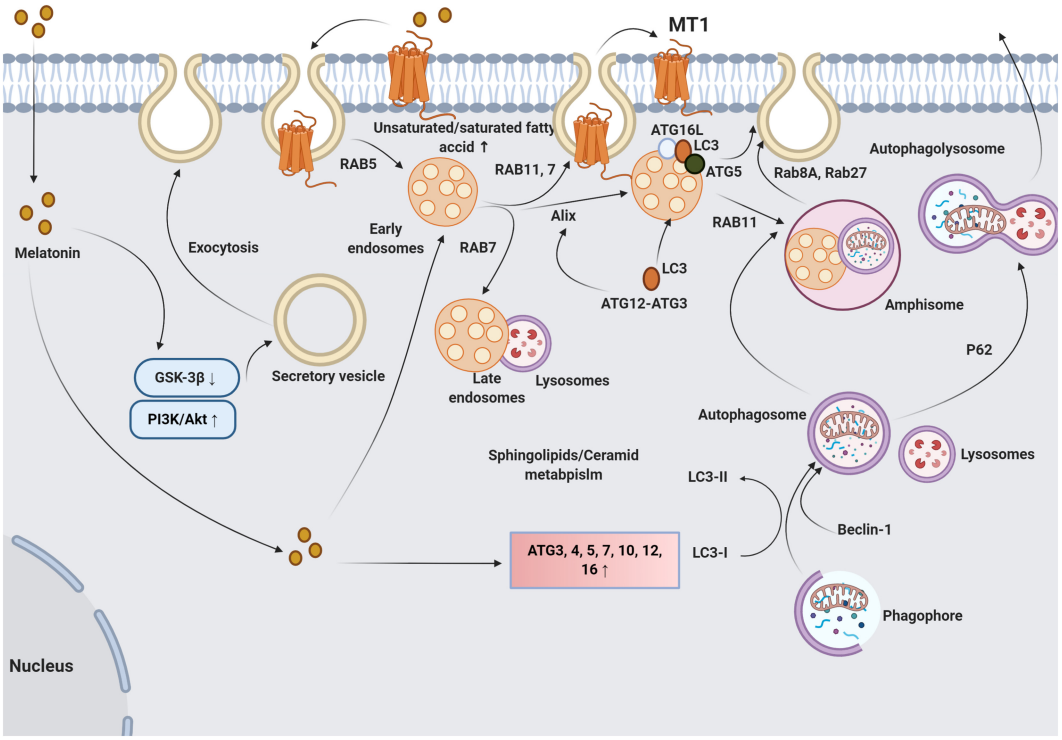

FIGURE 5 | The multiple possible means of molecular cross-talk between melatonin and exosome synthesis machinery are summarized here. Irrespective of melatonin how melatonin enters cells, it activates PI3K/Akt complex and inhibits GSK-3β, leading to fusion of secretory vesicles with plasma membrane and exocytosis. However, the underlying mechanisms have not been fully established. Changes in plasma membrane fluidity by an alteration of fatty acid composition (unsaturated/saturate fatty acid ratio) facilitate the exosome release. Also, melatonin promotes specific GTPases including Rab7 and 11 which accelerate the fusion of late MVBs with the plasma membrane. Upon binding of melatonin to MT1, the melatonin-MT1 complex is transferred to the early endosomes via vacuolar sorting machinery such as Rab5. The activation of Rab7 and 11 promotes endosomal secretion and recycles MT1 to the plasma membrane. Further activation of Rab7 directs endosomes with MT1 toward lysosomes which regulate the innate cell response to melatonin. How Rab 7 determines the fate of endosomes with melatonin (secretion or enzymatic digestion) needs further explorations. The interplay between melatonin and autophagy signaling pathway also influences the activity of exosome molecular machinery. Melatonin stimulates autophagic response directly via the activation of ATG4, 5, 7, 10, 12, and 16 and increases the LC3II/I ratio. These features promote the formation of autophagolysosomes and autophagic exocytosis. Melatonin enhances the autophagic machinery including LC3, ATG3, 5, 12, and 16L on the late endosome membrane that facilitates the fusion of these elements with the plasma membrane. Melatonin also increases the intersection of autophagic vacuoles and exosomes into compartments named amphisomes which have multiple fates. Amphisomes can fuse with lysosomes via the activation of P62. The activity of Rab8 and 27a initiates the autophagic release of amphisomes to the ECM. GSK-3, glycogen synthase kinase 3; ATG, autophagy-related protein; P62, sequestosome 1; LC3, microtubule-associated protein 1A/1B-light chain 3; and PI3K/Akt, Phosphatidylinositol-3-kinase/Protein kinase B.

A quantitative analysis of multiples genes related to different signaling transduction pathways in *Saccharomyces cerevisiae* under oxidative stress revealed mild to moderate expression of 29 genes regulating transmembrane transport activity after treatment with melatonin (Sunyer-Figueres et al., 2020). It may be that whether and how simultaneous activation of MT1 and 2 influence exosome delivery is determined by the physiological state of the host cell. In addition to the molecular pathways that participate in exosome release, other findings indicate changes in the physicochemical properties of the cell membrane as a result of melatonin exposure (Sunyer-Figueres et al., 2020). The report claimed a moderate rise in the synthesis of unsaturated fatty acids and sphingolipids upon treatment with melatonin, indicating an increase in membrane flexibility and fluidity (Sunyer-Figueres et al., 2020). In our previous work, we found that melatonin can alter the unsaturated/saturated fatty acid ratio by increasing Arachidonic acid, Oleic acid, and Linoleic acid levels and change the flexibility of the cell membrane, leading to enhanced exosome delivery (Pournaghi et al., 2021).

This contrasts with the application of long-chain saturated fatty acids like palmitic acid on exosome release (Maly and Hofmann, 2020). It was suggested that the addition of 25 μM palmitic acid suppressed exosome release from prostatic carcinoma PC3 cells (Maly and Hofmann, 2020). The selective inhibition of sphingolipid-metabolizing enzymes such as neutral sphingomyelinase reduced exosome secretion from neural cell lineages (Yuyama et al., 2012). Collectively, the data suggest that an alteration in the metabolism of fatty acids by melatonin may be another molecular mechanism that influences exosome release from host cells.

It is also apparent that melatonin regulates exocytosis which is involved in the progression of apoptosis and autophagy (Luo et al., 2020). Based on the results of several different experiments, certain intracellular and cell-membrane bound

proteins are responsible for the fusion and transfer of multiple sets of vesicles. The emerging data point to the existence of subsets of molecular mechanisms shared between autophagy and exosome abscission (Xu et al., 2018). Autophagy-related proteins (ATG), consisting of different subsets, are key regulators of the autophagic response in the cytosol and plasma membrane (Hassanpour et al., 2018a). Data show that ATG5 and ATG16L1 are shared between autophagy signaling and exosome biogenesis (Guo et al., 2017). ATG5 separates vacuolar proton pumps, namely V_1V_o-ATPase, and inhibits acidification inside the MVBs, allowing the fusion of MVBs with the plasma membrane and release of ILVs (**Figure 5**; Xu et al., 2018). The treatment of endothelial progenitor cells with melatonin after exposure to advanced glycation end product decreased cell toxicity by autophagic response mediated by the up-regulation of P-62 and LC3II/I ratio (Jin et al., 2018). It is also suggested once the conjugation of LC3 is initiated via the activity of the ATG3-ATG12 complex, Alix, which belongs to the ESCRT complex, is provoked and interacts with LC3 (Murrow et al., 2015). Thus, cells with LC3 activity achieve the autophagic response and exosome abscission by the interaction of Alix with LC3, showing the integration of autophagy mechanism and exosome biogenesis. In the support of this claim, the inhibition of LC3 conjugation interrupts both exosome secretion and the autophagic response (Murrow et al., 2015). It should be noted, however, that the promotion of autophagy does not necessarily accelerate the secretion of ILVs.

It has been reported that the activation of autophagy-related machinery by rapamycin increased MVB-autophagosome fusion and generated hybrid vacuoles, referred to as amphisomes (Xu et al., 2018). Amphisomes release exosomal and autophagy contents using specific GTPases including Rab8a and Rab27a. Under some circumstances, amphisomes fuse with the cell membrane and are redirected toward lysosomes leading to the formation of autophagolysosomes and a reduction of exosome delivery (**Figure 5**; Villarroya-Beltri et al., 2016). It was suggested that the expression of GTPases such as Rab27a and Rab27b was increased in cumulus cells after treatment with melatonin for 7 days (Pournaghi et al., 2021).

Studies using endothelial progenitor cells treated with diabetic sera showed reduced exosome secretory capacity (Hassanpour et al., 2018b). Considering the shared machinery regulating exosome abscission and autophagy, the promotion of the autophagic response would be expected to stimulate exosome secretion in the presence of melatonin. However, direct evidence for autophagy-mediated exosome release after melatonin treatment is lacking.

To better understand the possible modulatory effect of melatonin on exosome biogenesis, we performed bioinformatic analyses using NetworkAnalyst version 3, and molecular networks were generated by the application of Network Visual Analytics (**Figure 6**). Based on our previous experience, the Wnt signaling pathway affects exosome biogenesis and secretion during physiological and pathological conditions of the endothelial lineage (Bagheri et al., 2018). To mine the relationship between melatonin and exosomes, we performed a bioinformatic analysis based on common genes related to the melatonin signaling pathway, exosomes biogenesis, and the Wnt cascade. Our analyses showed that transducin-like enhancer of split 4 (TLE4) is a common effector that cross-links these three pathways. TLE4 belongs to the TLE family of transcription co-repressors. The TLE family members do not directly attach to the DNA. These proteins could generate repressor complexes after binding to Runx2, Hes1, and T cell factor/lymphoid enhancer-binding factor (TCF/LEF) (Zhang et al., 2019). Upon the activation of toll-like receptors (TLRs)

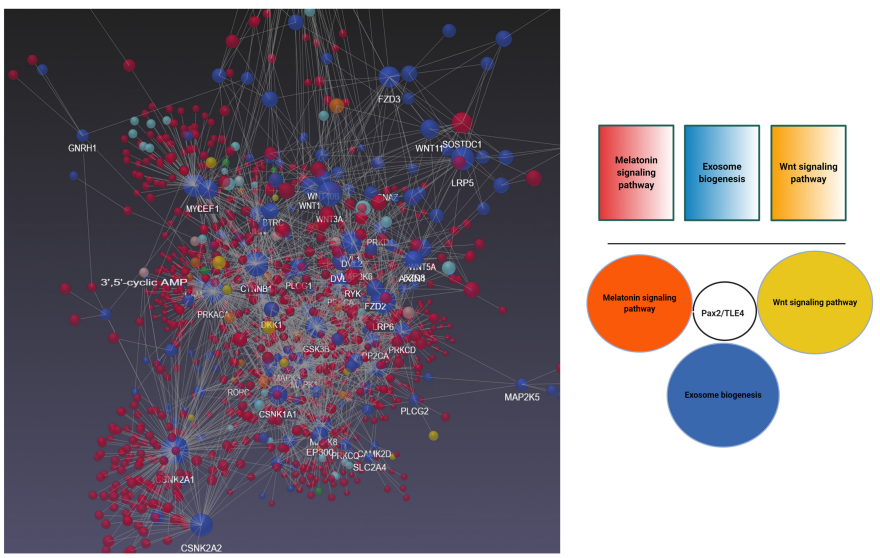

FIGURE 6 | Bioinformatics Analysis of Gene Expression Profiles of Wnt and melatonin signaling pathways with exosome biogenesis using NetworkAnalyst version 3. Data revealed shared Pax2/TLE4 interaction between Wnt, melatonin signaling pathway with exosome biogenesis.

TABLE 1 | Melatonin could alter exosomal cargo.

Type of study	Study design	Outcome	References
In vivo and *in vitro*	• Injection of bone marrow MSC-derived exosomes exposed to melatonin in a rat model of diabetic wound healing	IL-1β↓, TNF-α↓, and IL-10↑, Arg-1↓ and iNOS↓, Improved angiogenesis rate (CD31 and α-SMA↑), collagen synthesis↑, Increased M2 to M1 polarization via activation of PTEN/AKT signaling pathway	Liu et al., 2020
In vivo	• Hepatoprotection of adipocyte-derived exosomes in mice received melatonin compared to mice fed with a high-fat diet and resistin	Fatty acid accumulation in the liver↓, endoplasmic reticulum stress↓, hepatic steatosis↓, resistin-induced AMPKα phosphorylation↓, increased resistin mRNA degradation↑, Bmal1 transcriptional inhibition↑, and m^6 A RNA demethylation in adipocytes ↑	Rong et al., 2019
In vitro and in vivo	• Melatonin-treated hepatic carcinoma-exosomes effect on peritoneal macrophages immunosuppression capacity	Peritoneal macrophage phosphorylated STAT3↓, IL-6↓, IL-1β↓, IL-10↓, PD-L1↓, and TNF-α↓ in THP-1 cells,	Cheng et al., 2017
In vivo	• Maternal intraperitoneal of melatonin on lipopolysaccharide-induced neonatal brain inflammation	Microglial activity↓, Endoplasmic reticulum↓, Autophagy efflux↑, eIF2α phosphorylation↑, P62 and LC3↑, SIRT1↑, miR-34a↓, miR146a↓, and miR-126↓, Inflammatory response↓	Carloni et al., 2016
In vivo	• Injection of MSCs exosomes preconditioned with melatonin in a rat model of renal I/R injury	Tubular epithelial cell necrosis↓, Immune cell infiltration, and inflammation↓, BUN and creatinine levels ↓, Renal BUN and creatinine levels↑, MDA↓, NOx↓, HIF-1α↑, HO1↑, Apoptosis-related markers↓, Angiogenesis↑	Alzahrani, 2019

↓ Decrease; ↓ Increase; IL-1β, interleukin 1 beta; TNFα, tumor necrosis factor α; ARG1, arginase; iNOS, inducible nitric oxide synthase; αSMA, smooth muscle alpha-actin; CD31, platelet endothelial cell adhesion molecule; AMPKα, AMP-activated protein kinase α subunit; P62, sequestosome-1; LC3, microtubule-associated protein 1A/1B-light chain 3; PD-L1, programmed death-ligand 1; STAT3, signal transducer and activator of transcription 3; eIF2, eukaryotic initiation factor 2; BUN, blood urea nitrogen; MDA, malondialdehyde; NOx, nitrogen oxides; HIF-1α, hypoxia-inducible factor 1 alpha; HO-1, heme oxygenase-1.

including TLR2, 3, 4, and 7 by different ligands, the expression of TLE3 and 4 was initiated under pro-inflammatory status (Zhang et al., 2019). Based on our analyses, we found an interaction of TLE4 with Pax2 shared between melatonin and exosome biogenesis. Previously, the close interaction of melatonin and Wnt signaling pathways has been documented. As a result, the activation of Wnt4 through the ERK1/2-Pax2-Egr1 axis in preosteoblasts after exposure to melatonin increased bone formation capacity (Li et al., 2019). Whether activation of Pax2/TLE4 complex modulates the biogenesis of exosomes needs further investigations.

Research advances have confirmed the role of melatonin as a key player in the regulation of cell paracrine responses via exosome biogenesis. Further investigations should be directed at the characterization of the signaling pathways that regulate exosome biogenesis after treatment with melatonin. Identifying the molecular events by which melatonin modulates exosome biogenesis will likely soon become an active area of investigation.

EFFECT OF MELATONIN ON EXOSOME CARGO SORTING

Within the last decade, *in vivo* and *in vitro* evidence has shown that melatonin changes the molecular composition of exosome cargo (**Table 1**; Ozansoy et al., 2020). Progressive chronic changes such as chronic kidney disease, profoundly decrease the innate restorative capacity of MSCs (Zhao et al., 2020). Moreover, molecular analyses confirmed the existence of several factors, in the particular cellular prion protein (PrPC) and miR-4516, which participate in the regulation of angiogenesis (Alzahrani, 2019). These changes occurred concurrently with other desirable effects such as anti-aging actions and improvement of mitochondrial function after transplantation of MSCs treated with melatonin. These studies revealed that melatonin stimulates MSCs to release exosomes that are highly enriched with miR-4516-PrPC (Yoon et al., 2020). Other pro-angiogenic and anti-inflammatory factors have also been identified in MSC-derived exosomes pre-conditioned with melatonin (Liu et al., 2020). Exosomes isolated from melatonin-treated MSCs accelerated healing via an increase of microvascular density and suppression of inflammation in the rat model of diabetic wound healing (Liu et al., 2020).

Evidence for therapeutic effects of exosomes in hepatic disease has also been noted (Shen et al., 2014; Colica and Abenavoli, 2018). A recent study explored the hepato-protection of adipocyte-derived exosomes in mice who received melatonin (Rong et al., 2019). Compared to mice fed with resistin and a high-fat diet, melatonin application produced adipocyte-derived exosomes which are capable of reducing hepatic steatosis and endoplasmic reticulum stress (Rong et al., 2019). These data suggest that melatonin changes the exosome cargo and decreases phosphorylation of AMPK-α in Thr172 residue and that this activity prohibits endoplasmic reticulum and the development of hepatic steatosis (Rong et al., 2019). Owing to melatonin's pleiotropic effects, one scenario is that melatonin displays a regulatory mechanism on small molecules known as miRNAs which are subsequently released by exosomes (Hardeland, 2018a). Melatonin appears to alter m6 A RNA demethylation in adipocytes and changes the expression of resistin (Rong et al., 2019).

A large number of cancer cell exosomes, known also as oncosomes, containing multiple sets of miRNAs are involved in tumor metastasis and expansion (Cufaro et al., 2019; Jaiswal and Sedger, 2019). Melatonin is known to regulate

the transcription of certain miRNAs such as miR-155 and miR-21 in cancer cells. These miRNAs are responsible for tumor growth and metastasis (Hardeland, 2018b; Hunsaker et al., 2019). The alteration of exosomal miRNAs by melatonin not only inhibits the horizontal transfer of anaplastic-associated bio-information by exosomes but also recruits immune cells to the cancer site (Alfonsi et al., 2018; Wang et al., 2019). Studies have shown a moderate reduction in pro-inflammatory cytokines including TNF-α, IL-6, -10, -1β and programmed death-ligand 1 by macrophages incubated with hepatocellular carcinoma-derived exosomes pre-conditioned with melatonin (Cheng et al., 2017). The regulation of STAT3 may play a critical role in the immunomodulatory actions of carcinoma-derived exosomes (Cheng et al., 2017). Under other circumstances, such as lipopolysaccharide-induced Alzheimer's disease in rat neonates, melatonin decreases the pathological complications via the autophagy-SIRT-1 pathway and down-regulation of multiple miRNAs including miR-34a, -146a, and -126 (Meng et al., 2014; Carloni et al., 2016). Similarly, Heo et al. (2020) showed that melatonin-stimulated exosomes isolated from adipose-derived mesenchymal stem cells suppressed inflammation. These exosomes were enriched with multiple miRNAs such as miR-34a, -124, and -135b compared to non-treated melatonin exosomes.

Since various accessory factors are shared by autophagy and exosome signaling pathways, it is presumed that melatonin inhibits the progression of Alzheimer's disease by activation of exocytosis via both autophagy efflux and exosome secretion. This possibility as it relates to neurodegenerative diseases needs further analysis.

A recent study reported by Wang et al. (2020) injected blood-derived exosomes of melatonin-treated rats into the brain after focal cerebral ischemia. Melatonin changed the exosomal miRNAs profile and reduced ischemic changes via the promotion of angiogenesis, neurogenesis, and suppression of apoptosis. It is felt that melatonin alters cargo sorting in the exosomes. Attempts to investigate the effect of melatonin on exosome functions have not yielded a definition of the molecular mechanisms by which it controls exosome dynamics.

CONCLUDING REMARKS AND PERSPECTIVES

Research progress has led to the partial clarification of melatonin's efficacy in the modulation of exosomal biogenesis. What has been uncovered is that melatonin can alter the exosome biogenesis, intracellular trafficking, and abscission at the molecular levels by engaging different effectors. Further investigations should be focused on the identification of commonly shared pathways between exosome biogenesis and the melatonin signaling cascade. Based on the dose- and context-dependent activity of melatonin on the target cell populations, the findings related to these interactions will have to be interpreted with caution. Questions related to the heterogeneity and functions of effectors shared between two signaling pathways are still unanswered. Advancements in molecular biological analyses and improved technologies will be aids in clarifying melatonin-exosome interactions at different subcellular levels.

AUTHOR CONTRIBUTIONS

HA, AR, MHe, MHa, SH, and ES collected the data and prepared the draft. SG performed the bioinformatic analysis. RR and RJR edited and supervised the manuscript. All authors contributed to the article and approved the submitted version.

FUNDING

This study was approved and supported by the Student Research Committee, Tabriz University of Medical Sciences (Registration code: 66480).

ACKNOWLEDGMENTS

The authors thank the personnel of the Faculty of Advanced Medical Sciences for their support.

REFERENCES

Abd-Elhafeez, H. H., Mokhtar, D. M., and Hassan, A. H. (2017). Effect of melatonin on telocytes in the seminal vesicle of the Soay ram: an immunohistochemical, ultrastructural and morphometrical study. *Cells Tissues Organs* 203, 29–54. doi: 10.1159/000449500

Acuña-Castroviejo, D., Escames, G., Venegas, C., Diaz-Casado, M. E., Lima-Cabello, E., López, L. C., et al. (2014). Extrapineal melatonin: sources, regulation, and potential functions. *Cell. Mol. Life Sci.* 71, 2997–3025. doi: 10.1007/s00018-014-1579-2

Ageta, H., and Tsuchida, K. (2019). Post-translational modification and protein sorting to small extracellular vesicles including exosomes by ubiquitin and UBLs. *Cel. Mol. Life Sci.* 76, 4829–4848. doi: 10.1007/s00018-019-03246-7

Alfonsi, R., Grassi, L., Signore, M., and Bonci, D. (2018). The double face of exosome-carried microRNAs in cancer immunomodulation. *Int. J. Mol. Sci.* 19:1183. doi: 10.3390/ijms19041183

Alzahrani, F. A. (2019). Melatonin improves therapeutic potential of mesenchymal stem cells-derived exosomes against renal ischemia-reperfusion injury in rats. *Am. J. Transl. Res.* 11, 2887–2907.

Bagheri, H. S., Mousavi, M., Rezabakhsh, A., Rezaie, J., Rasta, S. H., Nourazarian, A., et al. (2018). Low-level laser irradiation at a high power intensity increased human endothelial cell exosome secretion via Wnt signaling. *Lasers Med. Sci.* 33, 1131–1145. doi: 10.1007/s10103-018-2495-8

Bang, O. Y., and Kim, E. H. (2019). Mesenchymal stem cell-derived extracellular vesicle therapy for stroke: challenges and progress. *Front. Neurol.* 10:211. doi: 10.3389/fneur.2019.00211

Birnbaumer, L. (2007). Expansion of signal transduction by G proteins: the second 15 years or so: from 3 to 16 α subunits plus βγ dimers. *Biochim. Biophys. Acta* 1768, 772–793.

Carloni, S., Favrais, G., Saliba, E., Albertini, M. C., Chalon, S., Longini, M., et al. (2016). Melatonin modulates neonatal brain inflammation through endoplasmic reticulum stress, autophagy, and miR-34a/silent information regulator 1 pathway. *J. Pineal Res.* 61, 370–380. doi: 10.1111/jpi.12354

Castillo, R. R., Quizon, G. R. A., Juco, M. J. M., Roman, A. D. E., de Leon, D. G., Punzalan, F. E. R., et al. (2020). Melatonin as adjuvant treatment for coronavirus disease 2019 pneumonia patients requiring hospitalization (MAC-19 PRO): a case series. *Melatonin Res.* 3, 297–310. doi: 10.32794/mr11250063

Cecon, E., Oishi, A., and Jockers, R. (2018). Melatonin receptors: molecular pharmacology and signalling in the context of system bias. *Br. J. Pharmacol.* 175, 3263–3280. doi: 10.1111/bph.13950

Chang, C.-L., Chen, C.-H., Chiang, J. Y., Sun, C.-K., Chen, Y.-L., Chen, K.-H., et al. (2019). Synergistic effect of combined melatonin and adipose-derived mesenchymal stem cell (ADMSC)-derived exosomes on amelioration of dextran sulfate sodium (DSS)-induced acute colitis. *Am. J. Transl. Res.* 11, 2706–2424.

Cheng, L., Liu, J., Liu, Q., Liu, Y., Fan, L., Wang, F., et al. (2017). Exosomes from melatonin treated hepatocellularcarcinoma cells alter the immunosupression status through STAT3 pathway in macrophages. *Int. J. Biol. Sci.* 13, 723–734. doi: 10.7150/ijbs.19642

Claustrat, B., and Leston, J. (2015). Melatonin: physiological effects in humans. *Neurochirurgie* 61, 77–84. doi: 10.1016/j.neuchi.2015.03.002

Colica, C., and Abenavoli, L. (2018). Resistin levels in non-alcoholic fatty liver disease pathogenesis. *J. Transl. Int. Med.* 6, 52–53. doi: 10.2478/jtim-2018-0011

Colombo, M., Moita, C., van Niel, G., Kowal, J., Vigneron, J., Benaroch, P., et al. (2013). Analysis of ESCRT functions in exosome biogenesis, composition and secretion highlights the heterogeneity of extracellular vesicles. *J. Cell Sci.* 126, 5553–5565. doi: 10.1242/jcs.128868

Colombo, M., Raposo, G., and Théry, C. (2014). Biogenesis, secretion, and intercellular interactions of exosomes and other extracellular vesicles. *Annu. Rev. Cell Dev. Biol.* 30, 255–289. doi: 10.1146/annurev-cellbio-101512-122326

Cufaro, M. C., Pieragostino, D., Lanuti, P., Rossi, C., Cicalini, I., Federici, L., et al. (2019). Extracellular vesicles and their potential use in monitoring cancer progression and therapy: the contribution of proteomics. *J. Oncol.* 2019:1639854.

Dubocovich, M. L., and Markowska, M. (2005). Functional MT 1 and MT 2 melatonin receptors in mammals. *Endocrine* 27, 101–110. doi: 10.1385/endo:27:2:101

Dupré, C., Bruno, O., Bonnaud, A., Giganti, A., Nosjean, O., Legros, C., et al. (2018). Assessments of cellular melatonin receptor signaling pathways: β-arrestin recruitment, receptor internalization, and impedance variations. *Eur. J. Pharmacol.* 818, 534–544. doi: 10.1016/j.ejphar.2017.11.022

Ellisdon, A. M., and Halls, M. L. (2016). Compartmentalization of GPCR signalling controls unique cellular responses. *Biochem. Soc. Trans.* 44, 562–567. doi: 10.1042/bst20150236

Emet, M., Ozcan, H., Ozel, L., Yayla, M., Halici, Z., and Hacimuftuoglu, A. (2016). A review of melatonin, its receptors and drugs. *Eurasian J. Med.* 48, 135–141. doi: 10.5152/eurasianjmed.2015.0267

Fitzner, D., Schnaars, M., van Rossum, D., Krishnamoorthy, G., Dibaj, P., Bakhti, M., et al. (2011). Selective transfer of exosomes from oligodendrocytes to microglia by macropinocytosis. *J. Cell Sci.* 124, 447–458. doi: 10.1242/jcs.074088

González, S., Moreno-Delgado, D., Moreno, E., Pérez-Capote, K., Franco, R., Mallol, J., et al. (2012). Circadian-related heteromerization of adrenergic and dopamine D4 receptors modulates melatonin synthesis and release in the pineal gland. *PLoS Biol.* 10:e1001347. doi: 10.1371/journal.pbio.1001347

Guo, H., Chitiprolu, M., Roncevic, L., Javalet, C., Hemming, F. J., Trung, M. T., et al. (2017). Atg5 disassociates the V_1V_0-ATPase to promote exosome production and tumor metastasis independent of canonical macroautophagy. *Dev. Cell* 43, 716.e7–730.e7.

Hardeland, R. (2009). Melatonin: signaling mechanisms of a pleiotropic agent. *Biofactors* 35, 183–192. doi: 10.1002/biof.23

Hardeland, R. (2018a). Extended signaling by melatonin. *Cell Cell Life Sci J.* 3:000123.

Hardeland, R. (2018b). Interactions of melatonin and microRNAs. *Biochem. Mol. Biol. J.* 4:7. doi: 10.21767/2471-8084.100056

Hassanpour, M., Rezabakhsh, A., Pezeshkian, M., Rahbarghazi, R., and Nouri, M. (2018a). Distinct role of autophagy on angiogenesis: highlights on the effect of autophagy in endothelial lineage and progenitor cells. *Stem Cell Res. Ther.* 9:305. doi: 10.1016/b978-0-12-405877-4.00021-4

Hassanpour, M., Cheraghi, O., Brazvan, B., Hiradfar, A., Aghamohammadzadeh, N., Rahbarghazi, R., et al. (2018b). Chronic exposure of human endothelial progenitor cells to diabetic condition abolished the regulated kinetics activity of exosomes. *Iranian J. Pharm. Res.* 17, 1068–1080.

He, B., Zhao, Y., Xu, L., Gao, L., Su, Y., Lin, N., et al. (2016). The nuclear melatonin receptor ROR α is a novel endogenous defender against myocardial ischemia/reperfusion injury. *J. Pineal Res.* 60, 313–326. doi: 10.1111/jpi.12312

Heo, J. S., Lim, J.-Y., Yoon, D. W., Pyo, S., and Kim, J. (2020). Exosome and Melatonin Additively Attenuates Inflammation by Transferring miR-34a, miR-124, and miR-135b. *Biomed Res. Int.* 2020:1621394.

Hessvik, N. P., and Llorente, A. (2018). Current knowledge on exosome biogenesis and release. *Cell. Mol. Life Sci.* 75, 193–208. doi: 10.1007/s00018-017-2595-9

Hooper, C., Sainz-Fuertes, R., Lynham, S., Hye, A., Killick, R., Warley, A., et al. (2020). Correction to: Wnt3a induces exosome secretion from primary cultured rat microglia. *BMC Neurosci.* 21:10. doi: 10.1186/s12868-020-0558-9

Huang-Doran, I., Zhang, C.-Y., and Vidal-Puig, A. (2017). Extracellular vesicles: novel mediators of cell communication in metabolic disease. *Trends Endocrinol. Metab.* 28, 3–18. doi: 10.1016/j.tem.2016.10.003

Hunsaker, M., Barba, G., Kingsley, K., and Howard, K. M. (2019). Differential microRNA expression of miR-21 and miR-155 within oral cancer extracellular vesicles in response to melatonin. *Dent. J.* 7, 48. doi: 10.3390/dj7020048

Hunt, A. E., Al-Ghoul, W. M., Gillette, M. U., and Dubocovich, M. L. (2001). Activation of MT2 melatonin receptors in rat suprachiasmatic nucleus phase advances the circadian clock. *Am. J. Physiol. Cell Physiol.* 280, C110–C118.

Hurley, J. H. (2015). ESCRTs are everywhere. *EMBO J.* 34, 2398–2407.

Jaiswal, R., and Sedger, L. M. (2019). Intercellular vesicular transfer by exosomes, microparticles and oncosomes-implications for cancer biology and treatments. *Front. Oncol.* 9:125. doi: 10.3389/fonc.2019.00125

Jin, H., Zhang, Z., Wang, C., Tang, Q., Wang, J., Bai, X., et al. (2018). Melatonin protects endothelial progenitor cells against AGE-induced apoptosis via autophagy flux stimulation and promotes wound healing in diabetic mice. *Exp. Mol. Med.* 50, 1–15. doi: 10.1038/s12276-018-0177-z

Jockers, R., Maurice, P., Boutin, J., and Delagrange, P. (2008). Melatonin receptors, heterodimerization, signal transduction and binding sites: what's new? *Br. J. Pharmacol.* 154, 1182–1195. doi: 10.1038/bjp.2008.184

Kamerkar, S., LeBleu, V. S., Sugimoto, H., Yang, S., Ruivo, C. F., Melo, S. A., et al. (2017). Exosomes facilitate therapeutic targeting of oncogenic KRAS in pancreatic cancer. *Nature* 546, 498–503. doi: 10.1038/nature22341

Li, X., Li, Z., Wang, J., Li, Z., Cui, H., Dai, G., et al. (2019). Wnt4 signaling mediates protective effects of melatonin on new bone formation in an inflammatory environment. *FASEB J.* 33, 10126–10139. doi: 10.1096/fj.201900093rr

Liu, D., Wei, N., Man, H. Y., Lu, Y., Zhu, L. Q., and Wang, J. Z. (2015). The MT2 receptor stimulates axonogenesis and enhances synaptic transmission by activating Akt signaling. *Cell Death Differ.* 22, 583–596. doi: 10.1038/cdd.2014.195

Liu, W., Yu, M., Xie, D., Wang, L., Ye, C., Zhu, Q., et al. (2020). Melatonin-stimulated MSC-derived exosomes improve diabetic wound healing through regulating macrophage M1 and M2 polarization by targeting the PTEN/AKT pathway. *Stem Cell Res. Ther.* 11:296.

Luo, F., Sandhu, A. F., Rungratanawanich, W., Williams, G. E., Akbar, M., Zhou, S., et al. (2020). Melatonin and autophagy in aging-related neurodegenerative diseases. *Int. J. Mol. Sci.* 21:7174. doi: 10.3390/ijms21197174

Maly, I. V., and Hofmann, W. A. (2020). Effect of palmitic acid on exosome-mediated secretion and invasive motility in prostate cancer cells. *Molecules* 25:2722. doi: 10.3390/molecules25122722

Manchester, L. C., Coto-Montes, A., Boga, J. A., Andersen, L. P. H., Zhou, Z., Galano, A., et al. (2015). Melatonin: an ancient molecule that makes oxygen metabolically tolerable. *J. Pineal Res.* 59, 403–419. doi: 10.1111/jpi.12267

Matar, E., McCarter, S. J., St Louis, E. K., and Lewis, S. J. G. (2021). Current concepts and controversies in the management of REM sleep behavior disorder. *Neurotherapeutics* doi: 10.1007/s13311-020-00983-7 Online ahead of print.

Mayo, J. C., Sainz, R. M., González-Menéndez, P., Hevia, D., and Cernuda-Cernuda, R. (2017). Melatonin transport into mitochondria. *Cell. Mol. Life Sci.* 74, 3927–3940. doi: 10.1007/s00018-017-2616-8

Meng, F., Dai, E., Yu, X., Zhang, Y., Chen, X., Liu, X., et al. (2014). Constructing and characterizing a bioactive small molecule and microRNA association network for Alzheimer's disease. *J. R. Soc. Interface* 11:20131057. doi: 10.1098/rsif.2013.1057

Minciacchi, V. R., Freeman, M. R., and Di Vizio, D. (2015). Extracellular vesicles in cancer: exosomes, microvesicles and the emerging role of large oncosomesed. *Semin. Cell Dev. Biol.* 40, 41–51. doi: 10.1016/j.semcdb.2015.02.010

Moreno, A. C. R., de Freitas Saito, R., Tiago, M., Massaro, R. R., Pagni, R. L., Pegoraro, R., et al. (2020). Melatonin inhibits human melanoma cells proliferation and invasion via cell cycle arrest and cytoskeleton remodeling. *Melatonin Res.* 3, 194–209. doi: 10.32794/mr11250057

Mulcahy, L. A., Pink, R. C., and Carter, D. R. F. (2014). Routes and mechanisms of extracellular vesicle uptake. *J. Extracell. Vesicles* 3:24641. doi: 10.3402/jev.v3.24641

Murrow, L., Malhotra, R., and Debnath, J. (2015). ATG12–ATG3 interacts with Alix to promote basal autophagic flux and late endosome function. *Nat. Cell Biol.* 17, 300–310. doi: 10.1038/ncb3112

Ozansoy, M., Ozansoy, M. B., Yulug, B., Cankaya, S., Kilic, E., Goktekin, S., et al. (2020). Melatonin affects the release of exosomes and tau-content in in vitro amyloid-beta toxicity model. *J. Clin. Neurosci.* 73, 237–244. doi: 10.1016/j.jocn.2019.11.046

Pandi-Perumal, S. R., Srinivasan, V., Maestroni, G., Cardinali, D., Poeggeler, B., and Hardeland, R. (2006). Melatonin: nature's most versatile biological signal? *FEBS J.* 273, 2813–2838. doi: 10.1111/j.1742-4658.2006.05322.x

Park, K.-S., Bandeira, E., Shelke, G. V., Lässer, C., and Lötvall, J. (2019). Enhancement of therapeutic potential of mesenchymal stem cell-derived extracellular vesicles. *Stem Cell Res. Ther.* 10:288.

Pfeffer, M., Korf, H.-W., and Wicht, H. (2018). Synchronizing effects of melatonin on diurnal and circadian rhythms. *Gen. Comp. Endocrinol.* 258, 215–221. doi: 10.1016/j.ygcen.2017.05.013

Pournaghi, M., Khodavirdilou, R., Saadatlou, M. A. E., Nasimi, F. S., Yousefi, S., Mobarak, H., et al. (2021). Effect of melatonin on exosomal dynamics in bovine cumulus cells. *Process Biochem.* 106, 78–87. doi: 10.1016/j.procbio.2021.03.008

Record, M. (2014). Intercellular communication by exosomes in placenta: a possible role in cell fusion? *Placenta* 35, 297–302. doi: 10.1016/j.placenta.2014.02.009

Reiter, R. J., Ma, Q., and Sharma, R. (2020). Melatonin in mitochondria: mitigating clear and present dangers. *Physiology* 35, 86–95. doi: 10.1152/physiol.00034.2019

Reiter, R. J., Tan, D. X., Kim, S. J., and Cruz, M. H. C. (2014). Delivery of pineal melatonin to the brain and SCN: role of canaliculi, cerebrospinal fluid, tanycytes and Virchow–Robin perivascular spaces. *Brain Struct. Funct.* 219, 1873–1887. doi: 10.1007/s00429-014-0719-7

Rezaie, J., Ajezi, S., Avci, ÇB., Karimipour, M., Geranmayeh, M. H., Nourazarian, A., et al. (2018). Exosomes and their application in biomedical field: difficulties and advantages. *Mol. Neurobiol.* 55, 3372–3393. doi: 10.1007/s12035-017-0582-7

Rimler, A., Jockers, R., Lupowitz, Z., and Zisapel, N. (2007). Gi and RGS proteins provide biochemical control of androgen receptor nuclear exclusion. *J. Mol. Neurosci.* 31, 1–12. doi: 10.1007/bf02686113

Rivera-Bermúdez, M. A., Masana, M. I., Brown, G. M., Earnest, D. J., and Dubocovich, M. L. (2004). Immortalized cells from the rat suprachiasmatic nucleus express functional melatonin receptors. *Brain Res.* 1002, 21–27. doi: 10.1016/j.brainres.2003.12.008

Rong, B., Feng, R., Liu, C., Wu, Q., and Sun, C. (2019). Reduced delivery of epididymal adipocyte-derived exosomal resistin is essential for melatonin ameliorating hepatic steatosis in mice. *J. Pineal Res.* 66:e12561. doi: 10.1111/jpi.12561

Sahu, R., Kaushik, S., Clement, C. C., Cannizzo, E. S., Scharf, B., Follenzi, A., et al. (2011). Microautophagy of cytosolic proteins by late endosomes. *Dev. Cell* 20, 131–139. doi: 10.1016/j.devcel.2010.12.003

Salon, J. A., Lodowski, D. T., and Palczewski, K. (2011). The significance of G protein-coupled receptor crystallography for drug discovery. *Pharmacol. Rev.* 63, 901–937. doi: 10.1124/pr.110.003350

Segura, E., Nicco, C., Lombard, B., Véron, P., Raposo, G., Batteux, F., et al. (2005). ICAM-1 on exosomes from mature dendritic cells is critical for efficient naive T-cell priming. *Blood* 106, 216–223. doi: 10.1182/blood-2005-01-0220

Shen, C., Zhao, C.-Y., Wang, W., Wang, Y.-D., Sun, H., Cao, W., et al. (2014). The relationship between hepatic resistin overexpression and inflammation in patients with nonalcoholic steatohepatitis. *BMC Gastroenterol.* 14:39.

Soekmadji, C., Riches, J. D., Russell, P. J., Ruelcke, J. E., McPherson, S., Wang, C., et al. (2017). Modulation of paracrine signaling by CD9 positive small extracellular vesicles mediates cellular growth of androgen deprived prostate cancer. *Oncotarget.* 8, 52237–52255. doi: 10.18632/oncotarget.11111

Sun, C.-K., Chen, C.-H., Chang, C.-L., Chiang, H.-J., Sung, P.-H., Chen, K.-H., et al. (2017). Melatonin treatment enhances therapeutic effects of exosomes against acute liver ischemia-reperfusion injury. *Am. J. Transl. Res.* 9, 1543–1560.

Sunyer-Figueres, M., Vázquez, J., Mas, A., Torija, M. J., and Beltran, G. (2020). Transcriptomic Insights into the effect of melatonin in saccharomyces cerevisiae in the presence and absence of oxidative stress. *Antioxidants* 9, 583–596.

Tan, D., Xu, B., Zhou, X., and Reiter, R. (2018). Pineal calcification, melatonin production, aging, associated health consequences and rejuvenation of the pineal gland. *Molecules* 23:301. doi: 10.3390/molecules23020301

Tan, D. X., Manchester, L. C., Liu, X., Rosales-Corral, S. A., Acuna-Castroviejo, D., and Reiter, R. J. (2013). Mitochondria and chloroplasts as the original sites of melatonin synthesis: a hypothesis related to melatonin's primary function and evolution in eukaryotes. *J. Pineal Res.* 54, 127–138. doi: 10.1111/jpi.12026

Théry, C., Ostrowski, M., and Segura, E. (2009). Membrane vesicles as conveyors of immune responses. *Nat. Rev. Immunol.* 9, 581–593. doi: 10.1038/nri2567

Tordjman, S., Chokron, S., Delorme, R., Charrier, A., Bellissant, E., Jaafari, N., et al. (2017). Melatonin: pharmacology, functions and therapeutic benefits. *Curr. Neuropharmacol.* 15, 434–443. doi: 10.2174/1570159x14666161228122115

Touitou, Y., Reinberg, A., and Touitou, D. (2017). Association between light at night, melatonin secretion, sleep deprivation, and the internal clock: health impacts and mechanisms of circadian disruption. *Life Sci.* 173, 94–106. doi: 10.1016/j.lfs.2017.02.008

Valadi, H., Ekström, K., Bossios, A., Sjöstrand, M., Lee, J. J., and Lötvall, J. O. (2007). Exosome-mediated transfer of mRNAs and microRNAs is a novel mechanism of genetic exchange between cells. *Nat. Cell Biol.* 9, 654–659. doi: 10.1038/ncb1596

Venegas, C., García, J. A., Escames, G., Ortiz, F., López, A., Doerrier, C., et al. (2012). Extrapineal melatonin: analysis of its subcellular distribution and daily fluctuations. *J. Pineal Res.* 52, 217–227. doi: 10.1111/j.1600-079x.2011.00931.x

Villarroya-Beltri, C., Baixauli, F., Mittelbrunn, M., Fernández-Delgado, I., Torralba, D., Moreno-Gonzalo, O., et al. (2016). ISGylation controls exosome secretion by promoting lysosomal degradation of MVB proteins. *Nat. Commun.* 7:13588.

Wang, K., Ru, J., Zhang, H., Chen, J., Lin, X., Lin, Z., et al. (2020). Melatonin enhances the therapeutic effect of plasma exosomes against cerebral ischemia-induced pyroptosis through the TLR4/NF-κB pathway. *Front. Neurosci.* 14:848. doi: 10.3389/fnins.2020.00848

Wang, T., Nasser, M. I., Shen, J., Qu, S., He, Q., and Zhao, M. (2019). Functions of Exosomes in the Triangular Relationship between the Tumor, Inflammation, and Immunity in the Tumor Microenvironment. *J. Immunol. Res.* 2019:4197829.

Wei, Y., Bai, Y., Cheng, X., Zhu, B., Reiter, R. J., and Shi, H. (2020). The dual roles of melatonin biosynthesis enzymes in the coordination of melatonin biosynthesis and autophagy in cassava. *J. Pineal Res.* 69:e12652.

Whitham, M., Parker, B. L., Friedrichsen, M., Hingst, J. R., Hjorth, M., Hughes, W. E., et al. (2018). Extracellular vesicles provide a means for tissue crosstalk during exercise. *Cell metab.* 27, 237.–251.

Xu, J., Camfield, R., and Gorski, S. M. (2018). The interplay between exosomes and autophagy – partners in crime. *J. Cell Sci.* 131:jcs215210.

Yáñez-Mó, M., Siljander, P. R.-M., Andreu, Z., Bedina Zavec, A., Borràs, F. E., Buzas, E. I., et al. (2015). Biological properties of extracellular vesicles and their physiological functions. *J. Extracell. Vesicles* 4:27066.

Yoon, Y. M., Lee, J. H., Song, K. H., Noh, H., and Lee, S. H. (2020). Melatonin-stimulated exosomes enhance the regenerative potential of chronic kidney disease-derived mesenchymal stem/stromal cells via cellular prion proteins. *J. Pineal Res.* 68:e12632.

Yuyama, K., Sun, H., Mitsutake, S., and Igarashi, Y. (2012). Sphingolipid-modulated exosome secretion promotes clearance of amyloid-β by microglia. *J. Biol. Chem.* 287, 10977–10989. doi: 10.1074/jbc.m111.324616

Zahran, R., Ghozy, A., Elkholy, S. S., El-Taweel, F., and El-Magd, M. A. (2020). Combination therapy with melatonin, stem cells and extracellular vesicles is effective in limiting renal ischemia–reperfusion injury in a rat model. *Int. J. Urol.* 27, 1039–1049. doi: 10.1111/iju.14345

Zhang, X., Li, X., Ning, F., Shang, Y., and Hu, X. (2019). TLE4 acts as a corepressor of Hes1 to inhibit inflammatory responses in macrophages. *Protein Cell* 10, 300–305. doi: 10.1007/s13238-018-0554-3

Zhao, D., Yu, Y., Shen, Y., Liu, Q., Zhao, Z., Sharma, R., et al. (2019). Melatonin synthesis and function: evolutionary history in animals and plants. *Front. Endocrinol.* 10:249. doi: 10.3389/fendo.2019.00249

Zhao, L., Hu, C., Zhang, P., Jiang, H., and Chen, J. (2019). Genetic communication by extracellular vesicles is an important mechanism underlying stem cell-based therapy-mediated protection against acute kidney injury. *Stem Cell Res. Ther.* 10:119.

Zhao, L., Hu, C., Zhang, P., Jiang, H., and Chen, J. (2020). Melatonin preconditioning is an effective strategy for mesenchymal stem cell-based therapy for kidney disease. *J. Cell Mol. Med.* 24, 25–33. doi: 10.1111/jcmm.14769

Zheng, Y., Hasan, A., Nejadi Babadaei, M. M., Behzadi, E., Nouri, M., Sharifi, M., et al. (2020). Exosomes: multiple-targeted multifunctional biological nanoparticles in the diagnosis, drug delivery, and imaging of cancer cells. *Biomed. Pharmacother.* 129:110442. doi: 10.1016/j.biopha.2020.110442

Zhou, H., Ma, Q., Zhu, P., Ren, J., Reiter, R. J., and Chen, Y. (2018). Protective role of melatonin in cardiac ischemia-reperfusion injury: from pathogenesis to targeted therapy. *J. Pineal Res.* 64:e12471. doi: 10.1111/jpi.12471

Conflict of Interest: The authors declare that the research was conducted in the absence of any commercial or financial relationships that could be construed as a potential conflict of interest.

frontiers in Cell and Developmental Biology

REVIEW
published: 09 June 2021
doi: 10.3389/fcell.2021.673677

Cell Death and Exosomes Regulation After Myocardial Infarction and Ischemia-Reperfusion

*Xun Wu[1], Chukwuemeka Daniel Iroegbu[1], Jun Peng[2], Jianjun Guo[3], Jinfu Yang[1] and Chengming Fan[1,2,3]**

[1] Department of Cardiovascular Surgery, The Second Xiangya Hospital, Central South University, Changsha, China, [2] Hunan Provincial Key Laboratory of Cardiovascular Research, Changsha, China, [3] Hunan Fangsheng Pharmaceutical Co., Ltd., Changsha, China

Cardiovascular disease (CVD) is the leading cause of death in the global population, accounting for about one-third of all deaths each year. Notably, with CVDs, myocardial damages result from myocardial infarction (MI) or cardiac arrhythmias caused by interrupted blood flow. Significantly, in the process of MI or myocardial ischemic-reperfusion (I/R) injury, both regulated and non-regulated cell death methods are involved. The critical factor for patients' prognosis is the infarct area's size, which determines the myocardial cells' survival. Cell therapy for MI has been a research hotspot in recent years; however, exosomes secreted by cells have attracted much attention following shortcomings concerning immunogens. Exosomes are extracellular vesicles containing several biologically active substances such as lipids, nucleic acids, and proteins. New evidence suggests that exosomes play a crucial role in regulating cell death after MI as exosomes of various stem cells can participate in the cell damage process after MI. Hence, in the review herein, we focused on introducing various cell-derived exosomes to reduce cell death after MI by regulating the cell death pathway to understand myocardial repair mechanisms better and provide a reference for clinical treatment.

Keywords: myocardial infarction, apoptosis, autophagy-dependent death, pyroptosis, ferroptosis, exosomes, microRNA, myocardial protection

OPEN ACCESS

Edited by:
Xinlei Li,
Nationwide Children's Hospital, United States

Reviewed by:
Ming Dong,
Guangzhou Institutes of Biomedicine and Health (CAS), China
Philippe Menasché,
Assistance Publique Hopitaux De Paris, France

***Correspondence:**
Chengming Fan
fanchengming@csu.edu.cn

Specialty section:
This article was submitted to Molecular Medicine, a section of the journal Frontiers in Cell and Developmental Biology

Received: *28 February 2021*
Accepted: *18 May 2021*
Published: *09 June 2021*

Citation:
Wu X, Iroegbu CD, Peng J, Guo J, Yang J and Fan C (2021) Cell Death and Exosomes Regulation After Myocardial Infarction and Ischemia-Reperfusion. Front. Cell Dev. Biol. 9:673677. doi: 10.3389/fcell.2021.673677

INTRODUCTION

Despite the considerable improvements in healthcare worldwide, acute myocardial infarction (MI) has long been the primary cause of death from coronary heart diseases (Roth et al., 2017). Endogenous cardiomyocytes have limited renewal potentials following MI, which leads to the irreversible loss of a significant number of cardiomyocytes, left ventricular remodeling, and

Abbreviations: 3′UTR, 3′untranslated region; ALDH2, aldehyde dehydrogenase 2; AMPK, AMP-activated protein kinase; Atgs, autophagy-related genes; CVD, Cardiovascular disease; DFO, desferrioxamine; DMT1, divalent metal transporter 1; EGR1, early growth response factor 1; ESCRT, endosomal sorting complex; GATA-4, GATA binding protein-4; GSDMD, gasdermin D; HSPs, heat shock proteins; I/R, ischemic-reperfusion; LPS, lipopolysaccharide; MI, myocardial infarction; mTOR, mammalian target of rapamycin; nSMase2, neutral sphingomyelinase 2; PAMPs, athogen-related molecular patterns; SDF1, stromal-derived factor 1; Steap3, six-transmembrane epithelial antigen of prostate 3; TIMP2, Tissue inhibitor of matrix metalloproteinase 2; NLR, nucleotide-binding oligomerization domain (NOD)-like receptor; TNF-α, tumor necrosis factor-α; TLRs, Toll-like receptors; TXNIP, thioredoxin-interacting protein.

progressive heart failure (Buja and Vela, 2008). Therefore, rescuing damaged cardiomyocytes becomes a potential strategy to preventing myocardial dysfunction and heart failure after MI.

Exosomes are small-membrane fragments with a diameter of 30–150 nm, secreted by almost all mammalian cells. Exosomes arise from a multivesicular endosomal pathway by fusion of multivesicular bodies (MVBs) with the plasma membrane, resulting in the release of vesicles as exosomes into the extracellular space. The generation of exosomes in MVBs can be divided into endosomal independent sorting complexes required for transport (ESCRT) and ESCRT-dependent mechanisms (Hurley, 2008; Stuffers et al., 2009). For example, cytoplasmic proteins' isolation into exosomes may result from co-classification with other proteins, for which heat shock protein70 (HSP70) plays an essential role (Théry et al., 2001). RNAs may also be classified into exosomes with complex mechanisms, including binding ESCRT-II subcomplex to RNA (Irion and St Johnston, 2007) and the sumoylation of hnRNPA2B1 (Villarroya-Beltri et al., 2013). The secretion of exosomes also requires MVBs to fuse with the plasma membrane. The process may be mediated by SNARE proteins and members of the synaptotagmin family (Jahn and Scheller, 2006). Exosomes are characterized by lipid bilayers, annexin, GTPase, Rab, transmembrane, and non-membrane-bound proteins, flotillin proteins, and ESCRT components, which include Alix, HSPs, Tsg101, integrins, and transmembrane proteins (CD63, CD81, and CD82). Exosomes also express secretory cell markers. Besides, exosomes are also rich in RNA from different sources (Théry et al., 2002).

The study herein reviews the potential mechanism of cell-derived exosomes in repairing damaged cardiomyocytes and provides a reference point for future clinical treatment of patients with cardiac ischemic diseases. It should be noted that that exosome is a two-edged sword during medical therapy. Following MI, exosomes may simultaneously enhance blood vessels' regeneration and damaged myocardium in the area around the infarcted site. The review aims to illustrate the therapeutic effect (anti-cell death) and potential molecular mechanism after myocardial ischemia.

TYPES OF CARDIOMYOCYTE DEATH AND THE POTENTIAL MECHANISMS AND KEY MEDIATORS OF CELL DEATH IN CARDIAC DISEASES

Following MI, cardiac I/R injury, heart failure, and other heart diseases, cell death can occur in regulated and non-regulated forms (Moe and Marín-García, 2016; Shekhar et al., 2018). Significantly, MI is caused by acute or chronic tissue deficiency of oxygen, nutrients, and growth factors. Although related imbalances following a series of MI could arise from several pathological cascades, the most common cause is acute or prolonged ischemia, with the rupture of coronary atherosclerotic plaques being the primary cause (Libby and Pasterkamp, 2015). In the 1990s, the implantation of thrombolysis or stents was considered an effective way to reduce the size of MI (Nabel and Braunwald, 2012). Although the potential risk of perfusion is still questionable after a few years, it is clear that the perfusion process will cause cell death via oxidative stress, calcium overload, and inflammation (Yellon and Hausenloy, 2007). Notwithstanding, it is difficult to assess the significant role ischemic duration and reperfusion play in the damaged myocytes. In most cases, genetic and pharmacological inhibition of cell death signaling reduces cardiomyocyte death and infarct size only in the context of myocardial ischemia-reperfusion. However, such changes are uncommon in permanent ischemia models. Remarkably, the primary reason will be the change from initially regulated cell death to unregulated cell death if the death stimulus persists (Del Re et al., 2019). Notably, extensive studies have been conducted on MI; it is still unclear which death process is dominant.

Morphological criteria consider that cell necrosis is the primary mode of myocardial cell death after MI. In contrast, apoptosis is considered to be the first regulated cell death process. Several studies have shown that the inhibition of apoptosis receptors and the reduction of mitochondrial apoptosis reduce apoptosis of cardiomyocytes and reduce the size of MII (Jeremias et al., 2000; Chen et al., 2001). Apart from apoptosis, studies show that necroptosis (Newton et al., 2016), pyroptosis (Kawaguchi et al., 2011), ferroptosis (Fang et al., 2019), parthanatos (Yang et al., 2000), autophagy-dependent cell death (Matsui et al., 2007), and mitochondrial-dependent necrosis (Baines et al., 2005) are all involved in cell death during MI. Thus, intervention is crucial as it can significantly mitigate the number of dead cardiomyocytes in peri-infarcted areas. These studies indicated that cardiomyocytes' death during MI was not based on a specific individual death pathway.

APOPTOSIS

Apoptosis, a kind of programmed death, is a different way of cell death from necrosis Apoptotic cells undergo structural changes, including cell shrinkage, nuclear pyknosis, and fragmentation (Edinger and Thompson, 2004). Studies have shown that cardiomyocyte apoptosis begins after prolonged myocardial ischemia or reperfusion after short-term ischemia (Kajstura et al., 1996). Activation of pro-apoptotic factors and caspase can be detected in the absence of DNA breakage during ischemia, followed by a substantial increase during reperfusion, suggesting that the apoptotic cascade begins during ischemia but fully implemented during reperfusion (Lazou et al., 2006). Clinical studies have confirmed apoptotic cardiomyocytes in the marginal regions of an infarcted area within hours to days after acute infarction (Saraste et al., 1997).

Apoptosis is mediated by two well-defined pathways, extrinsic and intrinsic, both of which are activated in cardiomyocytes under pathophysiological conditions (Youle and Strasser, 2008). In the exogenous pathway, cell death is induced by the activation of death domain receptors on the cell membrane. It is triggered by Fas ligand or tumor necrosis factor (TNF)-α (Ashkenazi and Dixit, 1998). Increased expression of Fas and TNF-α is associated with increased apoptosis in cardiomyocytes in a model

of I/R heart disease. Both Fas and TNF receptors have an intracellular death domain that recruits and activates caspase-8 in the cell membrane. The recruitment of caspase-8 then activates downstream caspases (including caspase-3) (Torre-Amione et al., 1996). Intrinsic pathways are activated by intracellular stress signals, such as hypoxia, oxidative stress, and DNA damage (Edinger and Thompson, 2004). The intrinsic pathway is regulated by the Bcl-2 protein family (Adams and Cory, 1998). Oligomerization of Bax and Bak in the Bcl-2 family results in pores formation, leading to the release of cytotoxic proteins from the mitochondria such as cytochrome C. Cytochrome C then activate procaspase-9, and the activated caspase-9 then cleaves and activates caspase-3 and caspase-7 (Adams and Cory, 1998).

AUTOPHAGY

Autophagy is an essential metabolic process where aging or damaged proteins and organelles are broken down into amino acids and fatty acids for energy generation and recycling (Cătană et al., 2018). These metabolic processes are activated during nutrient deficiency or metabolic stress to maintain tissue function and dynamic balance (Dong et al., 2018). It has been proved that autophagy is essential for maintaining normal heart function (Zhang Q. Y. et al., 2018). Amongst scholars, it is believed that autophagy is an essential lysosome-dependent catabolic mechanism (Hewitt and Korolchuk, 2017). According to lysosomes' transport mode and physiological function, autophagy is primarily divided into three types: macroautophagy, microautophagy, and chaperone-mediated autophagy (Zhang X. et al., 2018). Macroautophagy is the most widely studied form of autophagy. Nonetheless, over 30 autophagy-related genes (Atgs) and proteins have been found to participate in the process of autophagy (Díaz et al., 2017).

Presently, two classic signaling pathways from the entire autophagy signaling network have been described to inhibit or promote cell autophagy (Inoki et al., 2012; Shao et al., 2016). Type I PI3K-mammalian target of rapamycin (mTOR) signaling pathway is a classic inhibitory pathway. It is triggered under nutrient-rich conditions and stimulates mTOR and mTOR complex (MTORC1) via the protein kinase-B (also known as Akt) pathway, which then inhibits the formation of Atg1 complex (Kaur and Sharma, 2017). Another classic autophagy signaling pathway is induced by AMP-activated protein kinase (AMPK). AMPK is a sensor of stress and nutrient input. It activates ULK1 by inactivating mTORC1 or phosphorylating ULK1 at different residue serine kinase complexes to promote the autophagy process (Zhao et al., 2018). A study by Sciarretta et al. (2018) showed that autophagy plays a crucial role in inhibiting the occurrence and development of cardiovascular diseases such as MI, heart failure, and atherosclerosis. On the other hand, over-induction of the autophagy process may cause adverse effects to cells, the so-called "autophagy-dependent cell death" in the organism, which indicates the importance of controlling the degree of autophagy induction in disease treatment (Lambelet et al., 2018; Wang P. et al., 2018). Thus, autophagy seems to be a double-edged sword in the treatment of MI. Baseline autophagy can limit the death of cardiomyocytes, while excessive autophagy can aggravate the damage of cardiomyocytes. Demircan et al. (2018) also reported that patients with coronary heart disease or acute MI had an over-regulation of autophagy than the healthy controls. However, decreased autophagy and mitochondrial damage may lead to a weakened host's response to hypoxic-ischemic injury, thereby adversely affecting cardiomyocytes (Ham and Raju, 2017). Laboratory research on rat models showed that autophagy could reduce the scope of acute MI after ligation of the left anterior descending artery (Aisa et al., 2017). Studies have shown that the basic autophagy process in cardiomyocytes is upregulated via the AMPK-mTOR signaling pathway, leading to reduced MI in animal models of acute MI (Foglio et al., 2017). As mentioned above, baseline autophagy or appropriately induced autophagy protects cardiomyocyte ATP production by maintaining cell homeostasis, degrading organelles or misfolded proteins, thereby protecting against ischemic injury. However, it is reported that under severe ischemia, excessive autophagy of the heart promotes cell death and worsens heart function (Li et al., 2018; Liu C. Y. et al., 2018). Interestingly, mitochondrial aldehyde dehydrogenase 2 (ALDH2) is an enzyme known to catalyze aldehyde oxidation. It can significantly promote the autophagy process during ischemia by activating AMPK and down-regulating mTOR, thereby producing cardioprotection. On the contrary, during reperfusion, ALDH2 can inhibit autophagy by activating Akt and mTOR, thereby protecting cardiomyocytes from cell death caused by hypoxia and reoxygenation (Ma et al., 2011). In summary, these studies all show that severe ischemia-induced excessive autophagy could aggravate acute MI.

PYROPTOSIS

Pyroptosis is a regulated form of cell death closely associated with innate immune responses, characterized by plasma membrane permeability and the extracellular release of inflammatory cytokines and rupture of the plasma membrane mediated by gasdermin-D (GSDMD) (Shi et al., 2017). Regards morphology, cell pyroptosis, combines the characteristics of necrosis and apoptosis, including the formation of necrotic cell membrane pores, cell swelling, and membrane rupture, resulting in cytoplasmic content leakage nuclear condensation, and DNA fragmentation during apoptosis. In contrast to apoptosis, pyroptosis does not involve releasing cytochromes, and the mitochondrial integrity is maintained (Fink and Cookson, 2006; Cervantes et al., 2008). In a typical pyrophosphate signaling pathway, pathogen-related molecular patterns (PAMPs) or risk-related molecular patterns (DAMPs) are detected by different inflammasomes, which are composed of nucleotide-binding oligomerization domain (NOD), NOD-like receptors (NLR) family (NLRP3, NLRP1, NLRC4, NLRP9, and NLRP6), PYHIN protein family, and pyrin protein composition. These activated inflammasomes trigger the activation of caspase-1, which eventually leads to pyroptosis (Heilig and Broz, 2018). To trigger pyrolysis, the signal domains of NLR, AIM2, and pyrin (such as PYD) bind to ASC, while ASC recruits and activates pro-caspase-1, producing active caspase-1 (Aachoui et al., 2013).

Activated caspase-1 not only processes and maturates IL-1β/18 but also cleaves the GSDMD intermediate junction, releasing intramolecular inhibition of the gasdermin-N domain and inducing cell pyroptosis by forming a 10–15 nm diameter pore on the cell membrane (Shi et al., 2015; Ding et al., 2016).

In the atypical pyroptosis pathway, caspase-11 and caspase-4/5 are primarily involved and activated by cytoplasmic lipopolysaccharide (LPS), where the CARD domain recognizes the lipid part of LPS (Yang J. et al., 2015; Abu Khweek and Amer, 2020). Activated caspase-4/5/11 directly triggers pyrolysis and the release of IL-1α and HMGB1 after cutting the GSDMD-induced membrane pore formation and subsequent cell membrane rupture. Activated caspase-4/5/11 also indirectly processes IL-1β through the atypical NLRP 3/ASC/caspase-1 pathway, which is formed by GSDMD pore formation/K + efflux or through vascular wall protein-1 cleavage/ATP release/P2 × 7/K + release mediated (Kayagaki et al., 2015; Rühl and Broz, 2015).

MI is associated with a sterile inflammatory response that leads to white blood cell aggregation (Takahashi, 2010). The white blood cells that accumulate at the MI site, including neutrophils and macrophages, release inflammatory cytokines, chemokines, and proteases, further aggravating the inflammatory response after MI, promoting myocardial injury, and remodeling. This sterile inflammatory response may be mediated by Toll-like receptors (TLRs) and NLRs. NLR is an integral part of the inflammasome that mediates the release of IL-1β (Shi et al., 2015). Studies have shown that the NLRP3 inflammasome plays a vital role in MI (Toldo and Abbate, 2018). During MI, activation of NLRP3 is associated with the leakage of lysosomal cathepsin-B, induction of K + outflow, ROS production, and other mediators (Liu et al., 2017). Inflammatory bodies were observed in a mouse model of acute MI, with increased ASC, NLRP3, and Caspase-1 in scar tissue and the cytoplasm of adjacent myocardial cells in the infarction area (Mezzaroma et al., 2011). Besides, oxidative stress induced by MI can also cause cell pyroptosis. The inhibition of oxidative stress can reduce pyroptosis and decrease the activities of NF-κB and GSDMD. Inhibition of NF-κB also inhibits oxidative stress-regulated pyrogen death by reducing GSDMD (Lei et al., 2018). These results suggest that myocardial cell damage during MI is partly related to pyroptosis.

FERROPTOSIS

Ferroptosis is a form of regulatory cell death caused by iron-dependent lipid peroxidation (Stockwell et al., 2017). Among the members of the GPX family, Gpx4 is believed to specifically catalyze the reduction of lipid peroxides, thereby scavenging lipid reactive oxygen species (Stockwell et al., 2017). The absence of Gpx4 causes lipid peroxides and lipid ROS accumulation and in a 12/15-lipoxygenase (12/15LOX) dependent manner, leading to cell death (Seiler et al., 2008). On the other hand, the reduction of lipid peroxides by GPX4 requires the oxidation of glutathione. Glutathione is primarily synthesized by cysteine and inhibits the cystine-glutamate transporter (xCT), or cysteine deprivation will cause glutathione depletion, which will induce ferroptosis (Jiang et al., 2015). The recently discovered iron death inhibitor protein-1 (FSP1) (previously known as apoptosis-inducing factor mitochondria-2, AIFM2), an influential ferroptosis resistance factor, is believed to be a vital component of a non-mitochondrial CoQ antioxidant system, which is parallel to the typical glutathione-based GPX4 pathway anti-ferroptosis system.

EXOSOMES REDUCE CARDIOMYOCYTE DEATH AFTER MYOCARDIAC INJURY

Recent studies have shown that the myocardial protective effect of the injected stem cells is not produced by direct differentiation itself but mediated by exosomes secreted from stem cells (Kishore and Khan, 2016; Jung et al., 2017). Thus, exosomes may be an effective alteration to overcome the shortcomings of cell therapy. Exosomes with significant cargos may merge their membrane contents into the recipient cell membrane and transport complex signal molecules into the recipient cell (Valadi et al., 2007). Exosomes play an essential role in cell-to-cell communication, regulating various cellular processes in target cells, including adjacent cells and cells in remote parts (Stoorvogel, 2012). Several studies have reported that stem cell-derived exosomes could be used to treat ischemic disease (Lai et al., 2010; Arslan et al., 2013; Ibrahim et al., 2014; **Figure 1**).

Besides, exosome therapy has advantages where tumorigenesis and embolism caused by cell transplantation are significantly lower when using exosomes because they are much smaller than cells (Park K. S. et al., 2019). Also, the membrane of exosomes is primarily a lipid bilayer with fewer binding proteins. Thus, their immunogenicity is lower than that of cells and could reduce the recognition and phagocytosis of immune cells (Hood and Wickline, 2012). Moreover, with exosomes, there is (i) no self-metabolism and changes in the body temperature will not affect its biological activity where it could better exert its functional characteristics (Lai et al., 2013) and (ii) exosomes are lipid-bound nano-scale vesicles that can freely pass through the blood-brain barrier (Konala et al., 2016). Furthermore, due to their stable nature, they are thus, (i) suitable for storage and transportation as exosomes can be stored at −80°C for 4 weeks without losing their physical properties (Agrawal et al., 2017). Finally, the double-layer lipid membrane of the exosome can encapsulate and protect its contents, hence preventing the rapid degradation of cytokines and RNA and deliver therapeutic agents to the target site (Didiot et al., 2016). Generally speaking, molecular carriers with biological activity in exosomes include lipids, proteins, and nucleic acids, such as DNA, mRNA, miRNA, and lncRNA. Though exosomes have these advantages and have great potential in treating cardiovascular diseases, there are also some problems in practice. For example, the extraction of exosomes is complicated and time-consuming, and uneven purification can cause significant differences in therapeutic effects (Kishore and Khan, 2017). Potential therapeutic advances of exosomes include their role in promoting angiogenesis, anti-apoptosis, anti-immunogenicity, proliferation, and anti-fibrosis (Chaput and Théry, 2011; Wang Y. et al., 2015; Yang, 2018; Ye et al., 2019).

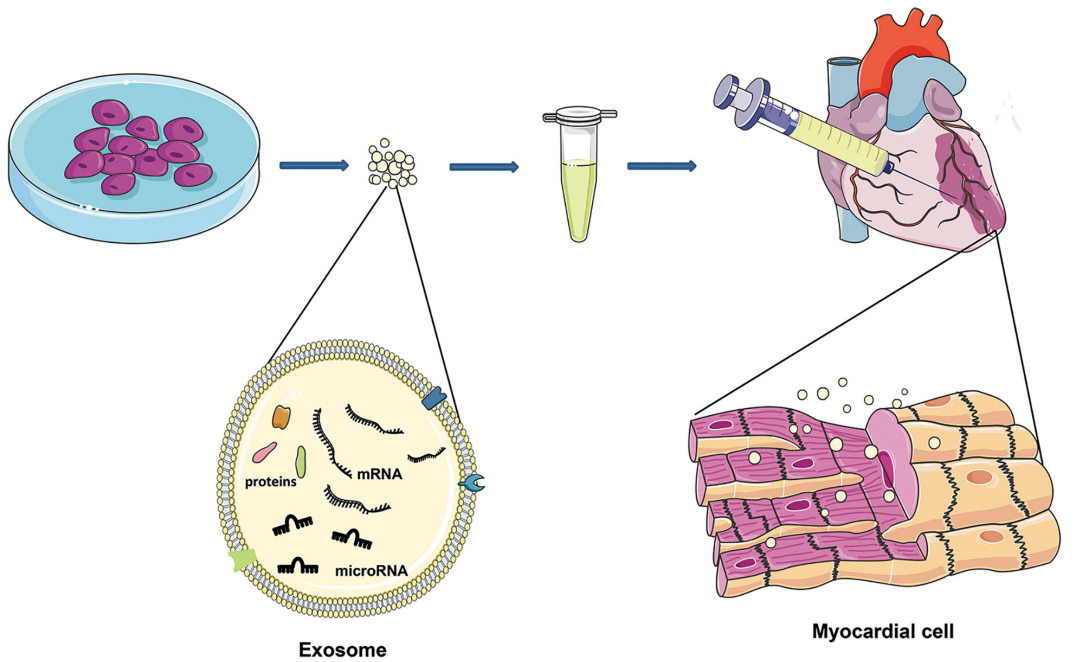

FIGURE 1 | After MI, exosomes of different cell sources are injected around the infarction site, and exosomes can enter the damaged cardiomyocytes to reduce cardiomyocyte death. Exosomes are characterized by lipid bilayers, transmembrane and non-membrane binding proteins, and a high concentration of nucleic acids (DNA, mRNA, microRNA, and lncRNA).

TABLE 1 | Mechanisms of exosomes from different cell sources against cardiomyocyte apoptosis.

Derivation of exosome	Stimulus	Molecular mediator(s)	Mechanisms	Biological effects	References
BMMSCs	–	miR-486-5p	miR-486-5p/ PTEN/PI3K/AKT	Apoptosis↓	Sun et al., 2019
BMMSCs	Hypoxia	miR-214	miR-214/CaMk2	Apoptosis↓, oxidative stress↓	Wang Y. et al., 2018
BMMSCs	Hypoxia	miR-125b-5p	miR-125b-5p/p53andBAK1	Apoptosis↓	Zhu et al., 2018
BMMSCs	Hypoxia	miR-210and miR-24	Not investigated	Apoptosis↓	Zhu et al., 2018
BMMSCs	Transduction with GATA-4	miR-19a	miR-19a/PTEN/AKT miR-19a/BIM	Apoptosis↓	Yu et al., 2015
BMMSCs	Transduction with SDF1	SDF1	SDF1/PI3K/mTOM	Apoptosis↓, microvascular regeneration	Gong et al., 2019
BMMSCs	Transduction with miR-125b	miR-125b	miR-125b/SIRT7	Apoptosis↓, inflammatory factor↓	Chen et al., 2020
ADMSCs	–	Not investigated	S1P/SK1/S1PR1	Apoptosis↓, fibrosis↓, M2 macrophages polarization	Deng et al., 2019
ADMSCs	–	miR-214	miR-214/Bcl2L11 miR-214/SLC8a1	Apoptosis↓	Eguchi et al., 2019
ADMSCs	Transduction with miR-146a	miR-146a	miR-146a/EGR1/TLR4/NFκB	Apoptosis↓	Pan et al., 2019
hucMSCs	–	miR-19a	miR-19a/SOX6/AKT/JNK3 /Caspase3	Apoptosis↓	Huang et al., 2020
hucMSCs	Transduction with TIMP2	Not investigated	AKT/sfrp2	Apoptosis↓, oxidative stress↓angiogenesis?	Ni et al., 2019
IPSCs	–	miR-21 miR-210	Not investigated	Apoptosis↓	Adamiak et al., 2018

It is essential to note that MI and I/R injury could lead to myocardial injury. Various types of cell-derived exosomes play a crucial role in repairing cell damage after myocardial tissue injury. Here we describe several programmed death of cardiomyocytes after MI and I/R injury and the regulatory mechanisms of exosomes.

Exosomes Reduce Apoptosis

The mechanism of exosomes from different cell sources about the anti-apoptosis of cardiomyocytes was summarized in **Table 1**. Bone marrow mesenchymal stem cell (BMMSC)-derived exosomes play a key role in repairing myocardial injury caused by tissue reperfusion, and the exosomal miR-486-5p inhibit myocardial apoptosis by PTEN de-activation and through PI3K/Akt pathway (Sun et al., 2019). In addition, a variety of pretreatments with BMMSCs can change the composition of the secreted exosomes. In which the most common used method is hypoxic pretreatment. Studies have found that with hypoxia pretreatment of BMMSCs, the miR-214 in secreted exosomes is significantly increased, and further confirmed that the exosomal miR-214 is transferred to cardiomyocytes and inhibit the expression of CaMKII (Wang Y. et al., 2018). Another study showed that hypoxic pretreatment of mouse BMMSCs increased the expression of miR-125b-5p in their exosomes. After injected into the infarcted area, the ability of cardiomyocytes to resist apoptosis were significantly enhanced through the inhibition of p53 and BAK1 (Zhu et al., 2018). Furthermore, the increased expression of miR-24 and miR-210 in the exosomes of hypoxic BMMSCs can also increase the anti-apoptotic potency of cardiomyocytes. The specific anti-apoptotic mechanism has not been elucidated, but the expression of exosomal miR-210 depends on the amount of neutral sphingomyelinase 2 (nSMase2). It is believed that gene or microRNA modified exosomes may convert the ability of these exosomes to resist cardiomyocyte apoptosis. Studies have found that GATA binding protein-4 (GATA-4) regulates the expression of miR-15 family members in BMMSCs and improves their survival rate in an ischemic environment (Yu et al., 2013). Other methods including miR-125b overexpression in exosomes via transfecting miR-125b into BMMSCs to achieve the effect of anti-cardiomyocyte apoptosis (Chen et al., 2020). The target of miR-125b is SIRT7, which is involved in the regulation of cardiac cell apoptosis (Araki et al., 2015). All of the above are the effects of exosomes derived from BMMSCs against cardiomyocyte apoptosis after ischemia.

Exosomes derived from other stem cells have also been extensively studied. Studies have found that exosomes derived from adipose-derived mesenchymal stem cells (ADMSCs) can regulate S1P/SK1/S1PR1 signals (Deng et al., 2019). Because miR-214 is highly expressed in exosomes derived from ADMSCs, they could inhibits the expression of Bcl2L11 and SLC8a1 after delivered into the myocardiac infarcted site (Eguchi et al., 2019). The protein encoded by Bcl2L11 may induces apoptosis through bax activation or anti-apoptotic proteins neutralization (Shukla et al., 2017). The sodium/calcium

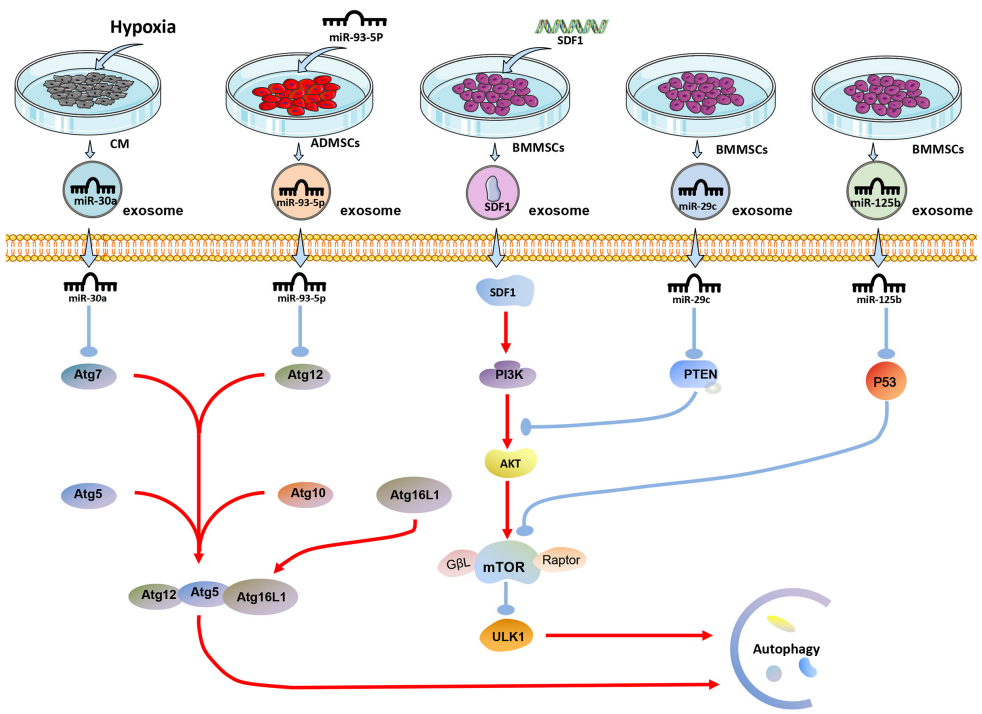

FIGURE 2 | The effect of exosomes derived from differently treated cells on autophagy of cardiomyocytes after MI. The miR-30a in exosomes secreted by cardiomyocytes after hypoxia is targeted to Atg7 for anti-autophagy; miR-93-5P in exosomes secreted by ADMSCs transfected with miR-93-5P targeted Atg12 for anti-autophagy; SDF1 protein secreted by BMMSCs transfected with SDF gene activates PI3K/AKT pathway to resist autophagy; miR-29c and miR-125b in exosomes derived from BMMSCs target PTEN and P53, respectively, to resist autophagy.

exchange protein encoded by SLC8A1 causes cardiomyocyte calcium overload-related apoptosis under cardiac stress (Aurora et al., 2012). Studies have showed the anti-apoptotic ability of hypoxic cardiomyocytes by overexpressing miR-146a in ADMSCs derived exosomes. The anti-apoptotic effect of miR-146a mainly caused by the inhibition of early growth response factor 1 (EGR1) in I/R injured tissue (Yang L. et al., 2015; Pan et al., 2019). Overexpressing miR-19 in exosomes derived from umbilical cord MSCs could regulate the AKT/JNK3/caspase-3 axis via inhibiting the expression of SOX6, which may lead to the decrease of hypoxic cardiomyocyte apoptosis (Huang et al., 2020). Exosomes derived from TIMP2 overexpressed umbilical cord MSCs significantly enhance the anti-apoptotic ability of hypoxic cardiomyocytes via the inhibition of Bax and pro-caspase expression (Ni et al., 2019). Exosomes derived from iPSCs also play a key role in resisting hypoxic myocardial apoptosis. Studies have shown that exosomal miR-21 and miR-210 may be key factors in anti-cardiomyocyte apoptosis (Wang Y. et al., 2015; Adamiak et al., 2018). Previous studies reported that miR-21 inhibits apoptosis by targeting PDCD4/AP-1 in infarcted cardiomyocytes (Xiao et al., 2016). Interestingly, a study showed that exercise can rapidly increase the exosomes in plasma, which could effectively resist cardiomyocyte apoptosis via activating ERK1/2 and HSP27 in hypoxia-reoxygenated cells (Bei et al., 2017).

Exosomes Regulate Autophagy-Dependent Cell Death

Studies have shown that exosomes can reduce myocardial autophagy and death during MI or I/R injury (**Figure 2**). In 2018, it was discovered that exosomes derived from human MSCs reduce I/R injury by inhibiting cardiomyocyte autophagy, but the specific mechanism has not been proved (Jiang et al., 2018). Experiments have shown that miR-125b-5p is highly expressed in exosomes derived from BMMSCs. Exosomal miR-125b-5p inhibits the expression of P53 and reduces the autophagy of myocardial cells in the infarcted site when delivered to the MI heart (Xiao et al., 2018). In the mouse myocardial I/R injury model, the expression of miR-29c decreased, and the autophagy flow of myocardial cells increased. The high expression of miR-29c can reduce the excessive autophagy of hypoxic myocardium by directly inhibiting the expression of PTEN, thus inhibiting

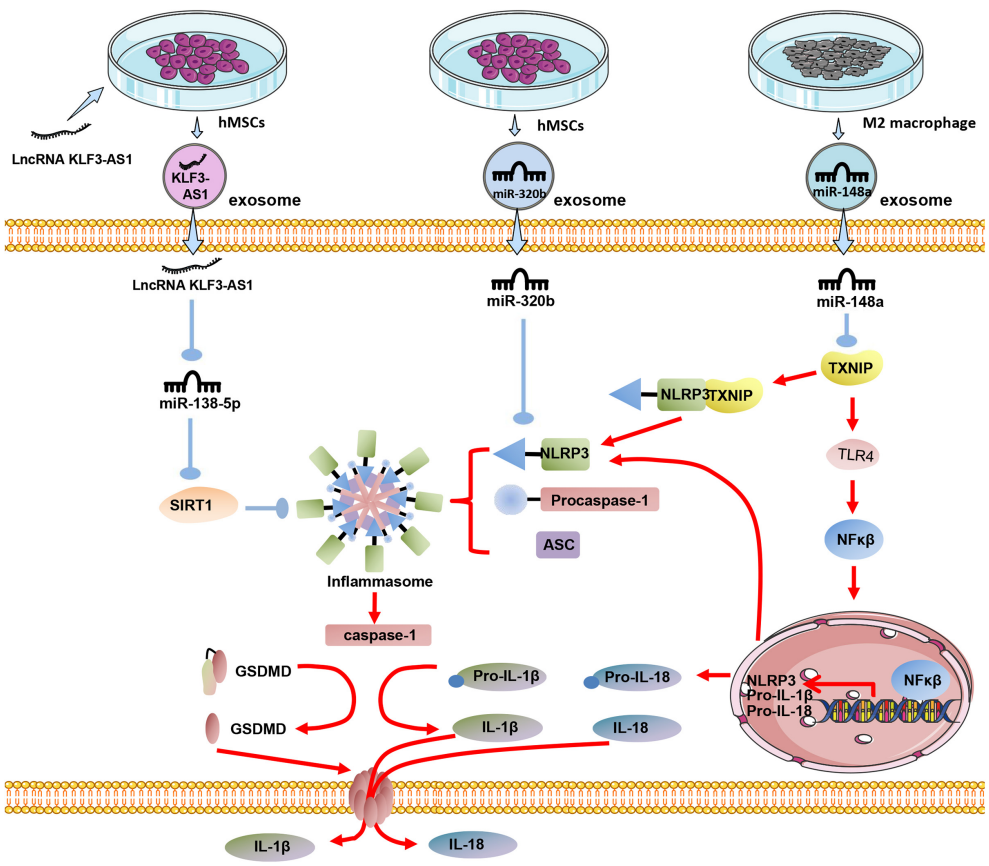

FIGURE 3 | The effect of exosomes derived from differently treated cells on the pyrolysis of cardiomyocytes after MI. Human MSCs are transfected with LncRNA KLF3-AS1, and the secreted exosomal LncRNA KLF3-AS1 are highly expressed. LncRNA KLF3-AS1 inhibits miR-138-5p then inhibits pyroptosis; Exosomal miR-320b derived from unmodified human MSCs targets NLRP3 to inhibit cardiomyocyte pyroptosis; Exosomal miR-148a in exosomes derived from M2 macrophages inhibits TXINP expression to protect against cardiomyocyte pyroptosis.

the I/R-induced excessive autophagy via the PTEN/AKT/mTOR signaling pathway (Li et al., 2020). Besides, through transfection, over expression of miR-301 in BMMSCs increases the expression of exosomal miR-301, which significantly reduces the ratio of LC3-II/LC3-I and increases P62 relative expression in the infarcted myocardial tissue. Notably, the ratio of LC3-II/LC3-I increased, and the expression level of P62 decreased when the degree of autophagy was enhanced (Li Y. et al., 2019).

Similarly, by overexpressing SDF1 in BMMSCs, the expression of SDF1 in exosomes was significantly increased, which significantly increased the expression of Bcl-2 in hypoxic cardiomyocytes. On the other hand, Bax, Beclin-1, LC3, and LC3II/LC3I ratio were significantly reduced, reducing excessive autophagy in cardiomyocytes (Gong et al., 2019). Studies have shown that ADMSCs overexpressing miR-93-5p can effective package miR-93-5p into exosomes. The exosomes would essentially deliver exosomal miR-93-5p to the site of MI to inhibit excessive autophagy. *In vitro* experiments show that miR-93-5p achieves these results by targeting Atg7 (Liu J. et al., 2018). Another interesting study found that miR-30a is highly enriched in exosomes in the serum of patients with acute MI. Exosomes are an important communication route among hypoxic cardiomyocytes, and exosomal miR-30a may inhibit autophagy in hypoxic cardiomyocytes by inhibiting Beclin-1 and Atg12 (Yang Y. et al., 2016).

Exosomes Reduce Pyroptosis

In the process of MI, NLRP3 is one of the critical molecules for myocardial cell pyroptosis. Studies have shown that exosomes derived from human MSCs can significantly reduce the expression of NLRP3 and Caspase-1 in the I/R myocardium, then reduce the myocardial pyroptosis. It has been proven that miR-320b in exosomes played a crucial role in myocardial cell pyroptosis, with NLRP3 being the target gene of miR-320b (Tang et al., 2020). Macrophage-derived exosomes occupy a large part of the circulating microcapsules in the blood (McDonald et al., 2014). Studies have found that exosomes derived from M2 macrophages can reduce myocardial damage caused by I/R injury via the high expression of exosomal miR-148a and through TXNIP-NLRP3-caspase-1 path way (McDonald et al., 2014). SIRT1 plays a central role in regulating various cellular processes related to heart development and cardiovascular diseases (Chen et al., 2010). SIRT1 expression is down-regulated in MI, and overexpression of SIRT1 can effectively reduce myocardial damage caused by MI (Mori et al., 2014).

Overexpressing LncRNA KLF3-AS1 in BMMSCs might increase the expression of LncRNA KLF3-AS1 in exosomes. LncRNA KLF3-AS1 acts as a sponge of miR-138-5p in ischemic cardiomyocytes, and the absorption of miR-138-5p increases the expression of SIRT1 in cardiomyocytes. Besides the inhibition of Caspase-1, inflammatory cytokine IL-1β, SIRT1 can also inhibit

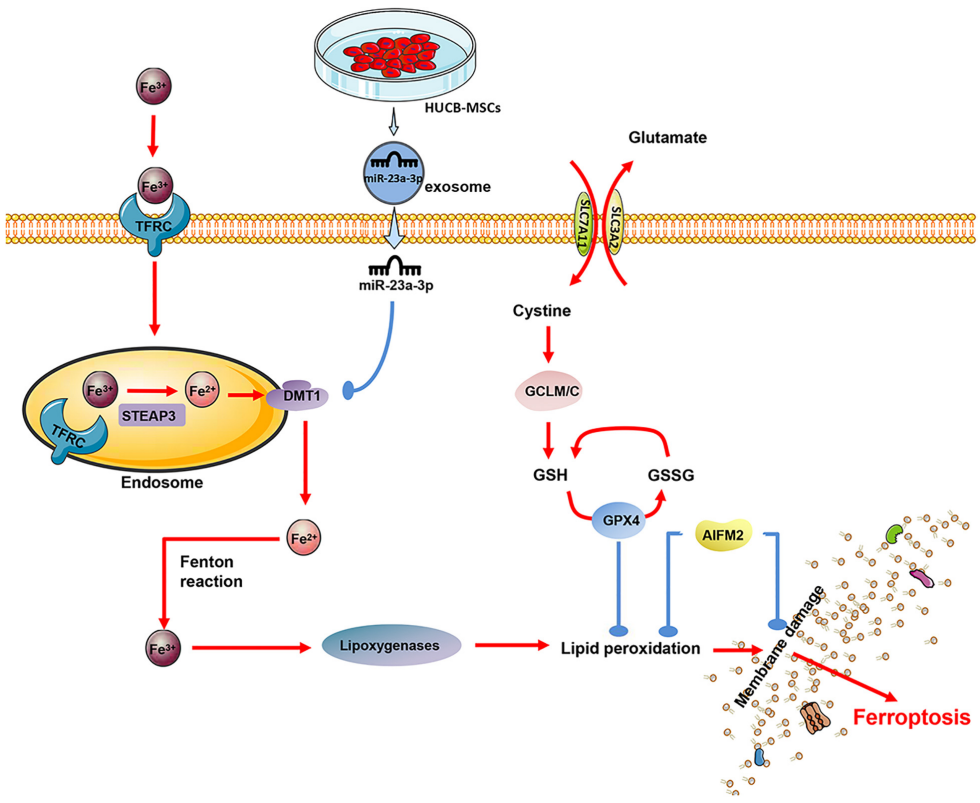

FIGURE 4 | The exosomes derived from human umbilical cord blood (MSCs) contain a significant amount of miR-23a-3p, which inhibits the expression of DMT1 after entering the cardiomyocytes, thereby reducing intracellular lipid oxidation and inhibiting the ferroptosis of cardiomyocytes.

the expression of NLRP3 and Asc, thus reducing the pyroptosis of cardiomyocytes (Mao et al., 2019; **Figure 3**).

Exosomes Reduce Ferroptosis

In a mouse model of cardiac I/R injury, both the iron chelator desferrioxamine (DFO) and the glutamine decomposition inhibitor compound-968 inhibit ferroptosis, reduce the size of MI, and improve heart function (Gao et al., 2015). Another study showed that treatment with Ferrostatin-1 or the iron chelator dexrazoxane in mice reduced the size of infarction and serum markers of myocardial injury during I/R (Fang et al., 2019). Proteomics showed that the protein level of GPX4 in myocardial cells decreased the first day and 1 week after MI in mice. The GPX4, however, slightly increased 8 weeks after infarction. RNA-seq and qRT-PCR analysis showed that the down-regulation of GPX4 occurred at the transcription level, and the down-regulation of GPX4 would cause ferroptosis of cardiomyocytes during MI (Park T. J. et al., 2019).

Significantly, $Fe3^{+}$ is introduced via the transferrin receptor (TR). In the endosome, Fe3 + is first converted to $Fe2^{+}$ via the Metallo-reductase six-transmembrane epithelial antigen of prostate 3 (Steap3) and later released from the endosome via the divalent metal transporter-1 (DMT1) (Xue et al., 2016; Pujol-Giménez et al., 2017). It is reported that the ferroptosis of cells is related to the up-regulation of DMT1 (Li L. B. et al., 2019; Yu et al., 2019). Notably, the expression of DMT1 in acute MI mice at 24 and 48-h was significantly higher than that in the sham operation group, while miR-23a-3p was highly expressed in exosomes derived from human MSCs (Ferguson et al., 2018). By transplanting exosomes, miR-23a-3p suppresses the iron death of myocardial cells by targeting DMT1 and improving MI's cardiac function (Song et al., 2020; **Figure 4**).

CONCLUSION

In the review herein, we discussed the anti-cell death potential of various exosomes from different cells, primarily stem cells for heart injury caused by MI or I/R. The above research shows that the same cell undergoes different treatments to change the type and proportion of the content in the exosomes from which it originates. Significantly after hypoxic treatment of stem cells, the protective substances in their exosomes increase. Studies have found that after LPS pretreated stem cells, their exosomes can enhance the M1 polarization of macrophages (Kang et al., 2018). All these indicate that modified and/or unmodified stem cells can increase the production of protective substances when they perceive danger signals, and exosomes serve as media to deliver protective substances. For the miRNAs and proteins, we believe can play a protective role, the cells are overexpressed by transfection, and these substances can also be delivered through exosomes as a medium to achieve cytoprotective effects. After modification of non-stem cells, can these cell-derived exosomes achieve the same protective effect? We believe that MSC and other stem cell-derived exosomes may be superior to other cells, because a large number of experiments have shown that stem cell-derived exosomes can play a protective role in cells, and the enhancement of protective factors can improve their ability. Besides, stem cell-derived exosomal microRNAs are potent regulators of cardiomyocytes' survival and functional properties, cardiomyocyte progenitor cells, and endothelial cells. The exocytosis of other cells including exosomes derived from cardiac lineage-committed cells (cardiospheres, cardiac cells differentiated from pluripotent stem cells) is also worthy of attention. The exosomes naturally produced by cells have been proven to produce the desired effect. Thus, the research for engineered exosomes that can produce potent effects to optimize cardioprotection should be the next step of action. The purpose of the modification is to produce exosomes that encapsulate the desired molecule. Future research in this area should focus on identifying the role of specific molecules in exosomes. Also, exploring the mechanism of the exosome loading process will be a valuable addition. Simultaneously, it is also necessary to consider that different microRNA target combinations should be tested in different cell types and different cardiovascular environments while paying attention to safety and effectiveness.

Despite the composition of exosomal contents, keen attention should be paid to saving cardiomyocytes, particularly those involved in multiple programmed deaths. For instance, p53 participates in apoptosis and autophagy death after MI, as one of the most common natural stresses of p53 activation is hypoxia. Under hypoxic conditions, neonatal rat cardiomyocytes may lead to intranuclear cleavage of genomic DNA, accompanied by increased p53 trans-activation activity and p53 protein accumulation (Kirshenbaum and de Moissac, 1997). The heterotopic expression of the anti-apoptotic gene Bcl-2 is sufficient to antagonize p53 induced apoptosis (Ng et al., 1999). Over-activation of p53-myocardin signaling in autophagy during myocardial infarction leads to the death of myocardial cells and accelerated ischemic injury (Liu C. Y. et al., 2018). The overexpression of p53 after MI may enhance apoptosis and autophagy of cardiomyocytes, and the inhibition of this target can achieve double the result with half the effort. Therefore, for the increase of protective substances in exosomes, the typical target of cardiomyocyte hypoxia death should be significantly considered to achieve maximum effectiveness.

AUTHOR CONTRIBUTIONS

XW and CF carried out the data collection and assembly of data, data analysis, and wrote the manuscript. XW, JP, and JG carried out the data collection and assembly. XW, CI, and JY carried out data analysis and interpretation, and manuscript revising. CF carried out the conception and design, and manuscript revising. All authors read and approved the final manuscript.

FUNDING

This work was supported by the Major Research Plan of the National Natural Science Foundation of China (No. 91539111 to JY) and the Key Project of Science and Technology of Hunan Province (No. 2020SK53420 to JY).

REFERENCES

Aachoui, Y., Sagulenko, V., Miao, E. A., and Stacey, K. J. (2013). Inflammasome-mediated pyroptotic and apoptotic cell death, and defense against infection. *Curr. Opin. Microbiol.* 16, 319–326. doi: 10.1016/j.mib.2013.04.004

Abu Khweek, A., and Amer, A. O. (2020). Pyroptotic and non-pyroptotic effector functions of caspase-11. *Immunol. Rev.* 297, 39–52. doi: 10.1111/imr.12910

Adamiak, M., Cheng, G., Bobis-Wozowicz, S., Zhao, L., Kedracka-Krok, S., Samanta, A., et al. (2018). Induced pluripotent stem cell (iPSC)-derived extracellular vesicles are safer and more effective for cardiac repair than iPSCs. *Circ. Res.* 122, 296–309. doi: 10.1161/circresaha.117.311769

Adams, J. M., and Cory, S. (1998). The Bcl-2 protein family: arbiters of cell survival. *Science (New York, N.Y.)* 281, 1322–1326. doi: 10.1126/science.281.5381.1322

Agrawal, A. K., Aqil, F., Jeyabalan, J., Spencer, W. A., Beck, J., Gachuki, B. W., et al. (2017). Milk-derived exosomes for oral delivery of paclitaxel. *Nanomed. Nanotechnol. Biol. Med.* 13, 1627–1636. doi: 10.1016/j.nano.2017.03.001

Aisa, Z., Liao, G. C., Shen, X. L., Chen, J., Li, L., and Jiang, S. B. (2017). Effect of autophagy on myocardial infarction and its mechanism. *Eur. Rev. Med. Pharmacol. Sci.* 21, 3705–3713.

Araki, S., Izumiya, Y., Rokutanda, T., Ianni, A., Hanatani, S., Kimura, Y., et al. (2015). Sirt7 contributes to myocardial tissue repair by maintaining transforming growth factor-β signaling pathway. *Circulation* 132, 1081–1093. doi: 10.1161/circulationaha.114.014821

Arslan, F., Lai, R. C., Smeets, M. B., Akeroyd, L., Choo, A., Aguor, E. N., et al. (2013). Mesenchymal stem cell-derived exosomes increase ATP levels, decrease oxidative stress and activate PI3K/Akt pathway to enhance myocardial viability and prevent adverse remodeling after myocardial ischemia/reperfusion injury. *Stem Cell Res.* 10, 301–312. doi: 10.1016/j.scr.2013.01.002

Ashkenazi, A., and Dixit, V. M. (1998). Death receptors: signaling and modulation. *Science (New York, N.Y.)* 281, 1305–1308. doi: 10.1126/science.281.5381.1305

Aurora, A. B., Mahmoud, A. I., Luo, X., Johnson, B. A., van Rooij, E., Matsuzaki, S., et al. (2012). MicroRNA-214 protects the mouse heart from ischemic injury by controlling $Ca+^2$ overload and cell death. *J. Clin. Invest.* 122, 1222–1232. doi: 10.1172/jci59327

Baines, C. P., Kaiser, R. A., Purcell, N. H., Blair, N. S., Osinska, H., Hambleton, M. A., et al. (2005). Loss of cyclophilin D reveals a critical role for mitochondrial permeability transition in cell death. *Nature* 434, 658–662. doi: 10.1038/nature03434

Bei, Y., Xu, T., Lv, D., Yu, P., Xu, J., Che, L., et al. (2017). Exercise-induced circulating extracellular vesicles protect against cardiac ischemia-reperfusion injury. *Basic Res. Cardiol.* 112:38. doi: 10.1007/s00395-017-0628-z

Buja, L. M., and Vela, D. (2008). Cardiomyocyte death and renewal in the normal and diseased heart. *Cardiovasc. Pathol.* 17, 349–374. doi: 10.1016/j.carpath.2008.02.004

Cătană, C. S., Atanasov, A. G., and Berindan-Neagoe, I. (2018). Natural products with anti-aging potential: affected targets and molecular mechanisms. *Biotechnol. Adv.* 36, 1649–1656. doi: 10.1016/j.biotechadv.2018.03.012

Cervantes, J., Nagata, T., Uchijima, M., Shibata, K., and Koide, Y. (2008). Intracytosolic Listeria monocytogenes induces cell death through caspase-1 activation in murine macrophages. *Cell. Microbiol.* 10, 41–52. doi: 10.1111/j.1462-5822.2007.01012.x

Chaput, N., and Théry, C. (2011). Exosomes: immune properties and potential clinical implementations. *Semin. Immunopathol.* 33, 419–440.

Chen, Q., Liu, Y., Ding, X., Li, Q., Qiu, F., Wang, M., et al. (2020). Bone marrow mesenchymal stem cell-secreted exosomes carrying microRNA-125b protect against myocardial ischemia reperfusion injury via targeting SIRT7. *Mol. Cell. Biochem.* 465, 103–114. doi: 10.1007/s11010-019-03671-z

Chen, Z., Chua, C. C., Ho, Y. S., Hamdy, R. C., and Chua, B. H. (2001). Overexpression of Bcl-2 attenuates apoptosis and protects against myocardial I/R injury in transgenic mice. *Am. J. Physiol. Heart Circ. Physiol.* 280, H2313–H2320. doi: 10.1152/ajpheart.2001.280.5.H2313

Chen, Z., Peng, I. C., Cui, X., Li, Y. S., Chien, S., and Shyy, J. Y. (2010). Shear stress, SIRT1, and vascular homeostasis. *Proc. Natl. Acad. Sci. U.S.A.* 107, 10268–10273. doi: 10.1073/pnas.1003833107

Del Re, D. P., Amgalan, D., Linkermann, A., Liu, Q., and Kitsis, R. N. (2019). Fundamental mechanisms of regulated cell death and implications for heart disease. *Physiol. Rev.* 99, 1765–1817. doi: 10.1152/physrev.00022.2018

Demircan, G., Kaplan, O., and Ozdas, S. B. (2018). Role of autophagy in the progress of coronary total occlusion. *Bratislavske Lekarske Listy* 119:103. doi: 10.4149/bll_2018_019

Deng, S., Zhou, X., Ge, Z., Song, Y., Wang, H., Liu, X., et al. (2019). Exosomes from adipose-derived mesenchymal stem cells ameliorate cardiac damage after myocardial infarction by activating S1P/SK1/S1PR1 signaling and promoting macrophage M2 polarization. *Int. J. Biochem. Cell Biol.* 114:105564. doi: 10.1016/j.biocel.2019.105564

Díaz, M., García, C., Sebastiani, G., de Zegher, F., López-Bermejo, A., and Ibáñez, L. (2017). Placental and cord blood methylation of genes involved in energy homeostasis: association with fetal growth and neonatal body composition. *Diabetes* 66, 779–784. doi: 10.2337/db16-0776

Didiot, M. C., Hall, L. M., Coles, A. H., Haraszti, R. A., Godinho, B. M., Chase, K., et al. (2016). Exosome-mediated delivery of hydrophobically modified siRNA for huntingtin mRNA silencing. *Mol. Ther.* 24, 1836–1847. doi: 10.1038/mt.2016.126

Ding, J., Wang, K., Liu, W., She, Y., Sun, Q., Shi, J., et al. (2016). Pore-forming activity and structural autoinhibition of the gasdermin family. *Nature* 535, 111–116. doi: 10.1038/nature18590

Dong, Z., Chu, G., Sima, Y., and Chen, G. (2018). Djhsp90s are crucial regulators during planarian regeneration and tissue homeostasis. *Biochem. Biophys. Res. Commun.* 498, 723–728. doi: 10.1016/j.bbrc.2018.03.047

Edinger, A. L., and Thompson, C. B. (2004). Death by design: apoptosis, necrosis and autophagy. *Curr. Opin. Cell Biol.* 16, 663–669. doi: 10.1016/j.ceb.2004.09.011

Eguchi, S., Takefuji, M., Sakaguchi, T., Ishihama, S., Mori, Y., Tsuda, T., et al. (2019). Cardiomyocytes capture stem cell-derived, anti-apoptotic microRNA-214 via clathrin-mediated endocytosis in acute myocardial infarction. *J. Biol. Chem.* 294, 11665–11674. doi: 10.1074/jbc.RA119.007537

Fang, X., Wang, H., Han, D., Xie, E., Yang, X., Wei, J., et al. (2019). Ferroptosis as a target for protection against cardiomyopathy. *Proc. Natl. Acad. Sci. U.S.A.* 116, 2672–2680. doi: 10.1073/pnas.1821022116

Ferguson, S. W., Wang, J., Lee, C. J., Liu, M., Neelamegham, S., Canty, J. M., et al. (2018). The microRNA regulatory landscape of MSC-derived exosomes: a systems view. *Sci. Rep.* 8:1419. doi: 10.1038/s41598-018-19581-x

Fink, S. L., and Cookson, B. T. (2006). Caspase-1-dependent pore formation during pyroptosis leads to osmotic lysis of infected host macrophages. *Cell. Microbiol.* 8, 1812–1825. doi: 10.1111/j.1462-5822.2006.00751.x

Foglio, E., Puddighinu, G., Germani, A., Russo, M. A., and Limana, F. (2017). HMGB1 inhibits apoptosis following MI and induces autophagy via mTORC1 inhibition. *J. Cell. Physiol.* 232, 1135–1143. doi: 10.1002/jcp.25576

Gao, M., Monian, P., Quadri, N., Ramasamy, R., and Jiang, X. (2015). Glutaminolysis and transferrin regulate ferroptosis. *Mol. Cell* 59, 298–308. doi: 10.1016/j.molcel.2015.06.011

Gong, X. H., Liu, H., Wang, S. J., Liang, S. W., and Wang, G. G. (2019). Exosomes derived from SDF1-overexpressing mesenchymal stem cells inhibit ischemic myocardial cell apoptosis and promote cardiac endothelial microvascular regeneration in mice with myocardial infarction. *J. Cell. Physiol.* 234, 13878–13893. doi: 10.1002/jcp.28070

Ham, P. B. III, and Raju, R. (2017). Mitochondrial function in hypoxic ischemic injury and influence of aging. *Prog. Neurobiol.* 157, 92–116. doi: 10.1016/j.pneurobio.2016.06.006

Heilig, R., and Broz, P. (2018). Function and mechanism of the pyrin inflammasome. *Eur. J. Immunol.* 48, 230–238. doi: 10.1002/eji.201746947

Hewitt, G., and Korolchuk, V. I. (2017). Repair, reuse, recycle: the expanding role of autophagy in genome maintenance. *Trends Cell Biol.* 27, 340–351. doi: 10.1016/j.tcb.2016.11.011

Hood, J. L., and Wickline, S. A. (2012). A systematic approach to exosome-based translational nanomedicine. *Wiley Interdiscip. Rev. Nanomed. Nanobiotechnol.* 4, 458–467. doi: 10.1002/wnan.1174

Huang, L., Yang, L., Ding, Y., Jiang, X., Xia, Z., and You, Z. (2020). Human umbilical cord mesenchymal stem cells-derived exosomes transfers microRNA-19a to protect cardiomyocytes from acute myocardial infarction by targeting SOX6. *Cell Cycle (Georgetown, Tex.)* 19, 339–353. doi: 10.1080/15384101.2019.1711305

Hurley, J. H. (2008). ESCRT complexes and the biogenesis of multivesicular bodies. *Curr. Opin. Cell Biol.* 20, 4–11. doi: 10.1016/j.ceb.2007.12.002

Ibrahim, A. G., Cheng, K., and Marbán, E. (2014). Exosomes as critical agents of cardiac regeneration triggered by cell therapy. *Stem Cell Rep.* 2, 606–619. doi: 10.1016/j.stemcr.2014.04.006

Inoki, K., Kim, J., and Guan, K. L. (2012). AMPK and mTOR in cellular energy homeostasis and drug targets. *Annu. Rev. Pharmacol. Toxicol.* 52, 381–400. doi: 10.1146/annurev-pharmtox-010611-134537

Irion, U., and St Johnston, D. (2007). bicoid RNA localization requires specific binding of an endosomal sorting complex. *Nature* 445, 554–558. doi: 10.1038/nature05503

Jahn, R., and Scheller, R. H. (2006). SNAREs–engines for membrane fusion. *Nat. Rev. Mol. Cell Biol.* 7, 631–643. doi: 10.1038/nrm2002

Jeremias, I., Kupatt, C., Martin-Villalba, A., Habazettl, H., Schenkel, J., Boekstegers, P., et al. (2000). Involvement of CD95/Apo1/Fas in cell death after myocardial ischemia. *Circulation* 102, 915–920. doi: 10.1161/01.cir.102.8.915

Jiang, L., Kon, N., Li, T., Wang, S. J., Su, T., Hibshoosh, H., et al. (2015). Ferroptosis as a p53-mediated activity during tumour suppression. *Nature* 520, 57–62. doi: 10.1038/nature14344

Jiang, X., Lew, K. S., Chen, Q., Richards, A. M., and Wang, P. (2018). human mesenchymal stem cell-derived exosomes reduce ischemia/reperfusion injury by the inhibitions of apoptosis and autophagy. *Curr. Pharma. Design* 24, 5334–5341. doi: 10.2174/1381612825666190119130441

Jung, J. H., Fu, X., and Yang, P. C. (2017). Exosomes generated from iPSC-derivatives: new direction for stem cell therapy in human heart diseases. *Circ. Res.* 120, 407–417. doi: 10.1161/circresaha.116.309307

Kajstura, J., Cheng, W., Reiss, K., Clark, W. A., Sonnenblick, E. H., Krajewski, S., et al. (1996). Apoptotic and necrotic myocyte cell deaths are independent contributing variables of infarct size in rats. *Lab. Invest. J. Technical Methods Pathol.* 74, 86–107.

Kang, H., Lee, M. J., Park, S. J., and Lee, M. S. (2018). Lipopolysaccharide-preconditioned periodontal ligament stem cells induce M1 polarization of macrophages through extracellular vesicles. *Int. J. Mol. Sci.* 19:3843. doi: 10.3390/ijms19123843

Kaur, A., and Sharma, S. (2017). Mammalian target of rapamycin (mTOR) as a potential therapeutic target in various diseases. *Inflammopharmacology* 25, 293–312. doi: 10.1007/s10787-017-0336-1

Kawaguchi, M., Takahashi, M., Hata, T., Kashima, Y., Usui, F., Morimoto, H., et al. (2011). Inflammasome activation of cardiac fibroblasts is essential for myocardial ischemia/reperfusion injury. *Circulation* 123, 594–604. doi: 10.1161/circulationaha.110.982777

Kayagaki, N., Stowe, I. B., Lee, B. L., O'Rourke, K., Anderson, K., Warming, S., et al. (2015). Caspase-11 cleaves gasdermin D for non-canonical inflammasome signalling. *Nature* 526, 666–671. doi: 10.1038/nature15541

Kirshenbaum, L. A., and de Moissac, D. (1997). The bcl-2 gene product prevents programmed cell death of ventricular myocytes. *Circulation* 96, 1580–1585. doi: 10.1161/01.cir.96.5.1580

Kishore, R., and Khan, M. (2016). More than tiny sacks: stem cell exosomes as cell-free modality for cardiac repair. *Circ. Res.* 118, 330–343. doi: 10.1161/circresaha.115.307654

Kishore, R., and Khan, M. (2017). Cardiac cell-derived exosomes: changing face of regenerative biology. *Eur. Heart J.* 38, 212–215. doi: 10.1093/eurheartj/ehw324

Konala, V. B., Mamidi, M. K., Bhonde, R., Das, A. K., Pochampally, R., and Pal, R. (2016). The current landscape of the mesenchymal stromal cell secretome: a new paradigm for cell-free regeneration. *Cytotherapy* 18, 13–24. doi: 10.1016/j.jcyt.2015.10.008

Lai, R. C., Arslan, F., Lee, M. M., Sze, N. S., Choo, A., Chen, T. S., et al. (2010). Exosome secreted by MSC reduces myocardial ischemia/reperfusion injury. *Stem Cell Res.* 4, 214–222. doi: 10.1016/j.scr.2009.12.003

Lai, R. C., Yeo, R. W., Tan, K. H., and Lim, S. K. (2013). Exosomes for drug delivery - a novel application for the mesenchymal stem cell. *Biotechnol. Adv.* 31, 543–551. doi: 10.1016/j.biotechadv.2012.08.008

Lambelet, M., Terra, L. F., Fukaya, M., Meyerovich, K., Labriola, L., Cardozo, A. K., et al. (2018). Dysfunctional autophagy following exposure to pro-inflammatory cytokines contributes to pancreatic β-cell apoptosis. *Cell Death Dis.* 9:96. doi: 10.1038/s41419-017-0121-5

Lazou, A., Iliodromitis, E. K., Cieslak, D., Voskarides, K., Mousikos, S., Bofilis, E., et al. (2006). Ischemic but not mechanical preconditioning attenuates ischemia/reperfusion induced myocardial apoptosis in anaesthetized rabbits: the role of Bcl-2 family proteins and ERK1/2. *Apoptosis* 11, 2195–2204. doi: 10.1007/s10495-006-0292-5

Lei, Q., Yi, T., and Chen, C. (2018). NF-κB-Gasdermin D (GSDMD) axis couples oxidative stress and NACHT, LRR and PYD domains-containing protein 3 (NLRP3) inflammasome-mediated cardiomyocyte pyroptosis following myocardial infarction. *Med. Sci. Monit.* 24, 6044–6052. doi: 10.12659/msm.908529

Li, J., Zhang, D., Wiersma, M., and Brundel, B. (2018). Role of autophagy in proteostasis: friend and foe in cardiac diseases. *Cells* 7:279. doi: 10.3390/cells7120279

Li, L. B., Chai, R., Zhang, S., Xu, S. F., Zhang, Y. H., Li, H. L., et al. (2019). Iron exposure and the cellular mechanisms linked to neuron degeneration in adult mice. *Cells* 8:198. doi: 10.3390/cells8020198

Li, T., Gu, J., Yang, O., Wang, J., Wang, Y., and Kong, J. (2020). Bone marrow mesenchymal stem cell-derived exosomal miRNA-29c decreases cardiac ischemia/reperfusion injury through inhibition of excessive autophagy via the PTEN/Akt/mTOR signaling pathway. *Circ. J.* 84, 1304–1311. doi: 10.1253/circj.CJ-19-1060

Li, Y., Yang, R., Guo, B., Zhang, H., Zhang, H., Liu, S., et al. (2019). Exosomal miR-301 derived from mesenchymal stem cells protects myocardial infarction by inhibiting myocardial autophagy. *Biochem. Biophys. Res. Commun.* 514, 323–328. doi: 10.1016/j.bbrc.2019.04.138

Libby, P., and Pasterkamp, G. (2015). Requiem for the 'vulnerable plaque'. *Eur. Heart J.* 36, 2984–2987. doi: 10.1093/eurheartj/ehv349

Liu, A., Gao, X., Zhang, Q., and Cui, L. (2017). [Retracted] Cathepsin B inhibition attenuates cardiac dysfunction and remodeling following myocardial infarction by inhibiting the NLRP3 pathway. *Mol. Med. Rep.* 16:7873. doi: 10.3892/mmr.2017.7551

Liu, C. Y., Zhang, Y. H., Li, R. B., Zhou, L. Y., An, T., Zhang, R. C., et al. (2018). LncRNA CAIF inhibits autophagy and attenuates myocardial infarction by blocking p53-mediated myocardin transcription. *Nat. Commun.* 9:29. doi: 10.1038/s41467-017-02280-y

Liu, J., Jiang, M., Deng, S., Lu, J., Huang, H., Zhang, Y., et al. (2018). miR-93-5p-containing exosomes treatment attenuates acute myocardial infarction-induced myocardial damage. *Mol. Ther. Nucleic Acids* 11, 103–115. doi: 10.1016/j.omtn.2018.01.010

Ma, H., Guo, R., Yu, L., Zhang, Y., and Ren, J. (2011). Aldehyde dehydrogenase 2 (ALDH2) rescues myocardial ischaemia/reperfusion injury: role of autophagy paradox and toxic aldehyde. *Eur. Heart J.* 32, 1025–1038. doi: 10.1093/eurheartj/ehq253

Mao, Q., Liang, X. L., Zhang, C. L., Pang, Y. H., and Lu, Y. X. (2019). LncRNA KLF3-AS1 in human mesenchymal stem cell-derived exosomes ameliorates pyroptosis of cardiomyocytes and myocardial infarction through miR-138-5p/Sirt1 axis. *Stem Cell Res. Ther.* 10:393. doi: 10.1186/s13287-019-1522-4

Matsui, Y., Takagi, H., Qu, X., Abdellatif, M., Sakoda, H., Asano, T., et al. (2007). Distinct roles of autophagy in the heart during ischemia and reperfusion: roles of AMP-activated protein kinase and Beclin 1 in mediating autophagy. *Circ. Res.* 100, 914–922. doi: 10.1161/01.Res.0000261924.76669.36

McDonald, M. K., Tian, Y., Qureshi, R. A., Gormley, M., Ertel, A., Gao, R., et al. (2014). Functional significance of macrophage-derived exosomes in inflammation and pain. *Pain* 155, 1527–1539. doi: 10.1016/j.pain.2014.04.029

Mezzaroma, E., Toldo, S., Farkas, D., Seropian, I. M., Van Tassell, B. W., Salloum, F. N., et al. (2011). The inflammasome promotes adverse cardiac remodeling following acute myocardial infarction in the mouse. *Proc. Natl. Acad. Sci. U.S.A.* 108, 19725–19730. doi: 10.1073/pnas.1108586108

Moe, G. W., and Marín-García, J. (2016). Role of cell death in the progression of heart failure. *Heart Fail. Rev.* 21, 157–167. doi: 10.1007/s10741-016-9532-0

Mori, J., Patel, V. B., Abo Alrob, O., Basu, R., Altamimi, T., Desaulniers, J., et al. (2014). Angiotensin 1-7 ameliorates diabetic cardiomyopathy and diastolic dysfunction in db/db mice by reducing lipotoxicity and inflammation. *Circ. Heart Fail.* 7, 327–339. doi: 10.1161/circheartfailure.113.000672

Nabel, E. G., and Braunwald, E. (2012). A tale of coronary artery disease and myocardial infarction. *N. Engl. J. Med.* 366, 54–63. doi: 10.1056/NEJMra1112570

Newton, K., Dugger, D. L., Maltzman, A., Greve, J. M., Hedehus, M., Martin-McNulty, B., et al. (2016). RIPK3 deficiency or catalytically inactive RIPK1 provides greater benefit than MLKL deficiency in mouse models of

inflammation and tissue injury. *Cell Death Differ.* 23, 1565–1576. doi: 10.1038/cdd.2016.46

Ng, I., Yeo, T. T., Soong, R., Tang, W. T., Ong, P. L., Lew, T., et al. (1999). Young Investigator's Award: induction of apoptosis following traumatic head injury in humans. *Ann. Acad. Med. Singapore* 28, 363–365.

Ni, J., Liu, X., Yin, Y., Zhang, P., Xu, Y. W., and Liu, Z. (2019). Exosomes derived from TIMP2-modified human umbilical cord mesenchymal stem cells enhance the repair effect in rat model with myocardial infarction possibly by the Akt/Sfrp2 pathway. *Oxid. Med. Cell. Longev.* 2019:1958941. doi: 10.1155/2019/1958941

Pan, J., Alimujiang, M., Chen, Q., Shi, H., and Luo, X. (2019). Exosomes derived from miR-146a-modified adipose-derived stem cells attenuate acute myocardial infarction-induced myocardial damage via downregulation of early growth response factor 1. *J. Cell. Biochem.* 120, 4433–4443. doi: 10.1002/jcb.27731

Park, K. S., Bandeira, E., Shelke, G. V., Lässer, C., and Lötvall, J. (2019). Enhancement of therapeutic potential of mesenchymal stem cell-derived extracellular vesicles. *Stem Cell Res. Ther.* 10:288. doi: 10.1186/s13287-019-1398-3

Park, T. J., Park, J. H., Lee, G. S., Lee, J. Y., Shin, J. H., Kim, M. W., et al. (2019). Quantitative proteomic analyses reveal that GPX4 downregulation during myocardial infarction contributes to ferroptosis in cardiomyocytes. *Cell Death Dis.* 10:835. doi: 10.1038/s41419-019-2061-8

Pujol-Giménez, J., Hediger, M. A., and Gyimesi, G. (2017). A novel proton transfer mechanism in the SLC11 family of divalent metal ion transporters. *Sci. Rep.* 7:6194. doi: 10.1038/s41598-017-06446-y

Roth, G. A., Johnson, C., Abajobir, A., Abd-Allah, F., Abera, S. F., Abyu, G., et al. (2017). Global, regional, and national burden of cardiovascular diseases for 10 causes, 1990 to 2015. *J. Am. Coll. Cardiol.* 70, 1–25. doi: 10.1016/j.jacc.2017.04.052

Rühl, S., and Broz, P. (2015). Caspase-11 activates a canonical NLRP3 inflammasome by promoting K(+) efflux. *Eur. J. Immunol.* 45, 2927–2936. doi: 10.1002/eji.201545772

Saraste, A., Pulkki, K., Kallajoki, M., Henriksen, K., Parvinen, M., and Voipio-Pulkki, L. M. (1997). Apoptosis in human acute myocardial infarction. *Circulation* 95, 320–323. doi: 10.1161/01.cir.95.2.320

Sciarretta, S., Forte, M., Frati, G., and Sadoshima, J. (2018). New insights into the role of mTOR signaling in the cardiovascular system. *Circ. Res.* 122, 489–505. doi: 10.1161/circresaha.117.311147

Seiler, A., Schneider, M., Förster, H., Roth, S., Wirth, E. K., Culmsee, C., et al. (2008). Glutathione peroxidase 4 senses and translates oxidative stress into 12/15-lipoxygenase dependent- and AIF-mediated cell death. *Cell Metab.* 8, 237–248. doi: 10.1016/j.cmet.2008.07.005

Shao, B. Z., Han, B. Z., Zeng, Y. X., Su, D. F., and Liu, C. (2016). The roles of macrophage autophagy in atherosclerosis. *Acta Pharmacol. Sin.* 37, 150–156. doi: 10.1038/aps.2015.87

Shekhar, A., Heeger, P., Reutelingsperger, C., Arbustini, E., Narula, N., Hofstra, L., et al. (2018). Targeted imaging for cell death in cardiovascular disorders. *JACC. Cardiovasc. Imaging* 11, 476–493. doi: 10.1016/j.jcmg.2017.11.018

Shi, J., Gao, W., and Shao, F. (2017). Pyroptosis: gasdermin-mediated programmed necrotic cell death. *Trends Biochem. Sci.* 42, 245–254. doi: 10.1016/j.tibs.2016.10.004

Shi, J., Zhao, Y., Wang, K., Shi, X., Wang, Y., Huang, H., et al. (2015). Cleavage of GSDMD by inflammatory caspases determines pyroptotic cell death. *Nature* 526, 660–665. doi: 10.1038/nature15514

Shukla, S., Saxena, S., Singh, B. K., and Kakkar, P. (2017). BH3-only protein BIM: an emerging target in chemotherapy. *Eur. J. Cell Biol.* 96, 728–738. doi: 10.1016/j.ejcb.2017.09.002

Song, Y., Wang, B., Zhu, X., Hu, J., Sun, J., Xuan, J., et al. (2020). Human umbilical cord blood-derived MSCs exosome attenuate myocardial injury by inhibiting ferroptosis in acute myocardial infarction mice. *Cell Biol. Toxicol.* 37, 51–64. doi: 10.1007/s10565-020-09530-8

Stockwell, B. R., Friedmann Angeli, J. P., Bayir, H., Bush, A. I., Conrad, M., Dixon, S. J., et al. (2017). Ferroptosis: a regulated cell death nexus linking metabolism, redox biology, and disease. *Cell* 171, 273–285. doi: 10.1016/j.cell.2017.09.021

Stoorvogel, W. (2012). Functional transfer of microRNA by exosomes. *Blood* 119, 646–648. doi: 10.1182/blood-2011-11-389478

Stuffers, S., Sem Wegner, C., Stenmark, H., and Brech, A. (2009). Multivesicular endosome biogenesis in the absence of ESCRTs. *Traffic (Copenhagen, Denmark)* 10, 925–937. doi: 10.1111/j.1600-0854.2009.00920.x

Sun, X. H., Wang, X., Zhang, Y., and Hui, J. (2019). Exosomes of bone-marrow stromal cells inhibit cardiomyocyte apoptosis under ischemic and hypoxic conditions via miR-486-5p targeting the PTEN/PI3K/AKT signaling pathway. *Thrombosis Res.* 177, 23–32. doi: 10.1016/j.thromres.2019.02.002

Takahashi, M. (2010). Role of the SDF-1/CXCR4 system in myocardial infarction. *Circ. J.* 74, 418–423. doi: 10.1253/circj.cj-09-1021

Tang, J., Jin, L., Liu, Y., Li, L., Ma, Y., Lu, L., et al. (2020). Exosomes derived from mesenchymal stem cells protect the myocardium against ischemia/reperfusion injury through inhibiting pyroptosis. *Drug Design Dev. Ther.* 14, 3765–3775. doi: 10.2147/dddt.S239546

Théry, C., Boussac, M., Véron, P., Ricciardi-Castagnoli, P., Raposo, G., Garin, J., et al. (2001). Proteomic analysis of dendritic cell-derived exosomes: a secreted subcellular compartment distinct from apoptotic vesicles. *J. Immunol. (Baltimore, Md. 1950)* 166, 7309–7318. doi: 10.4049/jimmunol.166.12.7309

Théry, C., Zitvogel, L., and Amigorena, S. (2002). Exosomes: composition, biogenesis and function. *Nat. Rev. Immunol.* 2, 569–579. doi: 10.1038/nri855

Toldo, S., and Abbate, A. (2018). The NLRP3 inflammasome in acute myocardial infarction. *Nat. Rev. Cardiol.* 15, 203–214. doi: 10.1038/nrcardio.2017.161

Torre-Amione, G., Kapadia, S., Lee, J., Durand, J. B., Bies, R. D., Young, J. B., et al. (1996). Tumor necrosis factor-alpha and tumor necrosis factor receptors in the failing human heart. *Circulation* 93, 704–711. doi: 10.1161/01.cir.93.4.704

Valadi, H., Ekström, K., Bossios, A., Sjöstrand, M., Lee, J. J., and Lötvall, J. O. (2007). Exosome-mediated transfer of mRNAs and microRNAs is a novel mechanism of genetic exchange between cells. *Nat. Cell Biol.* 9, 654–659. doi: 10.1038/ncb1596

Villarroya-Beltri, C., Gutiérrez-Vázquez, C., Sánchez-Cabo, F., Pérez-Hernández, D., Vázquez, J., Martin-Cofreces, N., et al. (2013). Sumoylated hnRNPA2B1 controls the sorting of miRNAs into exosomes through binding to specific motifs. *Nat. Commun.* 4:2980. doi: 10.1038/ncomms3980

Wang, P., Shao, B. Z., Deng, Z., Chen, S., Yue, Z., and Miao, C. Y. (2018). Autophagy in ischemic stroke. *Prog. Neurobiol.* 163-164, 98–117. doi: 10.1016/j.pneurobio.2018.01.001

Wang, Y., Zhang, L., Li, Y., Chen, L., Wang, X., Guo, W., et al. (2015). Exosomes/microvesicles from induced pluripotent stem cells deliver cardioprotective miRNAs and prevent cardiomyocyte apoptosis in the ischemic myocardium. *Int. J. Cardiol.* 192, 61–69. doi: 10.1016/j.ijcard.2015.05.020

Wang, Y., Zhao, R., Liu, D., Deng, W., Xu, G., Liu, W., et al. (2018). Exosomes derived from miR-214-enriched bone marrow-derived mesenchymal stem cells regulate oxidative damage in cardiac stem cells by targeting CaMKII. *Oxid. Med. Cell. Longev.* 2018:4971261. doi: 10.1155/2018/4971261

Xiao, C., Wang, K., Xu, Y., Hu, H., Zhang, N., Wang, Y., et al. (2018). Transplanted mesenchymal stem cells reduce autophagic flux in infarcted hearts via the exosomal transfer of miR-125b. *Circ. Res.* 123, 564–578. doi: 10.1161/CIRCRESAHA.118.312758

Xiao, J., Pan, Y., Li, X. H., Yang, X. Y., Feng, Y. L., Tan, H. H., et al. (2016). Cardiac progenitor cell-derived exosomes prevent cardiomyocytes apoptosis through exosomal miR-21 by targeting PDCD4. *Cell Death Dis.* 7:e2277. doi: 10.1038/cddis.2016.181

Xue, X., Ramakrishnan, S. K., Weisz, K., Triner, D., Xie, L., Attili, D., et al. (2016). Iron uptake via DMT1 integrates cell cycle with JAK-STAT3 signaling to promote colorectal tumorigenesis. *Cell Metab.* 24, 447–461. doi: 10.1016/j.cmet.2016.07.015

Yang, J., Zhao, Y., and Shao, F. (2015). Non-canonical activation of inflammatory caspases by cytosolic LPS in innate immunity. *Curr. Opin. Immunol.* 32, 78–83. doi: 10.1016/j.coi.2015.01.007

Yang, L., Jiang, Y., Wen, Z., Xu, X., Xu, X., Zhu, J., et al. (2015). Over-expressed EGR1 may exaggerate ischemic injury after experimental stroke by decreasing BDNF expression. *Neuroscience* 290, 509–517. doi: 10.1016/j.neuroscience.2015.01.020

Yang, P. C. (2018). Induced pluripotent stem cell (iPSC)–derived exosomes for precision medicine in heart failure. *Circ. Res.* 122, 661–663.

Yang, Y., Li, Y., Chen, X., Cheng, X., Liao, Y., and Yu, X. (2016). Exosomal transfer of miR-30a between cardiomyocytes regulates autophagy after hypoxia. *J. Mol. Med. (Berlin, Germany)* 94, 711–724. doi: 10.1007/s00109-016-1387-2

Yang, Z., Zingarelli, B., and Szabó, C. (2000). Effect of genetic disruption of poly (ADP-ribose) synthetase on delayed production of inflammatory mediators and delayed necrosis during myocardial ischemia-reperfusion injury. *Shock (Augusta, Ga.)* 13, 60–66. doi: 10.1097/00024382-200013010-00011

Ye, M., Ni, Q., Qi, H., Qian, X., Chen, J., Guo, X., et al. (2019). Exosomes derived from human induced pluripotent stem cells-endothelia cells promotes postnatal angiogenesis in mice bearing ischemic limbs. *Int. J. Biol. Sci.* 15, 158–168.

Yellon, D. M., and Hausenloy, D. J. (2007). Myocardial reperfusion injury. *N. Engl. J. Med.* 357, 1121–1135. doi: 10.1056/NEJMra071667

Youle, R. J., and Strasser, A. (2008). The BCL-2 protein family: opposing activities that mediate cell death. *Nat. Rev. Mol. Cell Biol.* 9, 47–59. doi: 10.1038/nrm2308

Yu, B., Gong, M., He, Z., Wang, Y. G., Millard, R. W., Ashraf, M., et al. (2013). Enhanced mesenchymal stem cell survival induced by GATA-4 overexpression is partially mediated by regulation of the miR-15 family. *Int. J. Biochem. Cell Biol.* 45, 2724–2735. doi: 10.1016/j.biocel.2013.09.007

Yu, B., Kim, H. W., Gong, M., Wang, J., Millard, R. W., Wang, Y., et al. (2015). Exosomes secreted from GATA-4 overexpressing mesenchymal stem cells serve as a reservoir of anti-apoptotic microRNAs for cardioprotection. *Int. J. Cardiol.* 182, 349–360. doi: 10.1016/j.ijcard.2014.12.043

Yu, H., Yang, C., Jian, L., Guo, S., Chen, R., Li, K., et al. (2019). Sulfasalazine-induced ferroptosis in breast cancer cells is reduced by the inhibitory effect of estrogen receptor on the transferrin receptor. *Oncol. Rep.* 42, 826–838. doi: 10.3892/or.2019.7189

Zhang, Q. Y., Jin, H. F., Chen, S., Chen, Q. H., Tang, C. S., Du, J. B., et al. (2018). Hydrogen sulfide regulating myocardial structure and function by targeting cardiomyocyte autophagy. *Chin. Med. J.* 131, 839–844. doi: 10.4103/0366-6999.228249

Zhang, X., Evans, T. D., Jeong, S. J., and Razani, B. (2018). Classical and alternative roles for autophagy in lipid metabolism. *Curr. Opin. Lipidol.* 29, 203–211. doi: 10.1097/mol.0000000000000509

Zhao, X., Luo, G., Cheng, Y., Yu, W., Chen, R., Xiao, B., et al. (2018). Compound C induces protective autophagy in human cholangiocarcinoma cells via Akt/mTOR-independent pathway. *J. Cell. Biochem.* 119, 5538–5550. doi: 10.1002/jcb.26723

Zhu, L. P., Tian, T., Wang, J. Y., He, J. N., Chen, T., Pan, M., et al. (2018). Hypoxia-elicited mesenchymal stem cell-derived exosomes facilitates cardiac repair through miR-125b-mediated prevention of cell death in myocardial infarction. *Theranostics* 8, 6163–6177. doi: 10.7150/thno.28021

Conflict of Interest: JG was employed by the company Hunan Fangsheng Pharmaceutical Co. Ltd.

The remaining authors declare that the research was conducted in the absence of any commercial or financial relationships that could be construed as a potential conflict of interest.

frontiers in Cell and Developmental Biology

BRIEF RESEARCH REPORT
published: 23 July 2021
doi: 10.3389/fcell.2021.697939

Extracellular Vesicle-Based Detection of Pancreatic Cancer

Yesim Verel-Yilmaz[1†], Juan Pablo Fernández[1†], Agnes Schäfer[2], Sheila Nevermann[1], Lena Cook[2], Norman Gercke[1], Frederik Helmprobst[3,4], Christian Jaworek[2], Elke Pogge von Strandmann[5], Axel Pagenstecher[3], Detlef K. Bartsch[1], Jörg W. Bartsch[2†] and Emily P. Slater[1†]*

[1] Department of Visceral, Thoracic and Vascular Surgery, Philipps University Marburg, Marburg, Germany, [2] Department of Neurosurgery, Philipps University Marburg, Marburg, Germany, [3] Department of Neuropathology, Philipps University Marburg, Marburg, Germany, [4] Core Facility-Mouse Pathology and Electron Microscopy (MPEM), Philipps University Marburg, Marburg, Germany, [5] Institute for Tumorimmunology, Philipps University Marburg, Marburg, Germany

Due to a grim prognosis, there is an urgent need to detect pancreatic ductal adenocarcinoma (PDAC) prior to metastasis. However, reliable diagnostic imaging methods or biomarkers for PDAC or its precursor lesions are still scarce. ADAM8, a metalloprotease-disintegrin, is highly expressed in PDAC tissue and negatively correlates with patient survival. The aim of our study was to determine the ability of ADAM8-positive extracellular vesicles (EVs) and cargo microRNAs (miRNAs) to discriminate precursor lesions or PDAC from healthy controls. In order to investigate enrichment of ADAM8 on EVs, these were isolated from serum of patients with PDAC (n = 52), precursor lesions (n = 7) and healthy individuals (n = 20). Nanoparticle Tracking Analysis and electron microscopy indicated successful preparation of EVs that were analyzed for ADAM8 by FACS. Additionally, EV cargo analyses of miRNAs from the same serum samples revealed the presence of miR-720 and miR-451 by qPCR and was validated in 20 additional PDAC samples. Statistical analyses included Wilcoxon rank test and ROC curves. FACS analysis detected significant enrichment of ADAM8 in EVs from patients with PDAC or precursor lesions compared to healthy individuals (p = 0.0005). ADAM8-dependent co-variates, miR-451 and miR-720 were also diagnostic, as patients with PDAC had significantly higher serum levels of miR-451 and lower serum levels of miR-720 than healthy controls and reached high sensitivity and specificity (AUC = 0.93 and 1.00, respectively) to discriminate PDAC from healthy control. Thus, detection of ADAM8-positive EVs and related cargo miR-720 and miR-451 may constitute a specific biomarker set for screening individuals at risk for PDAC.

Keywords: pancreatic cancer, extracellular vesicles, ADAM8, serum biomarkers, miRNA

OPEN ACCESS

Edited by:
Jeffrey David Galley, The Ohio State University, United States

Reviewed by:
Cheng Wang, Nanjing University, China
Xinlei Li, Nationwide Children's Hospital, United States

****Correspondence:***
Emily P. Slater
slater@med.uni-marburg.de

† These authors have contributed equally to this work

Specialty section:
This article was submitted to Molecular and Cellular Pathology, a section of the journal Frontiers in Cell and Developmental Biology

Received: *20 April 2021*
Accepted: *29 June 2021*
Published: *23 July 2021*

Citation:
Verel-Yilmaz Y, Fernández JP, Schäfer A, Nevermann S, Cook L, Gercke N, Helmprobst F, Jaworek C, Pogge von Strandmann E, Pagenstecher A, Bartsch DK, Bartsch JW and Slater EP (2021) Extracellular Vesicle-Based Detection of Pancreatic Cancer. Front. Cell Dev. Biol. 9:697939. doi: 10.3389/fcell.2021.697939

INTRODUCTION

Pancreatic cancer is the fourth leading cause of cancer-related deaths in the world with an incidence of 45 in 100,000 and a 5-year survival rate of around 9% (Siegel et al., 2020). Among pancreatic cancer, pancreatic ductal adenocarcinoma (PDAC) is the most common type with more than 90% of all cases. A number of factors are responsible for the poor prognosis of PDAC that combines the difficulties in detecting the tumor in early stages, an aggressive biological behavior to account

for metastasis and the resistance to existing adjuvant therapies. To detect PDAC in early stages, only a few biomarkers are used routinely that are able to detect its presence and the lesions prior to its derivation (Bartsch et al., 2018). Exosomes are a defined type of extracellular vesicle (EV) ranging in size from 30 to 100 nm and secreted by all cell types including cancer cells. In the context of cancer, exosomes produced in tumor cells contain an abundance of cell-specific molecules that may facilitate the discrimination between cancer afflicted patients and healthy individuals (Sumrin et al., 2018).

Exosome cargo consists of proteins, nucleic acids and lipids (Colombo et al., 2014). Their composition is not only a reflection of the cell they originated from, but also appears to be a regulated process that remains not completely understood (Minciacchi et al., 2015). Content sorting and exosome release seem to not only depend on the type of donor cell, but also on its physiological or pathological state, different stimuli and the pathway of exosome biogenesis (Minciacchi et al., 2015). There are, however, marker proteins that have been found to be specific to EVs because they are related to their pathway of biogenesis. These proteins are, for example, members of the tetraspanin family (CD9, CD81) that are characteristic to exosomes, or flotillins (flotillin-1–2), which are frequently observed in exosomes and microvesicles alike (Kowal et al., 2016). Because exosome content is specific to their donor cell and exosomes can be isolated from bodily fluids such as blood, saliva, ascites or urine, they make promising candidates for early tumor diagnostics.

One rationale to use EVs as early diagnostic markers is their potential to transport tumor-associated micro RNAs (miRNAs) encapsulated in serum exosomes. MiRNAs are small non-coding RNAs of about 18–22 nt long that can be transferred to adjacent cells in the tumor microenvironment to modulate gene expression (Zonari et al., 2013; Su et al., 2016).

As protein cargo, membrane proteins involved in extracellular communication and remodeling are excellent candidates for exosome loading. Among these proteins metalloprotease-disintegrins (ADAM) are potential cargo proteins (reviewed in Shimoda and Khokha, 2017). Due to the interaction with the exosomal marker protein CD9, ADAM10 was one of the first members of the ADAM protease family found to be associated with exosomes (Keller et al., 2009). In previous studies, ADAM8 was defined as an ADAM protease associated with tumor progression and metastasis formation in PDAC (Valkovskaya et al., 2007; Schlomann et al., 2015). In addition, ADAM8 is expressed in tumor associated immune cells such as macrophages, NK cells and neutrophils (Jaworek et al., 2021). These data suggest that ADAM8 itself could be a diffusible molecule that is, similarly to the ADAM protease ADAM10, released in exosomes. Recently, much attention has been addressed to EVs, which may serve as a strategy of monitoring and managing disease status (Cufaro et al., 2019). Since ADAM8 expression is high in PDAC, it is likely that EVs isolated from its precursor lesions, Pancreatic intraepithelial Neoplasia (PanINs) types 2 and 3, could be packed with ADAM8 and ADAM8-associated molecular markers such as miRNAs as shown for breast cancer with correlated expression levels of ADAM8 and miRNA-720 (Das et al., 2016). MiRNAs are integral components of almost every cancer-related biological process, including cellular differentiation, proliferation, migration, apoptosis, EMT and angiogenesis. Here we hypothesized that high ADAM8 expression levels in pancreatic cancer is reflected by release of EVs expressing ADAM8 on their surface and that ADAM8 expression might cause miRNAs associated with ADAM8 expression to be cargo for ADAM8-positive EVs, so that these EVs can be used to detect pancreatic cancer in patient serum at early stages.

MATERIALS AND METHODS

Patient Cohort

Patients with familial pancreatic cancer (FPC) or PDAC treated at the Department of Visceral Surgery at University Hospital Marburg were enrolled in our study. All patients provided written informed consent prior to participating in this study. Ethical approval was granted from the local ethics committee at Marburg University, Faculty of Medicine (File No. 5/03). All tumors were histologically staged by an experienced pathologist according to the UICC-TNM (Union for International Cancer Control; tumor, node, metastasis) classification 2017 (Gospodarowicz and Brierley, 2017).

Extracellular Vesicle Preparation

250 µl of serum were diluted with 4.5 ml Hank's Salt Saline Buffer in a 15 ml falcon tube in order to lower sample viscosity and centrifuged at 800 × g for 5 min in order to eliminate any remaining cells. The supernatant was transferred to a new 15 ml falcon tube and centrifuged at 2,000 × g for 10 min to remove dead cells or cell debris (Théry et al., 2006; Melo et al., 2015). The supernatant was then transferred to a 5 ml syringe and filtered through a 0.2 µm pore filter and transferred to a 6.0 ml polypropylene bell-top quick-seal centrifuge tube and filled with Hank's Balanced Salt Solution (HBSS). The tubes were centrifuged at 100,000 × g and 4°C for 70 min. The pellet was resuspended in HBSS and transferred to a polypropylene 1.5 ml microcentrifuge tube and was centrifuged with an Optima MAX-XP Ultracentrifuge in a TLA-55 fixed angle rotor at 100,000 × g and 4°C for 100 min. The supernatant was discarded, and the pellet resuspended with 50 µl HBSS. Samples were stored at –80°C. In order to determine the particle size and concentration of isolated EVs, NTA was performed with the ZetaView® BASIC PMX-120 and the corresponding software ZetaView®.

Western Blot Analysis

To further phenotype isolated EVs, enriched proteins were detected in Western blots. Twenty µg protein determined by standard BCA were boiled in Laemmli buffer without β-Mercaptoethanol (60 mM Tris-HCl, pH = 6.8; 2% SDS; 10% Glycerol; 0.01% Bromphenol-Blue) for 5 min. Protein separation was performed by SDS-PAGE followed by a transfer onto PVDF membranes. Successful transfer was confirmed by Ponceau S staining. To block unspecific binding, membranes were immersed in 4% BSA in TBST (50 mM

Tris, pH = 7.5; 150 mM NaCl; 0.1% Tween-20) for 1 h, followed by incubation with primary antibody against CD9 (CBL162; Chemicon International, Temecula, CA, United States, 1:1,000 in 4% BSA in TBST) at 4°C overnight. After washing three times, blots were incubated with the respective secondary antibody for 1 h. After an additional washing step, signals were detected with SuperSignal™ West Pico PLUS Chemiluminescent Substrate (Thermo Fisher Scientific, Rockford, IL, United States). Additional antibodies were used to characterize the EVs isolated. These included CD81 (sc-166029; Santa Cruz Biotechnology), Flotillin-1 (PA5-18053; Thermo Fisher Scientific), hADAM8 (MAB10311; R&D Systems) and Calnexin (2679; Cell Signaling Technology).

FACS Analyses

FACS analyses were performed as previously described (Bartsch et al., 2018). Briefly, 1.5×10^9 EVs were coupled to 10 µl of 4 µm aldehyde/sulfate latex beads, 4% w/v in 100 µl PBS and incubated for 15 min at room temperature. Then 900 µl of PBS were added to reach a final volume of 1,000 µl and EVs and beads were incubated for another 30 min at room temperature. Beads were then blocked by adding 50 µl 10% BSA. Samples were centrifuged at 9,900 rpm for 1 min. Supernatant was discarded leaving a volume of 100 µl in the tubes. Samples were further blocked by incubation with 5 µl Human True Stain FcX Blocking Solution for 10 min at room temperature. Samples were then centrifuged again at 9,000 rpm for 1 min and the supernatant was discarded. Pellets were resuspended in 20 µl 2% BSA. Now, one half of the samples was incubated with 3 µl anti-ADAM8 (MAB10311, R&D Systems) at 4°C overnight. The next day, all samples were washed in 1 ml 2% BSA and centrifuged at 9,900 rpm for 1 min. All samples were treated with 20 µl of a blocking solution consisting of Human True Stain FcX Blocking Solution (BioLegend, San Diego, CA, United States) and 2% BSA and incubated with 3 µl alexa-488-tagged secondary antibody (Abcam, Cambridge, United Kingdom) at 4°C for 1 h. In a final step, samples were washed twice in 1 ml 2% BSA. The final bead pellet was resuspended in 1 ml PBS and transferred to 5 ml Flow Cytometry Tubes. Samples were stored at 4°C in the dark until measurement. The percentage of ADAM8-positive beads out of 100,000 total events was then calculated in a FACS analysis.

Electron Microscopy

EVs were stained for electron microscopy as previously described (Théry et al., 2006). Briefly, purified extracellular vesicles were fixed with an equal amount of 4% PFA. An amount of 5–7 µl was placed on a Formvar/carbon coated 200 mesh copper (Ted Pella Inc., Redding, CA) electron microscopy grid and incubated for 20 min. After the membrane adsorbed the vesicles the grids were washed with sterile filtered PBS and fixed for 5 min with 1% glutaraldehyde. The grids were washed 8 times for 2 min with sterile filtered water and then incubated with 1% uranyl acetate for 5 min. After an additional incubation with 2% methyl cellulose supplemented with 4% uranyl acetate (ratio 9:1) on ice, the excess fluid was removed with filter paper and the grids were air dried for up to 10 min. The exosomes were imaged with a Zeiss EM 900 at 80 kV.

Protease Activity Assay

Serum EVs isolated from either PDAC patients or healthy individuals were tested for ADAM8 activity by determining cleavage of a FRET-based polypeptide substrate with a high Kcat/Km for ADAM8 (PEPDab13, BioZyme, Inc., North Carolina, United States) as previously described (Schlomann et al., 2019). Briefly, 10 µM of PEPDab13 in 50 µl assay buffer (1 mM $ZnCl_2$, 20 mM Tris-HCl pH 8.0, 10 mM $CaCl_2$, 150 mM NaCl, 0.0006% Brij-35) was incubated with 3.75×10^8 EVs in a total volume of 100 µl. Resulting fluorescence was monitored every 2 min for 6 h at 37°C with a multiwell plate reader (FLUOstar OPTIMA, BMG Labtech, Offenburg, Germany) using λ_{ex} of 485 nm and an λ_{em} of 530 nm.

Serum Exosome miRNA Analysis

Total RNA carried by exosomes or other EVs in 250 µl of serum was extracted using the ExoRNeasy Serum/Plasma Midi Kit from Qiagen (Hilden, Germany) with the addition of a spike of 25 fmol of synthetic cel-miR-54 DNA as recommended by the manufacturer. The RNA was converted to cDNA using the miRNA Reverse Transcription Kit, miScript II RT Kit, also from Qiagen. The cDNA synthesis reaction was diluted and incubated with QuantiTect® SYBR Green PCR Master Mix, miScript Universal Primer and specific miScript Primer Assays. The real-time PCR reactions were run in a StepOnePlus Real time PCR System from Applied Biosystems (Darmstadt, Germany). The Δ threshold cycle (Ct) values were then calculated by subtracting the *cel*-miR-54 Ct value from the specific miRNA Ct value. For the analyses of cell lines SNORD95 was chosen as the endogenous control as previously described (Sperveslage et al., 2014). Ct values of each target miRNA transcript were normalized against the Ct value of SNORD95. Relative change in exosomal miRNA expression comparing wild type and knock-out cells was calculated using the ΔΔCt method.

Statistical Analyses

A Wilcoxon signed-rank test and a *t*-test were performed to assess whether the patient values were significantly different from control samples. A p-value of < 0.05 was considered to be statistically significant. The receiver operating characteristic curve analyses were performed using GraphPad Prism version 6 (GraphPad Software, La Jolla, CA, United States).

RESULTS

Clinicopathological Characteristics of the Recruited Patients, Including IAR With High-Risk Precursor Lesions

The characteristics of the 72 PDAC patients that were included in the study are presented in **Table 1**.

Preparation of Extracellular Vesicles From Patient Serum Samples

Extracellular vesicles including exosomes with an average diameter < 120 nm were isolated from patient serum using

TABLE 1 | Clinicopathological characteristics of the recruited patients.

		Cohort (*n* = 72)
Gender		
	Males (%)	37 (51%)
	Females (%)	35 (49%)
Median age at surgery, years (range)		68 (47–85)
UICC stage		
	I	11 (15.3%)
	II	10 (13.9%)
	III	46 (63.9%)
	IV	5 (6.9%)
Median survival, months (range)		22 (1–92)
Location	Pancreas	
	Head	65 (90.3%)
	body or tail	7 (9.7%)

In addition, 7 individuals at risk (IAR) who had undergone surgery for removal of precursor lesions were also recruited. These included 2 males and 5 females with a median age of 54 years. Histologically verified precursor lesions included 1 main duct intraductal papillary mucinous neoplasm (IPMN) with high grade dysplasia, 2 PanIN 3 and 4 PanIN 2. The healthy controls (n = 20) had a median age of 40 years and included 10 males and 10 females.

a range of purification steps including ultracentrifugation and filtration. The exosomes present in these preparations were identified by a number of analytical methods including ZetaView® analyses and electron microscopy to confirm existence of a double membrane and the proper size corresponding to exosomes (**Figures 1A–C**). The particle size and vesicle concentration did not vary among the preparations from the different sources (**Figures 1D,E**). In addition, CD9 was found in all preparations. However, whereas the control samples had relatively constant amounts of CD9 (**Figure 1F**), the tumor samples varied in abundance (**Figure 1G**). Additional markers were also tested to characterize the EVs. The preparations were also positive for CD81, Flotillin-1 and ADAM8, but were negative for calnexin (**Supplementary Figure 1**).

Diagnostic FACS Analysis of ADAM8 in Exosomes

In order to detect ADAM8 on the surface of exosomes, a bead-coupled FACS analysis was performed (**Figure 2**). Positive ADAM8 signals were observed both in control individuals and in PDAC patients. However, their proportion was significantly different, so that an enrichment of ADAM8 in serum exosomes from patients with PDAC or its precursor lesions compared to healthy individuals was observed ($p < 0.0001$ or $p = 0.0139$, respectively).

Cargo Analysis of Serum Derived EVs From Control and PDAC Patients

Since ADAM8 is located on EVs as shown by bead-coupled FACS analysis, we investigated whether ADAM8 confers enzymatic activity to EVs enriched in ADAM8. Activity of ADAM8 can

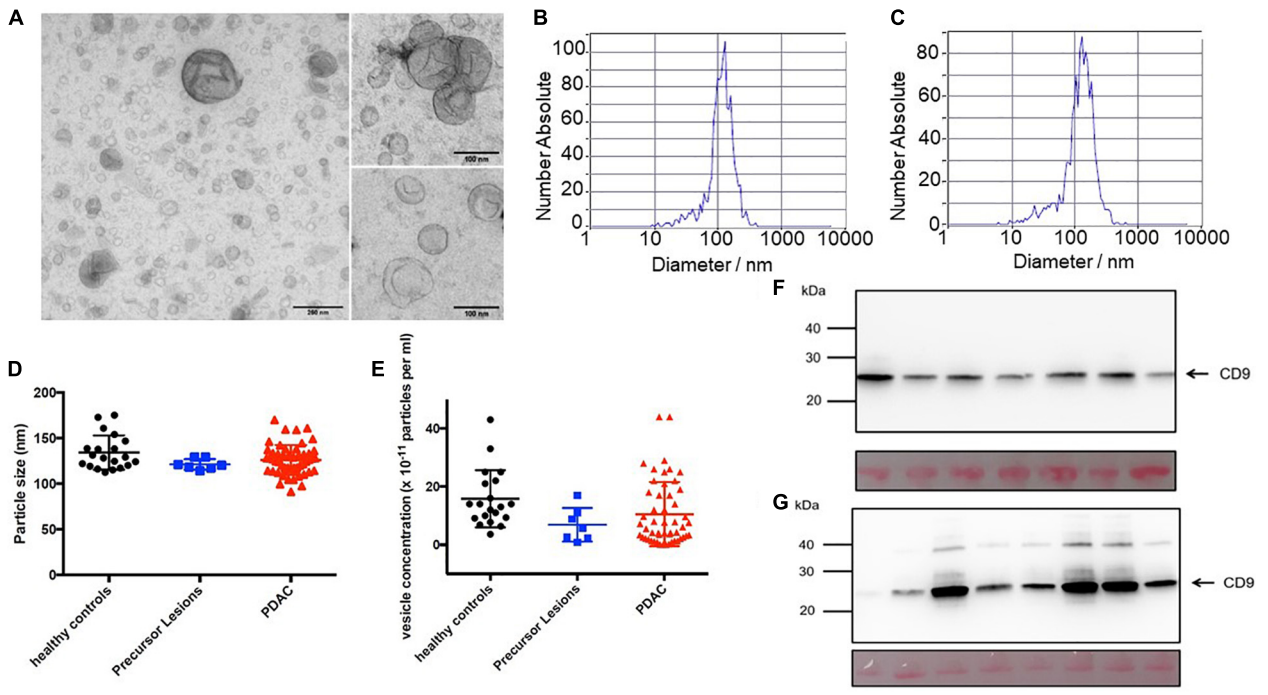

FIGURE 1 | Extracellular vesicles prepared from serum. Electron micrograph of EVs isolated from PDAC patient's serum **(A)**. Border is clearly delimited. ZetaView measurements of serum EVs isolated from healthy control **(B)** and PDAC patient **(C)**. Mean particle size **(D)** and mean vesicle concentration **(E)** of serum EVs from 7 patients with pancreatic precursor lesions (blue) and 52 patients with PDAC (red) compared to 20 healthy individuals (black). Immunoblots of serum EVs isolated from healthy individuals ($n = 7$, **F**) and PDAC patients ($n = 8$, **G**). Twenty μg protein determined by standard BCA were separated in an SDS-PAGE, blotted to PVDF membranes, stained with Ponceau S to confirm equal loading (lanes below), and probed with antibody against exosomal protein CD9.

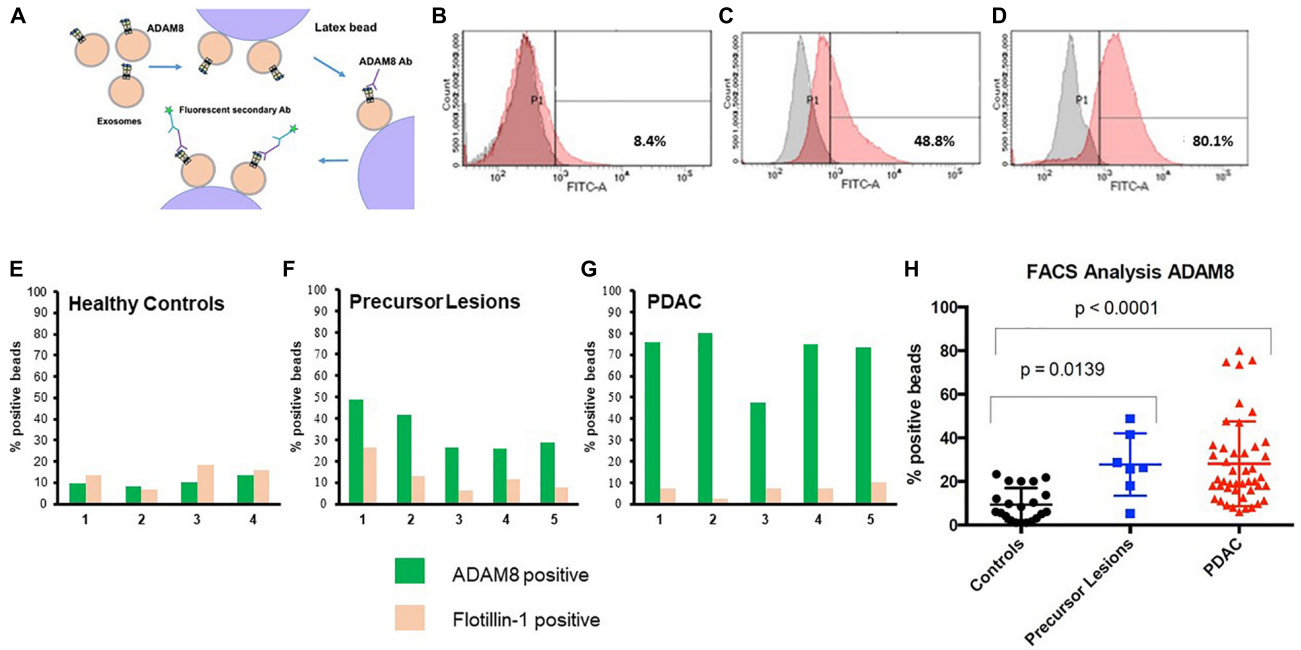

FIGURE 2 | Cartoon of protocol for flow cytometry (FACS) **(A)**. FACS analyses of serum EVs isolated from healthy individuals **(B)**, patients with precursor lesions **(C)** or PDAC **(D)**, attached to beads and detected with ADAM8 antibody. Results with secondary antibody alone appear in gray and those with both ADAM8 antibody and secondary antibody appear in red. Exemplary comparison of results for FACS analyses of serum exosomes from healthy controls (n = 4, **E**), precursor lesions (n = 5, **F**) or PDAC (n = 5, **G**) with ADAM8 (green) or Flotillin-1 (ochre) antibodies. Graphic representation of results from FACS analysis of EVs isolated from healthy individuals, patients with precursor lesions or PDAC from the total cohort, attached to beads and detected with ADAM8 antibody **(H)**.

be detected by using a FRET-based peptide representing the cleavage site of CD23 (Schlomann et al., 2019). Cleavage analysis of EVs isolated from either a control individual or a PDAC patient revealed a strongly enhanced proteolytic activity in EVs from the PDAC patient (**Figures 3A,B**). Although the FRET-based peptide is not specific for ADAM8 activity, it is very likely that the increased activity originates from ADAM8 as a protease with enhanced expression in EVs from PDAC patients as the FACS analysis suggests. In addition to the protein cargo analysis, a systematic screening for miRNAs was performed on EVs derived from control individuals and PDAC patients (**Figure 3C**). Interestingly, a set of 7 oncomiRNAs were found to be differentially regulated with the strongest upregulation for miRNA-451 and the strongest down-regulation for miRNA-720 (**Figure 3C**). To confirm differential regulation of these miRNAs in the PDAC patient cohort, exosomal miRNAs were isolated from the same serum samples and analyzed for miR-720 and miR-451 by semi-quantitative real time RT-PCR. Serum samples had been spiked with synthetic *C. elegans* miR-54 before miRNA isolation to be used as a normalization control. Statistical analyses were performed using the Wilcoxon rank test and ROC curve analysis. The miR-720 and miR-451 were also diagnostic, as patients with PDAC had significantly higher serum exosome levels of miR-451 and lower serum exosome levels of miR-720 than healthy controls and reached high sensitivity and specificity with an AUC = 0.9329 and 1.000, respectively, to discriminate PDAC (**Figures 3D–G**). In addition, serum exosomes were also isolated from patients with chronic pancreatitis (CP; n = 10) and precursor lesions (n = 7). Whereas serum exosomes from patients with precursor lesions had increased levels of miR-451, approaching the levels found in PDACs, CP patient serum exosomes did not. In contrast, the serum exosomes isolated from CP patients had lower levels of miR-720, similar to the PDAC serum exosomes, while the exosomes derived from serum of patients with precursor lesions had levels comparable to the healthy controls. Analysis of these miRNAs in Panc89 wild type and ADAM8 knock-out cells demonstrated that the levels of exosomal miR-451 decrease and the levels of exosomal miR-720 increase upon knock-out of ADAM8, suggesting a regulatory component of ADAM8 on these miRNAs (**Figure 3H**).

DISCUSSION

EV based serum diagnostics provides an additional and powerful diagnostic component in the field of liquid biopsies (Yee et al., 2020). With regard to EV diagnostic in PDAC, the concentration and size of EVs in patient serum has been correlated with tumor differentiation and overall survival in PDAC patients (Badovinac et al., 2021), but no specific cargo analysis of "diagnostic" EVs in serum has been reported up to now. In this respect, our results provide some novelties: First of all, we identified ADAM8, a protease with a therapeutic potential in PDAC, to be located in EVs that meet all criteria for exosomes. By establishing a bead-supported FACS analysis method to analyze surface located ADAM8 in EVs, we demonstrated that ADAM8-positive EVs

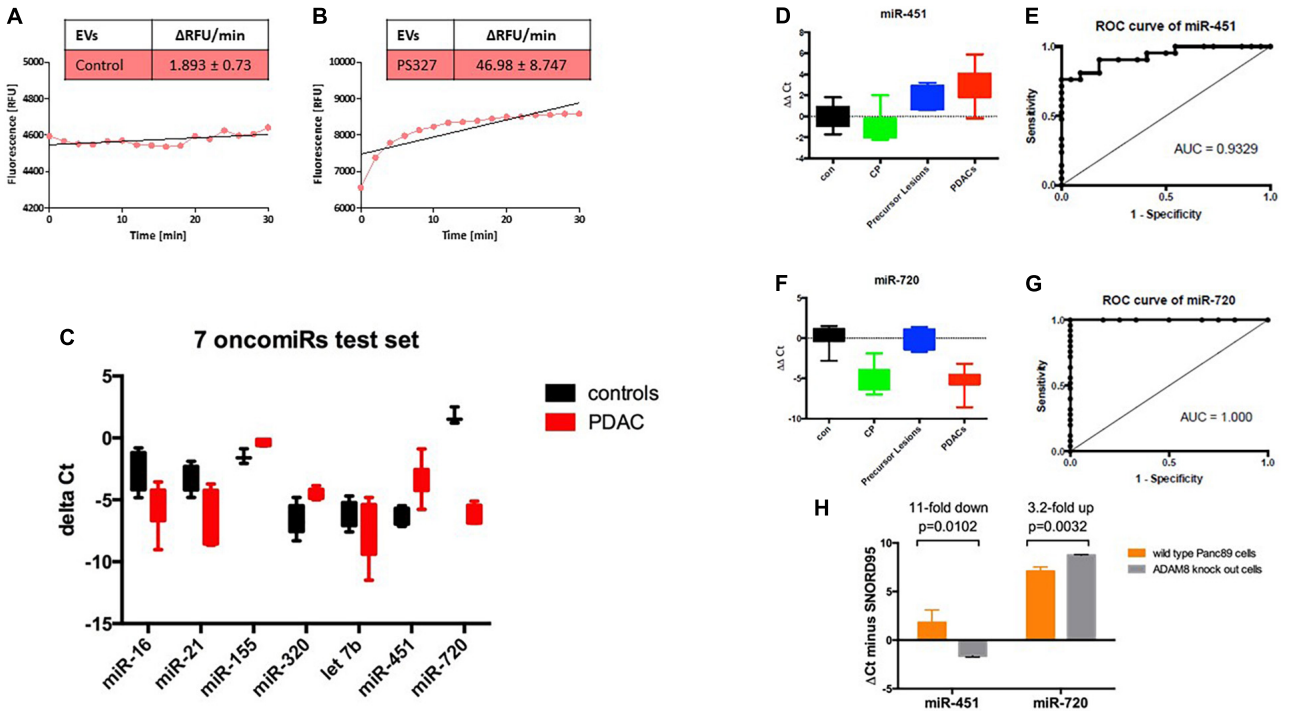

FIGURE 3 | Activity assay of ADAM8 in serum EVs isolated from healthy control **(A)** or PDAC patient **(B)**. Results of the test set using 7 oncomiRs with black boxes, controls, and red boxes, PDAC patients **(C)**. Boxplots of the (miR-451–*Cel*-54) **(D)** and (miR-720—*Cel*-54) **(F)** ΔΔCt values (patient minus healthy control) in the four groups (con, healthy control; CP, chronic pancreatitis; precursor lesions; and PDACs, pancreatic ductal adenocarcinoma). ROC curves for the comparison of exo-miR-451 **(E)** and exo-miR-720 **(G)** expression levels between patients with PDAC and healthy controls. ΔCt values for miRNAs isolated from EVs secreted by wild type Panc89 (orange) and ADAM8 knock-out cells (gray) **(H)**.

were significantly enriched in PDAC patients and were gradually increased with increasing tumor staging, at least when comparing precursor lesions with fully developed adenocarcinoma. From the biochemical point of view, we hypothesized that ADAM8 integrated in EV membranes should be enzymatically active. By peptide cleavage assays, we were able to confirm that ADAM8-enriched EVs show remarkable activities compared to those EVs from control individuals. These data support the notion that a FACS based analysis of EVs from PDAC patients can be performed to detect membrane proteins that are topologically oriented to the extracellular compartment.

In addition to the pure presence of ADAM8, we investigated potential exosomal miRNAs as EV cargo that could be regulated by ADAM8. A panel of "oncomiRNAs" including let-7b was screened from exosomal miRNAs extracted from healthy control individuals and PDAC patients, respectively. We found that ADAM8-positive EVs are specifically equipped with miRNAs that show a functional relevance in PDAC as exemplified by the results with miR-451 and miR-720 in serum EVs from these patients. From all miRNAs examined, exosomal (exo)-miRNA-720 and exo-miRNA-451 were the most significantly dysregulated. Exosomal miRNA-720 was significantly down-regulated in serum samples from chronic pancreatitis and PDAC patients and therefore suggested perfect accuracy in the diagnosis of CP and PDAC either in its hereditary or sporadic form (AUC = 1), exosomal miRNA-451 showed the highest up-regulation in precursor lesions and in PDAC, but not in samples from CP patients and was able to discriminate between precursor lesion or PDAC-afflicted patients and healthy individuals with relatively high accuracy and an AUC of 0.9329.

To further analyze the correlation of ADAM8 expression with miRNA expression levels, we used the PDAC cell line Panc89 with a genetic knockout of the *ADAM8* gene (Cook et al., manuscript in preparation). Using these cell lines, we further demonstrate that the regulation of miRNA-451 and miRNA-720 is dependent on ADAM8 expression levels, respectively. ADAM8 expression is inversely correlated with miRNA-720 levels, as an ADAM8-knockout in Panc89 cells leads to an increase in miRNA-720 levels (average 3.2-fold higher in Panc89_A8KO cells vs. Panc89_A8Ctrl cells), in accordance with the finding that we found decreased levels of miRNA-720 and increased ADAM8 levels in PDAC patients compared to control individuals. In contrast, miRNA-451 is positively correlated with ADAM8 expression levels, as this miRNA is decreased in Panc89_A8KO cells vs. Panc89_A8Ctrl cells. Similarly, we found increased miRNA-451 levels in PDAC patients with a higher ADAM8 expression. For both these miRNAs, functional roles in PDAC were reported that are in accordance with their described abundance in PDAC patient sera. In particular, it was shown that miRNA-720 inhibits pancreatic cancer cell proliferation and invasion by directly targeting cyclin D1 (Zhang et al., 2017)

so that down-regulation of miRNA-720 as observed in PDAC patients compared to healthy individuals has a potential tumor-promoting effect. ADAM8-dependent regulation of miRNA-720 was reported earlier in the breast cancer cell line MDA-MB-231 (Das et al., 2016) however in the opposite direction, an observation that we could reproduce with a CRISPR/Cas9 generated knockout of *ADAM8* in this cell line. In contrast, miRNA-451 can promote cell proliferation and metastasis in PDAC by down-regulating CAB39 (Calcium binding protein 39), a tumor suppressor upstream of STK11 (serine-threonine kinase 11) (Guo et al., 2017). Thus, as observed here, upregulation of miRNA-451 downregulated a tumor suppressor pathway. With miRNA-451 detecting precursor lesions and PDAC, but not chronic pancreatitis (CP) and miRNA 720 detecting CP but not precursor lesions in conjunction with ADAM8-positive EVs, we can achieve a high degree of specificity and sensitivity in serum EV analysis to predict pancreatic precursor lesion and PDAC while discriminating between chronic pancreatitis patients and healthy individuals.

CONCLUSION

Enrichment of ADAM8 in serum exosomes as well as the measurement of exosomal miRNAs, miR-720 and miR-451, may contribute to a biomarker profile for the screening of individuals for PDAC. More generally, our data provide evidence for an EV based communication in the PDAC tumor microenvironment that can be triggered in the pro-oncogenic direction by the presence of ADAM8. This biological signature in turn can be exploited for diagnostic purposes to detect PDAC lesions and fully developed PDAC, as demonstrated here.

DATA AVAILABILITY STATEMENT

The raw data supporting the conclusions of this article will be made available by the authors, without undue reservation.

ETHICS STATEMENT

The studies involving human participants were reviewed and approved by the Ethics Committee of the Marburg University, Faculty of Medicine (File No. 5/03). The patients/participants provided their written informed consent to participate in this study.

AUTHOR CONTRIBUTIONS

ES, DB, and JB conceived the study. YV-Y, JF, AS, SN, LC, NG, FH, CJ, EP, and AP performed the experiments and provided resources. ES and JB wrote the manuscript. All authors approved the submitted version.

FUNDING

Work was supported by the Deutsche Forschungsgemeinschaft (DFG) with a Clinical Research Unit grant (CRU 325) and grants to JB (BA-1606/4-1), to ES (SL-17/5-1), to DB (BA-1467/6-1), and to EP (PO-1408/14-1 and GRK 2573/1).

ACKNOWLEDGMENTS

We wish to thank all patients for participation in the study, Günter Klöppel for histological verification of precursor lesions and all members of the Department of Pathology, Marburg University, in particular Annette Ramaswamy, Corinna Keber and Carsten Denkert.

SUPPLEMENTARY MATERIAL

The Supplementary Material for this article can be found online at: https://www.frontiersin.org/articles/10.3389/fcell.2021.697939/full#supplementary-material

REFERENCES

Badovinac, D., Gorièar, K., Zavrtanik, H., Petriè, M., Lavrin, T., Mavec, N., et al. (2021). Plasma extracellular vesicle characteristics correlate with tumor differentiation and predict overall survival in patients with pancreatic ductal adenocarcinoma undergoing surgery with curative intent. *J. Pers. Med.* 11:77. doi: 10.3390/jpm11020077

Bartsch, D. K., Gercke, N., Strauch, K., Wieboldt, R., Matthäi, E., Wagner, V., et al. (2018). The combination of MiRNA-196b, LCN2, and TIMP1 is a potential set of circulating biomarkers for screening individuals at risk for familial pancreatic cancer. *J. Clin. Med.* 7:295. doi: 10.3390/jcm7100295

Colombo, M., Raposo, G., and Théry, C. (2014). Biogenesis, secretion, and intercellular interactions of exosomes and other extracellular vesicles. *Annu. Rev. Cell Dev. Biol.* 30, 255–289. doi: 10.1146/annurev-cellbio-101512-122326

Cufaro, M. C., Pieragostino, D., Lanuti, P., Rossi, C., Cicalini, I., Federici, L., et al. (2019). Extracellular vesicles and their potential use in monitoring cancer progression and therapy: the contribution of proteomics. *J. Oncol.* 2019:1639854. doi: 10.1155/2019/1639854

Das, S. G., Romagnoli, M., Mineva, N. D., Barillé-Nion, S., Jézéquel, P., Campone, M., et al. (2016). miR-720 is a downstream target of an ADAM8-induced ERK signaling cascade that promotes the migratory and invasive phenotype of triple-negative breast cancer cells. *Breast Cancer Res.* 18:40. doi: 10.1186/s13058-016-0699-z

Gospodarowicz, M. K., and Brierley, J. D. (2017). *TNM Classification of Malignant Tumors*. Oxford: Wiley-Blackwell.

Guo, R., Gu, J., Zhang, Z., Wang, Y., and Gu, C. (2017). MiR-451 promotes cell proliferation and metastasis in pancreatic cancer through targeting CAB39. *Biomed. Res. Int.* 2017:2381482. doi: 10.1155/2017/2381482

Jaworek, C., Verel-Yilmaz, Y., Driesch, S., Ostgathe, S., Cook, L., Wagner, S., et al. (2021). Cohort analysis of ADAM8 expression in the PDAC tumor stroma. *J. Pers. Med.* 11:113. doi: 10.3390/jpm11020113

Keller, S., König, A.-K., Marmé, F., Runz, S., Wolterink, S., Koensgen, D., et al. (2009). Systemic presence and tumor-growth promoting effect of ovarian carcinoma released exosomes. *Cancer Lett.* 278, 73–81. doi: 10.1016/j.canlet.2008.12.028

Kowal, J., Arras, G., Colombo, M., Jouve, M., Morath, J. P., Primdal-Bengtson, B., et al. (2016). Proteomic comparison defines novel markers to characterize heterogeneous populations of extracellular vesicle subtypes. *Proc. Natl. Acad. Sci. U.S.A.* 113, E968–E977. doi: 10.1073/pnas.1521230113

Melo, S. A., Luecke, L. B., Kahlert, C., Fernandez, A. F., Gammon, S. T., Kaye, J., et al. (2015). Glypican-1 identifies cancer exosomes and detects early pancreatic cancer. *Nature* 523, 177–182. doi: 10.1038/nature14581

Minciacchi, V. R., You, S., Spinelli, C., Morley, S., Zandian, M., Aspuria, P. J., et al. (2015). Large oncosomes contain distinct protein cargo and represent a separate functional class of tumor-derived extracellular vesicles. *Oncotarget* 6, 11327–11341. doi: 10.18632/oncotarget.3598

Schlomann, U., Dorzweiler, K., Nuti, E., Tuccinardi, T., Rossello, A., and Bartsch, J. W. (2019). Metalloprotease inhibitor profiles of human ADAM8 in vitro and in cell-based assays. *Biol. Chem.* 400, 801–810. doi: 10.1515/hsz-2018-0396

Schlomann, U., Koller, G., Conrad, C., Ferdous, T., Golfi, P., Garcia, A. M., et al. (2015). ADAM8 as a drug target in pancreatic cancer. *Nat. Commun.* 6:6175. doi: 10.1038/ncomms7175

Shimoda, M., and Khokha, R. (2017). Metalloproteinases in extracellular vesicles. *Biochim. Biophys. Acta Mol. Cell Res.* 1864(11 Pt A), 1989–2000. doi: 10.1016/j.bbamcr.2017.05.027

Siegel, R. L., Miller, K. D., and Jemal, A. (2020). Cancer statistics, 2020. *CA Cancer J. Clin.* 70, 7–30. doi: 10.3322/caac.21590

Sperveslage, J., Hoffmeister, M., Henopp, T., Klöppel, G., and Sipos, B. (2014). Establishment of robust controls for the normalization of miRNA expression in neuroendocrine tumors of the ileum and pancreas. *Endocrine* 46, 226–230. doi: 10.1007/s12020-014-0202-

Su, M.-J., Aldawsari, H., and Amiji, M. (2016). Pancreatic cancer cell exosome-mediated macrophage reprogramming and the role of microRNAs 155 and 125b2 transfection using nanoparticle delivery systems. *Sci. Rep.* 6:30110. doi: 10.1038/srep30110

Sumrin, A., Moazzam, S., Khan, A. A., Ramzan, I., Batool, Z., Kaleem, S., et al. (2018). Exosomes as biomarker of cancer. *Braz. Arch. Biol. Technol.* 61. doi: 10.1590/1678-4324-2018160730

Théry, C., Amigorena, S., Raposo, G., and Clayton, A. (2006). Isolation and characterization of exosomes from cell culture supernatants and biological fluids. *Curr. Protoc. Cell Biol.* 30, 3.22.21–23.22.29.

Valkovskaya, N., Kayed, H., Felix, K., Hartmann, D., Giese, N. A., Osinsky, S. P., et al. (2007). ADAM8 expression is associated with increased invasiveness and reduced patient survival in pancreatic cancer. *J. Cell Mol. Med.* 11, 1162–1174. doi: 10.1111/j.1582-4934.2007.00082.x

Yee, N. S., Zhang, S., He, H.-Z., and Zheng, S.-Y. (2020). Extracellular vesicles as potential biomarkers for early detection and diagnosis of pancreatic cancer. *Biomedicines* 8:581. doi: 10.3390/biomedicines8120581

Zhang, Y., Su, Y., Zhao, Y., Lv, G., and Luo, Y. (2017). MicroRNA-720 inhibits pancreatic cancer cell proliferation and invasion by directly targeting cyclin D1. *Mol. Med. Rep.* 16, 9256–9262. doi: 10.3892/mmr.2017.7732

Zonari, E., Pucci, F., Saini, M., Mazzieri, R., Politi, L. S., Gentner, B., et al. (2013). A role for miR-155 in enabling tumor-infiltrating innate immune cells to mount effective antitumor responses in mice. *Blood* 122, 243–252. doi: 10.1182/blood-2012-08-449306

Conflict of Interest: The authors declare that the research was conducted in the absence of any commercial or financial relationships that could be construed as a potential conflict of interest.

Publisher's Note: All claims expressed in this article are solely those of the authors and do not necessarily represent those of their affiliated organizations, or those of the publisher, the editors and the reviewers. Any product that may be evaluated in this article, or claim that may be made by its manufacturer, is not guaranteed or endorsed by the publisher.

frontiers in Cell and Developmental Biology

BRIEF RESEARCH REPORT
published: 01 October 2021
doi: 10.3389/fcell.2021.734950

Extracellular Vesicle Proteomes Shed Light on the Evolutionary, Interactive, and Functional Divergence of Their Biogenesis Mechanisms

Hyobin Julianne Lim[1†], Haejin Yoon[2†], Hyeyeon Kim[3†], Yun-Won Kang[1], Ji-Eun Kim[4,5], Oh Youn Kim[6], Eun-Young Lee[7], Jean-Claude Twizere[8,9], Janusz Rak[10‡] and Dae-Kyum Kim[1*‡]*

[1] Center for Personalized Medicine, Roswell Park Comprehensive Cancer Center, Buffalo, NY, United States, [2] Department of Cell Biology, Blavatnik Institute and Harvard Medical School, Boston, MA, United States, [3] Princess Margaret Cancer Centre, University Health Network, Toronto, ON, Canada, [4] Program in Developmental and Stem Cell Biology, The Hospital for Sick Children, Toronto, ON, Canada, [5] Department of Molecular Genetics, University of Toronto, Toronto, ON, Canada, [6] College of Medicine, Yonsei University, Seoul, South Korea, [7] Infection and Immunity Research Laboratory, Metabolic Regulation Research Center, Korea Research Institute of Bioscience and Biotechnology, Daejeon, South Korea, [8] Laboratory of Viral Interactomes, GIGA Institute, University of Liège, Liege, Belgium, [9] TERRA Teaching and Research Centre, University of Liège, Liege, Belgium, [10] Research Institute of the McGill University Health Centre, Glen Site, McGill University, Montreal, QC, Canada

OPEN ACCESS

Edited by:
Xinlei Li,
Nationwide Children's Hospital, United States

Reviewed by:
Eduardo Martínez-Martínez, Instituto Nacional de Medicina Genómica (INMEGEN), Mexico
Jeffrey David Galley, The Ohio State University, United States

***Correspondence:**
Janusz Rak
janusz.rak@mcgill.ca
Dae-Kyum Kim
daekyumkim@gmail.com

† These authors have contributed equally to this work and share first authorship

‡ These authors have contributed equally to this work and share last authorship

Specialty section:
This article was submitted to Molecular and Cellular Pathology, a section of the journal Frontiers in Cell and Developmental Biology

Received: *01 July 2021*
Accepted: *09 September 2021*
Published: *01 October 2021*

Citation:
Lim HJ, Yoon H, Kim H, Kang Y-W, Kim J-E, Kim OY, Lee E-Y, Twizere J-C, Rak J and Kim D-K (2021) Extracellular Vesicle Proteomes Shed Light on the Evolutionary, Interactive, and Functional Divergence of Their Biogenesis Mechanisms. Front. Cell Dev. Biol. 9:734950. doi: 10.3389/fcell.2021.734950

Extracellular vesicles (EVs) are membranous structures containing bioactive molecules, secreted by most cells into the extracellular environment. EVs are classified by their biogenesis mechanisms into two major subtypes: ectosomes (enriched in large EVs; lEVs), budding directly from the plasma membrane, which is common in both prokaryotes and eukaryotes, and exosomes (enriched in small EVs; sEVs) generated through the multivesicular bodies via the endomembrane system, which is unique to eukaryotes. Even though recent proteomic analyses have identified key proteins associated with EV subtypes, there has been no systematic analysis, thus far, to support the general validity and utility of current EV subtype separation methods, still largely dependent on physical properties, such as vesicular size and sedimentation. Here, we classified human EV proteomic datasets into two main categories based on distinct centrifugation protocols commonly used for isolating sEV or lEV fractions. We found characteristic, evolutionarily conserved profiles of sEV and lEV proteins linked to their respective biogenetic origins. This may suggest that the evolutionary trajectory of vesicular proteins may result in a membership bias toward specific EV subtypes. Protein–protein interaction (PPI) network analysis showed that vesicular proteins formed distinct clusters with proteins in the same EV fraction, providing evidence for the existence of EV subtype-specific protein recruiters. Moreover, we identified functional modules enriched in each fraction, including multivesicular body sorting for sEV, and mitochondria cellular respiration for lEV proteins. Our analysis successfully captured novel features of EVs embedded in heterogeneous proteomics studies and suggests specific protein markers and signatures to be used as quality controllers in the isolation procedure for subtype-enriched EV fractions.

Keywords: extracellular vesicle, biogenesis, purification, evolution, network

INTRODUCTION

Extracellular vesicles (EVs) are membrane-bound particles that are secreted by cells across the evolutionary spectrum (Gill et al., 2019). EVs enable the export of proteins, RNAs, lipids, and other biomolecules (Oliveira et al., 2010), protected from degradation by proteases and RNases in the extracellular fluid (O'Brien et al., 2020). EVs mediate communications systemically between organs or locally between cells (Al-Nedawi et al., 2008). However, EVs are immensely heterogeneous and our understanding of how their different subtypes are formed and how specific cargoes are selected for transport and delivered remains limited. Thus, it is important to differentiate the heterogeneous populations of EVs to understand the physiology of vesicles and their potential use, including specific biomarkers in disease.

There are two major subtypes of EVs based on their biogenesis and size (Cocucci and Meldolesi, 2015): (i) Ectosomes (100–1000 nm in diameter) bud from the cellular surface and are frequently referred to as microvesicles in eukaryotes, or as outer membrane vesicles in prokaryotes and (ii) exosomes (30–100 nm) arise within endosome-related intraluminal vesicles, which are then released from cells upon recruitment of multivesicular bodies to the inner layer of the plasma membrane (Colombo et al., 2014; van Niel et al., 2018). Both prokaryotic and eukaryotic cells secrete EVs, even though the biogenesis of exosomes is thought to be specific to eukaryotic cells due to the requirement for endosomal compartment (Deatherage and Cookson, 2012). However, the impact of evolutionary characteristics of biogenesis mechanisms on the vesicular cargo composition has not been explored.

To uncover mechanisms of EV biogenesis, a myriad of EV proteomic studies have been conducted under various conditions, from different cellular sources, and on different subtypes of EVs. EV subtypes may have different physiological roles and compositions (Kanada et al., 2015; Kowal et al., 2016), but it is difficult to dissect their differences on an empirical basis. Indeed, current isolation methods are limited in separating EV subtypes exclusively (Li et al., 2019), and the true predicted heterogeneity of EVs probably exceeds the traditional classification by orders of magnitude (Choi et al., 2019). Differential ultracentrifugation (DUC) is most commonly used to pre-clear debris and unwanted EV subtypes and/or concentrate the target EV subtype (Choi et al., 2013, 2015; Meldolesi, 2018). Although it is recommended to combine DUC methods with other purification methods, such as size-exclusion chromatography and affinity purification (Jeppesen et al., 2019), the choices of molecular markers used to pull down the desired EV subpopulations are often arbitrary and result in biased sampling that might introduce experimental artifacts and skew EV profiles. This emerging challenge may be addressed by integrating multiple datasets from various sources to validate common isolation methods and markers.

We hypothesize that the proteomic composition of ectosomes and exosomes fundamentally differs in an evolutionary, functional, and network-topological manner, due to their distinct core biogenesis mechanisms. We classified EV proteomic datasets available in the EVpedia database (Kim et al., 2013, 2015a,b) into two datasets – a smaller exosome-enriched fraction (small EV; sEV) and a larger ectosome-enriched fraction (large EV; lEV) – using the frequently used DUC cutoffs for analyzing specific EV subtypes. We validated our approach by comparing the identification frequency of popular exosomal and ectosomal markers in our classified sEV and lEV datasets. Moreover, our findings demonstrate that sEV and lEV datasets exhibit significant differences in: (i) degree of evolutionary conservation of proteins, (ii) topology of protein–protein interactions (PPIs), and (iii) enrichment in biological functions. While EVs are more readily secreted by cancer cells and represent a promising diagnostic analyte (Kosaka et al., 2019; Hoshino et al., 2020; Kalluri and LeBleu, 2020), differential expression of biomarkers between a diseased and normal cell may arise from cross-contamination between EV subtypes. Therefore, an integrated computational approach for analyzing their larger protein networks not only validates isolation methods but may also reveal a more comprehensive understanding of EV subtypes beyond the detection of individual protein markers, enabling discovery of novel cancer signatures and potential therapeutic targets.

MATERIALS AND METHODS

Classification of Extracellular Vesicle Proteomic Datasets Into Small Extracellular Vesicle and Large Extracellular Vesicle Datasets Based on Differential Ultracentrifugation Methods

We constructed an integrated EV proteomic dataset by compiling the entire list of shotgun proteomic datasets (**Supplementary Table 1A**) from EVpedia (Kim et al., 2013, 2015a,b), updated on April 30, 2018. We classified 485 human datasets based on DUC conditions used for purifying the EV samples. Given several methods to enrich lEVs at 10,000 × *g* (Kowal et al., 2016), we assumed that if the EV fraction has undergone pre-clearing of 10,000 × *g* or more, the sample has been cleared of most lEVs. We set the ultracentrifugation speed cut-off under 20,000 × *g* for sedimenting lEVs and over 100,000 × *g* for sEVs. Standards for classification can be found in detail in **Supplementary Table 1B**, and methods that did not meet these standards were excluded (**Supplementary Table 1C**). Common Tree tool from NCBI taxonomy database (latest updated on August 22, 2021) (Schoch et al., 2020) was used to generate a phylogenetic tree of species included in the EVpedia database (Kim et al., 2013, 2015a,b) and further visualized with the iTOL tool (version 5) (Letunic and Bork, 2021).

Analysis of Exosomal and Ectosomal Markers in Large Extracellular Vesicle and Small Extracellular Vesicle Proteomes

We identified 10 conventional molecular markers each for human ectosomes and exosomes from an extensive literature search (Muralidharan-Chari et al., 2009; Lee et al., 2012;

Surman et al., 2017; Meldolesi, 2018; Jeppesen et al., 2019; Rogers et al., 2020). We defined "Identification frequency in sEV datasets (fsEV)" and "Identification frequency in lEV datasets (flEV)" of every vesicular protein in the integrated dataset, which is the number of times that the protein was identified in a particular subset, divided by the total number of sEV or lEV studies in the subset, respectively (**Supplementary Table 2**). We used Fisher's exact test in MatLab (version 2016a) to compare individual markers between the datasets and Mann–Whitney *U* test to compare the identification of all the markers via GraphPad Prism (version 8.2). A scatter plot of fsEV and flEV was visualized in MatLab.

Evaluation of Evolutionary Conservation of Small Extracellular Vesicle and Large Extracellular Vesicle Protein Components

To evaluate the evolutionary conservation of proteins enriched in sEV and lEV, we used identification counts (ICs) of orthologous proteins in prokaryotes and eukaryotes across the entire dataset from EVpedia (**Supplementary Table 2**). IC_{eu} (identification count in eukaryotic EV datasets) and IC_{pro} (identification count in prokaryotic EV datasets) for proteins that showed higher identification frequency in each subset [log2(fsEV/flEV) $>$ 0.1 for sEV; log2(fsEV/flEV) $<$ -0.1 for lEV] were used for analysis. Statistical analysis was performed using Mann–Whitney *U* test in GraphPad Prism (version 8.2).

Protein–Protein Interaction Network Analysis of Vesicular Proteins

To construct a unified protein–protein interactome network, we integrated Affinity Purification-Mass Spectrometry (AP-MS)-based network from the BioPlex project (version 3.0) based on two distinct cell lines of HEK293T and HCT112 (Huttlin et al., 2015, 2017, 2021) and Yeast Two-Hybrid (Y2H)-based network from Human Reference Interactome (HuRI) project (Rual et al., 2005; Rolland et al., 2014; Luck et al., 2020; **Supplementary Table 3**). The Spearman correlation of fsEV/flEV ratio between bait and prey proteins of interacting pairs and their *P*-value were calculated by MatLab (version 2016a). The network was visualized by Cytoscape (version 3.8.2) (Shannon et al., 2003).

Functional Enrichment by Gene Set Enrichment Analysis

We constructed two separate gene lists ranked by (i) relative identification in sEV and lEV datasets [log2(fsEV/flEV)] or (ii) relative identification counts in human vesicular proteomes (IC_{human} - an average of IC_{human}) for proteins that were equally abundant [$|$ log2(fsEV/flEV)$|$ $<$ 0.1] in sEV and lEV datasets. Biological functions enriched in each classification category were determined using Gene Set Enrichment Analysis (GSEA; version 4.1.0) (Subramanian et al., 2005). Functional annotations that were significantly enriched (false discovery rate $<$ 0.05) were visualized using Cytoscape (version 3.8.2) (Shannon et al., 2003) apps, EnrichmentMap (version 3.3.2) (Merico et al., 2010), and AutoAnnotate (version 1.3.3) (Kucera et al., 2016).

RESULTS

Small Extracellular Vesicle and Large Extracellular Vesicle Datasets Exhibit a Differential Separation of Exosomal and Ectosomal Markers

DUC is a widely used purification method to separate exosome- or ectosome-enriched EV fractions (Kowal et al., 2016). Ectosome-enriched lEV fraction is often sedimented under 10,000 $\times$ *g* centrifugal force and exosome-enriched sEVs require over 100,000 $\times$ *g* preceded by pre-clearance of lEVs (Greening et al., 2015; Jeppesen et al., 2019). To maximize the size of input data for proper statistical testing, we set slightly more permissive standards of $\geq$100,000 $\times$ *g* with $\geq$10,000 $\times$ *g* of pre-clearance for sEV datasets and $\leq$20,000 $\times$ *g* and $<$10,000 $\times$ *g* pre-clearance for lEV datasets (**Figure 1A** and **Supplementary Tables 1B,C**). We performed our analyses on human datasets to account for variability of size and density between EVs of different species. A total of 485 human proteomic datasets have been classified into 51 lEV and 203 sEV datasets (**Supplementary Table 1A**). We then defined "Identification frequency in sEV datasets (fsEV)" and "Identification frequency in lEV datasets (flEV)" of every vesicular protein identified in the integrated 254 human datasets in which the number of datasets that identified the protein divided by the whole number of sEV or lEV datasets, respectively. These measures might provide us with a systematic evaluation of each protein's tendency to be present in sEVs or lEVs.

With an intent to validate our classification strategy while also evaluating the robustness of the common markers used, we examined enrichments of previously known exosomal and ectosomal markers in each fraction (Muralidharan-Chari et al., 2009; Lee et al., 2012; Surman et al., 2017; Meldolesi, 2018; Jeppesen et al., 2019; Kalluri and LeBleu, 2020; Rogers et al., 2020). Exosomal markers are generally restricted to the endocytic pathway. However, ectosomal markers are more diverse and the enriched proteins depend heavily on the samples and cell types from which they have originated (Lee et al., 2012; Liu and Williams, 2012; Sluijter et al., 2014). Markers representing exosomes included tetraspanins (CD63, CD81, and CD9), endomembrane network-associated proteins (FLOT1, PDCD6IP, SDCBP, TSG101, and YWHAE), and heat shock proteins (HSPA8 and HSP90AA1). Although molecular markers that distinguish ectosomes are less well defined, we selected actins (ACTB and ACTN4), myosins (MYLK and TPM3), selectin (SELP), lipid membrane remodeling molecule (ARF6), protease (MMP9), integrin (ITGB1), mitochondrial protein (IMMT), and annexin (ANXA1) as relatively ectosome-specific markers. Overall, we saw significant differences in the expression of markers between sEV and lEV fractions (**Figure 1B**). We showed that the most common exosome-specific markers were more readily identified in sEV datasets (**Figure 1B** and **Supplementary Figure 1A**). Some ectosomal markers such as TPM3 showed

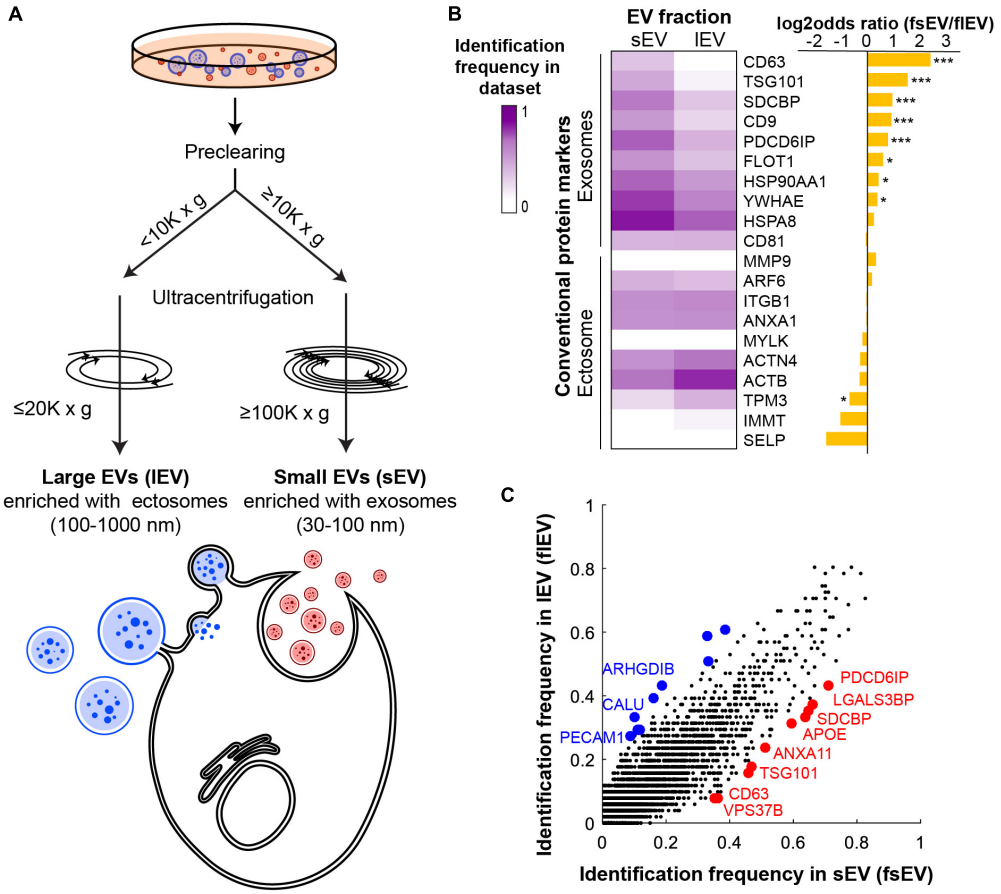

FIGURE 1 | Protein markers of ectosomes and exosomes show different identification frequencies in human small extracellular vesicle (sEV) and large EV (lEV) proteomic datasets. **(A)** Schematic of DUC criteria shows how we classified human proteomic datasets into sEV and lEV datasets. **(B)** Identification frequency of literature-surveyed EV protein markers in sEV (fsEV) and lEV (flEV) datasets supports the validity of our classification methods. $^{*}P < 0.05$; $^{***}P < 0.001$. **(C)** A scatter plot comparing fsEV and flEV of all human vesicular proteins deposited in EVpedia shows that known exosomal and ectosomal markers correctly identify EV subtype enriched in each fraction. Protein markers with the 10 highest differences between their identification frequencies in sEV and lEV are highlighted by red and blue for fsEV and flEV, respectively.

higher identification in lEV datasets (**Figure 1B**), but the overall identification frequency of 10 ectosomal markers was not significantly enriched in lEV compared to sEV datasets (**Supplementary Figure 1B**). Surprisingly, CD81 and ARF6, which are among the most common markers for exosomes and ectosomes, respectively, did not show a statistical difference between the datasets. While CD63 and TPM3 show high exclusivity in their respective datasets, they have a low frequency of identification. Therefore, we propose that multiple markers should be considered together when isolating EVs using affinity purification, as there are no good stand-alone markers that ensure high identification and specificity across sample sets.

We next compared fsEV and flEV for all the vesicular proteins deposited in EVpedia (**Figure 1C**). Among the top 10 proteins enriched in lEVs (colored blue in **Figure 1C**; $P < 0.001$ by Fisher's exact test), only two proteins were previously known as ectosomal markers: ARHGDIB (Cocucci and Meldolesi, 2011; Surman et al., 2017; Meldolesi, 2018) and PECAM1 (Kalra et al., 2016; Meldolesi, 2018; Słomka et al., 2018). CALU is a calcium-binding protein, which has been shown to regulate ectosomal budding at the plasma membrane (Surman et al., 2017). All seven remaining proteins are mitochondrial proteins (ATP5F1B, HSPD1, ATP5F1A, GOT2, ATP5PO, DLD, and UQCRC2), previously reported to be loaded into ectosomes (Mittelbrunn and Sánchez-Madrid, 2012; Phinney et al., 2015; Torralba et al., 2016). Among the top 10 enriched proteins in exosomes (colored red in **Figure 1C**), we found five endosomal pathway regulators (PDCD6IP, SDCBP, ANXA11, TSG101, and VPS37B) which are pivotal for exosome biogenesis, and CD63, a widely known exosomal tetraspanin marker. LGALS3BP has been found in diverse cancer-derived exosomes (Escrevente et al., 2013; Ung et al., 2014; Dutta et al., 2015; Gomes et al., 2015; Song et al., 2021), and APOE has been found in exosomes released from macrophages (Zheng et al., 2018) and neurons (Nikitidou et al., 2017; Mathews and Levy, 2019; Peng et al., 2019). This comparative analysis shows that our classification pipeline can successfully categorize proteomic datasets and suggests that systematic analysis of published proteomic studies

is a valuable approach for discovering novel markers for ectosome and exosomes.

Proteins Enriched in Large Extracellular Vesicles and Small Extracellular Vesicles Have Differential Evolutionary Conservation Profiles

Exosome forms in the late endosome, an organelle unique to eukaryotes, and transmits small intraluminal vesicle contents to the lysosome or the plasma membrane (Harris, 1986; Edgar, 2016). In contrast, ectosomes bud directly from the plasma membrane (Cocucci and Meldolesi, 2011), a mechanism used by both eukaryotes and prokaryotes (Deatherage and Cookson, 2012). Therefore, we hypothesized that the biogenesis mechanisms of EV subtypes correlate with kingdom-specific evolutionary conservation of proteins that are secreted via EVs (**Figure 2A**). To define a measure for the kingdom-specific evolutionary conservation, we used the identification count provided by EVpedia of proteins that had a higher tendency to be in sEV or lEV fraction. For example, "identification count in prokaryotes (IC_{pro})" indicates the number of prokaryotic EV proteomic datasets that had identified a particular protein's orthologs, as defined by the EggNOG database (Jensen et al., 2008; **Supplementary Table 2**). A higher identification count indicates that the EV protein is more conserved within the EVs of eukaryotes or prokaryotes. The phylogenetic tree shows how species that have EV proteomes available in EVpedia are evolutionarily related (**Figure 2A**, right). In general, identification counts for prokaryotic proteins are lower, meaning that most human EV proteins were not well conserved in prokaryotes. As we predicted, ectosome-enriched lEV proteins show higher conservation in prokaryotes (**Figure 2B**) and lower conservation in eukaryotes (**Figure 2C**). Conversely, exosome-enriched sEV proteins are conserved more in eukaryotes and less in prokaryotes (**Figures 2B,C**). Despite being significantly different, the differences may be small due to EV proteins that do not participate in biogenesis mechanisms being conserved in both sEV and lEV fractions. Nevertheless, our result demonstrates that the current purification methods for EV subtypes provide us with the evolutionarily distinct EV proteomes and further suggests that evolutionary trajectories of vesicular proteins may be an important determinant influencing cargo selection.

Network Analyses Reveal That Protein–Protein Interaction Networks of Small Extracellular Vesicles and Large Extracellular Vesicles Proteins Have High Intra-Fractional and Low Inter-Fractional Enrichment of Interactions

A biased PPI network resulting from the over-representation of popular genes may limit our ability to explore new biological information (Gillis et al., 2014). However, recent systematic

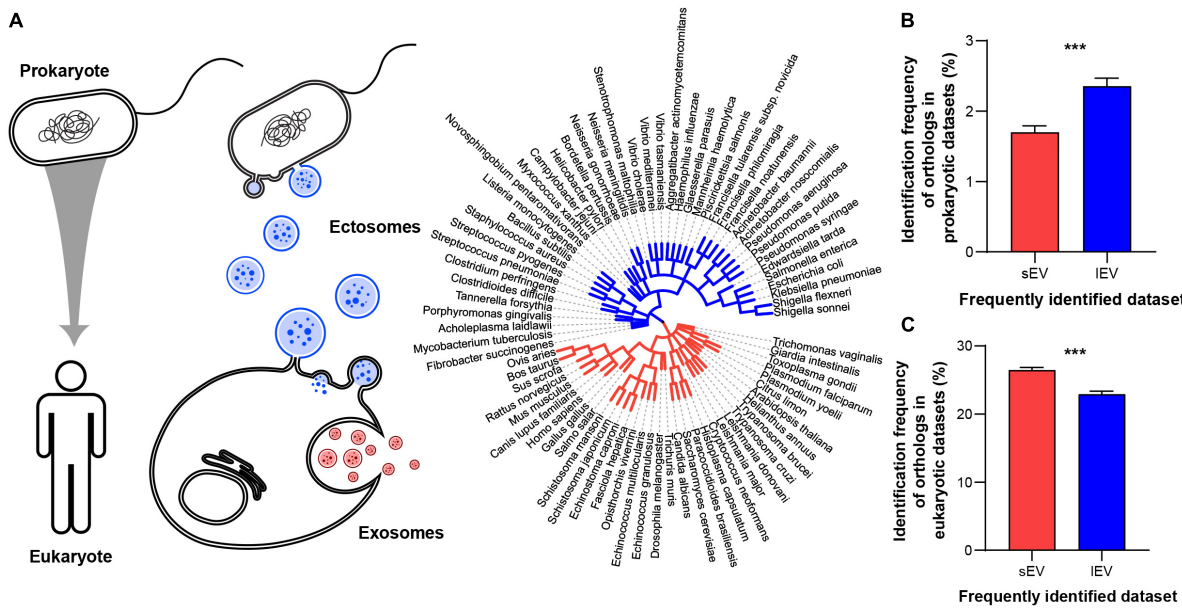

FIGURE 2 | Protein components of sEVs and lEVs show different evolutionary conservation. **(A)** Schematic diagram of EV evolutionary conservation (left two panels). EVs derived from different biogenesis mechanisms show different availability in two different kingdoms. Phylogenetic tree (right panel) illustrates the evolutionary trajectory of species included in the EVpedia database. The topology is based on EVpedia (Kim et al., 2013, 2015a,b). Branch lengths are proportional to the number of non-synonymous substitutions per site. Red and blue branches represent eukaryotes and prokaryotes, respectively. **(B)** Proteins that are more frequently identified in lEV fractions are more conserved in the prokaryotic (IC_{pro}/141 prokaryotic datasets) kingdom, **(C)** while proteins that are more frequently identified in sEV fraction are more conserved within the eukaryotic (IC_{eu}/656 eukaryotic datasets) kingdom. $^{***}P < 0.001$, $n = 3361$ and 3028 proteins specifically enriched in small and large EV fractions, respectively.

approaches to explore PPI via AP-MS called BioPlex (Huttlin et al., 2015, 2017, 2021) and Y2H called HuRI (Rual et al., 2005; Rolland et al., 2014; Luck et al., 2020) have enabled an unbiased proteome-wide analysis of PPIs (**Supplementary Table 3**). BioPlex and HuRI are highly valuable interactomes for analyzing EV PPIs as they appear to have a lower localization bias compared to other networks (Luck et al., 2020). This work identified a PPI "community" of vesicular proteins, which are unbiased subnetworks significantly enriched for EV localization (Luck et al., 2020). We hypothesized that key control elements in EV biogenesis or recruitment of specific cargo would be the possible "seed protein" candidates, which exist as hub proteins that link their interacting proteins within the same EV subtypes. We predict that if these "seed proteins" exist, PPI may occur more frequently between exosomal proteins and between ectosomal proteins, than between the two of them (**Figure 3A**). We showed that protein interaction partners share a similar tendency to be included in sEV or lEV, showing a positive correlation between fsEV/flEV ratios of bait and prey proteins of interacting protein pairs (**Figure 3B**; Spearman correlation $\rho = 0.1319$ with $P < 10^{-42}$). Moreover, a network analysis of EV proteins (proteins identified more than 50 times in EVpedia) shows that sEV proteins and lEV proteins clusters are significantly separated in space, sEV (red) and lEV (blue) proteins located in the left upper corner and right lower corner, respectively (**Figure 3C**). In particular, we found two examples of "seed proteins," whose PPI subnetworks are enriched with proteins that have a higher tendency to exist in corresponding EV subtypes: SDCBP for sEVs (**Figure 3D**) and ATP5ME for lEVs (**Figure 3E**).

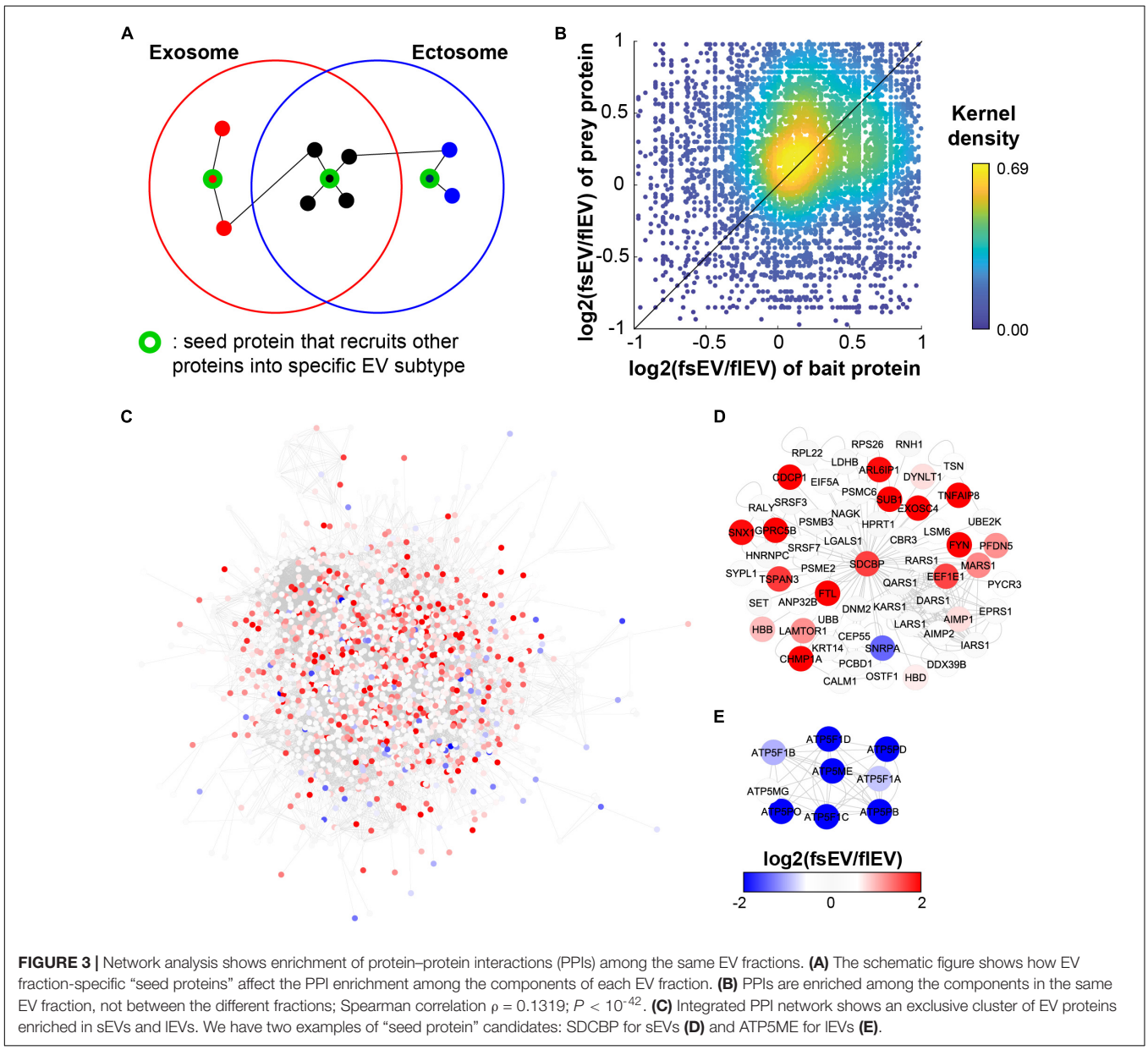

FIGURE 3 | Network analysis shows enrichment of protein–protein interactions (PPIs) among the same EV fractions. **(A)** The schematic figure shows how EV fraction-specific "seed proteins" affect the PPI enrichment among the components of each EV fraction. **(B)** PPIs are enriched among the components in the same EV fraction, not between the different fractions; Spearman correlation $\rho = 0.1319$; $P < 10^{-42}$. **(C)** Integrated PPI network shows an exclusive cluster of EV proteins enriched in sEVs and lEVs. We have two examples of "seed protein" candidates: SDCBP for sEVs **(D)** and ATP5ME for lEVs **(E)**.

In our previous interactome study (Luck et al., 2020), we validated SDCBP as a hub protein whose knock-out can downregulate the abundance of its interactors in EVs, alluding to the notion that SDCBP is involved in the recruitment of other proteins into EVs. Further, there were several SDCBP-interacting proteins whose expressions were downregulated by SCDBP knockout. These downregulated proteins included CEP55, which interacts with TSG101 (Lee et al., 2008) and CALM1, and HPRT1 that were proposed as novel EV cargoes recruited by PDZ domains of SDCBP (Garrido-Urbani et al., 2016). Meanwhile, ARF proteins (especially ARF6) – which are related to ectosome biogenesis – remain enriched in EV isolates (sedimented at 100,000 $\times$ g without pre-clearance) after SDCBP knockout, further supporting our "seed protein" hypothesis. In conclusion, these proteomic analyses suggest that overall proteomic profiles of each EV subtype are influenced by interactions of recruiter proteins involved in biogenesis.

The Components of Small Extracellular Vesicles and Large Extracellular Vesicles Have a Specific Biological Signature in Functional Enrichment

The difference in biogenesis mechanism between exosomes and ectosomes also explains the changes in the functional enrichment in their proteomes. We sorted EV proteins according to a rank score [log2(fsEV/flEV)] that describes the tendency of vesicular proteins to be identified in sEV (positive score) or lEV (negative score) datasets. Despite the differences in EV-secreting cell types, there are specific protein cargoes enriched within each EV fraction, suggesting a functional divergence between ectosomes and exosomes (**Figure 4**, **Supplementary Figure 2A**, and **Supplementary Tables 4A,B**). sEV proteins showed enrichment for functions relevant to their biogenesis such as multivesicular body sorting and vacuolar transport, while also showing enrichment for cell division and extracellular signaling pathways. Proteins in lEV showed strong enrichment for mitochondrial functions (**Figure 4**), further supporting their previously proposed role in supplying energy to tumor microenvironments (Lazar et al., 2018). The differences in functional enrichment raise a need of studying the physiological functions of the subtypes separately, thus further highlighting a necessity for establishing robust isolation methods of EVs to fully understand their biological roles.

We also performed a functional enrichment analysis of equally abundant proteins in both lEV and sEV to reveal common biological functions shared by all EVs (**Supplementary Figure 3**). We filtered the dataset for proteins that showed relatively similar identifications [$|\log2(\text{fsEV/flEV})| \leq 0.1$] and ranked them by their abundance in the human datasets (IC_{human}). Interestingly, nucleoside metabolic processes and immune-related functional modules were highly enriched which were also independently enriched for sEV and lEV proteins along with other functions like viral protein processing (lEV) and viral transport (sEV). This finding aligns with the previously proposed dual role of EVs during viral infection in increasing host immune responses as well as the virulence of viruses (Rybak and Robatzek, 2019; Ipinmoroti and Matthews, 2020). The EV proteins were also enriched in functions such as protein folding, localization to ER, and translation (**Supplementary Table 4C**), suggesting that ER proteins may be loaded into EVs through interactions with common "seed proteins" related to EV secretion. Consistent with previous findings, EVs showed enrichments for exocytosis (Lin et al., 2019), secretion, and signal transduction pathways including EGF and WNT signaling pathways (Al-Nedawi et al., 2008; Li et al., 2012; Latifkar et al., 2019; **Supplementary Figure 2B**). Altogether, functional enrichment analysis of proteomic data can be used to investigate the underlying biological role of EVs. Furthermore, our findings suggest that we may be able to identify specific biomarkers that are upregulated in a particular disease by analyzing the differential expression in sets of functionally related proteins, rather than single target proteins.

DISCUSSION

Recent studies suggest that the biological properties of EVs could be exploited as a new strategy for novel biomarkers and treatment of diseases, and yet a systematic approach to validate molecular classifications of EV subtypes has been lacking. To address this need, we performed a systemic analysis of the available EV datasets to explore defining proteomic characteristics of lEVs and sEVs. Our analysis suggests that we can infer unique functions and biogenesis elements of EV subtypes from published EV proteomes, questions which were rarely explored in related studies. These results also revealed several other core features of EVs such as (i) evolutionary conservation, (ii) functional categories, and (iii) PPI networks that could be demonstrated using extensive statistical and systematic approaches.

We defined the identification frequency of proteins in sEV and lEV according to differential ultracentrifugation (DUC) speeds (**Figure 1A**). We used centrifugation speeds that are commonly used for separating and concentrating EVs (Kowal et al., 2016), which are referred to as sEV and lEVs instead of more specific subtypes. Although the protocols used in each proteomics study are not consistent including centrifugation steps, the ultracentrifugation speeds successfully divided datasets into sEV and lEV fractions, which had statistically significant differences in the expression of several exosome markers. There are only a handful of datasets that combined other methods along with centrifugation; therefore, it was not possible to perform meaningful analysis on this material. Instead, to allow us to use datasets to discover general characteristics of sEV and lEV proteins, we validated our classification system using the identification of the most common exosome-specific markers in the datasets (**Figure 1**). However, the remaining challenge of this work is that due to availability of relevant details in pertinent publications, we have not been able to include EV proteome datasets dealing exclusively with DUC or validate the status of EV quality controls mentioned in a recent publication (Théry et al., 2018).

While our method does not define EV biogenesis mechanisms, it allows a separation of EV subsets that are clearly different,

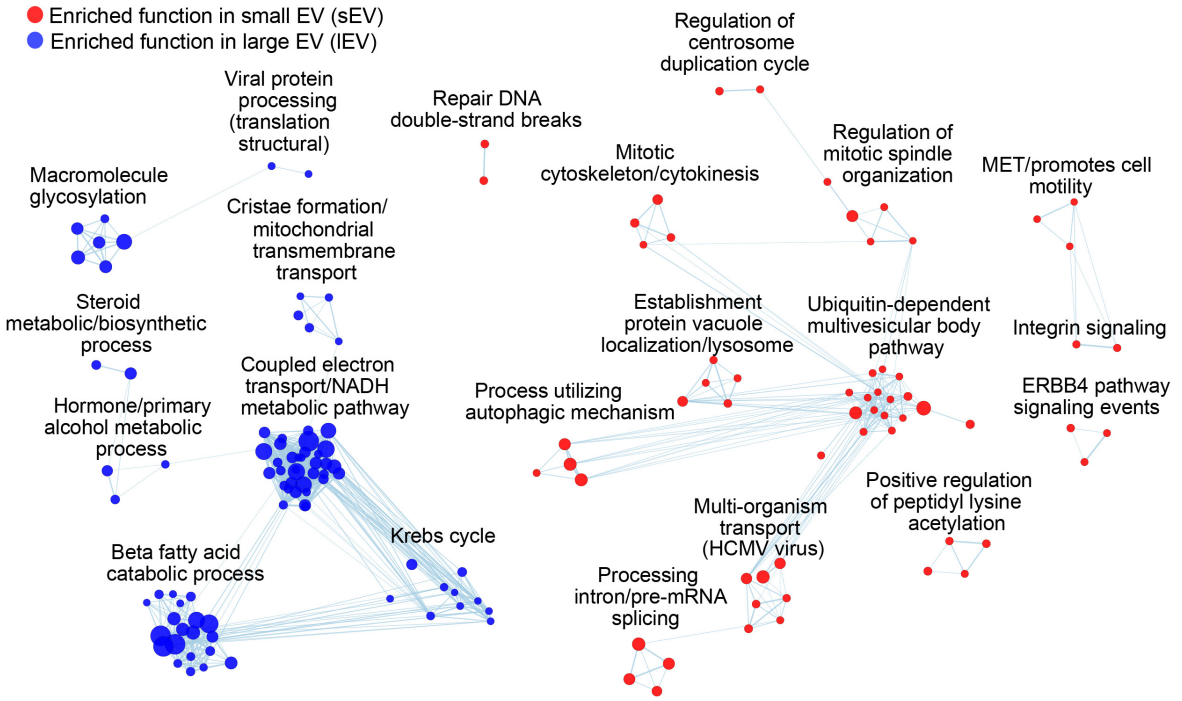

FIGURE 4 | sEV and lEV proteomes are enriched with distinct biological functions and processes. Each node represents a functional annotation, where node size reflects the enrichment score. Overlapping terms are further grouped using EnrichmentMap. Functions enriched for higher identification frequencies in sEVs and lEVs are colored with red and blue, respectively.

a notion which has been supported by respective enrichment of known exosomal and ectosomal markers (**Figures 1B,C**). Despite this consistency, DUC still carries remaining limitations as an independent method to separate the EV subtypes (Witwer et al., 2013). While newer Absolute Protein Expression (APEX) Quantitative Proteomics Tool might show significant differences in the relative inclusion of markers between sEV and lEV fractions, protein concentrations are often not considered in recovered EV fractions (Braisted et al., 2008). Another impediment posed by the current purification schemes is the protein overlap between sEV and lEV fractions which is evident from our functional annotation analysis (**Supplementary Figure 3**). Therefore, there is a need for additional criteria to identify markers that could distinguish EV subtypes more clearly.

Little is known about the role of vesiculation in the evolutionary leap from a simple prokaryotic cell to a more complex eukaryotic cell (Embley and Martin, 2006). Indeed, mitochondria are likely evolved from engulfed prokaryotes that once lived as independent organisms (Gray et al., 1999). This hypothesis is supported by our evolutionary and functional enrichment analysis that demonstrated the inclusion of prokaryotic and mitochondrial proteins in ectosomes. Likewise, the export of cellular fragments, such as EVs, has evolved from a primordial and conserved membrane budding mechanism to a more complex pathway of exosome biogenesis (van Niel et al., 2018). We suggest that the current EV purification method, even as simple as DUC, is sufficiently robust to capture the salient differences in protein networks that separate distinct EV subtypes and their evolutionary trajectory (**Figure 2**). In this regard, we show that lEVs contain conserved proteins characteristic of both prokaryotes and eukaryotes, as is the process of membrane budding. In contrast, sEV proteins are characterized as being mostly eukaryotic, reflecting a more recent emergence of the endosomal vesiculation process. These correspond to our functional annotation of sEV and lEV fractions (**Figure 4**). Indeed, lEVs comprise proteins involved in mitochondrial function, including energy synthesis, and sEV proteins mostly function in the synthesis of intracellular building blocks and signaling pathways (**Figure 4**). Recent studies using TEM showed that mitochondria are transferred through microvesicles (ectosome) (Phinney et al., 2015; Liu et al., 2021). Moreover, it is also known that damaged mitochondria are transported into migrasomes to maintain the quality of the mitochondrial pool (Jiao et al., 2021). Indeed, our data demonstrate that large vesicles may contain and transfer mitochondria. Interestingly, the genes related to cellular homeostasis and stress response including control of cellular proliferation and death and control of metabolic function (protein localization, biosynthetic and processes of organic compounds, regulation of catabolic processes, and actin reorganization) are not changed between sEV and lEV (**Supplementary Figure 3**). This functional segregation of proteins among EV subtypes and across a large population of databases demonstrates that our method may offer a new explanation to the emergence of different classes of EVs, some of which may be relevant to the evolutionary hypothesis of an endosymbiotic relationship between cellular as well as extracellular organelles.

Due to significant differences in fsEV versus flEV, we believe that there is an apparent set of EV type-specific recruiters that divide ectosomal and exosomal components. By extensive network analysis, we showed the existence of recruiter candidates and proposed mutually exclusive EV markers, some of which were previously reported. The limitation of this work is that we have integrated EV proteomics from various cellular contexts, thereby making it difficult to apply to all EV types from all cells and organisms of origin. Since EV composition is dependent on several factors, such as the cell of origin, metabolic activity, and health and pathologic conditions, a more focused EV analysis method is needed to control for known covariates. We highlight that we can utilize distinctive proteomic characteristics of exosomes and ectosomes as an alternative to using specific molecular markers for assessing the relative abundance of the EV subtypes in the purified EV sample and validating its purity.

Due to the fundamentally divergent biogenesis of exosomes and ectosomes, it is highly probable that a set of EV subtype-specific recruiters may distinguish ectosomal and exosomal components and is subject to evolutionary changes. By extensive network analysis, we showed the existence of recruiter candidates and identified mutually exclusive EV markers (**Figure 3**), some of which were shown by an independent experimental study (Kugeratski et al., 2021). We demonstrate that distinctive characteristics of the sEV and lEV proteomes can offer a high granularity alternative to traditionally used singular molecular markers in assessing EV subtypes and their functions. Taken together, this method can be applied to developing new analytical approaches that, in concert with metabolomics and transcriptomics, may offer unprecedented insights into the biology, functions, and clinical applications of EVs.

DATA AVAILABILITY STATEMENT

The original contributions presented in the study are included in the article/**Supplementary Material**, further inquiries can be directed to the corresponding authors.

AUTHOR CONTRIBUTIONS

D-KK got the invitation of manuscript submission for this special issue. HL and D-KK organized the first draft of the abstract and got an acceptance from the editorial board for this special issue. HL, HY, and HK performed overall bioinformatics analyses and organized the manuscript. Y-WK, J-EK, OK, E-YL, and J-CT revised the manuscript. JR and D-KK organized the study design and finalized the manuscript. All authors contributed to the article and approved the submitted version.

FUNDING

This study was supported by a start-up grant from Roswell Park Comprehensive Cancer Center. E-YL was supported by a grant from the National Research Foundation (NRF) of Korea (2015M3C9A4053394). J-CT is a Maitre de Recherche of the Fonds National de Recherche Scientifique (FNRS) supported by the Belgium Government. JR, who is a recipient of the Jack Cole Chair in Pediatric Hematology/Oncology, was supported by Foundation Grant (FDN 143322) from Canadian Institutes for Health Research (CIHR), grants from the Canadian Cancer Society (CRS), Genome Canada (GC79694), and McGill Interdisciplinary Initiative in Infection and Immunity (MI4) and Infrastructure funds from the Fonds de Recherche en Santé du Québec (FRSQ), and CAN program from the Canadian Foundation for Innovation (CFI). D-KK was supported by a Banting Post-doctoral Fellowship through the Natural Sciences and Engineering Research Council (NSERC) of Canada.

ACKNOWLEDGMENTS

We thank Suchul Jang (Codiak BioSciences, Cambridge, MA, United States), Jaewook Lee (Rosetta Exosome Co., Ltd., Seoul, South Korea), Yeojin Lee (Columbia University, New York, NY, United States), and Sae Rom Kim (Samsung Bioepis, Incheon, South Korea) for the discussions and review of this manuscript.

SUPPLEMENTARY MATERIAL

The Supplementary Material for this article can be found online at: https://www.frontiersin.org/articles/10.3389/fcell.2021.734950/full#supplementary-material

Supplementary Figure 1 | Comparison of the identification frequencies of conventional exosomal and ectosomal markers in **(A)** large extracellular vesicles (lEVs) and **(B)** small EVs (sEVs) datasets. n.s., not significant; $^*P < 0.05$.

Supplementary Figure 2 | Score plots from Gene Set Enrichment Analysis (GSEA) for **(A)** sEV (top) and lEV (bottom) proteins. **(B)** Enrichment score plots for vesicular proteins with similar identification frequencies in lEV and sEVs, using identification counts across human datasets. Upper panel, frequently identified EV proteins; lower panel, rarely identified ones.

Supplementary Figure 3 | Gene Set Enrichment Analysis (GSEA) reveals functions of proteins similarly abundant in both EV subtypes.

Supplementary Table 1 | An integrated EV proteomic dataset by compiling the entire list of shotgun proteomic datasets including a detailed description of the table. **(A)** Description of the proteomic datasets in EVpedia used in this study. **(B)** Definition of differential ultracentrifugation (DUC) criteria used for classifying datasets. **(C)** A list of methods used for isolation of EVs for proteomic datasets in EVpedia, and how they were classified.

Supplementary Table 2 | Identification frequencies of human vesicular proteins in EVpedia. fsEV and flEV indicate the number of times the protein was identified in an sEV or lEV dataset, divided by the total number of datasets, and IC_{pro} and IC_{eu} indicate the number of times an ortholog of the protein was identified in prokaryotic or eukaryotic dataset in EVpedia.

Supplementary Table 3 | List of interacting protein pairs from integrating Affinity Purification-Mass Spectrometry (AP-MS; BioPlex) and Yeast Two-Hybrid (Y2H; HuRI) datasets, including table description and details of the table.

Supplementary Table 4 | List of functional annotations enriched in proteins more frequently identified in **(A)** sEV and **(B)** lEV datasets. **(C)** Functional enrichment for proteins similarly identified in sEV and lEV was analyzed using their identification count across human datasets in EVpedia. The table contains a detailed description of the table. ES, enrichment score; NES, normalized enrichment score; NOM, nominal; FDR, false discovery rate; FWER, family-wise error rate.

REFERENCES

Al-Nedawi, K., Meehan, B., Micallef, J., Lhotak, V., May, L., Guha, A., et al. (2008). Intercellular transfer of the oncogenic receptor EGFRvIII by microvesicles derived from tumour cells. *Nat. Cell Biol.* 10, 619–624. doi: 10.1038/ncb1725

Braisted, J. C., Kuntumalla, S., Vogel, C., Marcotte, E. M., Rodrigues, A. R., Wang, R., et al. (2008). The APEX quantitative proteomics tool: generating protein quantitation estimates from LC-MS/MS proteomics results. *BMC Bioinformatics* 9:529. doi: 10.1186/1471-2105-9-529

Choi, D., Montermini, L., Jeong, H., Sharma, S., Meehan, B., and Rak, J. (2019). Mapping subpopulations of cancer cell-derived extracellular vesicles and particles by nano-flow cytometry. *ACS Nano* 13, 10499–10511. doi: 10.1021/acsnano.9b04480

Choi, D.-S., Kim, D.-K., Kim, Y.-K., and Gho, Y. S. (2013). Proteomics, transcriptomics and lipidomics of exosomes and ectosomes. *Proteomics* 13, 1554–1571. doi: 10.1002/pmic.201200329

Choi, D.-S., Kim, D.-K., Kim, Y.-K., and Gho, Y. S. (2015). Proteomics of extracellular vesicles: exosomes and ectosomes. *Mass Spectrom. Rev.* 34, 474–490. doi: 10.1002/mas.21420

Cocucci, E., and Meldolesi, J. (2011). Ectosomes. *Curr. Biol.* 21, R940–R941. doi: 10.1016/j.cub.2011.10.011

Cocucci, E., and Meldolesi, J. (2015). Ectosomes and exosomes: shedding the confusion between extracellular vesicles. *Trends Cell Biol.* 25, 364–372. doi: 10.1016/j.tcb.2015.01.004

Colombo, M., Raposo, G., and Théry, C. (2014). Biogenesis, secretion, and intercellular interactions of exosomes and other extracellular vesicles. *Annu. Rev. Cell Dev. Biol.* 30, 255–289. doi: 10.1146/annurev-cellbio-101512-122326

Deatherage, B. L., and Cookson, B. T. (2012). Membrane vesicle release in bacteria, eukaryotes, and archaea: a conserved yet underappreciated aspect of microbial life. *Infect. Immun.* 80, 1948–1957. doi: 10.1128/IAI.06014-11

Dutta, S., Reamtong, O., Panvongsa, W., Kitdumrongthum, S., Janpipatkul, K., Sangvanich, P., et al. (2015). Proteomics profiling of cholangiocarcinoma exosomes: a potential role of oncogenic protein transferring in cancer progression. *Biochim. Biophys. Acta* 1852, 1989–1999. doi: 10.1016/j.bbadis.2015.06.024

Edgar, J. R. (2016). Q&A: what are exosomes, exactly? *BMC Biol.* 14:46. doi: 10.1186/s12915-016-0268-z

Embley, T. M., and Martin, W. (2006). Eukaryotic evolution, changes and challenges. *Nature* 440, 623–630. doi: 10.1038/nature04546

Escrevente, C., Grammel, N., Kandzia, S., Zeiser, J., Tranfield, E. M., Conradt, H. S., et al. (2013). Sialoglycoproteins and N-glycans from secreted exosomes of ovarian carcinoma cells. *PLoS One* 8:e78631. doi: 10.1371/journal.pone.0078631

Garrido-Urbani, S., Garg, P., Ghossoub, R., Arnold, R., Lembo, F., Sundell, G. N., et al. (2016). Proteomic peptide phage display uncovers novel interactions of the PDZ1-2 supramodule of syntenin. *FEBS Lett.* 590, 3–12. doi: 10.1002/1873-3468.12037

Gill, S., Catchpole, R., and Forterre, P. (2019). Extracellular membrane vesicles in the three domains of life and beyond. *FEMS Microbiol. Rev.* 43, 273–303. doi: 10.1093/femsre/fuy042

Gillis, J., Ballouz, S., and Pavlidis, P. (2014). Bias tradeoffs in the creation and analysis of protein-protein interaction networks. *J. Proteomics* 100, 44–54. doi: 10.1016/j.jprot.2014.01.020

Gomes, J., Gomes-Alves, P., Carvalho, S. B., Peixoto, C., Alves, P. M., Altevogt, P., et al. (2015). Extracellular vesicles from ovarian carcinoma cells display specific glycosignatures. *Biomolecules* 5, 1741–1761. doi: 10.3390/biom5031741

Gray, M. W., Burger, G., and Lang, B. F. (1999). Mitochondrial evolution. *Science* 283, 1476–1481. doi: 10.1126/science.283.5407.1476

Greening, D. W., Xu, R., Ji, H., Tauro, B. J., and Simpson, R. J. (2015). "A protocol for exosome isolation and characterization: evaluation of ultracentrifugation, density-gradient separation, and immunoaffinity capture methods," in *Proteomic Profiling: Methods and Protocols*, ed. A. Posch (New York, NY: Springer New York), 179–209. doi: 10.1007/978-1-4939-2550-6_15

Harris, N. (1986). Organization of the endomembrane system. *Annu. Rev. Plant Physiol.* 37, 73–92. doi: 10.1146/annurev.pp.37.060186.000445

Hoshino, A., Kim, H. S., Bojmar, L., Gyan, K. E., Cioffi, M., Hernandez, J., et al. (2020). Extracellular vesicle and particle biomarkers define multiple human cancers. *Cell* 182, 1044.e–1061.e.

Huttlin, E. L., Bruckner, R. J., Navarrete-Perea, J., Cannon, J. R., Baltier, K., Gebreab, F., et al. (2021). Dual proteome-scale networks reveal cell-specific remodeling of the human interactome. *Cell* 184, 3022.e–3040.e. doi: 10.1016/j.cell.2021.04.011

Huttlin, E. L., Bruckner, R. J., Paulo, J. A., Cannon, J. R., Ting, L., Baltier, K., et al. (2017). Architecture of the human interactome defines protein communities and disease networks. *Nature* 545, 505–509. doi: 10.1038/nature22366

Huttlin, E. L., Ting, L., Bruckner, R. J., Gebreab, F., Gygi, M. P., Szpyt, J., et al. (2015). The BioPlex network: a systematic exploration of the human interactome. *Cell* 162, 425–440. doi: 10.1016/j.cell.2015.06.043

Ipinmoroti, A. O., and Matthews, Q. L. (2020). Extracellular vesicles: roles in human viral infections, immune-diagnostic, and therapeutic applications. *Pathogens* 9:1056. doi: 10.3390/pathogens9121056

Jensen, L. J., Julien, P., Kuhn, M., von Mering, C., Muller, J., Doerks, T., et al. (2008). eggNOG: automated construction and annotation of orthologous groups of genes. *Nucleic Acids Res.* 36, D250–D254. doi: 10.1093/nar/gkm796

Jeppesen, D. K., Fenix, A. M., Franklin, J. L., Higginbotham, J. N., Zhang, Q., Zimmerman, L. J., et al. (2019). Reassessment of exosome composition. *Cell* 177, 428.e–445.e. doi: 10.1016/j.cell.2019.02.029

Jiao, H., Jiang, D., Hu, X., Du, W., Ji, L., Yang, Y., et al. (2021). Mitocytosis, a migrasome-mediated mitochondrial quality-control process. *Cell* 184, 2896.e–2910.e. doi: 10.1016/j.cell.2021.04.027

Kalluri, R., and LeBleu, V. S. (2020). The biology, function, and biomedical applications of exosomes. *Science* 367:eaau6977. doi: 10.1126/science.aau6977

Kalra, H., Drummen, G. P. C., and Mathivanan, S. (2016). Focus on extracellular vesicles: introducing the next small big thing. *Int. J. Mol. Sci.* 17:170. doi: 10.3390/ijms17020170

Kanada, M., Bachmann, M. H., Hardy, J. W., Frimannson, D. O., Bronsart, L., Wang, A., et al. (2015). Differential fates of biomolecules delivered to target cells via extracellular vesicles. *Proc. Natl. Acad. Sci. U.S.A.* 112, E1433–E1442. doi: 10.1073/pnas.1418401112

Kim, D.-K., Kang, B., Kim, O. Y., Choi, D.-S., Lee, J., Kim, S. R., et al. (2013). EVpedia: an integrated database of high-throughput data for systemic analyses of extracellular vesicles. *J. Extracell. Vesicles* 2:20384. doi: 10.3402/jev.v2i0.20384

Kim, D.-K., Lee, J., Kim, S. R., Choi, D.-S., Yoon, Y. J., Kim, J. H., et al. (2015a). EVpedia: a community web portal for extracellular vesicles research. *Bioinformatics* 31, 933–939.

Kim, D.-K., Lee, J., Simpson, R. J., Lötvall, J., and Gho, Y. S. (2015b). EVpedia: a community web resource for prokaryotic and eukaryotic extracellular vesicles research. *Semin. Cell Dev. Biol.* 40, 4–7. doi: 10.1016/j.semcdb.2015.02.005

Kosaka, N., Kogure, A., Yamamoto, T., Urabe, F., Usuba, W., Prieto-Vila, M., et al. (2019). Exploiting the message from cancer: the diagnostic value of extracellular vesicles for clinical applications. *Exp. Mol. Med.* 51, 1–9. doi: 10.1038/s12276-019-0219-1

Kowal, J., Arras, G., Colombo, M., Jouve, M., Morath, J. P., Primdal-Bengtson, B., et al. (2016). Proteomic comparison defines novel markers to characterize heterogeneous populations of extracellular vesicle subtypes. *Proc. Natl. Acad. Sci. U.S.A.* 113, E968–E977. doi: 10.1073/pnas.1521230113

Kucera, M., Isserlin, R., Arkhangorodsky, A., and Bader, G. D. (2016). AutoAnnotate: a Cytoscape app for summarizing networks with semantic annotations. *F1000Res.* 5:1717. doi: 10.12688/f1000research.9090.1

Kugeratski, F. G., Hodge, K., Lilla, S., McAndrews, K. M., Zhou, X., Hwang, R. F., et al. (2021). Quantitative proteomics identifies the core proteome of exosomes with syntenin-1 as the highest abundant protein and a putative universal biomarker. *Nat. Cell Biol.* 23, 631–641. doi10.1038/s41556-021-00693-y

Latifkar, A., Hur, Y. H., Sanchez, J. C., Cerione, R. A., and Antonyak, M. A. (2019). New insights into extracellular vesicle biogenesis and function. *J. Cell Sci.* 132:jcs222406. doi: 10.1242/jcs.222406

Lazar, I., Clement, E., Attane, C., Muller, C., and Nieto, L. (2018). A new role for extracellular vesicles: how small vesicles can feed tumors' big appetite. *J. Lipid Res.* 59, 1793–1804. doi: 10.1194/jlr.R083725

Lee, H. H., Elia, N., Ghirlando, R., Lippincott-Schwartz, J., and Hurley, J. H. (2008). Midbody targeting of the ESCRT machinery by a noncanonical coiled coil in CEP55. *Science* 322, 576–580. doi: 10.1126/science.1162042

Lee, Y., El Andaloussi, S., and Wood, M. J. A. (2012). Exosomes and microvesicles: extracellular vesicles for genetic information transfer and gene therapy. *Hum. Mol. Genet.* 21, R125–R134. doi: 10.1093/hmg/dds317

Letunic, I., and Bork, P. (2021). Interactive Tree Of Life (iTOL) v5: an online tool for phylogenetic tree display and annotation. *Nucleic Acids Res.* 49, W293–W296. doi: 10.1093/nar/gkab301

Li, B., Antonyak, M. A., Zhang, J., and Cerione, R. A. (2012). RHOA triggers a specific signaling pathway that generates transforming microvesicles in cancer cells. *Oncogene* 31, 4740–4749. doi: 10.1038/onc.2011.636

Li, J., He, X., Deng, Y., and Yang, C. (2019). An update on isolation methods for proteomic studies of extracellular vesicles in biofluids. *Molecules* 24:3516. doi: 10.3390/molecules24193516

Lin, Y., Liang, A., He, Y., Li, Z., Li, Z., Wang, G., et al. (2019). Proteomic analysis of seminal extracellular vesicle proteins involved in asthenozoospermia by iTRAQ. *Mol. Reprod. Dev.* 86, 1094–1105. doi: 10.1002/mrd.23224

Liu, D., Gao, Y., Liu, J., Huang, Y., Yin, J., Feng, Y., et al. (2021). Intercellular mitochondrial transfer as a means of tissue revitalization. *Signal. Transduct. Target Ther.* 6:65. doi: 10.1038/s41392-020-00440-z

Liu, M.-L., and Williams, K. J. (2012). Microvesicles: potential markers and mediators of endothelial dysfunction. *Curr. Opin. Endocrinol. Diabetes Obes.* 19, 121–127. doi: 10.1097/MED.0b013e32835057e9

Luck, K., Kim, D.-K., Lambourne, L., Spirohn, K., Begg, B. E., Bian, W., et al. (2020). A reference map of the human binary protein interactome. *Nature* 580, 402–408. doi: 10.1038/s41586-020-2188-x

Mathews, P. M., and Levy, E. (2019). Exosome production is key to neuronal endosomal pathway integrity in neurodegenerative diseases. *Front. Neurosci.* 13:1347. doi: 10.3389/fnins.2019.01347

Meldolesi, J. (2018). Exosomes and ectosomes in intercellular communication. *Curr. Biol.* 28, R435–R444. doi: 10.1016/j.cub.2018.01.059

Merico, D., Isserlin, R., Stueker, O., Emili, A., and Bader, G. D. (2010). Enrichment map: a network-based method for gene-set enrichment visualization and interpretation. *PLoS One* 5:e13984. doi: 10.1371/journal.pone.0013984

Mittelbrunn, M., and Sánchez-Madrid, F. (2012). Intercellular communication: diverse structures for exchange of genetic information. *Nat. Rev. Mol. Cell Biol.* 13, 328–335. doi: 10.1038/nrm3335

Muralidharan-Chari, V., Clancy, J., Plou, C., Romao, M., Chavrier, P., Raposo, G., et al. (2009). ARF6-regulated shedding of tumor cell-derived plasma membrane microvesicles. *Curr. Biol.* 19, 1875–1885. doi: 10.1016/j.cub.2009.09.059

Nikitidou, E., Khoonsari, P. E., Shevchenko, G., Ingelsson, M., Kultima, K., and Erlandsson, A. (2017). Increased release of Apolipoprotein E in extracellular vesicles following amyloid-β protofibril exposure of neuroglial co-cultures. *J. Alzheimers. Dis.* 60, 305–321. doi: 10.3233/JAD-170278

O'Brien, K., Breyne, K., Ughetto, S., Laurent, L. C., and Breakefield, X. O. (2020). RNA delivery by extracellular vesicles in mammalian cells and its applications. *Nat. Rev. Mol. Cell Biol.* 21, 585–606. doi: 10.1038/s41580-020-0251-y

Oliveira, D. L., Nakayasu, E. S., Joffe, L. S., Guimarães, A. J., Sobreira, T. J., Nosanchuk, J. D., et al. (2010). Biogenesis of extracellular vesicles in yeast: many questions with few answers. *Commun. Integr. Biol.* 3, 533–535. doi: 10.4161/cib.3.6.12756

Peng, K. Y., Pérez-González, R., Alldred, M. J., Goulbourne, C. N., Morales-Corraliza, J., Saito, M., et al. (2019). Apolipoprotein E4 genotype compromises brain exosome production. *Brain* 142, 163–175. doi: 10.1093/brain/awy289

Phinney, D. G., Di Giuseppe, M., Njah, J., Sala, E., Shiva, S., St Croix, C. M., et al. (2015). Mesenchymal stem cells use extracellular vesicles to outsource mitophagy and shuttle microRNAs. *Nat. Commun.* 6:8472. doi: 10.1038/ncomms9472

Rogers, M. A., Buffolo, F., Schlotter, F., Atkins, S. K., Lee, L. H., Halu, A., et al. (2020). Annexin A1-dependent tethering promotes extracellular vesicle aggregation revealed with single-extracellular vesicle analysis. *Sci. Adv.* 6:eabb1244. doi: 10.1126/sciadv.abb1244

Rolland, T., Taşan, M., Charloteaux, B., Pevzner, S. J., Zhong, Q., Sahni, N., et al. (2014). A proteome-scale map of the human interactome network. *Cell* 159, 1212–1226. doi: 10.1016/j.cell.2014.10.050

Rual, J.-F., Venkatesan, K., Hao, T., Hirozane-Kishikawa, T., Dricot, A., Li, N., et al. (2005). Towards a proteome-scale map of the human protein–protein interaction network. *Nature* 437, 1173–1178. doi: 10.1038/nature04209

Rybak, K., and Robatzek, S. (2019). Functions of extracellular vesicles in immunity and virulence. *Plant Physiol.* 179, 1236–1247. doi: 10.1104/pp.18.01557

Schoch, C. L., Ciufo, S., Domrachev, M., Hotton, C. L., Kannan, S., Khovanskaya, R., et al. (2020). NCBI Taxonomy: a comprehensive update on curation, resources and tools. *Database* 2020:baaa062. doi: 10.1093/database/baa\breaka062

Shannon, P., Markiel, A., Ozier, O., Baliga, N. S., Wang, J. T., Ramage, D., et al. (2003). Cytoscape: a software environment for integrated models of biomolecular interaction networks. *Genome Res.* 13, 2498–2504. doi: 10.1101/gr.1239303

Słomka, A., Urban, S. K., Lukacs-Kornek, V., Żekanowska, E., and Kornek, M. (2018). Large extracellular vesicles: have we found the holy grail of inflammation? *Front. Immunol.* 9:2723. doi: 10.3389/fimmu.2018.02723

Sluijter, J. P. G., Verhage, V., Deddens, J. C., van den Akker, F., and Doevendans, P. A. (2014). Microvesicles and exosomes for intracardiac communication. *Cardiovasc. Res.* 102, 302–311. doi: 10.1093/cvr/cvu022

Song, Y., Wang, M., Tong, H., Tan, Y., Hu, X., Wang, K., et al. (2021). Plasma exosomes from endometrial cancer patients contain LGALS3BP to promote endometrial cancer progression. *Oncogene* 40, 633–646. doi: 10.1038/s41388-020-01555-x

Subramanian, A., Tamayo, P., Mootha, V. K., Mukherjee, S., Ebert, B. L., Gillette, M. A., et al. (2005). Gene set enrichment analysis: a knowledge-based approach for interpreting genome-wide expression profiles. *Proc. Natl. Acad. Sci. U.S.A.* 102, 15545–15550. doi: 10.1073/pnas.0506580102

Surman, M., Stępień, E., Hoja-Łukowicz, D., and Przybyło, M. (2017). Deciphering the role of ectosomes in cancer development and progression: focus on the proteome. *Clin. Exp. Metastasis* 34, 273–289. doi: 10.1007/s10585-017-9844-z

Théry, C., Witwer, K. W., Aikawa, E., Alcaraz, M. J., Anderson, J. D., Andriantsitohaina, R., et al. (2018). Minimal information for studies of extracellular vesicles 2018 (MISEV2018): a position statement of the International Society for Extracellular Vesicles and update of the MISEV2014 guidelines. *J. Extracell. Vesicles* 7:1535750. doi: 10.1080/20013078.2018.1535750

Torralba, D., Baixauli, F., and Sánchez-Madrid, F. (2016). Mitochondria know no boundaries: mechanisms and functions of intercellular mitochondrial transfer. *Front. Cell Dev. Biol* 4:107. doi: 10.3389/fcell.2016.00107

Ung, T. H., Madsen, H. J., Hellwinkel, J. E., Lencioni, A. M., and Graner, M. W. (2014). Exosome proteomics reveals transcriptional regulator proteins with potential to mediate downstream pathways. *Cancer Sci.* 105, 1384–1392. doi: 10.1111/cas.12534

van Niel, G., D'Angelo, G., and Raposo, G. (2018). Shedding light on the cell biology of extracellular vesicles. *Nat. Rev. Mol. Cell Biol.* 19, 213–228. doi: 10.1038/nrm.2017.125

Witwer, K. W., Buzás, E. I., Bemis, L. T., Bora, A., Lässer, C., Lötvall, J., et al. (2013). Standardization of sample collection, isolation and analysis methods in extracellular vesicle research. *J. Extracell. Vesicles* 2:20360. doi: 10.3402/jev.v2i0.20360

Zheng, P., Luo, Q., Wang, W., Li, J., Wang, T., Wang, P., et al. (2018). Tumor-associated macrophages-derived exosomes promote the migration of gastric cancer cells by transfer of functional Apolipoprotein E. *Cell Death Dis.* 9:434. doi: 10.1038/s41419-018-0465-5

Conflict of Interest: The authors declare that the research was conducted in the absence of any commercial or financial relationships that could be construed as a potential conflict of interest.

Publisher's Note: All claims expressed in this article are solely those of the authors and do not necessarily represent those of their affiliated organizations, or those of the publisher, the editors and the reviewers. Any product that may be evaluated in this article, or claim that may be made by its manufacturer, is not guaranteed or endorsed by the publisher.

frontiers in Cell and Developmental Biology

ORIGINAL RESEARCH
published: 06 October 2021
doi: 10.3389/fcell.2021.724389

Epidermal Growth Factor Receptor Mutations Carried in Extracellular Vesicle-Derived Cargo Mirror Disease Status in Metastatic Non-small Cell Lung Cancer

Emma Purcell[1,2†], Sarah Owen[1,2†], Emily Prantzalos[1,2], Abigail Radomski[1,2], Nayri Carman[1,2], Ting-Wen Lo[1,2], Mina Zeinali[1,2], Chitra Subramanian[3], Nithya Ramnath[4,5‡] and Sunitha Nagrath[1,2,6‡]*

[1] Department of Chemical Engineering, University of Michigan, Ann Arbor, MI, United States, [2] Biointerfaces Institute, University of Michigan, Ann Arbor, MI, United States, [3] Department of Surgery, University of Michigan, Ann Arbor, MI, United States, [4] Department of Internal Medicine, University of Michigan, Ann Arbor, MI, United States, [5] Veterans Affairs Ann Arbor Healthcare System, Ann Arbor, MI, United States, [6] Rogel Cancer Center, University of Michigan, Ann Arbor, MI, United States

In non-small cell lung cancer (NSCLC), identifying the presence of sensitizing and resistance epidermal growth factor receptor (EGFR) mutations dictates treatment plans. Extracellular vesicles (EVs) are emerging as abundant, stable potential liquid biopsy targets that offer the potential to quantify EGFR mutations in NSCLC patients at the RNA and protein level at multiple points through treatment. In this study, we present a systematic approach for serial mutation profiling of 34 EV samples from 10 metastatic NSCLC patients with known EGFR mutations through treatment. Using western blot and droplet digital PCR (ddPCR), sensitizing (exon 19 deletion, L858R) mutations were detected in EV-Protein, and both sensitizing and resistance (T790M) mutations were quantified in EV-RNA. EGFR mutations were detected in EV-Protein from four patients at multiple time points through treatment. Using EV-RNA, tumor biopsy matched sensitizing mutations were detected in 90% of patients and resistance mutations in 100% of patients. Finally, mutation burden in EV-RNA at each time point was compared to disease status, described as either stable or progressing. For 6/7 patients who were longitudinally monitored through treatment, EV mutation burden mirrored clinical trajectory. When comparing mutation detection between EV-RNA and ctDNA using ddPCR, EVs had a better detection rate for exon 19 deletions and the L858R point mutation. In conclusion, this study demonstrates that integrating EV analysis into liquid biopsy mutation screening has the potential to advance beyond the current standard of care "rule in" test. The multi-analyte testing allows future integration of EGFR mutation monitoring with additional EV-markers for a comprehensive patient monitoring biomarker.

Keywords: extracellular vesicle (EV), EGFR mutation, longitudinal monitoring, resistance mutation, non-small cell lung cancer, EV-protein, EV-RNA, tyrosine kinase inhibitor (TKI)

OPEN ACCESS

Edited by:
Xinlei Li,
Nationwide Children's Hospital, United States

Reviewed by:
Ikuhiko Nakase,
Osaka Prefecture University, Japan
Vito D'Agostino,
University of Trento, Italy

****Correspondence:***
Sunitha Nagrath
snagrath@umich.edu

† These authors have contributed equally to this work and share first authorship

‡ These authors have contributed equally to this work and share senior authorship

Specialty section:
This article was submitted to Molecular and Cellular Pathology, a section of the journal Frontiers in Cell and Developmental Biology

Received: *13 June 2021*
Accepted: *31 August 2021*
Published: *06 October 2021*

Citation:
Purcell E, Owen S, Prantzalos E, Radomski A, Carman N, Lo T-W, Zeinali M, Subramanian C, Ramnath N and Nagrath S (2021) Epidermal Growth Factor Receptor Mutations Carried in Extracellular Vesicle-Derived Cargo Mirror Disease Status in Metastatic Non-small Cell Lung Cancer. Front. Cell Dev. Biol. 9:724389. doi: 10.3389/fcell.2021.724389

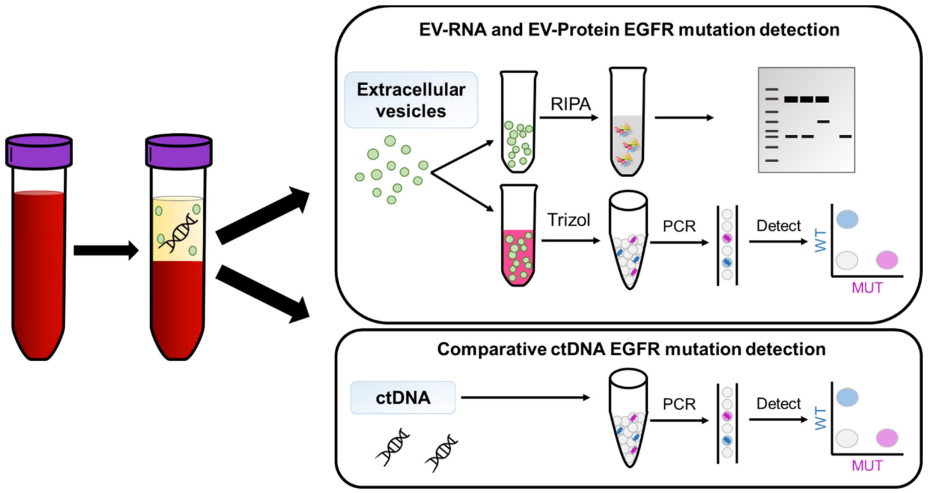

GRAPHICAL ABSTRACT | EVs are isolated from plasma collected from NSCLC patients harboring known EGFR mutations using ultracentrifugation. RNA and protein are extracted from the EV samples and tested for EGFR mutations using ddPCR and western blot, respectively.

INTRODUCTION

The widespread adoption of targeted therapies using small molecule tyrosine kinase inhibitors (TKIs) has greatly benefited the 10–30% of advanced non-small cell lung cancer (NSCLC) patients who have sensitizing epidermal growth factor receptor (EGFR) mutations in an otherwise challenging to treat cancer (Collisson et al., 2014; Zhang et al., 2016). This subset of NSCLC patients harboring sensitizing [L858R and exon 19 deletion (exon 19 del)] EGFR mutations have seen significantly improved survival due to TKIs; yet resistance often occurs in as few as 9 months, commonly through the secondary EGFR T790M mutation (Clark et al., 2005; Pao et al., 2005; Balak et al., 2006). While it has been documented that additional mutations arise during TKI treatment, traditional tumor monitoring technologies are not commonly used to monitor for these changes. To improve patient care, it is critical to have real-time knowledge of a patient's mutation status, thereby allowing clinicians to alter treatment strategies accordingly. As such, the development of a method for non-invasive longitudinal monitoring offers the potential to drastically improve real-time treatment personalization.

Due to the invasiveness and inherently localized sampling of tissue biopsies, they are not frequently used for repeated monitoring, may not result in enough material for testing, and may miss mutations carried in other tumor regions [National Comprehensive Cancer Network (NCCN)/NCCN Foundation, 2021]. To address these challenges, advancements in liquid biopsies have led to the clinical use of blood-based biomarkers, mostly commonly circulating tumor DNA (ctDNA), to monitor changes in the tumor non-invasively and longitudinally (Alix-Panabières and Pantel, 2016). Yet, ctDNA assays are limited by several notable technical challenges; ctDNA is shed only during cell death (Jahr et al., 2001) and suffers from low abundance (Diehl et al., 2005) and rapid clearance from circulation (Gauthier et al., 1996; Kustanovich et al., 2019). Hence, ctDNA has the potential to miss the most current molecular changes in tumor cells that are the most evasive leading to treatment resistant.

Extracellular vesicles (EVs), lipid bilayer bound nanovesicles approximately 30–150 nm in diameter, are a promising alternative blood-based biomarker offering increased abundance and stability compared to ctDNA (Jin et al., 2016; Kang et al., 2016). They are functional vesicles secreted from live cells as a mechanism of cell-cell communication and contain cargo from their originating cells, including DNA, RNA, and protein, which is protected by the lipid bilayer from exogenous degradation while in circulation (Théry, 2011). The stability of these vesicles in circulation is the key distinguishing factor compared to ctDNA.

Given the tiny amount of cargo carried by these nano-sized vesicles, the development of techniques that can analyze these important carriers is an active area of research. To date, research has largely been limited to microRNA or protein to glean information about a patient's disease, and to develop diagnostic and prognostic signatures (Rabinowits et al., 2009; Lobb et al., 2017). A final key benefit of using EVs for a liquid biopsy compared to ctDNA is the ability to perform multiplexed analysis of EV-derived RNA (EV-RNA) and EV-derived protein (EV-protein). However, thus far, the detection of mutations carried in EVs in either analyte has been reported by few groups and has been biased toward nucleic acid analysis, with few groups reporting the detection of mutant proteins in extracellular vesicles (Lobb et al., 2017).

Significantly, mutation profiling in extracellular vesicles is an emerging field, with the first studies focusing on the detection of cancer-specific mutations (Chen et al., 2013; Thakur et al., 2014; Figueroa et al., 2017). Mutations carried in EVs have been shown in glioblastoma, pancreatic cancer, and NSCLC. The clinical application has centered on improving detection rates compared to ctDNA alone, commonly by combining ctDNA with DNA and RNA derived from exosomes (a subset of small EVs) (Castellanos-Rizaldos et al., 2018; Krug et al., 2018). For example, Castellanos-Rizaldos et al. (2018) co-isolated exosomal RNA and cell-free

RNA for mutation detection from a panel of 30 EGFR mutations, achieving a higher sensitivity than with cell-free RNA alone. Similar to other studies, this work was limited based on the use of pre-amplification steps prior to qPCR, which can introduce signal strength bias, for mutation detection and was constrained to a single time point for evaluation. While increasing the detection rate of these rare mutations was achieved, these studies have not demonstrated their utility in a clinical setting and remain single-analyte analyses.

Several recent works have demonstrated the feasibility of using EV-RNA to detect EGFR mutations from blood (Dong et al., 2019; Pasini et al., 2021) and bronchoalveolar lavage fluid (Hur et al., 2019; Liam et al., 2020). Notably, a robust method was developed for detecting mutations in EV-RNA using droplet digital PCR (ddPCR) and was validated with Sanger sequencing with mutations found with over 90% sensitivity. The study profiled EVs before treatment and at the time of progression events in a cohort of metastatic NSCLC patients, further demonstrating the promise of using EV-RNA to monitor mutations through treatment (Pasini et al., 2021). There remains, however, a need to verify whether changes in mutation burden, at either the RNA or protein level, found within EVs, is a predictor of progression events as opposed to a result of disease progression.

The study presented here builds upon these previous works by following a cohort of metastatic NSCLC patients to quantify the EGFR mutation burden carried in both EV-RNA and EV-Protein. Specifically, ddPCR was used to analyze the EV-RNA without pre-amplification while mutated protein content of EVs was profiled using western blot. Patients carried at least one sensitizing EGFR mutation (exon 19 del, L858R) based on tumor biopsy and were receiving TKI therapy at the time of enrollment. Moreover, a subset of patients in this study already carried the resistance T790M mutation at the beginning of longitudinal monitoring. Resistance mutations would potentially decrease the efficacy of TKIs, although novel TKIs are being developed to target these mutations as well. Despite the predicted TKI sensitivity, patients had differing therapeutic responses, which is a well-known challenge of TKI therapies. As such, there is a need to develop an enhanced approach to predict who will have favorable outcomes, or who should receive an alternative therapy.

To this end, in this study the cohort was longitudinally monitored for EGFR mutation burden carried by EV-RNA and EV-protein. This study expanded upon previous works by monitoring patients serially, allowing for time points before, during, and after progression events. Finally, expanding beyond only EV-RNA profiling highlights the potential benefits of dual-monitoring both EV-RNA and EV-protein; distinct roles for EV-RNA and EV-protein were revealed.

RESULTS

Extracellular Vesicle Cargo Carries Mutations From Cells of Origin

To first establish experimental protocols and demonstrate the presence of EGFR mutations in EVs, EVs secreted from lung cancer cell lines with known EGFR mutations were tested for EGFR mutations. EV-RNA and EV-protein were tested using ddPCR and western blot, respectively. ddPCR offers a highly sensitive platform to directly quantify the number of mutant transcripts from bulk RNA without risk of pre-amplification bias (Owen et al., 2020), allowing for direct comparison between samples and patients. Briefly, the EVs were lysed using TRIzol^{TM} Reagent. The Norgen Single Cell RNA kit (Norgen Biotek Corp.) was used to purify and isolate the EV-RNA, due to the miniscule amount of RNA contained in these samples. RNA was reverse transcribed and directly loaded onto the RainDrop^{TM} (RainDance Technologies) ddPCR system for analysis.

Matching the cells of origin, EV-RNA derived from H3255 carried a heterozygous L858R mutation (**Figure 1A** and **Supplementary Figure 1**), EVs from H1975 carried heterozygous L858R and T790M mutations (**Figure 1A**), and EVs from H1650 carried exon 19 del (**Figure 1B**). As expected, the assay showed that the EVs were negative for EGFR mutations that were not present originally in their cell line of origin (**Figures 1A,B**). In healthy donor EV-RNA (1–3), there were 0.33 ± 0.47 ($n = 3$) L858R droplets and 0 ± 0 ($n = 3$) T790M droplets (**Figures 1A,B** and **Supplementary Figure 2**). However, when assaying healthy controls, the exon 19 del ddPCR assay showed an average background of 12.6 ± 2 ($n = 5$) droplets in healthy donor EV-RNA, similar to the background signal from the negative control cell line EV-RNA H1975. This assay simultaneously screens for 19 different deletion variants using pooled primers, resulting in increased background signal. A threshold for positive detection was determined based on the highest background signal observed among all negative control samples. This threshold for detection was used for all subsequent analysis for NSCLC patient EV-RNA.

Cell line derived EVs also carried mutant EGFR protein, as demonstrated using western blot. Specific identification of the two activating mutant proteins was achieved. L858R was detected exclusively in H3255 and H1975 derived EVs (**Figures 1C,D**), and exon 19 del only in H1650 derived EVs (**Figure 1D**). A validated T790M antibody is not yet commercially available, and therefore the samples were not tested for this mutation. Additionally, the cell line derived EVs were tested for total EGFR abundance probing for a conserved, wildtype region of EGFR (**Figure 1D**). Each EV-protein sample was additionally profiled for the EV marker CD9, and was shown to be free of cellular contamination based on calnexin (**Figure 1D**).

Protein intensity for each marker was normalized to the total protein loaded into each lane using Bio-Rad's Stain Free Gel technology. Each band was normalized to the total protein per lane, eliminating the need for housekeeping genes which are not equally present in all EVs due to their loading mechanisms and cells of origin (Théry et al., 2018). Stain Free Gels have been found to be more consistent than housekeeping proteins or Ponceau staining as a loading control and provide the added benefit of controlling for differential loading (Gilda and Gomes, 2013; Rivero-Gutiérrez et al., 2014). The samples were loaded based on a normalized starting cell number and EV biogenesis time, 3 million cells for 72 h incubation, which, for perspective

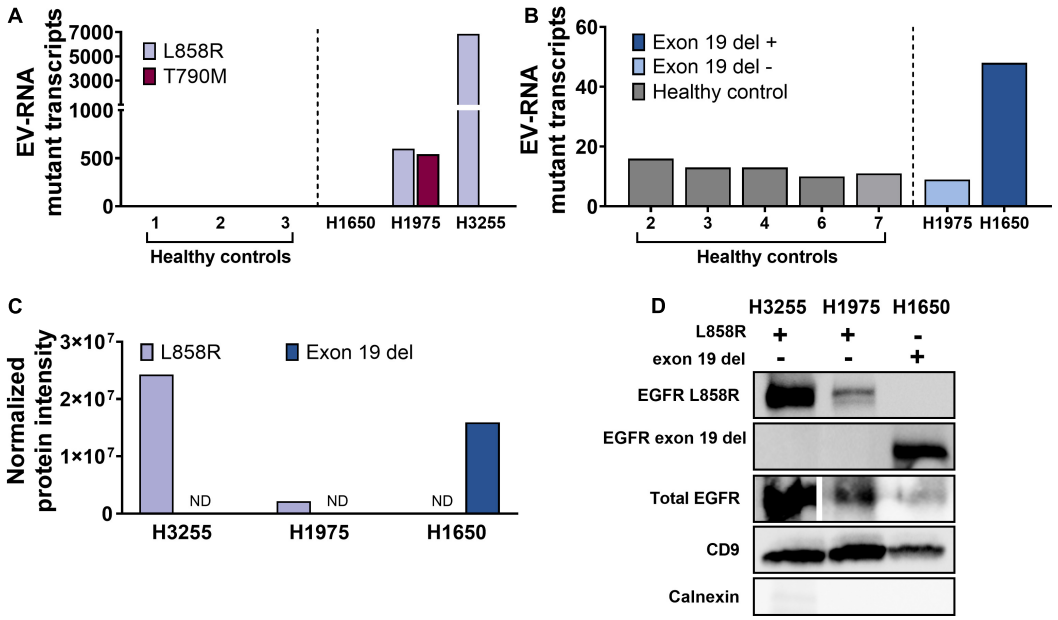

FIGURE 1 | EGFR mutations carried in RNA and protein from cell line derived EVs H1975 (L858R/T790M), H3255 (L858R), H1650 (exon 19 del). **(A,B)** EV-RNA ddPCR droplet counts of lung cancer cell line-derived and healthy plasma for **(A)** L858R and T790M point mutations and **(B)** exon 19 del. **(C)** Normalized protein intensity for L858R and exon 19 del EGFR mutations from cell line derived extracellular vesicles using western blots. Normalized protein intensity was calculated using Bio-Rad's Stain Free Blot technology to compare specific bands to the total protein of each lane. **(D)** Western blot of cell line derived EVs tested for L858R, exon 19 del, total EGFR, CD9, and calnexin. ND, not detected.

was quantified to be 7.5 μg for H3255 EVs, 3.5 μg for H1975 EVs, and 3.1 μg for H1650 EVs.

Metastatic Non-small Cell Lung Cancer Patient Cohort and Study Design for Epidermal Growth Factor Receptor Mutational Profiling in Extracellular Vesicles

The above established dual EV-RNA and EV-protein mutational profiling was applied to analyze EVs from blood plasma in a cohort of ten metastatic NSCLC patients with at least one known sensitizing EGFR mutation based on primary tumor biopsy. Patients were enrolled after consent and blood was collected under IRB approval. The cohort's median age was 64 years (range, 45–82 years) and was well distributed between male and female. Full patient demographics can be found in **Supplementary Table 1**.

Seven of the ten patients had samples collected at multiple time points, termed visits. The time between each visit varied depending on patient care, however, the time ranged from 26 to 231 days (mean = 89 ± 40 days) across all patients. The visit notation is used throughout this study to highlight general trends on the utility of patient monitoring using EVs to be compared across patients, however, patient specific details and timelines are shown in **Supplementary Figure 3** and **Supplementary Table 1**. The blood samples were preprocessed to isolate plasma using red blood cell depletion methods, validation experiments demonstrating this material can be utilized for EV analysis are shown in **Supplementary Figure 2**.

While a plethora of EV isolation methods have been widely developed, including ultracentrifugation (Théry et al., 2006), microfluidic devices for EV capture (Kanwar et al., 2014; Kang et al., 2019), and commercially available kits such as ExoQuick (System Biosciences), EVs in this study were isolated using ultracentrifugation, which offers the widest array of downstream applications and high purity compared to the above methods (Tang et al., 2017; Patel et al., 2019) and is compatible with a range of sample input volumes. After isolation, EV concentration and size was determined using nanoparticle tracking analysis (NTA), **Supplementary Table 2**. Each EV sample was tested for EGFR mutations matching the tumor biopsy result. Additionally, matching ctDNA samples, nine samples across five patients, were tested for the corresponding EGFR mutations to compare detection rates.

Longitudinal Detection of Epidermal Growth Factor Receptor Mutations in EV-Protein

EV-protein was isolated from the plasma of four patients over 2–4 visits. EV-protein was tested for sensitizing mutations exon 19 del or L858R based on initial biopsy. EGFR mutations in the EV-protein were detected using western blot in samples from 4/4 (100%) patients, two patients with exon 19 del mutations and two with L858R mutations. Patients L3 and L5 have moderately identifiable bands for exon 19 del, while having various levels of

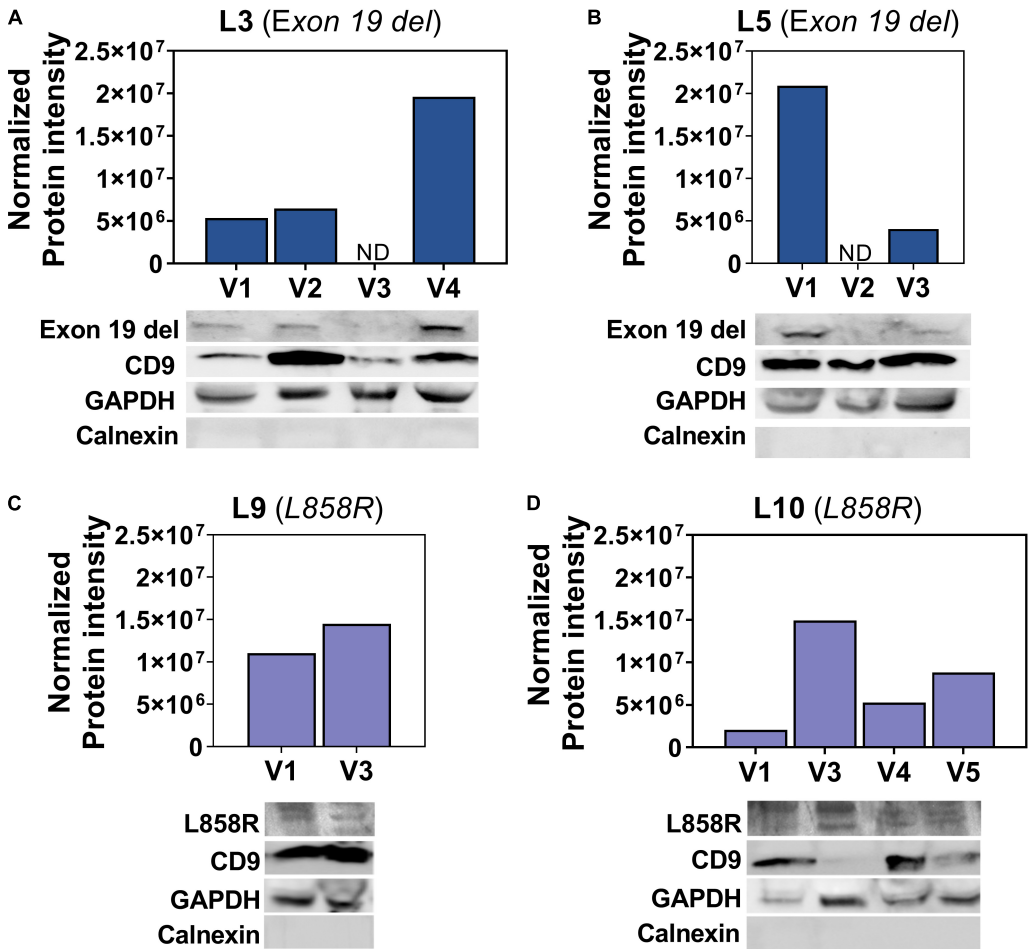

FIGURE 2 | Detection of EGFR mutations in EV-protein. **(A–D)** EV-protein with detected mutant EGFR from patients across multiple visits from **(A)** L3 with exon 19 del, **(B)** L5 with exon 19 del, **(C)** L9 with L858R, and **(D)** L10 with L858R. Samples were additionally screened for CD9, GAPDH, and calnexin. Normalized mutant EV-protein is quantified above each western blot using Bio-Rad's Stain Free Gel technology to normalize to the total protein as quantified by imaging the Stain Free Gel after transfer to a PVDF membrane. ND, not detected.

CD9 and similar GAPDH bands, **Figures 2A,B**. The two patients demonstrated similar detection rates, with one patient having exon 19 del EV-protein detected in 3/4 of samples (L3) and the second in 2/3 of samples (L5). Interestingly, one patient has a trending increase in their mutated EGFR EV-protein, while the other has a steady decrease, despite both being clinically stable through all time points.

Conversely, the L858R band is present in samples from patients L9 and L10, but less distinct compared to exon 19 del in L3 and L5, **Figures 2C,D**. While the bands are less distinct, there is L858R EV-protein at all the time points tested. The second patient, L10, shows a net increase in L858R EV-protein over time compared to visit one, although the amount does not increase at all visits. The less optimal bands could be the result of EV packaging, the protein itself, or several other challenges. However, the CD9 and GAPDH proteins are highly variable between samples for the patients with L858R and are less clean than would be expected from either cells or healthy EVs.

Epidermal growth factor receptor mutations found in EV-protein demonstrate the potential to use EVs as multiple cargo biomarkers. This finding marks the first demonstration of EGFR mutations detected in patient-derived EV-protein. Full western blots can be found in **Supplementary Figure 4**.

Epidermal Growth Factor Receptor Mutations in EV-RNA Detected in Metastatic Non-small Cell Lung Cancer Patients

In compliment, EV-RNA was isolated from 10 patients with multiple samples (n = 33 total samples) collected from each of these patients at different time points (up to six visits) through their course of treatment. The mutation burden was evaluated in each sample, defined as the number of mutant EGFR droplets detected using ddPCR normalized to 5 mL of starting blood volume. Exon 19 del was detected in 7/8 patients, **Figure 3A**. Patients varied as to the number of time points with exon 19 del

positive EV-RNA, with some patients having mutant EV-RNA at 100% of time points (L3, L4, L5, and L7), and one having no detected exon 19 del, L8, **Figure 3B**. It is important to note that the patients had varying numbers of visits, ranging from 1 to 5 (average = 2.88, n = 8). Taken together, the positivity rate across all samples for exon 19 del was 78% (n = 18/23).

The remaining two patients L9 and L10 co-harbored L858R and T790M mutations. Although the data is collected from only two patients, there was a larger range in the number of mutant transcripts detected for the two point mutations than were observed for exon 19 del. Patient L9 had a range of 0–80 T790M transcripts detected, compared to L10 with a range from 0 to 0.5 transcripts per 5 mL blood, **Figure 3C**. Additionally, the point mutations were detected less frequently per patient compared to the patients with exon 19 del. L858R was detected in 75% of time points in L9 and in 50% of time points in L10. Even more modest was the detection of T790M, found in 50% of visits in L9 and only 17% of visits in L10, **Figure 3D**.

For nine samples, matched ctDNA was tested alongside EV-RNA for the EGFR mutations using the same ddPCR technique. For patients with exon 19 del, ctDNA was found in only 1/4 samples tested, compared to 4/4 EV-RNA samples, **Figure 3E**. Similarly, five L858R/T790M samples had dual testing and results show that 3/5 samples tested positive for L858R in ctDNA, whereas 5/5 samples were positive for L858R in EV-RNA. The T790M was detected less frequently in both ctDNA and EV-RNA, with only 2/5 samples having mutations in both ctDNA and EV-RNA, one having only ctDNA mutations, and two having no detected T790M mutations, **Figure 3F**.

Finally, mutation burden between EV-RNA, EV-Protein, and ctDNA were analyzed to determine if there was a correlation between any of the three factors. Using a simple linear regression, it was found that the concentration of mutation burdens between the analytes (EV-RNA, EV-Protein, and ctDNA) were not correlated based off their R^2 values for the three mutations (exon 19 del, L858R, and T790M), **Supplementary Figure 5**.

Longitudinal Monitoring of Epidermal Growth Factor Receptor Mutations in EV-RNA Mirrors Disease Trajectory

To explore the utility of EV-RNA in patient care, transient mutant EGFR burden was compared to the clinical outcomes of seven patients across up to six visits, **Supplementary Figure 3**. At each time point, response to therapy is classified as either a stable (n = 17 samples) or progressing (n = 22 samples) based on available clinical data corresponding to each blood draw visit following the guidelines established in Response Evaluation Criteria in Solid Tumors (RECIST; Eisenhauer et al., 2009). EV-RNA was determined to mirror disease status when an increase in mutation burden occurred at the same time point as progression, or conversely if a decrease or no change in mutation burden occurred at a time point when a patient was determined to have stable disease, **Figure 4A**.

Each patient's progression was classified based on overall disease trajectory into one of three categories based on trend in EV-RNA burden over time: consistently progressing (n = 2 patients) **Figure 4B**, consistently stable (n = 3 patients), **Figure 4B**, and divergent (n = 2 patients), **Figure 4C**. The two patients with consistent progression, L1 and L2, both carried exon 19 del and had increasing EV-RNA mutation burden that mirrored disease progression, **Figure 4B**. Both patients had no detectable EV-RNA mutations in their first visits, however, as their disease progressed, the mutation burden increased with each visit. L1 had increased size of lung nodules between visits 2 and 3, which correlated with the onset of detectable exon 19 del in their EV-RNA. Between visits 3 and 4, the size and number of lung nodules both increased, corresponding with a mutation burden increase of 223%. Similarly, patient L2 had progressing disease between visit 1 and 2, which was reflected by the onset of EV-RNA mutation detection. While the patient was clinically stable between visit 2 and 3, only a modest 40% increase in mutation burden was observed. L2's disease further progressed after visit 3. Ultimately, both patients were placed in hospice shortly before their final time point in this study and are now both deceased.

The second category, comprised of patients L3–L5 who were consistently stable, all carried exon 19 del. They had sustained, clinically stable disease and showed a downward trend in their EV-RNA burden at nearly every time point, **Figure 4B**. L5 initially had brain metastases and high levels of EV-RNA, however, each subsequent time point demonstrated radiologically monitored resolution of brain metastases. This observation of sustained decreased EV-RNA burden is notably different than what was observed in L2, which showed a sustained increase in mutant EGFR burden, despite temporarily being classified as having clinically stable disease. All three patients with sustained clinical stability, L3–5, have been stable for 191, 182, and 204 days, respectively, since the final EV-RNA time point (**Supplementary Figure 3**).

In the last category, patients L9 and L10 each carried L858R and T790M and showed divergent clinical trajectories. L9 had undetectable levels of L858R and T790M EV-RNA at the initial visit and was clinically stable. However, as the patient progressed, EV-RNA burden of L858R and T790M increased between visits 3 and 4, 83 and 2460%, respectively (**Figure 4C**). At 87 days after the final blood draw, L9 has continued to show progression, and has brain metastasis (**Figure 4**). Conversely, L10 was progressing while on TKI therapy but did not have any detectable L858R or T790M EGFR burden. However, when the patient's therapy was switched to chemotherapy (pemetrexed) and the disease stabilized, the L858R mutation became detectable and increased by 672% between visits 5 and 6 in EV-RNA, **Figure 4C**. This patient has continued to be clinically stable for 133 days since the final blood draw (**Supplementary Figure 3**).

To summarize the overall effectiveness of using EV-RNA as a correlate for disease outcome, the change in EV-RNA mutation burden was calculated between each sequential pair of time points. It was then determined whether the patient remained stable or had disease progression between the two time points in question. Promisingly, change in EV-RNA exon 19 del burden mirrored clinical trajectories at 12/14 time points across all five patients who had 2+ time points, with the

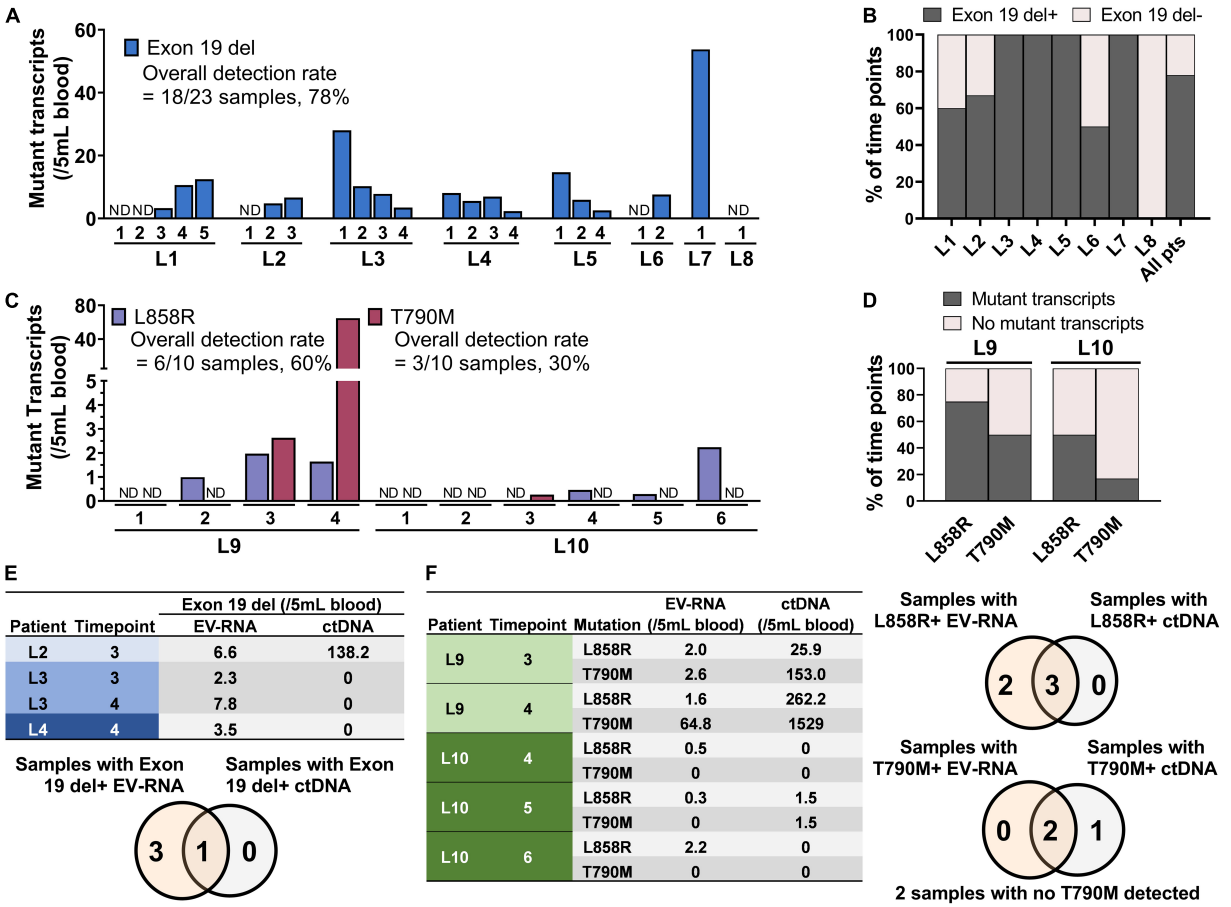

FIGURE 3 | Detection of EGFR mutations in EV-RNA samples from metastatic NSCLC patients. **(A)** EGFR exon 19 del transcript concentration per time point for the eight patients pre-identified as being exon 19 del positive. **(B)** Percent of time points that tested positive for EGFR exon 19 del mutations per patient. **(C)** Mutant EV-RNA concentration for both L858R and T790M mutations across time points for two patients. **(D)** Percent of time points that tested positive for L858R and T790M mutations by patient. **(E,F)** Comparative concentration of EGFR mutations found in ctDNA and EV-RNA along with Venn diagrams displaying the overlap in samples with detected mutations in EV-RNA and ctDNA for **(E)** four samples with known exon 19 del mutations and **(F)** five samples with known L858R and T790M mutations.

definition of mirroring being shown in **Figure 4A**. Patients ranged from having 67% to 100% of time points where EV-RNA mutation burden mirrored disease trajectory, **Figure 4D**. When quantitatively compared, the change in exon 19 del EV-RNA transcripts (ΔEV-RNA) between time points is significantly lower for patients who are stable compared to progressing (*p*-value = 0.0059), **Figure 4E**. Conversely, the two patients with L858R/T790M mutations saw 33 and 40% mirrored time points for L858R EV-RNA and 67 and 60% mirroring for T790M EV-RNA, **Figure 4F**. It is important to note that for both point mutations, especially for T790M, the detection rate was low, therefore conclusions cannot be accurately drawn about the relationship between ΔEV-RNA burden and disease progression. As a comparison, absolute quantity of EV mutation burden was quantified between stable and progressing time points for both all mutations summed and each individual mutation. It was found that the absolute EV-RNA mutation burden is not significantly different between the stable and progressing time points, **Supplementary Figure 6**. Therefore, it is critical to use the change in EV-RNA mutation burden within each individual patient as a determinant of disease status.

DISCUSSION

Using ddPCR and western blots, EVs isolated from lung cancer patient plasma were analyzed for EGFR mutations. In this pilot study, the utility of EV-RNA and EV-protein is demonstrated to not only screen for the presence of mutations, but to dynamically monitor patient disease status. Mutant EV-RNA was detected in 9/10 patients, and for 6/7 patients who were longitudinally monitored, mutant EV-RNA burden mirrored clinical trajectory. Within patients who had exon 19 del, ΔEV-RNA mutation burden strongly indicated disease trajectory, demonstrating that a single time point may be insufficient to assess patient status. The power of liquid biopsies enabled multiple time points from each patient to be collected.

While evidence from this pilot study suggests the rate of increase in EV-RNA mutation burden may be linked with progression severity, larger studies are needed to investigate this. For the patients with exon 19 deletion, both patients who had consistent progressive disease succumbed to their disease and are now deceased. These patients had a similarly consistent increase in EV-RNA mutation burden. Conversely, the three patients with decreasing EV-RNA exon 19 del burden have remained clinically stable for an average of 192 ± 9 days after the final blood draw. These patients saw consistently decreasing EV-RNA mutation burden that mirrored their stable disease status. This was further highlighted by the finding that there is a significant difference in the exon 19 del ΔEV-RNA burden between time points between stable and progressing patients. These results indicate that changes in EV-RNA mutant burden may be an early indicator of clinical stability and perhaps even indicate disease progression before clinical monitoring methods.

Of the two patients with L858R/T790M mutations, one patient's EV-RNA burden mirrored disease trajectory, while the other did not. L9 has had sustained progressive disease 87 days after the final blood draw. Conversely, L10, after switching from a TKI to chemotherapy between visits 4 and 5, has remained clinically stable for 133 days after the final blood draw, despite an increase in L858R EV-RNA. The change from TKI therapy to chemotherapy during this study could impact the utility of targetable mutations carried in EV-RNA for patient monitoring. Without the use of TKIs specifically targeting mutant EGFR, an increase mutant burden may not indicate treatment resistance in the tumor. Therefore, while EV-RNA may mirror disease trajectory for patients receiving targeted therapy, this may not extend to patients receiving other treatment types, such as chemotherapy and further studies are needed to investigate this.

Additional studies with larger cohorts are needed to validate these findings, however, this study presents initial evidence that

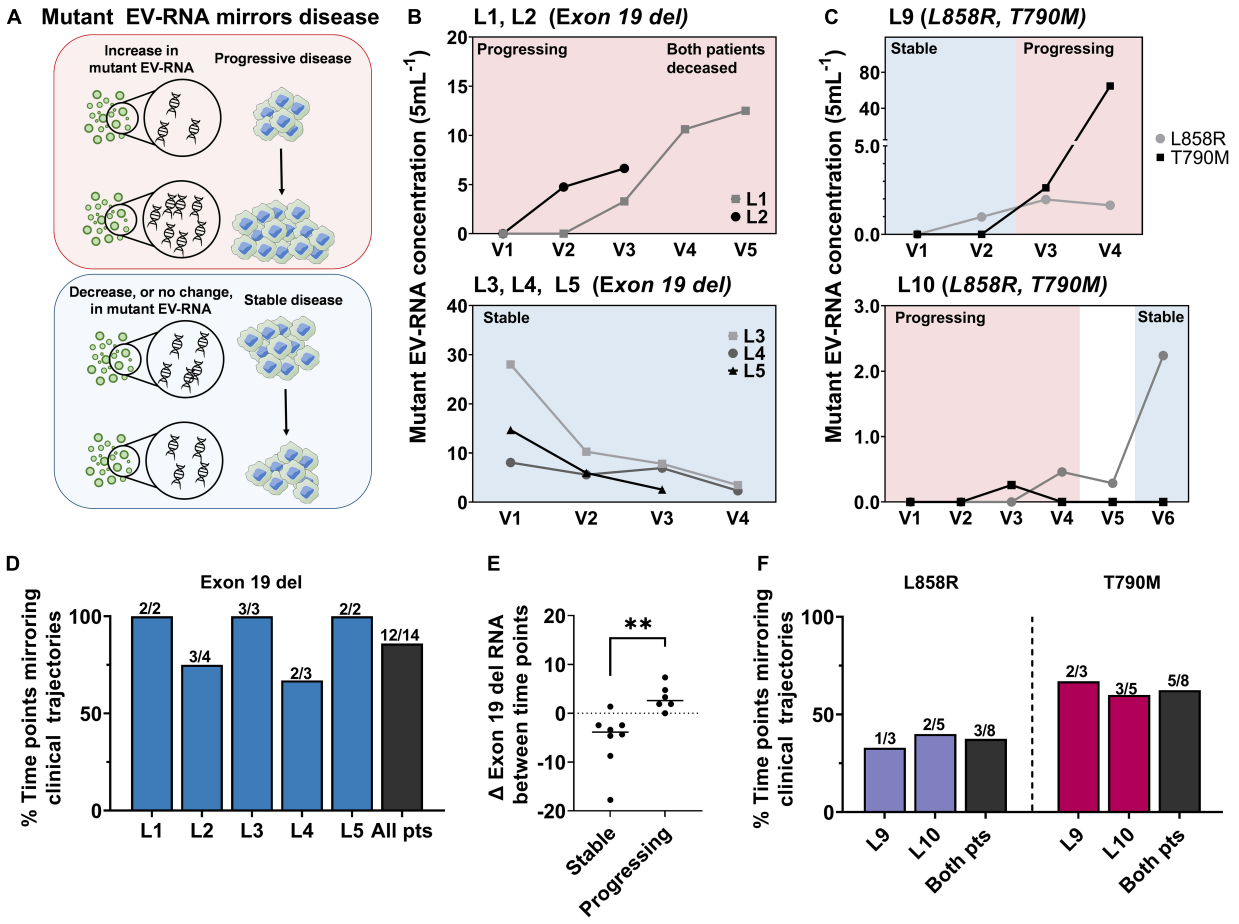

FIGURE 4 | Changes in EGFR mutation burden in EV-RNA mirror disease status. **(A)** Schematic demonstrating EV-RNA mirroring disease status. An increase in mutant EV-RNA mirrors progressive disease, while a decrease or no change in EV-RNA would mirror stable disease. **(B)** Mutant EV-RNA concentration for exon 19 del patients across multiple visits for patients with consistently progressive (top) or consistently stable (bottom) disease. **(C)** Mutant EV-RNA concentration for L858R/T790M in divergent patients, L9 (top) and L10 (bottom) across multiple visits. **(D)** Percent of EV-RNA samples drawn at a time point when EV-RNA mutation burden mirrors disease status for patients with exon 19 del. **(E)** Change (Δ) exon 19 deletion mutation burden in EV-RNA between time points for patients who are clinically stable compared to progressing, p-value = 0.0059 using an unpaired t-test. **(F)** Percent of EV-RNA samples drawn at a time point when EV-RNA mutation burden mirrors disease status for patients with L858R and T790M mutations. $^{**}p$-value ≤ 0.01.

increase in EV-RNA indicates progression for patients receiving targeted therapy. Future studies are needed to determine if EV-RNA can be used to detect progression prior to current techniques. Of interest, L6, only had two time points collected but saw an upward trend in their burden despite being clinically stable thus far, **Supplementary Table 2**. The preliminary findings presented here warrant a recommendation that the clinical trajectory of this patient should closely be monitored for indicators of disease progression.

While EV-protein was detected in samples from four patients, there was not an observed correlation between EV-protein burden and EV-RNA burden and there were too few patients to make assessments of correlation to disease. This could be due to the differences in EV packing of RNA cargo to protein cargo, which are largely poorly understood, especially in the ever-changing physiological states found during cancer immunotherapies. Beyond EV packaging differences, interestingly, previous studies in cell lines have shown that when exposed to TKIs, EGFR mutations result in differential protein stability compared to wildtype (Ray et al., 2016); Treatment with the TKI erlotinib led to protein degradation in a mutant dependent manner, without significantly changing the transcriptomic expression. Additionally, osimertinib, the primary TKI the patients in this study were receiving, has been suggested to reduce protein stability in both wildtype and T790M mutant EGFR. The decreased stability of EGFR protein due to TKI treatment could lead to increased cellular protein turnover thereby either (1) reducing the amount of protein packaged into EVs or (2) leading to increased degradation of either cellular protein or EV-protein, both of which would reduce the quality of the proteins found in EVs, as seen in this study (Ray et al., 2016). To answer this question, future studies could investigate the ratio of EGFR wildtype to EGFR mutated protein found within specifically tumor derived EVs through treatment to elucidate the stability of these mutated proteins. Further studies will need to be performed to elucidate information about the mutated protein found in EVs.

Liquid biopsies hold the potential to address spatial heterogeneity and longitudinal monitoring limitations. However, the only FDA-approved liquid biopsy test, the Cobas v2, for mutation detection, relies on ctDNA. While capable at detecting the presence of new mutations, this test is still currently considered a "rule in" test, with the recommendation of a tissue biopsy to confirm a mutant negative result (Odogwu et al., 2018). Compared to ctDNA, EVs demonstrated a more robust detection of exon 19 del and L858R point mutation, and similar detection rates for the point mutation T790M, **Figures 4E,F**. To avoid splitting the sample or using pre-amplification steps, this study screened solely for EGFR mutations detected by tumor biopsy, therefore future studies are needed to expand further to screening for mutations in EV-RNA not originally detected by tumor biopsy. By instead using EVs, liquid biopsy mutation screening has the potential to advance beyond the current "rule in" test.

This work lays the groundwork for future studies to establish the utility of mutations found in EV cargo for patient care. In this novel proof of concept study, EVs were screened for previously identified EGFR mutations carried by each patient. Changes in EV-RNA correlated with disease trajectory; however, the clinical implications of EV-protein remain unclear. The utility of EV mutation monitoring warrants further investigations across additional mutations and cancer types. Further, the dual analysis of EV-derived cargo has the potential to go beyond monitoring and be used in lieu of a tumor biopsy for non-invasive screening for both sensitizing and resistance mutations in EGFR across a patient's treatment course. This minimally invasive approach could be integrated into the standard of care enable more rapid identification of treatment resistance and allow for timely treatment changes, overall improving patient care.

MATERIALS AND METHODS

Cell Culture

H1975, H3255, and H1650 cells were grown in RPMI-1640 (Gibco) supplemented with 10% fetal bovine serum (FBS) (Sigma-Aldrich) and 1% Antibiotic-antimycotic (Gibco). Cells were grown to 80% confluence before subculturing using 0.05% Trypsin-EDTA (Gibco). To prepare extracellular vesicles, cells were seeded at 3,000,000 cells/100 mm dish (Sarstedt) in complete media. 24 h after seeding, cells were washed three times with phosphate-buffered saline (PBS) pH 7.4 (Gibco) and incubated for 72 h in serum-free RPMI-1640 media (Gibco). Cell culture media (CCM) was centrifuged at 2,000 × *g* for 15 min and frozen at −20°C.

Patient Enrollment

All blood was collected following IRB (HUM00119934) approval, and all patients gave their informed, written consent to participate in the study. All patients had metastatic lung adenocarcinoma. The cohort of patients in this study had known EGFR mutations.

Blood Preparation

Plasma was prepared for EV isolation using one of the following three methods and was stored in the −80°C freezer until use.

Plasma prep 1 (Ficoll): Whole blood was collected in EDTA tubes. Samples were prepared using Ficoll-Paque^{TM} PLUS (GE Healthcare) following the manufacturer's protocol. The plasma and leukocyte layers were collected for CTC isolation and effluents were centrifuged following the plasma prep 3 protocol.

Plasma prep 2 (Dextran): Whole blood was collected in EDTA tubes. 1 mL of 6% dextran solution (w/v) was mixed into 5 mL whole blood. The sample sat 1–1.5 h at room temperature to allow the red blood cells sedimentation. The supernatant was collected for CTC isolation and the effluent was centrifuged following the plasma prep 3 protocol.

Plasma prep 3: Whole blood was collected in EDTA tubes was centrifuged at 2,000 × *g* for 15 min at room temperature. The plasma supernatant was collected and frozen at −20°C for up to 30 days.

Extracellular Vesicle Isolation Using Differential and Ultracentrifugation

Plasma prep or CCM was centrifuged at 12,000 × *g* for 20 min to remove cellular debris. The supernatant was then ultracentrifuged at 100,000 × *g* for 90 min to pellet the EVs using 36 mL Polyethylene terephthalate (PET) tubes (Thermo Fisher Scientific). Excess tube volume was filled with sterile PBS pH 7.4 (Gibco). The extracellular vesicle-pellet was washed with PBS and centrifuged at 100,000 × *g* for 90 min. Extracellular vesicles were suspended in 100 μL PBS pH 7.4 or RIPA with protease inhibitor cocktail (Thermo Fisher Scientific) and frozen at −20°C. EVs stored in PBS were then used for nanoparticle tracking analysis along with RNA extraction and characterization, while EVs in RIPA were used for western blot analysis.

Extracellular Vesicle Quantification

Following isolation, extracellular vesicles were quantified for size and concentration using NTA using Malvern's NanoSight. Quantification was performed using five-30 s runs at a flow rate of 20 using the brightness setting of 15. The camera detection was set to a level of 4 for all runs. Runs were then averaged with the average and standard deviation between the runs being reported.

RNA Extraction and Reverse Transcription

Ultracentrifuged extracellular vesicles were lysed using TRIzol™ Reagent (TRIzol) (Invitrogen) at a 1:10 ratio of extracellular vesicle suspension to TRIzol and incubated at room temperature for 5 min. A 1:5 ratio of chloroform (Sigma-Aldrich) to TRIzol was added and briefly vortexed to mix, then incubated for 2–3 min at room temperature. The sample was centrifuged at 12,000 × *g* for 15 min. The aqueous phase was collected and mixed in a 1:1 ratio with 70% ethanol (Sigma-Aldrich). Total RNA was purified using the Norgen Single Cell RNA isolation kit (Norgen Biotek Corp.). cDNA was prepared using SuperScript IV VILO Master Mix with ezDNase Enzyme (Invitrogen) following the manufacturer's protocol. All purified RNA and cDNA products were handled in a PCR workstation to prevent contamination.

RT-qPCR

Twenty microliter TaqMan™ gene expression PCR reactions were prepared using TaqMan™ Fast Advanced Master Mix (Applied Biosystems) in 96-well MicroAmp Fast Optical Plates (Applied Biosystems) and processed on a QuantStudio 3 (Applied Biosystems) using fast cycling conditions. Each mRNA: sample pair was analyzed in technical triplicates.

TaqMan™ gene expression assay IDs

Gene	Assay ID
ACTB	Hs01060665_g1
GAPDH	Hs03929097_g1

Cell-Free DNA Extraction

Cell-free DNA (cfDNA) was isolated from the plasma using the QIAamp Circulating Nucleic Acid Kit (Qiagen) following the manufacturer's processing protocol. cfDNA was eluted into 15 μL for ddPCR mutation detection.

Mutation Detection by Droplet Digital PCR

Epidermal growth factor receptor mutations were identified by using RainDrop™ ddPCR (RainDance Technologies). In brief 25 μL reactions were prepared using TaqMan™ SNP Assay (Life Technologies), 2x TaqMan Genotyping Master Mix (Applied Biosystems), and droplet stabilizer (RainDance Technologies). Maximum cDNA was loaded into each dPCR reaction. The PCR reaction was loaded onto the Source Chip (RainDance Technologies) to for droplet generation and collected into an 8-tube PCR strip (Axygen). The PCR tubes were transferred to the thermocycler for 45 rounds of PCR amplification (Bio-Rad). The PCR tubes, containing the samples, were then transferred onto the Sense Machine (RainDance Technologies) where the fluorescence intensity of each droplet was measured.

For the point mutations, L858R and T790M, mutations were considered present based on the detection of one or more positive droplets within the pre-established gates based on positive EV-RNA controls. For exon 19 del, deletions were considered present based on the detection of one or more positive droplets above the threshold. A threshold for detection was determined based on the number of false positive droplets detected using EV-RNA negative controls. The maximum number of false positive droplets detected in any negative control (16 droplets) was used as the threshold for detection. All presented data is represented as the threshold subtracted from the total number of mutant positive droplets counted and any further normalization specified in the respective figure.

TaqMan™ EGFR mutation detection assay IDs

Gene	Assay ID
L858R	AHRSRSV
T790M	AHRSROS
Exon 19 deletion	Hs00000228_mu

Protein Extraction, Quantification, Normalization

Extracellular vesicles were isolated from ultracentrifugation into 150 μL RIPA buffer (Thermo Fisher Scientific, cat #89900), protein concentration was measured by Micro BCA™ Protein Assay Kit (Thermo Fisher Scientific cat #23235). Western blot loading was normalized by using 5 mL blood volume for extracellular vesicle isolation, loading the maximum protein (37.5 μL) in each lane, and using Bio-Rad's Stain Free gels to allow normalization. Briefly, the protein was separated at 250 V for 30 min. Semi-dry transfer was then performed using Trans-Blot Turbo Transfer System (Bio-Rad) to a high fluorescence PVFD membrane (Bio-Rad, cat #1620261). The membrane was imaged using Bio-Rad's ChemiDoc to quantify total protein per lane. The membrane was blocked and incubated overnight with

primary antibody in 5 mL of 5% bovine serum albumin (Sigma-Aldrich) in Tris Buffered Saline (TBS) (Bio-Rad) with 1% Tween 20 (Sigma-Aldrich) (TBST). The membrane was then washed thoroughly before incubating with HRP-secondary antibody in 3% non-fat milk in TBST for 90 min followed again by additional washes. Measurement was performed using SuperSignal™ West Pico PLUS Chemiluminescent Substrate (Bio-Rad, Cat #34579) and SuperSignal West Femto (Thermo Fisher Scientific, cat #34096) and imaged on the ChemiDoc.

Antibodies used for Western Blot

Target	Dilution	Catalog number (Cell Signaling)
CD9	1:1000	#13174
ACTB	1:1000	#4970
GAPDH	1:1000	#5174S
Calnexin	1:1000	#2679
EGF Receptor L858R Mutant Specific	1:1000	#3197
EGF Receptor exon 19 E746-A750 del specific	1:1000	#2085
Anti-rabbit IgG, HRP-linked Antibody	1:1500	#7074S

Normalization was performed following Bio-Rad's Stain Free Gel analysis protocols. Briefly, following protein separation and transfer, the blot is imaged using Bio-Rad's Stain Free Blot imaging setting to capture the total protein per lane. Using Bio-Rad's Image Lab 6.0.1 software, the total protein in each lane is compared and a normalization coefficient determined. After blotting for specific proteins, each band is compared to the total protein of the lane, adjusted using the normalization coefficient, and quantified as a Normalized Protein Intensity.

Statistical Analysis

All analysis was performed in GraphPad Prism V9. *P* values were calculated using unpaired, two tailed, *t*-tests.

DATA AVAILABILITY STATEMENT

The original contributions presented in the study are included in the article/**Supplementary Material**, further inquiries can be directed to the corresponding author.

ETHICS STATEMENT

The studies involving human participants were reviewed and approved by the University of Michigan Institutional Review Board #HUM00119934. The patients/participants provided their written informed consent to participate in this study.

AUTHOR CONTRIBUTIONS

EPu and SO designed the study, interpreted the data, and co-wrote the manuscript. EPu, AR, NC, and CS developed the protocols and performed the western blots and NTA. SO and EPr performed the ddPCR experiments. T-WL performed the SEM. MZ reserved the CTC isolation effluent for use in this study. NR and SN oversaw the study, managed ethical patient enrollment and sample collection, and revised the manuscript. All authors contributed to the article and approved the submitted version.

FUNDING

This work was supported in part by grants from the National Institutes of Health (NIH) (5-R33-CA-202867-02 to SN and NR and U01CA210152, 1-R01-CA-208335-01-A1 to SN). SO was supported by the National Science Foundation (NSF) (DGE 1256260) and EPu was supported by the National Institutes of Health (NIH) (NIH-MBSTP T32 EB005582). The authors acknowledge the financial support of the University of Michigan College of Engineering and NSF grant #DMR-0320740, and technical support from the Michigan Center for Materials Characterization.

ACKNOWLEDGMENTS

The authors would like to thank the Dipankar Ray Laboratory at the University of Michigan for their generous gift of the H3255 lung cancer cell line. The authors would also like to thank Yoon-Tae Kang for his valuable feedback on the manuscript.

SUPPLEMENTARY MATERIAL

The Supplementary Material for this article can be found online at: https://www.frontiersin.org/articles/10.3389/fcell.2021.724389/full#supplementary-material

REFERENCES

Alix-Panabières, C., and Pantel, K. (2016). Clinical applications of circulating tumor cells and circulating tumor DNA as liquid biopsy. *Cancer Discov.* 6, 479–491. doi: 10.1158/2159-8290.CD-15-1483

Balak, M. N., Gong, Y., Riely, G. J., Somwar, R., Li, A. R., Zakowski, M. F., et al. (2006). Novel D761Y and common secondary T790M mutations in epidermal growth factor receptor-mutant lung adenocarcinomas with acquired resistance to kinase inhibitors. *Clin. Cancer Res.* 12, 6494–6501. doi: 10.1158/1078-0432.ccr-06-1570

Castellanos-Rizaldos, E., Grimm, D. G., Tadigotla, V., Hurley, J., Healy, J., Neal, P. L., et al. (2018). Exosome-based detection of EGFR T790M in plasma from non–small cell lung cancer patients. *Clin. Cancer Res.* 24, 2944–2950.

Chen, W. W., Balaj, L., Liau, L. M., Samuels, M. L., Kotsopoulos, S. K., Maguire, C. A., et al. (2013). Beaming and droplet digital pcr analysis of mutant idh1 mrna in glioma patient serum and cerebrospinal fluid extracellular vesicles. *Mol. Ther. Nucleic Acids* 2:e109. doi: 10.1038/mtna.2013.28

Clark, J., Cools, J., and Gilliland, D. G. (2005). EGFR inhibition in non-small cell lung cancer: resistance, once again, rears its ugly head. *PLoS Med.* 2:e75. doi: 10.1371/journal.pmed.0020075

Collisson, E. A., Campbell, J. D., Brooks, A. N., Berger, A. H., Lee, W., Chmielecki, J., et al. (2014). Comprehensive molecular profiling of lung adenocarcinoma: the cancer genome atlas research network. *Nature* 511, 543–550. doi: 10.1038/nature13385

Diehl, F., Li, M., Dressman, D., He, Y., Shen, D., Szabo, S., et al. (2005). Detection and quantification of mutations in the plasma of patients with colorectal tumors. *Proc. Natl. Acad. Sci. U. S. A.* 102, 16368–16373. doi: 10.1073/pnas.0507904102

Dong, J., Zhang, R. Y., Sun, N., Smalley, M., Wu, Z., Zhou, A., et al. (2019). Bio-inspired NanoVilli chips for enhanced capture of tumor-derived extracellular vesicles: toward non-invasive detection of gene alterations in non-small cell lung cancer. *ACS Appl. Mater. Interfaces* 11, 13973–13983.

Eisenhauer, E. A., Therasse, P., Bogaerts, J., Schwartz, L. H., Sargent, D., Ford, R., et al. (2009). New response evaluation criteria in solid tumours: revised RECIST guideline (version 1.1). *Eur. J. Cancer* 45, 228–247. doi: 10.1016/j.ejca.2008.10.026

Figueroa, J. M., Skog, J., Akers, J., Li, H., Komotar, R., Jensen, R., et al. (2017). Detection of wild-Type EGFR amplification and EGFRvIII mutation in CSF-derived extracellular vesicles of glioblastoma patients. *Neuro. Oncol.* 19, 1494–1502. doi: 10.1093/neuonc/nox085

Gauthier, V. J., Tyler, L. N., and Mannik, M. (1996). Blood clearance kinetics and liver uptake of mononucleosomes in mice. *J. Immunol.* 156, 1151–1156.

Gilda, J. E., and Gomes, A. V. (2013). Stain-free total protein staining is a superior loading control to b-actin for Western blots. *Anal. Biochem.* 440, 186–188.

Hur, J. Y., Lee, J. S., Kim, I. A., Kim, H. J., Kim, W. S., Lee, K. Y., et al. (2019). Extracellular vesicle-based EGFR genotyping in bronchoalveolar lavage fluid from treatment-naive non-small cell lung cancer patients. *Transl. Lung Cancer Res.* 8, 1051–1060. doi: 10.21037/tlcr.2019.12.16

Jahr, S., Hentze, H., Englisch, S., Hardt, D., Fackelmayer, F. O., Hesch, R. D., et al. (2001). DNA fragments in the blood plasma of cancer patients: quantitations and evidence for their origin from apoptotic and necrotic cells. *Cancer Res.* 61, 1659–1665.

Jin, Y., Chen, K., Wang, Z., Wang, Y., Liu, J., Lin, L., et al. (2016). DNA in serum extracellular vesicles is stable under different storage conditions. *BMC Cancer* 16:753. doi: 10.1186/s12885-016-2783-2

Kang, Q., Henry, N. L., Paoletti, C., Jiang, H., Vats, P., Chinnaiyan, A. M., et al. (2016). Comparative analysis of circulating tumor DNA stability In K3EDTA, streck, and cellsave blood collection tubes. *Clin. Biochem.* 49, 1354–1360. doi: 10.1016/j.clinbiochem.2016.03.012

Kang, Y. T., Purcell, E., Hadlock, T., Lo, T. W., Mutukuri, A., Jolly, S., et al. (2019). Multiplex isolation and profiling of extracellular vesicles using a microfluidic DICE device. *Analyst* 144, 5785–5793. doi: 10.1039/c9an01235d

Kanwar, S. S., Dunlay, C. J., Simeone, D. M., and Nagrath, S. (2014). Microfluidic device (ExoChip) for on-chip isolation, quantification and characterization of circulating exosomes. *Lab. Chip.* 14, 1891–1900. doi: 10.1039/c4lc00136b

Krug, A. K., Enderle, D., Karlovich, C., Priewasser, T., Bentink, S., Spiel, A., et al. (2018). Improved EGFR mutation detection using combined exosomal RNA and circulating tumor DNA in NSCLC patient plasma. *Ann. Oncol.* 29, 2143. doi: 10.1093/annonc/mdy261

Kustanovich, A., Schwartz, R., Peretz, T., and Grinshpun, A. (2019). Life and death of circulating cell-free DNA. *Cancer Biol. Ther.* 20, 1057–1067. doi: 10.1080/15384047.2019.1598759

Liam, C. K., Liam, Y. S., and Wong, C. K. (2020). Extracellular vesicle-based EGFR genotyping in bronchoalveolar lavage fluid. *Transl. Lung Cancer Res.* 9, 168–171.

Lobb, R. J., Hastie, M. L., Norris, E. L., van Amerongen, R., Gorman, J. J., and Möller, A. (2017). Oncogenic transformation of lung cells results in distinct exosome protein profile similar to the cell of origin. *Proteomics* 17:1600432. doi: 10.1002/pmic.201600432

National Comprehensive Cancer Network (NCCN)/NCCN Foundation (2020). *CCN Clinical Practice Guidelines in Oncology (NCCN Guidelines) for Non-Small Cell Lung Cancer (NSCLC), Version 3*. Plymouth Meeting, PA: National Comprehensive Cancer Network, Inc.

Odogwu, L., Mathieu, L., Goldberg, K. B., Blumenthal, G. M., Larkins, E., Fiero, M. H., et al. (2018). Benefit-risk assessment of osimertinib for the treatment of metastatic non-small cell lung cancer harboring epidermal growth factor receptor T790M mutation. *Oncologist* 23, 353–359. doi: 10.1634/theoncologist.2017-0425

Owen, S., Wen Lo, T., Fouladdel, S., Zeinali, M., Keller, E., Azizi, E., et al. (2020). Simultaneous single cell gene expression and EGFR mutation analysis of circulating tumor cells reveals distinct phenotypes in NSCLC. *Adv. Biosyst.* 2000110, 1–11.

Pao, W., Miller, V. A., Politi, K. A., Riely, G. J., Somwar, R., Zakowski, M. F., et al. (2005). Acquired resistance of lung adenocarcinomas to gefitinib or erlotinib is associated with a second mutation in the EGFR kinase domain. *PLoS Med.* 2:e73. doi: 10.1371/journal.pmed.0020073

Pasini, L., Notarangelo, M., Vagheggini, A., Burgio, M. A., Crinò, L., Chiadini, E., et al. (2021). Unveiling mutational dynamics in non-small cell lung cancer patients by quantitative EGFR profiling in vesicular RNA. *Mol. Oncol.* 15, 2423–2438. doi: 10.1002/1878-0261.12976

Patel, G. K., Khan, M. A., Zubair, H., Srivastava, S. K., Khushman, M., Singh, S., et al. (2019). Comparative analysis of exosome isolation methods using culture supernatant for optimum yield, purity and downstream applications. *Sci. Rep.* 9, 1–10.

Rabinowits, G., Gerçel-Taylor, C., Day, J. M., Taylor, D. D., and Kloecker, G. H. (2009). Exosomal microRNA: a diagnostic marker for lung cancer. *Clin. Lung Cancer* 10, 42–46. doi: 10.3816/clc.2009.n.006

Ray, P., Tan, Y. S., Somnay, V., Mehta, R., Sitto, M., Ahsan, A., et al. (2016). Differential protein stability of EGFR mutants determines responsiveness to tyrosine kinase inhibitors. *Oncotarget* 19, 68597–68613. doi: 10.18632/oncotarget.11860

Rivero-Gutiérrez, B., Anzola, A., Martínez-Augustin, O., and De Medina, F. S. (2014). Stain-free detection as loading control alternative to Ponceau and housekeeping protein immunodetection in Western blotting. *Anal. Biochem.* 467, 1–3. doi: 10.1016/j.ab.2014.08.027

Tang, Y. T., Huang, Y. Y., Zheng, L., Qin, S. H., Xu, X. P., An, T. X., et al. (2017). Comparison of isolation methods of exosomes and exosomal RNA from cell culture medium and serum. *Int. J. Mol. Med.* 40, 834–844. doi: 10.3892/ijmm.2017.3080

Thakur, B. K., Zhang, H., Becker, A., Matei, I., Huang, Y., Costa-Silva, B., et al. (2014). Double-stranded DNA in exosomes: a novel biomarker in cancer detection. *Cell Res.* 24, 766–769. doi: 10.1038/cr.2014.44

Théry, C. (2011). Exosomes: secreted vesicles and intercellular communications. *Biol. Rep.* 3:15.

Théry, C., Clayton, A., Amigorena, S., Raposo, G., and Clayton, A. (2006). Isolation and characterization of exosomes from cell culture supernatants. *Curr. Protoc. Cell Biol. Chapter* 3, 1–29.

Théry, C., Witwer, K. W., Aikawa, E., Alcaraz, M. J., Anderson, J. D., Andriantsitohaina, R., et al. (2018). Minimal information for studies of extracellular vesicles 2018 (MISEV2018): a position statement of the international society for extracellular vesicles and update of the MISEV2014 guidelines. *J. Extracell. Vesicles* 7:1535750. doi: 10.1080/20013078.2018.1535750

Zhang, Y. L., Yuan, J. Q., Wang, K. F., Fu, X. H., Han, X. R., Threapleton, D., et al. (2016). The prevalence of EGFR mutation in patients with non-small cell lung cancer: a systematic review and meta-analysis. *Oncotarget* 7, 78985–78993. doi: 10.18632/oncotarget.12587

Conflict of Interest: The authors declare that the research was conducted in the absence of any commercial or financial relationships that could be construed as a potential conflict of interest.

Publisher's Note: All claims expressed in this article are solely those of the authors and do not necessarily represent those of their affiliated organizations, or those of the publisher, the editors and the reviewers. Any product that may be evaluated in this article, or claim that may be made by its manufacturer, is not guaranteed or endorsed by the publisher.

frontiers in Cell and Developmental Biology

MINI REVIEW
published: 08 October 2021
doi: 10.3389/fcell.2021.746432

Tumor-Derived Extracellular Vesicles: A Means of Co-opting Macrophage Polarization in the Tumor Microenvironment

*Theodore Reed, Jeffrey Schorey and Crislyn D'Souza-Schorey**

Department of Biological Sciences, University of Notre Dame, Notre Dame, IN, United States

Extracellular vesicles (EVs) are a heterogeneous population of membrane-bound parcels of bioactive proteins, nucleic acids, and lipids released from almost all cell types. The diversity of cargo packaged into EVs proffer the induction of an array of effects on recipient cells. EVs released from tumor cells have emerged as a vital means of communication and immune modulation within the tumor microenvironment (TME). Macrophages are an important contributor to the TME with seemingly paradoxical roles promoting either pro- or anti-tumoral immune function depending on their activated phenotypes. Here, we discuss the influence of tumor-derived extracellular vesicles on the functional plasticity of macrophages in tumor progression.

Keywords: extracellular vesicles, tumor microenvironment, intercellular communication, macrophages, polarization

OPEN ACCESS

Edited by:
Jeffrey David Galley, The Ohio State University, United States

Reviewed by:
Paolo Paganetti, Ente Ospedaliero Cantonale (EOC), Switzerland
Ronny Drapkin, University of Pennsylvania, United States

****Correspondence:***
Crislyn D'Souza-Schorey
cdsouzas@nd.edu

Specialty section:
This article was submitted to Molecular and Cellular Pathology, a section of the journal Frontiers in Cell and Developmental Biology

Received: *23 July 2021*
Accepted: *20 September 2021*
Published: *08 October 2021*

Citation:
Reed T, Schorey J and D'Souza-Schorey C (2021) Tumor-Derived Extracellular Vesicles: A Means of Co-opting Macrophage Polarization in the Tumor Microenvironment. Front. Cell Dev. Biol. 9:746432. doi: 10.3389/fcell.2021.746432

INTRODUCTION

Extracellular vesicles (EVs) are a heterogeneous population of cell-derived vesicles secreted by virtually all cell types. They range in size from 15 nm to a few microns in diameter (D'Souza-Schorey and Schorey, 2018). EVs have been often been subclassified on the basis of size and/or their mode of biogenesis (Zijlstra and Di Vizio, 2018; Sheehan and D'Souza-Schorey, 2019). For example, exosomes are derived from the fusion of the multivesicular bodies with the plasma membrane and release of the intraluminal vesicles into the extracellular space, whereas microvesicles, which are larger than exosomes, are derived from outward budding and pinching of the plasma membrane. The international society for extracellular vesicles (ISEV) has provided the field with guidelines as well as nomenclature for the classification of EVs (Théry et al., 2018). The intracellular routes of EV

Abbreviations: Arf6, ADP-ribosylation factor 6; Arg-1, arginase-1; CD, cluster of differentiation; CSF-1, colony stimulating factor 1; CRC, colorectal cancer; EGCG, epigallocatechin gallate; EGF, epidermal growth factor; EV, extracellular vesicle; GBM, glioblastoma; gp130, glycoprotein 130; HCC, hepatocellular carcinoma; HSP70, heat shock protein 70; ICAM-1, intercellular adhesion molecule 1; I-κB, inhibitor of nuclear factor κB; IL, interleukin; iNOS, inducible nitric oxide synthase; IRF, interferon regulatory factor; ISEV, international society of extracellular vesicles; MCP-1, monocyte chemoattractant protein 1; MDSCs, myeloid-derived suppressor cells; MMP, matrix metalloproteinase; miRNA, microRNA; MV, microvesicle; NF-κB, nuclear factor kappa-light-chain-enhancer of activated B cells; NK cells, natural killer cells; OSCC, oral squamous cell carcinoma; PDAC, pancreatic ductal adenocarcinoma; PD-L1, programmed death ligand 1; PD-1, programmed cell death protein 1; PI3K, phosphoinositide 3 kinase; PTEN, phosphate and tensin homolog; RNA, ribonucleic acid; sEV, small extracellular vesicle; STAT3, signal transducer and activator of transcription 3; TAM, tumor associated macrophage; THBS1, thrombospondin-1; TIL, tumor infiltrating lymphocyte; TLR7, toll-like receptor 7; TME, tumor microenvironment; TNBC, triple negative breast cancer; TNF-α, tumor necrosis factor alpha; TSG101, tumor susceptibility gene 101; T_H17, helper T cell 17; Treg, regulatory T cell; VEGF, vascular endothelial growth factor.

biogenesis in many ways dictate the composition of EV subtypes. As such, various protein markers are associated with the different EV subclasses. For example, exosomes are typically identified by the presence of CD63, CD9, CD81, TSG101, and HSP70 whereas markers of microvesicles (MVs) are less well understood but can include integrin receptors, ARF6, VAMP3, and MHC Class I as well as other components of the endosomal recycling pathway involved in their formation (Clancy et al., 2019; Jeppesen et al., 2019; Sheehan and D'Souza-Schorey, 2019). Most EV subclasses are thought to be loaded with bioactive cargo ranging from nucleic acids, cytoplasmic proteins, metabolites, and components of lipid rafts (Sheehan and D'Souza-Schorey, 2019) and with the expanding knowledge of the intracellular pathways that regulate EV loading (Clancy et al., 2019; Jeppesen et al., 2019; Lee et al., 2019; Kalluri and LeBleu, 2020), the mechanisms involved in cargo delivery remain an important and active area of investigation.

Over the past decade, EVs have emerged as important mediators of horizontal intercellular communication in both prokaryotes and higher eukaryotes, inducing a plethora of physiological processes and also disease pathologies (Boomgarden et al., 2020; and references therein). In the context of cancer, where EVs have been best characterized, many of the pathways leading to EV production are usurped (Clancy and D'Souza-Schorey, 2018; Kalluri and LeBleu, 2020). In fact, tumor cells have been thought to secrete EVs to a higher level compared to the normal parent populations and further the amounts shed increase with disease stage (Ginestra et al., 1998; Bebelman et al., 2018; and references therein). The removal of EVs from circulation limits tumor growth and metastasis, substantiating the importance of EVs in tumor progression (Bobrie et al., 2012; Peinado et al., 2012; Ortiz et al., 2019; Wortzel et al., 2019). There is burgeoning interest in how these vesicles may affect recipient cells in the tumor microenvironment (TME) including cancer-associated fibroblasts, cells of the tumor vasculature and infiltrating immune cells. In particular, the effects of EV signaling on immune responses has garnered increasing attention. The functions of T and B lymphocytes, macrophages, natural killer (NK) cells, monocytes, dendritic cells, neutrophils, and myeloid-derived suppressor cells (MDSCs) are all affected by EV signaling, and depending on the status of the immune cell type, EVs might trigger adaptive immune responses or suppress inflammation (Théry et al., 2009; Sheehan and D'Souza-Schorey, 2019; Droste et al., 2020).

Macrophages are one of the most abundant immune cell types found in the TME (Gleave et al., 1991). These professional phagocytes are a part of the innate immune response and some of the first cells to arrive at the site of tissue damage or infection. Macrophages aid in clearing damaged cells and tissues while simultaneously recruiting and activating other immune cells through various mechanisms including release of cytokines and chemokines, and antigen presentation (Unanue et al., 1976). In addition to these well-known functions, macrophages are also known for secreting angiogenic factors, aid in tissue repair and remodeling, and secreting growth and migration factors (Lin et al., 2002; Wyckoff et al., 2004). While the ability of macrophages to play a role in both clearing and repair is vital to the innate immune response, in the context of tumor associated macrophages (TAMs) these roles can in fact facilitate tumor progression. Indeed, macrophages can enhance intravasation, basement membrane degradation for successful invasion, and even support tumor cell migration (Lin et al., 2002; Wyckoff et al., 2004). Macrophages within the TME have been shown to engage in paracrine activating loops wherein macrophages secrete epidermal growth factor (EGF) and matrix metalloproteinases (MMPs) in response to the secretion of colony stimulating factor 1 (CSF-1) from tumors (Lin et al., 2002; Wyckoff et al., 2004; Goswami et al., 2005; Cardoso et al., 2014). As described below, tumors have demonstrated the ability to co-opt macrophage functions in order to promote tumor progression and this modulation of macrophage function is mediated, at least in part, by EVs. In the following sections, we discuss the mechanisms by which tumor-derived EVs affect macrophage activation and its impact on tumor progression, and begin with an overview of tumor-associated macrophage (TAM) polarization.

MACROPHAGE POLARIZATION IN THE TUMOR MICROENVIRONMENT

Tumor-associated macrophages have been shown to consistently react to signals received from tumors, including directly responding to tumor-derived EVs which can trigger multiple forms of macrophage activation and polarization (Arkhypov et al., 2020). Macrophages are activated by a myriad of factors that cause them to differentiate from their original monocyte progenitor. Once differentiated, macrophages undergo a secondary process called polarization, where they can take on either a proinflammatory phenotype traditionally referred to as M1, or an anti-inflammatory phenotype which is traditionally referred to as M2 (**Figure 1**). Macrophages are able to transition between these states depending on the signals they receive (Labonte et al., 2014). In the TME, this polarization and phenotype shift can be facilitated by EVs.

M1 macrophages produce factors associated with inflammation such as TNFα, IL-1β, iNOS, reactive oxygen species, IL-1, IL-6, and IL-12 (Labonte et al., 2014). Akt2 and PI3K-mediated signaling are major drivers of M1 polarization in various cancer models (Fang et al., 2004; Arranz et al., 2012; Labonte et al., 2014; Wang et al., 2014). Additionally, the transcription factor IRF5 has been shown to be active in proinflammatory macrophages (Vergadi et al., 2017). Another common feature of M1 macrophages is inflammasome activation. The inflammasome is involved in cleavage of pro-IL-1β resulting in its release from macrophages in its activated form (Lopez-Castejon and Brough, 2011). Although M1 macrophages are primarily considered anti-tumorigenic, their potential to induce a chronic inflammatory response can promote tumor progression as discussed later in this review.

Alternatively activated macrophages, also referred to as M2 macrophages, are associated with an anti-inflammatory and immunosuppressive response (Aminin and Wang, 2021). The M2 phenotype typically arises when the cause of tissue damage has been cleared and the immune response is no longer required.

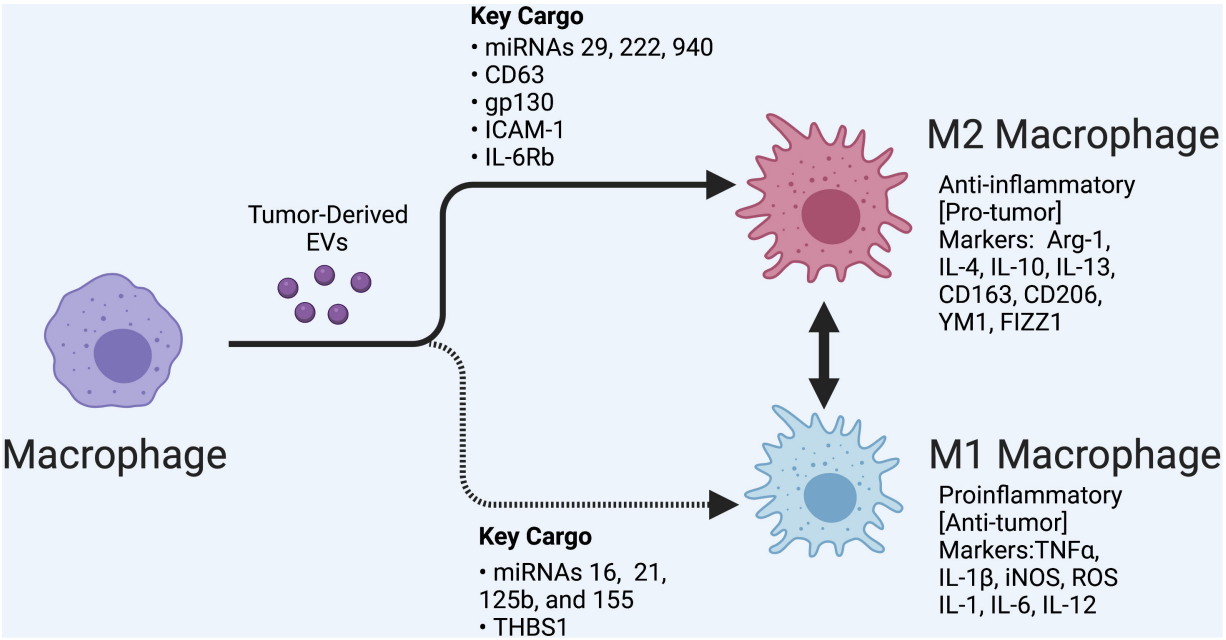

FIGURE 1 | Macrophage polarization regulated by tumor-derived extracellular vesicles (EVs). A variety of tumors release EVs that can modulate tumor-associated macrophages depending in part on their cargo, as shown. M1 and M2 subsets are shown along with classifying cell markers. EVs can also regulate the transition between these polarization states. In the tumor microenvironment, polarized states across a spectrum are likely observed. Created with BioRender.com.

The M2 phenotype can be induced directly from a circulating monocyte or by conversion of an M1 macrophage (Evans et al., 2018). The presence of M2 macrophages in the TME provides a means to limit or divert the immune response (Shields et al., 2020). Activation of Arg-1, IL-4, IL-10, IL-13, CD163, CD206, YM1, and FIZZ1 are typically used as indicators of M2 polarization (Labonte et al., 2014). There are several known signaling molecules associated with this alternate macrophage activation including PI3K/Akt1 (Arranz et al., 2012; Vergadi et al., 2017). Further, IRF4 activation has been shown to contribute to the immunosuppressive macrophage phenotype (Wang et al., 2014).

M1 POLARIZATION-MEDIATED BY EXTRACELLULAR VESICLES

Since EVs contain a multitude of bioactive cargos, it is not surprising that their release from tumors have the capacity to modulate how macrophages respond in the TME. In several different types of cancer including oral squamous cell carcinoma (OSCC), brain cancer, pancreatic ductal adenocarcinoma (PDAC), and colorectal cancer (CRC), tumor cells have been shown to directly trigger M1 polarization through their secreted EVs (Jang et al., 2013; Su et al., 2016; Shao et al., 2018; Xiao et al., 2018). Investigations have begun to elucidate a list of bioactive cargos contained within EVs that can trigger this M1 polarization in recipient macrophages. The glycoprotein thrombosondin-1 (THBS1) and miRNAs 16, 21, 125b, and 155 have been shown to be transferred to macrophages through tumor EVs and induce M1 polarization in OSCC, breast cancer, PDAC, and CRC, respectively (Jang et al., 2013; Su et al., 2016; Shao et al., 2018; Xiao et al., 2018).

M1 macrophages release various factors that can induce tumor cell death, recruit and activate additional immune cell types, and directly remodel or degrade the surrounding tissue (Najafi et al., 2019). However, while classically activated macrophages are typically considered "anti-tumor," some functions may in fact promote cancer progression. As example, immune cell recruitment can trigger inflammation in the TME and can stimulate vasodilation (Pober and Sessa, 2014) resulting in increase in blood vessel leakage and local angiogenesis creates an opportunity for tumor cells to gain access to the vascular space and thus contribute to metastatic potential. In the study performed by Xiao et al. (2018), exosomes loaded with THBS1 from OSCC were able to increase the transcription and subsequent protein secretion of typical the M1 markers TNF-α, IL-1β, and IL-6. Further, this same study showed that when conditioned media collected from macrophages previously treated with OSCC-derived EVs was added to OSCC cells it resulted in a statistically significant increase in OSCC cell migration relative to OSCC cells exposed to condition media from untreated macrophages (Xiao et al., 2018). Similarly, Shao et al. (2018) showed that small extracellular vesicles (sEVs) derived from CRC established an inflammatory, premetastatic niche for liver metastasis in part through the polarization of macrophages to an M1 phenotype. MiRNA-21 in sEVs was shown to stimulate M1 macrophages through a TLR7-mediated pathway (Shao et al., 2018). This inflammation, attributed to M1 activated macrophages, was confirmed in a retrospective

study performed on patient serum samples, ultimately linking metastasis to the upregulation of proinflammatory cytokine, IL-6 (Shao et al., 2018). Another study performed in a breast cancer model found that 4T1 breast cancer cells when treated with epigallocatechin gallate (EGCG), a catechin with known anti-tumor effects, released EVs containing miRNA-16 (Jang et al., 2013). Exosomal miRNA-16 prevents TAM infiltration and inhibits M2 polarization. The study showed that miRNA-16 mediated this activity by down regulating IKKα resulting in the suppression of NF-κB and accumulation of Iκ-B. Similar findings of were made in several other studies pertaining to M1 polarization of TAMs and are summarized in **Table 1**.

M2 POLARIZATION-MEDIATED BY EXTRACELLULAR VESICLES

M2 polarization is deemed "pro-tumor," as it has the ability to reduce inflammation and diminish immune cell activity through secretion of cytokines and other inhibitory factors (Aminin and Wang, 2021). Tumors are known to evade the immune response through several mechanisms, including recruiting/inducing tumor infiltrating lymphocytes (TILs) which have an immunosuppressive phenotype, such as M2 macrophages, T_{reg} cells, and T_H17 cells (Sakaguchi et al., 2008). EVs released from tumors, when taken up by immune cells in the TME can be the direct cause of this immune suppression. This suppression of the immune system allows tumors to evade detection and subsequent destruction. It also allows for tumor expansion through cell proliferation, which also facilitates generation of additional protumor mutations over time. In addition, expression of various checkpoint inhibitors by tumor cells can suppress the anti-tumor immune response (Russell et al., 2021). Checkpoint inhibitors on EVs released from tumors can drive this immune suppression by serving as decoys (Lawler et al., 2020). Chen et al. (2018) identifies PD-L1 on EVs using *in vivo* models as well as patient serum and showed EV PD-L1 interacting with PD-1 on CD8 T cells in a manner that inhibited T cell cytotoxic function. PD-1 has also been shown to be expressed on TAMs and is associated with increased phagocytosis, reduction of tumor size, and increased survival in mice (Gordon et al., 2017). Previous studies have shown that specific EVs can upregulate PD-L1 expression on a variety of immune cell types, including neutrophils (Zhang et al., 2020) and myeloid cells (Fleming et al., 2019). This phenomenon is also observed in macrophages. In a more recent study, Liu et al. (2015) showed that HCC cancer cells released EV-associated miRNA-23a-3p in response to endoplasmic reticulum (ER) stress which led to an increase in macrophage PD-L1 expression (Liu et al., 2020). The study demonstrated an increase in PD-L1 on macrophage cell surfaces in patient samples as well as in *in vitro* studies. Interactions between immune checkpoint receptors and ligands are an important aspect of communication within the TME and can be modulated by the release of EVs or the presence of these ligands on EVs.

Extracellular vesicles-mediated M2 polarization of macrophages has been demonstrated in models of triple negative breast cancer (TNBC), hepatocellular carcinoma (HCC), lung cancer, prostate cancer, OSCC, epithelial ovarian cancer, glioblastoma (GBM), and CRC (Li et al., 2016, 2018; Chen et al., 2017; Piao et al., 2017; Takano et al., 2017; Gabrusiewicz et al., 2018; Hsu et al., 2018). Several EV-specific cargos have been linked to this alternate activation of macrophages, including miRNAs 29, 222, and 940, CD63, gp130, ICAM-1, IL-6Rb, proteins involved in focal adhesion, proteins involved in leukocyte transendothelial migration, and cytoskeleton-centric proteins (Baig et al., 2020). In a study conducted by Piao et al. (2017), TNBC cells release CD63-containing EVs which were able to induce macrophage polarization to an M2 phenotype both *in vitro* and *in vivo*. This polarization was shown to contribute to axillary lymph node metastases in an orthotopic breast cancer model by increasing the M2 to M1 ratio. Another study demonstrated that lung cancer-derived EVs can polarize monocytes toward an M2 phenotype, which subsequently increased the oncogenic effects of macrophages through the horizontal transfer of miRNA-103a. Recipient macrophages stimulated angiogenesis in this cancer model through the targeting of PTEN and activation of the PI3 kinase as well as STAT3 signaling pathways (Hsu et al., 2018). Another study by Linton et al. (2018) found that EVs derived from PDAC and containing ICAM-1 and arachidonic acid were

TABLE 1 | Tumor-derived extracellular vesicles (EVs) and their effect on macrophage polarization based on their cargo.

Polarization	Tumor source of EVs	Key cargo	References
MI	Oral squamous cell carcinoma (OSCC)	THBS1	Xiao et al., 2018
	Breast cancer	MiRNA-16	Jang et al., 2013
	Pancreatic ductal adenocarcinoma (PDAC)	MiRNA-155, miRNA-125b	Su et al., 2016
	Colorectal cancer (CRC)	MiRNA-21	Popēna et al., 2018; Shao et al., 2018
M2	Triple negative breast cancer (TNBC)	CD63	Piao et al., 2017
	Hepatocellular carcinoma (HCC)	LncRNAs	Li et al., 2018
	Lung cancer	MiR-103a, TRIM59	Hsu et al., 2018; Liang et al., 2020; Pritchard et al., 2020
	Epithelial ovarian cancer	MiRNA-222	Ying et al., 2016
	Glioblastoma (GBM)	Focal adhesion proteins, leukocyte transendothelial migration proteins, miRNA-1246	Gabrusiewicz et al., 2018; Qian et al., 2020
	Oral squamous cell carcinoma (OSCC)	MiRNA-21, miRNA-29a-3p	Li et al., 2016; Cai et al., 2019
	Colorectal cancer (CRC)	MiRNA-203, miRNA-934	Takano et al., 2017; Wang et al., 2020; Zhao et al., 2020

able to trigger macrophages to polarize to an M2 phenotype and secrete pro-tumorigenic factors including VEGF, MCP-1, IL-6, IL-1β, MMP-9, and TNF-α. These factors are known to induce angiogenesis, lymphocyte recruitment and infiltration, tumor fibrosis, and metastasis in PDAC (Linton et al., 2018). Several additional studies, as summarized in **Table 1**, have also shown tumor-derived EVs to induce M2 polarization and tumor progression.

DISCUSSION

Macrophages are recipients of EVs released from tumors but their response is heterogeneous and dependent on the cargo of the tumor EV. EV-mediated intercellular communication within the tumor microenvironment has been shown to promote the production of tumor-promoting factors even in M1 macrophages that are classically categorized as "anti-cancer" (Pober and Sessa, 2014; Shao et al., 2018; Xiao et al., 2018). Macrophages are important in the TME based on their capacity to recruit immune cells, remodel tissues, and secrete angiogenic factors. Conditioning of macrophages mediated through EVs changes the TME in ways that can be advantageous for tumor growth and metastases. Understanding how tumor EVs co-opt macrophage function has the potential to uncover not only important information about EVs themselves but also helps broaden our understanding of tumor invasion and metastasis, potentially revealing new diagnostic or prognostic biomarkers or new targets for directed therapies. The field would also benefit from longitudinal studies pertaining to the effects of tumor derived-EVs on macrophages.

As early responders in the immune response, macrophages are extremely sensitive to their surrounding environments. M1 polarization is typically associated with clearing infections and promoting inflammation. As described above, when this function is controlled by tumors through EV secretion, macrophages characteristically referred to as anti-tumor can actually promote tumor invasion and dissemination through tissue remodeling and stimulating angiogenesis. M2 polarization has been a well-documented polarization state within tumors as this activation state aids in local immunosuppression. The conversion of M1 to M2 macrophages is well documented within the TME, and EV secretion from tumors, as described above, is a strong facilitator of this change. Thus, the M1 and M2 cell phenotype provide only a snapshot at any given point in time. Further, the phenotype of an activated macrophage is not necessarily an indicator of its function. Indeed, there is emerging evidence for even further subclassifications of macrophage polarization states as techniques such as single cell sequencing are applied to further probe the transcript and protein profiles of activated macrophages. As these profiles are revealed, new markers and subsequently new panels of assays will become available to assess macrophage content and function and better understand polarization heterogeneity. These new discoveries need to be applied to our understanding of EVs so as to paint a more complete picture of the role of EVs in modulating macrophage function within the TME.

While not discussed in this review, it is important to note that macrophages also secrete EVs within the TME that are able to drive or inhibit tumor progression (Goughnour et al., 2020; Zhang et al., 2020; Chang et al., 2021; Liu et al., 2021; Xavier et al., 2021). This cross-talk between tumors and macrophages, can result in complex paracrine and autocrine circuits that affect disease progression. Moreover, the majority of studies have done little to address the role of the different EV subpopulations. Macrophage polarization by EVs has been defined, almost exclusively through the study of either exosomes or largely undefined EVs. New insights into the specific roles of exomeres, microvesicles and oncosomes, in addition to exosomes, in macrophage polarization may generate a very different picture on the current TME/immune cell landscape. The effects of these different EVs and their cargo will require further investigation but the result of this work will provide a better understanding of how the immune system is regulated by and responds to the TME.

AUTHOR CONTRIBUTIONS

All authors listed have made a substantial, direct and intellectual contribution to the work, and approved it for publication.

FUNDING

We acknowledge support from the NIH/NCI, the Boler Foundation, The Catherine Peachey Foundation to CDS and the NIH/NIAID and the Bill and Melinda Gates Foundation to JS, for EV-related research in our laboratories.

REFERENCES

Aminin, D., and Wang, Y. M. (2021). Macrophages as a "weapon" in anticancer cellular immunotherapy. *Kaohsiung J. Med. Sci.* 37, 749–758. doi: 10.1002/kjm2.12405

Arkhypov, I., Lasser, S., Petrova, V., Weber, R., Groth, C., Utikal, J., et al. (2020). Myeloid cell modulation by tumor-derived extracellular vesicles. *Int. J. Mol. Sci.* 21:6319. doi: 10.3390/ijms21176319

Arranz, A., Doxaki, C., Vergadi, E., Martinez de la Torre, Y., Vaporidi, K., Lagoudaki, E. D., et al. (2012). Akt1 and Akt2 protein kinases differentially contribute to macrophage polarization. *Proc. Natl. Acad. Sci. U.S.A.* 109, 9517–9522. doi: 10.1073/pnas.1119038109

Baig, M. S., Roy, A., Rajpoot, S., Liu, D., Savai, R., Banerjee, S., et al. (2020). Tumor-derived exosomes in the regulation of macrophage polarization. *Inflamm. Res.* 69, 435–451. doi: 10.1007/s00011-020-01318-0

Bebelman, M. P., Smit, M. J., Pegtel, D. M., and Baglio, S. R. (2018). Biogenesis and function of extracellular vesicles in cancer. *Pharmacol. Ther.* 188, 1–11. doi: 10.1016/j.pharmthera.2018.02.013

Bobrie, A., Krumeich, S., Reyal, F., Recchi, C., Moita, L. F., Seabra, M. C., et al. (2012). Rab27a supports exosome-dependent and -independent mechanisms that modify the tumor microenvironment and can promote tumor progression. *Cancer Res.* 72, 4920–4930. doi: 10.1158/0008-5472.CAN-12-0925

Boomgarden, A. C., Sheehan, C., and D'Souza-Schorey, C. (2020). Extracellular vesicles in the tumor microenvironment: various implications in tumor

progression. *Adv. Exp. Med. Biol.* 1259, 155–170. doi: 10.1007/978-3-030-43093-1_9

Cai, J., Qiao, B., Gao, N., Lin, N., and He, W. (2019). Oral squamous cell carcinoma-derived exosomes promote M2 subtype macrophage polarization mediated by exosome-enclosed miR-29a-3p. *Am. J. Physiol. Cell Physiol.* 316, C731–C740. doi: 10.1152/ajpcell.00366.2018

Cardoso, A. P., Pinto, M. L., Pinto, A. T., Oliveira, M. I., Pinto, M. T., Gonçalves, R., et al. (2014). Macrophages stimulate gastric and colorectal cancer invasion through EGFR Y(1086), c-Src, Erk1/2 and Akt phosphorylation and smallGTPase activity. *Oncogene* 33, 2123–2133. doi: 10.1038/onc.2013.154

Chang, J., Li, H., Zhu, Z., Mei, P., Hu, W., Xiong, X., et al. (2021). microRNA-21-5p from M2 macrophage-derived extracellular vesicles promotes the differentiation and activity of pancreatic cancer stem cells by mediating KLF3. *Cell Biol. Toxicol.* doi: 10.1007/s10565-021-09597-x

Chen, G., Huang, A. C., Zhang, W., Zhang, G., Wu, M., Xu, W., et al. (2018). Exosomal PD-L1 contributes to immunosuppression and is associated with anti-PD-1 response. *Nature* 560, 382–386. doi: 10.1038/s41586-018-0392-8

Chen, X., Ying, X., Wang, X., Wu, X., Zhu, Q., and Wang, X. (2017). Exosomes derived from hypoxic epithelial ovarian cancer deliver microRNA-940 to induce macrophage M2 polarization. *Oncol. Rep.* 38, 522–528. doi: 10.3892/or.2017.5697

Clancy, J. W., Zhang, Y., Sheehan, C., and D'Souza-Schorey, C. (2019). An ARF6-exportin-5 axis delivers pre-miRNA cargo to tumour microvesicles. *Nat. Cell Biol.* 21, 856–866. doi: 10.1038/s41556-019-0345-y

Clancy, J., and D'Souza-Schorey, C. (2018). Extracellular vesicles in cancer: purpose and promise. *Cancer J.* 24, 65–69. doi: 10.1097/PPO.0000000000000306

Droste, M., Thakur, B. K., and Eliceiri, B. P. (2020). Tumor-derived extracellular vesicles and the immune system-lessons from immune-competent mouse-tumor models. *Front. Immunol.* 11:606859. doi: 10.3389/fimmu.2020.606859

D'Souza-Schorey, C., and Schorey, J. S. (2018). Regulation and mechanisms of extracellular vesicle biogenesis and secretion. *Essays Biochem.* 62, 125–133. doi: 10.1042/EBC20170078

Evans, M. A., Huang, P. J., Iwamoto, Y., Ibsen, K. N., Chan, E. M., Hitomi, Y., et al. (2018). Macrophage-mediated delivery of light activated nitric oxide prodrugs with spatial, temporal and concentration control. *Chem. Sci.* 9, 3729–3741. doi: 10.1039/c8sc00015h

Fang, H., Pengal, R. A., Cao, X., Ganesan, L. P., Wewers, M. D., Marsh, C. B., et al. (2004). Lipopolysaccharide-induced macrophage inflammatory response is regulated by SHIP. *J. Immunol.* 173, 360–366. doi: 10.4049/jimmunol.173.1.360

Fleming, V., Hu, X., Weller, C., Weber, R., Groth, C., Riester, Z., et al. (2019). Melanoma extracellular vesicles generate immunosuppressive myeloid cells by upregulating PD-L1 *via* TLR4 signaling. *Cancer Res.* 79, 4715–4728. doi: 10.1158/0008-5472

Gabrusiewicz, K., Li, X., Wei, J., Hashimoto, Y., Marisetty, A. L., Ott, M., et al. (2018). Glioblastoma stem cell-derived exosomes induce M2 macrophages and PD-L1 expression on human monocytes. *Oncoimmunology* 7:e1412909. doi: 10.1080/2162402X.2017.1412909

Ginestra, A., La Placa, M. D., Saladino, F., Cassarà, D., Nagase, H., and Vittorelli, M. L. (1998). The amount and proteolytic content of vesicles shed by human cancer cell lines correlates with their in vitro invasiveness. *Anticancer Res.* 18, 3433–3437.

Gleave, M., Hsieh, J. T., Gao, C. A., von Eschenbach, A. C., and Chung, L. W. (1991). Acceleration of human prostate cancer growth in vivo by factors produced by prostate and bone fibroblasts. *Cancer Res.* 51, 3753–3761.

Gordon, S. R., Maute, R. L., Dulken, B. W., Hutter, G., George, B. M., McCracken, M. N., et al. (2017). PD-1 expression by tumour-associated macrophages inhibits phagocytosis and tumour immunity. *Nature* 545, 495–499. doi: 10.1038/nature22396

Goswami, S., Sahai, E., Wyckoff, J. B., Cammer, M., Cox, D., Pixley, F. J., et al. (2005). Macrophages promote the invasion of breast carcinoma cells via a colony-stimulating factor-1/epidermal growth factor paracrine loop. *Cancer Res.* 65, 5278–5283. doi: 10.1158/0008-5472.CAN-04-1853

Goughnour, P. C., Park, M. C., Kim, S. B., Jun, S., Yang, W. S., Chae, S., et al. (2020). Extracellular vesicles derived from macrophages display glycyl-tRNA synthetase 1 and exhibit anti-cancer activity. *J. Extracell. Vesicles* 10:e12029. doi: 10.1002/jev2.12029

Hsu, Y. L., Hung, J. Y., Chang, W. A., Jian, S. F., Lin, Y. S., Pan, Y. C., et al. (2018). Hypoxic lung-cancer-derived extracellular vesicle microRNA-103a increases the oncogenic effects of macrophages by targeting PTEN. *Mol. Ther.* 26, 568–581. doi: 10.1016/j.ymthe.2017.11.016

Jang, J. Y., Lee, J. K., Jeon, Y. K., and Kim, C. W. (2013). Exosome derived from epigallocatechin gallate treated breast cancer cells suppresses tumor growth by inhibiting tumor-associated macrophage infiltration and M2 polarization. *BMC Cancer* 13:421. doi: 10.1186/1471-2407-13-421

Jeppesen, D. K., Fenix, A. M., Franklin, J. L., Higginbotham, J. N., Zhang, Q., Zimmerman, L. J., et al. (2019). Reassessment of exosome composition. *Cell* 177, 428–445.e18. doi: 10.1016/j.cell.2019.02.029

Kalluri, R., and LeBleu, V. S. (2020). The biology, function, and biomedical applications of exosomes. *Science* 367:eaau6977. doi: 10.1126/science.aau6977

Labonte, A. C., Tosello-Trampont, A. C., and Hahn, Y. S. (2014). The role of macrophage polarization in infectious and inflammatory diseases. *Mol. Cells* 37, 275–285. doi: 10.14348/molcells.2014.2374

Lawler, S. E., Nowicki, M. O., Ricklefs, F. L., and Chiocca, E. A. (2020). Immune escape mediated by exosomal PD-L1 in cancer. *Adv. Biosyst.* 4:e2000017. doi: 10.1002/adbi.202000017

Lee, H., Li, C., Zhang, Y., Zhang, D., Otterbein, L. E., and Jin, Y. (2019). Caveolin-1 selectively regulates microRNA sorting into microvesicles after noxious stimuli. *J. Exp. Med.* 216, 2202–2220. doi: 10.1084/jem.20182313

Li, L., Li, C., Wang, S., Wang, Z., Jiang, J., Wang, W., et al. (2016). Exosomes derived from hypoxic oral squamous cell carcinoma cells deliver miR-21 to normoxic cells to elicit a prometastatic phenotype. *Cancer Res.* 76, 1770–1780. doi: 10.1158/0008-5472.CAN-15-1625

Li, X., Lei, Y., Wu, M., and Li, N. (2018). Regulation of macrophage activation and polarization by HCC-derived exosomal lncRNA TUC339. *Int. J. Mol. Sci.* 19:2958. doi: 10.3390/ijms19102958

Liang, M., Chen, X., Wang, L., Qin, L., Wang, H., Sun, Z., et al. (2020). Cancer-derived exosomal TRIM59 regulates macrophage NLRP3 inflammasome activation to promote lung cancer progression. *J. Exp. Clin. Cancer Res.* 39:176. doi: 10.1186/s13046-020-01688-7

Lin, E. Y., Gouon-Evans, V., Nguyen, A. V., and Pollard, J. W. (2002). The macrophage growth factor CSF-1 in mammary gland development and tumor progression. *J. Mammary Gland Biol. Neoplasia* 7, 147–162. doi: 10.1023/a:1020399802795

Linton, S. S., Abraham, T., Liao, J., Clawson, G. A., Butler, P. J., Fox, T., et al. (2018). Tumor-promoting effects of pancreatic cancer cell exosomes on THP-1-derived macrophages. *PLoS One* 13:e0206759. doi: 10.1371/journal.pone.0206759

Liu, J., Fan, L., Yu, H., Zhang, J., He, Y., Feng, D., et al. (2020). Endoplasmic reticulum stress causes liver cancer cells to release exosomal miR-23a-3p and up-regulate programmed death ligand 1 expression in macrophages. *Hepatology* 70, 241–258. doi: 10.1002/hep.30607

Liu, J., Lin, P. C., and Zhou, B. P. (2015). Inflammation fuels tumor progress and metastasis. *Curr. Pharm. Des.* 21, 3032–3040. doi: 10.2174/1381612821666150514105741

Liu, Y., Lu, M., Chen, J., Li, S., Deng, Y., Yang, S., et al. (2021). Extracellular vesicles derived from lung cancer cells exposed to intermittent hypoxia upregulate programmed death ligand 1 expression in macrophages. *Sleep Breath* doi: 10.1007/s11325-021-02369-1

Lopez-Castejon, G., and Brough, D. (2011). Understanding the mechanism of IL-1β secretion. *Cytokine Growth Factor Rev.* 22, 189–195. doi: 10.1016/j.cytogfr.2011.10.001

Najafi, M., Hashemi Goradel, N., Farhood, B., Salehi, E., Nashtaei, M. S., Khanlarkhani, N., et al. (2019). Macrophage polarity in cancer: a review. *J. Cell. Biochem.* 120, 2756–2765. doi: 10.1002/jcb.27646

Ortiz, A., Gui, J., Zahedi, F., Yu, P., Cho, C., Bhattacharya, S., et al. (2019). An interferon-driven oxysterol-based defense against tumor-derived extracellular vesicles. *Cancer Cell* 35, 33–45.e6. doi: 10.1016/j.ccell.2018.12.001

Peinado, H., Alečković, M., Lavotshkin, S., Matei, I., Costa-Silva, B., Moreno-Bueno, G., et al. (2012). Melanoma exosomes educate bone marrow progenitor cells toward a pro-metastatic phenotype through MET. *Nat. Med.* 18, 883–891. doi: 10.1038/nm.2753

Piao, Y. J., Kim, H. S., Hwang, E. H., Woo, J., Zhang, M., and Moon, W. K. (2017). Breast cancer cell-derived exosomes and macrophage polarization are

associated with lymph node metastasis. *Oncotarget* 9, 7398–7410. doi: 10.18632/oncotarget.23238

Pober, J. S., and Sessa, W. C. (2014). Inflammation and the blood microvascular system. *Cold Spring Harb. Perspect. Biol.* 7:a016345. doi: 10.1101/cshperspect.a016345

Popēna, I., Âbols, A., Saulîte, L., Pleiko, K., Zandberga, E., Jēkabsons, K., et al. (2018). Effect of colorectal cancer-derived extracellular vesicles on the immunophenotype and cytokine secretion profile of monocytes and macrophages. *Cell Commun. Signal.* 16:17. doi: 10.1186/s12964-018-0229-y

Pritchard, A., Tousif, S., Wang, Y., Hough, K., Khan, S., Strenkowski, J., et al. (2020). Lung tumor cell-derived exosomes promote M2 macrophage polarization. *Cells* 9:1303. doi: 10.3390/cells9051303

Qian, M., Wang, S., Guo, X., Wang, J., Zhang, Z., Qiu, W., et al. (2020). Hypoxic glioma-derived exosomes deliver microRNA-1246 to induce M2 macrophage polarization by targeting TERF2IP via the STAT3 and NF-κB pathways. *Oncogene* 39, 428–442. doi: 10.1038/s41388-019-0996-y

Russell, B. L., Sooklal, S. A., Malindisa, S. T., Daka, L. J., and Ntwasa, M. (2021). The tumor microenvironment factors that promote resistance to immune checkpoint blockade therapy. *Front. Oncol.* 11:641428. doi: 10.3389/fonc.2021.641428

Sakaguchi, S., Yamaguchi, T., Nomura, T., and Ono, M. (2008). Regulatory T cells and immune tolerance. *Cell* 133, 775–787. doi: 10.1016/j.cell.2008.05.009

Shao, Y., Chen, T., Zheng, X., Yang, S., Xu, K., Chen, X., et al. (2018). Colorectal cancer-derived small extracellular vesicles establish an inflammatory premetastatic niche in liver metastasis. *Carcinogenesis* 39, 1368–1379. doi: 10.1093/carcin/bgy115

Sheehan, C., and D'Souza-Schorey, C. (2019). Tumor-derived extracellular vesicles: molecular parcels that enable regulation of the immune response in cancer. *J. Cell Sci.* 132:jcs235085. doi: 10.1242/jcs.235085

Shields, C. W. IV, Evans, M. A., Wang, L. L., Baugh, N., Iyer, S., Wu, D., et al. (2020). Cellular backpacks for macrophage immunotherapy. *Sci. Adv.* 6:eaaz6579. doi: 10.1126/sciadv.aaz6579

Su, M. J., Aldawsari, H., and Amiji, M. (2016). Pancreatic cancer cell exosome-mediated macrophage reprogramming and the role of microRNAs 155 and 125b2 transfection using nanoparticle delivery systems. *Sci. Rep.* 6:30110. doi: 10.1038/srep30110

Takano, Y., Masuda, T., Iinuma, H., Yamaguchi, R., Sato, K., Tobo, T., et al. (2017). Circulating exosomal microRNA-203 is associated with metastasis possibly via inducing tumor-associated macrophages in colorectal cancer. *Oncotarget* 8, 78598–78613. doi: 10.18632/oncotarget.20009

Théry, C., Ostrowski, M., and Segura, E. (2009). Membrane vesicles as conveyors of immune responses. *Nat. Rev. Immunol.* 9, 581–593. doi: 10.1038/nri2567

Théry, C., Witwer, K. W., Aikawa, E., Alcaraz, M. J., Anderson, J. D., Andriantsitohaina, R., et al. (2018). Minimal information for studies of extracellular vesicles 2018 (MISEV2018): a position statement of the international society for extracellular vesicles and update of the MISEV2014 guidelines. *J. Extracell. Vesicles* 7:1535750. doi: 10.1080/20013078.2018.1535750

Unanue, E. R., Beller, D. I., Calderon, J., Kiely, J. M., and Stadecker, M. J. (1976). Regulation of immunity and inflammation by mediators from macrophages. *Am. J. Pathol.* 85, 465–478.

Vergadi, E., Ieronymaki, E., Lyroni, K., Vaporidi, K., and Tsatsanis, C. (2017). Akt signaling pathway in macrophage activation and M1/M2 polarization. *J. Immunol.* 198, 1006–1014. doi: 10.4049/jimmunol.1601515

Wang, D., Wang, X., Si, M., Yang, J., Sun, S., Wu, H., et al. (2020). Exosome-encapsulated miRNAs contribute to CXCL12/CXCR4-induced liver metastasis of colorectal cancer by enhancing M2 polarization of macrophages. *Cancer Lett.* 474, 36–52. doi: 10.1016/j.canlet.2020.01.005

Wang, N., Liang, H., and Zen, K. (2014). Molecular mechanisms that influence the macrophage m1-m2 polarization balance. *Front. Immunol.* 5:614. doi: 10.3389/fimmu.2014.00614

Wortzel, I., Dror, S., Kenific, C. M., and Lyden, D. (2019). Exosome-mediated metastasis: communication from a distance. *Dev. Cell* 49, 347–360. doi: 10.1016/j.devcel.2019.04.011

Wyckoff, J., Wang, W., Lin, E. Y., Wang, Y., Pixley, F., Stanley, E. R., et al. (2004). A paracrine loop between tumor cells and macrophages is required for tumor cell migration in mammary tumors. *Cancer Res.* 64, 7022–7029. doi: 10.1158/0008-5472.CAN-04-1449

Xavier, C. P. R., Castro, I., Caires, H. R., Ferreira, D., Cavadas, B., Pereira, L., et al. (2021). Chitinase 3-like-1 and fibronectin in the cargo of extracellular vesicles shed by human macrophages influence pancreatic cancer cellular response to gemcitabine. *Cancer Lett.* 501, 210–223. doi: 10.1016/j.canlet.2020.11.013

Xiao, M., Zhang, J., Chen, W., and Chen, W. (2018). M1-like tumor-associated macrophages activated by exosome-transferred THBS1 promote malignant migration in oral squamous cell carcinoma. *J. Exp. Clin. Cancer Res.* 37:143. doi: 10.1186/s13046-018-0815-2

Ying, X., Wu, Q., Wu, X., Zhu, Q., Wang, X., Jiang, L., et al. (2016). Epithelial ovarian cancer-secreted exosomal miR-222-3p induces polarization of tumor-associated macrophages. *Oncotarget* 7, 43076–43087. doi: 10.18632/oncotarget.9246

Zhang, Y., Meng, W., Yue, P., and Li, X. (2020). M2 macrophage-derived extracellular vesicles promote gastric cancer progression via a microRNA-130b-3p/MLL3/GRHL2 signaling cascade. *J. Exp. Clin. Cancer Res.* 39:134. doi: 10.1186/s13046-020-01626-7

Zhao, S., Mi, Y., Guan, B., Zheng, B., Wei, P., Gu, Y., et al. (2020). Tumor-derived exosomal miR-934 induces macrophage M2 polarization to promote liver metastasis of colorectal cancer. *J. Hematol. Oncol.* 13:156. doi: 10.1186/s13045-020-00991-2

Zijlstra, A., and Di Vizio, D. (2018). Size matters in nanoscale communication. *Nat. Cell Biol.* 20, 228–230. doi: 10.1038/s41556-018-0049-8

Conflict of Interest: The authors declare that the research was conducted in the absence of any commercial or financial relationships that could be construed as a potential conflict of interest.

Publisher's Note: All claims expressed in this article are solely those of the authors and do not necessarily represent those of their affiliated organizations, or those of the publisher, the editors and the reviewers. Any product that may be evaluated in this article, or claim that may be made by its manufacturer, is not guaranteed or endorsed by the publisher.

frontiers in Cell and Developmental Biology

ORIGINAL RESEARCH
published: 11 October 2021
doi: 10.3389/fcell.2021.727370

Higher Urine Exosomal miR-193a Is Associated With a Higher Probability of Primary Focal Segmental Glomerulosclerosis and an Increased Risk of Poor Prognosis Among Children With Nephrotic Syndrome

Lixia Wang[1,2†], Jie Wang[1†], Zhimin Wang[1], Jianhua Zhou[1] and Yu Zhang[1]*

[1] Department of Pediatrics, Tongji Hospital, Tongji Medical College, Huazhong University of Science and Technology, Wuhan, China, [2] Department of Neonatology, Maternal and Child Health Hospital of Hubei Province, Tongji Medical College, Huazhong University of Science and Technology, Wuhan, China

OPEN ACCESS

Edited by:
Ming Dong,
Guangzhou Institutes of Biomedicine and Health, Chinese Academy of Sciences (CAS), China

Reviewed by:
Thomas Kitzler,
McGill University, Canada
George William Burke,
University of Miami, United States

***Correspondence:**
Yu Zhang
yuzhang497@163.com

† These authors have contributed equally to this work

Specialty section:
This article was submitted to Molecular and Cellular Pathology, a section of the journal Frontiers in Cell and Developmental Biology

Received: 18 June 2021
Accepted: 22 September 2021
Published: 11 October 2021

Citation:
Wang L, Wang J, Wang Z, Zhou J and Zhang Y (2021) Higher Urine Exosomal miR-193a Is Associated With a Higher Probability of Primary Focal Segmental Glomerulosclerosis and an Increased Risk of Poor Prognosis Among Children With Nephrotic Syndrome. Front. Cell Dev. Biol. 9:727370. doi: 10.3389/fcell.2021.727370

Background: In children, focal segmental glomerulosclerosis (FSGS) is one of the most common primary glomerular diseases leading to end-stage renal disease. Exosomes facilitate communication between cells by transporting proteins and microRNAs. We aimed to investigate the utility of urine exosomal miR-193a for diagnosis and prognosis estimation among patients with primary FSGS, and preliminarily explore the regulation mechanism of exosome secretion from podocytes.

Methods: Specimens of urine were obtained from patients with primary FSGS, minimal change nephropathy (MCN) and IgA nephropathy (IgAN), followed by exosome isolation. We quantified urine exosomal miR-193a based on quantitative reverse transcription-polymerase chain reaction, and evaluated its applicability using area-under-receiver-operating-characteristics curves (AUROCs). The semiquantitative glomerulosclerosis index (GSI) was used to evaluate the degree of glomerulosclerosis according to the method of Raij et al. We further used FAM-labeled miR-193a-5p to examine exosome shuttling using confocal microscopy for visualization, and explored the regulation mechanism of exosomes release from podocytes using Fluo-3AM dye.

Results: Urine exosomal miR-193a levels were significantly higher in patients with primary FSGS than those with MCN and IgAN. The AUROCs for discriminating between primary FSGS and MCN or IgAN were 0.85 and 0.821, respectively. Urine exosomal miR-193a levels positively correlated with GSI in patients with primary FSGS. We further found that kidney tissues from these patients had increased CD63 expression involving podocytes in non-sclerotic tufts. Exosomes from cultured podocytes could transport miR-193a-5p to recipient cells, potentially through a calcium-dependent release mechanism.

Conclusion: Urine exosomal miR-193a might be harnessed as a non-invasive marker for diagnosis and outcome assessment among patients with primary FSGS. Exosomes were potential vehicles for miRNAs shuttling between podocytes, and released from podocytes in a calcium-dependent manner.

Keywords: exosomes, microRNA-193a, focal segmental glomerulosclerosis, nephrotic syndrome, podocyte

INTRODUCTION

Primary focal segmental glomerulosclerosis (FSGS) is a frequent cause of nephrotic syndrome with a treatment-refractory course, and can be progressive. Having primary FSGS is associated with a 50% probability of developing end-stage renal disease (ESRD) after a mean duration of 5 to 8 years since biopsy, especially among patients not responsive to therapeutics or who were untreated (Korbet, 1999). Focal segmental glomerulosclerosis frequently recurs even after a successful renal transplantation, affecting up to 30% and 50% of adults and children, respectively (Vinai et al., 2010). From this perspective, earlier diagnosis and a timely treatment become an important goal if we want to improve patients' long-term outcomes. The golden standard for diagnosing and classifying FSGS currently remains renal biopsy, whose disadvantages include sampling insufficiency leading to missing glomerular abnormalities. It is not uncommon to have difficulty distinguishing findings between early FSGS and minimal change disease. In addition, the invasiveness of renal biopsy and its association with several adverse events including bleeding and infections is also of concern. Finally, serial renal biopsy for dynamically monitoring disease course is deemed impractical from the clinical ground. Consequently, we are in urgent need of reliable non-invasive biomarkers to facilitate a prompt diagnosis and prognosis estimation for patients with FSGS.

MicroRNAs (miRNAs) are promising disease biomarkers owing to their disease-specificity and biological stability in different kinds of body fluid. Cumulative clinical and experimental reports have shown that miRNAs play an important role in the pathophysiology of renal diseases (Chung and Lan, 2015; Bhatt et al., 2016; Denby and Baker, 2016; Ledeganck et al., 2019). Gebeshuber et al. revealed that mice with transgenic miR-193a expressions developed FSGS rapidly, presenting as the effacement of podocyte foot processes extensively. In their study, an up-regulation of miR-193a levels could be observed in glomeruli isolated from adults with FSGS (Gebeshuber et al., 2013). Later, another group found that miR-193a mediated the switch between the parietal epithelia phenotype and that of podocytes (Kietzmann et al., 2015). Furthermore, patients with FSGS had significantly higher plasma miR-193a levels than healthy controls (Zhang C. et al., 2015). Although increased expression of miR-193a has been described in patients with FSGS, it remains unclear whether miR-193a contributes to glomerulosclerosis or whether miR-193a can be harnessed for early diagnosis and outcome assessment.

Exosomes are a class of extracellular membrane-bound vesicles released from host cells by fusion of the multivesicular body with the cell membrane. Exosomes can be secreted by every epithelial cell type lining the urinary tract system in humans (Pisitkun et al., 2004; Morrison et al., 2016). Their sizes are 30-100 nm and they harbor precursor miRNAs, mature miRNAs, mRNAs, single- and double-stranded DNA (ssDNA and dsDNA), mitochondrial DNA (mtDNA), and proteins within (Morrison et al., 2016). Exosomes are capable of acting in a paracrine manner by transmitting messages not only to nearby cells but also to other organs body-wide. Upon stimulation, transcriptomic changes within cells may modulate the assortment of miRNAs into exosomes (Squadrito et al., 2014). Besides, exosomes have lipid bilayers and can protect their cargoes from the degradation of RNase (Miranda et al., 2010; Cheng et al., 2014). Consequently, exosomes may serve as a potential source for uncovering new biomarkers. Exosomes can be obtained non-invasively, which is another advantage. Ever since the first report of urine exosome isolation in 2004, subsequent studies have tried to test the utility of urine exosomes as sources of biomarkers discovery in patients with different diseases including renal, urogenital and others (Miranda et al., 2010; Erdbrügger and Le, 2016). Along with the above rationale, we attempted to investigate whether urine exosomal miR-193a might be a potential biomarker for achieving an early diagnosis of primary FSGS and for outcome assessment. In addition, we performed some pilot experiments regarding the mechanisms through which exosomes were secreted by podocytes.

MATERIALS AND METHODS

Patient Recruitment and Sampling

We recruited patients with primary FSGS (n = 8), IgA nephropathy (IgAN, n = 7), minimal change nephropathy (MCN) (n = 5), and healthy individuals (n = 5). The diagnosis of primary FSGS and IgAN was made based on input from expert pediatric nephrologists and pathologists who reviewed patients' medical history, physical examination results, laboratory data, whole exome sequencing data and renal biopsy findings. The diagnosis of MCN was achieved based on clinical manifestation and laboratory data only, because children with MCN usually have no renal biopsy as most of these patients are steroid-sensitive. Exclusion criteria of this study included genetic testing-proven genetic FSGS, secondary FSGS, urinary tract infection, those with a positive family history of kidney diseases, congenital anomalies of the kidney and urinary tract, secondary nephrotic syndrome, those with diabetes, hypertension, with non-nephrotic proteinuria, those with an estimated glomerular filtration rate (eGFR) lower than 90 mL/min/1.73 m^2 (using the Schwartz formula), and those receiving immunosuppressive

treatments. Healthy controls were selected based on the following criteria: being free of any systemic and non-systemic diseases according to patients' history and routine laboratory findings. To avoid selection bias, healthy controls and patients with different glomerulopathy were enrolled consecutively from January 2015 to July 2016.

The protocol of this study was approved by the Ethical Committee of Tongji Hospital, and written informed consent was obtained from all participants' parents.

Urine Sample Processing and Exosome Isolation

We obtained renal tissue specimens from renal biopsy prior treatment and collected morning urine samples from study patients at the day before biopsy. Ten milli-liters of first-time urine in the morning were centrifuged for 15 min at 3,000 g at 4°C for removing cells and/or debris. The remaining supernatants were stored at −80°C, followed by exosome isolation using the ExoQuick Exosome Precipitation Solution (System Biosciences, United States), according to the manufacturer's instruction. This was achieved through incubating supernatant with an equal volume of ExoQuick-TC Exosome Precipitation Solution for 12 h at 4°C. Samples were subsequently centrifuged at 1,500 g for 30 min at 4°C. After discarding the residual supernatant, we collected exosome pellets, resuspended them in nuclease-free water of one-tenth of the original volume, and stored specimens at −80°C until the next step.

Transmission Electron Microscopy Procedure

We fixed exosome-containing pellets in 100 μL glutaraldehyde and mounted them onto formvar/carbon-coated cooper grids. We removed excess fluid using a piece of dry filter paper. The loaded grids were transferred and stained with 0.75% uranyl formate for 30 s. Subsequently we dried them with filter paper and imaged the samples using a transmission electron microscopy (FEI Tecnai 20, Philips, United States), with sizes of exosomes measured by image.

Western Blot Analysis

During western blotting, we loaded proteins on 10% sodium dodecyl sulfate polyacrylamide gel electrophoresis (SDS-PAGE) gels and transferred them to polyvinylidene fluoride (PVDF) membranes. Blots were then incubated with primary antibodies against TSG101 or HSP70 (dilution 1:1000, Abcam, United States), and later with horseradish peroxidase (HRP)-conjugated secondary antibody (dilution 1:10000, Santa Cruz Biotechnology, United States). We used Clarity^{TM} Western ECL substate kit (Bio-Rad, United States) to develop the blots and measured the intensity of bands using densitometric scanning based on the ImageJ software.

Exosome RNA Extraction and Quantitation of miR-193a

We subjected 200 μL of resuspended exosome pellets to RNA extraction, using a Total Exosome RNA & Protein Isolation Kit (Applied Biosystems, United States), in compliance with the manufacturer's protocol. We measured RNA concentration and purity based on the relative absorbance ratio at 260/280 (Nanodrop 2000, Thermo, United States). Subsequently, 10 ng of total RNA was reverse transcribed to cDNA using a miRNA cDNA Synthesis Kit (ABM Inc., Canada), followed by quantitative polymerase chain reaction (qPCR) using EvaGreen qPCR Master mix (ABM Inc., Canada) for miRNAs. We obtained primer mixes of RNU6 and has-miR-193a-5p from Genecopoeia lnc, and performed qPCR using the following condition: cycling initially at 95°C for 10 min, then at 95°C for 10 s, 63°C for 15 s, and finally at 72°C for 32 s, with a 7500 Fast Real-Time PCR System (Applied Biosystems, United States). We analyzed qPCR results using the 7500 System SDS software (Applied Biosystems, United States), and normalized the relative expression values of exosomal miR-193a to RNU6 using the $2^{-\Delta\Delta Ct}$ method.

Histological and Immunohistochemical Studies

We fixed kidney tissues in neutral formalin, dehydrated and embedded them in paraffin, and cut the specimens in 2-μm-thick sections using a microtome. Sections were stained with hematoxylin & eosin (H&E), periodic acid-Schiff (PAS), and Masson's Trichrome as general histological examinations. For immunohistochemical staining, we incubated the sections with rabbit anti-human CD63 antibodies (1:200, Wuhan Boster Biological Technology Co., Ltd, China), and then dewaxed, rehydrated, retrieved antigen, inactivated sections with 3% H_2O_2, and blocked non-specific binding with 10% goat sera. Negative control sections were also incubated with the antibody dilution vehicle [0.01 M phosphate-buffered saline (PBS) containing 0.3% Triton X-100]. We added secondary antibodies to the sections using the EnVision kit (DAKO, Denmark) after an overnight incubation at 4°C. After DAB developed, sections underwent gradient dehydration, transparency, and mounting. We observed sections under a light microscope (Olympus, Japan), and analyzed images by the Image Pro Plus 6.0 software.

Calculating Glomerular Sclerosis Index

We measured the severity of glomerular sclerosis by a standard semiquantitative analysis, Glomerular Sclerosis Index (GSI), introduced by Raij et al. (1984). Briefly, at least 20 glomeruli in each specimen were assigned scores from 0, 1, 2, 3, to 4 if the glomeruli were normal, had less than 25, 25 to 50, 50, to 75, or more than 75% sclerosed area, respectively. We calculated GSI of each patient based on the following formula: $N1 \times 1 + N2 \times 2 + N3 \times 3 + N4 \times 4)/n$, in which N1, N2, N3, and N4 represented the numbers of glomeruli having grades 1, 2, 3, or 4, respectively, while n was the number of glomeruli assessed. Two independent observers (J.W. and Z.W.) blind to the experiment performed morphological analyses.

Cell Cultures and the Isolation of Exosomes

We obtained immortalized human podocyte cells (AB8/13) from Dr. Kang YL (Shanghai Children's Hospital, China), and cells

were cultured in RPMI 1640 medium with 10% fetal bovine serum (Life Technologies, United States), 100 U/mL penicillin and 100 μg/mL streptomycin (Sigma-Aldrich, United States). We propagated the podocytes at 33°C and treated cells with Insulin-Transferrin-Selenium (Life Technologies, United States) to maintain their proliferative ability. Once reaching 50–60% confluence, cells were harvested, washed and cultured in a type I collagen-coated plate at 37°C for at least 10 days to allow differentiation. The differentiated cells were used for the following experiments.

To isolate exosomes, we collected medium followed by sequential centrifugation at 300 g for 10 min, 3,000 g for 15 min, and then at 10,000 g for 70 min at 4°C firstly. We further treated the supernatant with ExoQuick-TC for final exosomes isolation. Pellets containing exosomes were dissolved in 500 μL of 1 × PBS.

Determining the Levels of Cytosolic $[Ca^{2+}]i$ by the Fluo-3AM Fluorescent Dye

This method has been described by Lencesova et al. (2013). In brief, we plated podocytes on a 24-well plate at the density of 4×10^4. After 24 h of treatment, cells were washed with 1 mL of serum-free medium and we added 2 μM Fluo-3AM [4-(6-acetoxymethoxy-2, 7-dichloro-3-oxo-9-xanthenyl)-4′-methyl-2, 2′(ethylendioxy) dianiline-N,N,N′,N′-tetraacetic acid tetrakis (acetoxy methyl)ester] (Sigma-Aldrich, United States) with 1 mM probenecid (Sigma-Aldrich, United States) dissolved in serum-free medium, for 30 min at 37°C with the condition of 5% CO_2 in darkness. Later, we washed cells with 1 mL of serum-free medium, and measured fluorescence using a flow cytometer at λ_{ex} 506 nm and λ_{em} 526 nm. We calculated results based on the mean fluorescence intensity. To chelate Ca^{2+} present in culture media, cells were incubated for several hours in the presence of 1.5 mM EGTA. BAPTA-AM was used to chelate intracellular Ca^{2+}.

Quantitation of Released Exosomes

We quantified the levels of exosomes through measuring acetylcholinesterase (AChE) activity, an enzyme specifically directed to these vesicles (Savina et al., 2002). In short, we suspended 25 μL of isolated exosomes in 100 μL of phosphate buffer and incubated them with 1.25 mM acetylthiocholine and 0.1 mM 5,5′-dithiobis (2-nitrobenzoic acid), achieving 1 mL as the final volume, in cuvettes at 37°C. We followed changes in absorbance at 412 nm continuously, and collected the enzymatic activity at 20 min after incubation as the results.

Statistical Analysis

We described data as median (if non-normally distributed data) or mean ± standard deviation (if normally distributed data), and our experimental results were obtained from triplicate experiments. We compared data between groups using Kruskal Wallis test (if non-parametric variables) or Fisher's least significant difference (LSD) test (if parametric variables). We evaluated the diagnostic performance of urine exosomal miR-193a for primary FSGS by calculating the sensitivity and specificity using the receiver-operating-characteristic (ROC) curves. We used one-dimensional regression to analyze the correlations between two parameters. A P value lower than 0.05 was considered statistically significant. We used the SPSS software package (version 13.0) for statistical analysis and created charts using the GraphPad Prism version 6 for Windows.

RESULTS

The Characteristics of Participants

We summarize baseline demographic and clinical features of study participants in **Table 1**. There were no significant differences in gender, race and eGFR between the primary FSGS group and other groups. Similarly, there were no significant differences in serum albumin, proteinuria and the doses of steroid between the FSGS, MCN, and IgAN groups. Significant differences existed in age between those of the MCN group and those of the other groups, because MCN is the most common origin of nephrotic syndrome among children aged between 1 and 6 years.

TABLE 1 | Clinical and laboratory characteristics of study subjects.

	FSGS (n = 8)	MCN (n = 5)	IgAN (n = 7)	Control (n = 5)
Demographic				
Age, year	8.2 ± 1.0*	2.8 ± 0.3	10.2 ± 0.98	5.9 ± 1.7
Sex, male/female	6/2	2/3	4/3	3/2
Race/ethnicity, n (%)				
Han	100%	100%	100%	100%
Laboratory parameters				
eGFR (mL/min)	> 90	> 90	> 90	> 90
Proteinuria (g/24h)	3.587 ± 1.484#	3.242 ± 1.631	3.590 ± 0.680	0
Serum albumin (g/L)	22.7 ± 3.5	20.2 ± 2.2	28.7 ± 3.4	40.5 ± 1.5
Treatment				
Dose of steroid	2 mg/kg/d	2 mg/kg/d	2 mg/kg/d	n.d.

*Values are means ± SE. eGFR, estimated glomerular filtration rate; n.d., not determinate. P-value refers to the comparison of the FSGS with healthy controls and the values in bracket referred to the comparison with MCN: Mann-Whitney U Test or Pearson χ^2 test. * FSGS vs. MCN $P < 0.05$, # FSGS vs. healthy controls $P < 0.05$.*

Characterizing Urine Exosomes

We examined urine exosomes using an electron microscopy, and found vesicles with an average of 65.44 ± 20.1 nm diameters and a typical spherical shape (**Figure 1A**). Results from Western blot showed that exosomal markers including TSG101 and HSP70 could be detected at molecular weight levels of 44 and 70 kDa, respectively (**Figure 1B**). The findings of our isolated vesicles were compatible with the typical features of exosomes (Zhang J. et al., 2015), and the quality could be satisfactory and suitable for subsequent experiments.

Urine Exosomal miR-193a in Patients With Primary Focal Segmental Glomerulosclerosis and the Control Groups

As shown in **Figure 2**, the expression levels of urine exosomal miR-193a were significantly higher in the primary FSGS group than those of other groups (FSGS: 1060.4 *vs.* MCN: 423.7, IgAN: 381.9, Control: 163.6). These findings suggested that urine exosomes could potential be utilized for identifying miR-193a, a biomarker capable of differentiating primary FSGS from other glomerular diseases including MCN.

Discriminative Power Using miR-193a for Identifying Primary Focal Segmental Glomerulosclerosis

To assess the diagnostic ability using urine exosomal miR-193a for primary FSGS, we used ROC curves for discriminating primary FSGS from other glomerular diseases. The areas under the ROC curve (AUCs) of using urine exosomal miR-193a for differentiating primary FSGS from MCN or IgAN were 0.85 and 0.821, respectively (**Figure 3**).

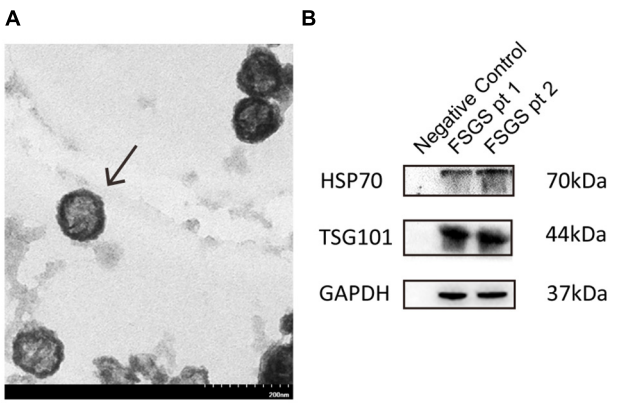

FIGURE 1 | Identification and characterization of exosomes. **(A)** Urine exosomes were isolated from urine by the ExoQuick exosome precipitation solution. Urine vesicles, showing the characteristic exosomal cup-shape and size, are shown in the representative electron micrographs; scale bar = 200 nm. **(B)** Expression of exosomal markers (HSP70, CD9) was assessed by immunoblotting in total protein extracts from isolated urinary exosomes.

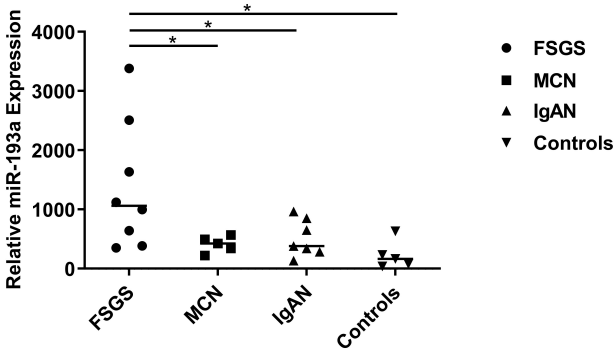

FIGURE 2 | Relative expression levels of urine exosomal miR-193a between patients with FSGS patients and controls. Relative expressions were shown which was calculated with the equation $2^{-deltaCt}$, normalized for RNU6 and relative to the control average. Scatter plot (middle line: median). *$P < 0.05$.

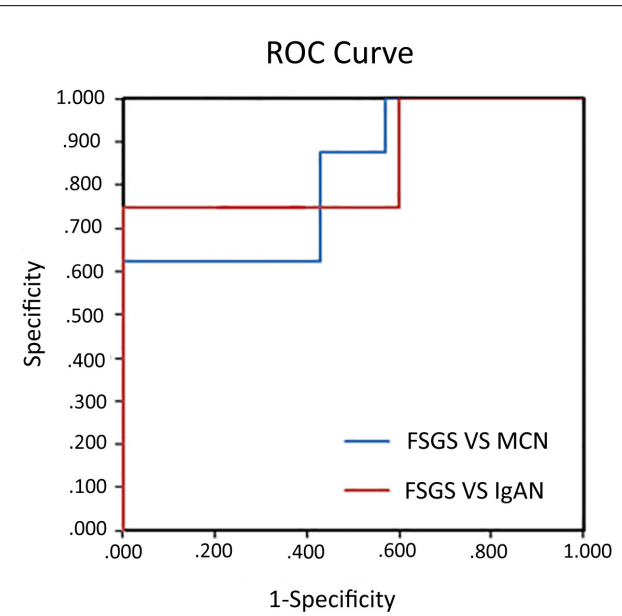

FIGURE 3 | Diagnostic values of urine exosomal miR-193a levels in patients with primary FSGS. ROC curve analysis of miR-193a expression to discriminate between primary FSGS patients and MCN or IgAN patients. The areas under the ROC curve were 0.85 and 0.821, respectively.

Urine Exosomal miR-193a Expression Correlates Positively With Glomerular Sclerosis Index in Patients With Primary Focal Segmental Glomerulosclerosis

We collected 8 renal tissue samples from patients with primary FSGS and calculated their GSI. **Figure 4A** shows the representative Masson trichrome staining results of renal sections from each group. Urine exosomal miR-193a expressions were positively correlated with the severity of glomerular sclerosis. Patients with a higher GSI had significantly higher levels of urine exosomal miR-193a compared to those with a low

GSI (**Figure 4B**). Among the spectrum of renal pathological changes, only glomerular sclerosis was correlated with miR-193a expressions, while there was no correlation between the degree of tubular atrophy or interstitial fibrosis and miR-193a expressions.

CD63 Expressions Increase Within Glomeruli From Patients With Primary Focal Segmental Glomerulosclerosis

To examine whether urine exosomal miR-193a came from podocytes and whether it could be used as a biomarker for diagnosing primary FSGS, we evaluated CD63 expressions (exosome marker) in the renal tissue sections. We found that renal CD63 expressions were significantly up-regulated in patients with FSGS compared to those with thin basement membrane disease (TBMD). In the FSGS cases, renal CD63 expressions were mainly located in podocyte cytoplasm within non-sclerotic tuft segments (**Figure 5**). This finding suggested that the formation of multivesicular bodies increased within the podocytes in patients with primary FSGS.

Podocyte-Derived Exosomes Can Deliver miR-193a to Recipient Cells *in vitro*

We further visualized the transfer of labeled miRNAs between podocytes *in vitro*. We first transfected podocytes with FAM-labeled miR-193a-5p. Twenty-four hours later, we used a fluorescent phosphatidyl ethanolamine analog, N-Rh-PE [1,2-dipalmitoyl-sn-glycero-3-phosphoethanolamine-N-(lissamine rhodamine B sulfonyl)], to label exosomes. We collected culture medium 1 day later for isolating exosomes. An independent set of recipient podocytes was then incubated with 10 μg of isolated exosomes for 24 h. We showed that N-Rh-PE-labeled exosomes were endocytosed, and FAM-labeled miR-193a-5p was localized in exosomes, as were visualized by a fluorescence microscopy (**Figure 6**). Our findings indicated that podocyte-derived exosomes could transport miRNAs to recipient cells.

A Calcium-Dependent Mechanism Is Involved in Exosome Release

Intracellular Ca^{2+} rise is found to be necessary for the induction of regulated secretion in most cell types (Gerber and Südhof, 2002; Wasle and Edwardson, 2002). During exocytosis under regulation, the membrane of secretory vesicle fuses with the plasma membrane precipitated by a tightly controlled Ca^{2+}-triggered reaction. Because monensin (MON), a membrane-permeable Na^{+} ionophore known to induce Ca^{2+} entry through reversed activity of the Na^{+}/Ca^{2+} exchanger (Wang et al., 1999), we tested the influence of MON on the release of exosomes from podocytes and observed whether Ca^{2+} was involved in this process. We harvested exosomes from culture media after 7 h of incubations with 7 μM MON and measured AChE activity. Monensin treatment was found to induce a marked increase in the amount of exosome released (**Figure 7B**). To assess whether the MON-induced exosome release was related to intracellular Ca^{2+} increase, we evaluated whether MON modified intracellular Ca^{2+} concentrations in cultured podocytes. We found a significant increased intensity of Fluo-3AM fluorescence (**Figure 7A**), suggesting that the increase in exosome release might be Ca^{2+} dependent. We also assessed whether the effect of MON effect could be prevented by Ca^{2+} chelators. Both EGTA and BAPTA-AM slightly decreased the basal levels of exosome release (**Figure 7B**). The MON-dependent increase was significantly abrogated by both Ca^{2+} chelators, indicating that Ca^{2+} present in culture media and also in intracellular space was required for exosome secretion from podocytes.

DISCUSSION

Focal segmental glomerulosclerosis (FSGS), a primary podocytopathy, is characterized histologically by extensive podocyte injury with segmental glomerular scarring. Podocytes, an important pathologic player, cover the outer layer of the glomerular basement membrane and assist in stabilizing

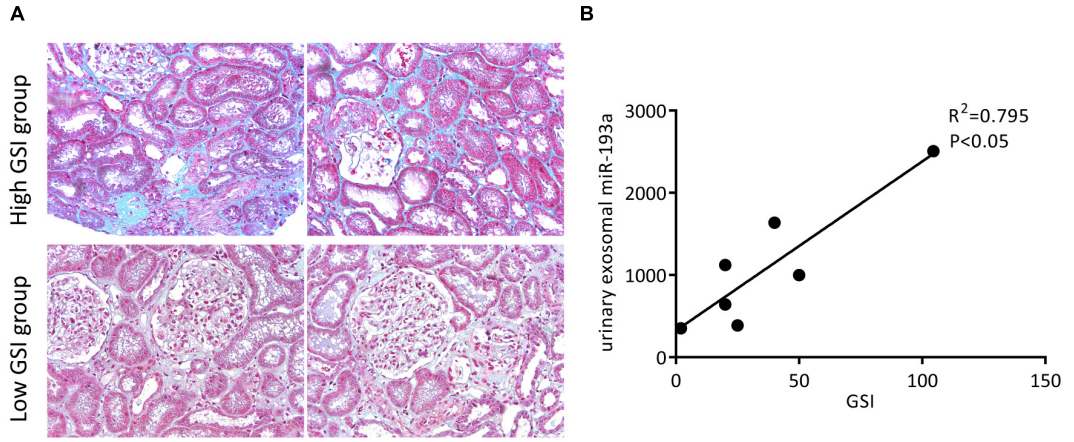

FIGURE 4 | Prognostic values of urine exosomal miR-193a levels in patients with primary FSGS. **(A)** Representative photomicrographs of the renal biopsy with Masson's trichrome staining (200×). **(B)** The correlation between the expression level of urine exosomal miR-193a with GSI in patients with primary FSGS.

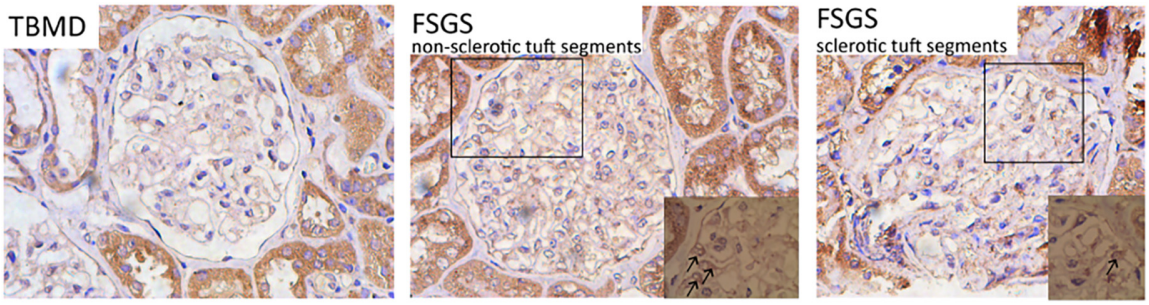

FIGURE 5 | Representative micrographs show renal CD63 staining (IHC, 400×). The expression level of CD63 was significantly up-regulated in patients with FSGS compared with TBMD, which was mainly located in the cytoplasm of podocytes within non-sclerotic tuft segments (indicated by black arrows).

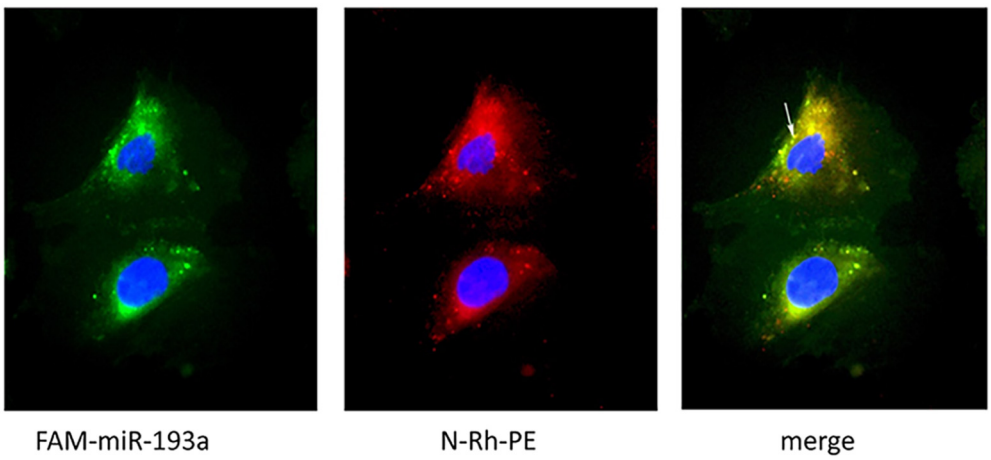

FIGURE 6 | Visualization of exosomes shuttling FAM-labeled miR-193a-5p to recipient podocytes. Recipient podocytes were incubated with donor podocytes-derived exosomes (10 μg/ml). Yellow fluorescent "specs" (indicated by white arrow) represent N-Rh-PE labeled exosomes containing FAM-miR-193a-5p taken up by the recipient podocytes.

glomerular architecture as well as function. Podocyte-origin exosomes have been shown to be detectable in urine from previous studies (Zhou et al., 2013; Hogan et al., 2014; Lv et al., 2014; Gámez-Valero et al., 2015). Similarly, we showed that patients with primary FSGS had podocytes with an increased exosome production if compared to those with TBMD. We also found massive quantities of detectable exosomes in the urine of patients with MCN and IgAN, suggesting that urine exosomes serve as potential sources of biomarkers for diagnosing glomerular diseases while sera or plasma may be inappropriate due to their containing exosomes of non-renal origin. Besides, functional cells can selectively incorporate miRNAs into exosomes followed by releasing them extracellularly, in response to multiple adverse stimulations (Zhang et al., 2010; Chen et al., 2012; Eirin et al., 2014; Nishida-Aoki and Ochiya, 2015). It is reasonable to hypothesize that urinary exosomal miRNAs could be used as a more excellent mirror to reflect the renal pathological change compared with miRNAs gained from whole urine sample. Unlike renal biopsy, the collection of urine exosomes is relatively non-invasive, convenient, and amenable to repeated performance. In addition, exosomes can protect their internal content from the degradation of RNases and proteinases. These biologic advantages suggest that using enriched urine exosomes as a source of biomarkers may increase the sensitivity, specificity and practicality of miRNA for predicting podocytopathy. So far, few reports addressed the utility of urine exosomal miRNAs as biomarker for diagnosing primary glomerular disorders. Lv et al. (2013) discovered that urine exosomal miR-29c was a biomarker correlating with renal function and fibrosis in patients with chronic kidney disease (CKD). Ramezani et al. (2015) reported that urine exosomal miR-1915 and miR-663 were downregulated while miR-155 was upregulated in patients with FSGS. We believe that more urine exosomal miRNAs as diagnostic biomarker are needed for patients with primary FSGS. Prior experiments showed that mice with transgenic miR-193a expressions developed FSGS (Gebeshuber et al., 2013), and we enrich their findings by showing the diagnostic and prognosis estimating ability of urine exosomal miR-193a for primary FSGS.

We used to establish a handy and reliable protocol for the isolation of exosomes from urine, and further showed that urine exosomal miR-193a significantly increased in patients with

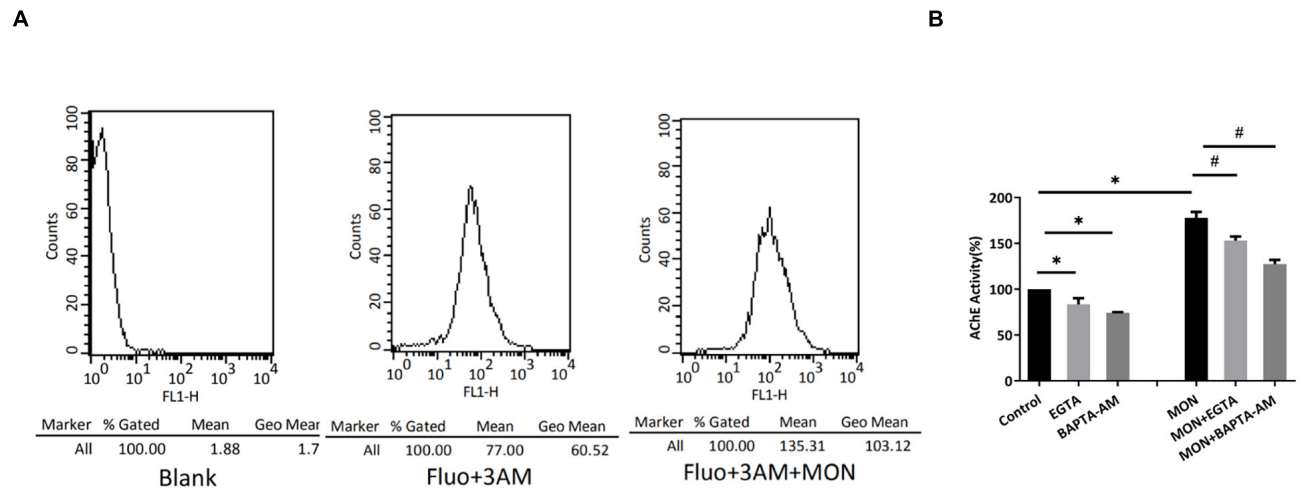

FIGURE 7 | Monensin stimulates exosome release by a calcium-dependent mechanism. **(A)** Podocytes were loaded with Fluo-3AM, and intracellular Ca^{2+} concentration was measured. Shown are changes in Ca^{2+} concentration elicited by 7 μM MON. Data are representative of at least three independent experiments. **(B)** Podocytes were incubated for 7 h in the presence of 1.5 mM EGTA, 30 μM BAPTA-AM, 7 μM MON, or the combination of 1.5 mM EGTA/7 μM MON (MON + EGTA) or 30 μM BAPTA-AM/7 μM MON (MON + BAPTA-AM). The secreted exosomes were collected and quantitated by measuring the AChE activity. * significantly different from the control, $P < 0.05$. # significantly different from the MON-treated cells, $P < 0.05$.

primary FSGS patients compared to those with MCN (Huang et al., 2017). In this study, we attempted to characterize the utility of urine exosomal miR-193a as a diagnostic marker for primary FSGS, through comparing their levels in those with primary FSGS to those of patients with other primary glomerulopathies including MCN and IgAN and those of healthy controls. We found that urine exosomal miR-193a levels were significantly higher in the primary FSGS group than those of other groups. Results of ROC analyses support the utility of urine exosomal miR-193a for discriminating primary FSGS from MCN and IgAN. Therefore, we believed that urine exosomal miR-193a might be a potential diagnostic biomarker for primary FSGS. In addition, urine exosomal miR-193a levels also correlated with GSI while not with tubular and interstitial lesions. Gebeshuber et al. (2013) revealed that miR-193a inhibited WT1 expressions, leading to the downregulation of WT1 targets including *PODXL* and *NPHS1*. This action exerts a catastrophic influence on the entire podocyte-stabilizing system. From this view, miR-193a plays a critical role in glomerular sclerosis development and urine exosomal miR-193a could be directly linked to the severity of podocyte injuries.

Matsusaka et al. (2011) established chimeric mice with 25–50% podocytes expressing immunotoxin LMB2 receptor hCD25, and the mice were subsequently stimulated to develop hCD25-positive podocytes-specific injuries through injecting recombinant immunotoxin LMB2. They demonstrated that, although LMB2 was rapidly metabolized with a half-life of 35 min, injuries to podocytes worsened over weeks, culminating in FSGS development 6 weeks after injection. Their findings clearly indicated that the expansion of segmental sclerosis involved gradual podocyte loss unrelated to the primary insult and were related to the autonomous propagation of podocyte-to-podocyte damages. Exosomes are purported as vital messengers participating in intercellular communication and exosomes secreted by one cell can interact with recipient cells, inducing adverse changes in recipient cells. According to findings of our study, significantly increased exosomes formation could be observed in podocytes from patients with primary FSGS compared to those from patients with TBMD. In order to identify whether exosomes could participate in the podocyte-to-podocyte transmission of damages, we conducted *in vitro* experiments to visualize the process of signal transmission by exosomes between podocytes. Using a confocal microscopy, we found that exosomes isolated from podocytes could deliver miR-193a to recipient podocytes. The induction of podocyte-secreted exosomes was calcium-dependent.

The main limitations in this study included the following: first, this study recruited relatively low number of patients, and future studies using a larger cohort will be necessary to validate our results. Second, we did not identify miRNA intrarenal expressions simultaneously. Third, our study is a cross-sectional one. Finally, the regulatory mechanisms of exosomes secretion from podocytes were not addressed in detail, and there are more to be explored.

CONCLUSION

The present study identified two important findings that were different from previous reports, with regard to the exact pathophysiologic role of miR-193a in FSGS. First, our study might be one of the few pilot reports focusing on both the diagnostic and prognostic value of urine exosomal miR-193a for patients with primary FSGS. Secondly, we showed that *in vitro*, exosomes could transport miRNAs between podocytes in a calcium-dependent manner.

DATA AVAILABILITY STATEMENT

The original contributions presented in the study are included in the article/supplementary material, further inquiries can be directed to the corresponding author.

ETHICS STATEMENT

The studies involving human participants were reviewed and approved by the Ethical Committee of Tongji Hospital. Written informed consent to participate in this study was provided by the participants' legal guardian/next of kin.

AUTHOR CONTRIBUTIONS

YZ contributed to conception and design of the study. LW and JW completed the experiment and performed the statistical analysis. YZ wrote the first draft of the manuscript. All authors contributed to manuscript revision, read, and approved the submitted version.

FUNDING

This work was supported by the grant from the National Natural Science Foundation of China (No. 81570641).

REFERENCES

Bhatt, K., Kato, M., and Natarajan, R. (2016). Mini-review: emerging roles of microRNAs in the pathophysiology of renal diseases. *Am. J. Physiol. Renal Physiol.* 310, F109–F118.

Chen, X., Liang, H., Zhang, J., Zen, K., and Zhang, C. Y. (2012). Secreted microRNAs: a new form of intercellular communication. *Trends Cell Biol.* 22, 125–132. doi: 10.1016/j.tcb.2011.12.001

Cheng, L., Sun, X., Scicluna, B. J., Coleman, B. M., and Hill, A. F. (2014). Characterization and deep sequencing analysis of exosomal and non-exosomal miRNA in human urine. *Kidney Int.* 86, 433–444. doi: 10.1038/ki.2013.502

Chung, A. C., and Lan, H. Y. (2015). MicroRNAs in renal fibrosis. *Front. Physiol.* 6:50. doi: 10.3389/fphys.2015.00050

Denby, L., and Baker, A. H. (2016). Targeting non-coding RNA for the therapy of renal disease. *Curr. Opin. Pharmacol.* 27, 70–77. doi: 10.1016/j.coph.2016.02.001

Eirin, A., Riester, S. M., Zhu, X. Y., Tang, H., Evans, J. M., O'Brien, D., et al. (2014). MicroRNA and mRNA cargo of extracellular vesicles from porcine adipose tissue-derived mesenchymal stem cells. *Gene* 551, 55–64. doi: 10.1016/j.gene.2014.08.041

Erdbrügger, U., and Le, T. H. (2016). Extracellular vesicles in renal diseases: more than novel biomarkers? *J. Am. Soc. Nephrol.* 27, 12–26. doi: 10.1681/asn.2015010074

Gámez-Valero, A., Lozano-Ramos, S. I., Bancu, I., Lauzurica-Valdemoros, R., and Borràs, F. E. (2015). Urinary extracellular vesicles as source of biomarkers in kidney diseases. *Front. Immunol.* 6:6. doi: 10.3389/fimmu.2015.00006

Gebeshuber, C. A., Kornauth, C., Dong, L., Sierig, R., Seibler, J., Reiss, M., et al. (2013). Focal segmental glomerulosclerosis is induced by microRNA-193a and its downregulation of WT1. *Nat. Med.* 19, 481–487. doi: 10.1038/nm.3142

Gerber, S. H., and Südhof, T. C. (2002). Molecular determinants of regulated exocytosis. *Diabetes* 51(Suppl. 1), S3–S11.

Hogan, M. C., Johnson, K. L., Zenka, R. M., Charlesworth, M. C., Madden, B. J., Mahoney, D. W., et al. (2014). Subfractionation, characterization, and in-depth proteomic analysis of glomerular membrane vesicles in human urine. *Kidney Int.* 85, 1225–1237. doi: 10.1038/ki.2013.422

Huang, Z., Zhang, Y., Zhou, J., and Zhang, Y. (2017). Urinary exosomal miR-193a can be a potential biomarker for the diagnosis of primary focal segmental glomerulosclerosis in children. *Biomed. Res. Int.* 2017:7298160.

Kietzmann, L., Guhr, S. S., Meyer, T. N., Ni, L., Sachs, M., Panzer, U., et al. (2015). MicroRNA-193a regulates the transdifferentiation of human parietal epithelial cells toward a podocyte phenotype. *J. Am. Soc. Nephrol.* 26, 1389–1401. doi: 10.1681/asn.2014020190

Korbet, S. M. (1999). Clinical picture and outcome of primary focal segmental glomerulosclerosis. *Nephrol. Dial. Transplant.* 14(Suppl. 3), 68–73. doi: 10.1093/ndt/14.suppl_3.68

Ledeganck, K. J., Gielis, E. M., Abramowicz, D., Stenvinkel, P., Shiels, P. G., and Van Craenenbroeck, A. H. (2019). MicroRNAs in AKI and kidney transplantation. *Clin. J. Am. Soc. Nephrol.* 14, 454–468.

Lencesova, L., Hudecova, S., Csaderova, L., Markova, J., Soltysova, A., Pastorek, M., et al. (2013). Sulphide signaling potentiates apoptosis through the up-regulation of IP3 receptor types 1 and 2. *Acta Physiol. (Oxf.)* 208, 350–361. doi: 10.1111/apha.12105

Lv, L. L., Cao, Y. H., Ni, H. F., Xu, M., Liu, D., Liu, H., et al. (2013). MicroRNA-29c in urinary exosome/microvesicle as a biomarker of renal fibrosis. *Am. J. Physiol. Renal. Physiol.* 305, F1220–F1227.

Lv, L. L., Cao, Y. H., Pan, M. M., Liu, H., Tang, R. N., Ma, K. L., et al. (2014). CD2AP mRNA in urinary exosome as biomarker of kidney disease. *Clin. Chim. Acta* 428, 26–31. doi: 10.1016/j.cca.2013.10.003

Matsusaka, T., Sandgren, E., Shintani, A., Kon, V., Pastan, I., Fogo, A. B., et al. (2011). Podocyte injury damages other podocytes. *J. Am. Soc. Nephrol.* 22, 1275–1285. doi: 10.1681/asn.2010090963

Miranda, K. C., Bond, D. T., McKee, M., Skog, J., Păunescu, T. G., Da Silva, N., et al. (2010). Nucleic acids within urinary exosomes/microvesicles are potential biomarkers for renal disease. *Kidney Int.* 78, 191–199. doi: 10.1038/ki.2010.106

Morrison, E. E., Bailey, M. A., and Dear, J. W. (2016). Renal extracellular vesicles: from physiology to clinical application. *J. Physiol.* 594, 5735–5748. doi: 10.1113/jp272182

Nishida-Aoki, N., and Ochiya, T. (2015). Interactions between cancer cells and normal cells via miRNAs in extracellular vesicles. *Cell Mol. Life Sci.* 72, 1849–1861. doi: 10.1007/s00018-014-1811-0

Pisitkun, T., Shen, R. F., and Knepper, M. A. (2004). Identification and proteomic profiling of exosomes in human urine. *Proc. Natl. Acad. Sci. U.S.A.* 101, 13368–13373.

Raij, L., Azar, S., and Keane, W. (1984). Mesangial immune injury, hypertension, and progressive glomerular damage in Dahl rats. *Kidney Int.* 26, 137–143. doi: 10.1038/ki.1984.147

Ramezani, A., Devaney, J. M., Cohen, S., Wing, M. R., Scott, R., Knoblach, S., et al. (2015). Circulating and urinary microRNA profile in focal segmental glomerulosclerosis: a pilot study. *Eur. J. Clin. Invest.* 45, 394–404. doi: 10.1111/eci.12420

Savina, A., Vidal, M., and Colombo, M. I. (2002). The exosome pathway in K562 cells is regulated by Rab11. *J. Cell Sci.* 115, 2505–2515. doi: 10.1242/jcs.115.12.2505

Squadrito, M. L., Baer, C., Burdet, F., Maderna, C., Gilfillan, G. D., Lyle, R., et al. (2014). Endogenous RNAs modulate microRNA sorting to exosomes and transfer to acceptor cells. *Cell Rep.* 8, 1432–1446. doi: 10.1016/j.celrep.2014.07.035

Vinai, M., Weber, P., and Seikaly, M. G. (2010). Recurrence of focal segmental glomerulosclerosis in renal allograft: An in-depth review. *Pediatr. .* 14, 314–325. doi: 10.1111/j.1399-3046.2009.01261.x

Wang, X. D., Kiang, J. G., Scheibel, L. W., and Smallridge, R. C. (1999). Phospholipase C activation by Na+/Ca2+ exchange is essential for monensin-induced Ca2+ influx and arachidonic acid release in FRTL-5 thyroid cells. *J. Investig. Med.* 47, 388–396.

Wasle, B., and Edwardson, J. M. (2002). The regulation of exocytosis in the pancreatic acinar cell. *Cell Signal.* 14, 191–197. doi: 10.1016/s0898-6568(01)00257-1

Zhang, C., Zhang, W., Chen, H. M., Liu, C., Wu, J., Shi, S., et al. (2015). Plasma microRNA-186 and proteinuria in focal segmental glomerulosclerosis. *Am. J. Kidney Dis.* 65, 223–232. doi: 10.1053/j.ajkd.2014.07.013

Zhang, J., Li, S., Li, L., Li, M., Guo, C., Yao, J., et al. (2015). Exosome and exosomal microRNA: trafficking, sorting, and function. *Genomics Proteomics Bioinformatics* 13, 17–24. doi: 10.1016/j.gpb.2015.02.001

Zhang, Y., Liu, D., Chen, X., Li, J., Li, L., Bian, Z., et al. (2010). Secreted monocytic miR-150 enhances targeted endothelial cell migration. *Mol. Cell.* 39, 133–144. doi: 10.1016/j.molcel.2010.06.010

Zhou, H., Kajiyama, H., Tsuji, T., Hu, X., Leelahavanichkul, A., Vento, S., et al. (2013). Urinary exosomal Wilms' tumor-1 as a potential biomarker for podocyte injury. *Am. J. Physiol. Renal. Physiol.* 305, F553–F559.

Conflict of Interest: The authors declare that the research was conducted in the absence of any commercial or financial relationships that could be construed as a potential conflict of interest.

Publisher's Note: All claims expressed in this article are solely those of the authors and do not necessarily represent those of their affiliated organizations, or those of the publisher, the editors and the reviewers. Any product that may be evaluated in this article, or claim that may be made by its manufacturer, is not guaranteed or endorsed by the publisher.

frontiers in Cell and Developmental Biology

ORIGINAL RESEARCH
published: 12 October 2021
doi: 10.3389/fcell.2021.729061

Detection of Atherosclerosis by Small RNA-Sequencing Analysis of Extracellular Vesicle Enriched Serum Samples

Alex Hildebrandt[1], Benedikt Kirchner[1], Agnes S. Meidert[2], Florian Brandes[2], Anja Lindemann[3], Gero Doose[4], Alexander Doege[2], Rolf Weidenhagen[5], Marlene Reithmair[3], Gustav Schelling[2] and Michael W. Pfaffl[1]*

[1] Division of Animal Physiology and Immunology, School of Life Sciences Weihenstephan, Technical University of Munich, Freising, Germany, [2] Department of Anesthesiology, University Hospital, Ludwig-Maximilians-University Munich, Munich, Germany, [3] Institute of Human Genetics, University Hospital, Ludwig-Maximilians-University Munich, Munich, Germany, [4] ecSeq Bioinformatics GmbH, Leipzig, Germany, [5] Department of Vascular Surgery, Klinikum Neuperlach, Muenchen-Kliniken, Munich, Germany

OPEN ACCESS

Edited by:
Xinlei Li,
Nationwide Children's Hospital,
United States

Reviewed by:
Laurent Metzinger,
University of Picardie Jules Verne,
France
Zhaohui Xu,
Nationwide Children's Hospital,
United States
Miguel Hueso,
Bellvitge University Hospital, Spain

***Correspondence:**
Alex Hildebrandt
alex.hildebrandt@tum.de

Specialty section:
This article was submitted to Molecular and Cellular Pathology, a section of the journal Frontiers in Cell and Developmental Biology

Received: 22 June 2021
Accepted: 14 September 2021
Published: 12 October 2021

Citation:
Hildebrandt A, Kirchner B, Meidert AS, Brandes F, Lindemann A, Doose G, Doege A, Weidenhagen R, Reithmair M, Schelling G and Pfaffl MW (2021) Detection of Atherosclerosis by Small RNA-Sequencing Analysis of Extracellular Vesicle Enriched Serum Samples. Front. Cell Dev. Biol. 9:729061. doi: 10.3389/fcell.2021.729061

Atherosclerosis can occur throughout the arterial vascular system and lead to various diseases. Early diagnosis of atherosclerotic processes and of individual disease patterns would be more likely to be successful if targeted therapies were available. For this, it is important to find reliable biomarkers that are easily accessible and with little inconvenience for patients. There are many cell culture, animal model or tissue studies that found biomarkers at the microRNA (miRNA) and mRNA level describing atherosclerotic processes. However, little is known about their potential as circulating and liquid biopsy markers in patients. In this study, we examined serum-derived miRNA – profiles from 129 patients and 28 volunteers to identify potential biomarkers. The patients had four different atherosclerotic manifestations: abdominal aneurysm (n = 35), coronary heart disease (n = 34), carotid artery stenosis (n = 24) and peripheral arterial disease (n = 36). The samples were processed with an extracellular vesicle enrichment protocol, total-RNA extraction and small RNA-sequencing were performed. A differential expression analysis was performed bioinformatically to find potentially regulated miRNA biomarkers. Resulting miRNA candidates served as a starting point for an overrepresentation analysis in which relevant target mRNAs were identified. The Gene Ontology database revealed relevant biological functions in relation to atherosclerotic processes. In patients, expression of specific miRNAs changed significantly compared to healthy volunteers; 27 differentially expressed miRNAs were identified. We were able to detect a group-specific miRNA fingerprint: miR-122-5p, miR-2110 and miR-483-5p for abdominal aortic aneurysm, miR-370-3p and miR-409-3p for coronary heart disease, miR-335-3p, miR-381-3p, miR493-5p and miR654-3p for carotid artery stenosis, miR-199a-5p, miR-215-5p, miR-3168, miR-582-3p and miR-769-5p for peripheral arterial disease. The results of the study show that some of the

identified miRNAs have already been associated with atherosclerosis in previous studies. Overrepresentation analysis on this data detected biological processes that are clearly relevant for atherosclerosis, its development and progression showing the potential of these miRNAs as biomarker candidates. In a next step, the relevance of these findings on the mRNA level is to be investigated and substantiated.

Keywords: atherosclerosis, extracellular vesicles, small RNA-sequencing, biomarker, gene ontology

INTRODUCTION

Atherosclerosis is a chronic arterial disease and a leading cause of vascular death worldwide. Although the vascular mortality risk has declined substantially over the last decades from 16% in 1980 to 4% in 2010 in high income countries, some countries (in particular Eastern Europe and parts of Asia) still report increases in mortality rates (Bennett et al., 2014; Moran et al., 2014). Despite these trends, atherosclerosis remains the leading cause of premature adult morbidity and mortality worldwide (GBD 2013 Mortality and Causes of Death Collaborators, 2015).

The pathophysiologic process leading to atherosclerosis starts with accumulation of low-density lipoproteins (LDL) in the intima (the innermost layer of arterial vessels) followed by activation of endothelial cells (ECs) and expression of adhesion molecules. Monocytes from the bloodstream attach to them and enter the intima. Here, monocytes mature into macrophages that devour lipoproteins and become foam cells (Vozenilek et al., 2018). During the inflammatory process, T lymphocytes also migrate into the intima and can trigger inflammatory processes that affect both ECs and smooth muscle cells (SMCs). It is believed that these immunological and cellular processes lead to the formation of the neointima, which causes plaque formation (Libby and Theroux, 2005). The growth of the neointima and the associated stenosis can lead to complete occlusion of the affected artery (Bentzon et al., 2014). The disease has a latency of many years and frequently coexists in more than one vascular bed. This leads to different clinical manifestations, which include ischemic heart disease, ischemic stroke, and peripheral arterial disease among others (Herrington et al., 2016). For the correct diagnosis of the various disease manifestations, it is necessary to find suitable biomarkers to apply a focused and optimized therapy. These should be easily accessible diagnostically by liquid biopsy and as specific as possible. Today, technological progress in molecular biology is leading to more and more knowledge in the context of circulating biomarkers, e.g., by analyzing extracellular vesicles (EVs) and the connected miRNAs of cardiovascular diseases. This makes EV-related miRNA biomarkers an interesting subject of investigation (Reithmair et al., 2017).

miRNAs are small single-stranded non-coding RNA molecules with a length of about 22 nucleotides. The biogenesis of miRNAs is a multistep process including endonucleolytic cleavages and hairpin formation before finally resulting in mature miRNA. These influence the synthesis of proteins by their interactions with mRNAs (Bartel, 2004). A changed expression of miRNAs can thus contribute to disease-relevant processes. Most miRNAs are located in the cell but they can also be present extracellularly in various biological fluids (circulating or extracellular miRNAs). In biofluids such as blood they can be found as cargo of EVs or bound to high-density lipoprotein cholesterol particles or Argonaut 2 proteins (Murillo et al., 2019). In this context, they are better protected from circulating RNAses and can be obtained through liquid biopsy and put into a diagnostic context.

EVs are considered to have great diagnostic potential because of their prospective role as signal transmitters in numerous physiological and pathological processes (Properzi et al., 2013; Zhang et al., 2019). It was noted that the miRNA level in EVs differs from that in the intercellular environment they were expelled from. Consequently, miRNAs are selectively packed into EVs and may regulate disease-specific mechanisms (Simeone et al., 2020).

A large number of miRNAs which control various actors and pathways involved in atherosclerosis are described (Lu et al., 2018). For instance, ECs can be influenced by suppressing the expression of the antisenescence factor SIRT1 by overexpression of, e.g., miR-34a (Deng et al., 2017). Thereby, EC senescence is associated with an increased likelihood of atherogenesis (Menghini et al., 2009). miR-217 and miR-146a are mentioned in this context as well (Sun et al., 2013; Kumar et al., 2014). Additionally, inflammatory processes can be induced by miRNAs within the endothelial layer which is enriching for the atherosclerotic environment (Libby, 2012). Smooth muscle cells can be dysregulated in their differentiation and proliferation behaviour by miRNAs like miR-22 which can cause a synthetic nature instead of a contractile one by suppressing important vascular genes and promoting disease progression (Leeper and Maegdefessel, 2018; Yang et al., 2018). Also, leukocytes such as macrophages are dysregulated by miRNAs like miR-33, leading to impaired lipid phagocytosis, cholesterol efflux, fatty acid oxidation and favouring the formation of foam cells (Karunakaran and Rayner, 2016; Ouimet et al., 2016; Ouimet et al., 2017). Some studies also point to the ability of individual miRNAs to control multiple biological processes relevant in progression of atherosclerosis. miR-21 is associated with the infiltration of macrophages into the intimate, with inflammatory reactions, proliferation of SMCs and senescence (Fan et al., 2014). Lipid uptake and inflammatory cytokine secretion are associated with miRNA-29a (Fan et al., 2014). The proliferation of SMCs and contractile gene transcription is linked to miR-221/222 (Fan et al., 2014). These and other studies suggest that a modified and disease-promoting expression level of miRNAs may be used to identify potential biomarkers for diagnosis and disease-monitoring.

The aim of this study was on the one hand to identify circulating miRNAs that can serve as biomarker candidates for atherosclerosis; on the other hand, to investigate whether a subgroup unique miRNA-profile can be determined for the four different atherosclerotic manifestations. Therefore, blood samples of 129 patients with atherosclerosis and of 28 healthy volunteers were processed with an EV enrichment protocol. The study sample included patients with abdominal aneurysm (aneu), coronary heart disease (chd), carotid stenosis (cs) and peripheral arterial disease (pad). To detect atherosclerotic processes early on and to be able to make a statement which manifestation of the disease is present could help to enable individual therapeutic approaches at an early disease stage.

TABLE 1 | Inclusion and exclusion criteria of patients participating in this study.

Inclusion	Exclusion
Cause of admission: - PAD (independent of stadium) - Carotis stenosis (independent of stadium) - Thoracal or abdominal aortic aneurysm - CHD (independent of stadium)	- No consent given - Under the age of 18 - HIV, Hepatitis B/C infection - active inflammatory focus - active malign tumor disease - limited life expectancy of less than 6 month independent of the acute atherosclerotic disease - immunosuppression - limited ability to give consent (e.g., because of mental disability)

Patients need to meet one of the inclusion criteria and none of the exclusion criteria to be eligible.

MATERIALS AND METHODS

Patient Recruitment

This study was comprised of 157 individuals, including 28 healthy volunteers (control) serving as a control group and 129 patients diagnosed with atherosclerosis (athero). The patients were recruited from the Department of Vascular Surgery of the Neuperlach Community Hospital of Munich and the University Hospital, Ludwig-Maximilians-University Munich as well as the Department of cardiac surgery of the University Hospital, Ludwig-Maximilians-University Munich.

The attending physician was responsible for the diagnosis and followed all respective guidelines. Patients were identified after the attending physician made the diagnosis of atherosclerotic disease and categorized the patients according to the presence of the following manifestations of the disorder: 34 patients had coronary heart disease (chd), 36 patients had peripheral artery disease (pad), 24 patients had carotid stenosis (cs), 35 patients had abdominal aortic aneurysm (aneu) severe enough to require surgical intervention. Patients were included into the study after evaluation for inclusion and exclusion criteria (see **Table 1**) and patients consent. For a comparison of the study population please see **Table 2**.

Most of the included patients had more than one atherosclerotic lesion. For all patients, their medical history was evaluated and noted. Please see **Table 3** for a detailed summary of secondary diagnosis besides the cause of admission.

Comparisons of the clinical and demographics data between volunteers and patients were done with either Chi^2-test for categorial comparisons or with Kruskal–Wallis one-way analysis of variance. A p-value < 0.05 was considered statistically significant. Statistical analysis was performed utilizing. Python Version 3.8 (Python Software Foundation, Beaverton, OR, United States). Libraries used in this study included: Numpy, Pandas and Scipy.

As very few studies on EVs and their miRNA cargo were previously performed and possible differences in EV miRNA expression levels between the different organ manifestations of atherosclerosis were not available, we had to base the sample size estimation in the statistical plan on a single but somewhat comparable study. In this study, which investigated the role of circulating extracellular vesicles (EVs), proteins, and microRNAs in ischaemic stroke, the inclusion of 81 patients with ischaemic stroke and 22 healthy controls resulted in a significant difference between expression values of a number of miRNAs between patients and healthy controls. We therefore assumed, that a further increase in the overall sample size to 129 patients and 28 volunteers would also result in statistically differences in expression values of selected miRNAs.

Blood Sampling, Sample Preparation and Sequencing

Blood samples were drawn from patients and volunteers via venipuncture. Serum was obtained by using 9 ml serum tubes (S-Monovette, Sarstedt, Germany), allowed to clot for 30 min and subsequently centrifuged at 3400 g for 10 min at 4°C. The samples were aliquoted and stored at −80°C. The enrichment of EVs was performed by a precipitation method according to the manufacturer's instruction (miRCURY Exosome Serum/Plasma Kit Qiagen, Venlo, the Netherlands). 1 ml of serum was used as starting volume. Cell-free total RNA was obtained with the NucleoSpin miRNA (Macherey-Nagel, Düren, Germany) in an elution volume of 30 µl. RNA yield and size distribution were determined using the RNA 6000 Pico Kit on the 2100 Bioanalyzer (Agilent Technologies, Santa Clara, United States). Total RNA was resubstituted in 8 µl of nuclease-free water after vacuum-induced centrifugal evaporation. The libraries for small RNA-sequencing were prepared with the NEBNext Multiplex Small RNA Library Prep Set for Illumina (New England Biolabs Inc, Ipswich, United States). cDNA amplification product was purified using the Monarch PCR&DNA Cleanup Kit (New England Biolabs Inc, Ipswich, United States). Yield was subsequently determined using the DNA 1000 Kit on the 2100 Bioanalyzer (Agilent Technologies, Santa Clara, United States). For each sequencing run the same amount of cDNA was pooled for electrophoretic size selection step. The extraction from the gel was carried out with the Monarch DNA Gel Extraction Kit (New England Biolabs Inc, Ipswich, United States). Bands harbouring the miRNA fraction occurred at about 147 bp and were excised. Yield and size distribution of pooled samples were assessed using the High Sensitivity DNA Kit on the 2100 Bioanalyzer (Agilent Technologies, Santa Clara, United States). Sequencing of all samples was performed in

TABLE 2 | Overview of the demographic, risk factors and medication of all participants in this study.

Demographics	Atherosclerosis	Healthy volunteer	P-value
N	129	28	
Age	71.0 (65.0 – 78.0)	39.0 (34.8 – 50.5)	< 0.001
BMI	28.0 (24.8 – 31.2)	25.5 (23.9 – 26.6)	0.003
Gender (Female / Male)	33 / 96	10 / 18	0.392
Study course			
ICU stay (No / Yes)	53 / 76	N/A	
Death while in study (No / Yes)	128 / 1	N/A	
Risk factors			
Smoking (No / Yes)	80 / 49	28 / 0	< 0.001
Alcohol (No / Yes)	120 / 9	28 / 0	0.322
Hypertension (No / Yes)	30 / 99	28 / 0	< 0.001
Diabetes (No / Yes)	79 / 50	28 / 0	< 0.001
Kidney insufficiency (No / Yes)	104 / 25	28 / 0	0.024
Liver insufficiency (No / Yes)	128 / 1	28 / 0	0.399
Medication			
Aspirin (No / Yes)	37 / 92	28 / 0	< 0.001
Direct anticoagulation (No / Yes)	116 / 13	28 / 0	0.169
Cumarines (No / Yes)	120 / 9	28 / 0	0.322
Dual antiplatelet (No / yes)	117 / 12	28 / 0	0.198
Oral anti-diabetics No / Yes)	90 / 39	28 / 0	0.002
Insulin (No / Yes)	120 / 9	28 / 0	0.322
Betablockers (No / Yes)	63 / 66	28 / 0	< 0.001
ACE Inhibitors (No / Yes)	59 / 70	28 / 0	< 0.001
Antidepressives (No / Yes)	118 / 11	28 / 0	0.232
Statins (No / Yes)	37 / 92	28 / 0	<0.001

All values are mean values and 25% and 75% quartiles.

four single-end sequencing runs in 50 cycles on the HiSeq2500 (Illumina Inc. San Diego, United States). A summary about the sample composition of each sequencing run is given in **Table 4**.

Bioinformatic Analysis of Small RNA-Sequencing Data

Data Processing

FastQC (version 0.11.9) was used to quality check each sequencing dataset. Adaptor sequences of reads were trimmed with btrim32 (version 0.3.0). Reads without any adaptor were removed as well as reads with less than 16 nucleotides in length. The mapping of reads was performed with bowtie (version 1.2.3). The cut off for reads was set to maximum one mismatch. Additional parameters that limit alignment to the sense strand (–norc) and output to the single best match in terms of mismatch quality (–best) were applied. References of non-coding RNA sequences for ribosomal RNA (rRNA), small nuclear RNA (snRNA), small nucleolar RNA (snoRNA) and transfer RNA (tRNA) were downloaded from RNACentral (release 12). miRNA references were obtained from miRBase (release 22.1). Mapping was performed sequential. First sequences of rRNA and tRNA were mapped and eliminated from the dataset. Subsequently miRNAs as well as snoRNAs and snRNAs were identified and counted. By mapping directly on mature sequences of the small RNA transcriptome, read counts were generated by calling the sum of reads matching each mature sequence. The miRNA analysis pipeline was frequently and successfully applied in various biomarker studies (Spornraft et al., 2014; Buschmann et al., 2016, 2018; Reithmair et al., 2017).

Differential Gene Expression Analysis

A differential gene expression (DGE) analysis was performed using R (version 4.0.3; R Core Team, 2020) and the DESeq2 (version 1.28.1; Love et al., 2014) package. Since we used four sequencing runs to collect all samples and each run had different sample distribution per group, in addition to different library sizes of the individual data sets, a normalization method and batch correction was used. All these possible biases were first balanced out by the normalization of raw reads by calculating a sample specific scaling factor using the mean of ratios methods while any batch effects were accounted for through linear modelling. The algorithms are implemented in the DESeq2 package. The Benjamin-Hochberg method was applied to correct for false discovery. Two result sets were obtained; a default set by filtering for p-value ≤ 0.1 and a more stringent one by filtering additionally for an absolute $\log_2$ fold change ($|\log2FC|$) ≥ 1 and base mean ≥ 50.

Overlap Analysis

Both the result tables with the default cut-off and the stricter filter criteria of the DGE analysis were used for the overlap analysis. The analysis was carried out using R (version 4.0.3; R Core Team, 2020) and the veccompare (version 0.1.0; Levernier and Wacha, 2017) package.

Unsupervised and Supervised Clustering

Unsupervised clustering was performed using principal component analysis (PCA) using R (version 4.0.3; R Core Team, 2020), stats (version 4.0.3, R Core Team, 2020) and ggplot2 (version 3.3.2, Wilkinson, 2011) packages for calculation and plotting. The dataset was also filtered to the 500 most variant miRNAs of the whole dataset. Supervised clustering was done by sparse partial-least-squares discriminant analysis (sPLS-DA) using R (version 4.0.3; R Core Team, 2020) and mixOmics (version 6.12.2, Rohart et al., 2017) package. PCA as well as sPLS-DA were carried out in two ways. First, the atherosclerotic group (n = 129) was compared with the control group (n = 28). Second, all four atherosclerotic subgroups and the control were given as input. To find optimal number of components for the sPLS-DA the distance was measured by three algorithms and ranked with the balanced error rate (BER) and the total error rate. Subsequently, optimal numbers of features (miRNAs) for each component were determined.

TABLE 3 | Detailed overview of all participating patients of the Arteriosclerosis cohort.

Cause of admission	Abdominal aortic aneurysm (aneu)	Coronary heart disease (chd)	Peripheral artery disease (pad)	Carotic stenosis (cs)
n	35	34	36	24
Age	71.5 (61.0 – 79.8)	71.0 (65.0 – 75.0)	69.0 (63.0 – 76.0)	75.0 (72.0 – 82.0)
BMI	24.8 (22.2 – 28.3)	30.7 (26.1 – 32.4)	29.0 (25.7 – 31.2)	29.2 (25.4 – 30.9)
Length of hospital stay	10.0 (8.0 – 12.2)	14.0 (11.0 – 16.0)	3.0 (2.0 – 10.0)	7.0 (6.0 – 8.0)
Gender (Female / Male)	8 / 27	10 / 24	9 / 27	6 / 18
Study course				
ICU stay (No / Yes)	7 / 28	2 / 32	31 / 5	13 / 11
Died in study (No / Yes)	35 / 0	33 / 1	36 / 0	24 / 0
Risk factors				
Smoking (No / Yes)	22 / 13	23 / 11	17 / 19	18 / 6
Alcohol (No / Yes)	34 / 1	28 / 6	35 / 1	23 / 1
Hypertension (No / Yes)	8 / 27	6 / 28	10 / 26	6 / 18
Diabetes (No / Yes)	30 / 5	23 / 11	15 / 21	11 / 13
Kidney insufficiency (No / Yes)	30 / 5	25 / 9	28 / 8	21 / 3
Liver insufficiency (No / Yes)	35 / 0	33 / 1	36 / 0	24 / 0
Medication				
Aspirin (No / Yes)	13 / 22	6 / 28	9 / 27	9 / 15
Direct anticoagulation (No / Yes)	32 / 3	30 / 4	30 / 6	24 / 0
Cumarines (No / Yes)	30 / 5	33 / 1	34 / 2	23 / 1
Dual antiplatelet (No / yes)	34 / 1	29 / 5	33 / 3	21 / 3
Oral anti-diabetics (No / Yes)	32 / 3	26 / 8	20 / 16	12 / 12
Insulin (No / Yes)	35 / 0	30 / 4	32 / 4	23 / 1
Betablocker (No / Yes)	18 / 17	14 / 20	18 / 18	13 / 11
ACE Inhibitors (No / Yes)	18 / 17	14 / 20	17 / 19	10 / 14
Antidepressives (No / Yes)	33 / 2	32 / 2	30 / 6	23 / 1
Statins (No / Yes)	14 / 21	9 / 25	8 / 28	6 / 18
Aneurysm*				
Diameter	52.0 (45.2 – 60.0)	–	–	–
Dissection (No / Unknown / Yes)	28 / 4 / 3	29 / 5 / 0	31 / 5 / 0	20 / 4 / 0
Aneurysm Clinical Symptoms (No / Unknown / Yes)	23 / 6 / 6	29 / 5 / 0	31 / 5 / 0	20 / 4 / 0
Coronary Heart Disease (CHD)*				
EF	56.5 (54.5 – 63.2)	56.5 (50.0 – 67.5)	34.0 (32.0 – 36.0)	–
NYHA (NYHA I / NYHA II / NYHA III / NYHA IV / No NYHA / Unknown)	2 / 1 / 4 / 1 / 20 / 7	3 / 7 / 10 / 8 / 4 / 2	0 / 0 / 2 / 1 / 24 / 9	1 / 0 / 0 / 0 / 18 / 5
Atrial Fibrillation (No / Unknown / Yes)	26 / 7 / 2	27 / 0 / 7	26 / 6 / 4	18 / 5 / 1
CHD Acute Infarction (No / Unknown / Yes)	28 / 7 / 0	32 / 0 / 2	30 / 6 / 0	20 / 4 / 0
Peripheral arterial disease (PAD)*				
PAD Fontaine stage (No PAD / Stage I / Stage IIb / Stage III / Stage IV / Unknown)	26 / 1 / 1 / 0 / 0 / 7	27 / 0 / 1 / 0 / 0 / 6	0 / 0 / 16 / 2 / 17 / 1	20 / 0 / 1 / 0 / 3
PAD therapy (Atherectomy / Bypass / No therapy and Lifestyle / PTA / Unknown	0 / 0 / 28 / 1 / 0 / 6	0 / 0 / 27 / 1 / 0 / 6	6 / 2 / 6 / 22 / 0	0 / 0 / 20 / 0 / 0 / 4

(Continued)

TABLE 3 | (Continued)

Cause of admission	Abdominal aortic aneurysm (aneu)	Coronary heart disease (chd)	Peripheral artery disease (pad)	Carotic stenosis (cs)
PAD therapy (Balloon / Both / No PTA / Stent / Unknown / unsuccessful)	1 / 28 / 0 / 6 / 0	0 / 26 / 1 / 6 / 0	12 / 5 / 11 / 3 / 3 / 2	0 / 0 / 20 / 0 / 4 / 0
Carotis stenosis (cs)*				
Symptomatic stenosis (No / Unknown / Yes)	29 / 6 / 0	29 / 5 / 0	32 / 4 / 0	13 / 3 / 8
Stenosis type (extracranial / ischemic stroke / no stroke / unknown)	0 / 1 / 28 / 6	0 / 0 / 30 / 3	1 / 0 / 31 / 4	0 / 4 / 17 / 3
Carotid stenosis (No / Unknown / Yes)	28 / 7 / 0	20 / 4 / 10	29 / 3 / 4	1 / 3 / 20
internal carotid artery stenosis (%)	–	50.0 (32.0 – 60.0)	85.0 (82.5 – 87.5)	80.0 (63.8 – 80.0)
Lab results				
Fasting Glucose levels	92.0 (86.0 – 93.0)	92.0 (90.5 – 97.0)	113.5 (93.8 – 130.5)	98.0 (94.0 – 111.0)
Cholesterine (All)	200.0 (170.0 – 218.0)	193.0 (162.0 – 235.5)	157.0 (145.0 – 224.0)	168.0 (167.0 – 190.0)
Cholesterine (Hdl)	62.0 (45.0 – 77.0)	54.0 (43.5 – 57.0)	50.0 (38.5 – 54.0)	46.0 (37.0 – 57.0)
Cholesterine (Ldl)	120.5 (103.0 – 173.8)	104.0 (85.5 – 157.5)	68.0 (64.0 – 135.5)	107.0 (97.0 – 109.0)
Triglycerides	128.0 (104.0 – 152.2)	162.0 (114.8 – 248.5)	115.0 (104.0 – 160.0)	132.5 (79.0 – 189.0)
White blood cell count (G/l))	7.4 (6.0 – 8.3)	6.3 (5.5 – 7.9)	8.1 (6.7 – 9.1)	8.0 (7.1 – 8.6)
International normalized ratio (INR)	1.0 (0.0 – 1.0)	1.0 (0.9 – 1.0)	0.0 (0.0 – 1.0)	0.0 (0.0 – 1.0)
Partial thromboplastin time (PTT) (s)	28.0 (25.8 – 30.0)	24.0 (23.0 – 26.5)	30.0 (28.0 – 31.5)	28.5 (27.0 – 30.8)
Creatinine (mg/dl)	1.0 (1.0 – 1.2)	1.1 (0.9 – 1.2)	0.9 (0.8 – 1.1)	1.0 (0.8 – 1.2)
C-reactive protein (CRP) (mg/dl)	0.2 (0.1 – 0.7)	0.2 (0.1 – 0.4)	0.6 (0.3 – 1.7)	0.4 (0.2 – 0.6)

All values are mean values and 25% and 75% quartiles. The highlighted fields correspond to the cause of admission.
**Patients with another cause of admission had this disease in the past patient history, but did not contribute to the current patient stay.*

TABLE 4 | Summary of sequenced and analysed samples per sequencing run.

Group	First sequencing run before | after filtering	Second sequencing run before | after filtering	Third sequencing run before | after filtering	Fourth sequencing run before | after filtering
Abdominal Aneurysm	13 | 13	8 | 7	5 | 4	9 | 6
Coronary Heart Disease	13 | 13	7 | 7	7 | 6	7 | 6
Carotid Stenosis	10 | 10	9 | 9	2 | 2	3 | 3
Peripheral Artery Disease	11 | 11	7 | 5	7 | 7	11 | 6
Control	0 | 0	16 | 16	4 | 4	8 | 5

Number on the left shows sequenced samples and number on the right analysed ones. Non-analysed samples did not meet the thresholds for a sufficient sequencing quality (A minimum of 500,000 reads altogether and 7% of mapped miRNA in relation to total library size).

Overrepresentation Analysis

Overrepresentation analysis was carried out with miRNAs resulting from the DGE analysis with the stricter filter criteria using R and clusterProfiler (version 3.16.1, Wu et al., 2021) package. The mRNA targets of miRNAs were determined using the miRTarBase database (release 8.0). The annotation of targets was supported by strong experimental evidences (reporter assay or western blot). Pathways and processes that targeted genes contributed to were identified using the Gene Ontology (GO) database for biological processes. To reduce redundant GO terms in the result, the *simplify* function implemented in the package was applied and filtering steps with the GO.db (version 3.11.4, Carlson, 2019) package for R 4.0.3 (R Core Team, 2020) were carried out.

Ethics Approval and Patient Consent for Study Participation

The study was approved by the Ethics Committee of the Medical Faculty of the University of Munich (protocol #17-572). The study was carried out according to the World Medical Association Declaration of Helsinki and all study samples were pseudonymized during analysis. Written informed consent for publication of blinded individual personal data was obtained from each participant.

RESULTS

Sequencing Quality and Mapping Distribution

Data processing resulted in a count table with the dimensions of 2165 miRNAs and 157 samples. For each miRNA, at least one read was counted in one sample. Next, samples with an insufficient sequencing result were determined and taken out from further analysis. A minimum of 500000 reads altogether and 7% of mapped miRNAs in relation to total library size were set as thresholds. This reduced the dimensions for further analysis to 2165 miRNAs and 140 samples. A summary of included samples of each sequencing run is given in **Table 4**. For all data sets the per-base sequence quality had a Phred score over 32. Highest mean library size was observed in the control group with 6.7 M reads. Fewer reads were assigned to the other groups (athero 5.7 M, aneu 5.9 M, chd 6 M, cs 5.2 M, pad 5.8 M) (**Figures 1A**, **2A**). Mean of reads mapped to miRNA reference for the athero and control group was nearly the same (athero 1.3 M, control 1.4 M) (**Figure 1B**). The aneu group showed with 1.6 M the highest number of mapped reads on average. In the other subgroups, 0.2 – 0.4 M reads less were mapped on average (**Figure 2B**). The relative mapping distributions of mapped read counts to different RNA species for the athero group and for the control group (**Figure 1C**) as well as for the individual subgroups (**Figure 2C**) were comparable. Beside different RNA species the reads were also classified as reads shorter than 16nt (Short), as reads without an adaptor (No Adapter) and as unmapped reads (Unmapped) (**Figures 1C**, **2C**). The aneu group showed the highest relative frequency of mapped miRNAs with 33.1%, followed by the cs and athero group with 26.6%, the control group with 24.6%, the pad group with 23.9% and the chd group with 23.4% (**Supplementary Table 1**). A detailed assignment of the individual components of the relative mapping distribution and its percentage of the standard error are given in the **Supplementary Tables 1,2**.

Bioinformatic Analysis of Small RNA-Sequencing Data

Differential Gene Expression Analysis With DESeq2

When comparing the athero group with the control group, the DGE with the default cut-off (adjusted p-value ≤ 0.1) resulted in 114 differentially expressed miRNAs (**Supplementary Table 3**). Filtering the results ($|\log2FC| \geq 1$, adjusted p-value ≤ 0.1 and base mean ≥ 50) yielded 12 differentially expressed miRNAs (**Supplementary Table 4**). The mean log2FC of all differentially expressed and filtered miRNAs for all group comparisons against the control was 1.38 ± 0.31. The highest $|\log2FC|$ was 2. When comparing the individual subgroups with the control group, the following numbers of differentially expressed miRNAs within filtering criteria were found: aneu vs. control ($n = 14$), chd vs. control ($n = 10$), cs vs. control ($n = 10$), pad vs. control ($n = 13$) (**Supplementary Tables 5–8**). The filtered results of the DGE analysis are summarized in **Figure 3**. A total of 27 miRNAs which

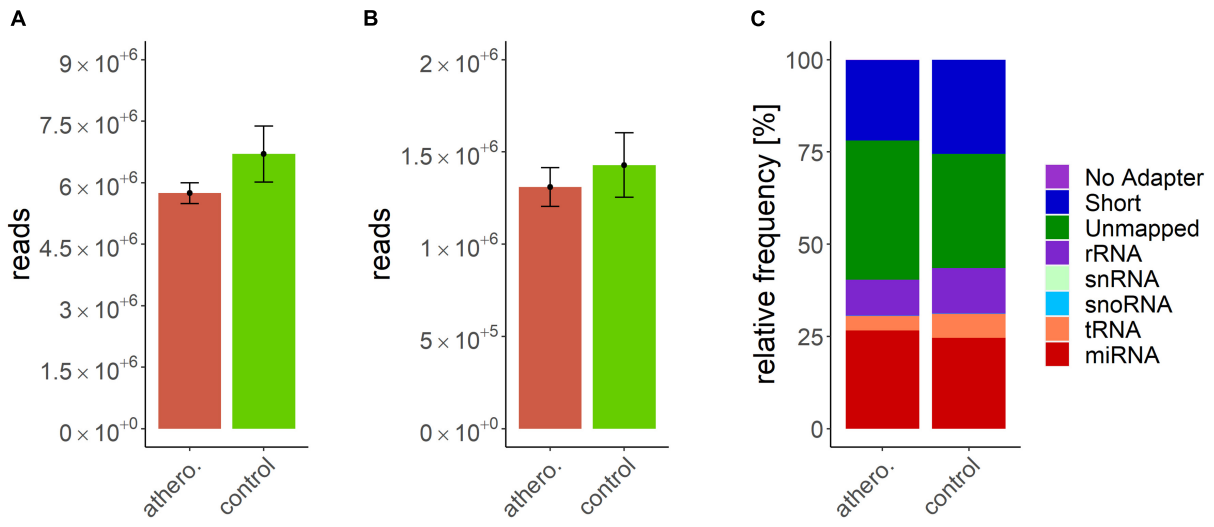

FIGURE 1 | (A) mean library size: athero: 5.74 ± 0.25 M.; control: 6.7 ± 0.69 M.; **(B)** mean of mapped miRNAs: athero: 1.31 ± 0.11 M.; controlr: 1.43 ± 0.17 M.; **(C)** mean relative frequency of mapped read counts. athero = atherosclerotic group; control = control group; No Adapter = reads without adapter; Short = reads smaller than 16 nt; Unmapped = reads which are not mapped to reference; rRNA = reads mapped as rRNA; snRNA = reads mapped as snRNA; snoRNA = reads mapped as snoRNA; tRNA = reads mapped as tRNA; miRNA = reads mapped as miRNA.

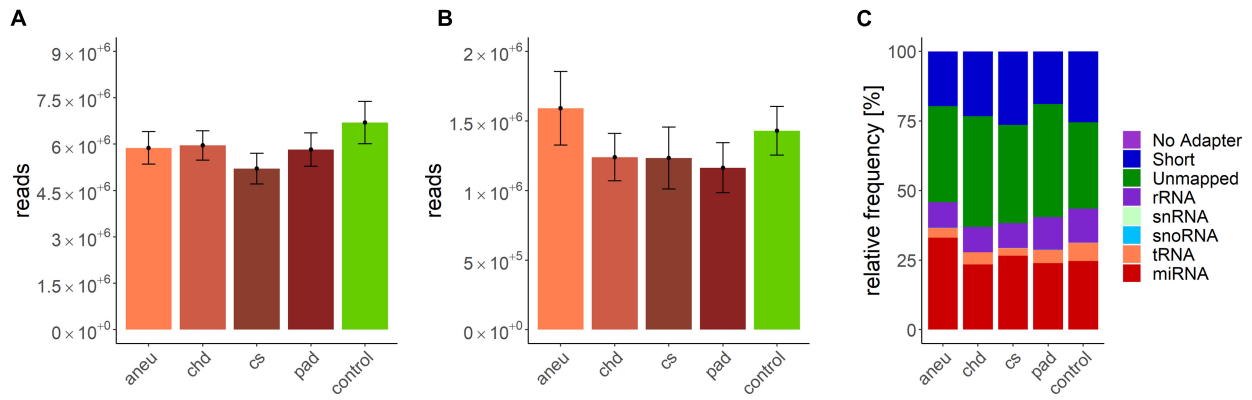

FIGURE 2 | (A) mean library size: aneu: 5.88 ± 0.53 M.; chd: 5.96 ± 0.47 M.; cs: 5.21 ± 0.49 M.; pad: 5.83 ± 0.54 M.; control: 6.7 ± 0.69; **(B)** mean of mapped miRNAs: aneu: 1.6 ± 0.26 M.; chd: 1.24 ± 0.17 M.; cs: 1.23 ± 0.22 M.; pad: 1.16 ± 0.18 M.; control: 1.43 ± 0.17; **(C)** mean relative frequency of mapped read counts. aneu = abdominal aneurysm; chd = coronary heart disease; cs = carotid stenosis; pad = peripheral artery disease; control = control group; No Adapter = reads without adapter; Short = reads smaller than 16 nt; Unmapped = reads which are not mapped to reference; rRNA = reads mapped as rRNA; snRNA = reads mapped as snRNA; snoRNA = reads mapped as snoRNA; tRNA = reads mapped as tRNA; miRNA = reads mapped as miRNA.

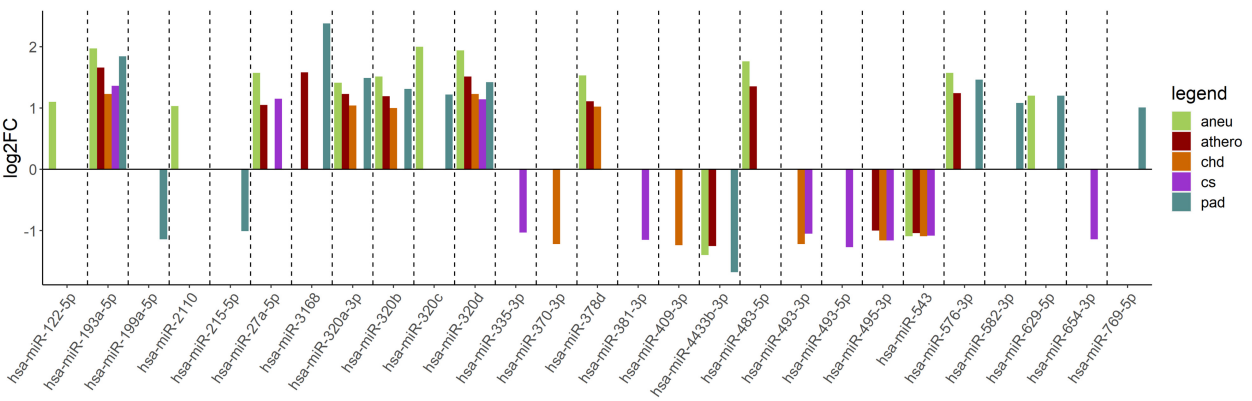

FIGURE 3 | Log2FC of summarized differentially expressed miRNAs from the comparison of each group vs. control. The log2FC is given on the y-axis. aneu = abdominal aneurysm, athero = atherosclerosis, chd = coronary heart disease, cs = carotid stenosis, pad = peripheral artery disease, log2FC = log2 fold change.

were expressed differentially in atherosclerotic groups compared to the control group were found. miR-193-5p and miR-320d were differentially expressed in all groups compared with the control.

Overlap Analysis of the Differentially Expressed miRNAs of the Individual Subgroups

The following overlap analysis was carried out with the resulting miRNAs of the DGE analysis applying stricter filter criteria ($|\log2FC| \geq 1$, adjusted p-value ≤ 0.1 and base mean ≥ 50). Overlapping and group-specific as well as uniquely differentially expressed miRNAs are summarized in **Table 5** and plotted as a Venn-diagram in **Figure 4**. Group-specific differentially expressed miRNAs were the ones that resulted under stricter filter criteria but were also found in other groups and had a adjusted *p*-value below 0.1. Uniquely differentially expressed miRNAs were the ones that were found exclusively in one group. miR-122-5p, miR-2110 and miR-483-5p were found to be group-specific to patients with aneu whereas miR-122-5p and miR-483-5p were exclusive. miR-335-3p, miR-381-3p, miR-493-5p and miR-654-3p were found in patients with cs. miR-654-3p was exclusive for this group. In patients with chd no unique miRNA was found but miR-370-3p and miR-409-3p were group-specific. miR-199a-5p, miR-215-5p, miR-3168, miR-582-3p and miR-769-5p were found in patients with pad whereas miR-3168, miR582-3p and miR-769-5p were found to be uniquely differentially expressed for this group. Common miRNAs of all groups which met the stricter filter criteria were miR-193-5p and miR-320d.

When using differentially expressed miRNAs that resulted with default cut-offs (adjusted p-value ≤ 0.1), 29 group-specific miRNAs were found for aneu, 16 for chd, 15 for cs and 34 for pad (**Supplementary Table 9**). 11 miRNAs (miR-125a-3p, miR-1306-5p, miR-193a-5p, miR-199a-5p, miR-22-3p, miR-22-5p, miR-320d, miR-378i, miR-543, miR-548ad-5p, miR-576-3p) were commonly differentially expressed in all subgroups. Some miRNAs could be assigned in both overlap analyses (default cut-offs and stricter filter criteria) to one group. miR-654-3p was

TABLE 5 | Differential expression of unique miRNAs for each atherosclerotic subgroup.

	Unique for coronary heart disease			Unique for carotid stenosis			Unique for abdominal aneurysm			Unique for peripheral arteria disease		
Gene	**group specific**	**log2FC**	**padj.**	**group specific**	**log2FC**	**padj.**	**group specific**	**log2FC**	**padj.**	**group specific**	**log2FC**	**padj.**
miR-370-3p	**yes**	−1.220	0.007	**no**	−0.972	0.076	**no**	–	–	**no**	–	–
miR-409-3p	**yes**	−1.241	0.006	**no**	−0.996	0.056	**no**	–	–	**no**	–	–
miR-335-3p	**no**	–	–	**yes**	−1.031	0.036	**no**	−0.828	0.042	**no**	–	–
miR-381-3p	**no**	−0.921	0.037	**yes**	−1.149	0.036	**no**	−0.782	0.081	**no**	–	–
miR-493-5p	**no**	–	–	**yes**	−1.271	0.045	**no**	−0.921	0.096	**no**	–	–
miR-654-3p	**no**	–	–	**yes**	−1.137	0.039	**no**	–	–	**no**	–	–
miR-122-5p	**no**	–	–	**no**	–	–	**yes**	1.098	0.050	**no**	–	–
miR-2110	**no**	–	–	**no**	–	–	**yes**	1.028	< 0.001	**no**	0.837	0.014
miR-483-5p	**no**	–	–	**no**	–	–	**yes**	1.765	0.027	**no**	–	–
miR-199a-5p	**no**	−0.820	0.036	**no**	−0.833	0.064	**no**	−0.730	0.061	**yes**	1.136	0.003
miR-215-5p	**no**	−0.988	0.007	**no**	–	–	**no**	−0.677	0.074	**yes**	1.006	0.005
miR-3168	**no**	–	–	**no**	–	–	**no**	–	–	**yes**	−2.380	0.004
miR-582-3p	**no**	–	–	**no**	–	–	**no**	–	–	**yes**	−1.081	0.013
miR-769-5p	**no**	–	–	**no**	–	–	**no**	–	–	**yes**	−1.012	0.052

Input for the overlap analysis was the resulted differentially expressed miRNAs of the DGE analysis with stricter filter criteria (adjusted p-value ≤ 0.1, log_2 fold change (|log2FC|) ≥ 1, base mean ≥ 50). Group specific miRNAs meet the stricter filter criteria. Genes in bold were only found in the corresponding group as significant differentially expressed (padj. < 0.1).

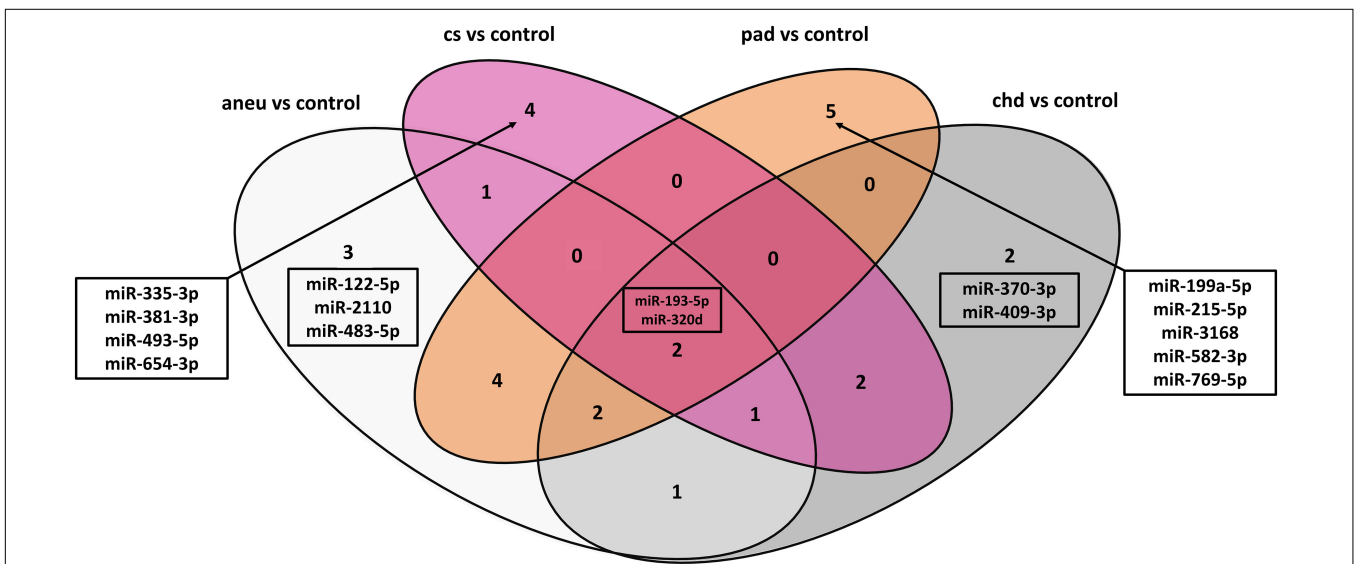

FIGURE 4 | Venn-diagram representing the result of the overlap analysis; aneu = abdominal aneurysm; chd = coronary heart disease; cs = carotid stenosis; pad = peripheral artery disease.

found in both analyses for the cs group. miR-122-5p and miR-483-5p were found for the aneu group, miR-3168, miR-583-3p, and miR-769-5p for the pad group and for the chd group the result did not overlap.

Unsupervised and Supervised Clustering

The unsupervised clustering was done by PCA. The data points of the different groups overlap in both comparisons. Even by reducing the dataset to the 500 most variant miRNAs as input for the analysis the expression variance between groups is overall too small. The results of the PCA analysis are shown as a plot in **Figure 5**. **Figure 5A** (PC1 and PC2) represents the comparison of atherosclerotic against control while **Figure 5B** (PC1 and PC2) displays the comparison of all subgroups and the control.

Supervised clustering of the multivariate dataset was carried out by a sPLS-DA. The analysis resulted in a differentiation between the athero and control group by nine miRNAs as discriminator (**Figure 6A**). One of the miRNAs (miR-193a-5p) was also determined by the DGE analysis with DESeq2. To differentiate between the individual subgroups and the control, 34 miRNAs (**Supplementary Table 11**) were determined by the sPLS-DA (**Figure 6B**). Three (miR-193a-5p, 199a-5p, 215-5p) out

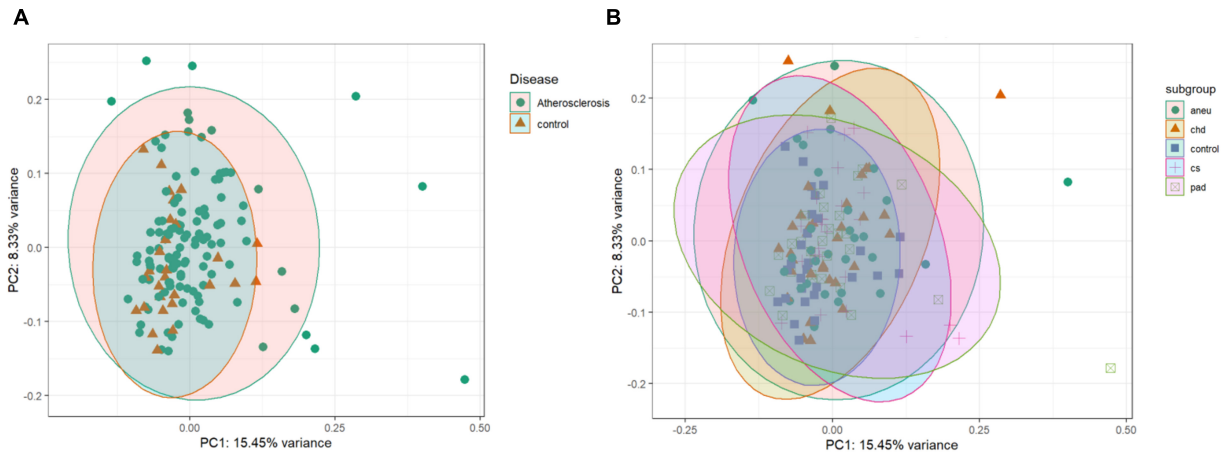

FIGURE 5 | Unsupervised clustering results: **(A)** is the principal component analysis (PCA) result of the comparison of the athero and control group. **(B)** is showing the results of the subgroups and control comparison. Dataset was reduced to the 500 most variant miRNAs; PC1 = principal component 1; PC2 = principal component 2; aneu = abdominal aneurysm; chd = coronary heart disease; cs = carotid stenosis; pad = peripheral artery disease.

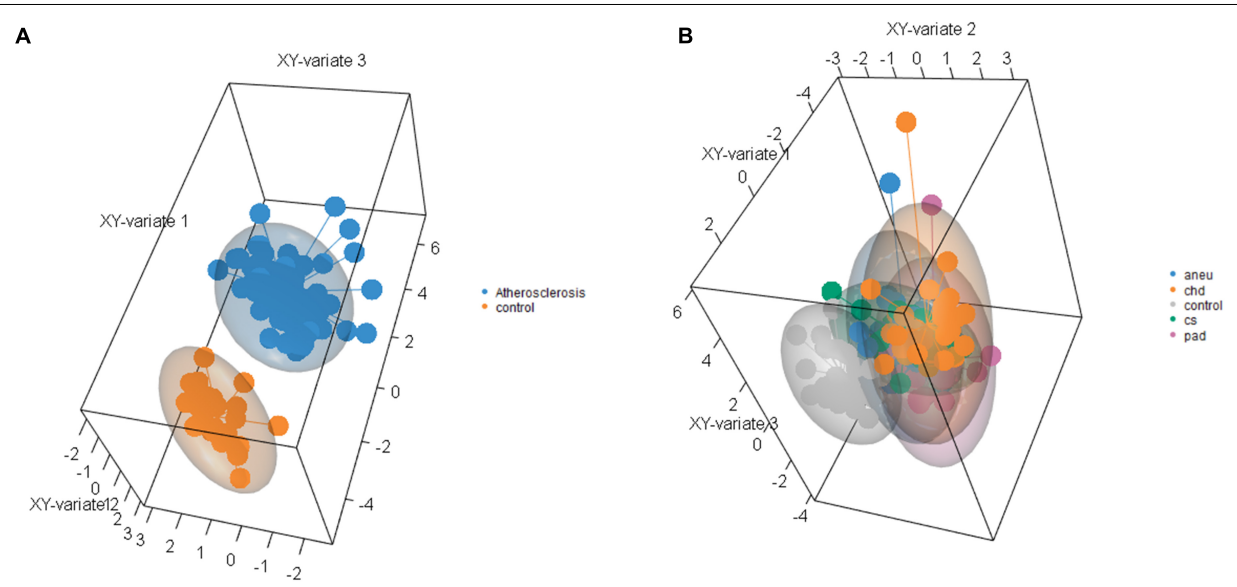

FIGURE 6 | Results of sparse partial-least-squares discriminant analysis for two components. **(A)** Comparing athero group and control group and **(B)** comparing subgroups and control; aneu = abdominal aneurysm; chd = coronary heart disease; cs = carotid stenosis; pad = peripheral artery disease.

of them were also obtained in the DGE analysis. Both results, one with the weighted coefficient of each miRNA and the other one with the principal component (PC) it is assigned to are summarized in **Supplementary Tables 10,11**.

Overrepresentation Analysis

Differentially expressed miRNAs which were detected in the DGE analysis were the starting point to determine mRNA targets (**Table 6**). Only annotations supported by strong experimental evidence from the miRTarBase database were used.

The biological processes controlled by these genes were determined using the GO database. The filtered results of the ORA for each group are summarized in **Supplementary Tables 12–16**. Part of the ORA result with the best ranked enriched GO terms of all individual groups is illustrated in a dot plot (**Figure 7**). Here 13 regulated biological processes were assigned to all groups. Group specific processes were found, too: 2 for the athero group, 2 for the aneu group, 1 for the chd group and 2 for the cs and pad group. Most of the GO terms presented in the dot plot could be linked to disease related processes of atherosclerosis.

For a better overview of the dot plot, further GO terms from the ORA analysis have been summarised in **Table 7**. Here, the individual GO terms were assigned to seven different biological processes that are associated with the development and progression of atherosclerosis. These are processes related to

TABLE 6 | Differentially expressed miRNAs and their targeted mRNAs.

miRNA	Log2FC	Adjusted p-value (FDR)	Targeted mRNAs
Atherosclerosis vs. Control			
miR-193a-5p	1.66	< 0.001	ERBB2, IGF2BP1, ING5, MTOR, NLN, PIK3R3, SRR, TFAP2A, TP73, WT1
miR-27a-5p	1.05	0.027	EGFR, GREM1, MXI1, PEBP1, PPARA, SFRP1 SNAP25, TXN2
miR-320b	1.19	0.002	DLX5, MYC, NOD2
miR-320d	1.51	< 0.001	GNAI1, RBFOX2
miR-483-5p	1.35	0.045	CKB, ALCAM, FAM160B2, MAPK3, RHOA, SRF, NOTCH3
miR-495-3p	−1	0.009	AKT1, ATP7A, BMI1, RUNX3, FOXC1, HSPA5, MAT1A, MEIS1, PBX3, ABCB1, CCL2, SOX9, HMGA2, SMR3B, PTP4A3, TBC1D9, MTA3
miR-543	−1.04	0.003	KRAS, MMP7, NOS3, PTK2, TWIST1, HMGA2, MTA1, SIRT1, FBXO11
miR-576-3p	1.24	< 0.001	CCND1
Abdominal aneurysm vs. Control			
miR-122-5p	1.10	0.050	ADAM10, ALDOA, ANK2, ANXA11, RHOA, ATP1A2, AXL, BAX, BCL2L1, BCL2L2, CCNG1, CDK4, CREB1, CYP7A1, DUSP2, EGFR, FUT8, GYS1, HMOX1, IGF1R, IL1A, MECP2, MEF2D, NCAM1, P4HA1, PDK4, PKM, PRKAB1, MAPK11, PTPN1, RAC1, SLC7A1, SRF, ADAM17, TPD52L2, VEGFC, WNT1, PRKRA, SOCS1, TBX19, NUMBL, ENTPD4, AKT3, TRIB1, SPRY2, AP3M2, FOXJ3, PEG10, LPIN1, XPO6, CTDNEP1, SLC7A11, DSTYK, CLIC4, FOXP1, NT5C3A, RAB6B, GALNT10, UBAP2, ZNF395, NOD2, AACS, FUNDC2, RAB11FIP1, NFATC2IP, G6PC3, EGLN3, ACVR1C, FAM117B
miR-193a-5p	1.97	< 0.001	ERBB2, IGF2BP1, ING5, MTOR, NLN, PIK3R3, SRR, TFAP2A, TP73, WT1
miR-27a-5p	1.57	0.002	EGFR, GREM1, MXI1, PEBP1, PPARA, SFRP1 SNAP25, TXN2
miR-320b	1.51	0.002	DLX5, MYC, NOD2
miR-320c	2.00	< 0.001	PRDM1, EZH2, GNAI1, IRF4, SMARCC1, XBP1, NOD2
miR-320d	1.94	< 0.001	GNAI1, RBFOX2
miR-483-5p	1.76	0.027	CKB, ALCAM, FAM160B2, MAPK3, RHOA, SRF, NOTCH3
miR-543	−1.09	0.026	KRAS, MMP7, NOS3, PTK2, TWIST1, HMGA2, MTA1, SIRT1, FBXO11
miR-576-3p	1.57	< 0.001	CCND1
miR-629-5p	1.2	< 0.001	HNF4A, TRIM33
Coronary heart disease vs. Control			
miR-193a-5p	1.23	0.003	ERBB2, IGF2BP1, ING5, MTOR, NLN, PIK3R3, SRR, TFAP2A, TP73, WT1
miR-320d	1.23	0.019	GNAI1, RBFOX2
miR-370-3p	−1.22	0.007	MAP3K8, CPT1A, CTNNB1, GADD45A, FOXM1, FOXO1, FOXO1, MGMT
miR-409-3p	−1.24	0.006	AKT1, ANG, CTNND1, ELF2, FGA, FGB, FGG, GAB1, IFNG, MET, MGMT
miR-493-3p	−1.22	0.017	RHOC, MXI1, MAP2K7, FZD4, DKK1
miR-495-3p	−1.16	0.018	AKT1, ATP7A, BMI1, RUNX3, FOXC1, HSPA5, MAT1A, MEIS1, PBX3, ABCB1, CCL2, SOX9, HMGA2, SMR3B, PTP4A3, TBC1D9, MTA3
miR-543	−1.09	0.017	KRAS, MMP7, NOS3, PTK2, TWIST1, HMGA2, MTA1, SIRT1, FBXO11
Carotid stenosis vs. Control			
miR-193a-5p	1.36	0.005	ERBB2, IGF2BP1, ING5, MTOR, NLN, PIK3R3, SRR, TFAP2A, TP73, WT1
miR-27a-5p	1.15	0.087	EGFR, GREM1, MXI1, PEBP1, PPARA, SFRP1 SNAP25, TXN2
miR-320d	1.14	0.067	GNAI1, RBFOX2
miR-335-3p	−1.03	0.036	ESR1, NOS3, PAX6

(Continued)

TABLE 6 | (Continued)

miRNA	Log2FC	Adjusted p-value (FDR)	Targeted mRNAs
miR-381-3p	−1.15	0.036	CD1C, GJA1, ID1, NFKBIA, P2RX5, TWIST1, WEE1, HDAC4, TBC1D9, ANO1
miR-493-3p	−1.05	0.084	RHOC, MXI1, MAP2K7, FZD4, DKK1
miR-495-3p	−1.16	0.045	AKT1, ATP7A, BMI1, RUNX3, FOXC1, HSPA5, MAT1A, MEIS1, PBX3, ABCB1, CCL2, SOX9, HMGA2, SMR3B, PTP4A3, TBC1D9, MTA3
miR-543	−1.08	0.045	KRAS, MMP7, NOS3, PTK2, TWIST1, HMGA2, MTA1, SIRT1, FBXO11
miR-654-3p	−1.14	0.039	CDKN1A
Peripheral artery disease vs. Control			
miR-193a-5p	1.84	< 0.001	ERBB2, IGF2BP1, ING5, MTOR, NLN, PIK3R3, SRR, TFAP2A, TP73, WT1
miR-199a-5p	−1.14	0.002	ACVR1B, JAG1, APOE, DDR1, CAV1, CD44, CDH1, CDH2, CDKN1C, CTSC, CLTC, CCR7, EDN1, ERBB2, ERBB3, ERN1, ETS1, EZH2, GSK3B, HIF1A, HK2, HSPA5, IKBKB, ITGA3, JUNB, KRAS, LDLR, LIF, SMAD3, SMAD4, MAP3K11, NFKB1, PDE4D, PIK3CD, PSMD9, PTGS2, NECTIN1, SMARCA2, SNAI1, SULT1E1, TGFB2, TGFBR1, UNG„ WNT2, LIN7A, VEGFA, WNT2, FZD4, FZD6, MAP4K3, BECN1, LIN7A, KL, MAFB, PIAS3, ATF6, RAB21, SIRT1, SIRT1, GPR78, RND1, SETD2, DRAM1, DNAJA4, WNK1, ARHGAP12, TMEM54, OSCP1, SLC27A1
miR-215-5p	−1.01	0.005	ACVR2B, ALCAM, XIAP, RUNX1, NID1, RB1, ZEB2, PTPRT, SIGLEC8, CTNNBIP1, WNK1, KDM1B
miR-320b	1.31	0.004	DLX5, MYC, NOD2
miR-320c	1.22	0.045	PRDM1, EZH2, GNAI1, IRF4, SMARCC1, XBP1, NOD2
miR-320d	1.42	0.007	GNAI1, RBFOX2
miR-576-3p	1.46	< 0.001	CCND1
miR-582-3p	1.08	0.011	SFRP1, AXIN2, DKK3
miR-629-5p	1.2	< 0.001	HNF4A, TRIM33
miR-769-5p	1.01	0.052	GSK3B, TRAPPC2B

Targets were determined using the miRTarBase database with annotations supported by strong experimental evidence. Log2FC and FDR were calculated by DGE analysis with DESeq2. Bold-marked miRNAs are exclusively differentially expressed. Log2FC = log_2 fold change; B-H p-value = adjusted p-value (Benjamini & Hochberg); FDR = false discovery rate.

the growth and development of endothelial cells which play an important role in the development of atherosclerosis, processes indicating immunological involvement and the presence of messenger substances, processes contributing to the remodeling and mineralization and hardening of tissue, processes related to the blood vessel system in general, processes related to the presence of oxidative stress, processes referred to the metabolism of lipids and glucose and generally to aging.

DISCUSSION

In this study, the transcriptional serum-derived miRNA fingerprint from EVs obtained from four atherosclerotic subgroups and a control group was analysed. These EV-associated miRNAs were investigated to determine a miRNA set serving as potential circulating biomarkers for the identification of atherosclerotic processes and distinguishing between different manifestations. On the one hand, the transcriptional profile of the atherosclerotic group was compared (n = 129) with the control group (n = 28) and on the other hand, each of the four subgroups was compared between each other and with the control group.

Differentially expressed miRNAs were found in the DGE analysis (filter criteria: $|\log2FC| \geq 1$, adjusted p-value ≤ 0.1 and base mean ≥ 50) between the individual subgroups and the control, indicating that a differentiation of the varying manifestations based on the miRNA profiles is possible. Furthermore, the overlap analysis revealed the presence of group-specific and uniquely differentially expressed miRNAs that can be used to characterize individual manifestations. These could be used as circulating candidate signatures to diagnostically assign individual patients to certain subgroups of atherosclerosis and thus to be able to pursue more targeted therapeutic approaches. Some of the differentially expressed miRNAs could also be determined in the supervised clustering, supporting the results of the DGE analysis. We did a cross validation (M-fold validation) within the sPLS-DA analysis. This serves to increase the statistical significance of the results. Other validation strategies are also possible. One option would be to collect independent samples with same manifestations and use RT-qPCR analysis with potential biomarkers from this study to check if they are present.

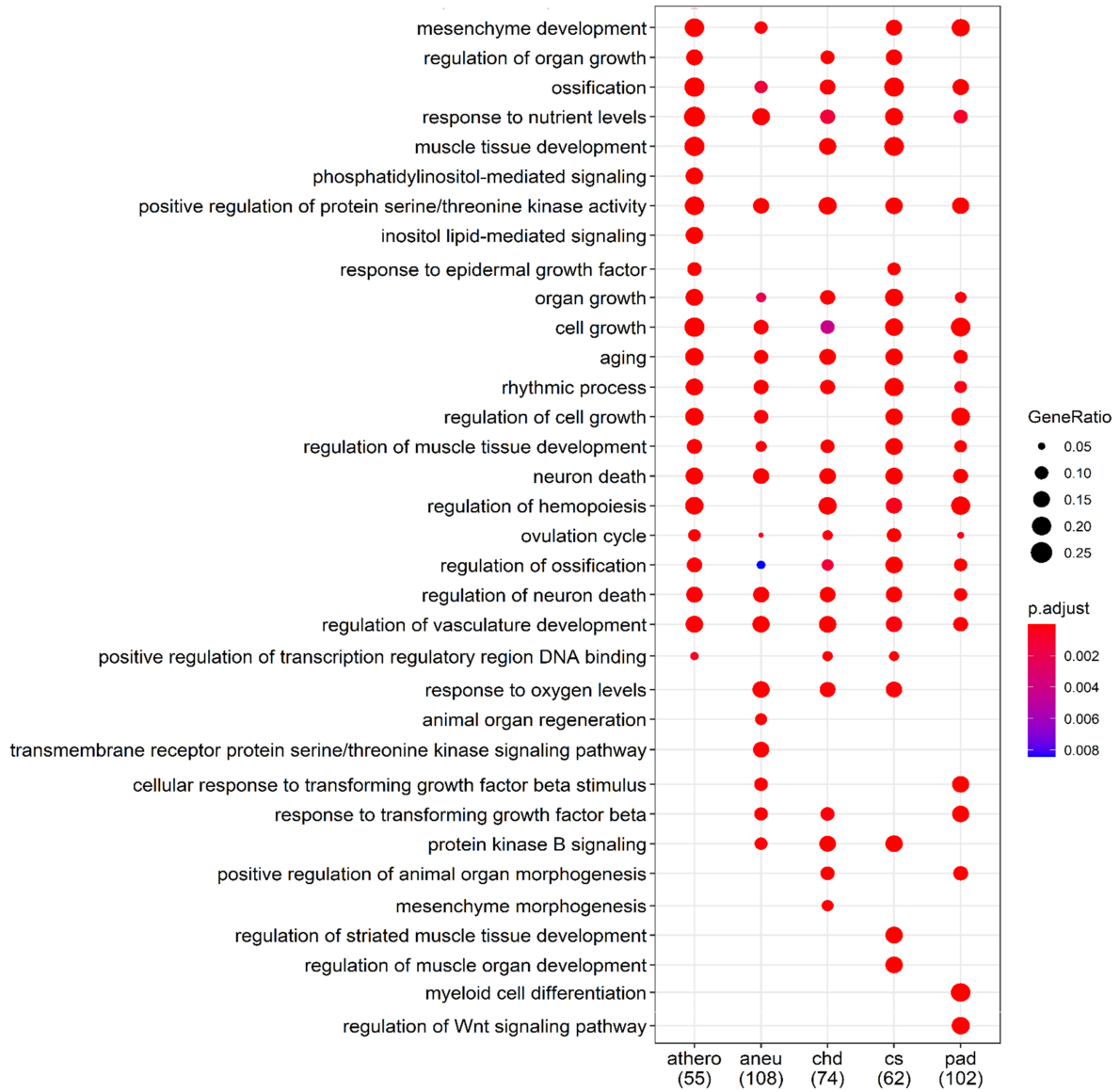

FIGURE 7 | Comparison of the first 34 most enriched GO terms across groups. Gene Ratio indicates the percentage of GO term annotated genes in the gene set. The numbers in brackets indicate the size of the gene set per group; athero = atherosclerosis; aneu = abdominal aneurysm; chd = coronary heart disease; cs = carotid stenosis; pad = peripheral artery disease.

Another way is to divide the samples from this study into a training set to identify biomarker candidates and a test set to validate the results using RT-qPCR analyses. However, this would reduce the statistical power of the DGE by reducing the number of samples for each group.

The relevance of this finding is confirmed by published studies describing miRNAs found in our study as biomarkers for atherosclerosis. miR-320b, which was differentially expressed in all group comparisons except for cs in our study, was associated as a potential biomarker for ischemic stroke (Zhang et al., 2016). miR-27a-5p appeared in our results as discriminator when comparing the aneu and cs group with the control. This miRNA was linked to atherosclerotic processes in various ways (Chen et al., 2012). miR-483-5p was found to be upregulated in patients with acute myocardial infarction (Li et al., 2019) and we assigned it uniquely differentially expressed in the aneu group. In a cell culture study with vascular smooth muscle cells it was shown that a reduced level of miR-381-3p could be associated with the atherosclerotic environment, e.g., in inflammatory reaction, oxidative stress, proliferation and migration of immune cells (Zhu et al., 2021). We found this miRNA differentially expressed in the cs group. In addition to these potential miRNA biomarkers for atherosclerotic processes mentioned in the literature, we were able to identify new candidates. For the aneu group miR-122-5p, miR-193a-5p, miR-543, miR-576-3p, and miR-629-5p were differentially expressed. miR-193a-5p,

miR-370-3p, miR-409-3p, miR-493-3p, miR-495-3p and miR-543 were found for the chd group. In the cs group miR-193a-5p, miR-493-3p, miR-495-3p, miR-543 and miR-654-3p were found to be differentially expressed. And in the pad group miR-193a-5p, miR-199a-5p, miR-215-5p, miR-576-3p, miR-582-3p, miR-629-5p and miR-769-5p were found.

In addition to the results of the DGE analysis with more stringent filter criteria (log2FC $\geq$ | 1|, adjusted p-value $\leq$ 0.1 and base mean $\geq$ 50), further potential miRNA candidates were found using default filter settings (adjusted p-value $\leq$ 0.1). The relevance of these miRNAs to atherosclerotic processes is shown in the following by means of selected literature references. miR-22-5p and -3p were found to be differentially expressed in the comparison of all subgroups against the control. This miRNA is described to play a role in the formation of the neointima through the regulation of artery vascular SMCs (Huang et al., 2017; Yang et al., 2018). In functional *in-vitro* studies it could be shown that the reduced expression of miR-335-5p had a regulative effect on macrophages that was beneficial for plaque formation (Sun et al., 2021). In our case, this miRNA was expressed differentially compared to the aneu group. Other miRNAs such as miR-132 were associated with inducing proliferation in SMCs

TABLE 7 | Biological processes that can be associated with atherosclerosis and the associated gene ontology (GO) terms of the overrepresentation analysis (ORA).

Biological processes related to atherosclerosis	GO Term found in ORA
Processes related to the growth and development of endothelial cells which play an important role in the development of atherosclerosis.	• cellular response to vascular endothelial growth factor stimulus • regulation of endothelial cell migration • vascular endothelial growth factor signaling pathway • endothelial cell differentiation • endothelial cell differentiation • endothelial cell activation
Processes indicating immunological involvement and the presence of messenger substances.	• regulation of leukocyte apoptotic process • leukocyte cell-cell adhesion • positive regulation of leukocyte chemotaxis • regulation of leukocyte migration • regulation of leukocyte differentiation • regulation of leukocyte apoptotic process • T cell differentiation • positive regulation of T cell activation • T cell differentiation • alpha-beta T cell activation involved in immune response • negative regulation of lymphocyte migration • lymphocyte differentiation • cytokine secretion • positive regulation of cytokine production • cytokine secretion involved in immune response • cellular response to interleukin-1 • cellular response to interleukin-6 • cellular response to transforming growth factor beta stimulus • cellular response to tumor necrosis factor • negative regulation of cellular response to growth factor stimulus
Processes that contribute to the remodeling and mineralization and hardening of tissue.	• regulation of ossification • osteoblast differentiation • regulation of osteoblast differentiation • regulation of osteoblast proliferation • negative regulation of osteoblast differentiation • regulation of biomineralization for plaque calcification • tissue remodeling • connective tissue development • regulation of tissue remodeling • regulation of muscle tissue development • tissue homeostasis
Processes related to the blood vessel system in general.	• regulation of vasculature development • cellular response to vascular endothelial growth factor stimulus • regulation of vasculature development • vasculogenesis • coronary vasculature morphogenesis • regulation of vascular permeability • artery morphogenesis, artery development
Processes related to the presence of oxidative stress.	• cellular response to oxidative stress • cellular response to hypoxia • negative regulation of oxidative stress-induced cell death

(Continued)

TABLE 7 | (Continued)

Biological processes related to atherosclerosis	GO Term found in ORA
Processes referred the metabolism of lipids and glucose.	• positive regulation of cholesterol efflux • cholesterol homeostasis • cholesterol transport regulation of fatty acid beta-oxidation • fatty acid homeostasis • response to fatty acid • regulation of fatty acid metabolic process • positive regulation of lipid metabolic process • regulation of lipid storage • regulation of phospholipid metabolic process • regulation of lipid kinase activity • regulation of triglyceride metabolic process • triglyceride homeostasis • cellular response to glucose stimulus • regulation of glucose metabolic process • cellular glucose homeostasis • regulation of fat cell differentiation
Processes generally concerned to aging.	• aging • negative regulation of cell aging • regulation of cell aging • regulation of cellular senescence • cellular senescence

(Reddy et al., 2016) and were assigned in our study to the aneu group (miR-132-3p) (**Supplementary Table 3**). It is also believed that miR-21 targets TPM1. A downregulation of that gene is associated with the regulation of the shape of SMCs which influence the cytoskeletal stability (Wang et al., 2011). We found this miRNA (miR-21-5p) (**Supplementary Table 3**) to be upregulated in the comparison of the chd group to the control. Upregulated miR-191 is linked to the use of antiplatelet therapy (prasugrel or aspirin) (Willeit et al., 2013) and could be found in all groups (miR-193-3p) except the aneu.

The ORA results showed and confirmed the plausibility of the miRNAs found in relation to atherosclerotic processes. Several of the thereby identified biological processes that are triggered by mRNAs targeted by the specifically differentially regulated miRNAs found in our patients could be linked to the formation and progression of atherosclerosis. One example is the formation of atherosclerotic plaques. It is initiated by the sub endothelial accumulation of lipoproteins (Libby et al., 2019). Identified GO terms which are linked to this are describing the homeostasis, transport and metabolism of lipoproteins (positive regulation of cholesterol efflux, cholesterol homeostasis and positive regulation of lipid metabolic process). Subsequently, the accumulation of lipoproteins in the endothelium results in an immunological reaction. Immune cells and their messenger substances create inflammation (Linton and Fazio, 2003; Libby et al., 2010). Gene Ontology terms linked to this process refer on the one hand to cellular immune response such as the differentiation and regulation of leukocytes and t-cells and on the other to activation of messenger substances such as interleukins and growth factors. Furthermore, endothelial–mesenchymal transition plays an important role in the development of atherosclerosis (Souilhol et al., 2018; Wesseling et al., 2018; Hao et al., 2019), as do aging and mineralization (Menghini et al., 2009; Shioi and Ikari, 2018). The associated annotations of the ORA relate to the proliferation, differentiation and regulation of endothelial cells (e. g. *regulation of endothelial cell migration, endothelial cell activation*), but also generally to the blood vessel system and the remodelling of tissue (e.g., *regulation of tissue remodeling, regulation of vasculature development, vasculogenesis, artery development*). Interestingly, several annotations are linked to ossification as histologic process behind calcification of atherosclerotic plaques.

Samples from four sequencing runs were included in this study. Care was taken to achieve an approximately equal distribution of the groups for each run to avoid batch effects. It should be noted that no control group was available in the first run. Both the variation due to the groups within the individual sequencing and the sequencing runs itself were considered and corrected using a suitable algorithm of the DESeq2 package.

One limitation of this study is that the analysed miRNA is not a "pure EV miRNA," as the EV precipitation method may also contain other miRNAs that are bound to other circulating co-isolates (Murillo et al., 2019). Co-isolates may include high- and low-density lipoproteins (HDL and LDL), Argonaut-2 protein complexes and other proteins binding circulating nucleic acids, including miRNAs. But as shown in previous studies, the EV precipitation methods result in the most abundant miRNA expression profiles with most stable biomarker signatures (Spornraft et al., 2014; Buschmann et al., 2016, 2018; Reithmair et al., 2017).

A further limitation of our study results from the fact that some of the identified miRNAs have low differential expression values between groups and that a second patient group for biologic validation of our findings was not available. Our study was designed as a hypothesis generating study, however, and aimed to identify only potential biomarkers for different vascular manifestations of systemic atherosclerosis and did not intend to present a full biomarker panel which need to be characterized in further studies. As any given miRNA can

potentially regulate a high number of mRNA transcripts and even small differences in miRNA expression values can have large biologic consequences, we believe that some of the identified miRNAs may indeed be useful for screening patients with clinically suspected atherosclerosis based on the presence of easily identifiable risk factor (e.g., the metabolic syndrome).

CONCLUSION

This study showed that different manifestations of atherosclerosis can be identified by differentiated miRNAs compared to the control group. In addition, group-specific miRNAs were found. The consistency of the results at the miRNA level is to be confirmed in a next step by additional differential mRNA expression analysis.

DATA AVAILABILITY STATEMENT

The miRNA-Seq. datasets generated and analyzed for this study can be found in https://www.ncbi.nlm.nih.gov/, with the accession number PRJNA739836.

ETHICS STATEMENT

The studies involving human participants were reviewed and approved by Ethics Committee of the Medical Faculty of the University of Munich (protocol #17-572). The patients/participants provided their written informed consent to participate in this study.

AUTHOR CONTRIBUTIONS

MP, GS, and MR: initiating the research idea and applying for funding. FB, AD, RW, and AM: patient recruitment and metadata collection. AH, MR, and AL: laboratory processing of samples. BK, AH, and GD: bioinformatic processing and evaluation of sequencing data. AH: wrote the first draft of the manuscript. AM, GS, MP, and BK: support the interpretation and classification of results. All authors discussed the results and contributed to the final manuscript.

FUNDING

This project was funded by the "Central Innovation Programme for small and medium-sized enterprises (SMEs)" by the Federal Ministry for Economic Affairs and Energy, ZIM grant number ZF4025030AW8 and by the European Research Council under the European Union's Seventh Framework Programme (FP/2007-2013)/ERC Grant Agreement Number (337581).

SUPPLEMENTARY MATERIAL

The Supplementary Material for this article can be found online at: https://www.frontiersin.org/articles/10.3389/fcell.2021.729061/full#supplementary-material

REFERENCES

Bartel, D. P. (2004). MicroRNAs: genomics, biogenesis, mechanism, and function. *Cell* 116, 281–297.

Bennett, D. A., Krishnamurthi, R. V., Barker-Collo, S., Forouzanfar, M. H., Naghavi, M., Connor, M., et al. (2014). The global burden of ischemic stroke. *Glob. Heart* 9, 107–112.

Bentzon, J. F., Otsuka, F., Virmani, R., and Falk, E. (2014). Mechanisms of plaque formation and rupture. *Circ. Res.* 114, 1852–1866.

Buschmann, D., Haberberger, A., Kirchner, B., Spornraft, M., Riedmaier, I., Schelling, G., et al. (2016). Toward reliable biomarker signatures in the age of liquid biopsies – how to standardize the small RNA-Seq workflow. *Nucleic Acids Res.* 44, 5995–6018. doi: 10.1093/nar/gkw545

Buschmann, D., Kirchner, B., Hermann, S., Märte, M., Wurmser, C., Brandes, F., et al. (2018). Evaluation of serum extracellular vesicle isolation methods for profiling miRNAs by next-generation sequencing. *J. Extracell. Vesicles* 7:1481321. doi: 10.1080/20013078.2018.1481321

Carlson, M. (2019). Bioconductor – GO.db [Internet]. Available online at: https://bioconductor.riken.jp/packages/3.10/data/annotation/html/GO.db.html (accessed Sep 22, 2021).

Chen, W. J., Yin, K., Zhao, G. J., Fu, Y. C., and Tang, C. K. (2012). The magic and mystery of MicroRNA-27 in atherosclerosis. *Atherosclerosis* 222, 314–323. doi: 10.1016/j.atherosclerosis.2012.01.020

Deng, S., Wang, H., Jia, C., Zhu, S., Chu, X., Ma, Q., et al. (2017). MicroRNA-146a induces lineage-negative bone marrow cell apoptosis and senescence by targeting polo-like kinase 2 expression. *Arterioscler. Thromb. Vasc. Biol.* 37, 280–290. doi: 10.1161/atvbaha.116.308378

Fan, X., Wang, E., Wang, X., Cong, X., and Chen, X. (2014). MicroRNA-21 is a unique signature associated with coronary plaque instability in humans by regulating matrix metalloproteinase-9 via reversion-inducing cysteine-rich protein with Kazal motifs. *Exp. Mol. Pathol.* 96, 242–249. doi: 10.1016/j.yexmp.2014.02.009

GBD 2013 Mortality and Causes of Death Collaborators (2015). Global, regional, and national age-sex specific all-cause and cause-specific mortality for 240 causes of death, 1990-2013: a systematic analysis for the Global Burden of Disease Study 2013. *Lancet (London, England)* 385, 117–171. doi: 10.1016/s0140-6736(14)61682-2

Hao, Y. M., Yuan, H. Q., Ren, Z., Qu, S. L., Liu, L. S., HengWei, D., et al. (2019). Endothelial to mesenchymal transition in atherosclerotic vascular remodeling. *Clin. Chim. Acta* 490, 34–38. doi: 10.1016/j.cca.2018.12.018

Herrington, W., Lacey, B., Sherliker, P., Armitage, J., and Lewington, S. (2016). Epidemiology of atherosclerosis and the potential to reduce the global burden of atherothrombotic disease. *Circ. Res.* 118, 535–546. doi: 10.1161/circresaha.115.307611

Huang, S., Wang, M., Wu, W., Wang, R., Cui, J., Li, W., et al. (2017). Mir-22-3p inhibits arterial smooth muscle cell proliferation and migration and neointimal hyperplasia by targeting HMGB1 in Arteriosclerosis obliterans. *Cell Physiol. Biochem.* 42, 2492–2506. doi: 10.1159/000480212

Karunakaran, D., and Rayner, K. J. (2016). Macrophage miRNAs in atherosclerosis. *Biochim. Biophys. Acta Mol. Cell Biol. Lipids* 1861(12 Pt B), 2087–2093. doi: 10.1016/j.bbalip.2016.02.006

Kumar, S., Kim, C. W., Simmons, R. D., and Jo, H. (2014). Role of flow-sensitive microRNAs in endothelial dysfunction and atherosclerosis. *Arterioscler. Thromb. Vasc. Biol.* 34, 2206–2216. doi: 10.1161/atvbaha.114.303425

Leeper, N. J., and Maegdefessel, L. (2018). Non-coding RNAs: key regulators of smooth muscle cell fate in vascular disease. *Cardiovasc. Res.* 114, 611–621. doi: 10.1093/cvr/cvx249

Levernier, J. G., and Wacha, H. G. (2017). *Perform Set Operations on Vectors, Automatically Generating All n-Wise Comparisons, and Create Markdown Output [R Package Veccompare Version 0.1.0]*. Available online at: https://cran.r-project.org/package=veccompare (accessed Sep 22, 2021).

Li, L., Li, S., Wu, M., Chi, C., Hu, D., Cui, Y., et al. (2019). Early diagnostic value of circulating microRNAs in patients with suspected acute myocardial infarction. *J. Cell Physiol.* 234, 13649–13658. doi: 10.1002/jcp.28045

Libby, P. (2012). Inflammation in atherosclerosis. *Arterioscler. Thromb. Vasc. Biol.* 32, 2045–2051.

Libby, P., and Theroux, P. (2005). Pathophysiology of coronary artery disease. *Circulation* 111, 3481–3488.

Libby, P., Buring, J. E., Badimon, L., Hansson, G. K., Deanfield, J., Bittencourt, M. S., et al. (2019). Atherosclerosis. *Nat. Rev. Dis. Prim.* 5, 1–18.

Libby, P., Okamoto, Y., Rocha, V. Z., and Folco, E. (2010). Inflammation in atherosclerosis: transition from theory to practice. *Circ. J.* 74, 213–220. doi: 10.1253/circj.cj-09-0706

Linton, M. F., and Fazio, S. (2003). Macrophages, inflammation, and atherosclerosis. *Int. J. Obes.* 27 Suppl 3, S35–S40.

Love, M. I., Huber, W., and Anders, S. (2014). Moderated estimation of fold change and dispersion for RNA-seq data with DESeq2. *Genome Biol.* 15:550. doi: 10.1186/s13059-014-0550-8

Lu, Y., Thavarajah, T., Gu, W., Cai, J., and Xu, Q. (2018). Impact of miRNA in atherosclerosis. *Arterioscler. Thromb. Vasc. Biol.* 38, e159–e170.

Menghini, R., Casagrande, V., Cardellini, M., Martelli, E., Terrinoni, A., Amati, F., et al. (2009). MicroRNA 217 modulates endothelial cell senescence via silent information regulator 1. *Circulation* 120, 1524–1532. doi: 10.1161/circulationaha.109.864629

Moran, A. E., Forouzanfar, M. H., Roth, G. A., Mensah, G. A., Ezzati, M., Murray, C. J. L., et al. (2014). Temporal trends in ischemic heart disease mortality in 21 world regions, 1980 to 2010: the Global Burden of Disease 2010 study. *Circulation [Internet]* 129, 1483–1492.

Murillo, O. D., Thistlethwaite, W., Rozowsky, J., Subramanian, S. L., Lucero, R., Shah, N., et al. (2019). exRNA atlas analysis reveals distinct extracellular RNA cargo types and their carriers present across human biofluids. *Cell* 177, 463–477.e15.

Ouimet, M., Ediriweera, H., Afonso, M. S., Ramkhelawon, B., Singaravelu, R., Liao, X., et al. (2017). MicroRNA-33 regulates macrophage autophagy in atherosclerosis. *Arterioscler. Thromb. Vasc. Biol.* 37, 1058–1067. doi: 10.1161/atvbaha.116.308916

Ouimet, M., Hennessy, E. J., Van Solingen, C., Koelwyn, G. J., Hussein, M. A., Ramkhelawon, B., et al. (2016). MiRNA targeting of oxysterol-binding protein-like 6 regulates cholesterol trafficking and efflux. *Arterioscler. Thromb. Vasc. Biol.* 36, 942–951. doi: 10.1161/atvbaha.116.307282

Properzi, F., Logozzi, M., and Fais, S. (2013). Exosomes: the future of biomarkers in medicine. *Biomark. Med.* 7, 769–778. doi: 10.2217/bmm.13.63

R Core Team (2020). *A Language and Environment for Statistical Computing*. Vienna: R Foundation for Statistical Computing. Available online at: http://www.r-project.org.

Reddy, M. A., Das, S., Zhuo, C., Jin, W., Wang, M., Lanting, L., et al. (2016). Regulation of vascular smooth muscle cell dysfunction under diabetic conditions by MIR-504. *Arterioscler. Thromb. Vasc. Biol.* 36, 864–873. doi: 10.1161/atvbaha.115.306770

Reithmair, M., Buschmann, D., Märte, M., Kirchner, B., Hagl, D., Kaufmann, I., et al. (2017). Cellular and extracellular miRNAs are blood-compartment-specific diagnostic targets in sepsis. *J. Cell Mol. Med.* 21, 2403–2411. doi: 10.1111/jcmm.13162

Rohart, F., Gautier, B., Singh, A., and Lê Cao, K. A. (2017). mixOmics: an r package for 'omics feature selection and multiple data integration. *PLoS Comput. Biol.* 13:e1005752. doi: 10.1371/journal.pcbi.1005752

Shioi, A., and Ikari, Y. (2018). Plaque calcification during atherosclerosis progression and regression [Internet]. *J. Atheroscler. Thromb.* 25, 294–303. doi: 10.5551/jat.rv17020

Simeone, P., Bologna, G., Lanuti, P., Pierdomenico, L., Guagnano, M. T., Pieragostino, D., et al. (2020). Extracellular vesicles as signaling mediators and disease biomarkers across biological barriers [Internet]. *Int. J. Mol. Sci.* 21:2514. doi: 10.3390/ijms21072514

Souilhol, C., Harmsen, M. C., Evans, P. C., and Krenning, G. (2018). Endothelial-mesenchymal transition in atherosclerosis. *Cardiovasc. Res.* 144, 565–577. doi: 10.1093/cvr/cvx253

Spornraft, M., Kirchner, B., Haase, B., Benes, V., Pfaffl, M. W., and Riedmaier, I. (2014). Optimization of extraction of circulating RNAs from plasma – enabling small RNA sequencing. *PLoS One* 9:e107259. doi: 10.1371/journal.pone.0107259

Sun, D., Ma, T., Zhang, Y., Zhang, F., and Cui, B. (2021). Overexpressed miR-335-5p reduces atherosclerotic vulnerable plaque formation in acute coronary syndrome. *J. Clin. Lab. Anal.* 35:e23608.

Sun, X., Belkin, N., and Feinberg, M. W. (2013). Endothelial microRNAs and atherosclerosis. *Curr. Atheroscler. Rep.* 15: 372.

Vozenilek, A. E., Navratil, A. R., Green, J. M., Coleman, D. T., Blackburn, C. M. R., Finney, A. C., et al. (2018). Macrophage-associated lipin-1 enzymatic activity contributes to modified low-density lipoprotein-induced proinflammatory signaling and atherosclerosis. *Arterioscler. Thromb. Vasc. Biol.* 38, 324–334. doi: 10.1161/atvbaha.117.310455

Wang, M., Li, W., Chang, G. Q., Ye, C. S., Ou, J. S., Li, X. X., et al. (2011). MicroRNA-21 regulates vascular smooth muscle cell function via targeting tropomyosin 1 in arteriosclerosis obliterans of lower extremities. *Arterioscler. Thromb. Vasc. Biol.* 31, 2044–2053. doi: 10.1161/atvbaha.111.229559

Wesseling, M., Sakkers, T. R., de Jager, S. C. A., Pasterkamp, G., and Goumans, M. J. (2018). The morphological and molecular mechanisms of epithelial/endothelial-to-mesenchymal transition and its involvement in atherosclerosis. *Vasc. Pharmacol.* 106, 1–8. doi: 10.1016/j.vph.2018.02.006

Willeit, P., Zampetaki, A., Dudek, K., Kaudewitz, D., King, A., Kirkby, N. S., et al. (2013). Circulating MicroRNAs as novel biomarkers for platelet activation. *Circ. Res.* 112, 595–600. doi: 10.1161/circresaha.111.300539

Wilkinson, L. (2011). ggplot2: elegant graphics for data analysis by WICKHAM, H. *Biometrics* 67, 678–679.

Wu, T., Hu, E., Xu, S., Chen, M., Guo, P., Dai, Z., et al. (2021). clusterProfiler 4.0: a universal enrichment tool for interpreting omics data. *Innovation* 2:100141.

Yang, F., Chen, Q., He, S., Yang, M., Maguire, E. M., An, W., et al. (2018). miR-22 is a novel mediator of vascular smooth muscle cell phenotypic modulation and neointima formation. *Circulation* 137, 1824–1841. doi: 10.1161/circulationaha.117.027799

Zhang, R., Qin, Y., Zhu, G., Li, Y., and Xue, J. (2016). Low serum miR-320b expression as a novel indicator of carotid atherosclerosis. *J. Clin. Neurosci.* 33, 252–258. doi: 10.1016/j.jocn.2016.03.034

Zhang, Y., Liu, Y., Liu, H., and Tang, W. H. (2019). Exosomes: biogenesis, biologic function and clinical potential. *Cell Biosci.* 9:19.

Zhu, X., Zhou, H., Yang, F., Zhang, H., and Ma, K. (2021). miR-381-3p inhibits high glucose-induced vascular smooth muscle cell proliferation and migration by targeting HMGB1. *J. Gene Med.* 23:e3274.

Conflict of Interest: GD is employed by ecSeq Bioinformatics GmbH.

The remaining authors declare that the research was conducted in the absence of any commercial or financial relationships that could be construed as a potential conflict of interest.

Publisher's Note: All claims expressed in this article are solely those of the authors and do not necessarily represent those of their affiliated organizations, or those of the publisher, the editors and the reviewers. Any product that may be evaluated in this article, or claim that may be made by its manufacturer, is not guaranteed or endorsed by the publisher.

frontiers in Cell and Developmental Biology

ORIGINAL RESEARCH
published: 13 October 2021
doi: 10.3389/fcell.2021.735888

Selective Surface and Intraluminal Localization of Wnt Ligands on Small Extracellular Vesicles Released by HT-22 Hippocampal Neurons

Viviana I. Torres[1†], Daniela P. Barrera[2†], Manuel Varas-Godoy[3], Duxan Arancibia[4] and Nibaldo C. Inestrosa[2,5*]*

[1] Departamento Bioquímica y Biología Molecular, Facultad de Ciencias Biológicas, Universidad de Concepción, Concepción, Chile, [2] Centro de Envejecimiento y Regeneración (CARE UC), Departamento de Biología Celular y Molecular, Facultad de Ciencias Biológicas, Pontificia Universidad Católica de Chile, Santiago, Chile, [3] Cancer Cell Biology Laboratory, Centro de Biología Celular y Biomedicina (CEBICEM), Facultad de Medicina y Ciencia, Universidad San Sebastián, Santiago, Chile, [4] Departamento Biomédico, Facultad de Ciencias de la Salud, Universidad de Antofagasta, Antofagasta, Chile, [5] Centro de Excelencia en Biomedicina de Magallanes (CEBIMA), Universidad de Magallanes, Punta Arenas, Chile

The Wnt signaling pathway induces various responses underlying the development and maturation of the nervous system. Wnt ligands are highly hydrophobic proteins that limit their diffusion through an aqueous extracellular medium to a target cell. Nevertheless, their attachment to small extracellular vesicles-like exosomes is one of the described mechanisms that allow their transport under this condition. Some Wnt ligands in these vehicles are expected to be dependent on post-translational modifications such as acylation. The mechanisms determining Wnt loading in exosomes and delivery to the target cells are largely unknown. Here, we took advantage of a cell model that secret a highly enriched population of small extracellular vesicles (sEVs), hippocampal HT-22 neurons. First, to establish the cell model, we characterized the morphological and biochemical properties of an enriched fraction of sEVs obtained from hippocampal HT-22 neurons that express NCAM-L1, a specific exosomal neuronal marker. Transmission electron microscopy showed a highly enriched fraction of exosome-like vesicles. Next, the exosomal presence of Wnt3a, Wnt5a, and Wnt7a was confirmed by western blot analysis and electron microscopy combined with immunogold. Also, we studied whether palmitoylation is a necessary post-translational modification for the transport Wnt in these vesicles. We found that proteinase-K treatment of exosomes selectively decreased their Wnt5a and Wnt7a content, suggesting that their expression is delimited to the exterior membrane surface. In contrast, Wnt3a remained attached, suggesting that it is localized within the exosome lumen. On the other hand, Wnt-C59, a specific inhibitor of porcupine O-acyltransferase (PORCN), decreased the association of Wnt with exosomes, suggesting that Wnt ligand acylation is necessary for them to be secreted by exosomes. These findings may help to understand the action of the Wnt ligands in the target cell, which could be defined during the packaging of the ligands in the secretory cell sEVs.

Keywords: exosomes, hippocampal cells, porcupine, Wnt-C59, Wnt ligand

OPEN ACCESS

Edited by:
Jeffrey David Galley, The Ohio State University, United States

Reviewed by:
Chandrasekar Raman, Joslin Diabetes Center and Harvard Medical School, United States
Xia Gao, Nanjing Drum Tower Hospital, China
Xinlei Li, Nationwide Children's Hospital, United States

***Correspondence:**
Viviana I. Torres
vtorresa@udec.cl
Nibaldo C. Inestrosa
ninestrosa@bio.puc.cl

† These authors have contributed equally to this work and share first authorship

Specialty section:
This article was submitted to Molecular and Cellular Pathology, a section of the journal Frontiers in Cell and Developmental Biology

Received: *03 July 2021*
Accepted: *23 September 2021*
Published: *13 October 2021*

Citation:
Torres VI, Barrera DP, Varas-Godoy M, Arancibia D and Inestrosa NC (2021) Selective Surface and Intraluminal Localization of Wnt Ligands on Small Extracellular Vesicles Released by HT-22 Hippocampal Neurons. Front. Cell Dev. Biol. 9:735888. doi: 10.3389/fcell.2021.735888

INTRODUCTION

Since its discovery, the Wnt signaling and related molecules have been shown to be essential for controlling the development and maturation of the central nervous system (CNS). Wnt ligands modulate several processes during development, such as neurogenesis, synapse formation, synaptic plasticity, and neuronal survival (Dickins and Salinas, 2013; Inestrosa and Varela-Nallar, 2015; McLeod and Salinas, 2018; Oliva et al., 2018). At an early developmental stage, failure of Wnt signaling can compromise synapse formation and consequently the establishment of neuronal circuits (Noelanders and Vleminckx, 2017; Torres et al., 2017; Oliva et al., 2018). In the classical mechanism of action Wnt ligands bind to extracellular receptors activating at least two pathways: the canonical or Wnt/β-catenin pathway and the non-canonical or independent β-catenin pathway (Niehrs, 2012; Nusse and Clevers, 2017). In the canonical β-catenin dependent pathway, Wnt proteins exert their function by binding to the extracellular domains of Frizzled receptors (Fz)/LRP5/6 co-receptor (MacDonald and He, 2012) and in the β-catenin independent pathway, Wnts bind RYK/Derailed, and ROR receptors (Green et al., 2014).

After synthesis, Wnt molecules undergo glycosylation and acylation at the endoplasmic reticulum (ER) and follow the secretory pathway (Takada et al., 2006; Herr and Basler, 2012; Torres et al., 2019). The role of glycosylation in secretion appears to be specific to the Wnt ligand. For example, it has been reported in a mouse cell line that any of the four asparagine(N)-linked glycosylations of Wnt1 are necessary for secretion (Mason et al., 1992). A similar observation was made in *Drosophila* with the Wnt homolog Wingless (Wg; Tang et al., 2012). On the contrary, site-directed mutagenesis of the four asparagine residues in Wnt5a did affect secretion into the extracellular matrix (ECM; Kurayoshi et al., 2007; Torres et al., 2019). The other modification that Wnt molecules undergo is the addition of a lipid moiety by the O-acyltransferase PORCN, which adds palmitoleic acid to specific serine residues of Wnts (Gao and Hannoush, 2014; Torres et al., 2019). Although several studies have suggested that acylation mediated by PORCN is necessary for Wnt secretion (Kadowaki et al., 1996; Barrott et al., 2011; Biechele et al., 2011), the latest findings in several cancer cells lines and a specific T cell seem to contradict that (Richards et al., 2014; Rao et al., 2019). A putative explanation for those opposed results is that Wnt acylation mediated by PORCN is only necessary for their association with specific Wnt transporters.

Once Wnts reach the extracellular milieu, they can act in an autocrine as well as in a paracrine fashion. In the latter, Wnt ligands act over long distances from a Wnt-producing cell (Zecca et al., 1996; Neumann and Cohen, 1997). Given this capability, it was hypothesized that instead of spreading to reach their targets, they could be transferred between cells by different mechanisms, which include: (i) specialized filopodia mechanism called cytonemes (Takada et al., 2017); (ii) lipoproteins or the SWIM protein (Mulligan et al., 2012; Kaiser et al., 2019); (iii) membranous structures designated as argosomes (Greco et al., 2001) which are lipoprotein particles surrounded by lipid particles; and (iv) small extracellular vesicles (sEVs) referred to as exosomes (Gross et al., 2012; Działo et al., 2019). These extracellular vesicles have a diameter of 50–150 nm, are secreted by most cell types (Raposo and Stoorvogel, 2013), and deliver macromolecules to their target cells in healthy and pathological conditions (Isola and Chen, 2017). What determines the extracellular transport mechanisms for Wnts is unclear which might be tissue, cell type or Wnt specific, but also the physiological stage of the secreting cell might play a role.

In the CNS, microglia, oligodendrocyte and neurons release exosomes (Potolicchio et al., 2005; Fauré et al., 2006; Krämer-Albers et al., 2007) and *in vitro* evidence demonstrates that changes in synaptic activity modulate the release of exosomes from neurons (Fauré et al., 2006; Lachenal et al., 2011). These exosomes can be reincorporated into other neurons, suggesting a new form of inter-neuronal communication. In *Drosophila,* Wg is associated with exosomes, and the protein GPR177/Evi transfers it from the presynapse to the postsynapse (Korkut et al., 2009; Beckett et al., 2013). In vertebrates, Wnt ligands also co-localize with exosomes (Gross et al., 2012; Działo et al., 2019) in physiological and pathological conditions (Zhang and Wrana, 2014; Działo et al., 2019), but in the CNS, to the best of our knowledge, there are no reports on neurons releasing Wnt containing exosomes.

Although Wnt molecules were described 40 years ago, many questions remain unanswered regarding the mechanism of intracellular sorting into the different putative cargoes, and less is known about the possible role of exosomes in mediating Wnt signaling protein transport from one cell to another. Here, we determined the association between Wnt ligands and sEVs. Also, we described how the inhibition of Wnt ligands palmitoylation affects their release associated with these vesicles. Finally, we show the topological localization of Wnt signaling proteins in the population of sEVs released from HT-22 cells.

MATERIALS AND METHODS

This study was not pre-registered. No blinding was performed. Institutional Ethical Approval was not required for the study.

Cell Culture and Small Extracellular Vesicle Preparation

The immortalized mouse hippocampal cell line HT-22 (passages 15–20) was cultured with the following Thermo Fisher Scientific Inc., reagents: Dulbecco's Modified Eagle Medium (Catalog Number: 11966025) supplemented with 4.5 g/L glucose, 10% Fetal Bovine Serum (FBS) (Catalog Number: 16000044), 2 mM glutamine (Catalog Number: 25030024), 100 I.U./ml penicillin-100 μg/ml Streptomycin (Catalog Number: 15140163), at 37°C under 5% CO_2. Once 60–70% confluency was reached, cells were washed twice with phosphate buffer saline (PBS) to remove any FBS. Then, cells were grown in the same medium but using 10% exosome depleted FBS (Thermo Fisher Scientific Inc., Catalog Number: A2720803). After 48 h, the conditioned medium (CM) of HT-22 cells was collected, and the cells were lysed with RIPA buffer containing Halt protease inhibitor cocktail (Thermo Fisher Scientific Inc., Catalog Number: 78445). The CM was subjected to

three consecutive centrifugations: 2,000× *g*, 10 min; 20,000× *g*, 20 min; and 100,000× *g*, for 2 h at 4°C. The final pellet, called P100 or EV (Kowal et al., 2016), was resuspended in 0.2 μm filtered PBS, pelleted again, and stored at −80°C until further analysis or used immediately for downstream analysis.

Electron Microscopy

P100 was re-suspended in PBS, re-pelleted and analyzed by transmission electron microscopy. To examine its fine structure, P100 was fixed in 2.5% glutaraldehyde/0.1 M sodium cacodylate buffer pH 7.4 at room temperature overnight (EMS, Catalog Number: 15960). Then it was washed with cacodylate buffer for 2 h and post-fixed with 1% aqueous osmium tetroxide for 2 h, rinsed with bidistilled water and stained with 1% uranyl acetate for 90 min. It was dehydrated twice stepwise with increasing acetone concentrations (50, 70, 95, and 100%) for 30 min each. Preinclusion was done with epon:acetone (1:1) overnight and then it was included in pure epon. The polymerization was carried out in an oven at 60°C for 48 h. Fine cuts of 80 nm thickness were obtained in a Leica Ultracut R Ultramicrotome, stained with 4% uranyl acetate in methanol for 2 min and with Reynolds's lead citrate for 5 min. The slices were observed in a Philips Tecnai 12 BioTwin microscope (Eindhoven, Netherlands) at 80 kV. All post-fixation treatments of a sample were performed in the advanced Pontificia Universidad Católica de Chile Microscopy Unit.

Immunogold

For immunogold analysis, P100 pellets were fixed in 4% paraformaldehyde (PFA) in 0.1 M phosphate buffer pH 7.0, 0.2% for at 4°C for 2 h, then rinsed for 30 min in phosphate buffer, dehydrated with 50, 70, 95, and 100% ethanol for 15 min each and then left overnight in ethanol/LR White 1:1. Then, P100 pellets were included in the resin in gelatin capsules and polymerized at 50°C for 8 h. A Leica Ultracut R Ultramicrotome was used to make fine 90 nm wide cuts, which were placed in nickel grids. A cut was blocked with PBS/0.1% BSA for 30 min, then incubated with a 1:20 dilution of a primary antibody (CD63, Santa Cruz Biotechnology, Inc., Catalog Number: sc-5275; Wnt3a, Thermo Fisher Scientific Inc., Catalog Number: PA5-44946; Wnt5a, Abcam, Catalog Number: ab174963; Santa Cruz Biotechnology, Inc., Wnt5a Catalog Number: sc-365370; Thermo Fisher Scientific Inc., Wnt7a, Catalog Number: PA5-80231; MyBioSource GPR177, Catalog Number: MBS769833, and washed three times with PBS/0.1% BSA/0.2% Triton X-100 for 20 min. Goat anti-Rabbit Gold 6 nm, (Abcam, Catalog Number: ab41498) or goat anti-mouse Gold 25 nm (EMS, Catalog Number: 25135) was used as secondary antibody and incubated for 1 h, then washed three times for 20 min with PBS/0.1% BSA/0.2% Triton X-100, and a rapid final wash in distilled water was done. A Philips Tecnai 12 BioTwin microscope (Eindhoven, Netherlands) at 80 kV was used to examine the sections stained with aqueous 1% uranyl acetate for 5 min.

Nanoparticle Tracking Analysis

A more precise size determination of the EV was obtained through performing NTA, which is a higher resolution technique than electron microscopy (Malloy, 2011). It is based on light scattering and Brownian motion behavior, which allows assessing nanoparticle size distribution and abundance of samples in liquid suspensions (NanoSight NS300, Malvern). The samples were diluted in sterile PBS allowing that the particle concentration is within the linear dynamic range of the equipment (10^6–10^9 particles/ml). The analysis was performed using the 532 nm laser, 565 nm long-pass filter, with a camera level set at 9 and a detection threshold of 3.

Western Blotting

Western blots were used to analyze the protein composition of P100 pellets. We used primary antibodies: (dilution used for all primary antibodies 1/300) for, GPR177 (MyBioSource, Catalog Number: MBS769833; Abcam, GM130 Catalog Number: ab52649; Thermo Fisher Scientific Inc., Wnt3a Catalog Number: PA5-44946; Abcam, Wnt5a Catalog Number: ab174963; Thermo Fisher Scientific Inc., Wnt7a Catalog Number: PA5-80231. All the following antibodies were from Santa Cruz Biotechnology, Inc., Wnt5a, Catalog Number: sc-365370; Alix, Catalog Number: sc-53540; TSG101, Catalog Number: sc-7694; NCAM-L1 Catalog Number: sc-374046; Flotillin-1, Catalog Number: sc-133153; Tubulin, Catalog Number: sc-8035; CD63, Catalog Number: sc-5275. Lysate of HT-22 cells were homogenized in RIPA buffer (10 mM Tris–HCl, 1 mM EDTA, 1% Triton X-100, 0.1% sodium deoxycholate, 0.1% SDS, 140 mM NaCl) supplemented with 1 mM PMSF, 7 μg/mL Pepstatin, 5–10 μg/mL Leupeptin, and 10 μg/mL Aprotinin. The protein content of the cell lysate and the P100 were determined by Pierce™ BCA Protein Assay Kit. An aliquot containing 30 μg of protein in both the lysate and the P100 was mixed with standard sample loading buffer loaded and ran in a 10% acrylamide gel. Proteins were transferred on to a PVDF membrane overnight at 4°C.

Wnt-C59 Treatment

HT-22 cells were cultured as described before to obtain the conditioned medium, but in parallel, the cells were incubated with 1 μM of the Wnt-C59 Porcupine inhibitor (Tocris, Catalog Number: 5148). The fresh drug was added after 24 h, and the CM was collected after 48 h to perform the enrichment procedure of EV as indicated above. As a stock of 20 mM of Wnt-C59 was prepared in DMSO, control cells were treated with 0.005% DMSO (vehicle) prepared in indicated cell media.

Proteinase K Assay

The sEVs were isolated by differential ultracentrifugation and resuspended in PBS. Samples were incubated in either PBS or 1.2 μg/ml Proteinase K (Promega, Catalog Number: V3021) in PBS, with or without 0.5% Triton X-100, in a final volume of 40 μl per sample for 5 min at 4°C. The assay was stopped by the addition of 8 μl 5X SDS-PAGE Loading Buffer and heating for 8 min at 97°C, and samples were analyzed by SDS-PAGE and immunoblotted.

Statistics

The GraphPad Prism program was used for statistical analysis. Data derived from the western blot analysis of the Wnt ligands

and other proteins were subjected to the Shapiro–Wilk test, which tested the normality of a data set since the sample size was less than 50. After confirming that all the data were normally distributed, a mismatched *t*-student test was performed. Error bars show SD. No sample size calculation was performed. No exclusion criteria were pre-determined.

RESULTS

Characterization of Extracellular Vesicles Released by the Hippocampal HT-22 Cell Line

To isolate extracellular vesicles, we used the mouse hippocampal cell line HT-22, a relevant model for studying glutamate and heavy metal neurotoxicity (Murphy et al., 1989; Fukui et al., 2009). The cell line HT-22 is accessible to culture and provides an *in vitro* model for biochemistry studies requiring large amounts of starting material. In fact, six to eight 150-mm culture plates were required to obtain 100 μg of protein in the P100 pellet. Transmission electron microscopy (TEM) was performed to morphologically characterize the vesicles in the P100 fraction (see section "Materials and Methods"). A representative image of the P100 pellet shows an enriched fraction of exosome-like vesicles containing a membrane with typical bilayer morphology and with an average diameter of 124.1 ± 6.8 nm (**Figures 1A,B**). Immunogold labeling allows us to visualize the CD63 exosomal signature marker (**Figure 1B**, right panel). The structure of the vesicles was partially lost due to a mild fixation used in immunogold studies to preserve protein epitopes. Considering that the fixation and dehydration of the sample for TEM analysis can cause deformation of the vesicles, a more precise size determination was obtained using NTA. Consistently, the NTA size distribution was similar to the reported size by TEM. The NTA profiles showed a peak of abundant vesicles of 127.4 ± 1.3 nm (**Figure 1C**; mode) and a population of vesicles with a size of <200 nm (defined as small extracellular vesicles, sEVs) representing 78% of the particles in the sample. The remaining 22% corresponds to medium or large extracellular vesicles (**Figures 1C,D**).

Then, we characterize the vesicles released by the HT-22 cells according to the International Society for Extracellular Vesicles (ISEV; Théry et al., 2018). **Figure 1E** shows a western blot analysis of the P100 protein content profile. The P100 pellet exosomal marker content was enriched relative to that of the lysate in the following rank order: Alix > TSG101 > CD63 > Flotillin-1 (**Figure 1F**). The neuronal origin of the vesicles released by HT-22 cells is corroborated by the presence of the adhesion molecule NCAM-L1, an accepted exosome biomarker of neuronal origin (Fauré et al., 2006; **Figure 1F**). Nevertheless, the *cis*-Golgi matrix protein, GM130, was absent from sEVs (**Figure 1E**), suggesting our preparation was not contaminated with intracellular membranes. Thus, our analysis revealed that vesicles released by HT-22 cells and collected in the P100 fraction effectively correspond to small extracellular vesicles like exosomes (size <200 nm) (Théry et al., 2018).

Canonical and Non-canonical Wnt Ligands Are Present in Small Extracellular Vesicles

The enrichment and homogeneous population of exosome-like vesicles prompt us to continue with this cell model to study the presence of Wnt ligands on those vesicles. Next, we examined whether the canonical Wnt3a and Wnt7a ligands and the non-canonical Wnt5a (Korkut et al., 2009; Beckett et al., 2013) were secreted in association with sEVs released by HT-22 cells. Western blot analysis of the sEVs containing fraction (P100) showed enrichment of Wnt5a and the Wnt chaperone, GPR177/Evi, relative to the cell lysate (**Figures 2A,B**). On the other hand, although present, Wnt3a and Wnt7a were not enriched in this fraction (**Figures 2A,B**). To corroborate the presence of Wnts in sEVs, immunogold analysis was performed, revealing that Wnt3a, Wnt5a, Wnt7a, and GPR177/Evi were present in the sEVs (**Figure 3B**). Also, a double immunogold analysis was performed, revealing that Wnt5a (red arrows) and GPR177/Evi (black arrows) were jointly secreted together by the same sEVs (**Figure 3D**). On the contrary, the IgG respective controls did not show any electrodense mark (**Figures 3A,C**). Although these data provide evidence of the presence of Wnt ligands in HT-22 secreted vesicles with exosomes characteristics, it was not possible to detect double labeling of Wnt3a or Wnt7a with GPR177/Evi.

Treatment of HT-22 Cells With the Porcupine Inhibitor Wnt-C59 Affects Wnt Ligands Content of Small Extracellular Vesicles

Porcupine O-acyltransferase is an O-acyltransferase whose activity affects Wnt ligand secretion in Wnt-producing cells (Kadowaki et al., 1996; Torres et al., 2019). It is unknown if inhibition of PORCN by Wnt-C59 affects only a single or all the secretory pathways that mediate Wnt release from cells (Proffitt et al., 2013; Bengoa-Vergniory et al., 2014). In the present work, we specifically assessed the effect of Wnt-C59 on Wnt ligand secretion associated with sEVs. Although this inhibitor should not affect the exosome formation and secretion pathways, we carried out control experiments. From now on, we will call control and Wnt-C59 the vesicles derived from the vehicle (DMSO) and Wnt-C59 treated cells, respectively. First, we evaluated whether treatment of HT-22 cells with Wnt-C59 alters the relative abundance of each of the vesicle subpopulations released by these cells. NTA was performed with the NanoSight NS300 system to analyze the microvesicle fraction content in the P100 pellet. **Figure 4A** provides a graphical description of the relationship between particle density (i.e., particles/ml) and their size distribution (nm). There were no significant differences between the control and Wnt-C59 extracellular vesicles (**Figure 4B**). For both the control and Wnt-C59, there is an enrichment of vesicles with a size of less than 200 nm, similar to the finding showed in **Figure 1C**. Even though there was a trend toward a decrease in the density of total particles, this decline was not significant (**Figure 4C**).

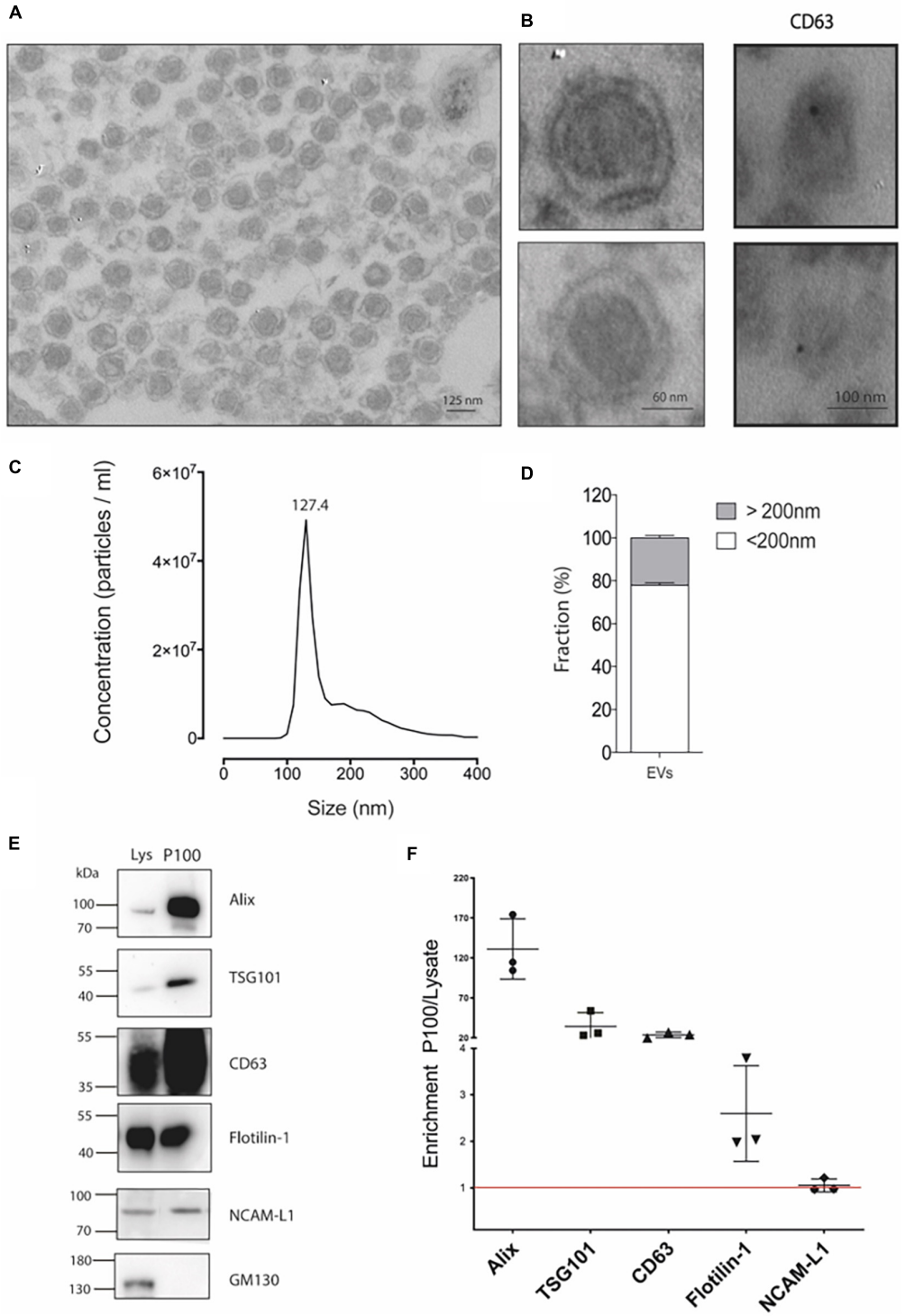

FIGURE 1 | Detailed characterization of P100 vesicles secreted from hippocampal HT-22 cells. **(A)** Representative transmission electron microscopy of P100 shows abundant vesicles with exosome-like appearance with an average diameter of 124.1 ± 6.8 nm of ($n = 31$; three independent cell culture preparations). **(B)** Close capture of single exosomes (left) and immunogold labeling of a selective exosomal biomarker, CD63 (right panel, black dot). **(C)** Nanoparticle tracking analyses show a mean peak at 127.4 ± 1.3 nm ($n = 5$; five independent cell culture preparations). **(D)** Abundance analysis shows that 77.88 ± 2.41% of the vesicles have a diameter of <200 nm and a 22.12 ± 2.41% >200 nm ($n = 4$; four-five independent cell culture preparations). **(E,F)** Western blot and Analysis enrichment (fold) of the protein content of the exosomal markers Alix, 131.08 ± 37.7; TSG101, 34.36 ± 17.00; CD63, 23.82 ± 3.50; Flotillin-1, 2.60 ± 1.03; NCAM-L1, 1.05 ± 0.14. The control GM130, a Golgi-associated protein, was absent. Enrichment is relative to their levels in the lysate. The values were obtained from three independent cell culture preparations.

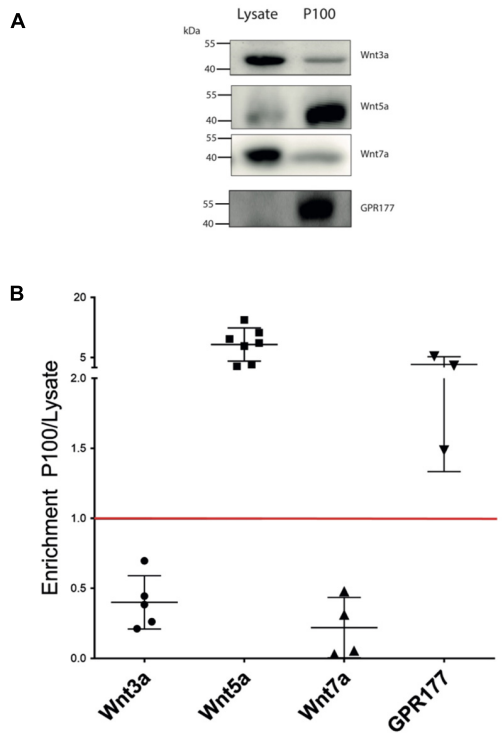

FIGURE 2 | Wnt ligand expression levels in HT-22 cells. **(A)** Comparison of western blot analysis of Wnt3a, Wnt5a, Wnt7a, and GPR177 protein content in cell lysate and P100 fraction. Each lane was loaded with 30 μg protein. **(B)** Summary densitometric measurement of band intensity showing enrichment (fold) of each protein in the P100 pellet relative to a corresponding lysate. Wnt3a, 0.4 ± 0.19 ($n = 5$); Wnt5a, 8.70 ± 4.14 ($n = 7$); Wnt7a, 0.22 ± 0.21 ($n = 4$; four independent cell culture preparations); GPR177 3.30 ± 1.93 ($n = 3$; independent cell culture preparations).

Similarly, no significant differences were observed in the mean distribution size (**Figure 4D**) and the mode distribution size (**Figure 4E**) between the control and Wnt-C59 vesicles. The mean distribution sizes were 166.6 ± 2.5 nm and 164.8 ± 3.9 nm for the control and Wnt-C59 vesicles, respectively (**Figure 4D**). Their mode distribution size was 128.5 ± 0.8 nm and 128.1 ± 0.4 nm for the control and Wnt-C59 vesicles, respectively (**Figure 4E**). Therefore, Wnt-C59 did not affect the secretion of sEVs by HT-22 cells.

Western blot analysis was then used as a second control experiment to determine whether Wnt-C59 alters the content of exosomal markers in the sEVs (**Figure 4F**). As concentration standards have not been described for sEVs protein normalization (Koritzinsky et al., 2017), a statistical analysis of the sEVs protein content with three replicates were performed as shown by others (Imjeti et al., 2017) in which the staining intensity of each band derived from non-treated samples was assigned a value of 100%. The value obtained in the Wnt-C59 sEVs, derived for treated cells, was compared with its respective non-treated control. A *t*-student test was performed on each data pair of a protein. The results show that Alix, CD63, TSG101, and NCAM-L1 expression levels were unaffected by Wnt-C59 treatment (**Figures 4F,G**). On the other hand, Wnt-C59 treatment significantly decreased ($p = 0.0011$) the Flotillin-1 exosomal content relative to its content in the Wnt-C59 exosomes. The purity of the sEVs preparation was corroborated by the absence of the Golgi protein GM130. Hence, the porcupine inhibitor Wnt-C59 has no effect on the amount, size distribution, or content of exosomal markers but Flotillin-1 in the sEVs.

Next, we performed a western blot analysis to determine if Wnt-C59 altered the content of Wnt3a, Wnt5a, Wnt7a, and GPR177/Evi proteins in the P100 fraction obtained from control cells and Wnt-C59 treated cells (**Figure 5A**). Quantification was carried out in the same way as it was done for **Figure 4**. The results showed that Wnt ligands and GPR177/Evi levels decreased significantly (**Figure 5B**). Then, to confirm this finding, a second analysis was performed where the intensity values of the band were normalized dividing them by the number of particles contained in 30 μg of protein loaded per well, as previously reported by others (Dismuke et al., 2016; Shu et al., 2020). Accordingly, the Student *t*-test results show that the Wnt3a, Wnt5a, Wnt7a, and GPR177/Evi protein content decreased significantly (∼50%) compared to the control group (**Figure 5C**). Therefore, these declines suggest that palmitoylation is a necessary post-translational modification that allows Wnt ligand secretion by sEVs.

Localization of Wnt Ligands in Small Extracellular Vesicles

To establish whether Wnt ligands are localized within different regions of sEVs, we used proteinase K to perform a "shaving" procedure (Escrevente et al., 2011; Wang et al., 2017). In this procedure, proteinase K only degrades proteins on the surface of the vesicles, since it does not penetrate the membranous lipid bilayer. However, if proteinase K and Triton X-100 are applied together, the detergent lyses the outer limiting vesicles membrane rendering all sEVs proteins accessible to proteolysis by proteinase K. Hence, the effect of proteinase K on sEVs protein content in the presence and absence of Triton X-100 was compared (see section "Materials and Methods"). Western blot data shows that proteinase K treatment alone did not degrade Wnt3a but Wnt5a, and Wnt7a were degraded (**Figure 6**). On the other hand, co-incubation with proteinase K plus Triton X-100 completely digested all these proteinaceous Wnt ligands. As a control we used the exosomal biomarker CD63 which is a tetraspanin transmembrane protein (Théry et al., 2018) sensitive to proteinase K treatment as demonstrated by others (Vlassov et al., 2012; Phoonsawat et al., 2014). As luminal control we used Alix which was still present after proteinase K digestion but underwent a shift to a lower molecular weight protein. A similar result was found for Alix for exosomes derived from neurons treated with proteinase K (Wang et al., 2017). Moreover, the presence of two bands for Alix has been previously documented in several cell lines (Shtanko et al., 2011; Bongiovanni et al., 2012; Lopes-Rodrigues et al., 2019), with the 97 kDa band representing the full-length protein and the 75 kDa band would represent a cathepsin digestion product (Impens et al., 2010;

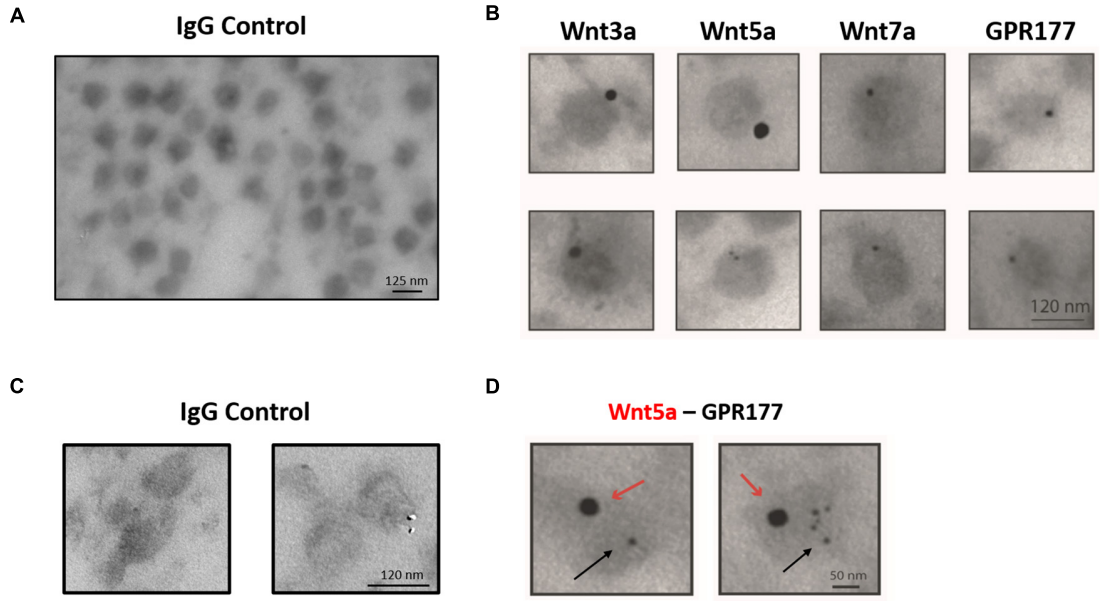

FIGURE 3 | Immunogold-TEM characterization of HT-22 exosomes. **(A)** IgG control for single immunogold labeling. **(B)** Single immunogold labeling shows that exosome-like vesicles secreted by HT-22 cells express Wnt3a, Wnt5a, Wnt7a, and GPR177. **(C)** IgG control for double immunogold. **(D)** Doubled immunogold analysis detected co-expression of Wnt5a and GPR177. Red and black arrows show the presence of Wnt5 and GPR177, respectively.

Lopes-Rodrigues et al., 2019) that have been found in exosomes (Fiandaca et al., 2015; Kanninen et al., 2016).

Taken together, these results are unique since they suggest that Wnt ligands are segregated into different compartments of exosome-like vesicles secreted by HT-22 cells. Accordingly, it is likely that Wnt3a is restricted to the luminal interior, while Wnt5a and Wnt7a are delimited to the outer limiting membrane.

DISCUSSION

NTA analysis of the P100 pellet vesicular fraction showed that approximately 80% of all the particles have an average diameter of 127.4 nm, which is within the range described for exosomes (Raposo and Stoorvogel, 2013). Furthermore, electron microscopic analysis showed a highly enriched type of vesicle (average diameter 124.1 nm) with a well-defined round shape similar to exosomes (**Figure 1**). As there are no specific and universal signature biomarkers of exosomes needed to confirm their presence, we instead relied on a battery of markers that have been suggested to be indicative of small extracellular vesicles (Théry et al., 2018). In this study, we used several sEVs markers proposed by Théry et al. (2018) in two categories, those belonging to category 1 that are indicative of lipid bilayer structure sandwiched between the outer membrane transmembrane proteins in the sEVs, like CD63, revealing the presence of tetraspanins. Furthermore, category 2 markers such as TSG101, Flotillin, and Alix reflect the cytosolic proteins involved in sEVs biogenesis. As the evaluation of the marker expression profile assesses the purity of preparation, we also quantified: (a) the GM130 expression level which is a *cis*-Golgi matrix protein (Théry et al., 2018); (b) tubulin the cytoskeletal protein, which were both absent from our micro-vesicular preparation indicating intracellular contaminants were entirely discarded following cell rupture (not shown). The confirmed presence of extracellular vesicles coupled with the exosome-like particle diameter morphology and biomarker content allows us to conclude that the particles are exosomes. Also, our purified sEVs showed expression of NCAM-L1, a neuronal adhesion molecule critical for neuronal development and found in exosomes released from neurons (Fauré et al., 2006). Concerning the Wnt3a, Wnt5a, and Wnt7a ligands, all were associated with the P100 fraction. However, only Wnt5a and GPR177/Evi were enriched, which is consistent with immunogold-TEM (**Figure 3**).

Wnt ligands are highly hydrophobic molecules that undergo acylation during their intracellular trafficking by the action of the enzyme PORCN (Torres et al., 2019). A role for PORCN in Wnt signaling was first suggested based on the similarity between the phenotype generated by Wnt gene mutations and that caused by a mutation in the PORCN gene of *Drosophila* (van den Heuvel et al., 1993; Kadowaki et al., 1996). Palmitoylation of Wnt ligands by the O-acyltransferase PORCN is considered essential for Wnt secretion (Barrott et al., 2011; Biechele et al., 2011), but this paradigm was challenged recently (Richards et al., 2014; Rao et al., 2019). Rao et al. (2019) showed that inhibition of the PORCN sometimes does not phenocopy the loss of specific Wnt molecules in some cancer cells, and both Wnt3a as Wnt4a secretion was PORCN independent. A PORCN-independent Wnt secretion and signaling was also observed in CD8+ T cells (Richards et al., 2014). The latter observation leads to a more specific question, is acylation a requirement for Wnt ligands to be secreted in any of the mechanisms so far documented. Here, we focused

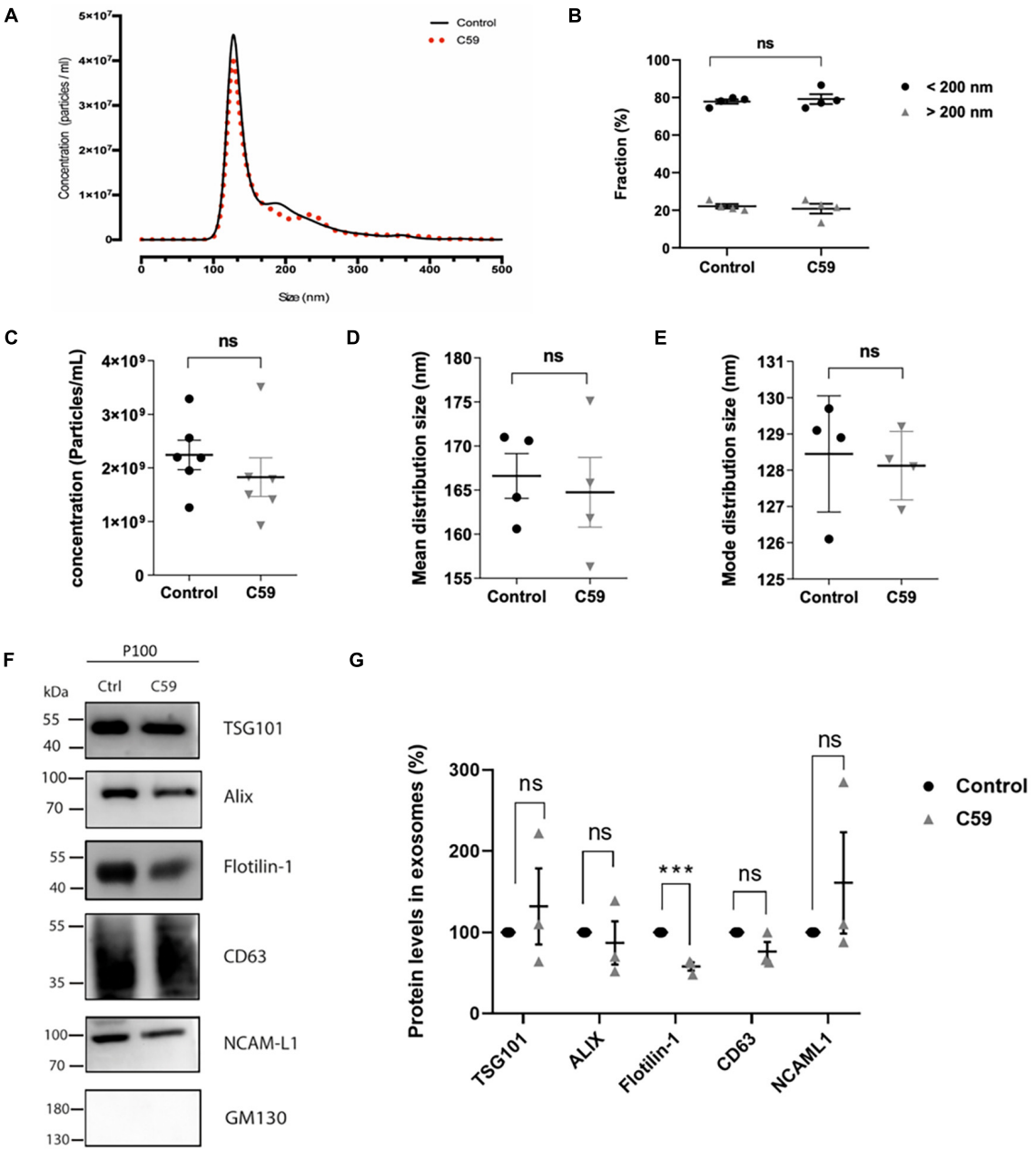

FIGURE 4 | Nanoparticle tracking analyses of exosomes secreted by control and Wnt-C59 treated HT-22 cells and the effect of Wnt-C59 on the content of exosomal markers in the P100 fraction. **(A)** Representative Nanoparticle tracking analyses show a mean peak for both control and Wnt-C59 samples. **(B)** Abundance analysis shows that 80% of the vesicles have a diameter of <200 nm (Control: 77.88 ± 2.41%, Wnt-C59: 79.20 ± 5.22; $n = 4$) and a 20% >200 nm (Control: 22.12 ± 2.41%, Wnt-C59: 20.83 ± 5.22; $n = 4$). **(C)** Concentration of particles. Shapiro–Wilk and KS tests showed that the data conformed to a normal distribution. Subsequently, the result of the Student unpaired *t*-test was $p = 0.8272$ with values of $2.3 \times 10^9 \pm 7.6 \times 10^8$ (control; $n = 7$) and $1.9 \times 10^9 \pm 8.3 \times 10^8$ (Wnt-C59; $n = 7$). **(D)** Mean distribution size of the total extracellular vesicles. Shapiro–Wilk and KS tests showed that the data conformed to a normal distribution. Subsequently, the result of the Student unpaired *t*-test was $p = 0.7602$ with values of 166.6 ± 2.5 (control; $n = 7$) and 164.8 ± 3.9 nm (Wnt-C59; $n = 7$). **(E)** Mode distribution size. As in **(D)**, values conform with a normal distribution. The student unpaired *t*-test result was $p = 0.7824$ with values of 128.5 ± 0.8 nm (control; $n = 7$) and 128.1 ± 0.4 nm (Wnt-C59; $n = 7$). *n* value means the number of independent cell culture preparations. **(F)** Representative western blot analysis of the protein content of TSG101, Alix, Flotillin-1, CD63, NCAM-L1 in P100 from control and C59 treated HT-22 cells. GM130 purity control is absent in the P100 fraction. **(G)** Relative protein expression levels of exosomal markers. The staining intensity of each band derived from control P100 was assigned a value of 100%, and the value obtained in the P100 from Wnt-C59 treatment was compared with its respective control. Flotillin-1 was the only exosomal marker whose expression level underwent a significant decrease in exosomes secreted by WntC59 treated HT-22 cells. TSG101 (Control: 100%, Wnt-C59: 132 ± 81.3%; $n = 3$; $p = 0.700$); Alix (Control: 100%, Wnt-C59: 87 ± 45.9%; $n = 3$; $p = 0.6496$); Flotillin-1 (Control: 100%, Wnt-C59: 58 ± 8.7%; $n = 3$; $p = 0.0011$); CD63 (100%, Wnt-C59: 76.3 ± 20.6; $n = 3$; $p = 0.0952$); NCAM-L1 (Control: 100%, Wnt-C59: 161 ± 157.9; $n = 3$; $p = 0.3831$). Mann–Whitney non-parametric *t*-student test (ns, not significant; $^{***}p < 0.005$).

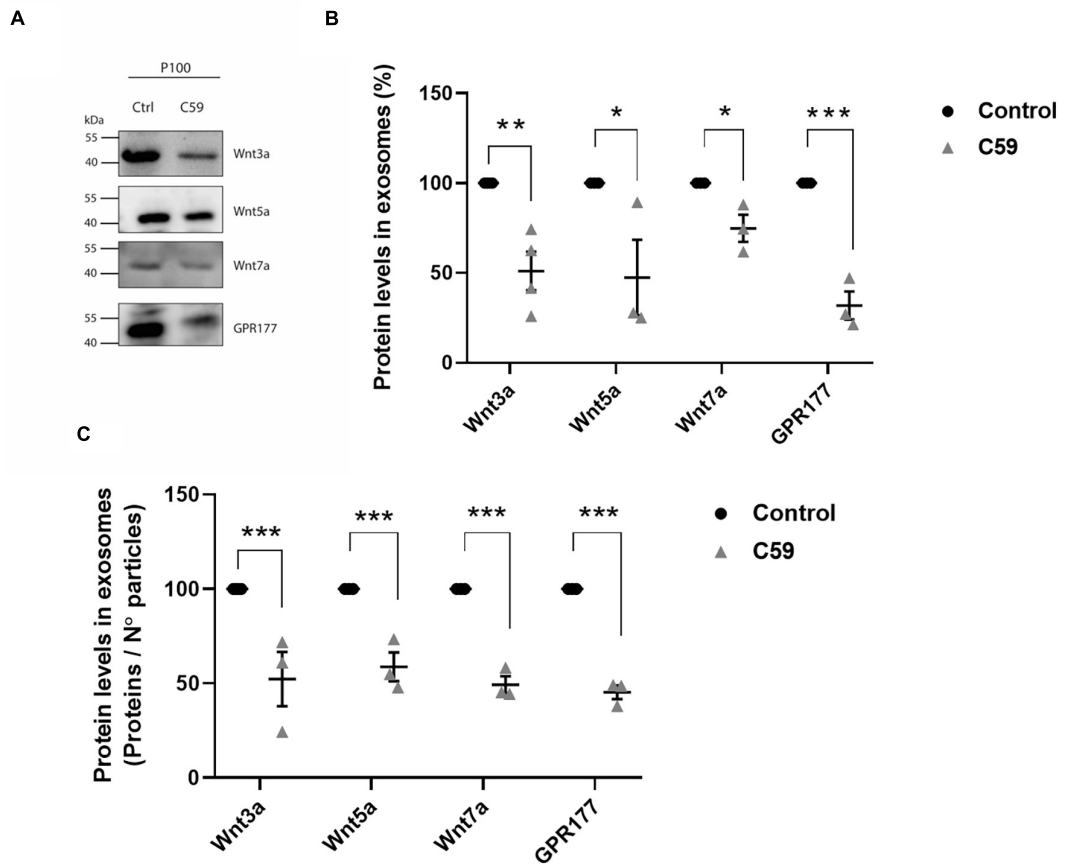

FIGURE 5 | Effects of Wnt-C59 on the content of Wnt ligands in the P100 fraction. **(A)** Comparison of the western blot analysis of Wnt3a, Wnt5a, Wnt7a, and GPR177 protein expression levels in the P100 fraction derived from control and Wnt-C59 treated cells (each lane was loaded with 30 μg protein). **(B)** Relative protein expression levels of Wnt ligands and GPR177 in the P100 fraction. The staining intensity of each band derived from control P100 was assigned a value of 100%, and the value obtained in the P100 from Wnt-C59 treatment was compared with its respective control. Wnt3a (Control: 100%, Wnt-C59: 51.1 ± 21.5%; $n = 3$; $p = 0.0039$); Wnt5a (Control: 100%, Wnt-C59: 39.1 ± 45.6%; $n = 3$; $p = 0.0404$); Wnt7a (Control: 100%, Wnt-C59: 74.82 ± 13.1%; $n = 3$; $p = 0.0291$); GPR177 (Control: 100%, Wnt-C59: 31.9 ± 13.6%; $n = 3$; $p = 0.001$). **(C)** Protein expression levels of Wnt ligands and GPR177 relative to the number of particles loaded per well. Control P100 was assigned a value of 100%, and the value obtained in the P100 from Wnt-C59 treatment was compared with its respective control. In both types of analysis of **(B,C)**, the Wnt3a, Wnt5a, Wnt7a, and GPR177 contents significantly decreased in the exosomes secreted by Wnt-C59 treated cells relative to their levels in the control cells based on the results of Mann–Whitney non-parametric *t*-student test (ns, not significant; $^{*}p < 0.05$; $^{**}p < 0.01$; $^{***}p < 0.005$). Wnt3a (Control: 100%, Wnt-C59: 52.4 ± 24.9%; $n = 3$; $p = 0.0295$); Wnt5a (Control: 100%, Wnt-C59: 58.8 ± 13.2%; $n = 3$; $p = 0.0056$); Wnt7a (Control: 100%, Wnt-C59: 49.4 ± 7.8%; $n = 3$; $p = 0.0004$); GPR177 (Control: 100%, Wnt-C59: 45.3 ± 6.2%; $n = 3$; $p = 0.0001$). *n* value means the number independent cell culture preparations.

on one of those mechanisms describing how Wnt palmitoylation inhibition specifically alters Wnt proteins association with small extracellular vesicles.

First, we exhaustively controlled any side effects of Wnt-C59 on the vesicle subpopulation obtained in the preparations (**Figure 4**). NanoSight analysis showed that the average diameter of the EVs secreted by control cells and treated with the drug was maintained. Under both conditions, approximately 80% of the vesicles present correspond to sEVs (small extracellular vesicles) whose diameter was less than 200 nm. Also, the concentration of secreted vesicles was not affected. Hence, Wnt-C59 did not affect the sEVs. Similarly, none of the exosome markers used to characterize these vesicles were altered in the presence of Wnt-C59. Surprisingly, we found that the amount of Flotillin-1 associated with sEVs decreases with the treatment of cells with Wnt-C59. Flotillins are hydrophobic proteins located in the inner part of the plasma membrane, where they play a fundamental role in the formation of lipid rafts (Bickel et al., 1997; Rajendran et al., 2007). Also, Flotillin microdomains have been described in recycling endosomes, as well as in exosomes (Meister and Tikkanen, 2014). Interestingly, palmitoylation is necessary for Wnt ligands to associate with lipid rafts (Zhai et al., 2004). Flotillin-2, although not specific for Wnt, is known to participate in the intracellular traffic of Wnt (Katanaev et al., 2008; Solis et al., 2013; Galli et al., 2016). Our observation suggests that there is probably a closer relationship between these proteins with the exocytosis of Wnt ligands. The intracellular trafficking and exocytosis model of Wnt ligands is incomplete, and the role played by proteins as Flotillins must be revisited. Regarding the ligand content, Wnt3a, Wnt5a, and Wnt7 ligands underwent a

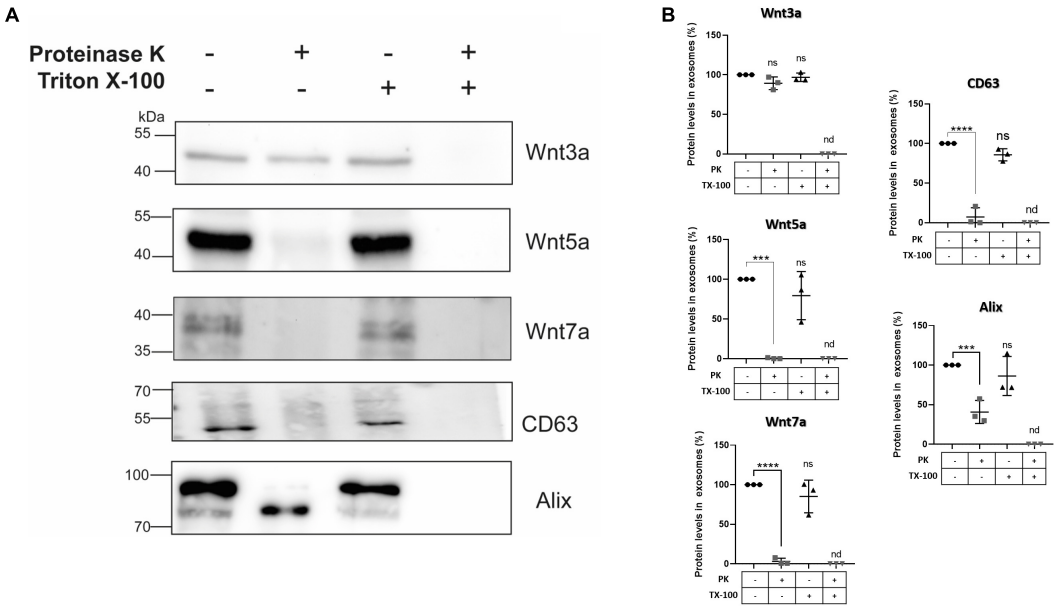

FIGURE 6 | Effects of proteinase K treatment on sEVs Wnt ligand contents. HT-22 cells-derived sEVs were treated with proteinase K in the absence and presence of Triton X-100 (see section "Materials and Methods"). **(A)** Proteinase K treatment did not affect the Wnt3a ligand presence. However, plasma membrane permeabilization with 0.5% Triton X-100 and co-treatment with proteinase K resulted in its disappearance. On the other hand, proteinase K treatment alone resulted in marked declines or even disappearance of Wnt5a, Wnt7a ligands, and the exosomal marker CD63. However, in the case of Alix, a band shift was produced (see comments in the section "Discussion"). Triton X-100 and co-treatment with proteinase K also resulted in the disappearance of CD63 and Alix. **(B)** The graphs show the relative protein expression levels with the different treatments. The staining intensity of each band derived from control P100 was assigned a value of 100%, and the value obtained in the P100 from the different treatments was compared with its respective control (100%). Wnt3a: 89.33 ± 8.02 (PK; $p = 0.0638$); 96.87 ± 5.32 (TX-100; $p = 0.7695$). Wnt5a: 0.41 ± 0.20 (PK; $p = 0.002$); 79.34 ± 30.33 (TX-100; $p = 0.2904$). Wnt7a: 3.02 ± 2.02 (PK; $p < 0.0001$); 85.14 ± 20.65 (TX-100; $p = 0.2673$). CD63: 7.23 ± 7.0 (PK; $p < 0.0001$); 85.73 ± 7.63 (TX-100; $p = 0.0842$). Alix: 40.72 ± 14.59 (PK; $p < 0.0025$); 86.23 ± 24.73 (TX-100; $p = 0.5365$). n.d., not detected; PK, proteinase K; TX-100, triton X-100. Mann–Whitney non-parametric *t*-student test (ns, not significant; ***$p < 0.005$; ****$p < 0.0001$). The images are representative of three independent cell culture preparations.

similar partial decrease in the sEVs derived from HT-22 cells treated with Wnt-C59. The levels of Wnt transport chaperone, GPR177/Evi, in sEVs also diminished with the drug treatment. Note that GPR177/Evi is not a PORCN target; therefore, this finding supports an interdependence among Wnt, GPR177/Evi and PORCN as suggested before (Bartscherer et al., 2006; Korkut et al., 2009; Glaeser et al., 2018). Regarding the ligand content, Wnt3a, Wnt5a, and Wnt7 ligands underwent a similar partial decrease in the sEVs derived from HT-22 cells treated with Wnt-C59. The levels of Wnt transport chaperone, GPR177/Evi, in sEVs also diminished with the drug treatment. Note that GPR177/Evi is not a PORCN target; therefore, this finding supports an interdependence among Wnt, GPR177/Evi, and PORCN as suggested before (Bartscherer et al., 2006; Korkut et al., 2009; Glaeser et al., 2018).

The way Wnt molecules diffuse at the extracellular space is still a subject of debate. One of the mechanisms is via exosomes, but how these vesicles deliver Wnt to a target cell is still unclear. A few studies suggest Wnt association with the outer face of exosomes (Gross et al., 2012; McBride et al., 2017), which mechanistically makes sense considering that Wnt ligands would activate extracellular receptors. Accordingly, we found Wnt5a and Wnt7a associated with the extracellular surface of HT-22 derived sEVs. However, an unexpected finding of the present work was the presence of Wnt3a inside the exosomes. Exosomes contain receptors and ligands at their outer membrane surface, whereas proteins and RNA are encapsulated inside (Théry et al., 2002; Valadi et al., 2007; Doyle and Wang, 2019). A mechanism of brain dissemination for Tau, a protein transported inside exosomes, has recently been postulated. The mechanism suggests that exosomes that contain Tau inside would be released first by a "parent" neuron, then captured intact by the soma of a second neuron through a transcytosis mechanism, which in turn would transport the intact vesicle intracellularly to be released by the axonal terminal. Then, a third synaptically connected neuron would take the exosome by endocytosis, releasing the content in its cytoplasm (Wang et al., 2017). This transcytosis mechanism has also been observed in some cancers, e.g., exosomes would support brain metastasis through transcytosis across the blood-brain barrier (Peinado et al., 2017; Morad et al., 2019). Similarly, under a physiological condition, transcytosis mediated by exosomes accounts for how folate is transported across the blood-cerebrospinal fluid barrier (Grapp et al., 2013). Transcytosis also was observed in vertebrate cells for Wnt3a and Hedgehog, another lipid-modified signaling protein (Gallet et al., 2008; Callejo et al., 2011; Yamamoto et al., 2013). However, none of those studies described the extracellular mechanism transporting the endocytosed/transcytosed Wnt

ligand. Therefore, the presence of Wnt3a inside exosomes opens new perspectives to explain long-range actions of Wnt.

CONCLUSION

The present work provides evidence that acylation is needed for Wnt ligands association to small extracellular vesicles, that according to our findings, they are exosomes. In addition, we found that Wnt ligands can be associated both to the outer surface and the luminal side of exosomes, which might provide clues to explain the diverse mechanisms of actions postulated for Wnt molecules. Many questions remain about how Wnt ligands induce target activation and signaling transduction. The same uncertainties apply to explain how Wnts are packed into exosomes prior to secretion. Clarifying these questions also requires considering the cellular context and the physiological state of the releasing and receiving cells.

DATA AVAILABILITY STATEMENT

The original contributions presented in the study are included in the article/supplementary material, further inquiries can be directed to the corresponding authors.

AUTHOR CONTRIBUTIONS

VT: conceptualization, methodology, writing-original draft preparation, investigation, supervision, writing-reviewing and editing, and funding acquisition. DB: methodology, writing-original draft preparation, and investigation. MV-G: methodology, investigation, and writing-reviewing and editing. DA: investigation and writing-reviewing and editing. NI: conceptualization, supervision, reviewing and editing, and funding acquisition. All authors contributed to the article and approved the submitted version.

FUNDING

This study was supported by grants Comisión Nacional de Investigación Científica y Tecnológica CONICYT grants: Basal Center of Excellence in Aging and Regeneration, AFB-170005 to NI; BMBF grant #20150065 to VT; FONDECYT#1190928 to MV-G.

ACKNOWLEDGMENTS

The authors thank Peter Reinach for proofreading the manuscript.

REFERENCES

Barrott, J. J., Cash, G. M., Smith, A. P., Barrow, J. R., and Murtaugh, L. C. (2011). Deletion of mouse *Porcn* blocks Wnt ligand secretion and reveals an ectodermal etiology of human focal dermal hypoplasia/Goltz syndrome. *Proc. Natl. Acad. Sci. U.S.A.* 108, 12752–12757. doi: 10.1073/pnas.1006437108

Bartscherer, K., Pelte, N., Ingelfinger, D., and Boutros, M. (2006). Secretion of Wnt ligands requires Evi, a conserved transmembrane protein. *Cell* 125, 523–533. doi: 10.1016/j.cell.2006.04.009

Beckett, K., Monier, S., Palmer, L., Alexandre, C., Green, H., Bonneil, E., et al. (2013). *Drosophila* S2 cells secrete wingless on exosome-like vesicles but the wingless gradient forms independently of exosomes: wingless is secreted on exosomes. *Traffic* 14, 82–96. doi: 10.1111/tra.12016

Bengoa-Vergniory, N., Gorroño-Etxebarria, I., González-Salazar, I., and Kypta, R. M. (2014). A switch from canonical to noncanonical Wnt signaling mediates early differentiation of human neural stem cells. *Stem Cells* 32, 3196–3208. doi: 10.1002/stem.1807

Bickel, P. E., Scherer, P. E., Schnitzer, J. E., Oh, P., Lisanti, M. P., and Lodish, H. F. (1997). Flotillin and epidermal surface antigen define a new family of caveolae-associated integral membrane proteins. *J. Biol. Chem.* 272, 13793–13802. doi: 10.1074/jbc.272.21.13793

Biechele, S., Cox, B. J., and Rossant, J. (2011). Porcupine homolog is required for canonical Wnt signaling and gastrulation in mouse embryos. *Dev. Biol.* 355, 275–285. doi: 10.1016/j.ydbio.2011.04.029

Bongiovanni, A., Romancino, D. P., Campos, Y., Paterniti, G., Qiu, X., Moshiach, S., et al. (2012). Alix protein is substrate of Ozz-E3 ligase and modulates actin remodeling in skeletal muscle. *J. Biol. Chem.* 287, 12159–12171. doi: 10.1074/jbc.m111.297036

Callejo, A., Bilioni, A., Mollica, E., Gorfinkiel, N., Andres, G., Ibanez, C., et al. (2011). Dispatched mediates Hedgehog basolateral release to form the long-range morphogenetic gradient in the *Drosophila* wing disk epithelium. *Proc. Natl. Acad. Sci. U.S.A.* 108, 12591–12598. doi: 10.1073/pnas.1106881108

Dickins, E. M., and Salinas, P. C. (2013). Wnts in action: from synapse formation to synaptic maintenance. *Front. Cell. Neurosci.* 7:162. doi: 10.3389/fncel.2013.00162

Dismuke, W. M., Klingeborn, M., and Stamer, W. D. (2016). Mechanism of fibronectin binding to human trabecular meshwork exosomes and its modulation by dexamethasone. *PLoS One* 11:e0165326. doi: 10.1371/journal.pone.0165326

Doyle, L. M., and Wang, M. Z. (2019). Overview of extracellular vesicles, their origin, composition, purpose, and methods for exosome isolation and analysis. *Cells* 8:727. doi: 10.3390/cells8070727

Działo, E., Rudnik, M., Koning, R. I., Czepiel, M., Tkacz, K., Baj-Krzyworzeka, M., et al. (2019). WNT3a and WNT5a transported by exosomes activate WNT signaling pathways in human cardiac fibroblasts. *Int. J. Mol. Sci.* 20:1436. doi: 10.3390/ijms20061436

Escrevente, C., Keller, S., Altevogt, P., and Costa, J. (2011). Interaction and uptake of exosomes by ovarian cancer cells. *BMC Cancer* 11:108. doi: 10.1186/1471-2407-11-108

Fauré, J., Lachenal, G., Court, M., Hirrlinger, J., Chatellard-Causse, C., Blot, B., et al. (2006). Exosomes are released by cultured cortical neurones. *Mol. Cell. Neurosci.* 31, 642–648. doi: 10.1016/j.mcn.2005.12.003

Fiandaca, M. S., Kapogiannis, D., Mapstone, M., Boxer, A., Eitan, E., Schwartz, J. B., et al. (2015). Identification of preclinical Alzheimer's disease by a profile of pathogenic proteins in neurally derived blood exosomes: a case-control study. *Alzheimers Dement.* 11, 600–607.e1.

Fukui, M., Song, J.-H., Choi, J., Choi, H. J., and Zhu, B. T. (2009). Mechanism of glutamate-induced neurotoxicity in HT22 mouse hippocampal cells. *Eur. J. Pharmacol.* 617, 1–11. doi: 10.1016/j.ejphar.2009.06.059

Gallet, A., Staccini-Lavenant, L., and Thérond, P. P. (2008). Cellular trafficking of the glypican dally-like is required for full-strength Hedgehog signaling and wingless transcytosis. *Dev. Cell* 14, 712–725. doi: 10.1016/j.devcel.2008.03.001

Galli, L. M., Zebarjadi, N., Li, L., Lingappa, V. R., and Burrus, L. W. (2016). Divergent effects of porcupine and Wntless on WNT1 trafficking, secretion, and signaling. *Exp. Cell Res.* 347, 171–183.

Gao, X., and Hannoush, R. N. (2014). Single-cell imaging of Wnt palmitoylation by the acyltransferase porcupine. *Nat. Chem. Biol.* 10, 61–68. doi: 10.1038/nchembio.1392

Glaeser, K., Urban, M., Fenech, E., Voloshanenko, O., Kranz, D., Lari, F., et al. (2018). ERAD-dependent control of the Wnt secretory factor Evi. *EMBO J.* 37:e97311.

Grapp, M., Wrede, A., Schweizer, M., Hüwel, S., Galla, H.-J., Snaidero, N., et al. (2013). Choroid plexus transcytosis and exosome shuttling deliver folate into brain parenchyma. *Nat. Commun.* 4:2123.

Greco, V., Hannus, M., and Eaton, S. (2001). Argosomes. *Cell* 106, 633–645. doi: 10.1016/s0092-8674(01)00484-6

Green, J., Nusse, R., and Amerongen, R. V. (2014). The role of Ryk and Ror receptor tyrosine kinases in Wnt signal transduction. *Cold Spring Harb. Perspect. Biol.* 6:a009175. doi: 10.1101/cshperspect.a009175

Gross, J. C., Chaudhary, V., Bartscherer, K., and Boutros, M. (2012). Active Wnt proteins are secreted on exosomes. *Nat. Cell Biol.* 14, 1036–1045. doi: 10.1038/ncb2574

Herr, P., and Basler, K. (2012). Porcupine-mediated lipidation is required for Wnt recognition by Wls. *Dev. Biol.* 361, 392–402. doi: 10.1016/j.ydbio.2011.11.003

Imjeti, N. S., Menck, K., Egea-Jimenez, A. L., Lecointre, C., Lembo, F., Bouguenina, H., et al. (2017). Syntenin mediates SRC function in exosomal cell-to-cell communication. *Proc. Natl. Acad. Sci. U.S.A.* 114, 12495–12500. doi: 10.1073/pnas.1713433114

Impens, F., Colaert, N., Helsens, K., Ghesquière, B., Timmerman, E., De Bock, P.-J., et al. (2010). A quantitative proteomics design for systematic identification of protease cleavage events. *Mol. Cell. Proteomics* 9, 2327–2333. doi: 10.1074/mcp.m110.001271

Inestrosa, N. C., and Varela-Nallar, L. (2015). Wnt signalling in neuronal differentiation and development. *Cell Tissue Res.* 359, 215–223. doi: 10.1007/s00441-014-1996-4

Isola, A. L., and Chen, S. (2017). Exosomes: the messengers of health and disease. *Curr. Neuropharmacol.* 15, 157–165. doi: 10.2174/1570159x14666160825160421

Kadowaki, T., Wilder, E., Klingensmith, J., Zachary, K., and Perrimon, N. (1996). The segment polarity gene porcupine encodes a putative multitransmembrane protein involved in wingless processing. *Genes Dev.* 10, 3116–3128. doi: 10.1101/gad.10.24.3116

Kaiser, K., Gyllborg, D., Procházka, J., Salašová, A., Kompaníková, P., Molina, F. L., et al. (2019). WNT5A is transported via lipoprotein particles in the cerebrospinal fluid to regulate hindbrain morphogenesis. *Nat. Commun.* 10:1498.

Kanninen, K. M., Bister, N., Koistinaho, J., and Malm, T. (2016). Exosomes as new diagnostic tools in CNS diseases. *Biochim. Biophys. Acta* 1862, 403–410. doi: 10.1016/j.bbadis.2015.09.020

Katanaev, V. L., Solis, G. P., Hausmann, G., Buestorf, S., Katanayeva, N., Schrock, Y., et al. (2008). Reggie-1/flotillin-2 promotes secretion of the long-range signalling forms of wingless and Hedgehog in *Drosophila*. *EMBO J.* 27, 509–521. doi: 10.1038/sj.emboj.7601981

Koritzinsky, E. H., Street, J. M., Star, R. A., and Yuen, P. S. T. (2017). Quantification of exosomes. *J. Cell. Physiol.* 232, 1587–1590. doi: 10.1002/jcp.25387

Korkut, C., Ataman, B., Ramachandran, P., Ashley, J., Barria, R., Gherbesi, N., et al. (2009). Trans-synaptic transmission of vesicular Wnt signals through Evi/Wntless. *Cell* 139, 393–404. doi: 10.1016/j.cell.2009.07.051

Kowal, J., Arras, G., Colombo, M., Jouve, M., Morath, J. P., Primdal-Bengtson, B., et al. (2016). Proteomic comparison defines novel markers to characterize heterogeneous populations of extracellular vesicle subtypes. *Proc. Natl. Acad. Sci. U.S.A.* 113, E968–E977.

Krämer-Albers, E.-M., Bretz, N., Tenzer, S., Winterstein, C., Möbius, W., Berger, H., et al. (2007). Oligodendrocytes secrete exosomes containing major myelin and stress-protective proteins: trophic support for axons? *Proteomics Clin. Appl.* 1, 1446–1461. doi: 10.1002/prca.200700522

Kurayoshi, M., Yamamoto, H., Izumi, S., and Kikuchi, A. (2007). Post-translational palmitoylation and glycosylation of Wnt-5a are necessary for its signalling. *Biochem. J.* 402, 515–523. doi: 10.1042/bj20061476

Lachenal, G., Pernet-Gallay, K., Chivet, M., Hemming, F. J., Belly, A., Bodon, G., et al. (2011). Release of exosomes from differentiated neurons and its regulation by synaptic glutamatergic activity. *Mol. Cell. Neurosci.* 46, 409–418. doi: 10.1016/j.mcn.2010.11.004

Lopes-Rodrigues, V., Cristina, P. R. X., Diana's, S., Osório, H., Yehuda, A., Raquel, T., et al. (2019). ALIX protein analysis: storage temperature may impair results. *J. Mol. Clin. Med.* 2, 29–34. doi: 10.31083/j.jmcm.2019.02.7161

MacDonald, B. T., and He, X. (2012). Frizzled and LRP5/6 receptors for Wnt/β-catenin signaling. *Cold Spring Harb. Perspect. Biol.* 4:a007880. doi: 10.1101/cshperspect.a007880

Malloy, A. (2011). Count, size and visualize nanoparticles. *Mater. Today* 14, 170–173. doi: 10.1016/s1369-7021(11)70089-x

Mason, J. O., Kitajewski, J., and Varmus, H. E. (1992). Mutational analysis of mouse Wnt-1 identifies two temperature-sensitive alleles and attributes of Wnt-1 protein essential for transformation of a mammary cell line. *Mol. Biol. Cell* 3, 521–533. doi: 10.1091/mbc.3.5.521

McBride, J. D., Rodriguez-Menocal, L., Guzman, W., Candanedo, A., Garcia-Contreras, M., and Badiavas, E. V. (2017). Bone marrow mesenchymal stem cell-derived CD63+ exosomes transport Wnt3a exteriorly and enhance dermal fibroblast proliferation, migration, and angiogenesis in vitro. *Stem Cells Dev.* 26, 1384–1398. doi: 10.1089/scd.2017.0087

McLeod, F., and Salinas, P. C. (2018). Wnt proteins as modulators of synaptic plasticity. *Curr. Opin. Neurobiol.* 53, 90–95. doi: 10.1016/j.conb.2018.06.003

Meister, M., and Tikkanen, R. (2014). Endocytic trafficking of membrane-bound cargo: a flotillin point of view. *Membranes* 4, 356–371. doi: 10.3390/membranes4030356

Morad, G., Carman, C. V., Hagedorn, E. J., Perlin, J. R., Zon, L. I., Mustafaoglu, N., et al. (2019). Tumor-derived extracellular vesicles breach the intact blood–brain barrier *via* transcytosis. *ACS Nano* 13, 13853–13865. doi: 10.1021/acsnano.9b04397

Mulligan, K. A., Fuerer, C., Ching, W., Fish, M., Willert, K., and Nusse, R. (2012). Secreted Wingless-interacting molecule (Swim) promotes long-range signaling by maintaining wingless solubility. *Proc. Natl. Acad. Sci.U.S.A.* 109, 370–377. doi: 10.1073/pnas.1119197109

Murphy, T. H., Miyamoto, M., Sastre, A., Schnaar, R. L., and Coyle, J. T. (1989). Glutamate toxicity in a neuronal cell line involves inhibition of cystine transport leading to oxidative stress. *Neuron* 2, 1547–1558. doi: 10.1016/0896-6273(89)90043-3

Neumann, C. J., and Cohen, S. M. (1997). Long-range action of wingless organizes the dorsal-ventral axis of the *Drosophila* wing. *Development* 124, 871–880. doi: 10.1242/dev.124.4.871

Niehrs, C. (2012). The complex world of WNT receptor signalling. *Nat. Rev. Mol. Cell Biol.* 13, 767–779. doi: 10.1038/nrm3470

Noelanders, R., and Vleminckx, K. (2017). How Wnt signaling builds the brain: bridging development and disease. *Neuroscientist* 23, 314–329. doi: 10.1177/1073858416667270

Nusse, R., and Clevers, H. (2017). Wnt/β-catenin signaling, disease, and emerging therapeutic modalities. *Cell* 169, 985–999. doi: 10.1016/j.cell.2017.05.016

Oliva, C. A., Montecinos-Oliva, C., and Inestrosa, N. C. (2018). Wnt signaling in the central nervous system: new insights in health and disease. *Prog. Mol. Biol. Transl. Sci.* 153, 81–130. doi: 10.1016/bs.pmbts.2017.11.018

Peinado, H., Zhang, H., Matei, I. R., Costa-Silva, B., Hoshino, A., Rodrigues, G., et al. (2017). Pre-metastatic niches: organ-specific homes for metastases. *Nat. Rev. Cancer* 17, 302–317. doi: 10.1038/nrc.2017.6

Phoonsawat, W., Aoki-Yoshida, A., Tsuruta, T., and Sonoyama, K. (2014). Adiponectin is partially associated with exosomes in mouse serum. *Biochem. Biophys. Res. Commun.* 448, 261–266. doi: 10.1016/j.bbrc.2014.04.114

Potolicchio, I., Carven, G. J., Xu, X., Stipp, C., Riese, R. J., Stern, L. J., et al. (2005). Proteomic analysis of microglia-derived exosomes: metabolic role of the aminopeptidase CD13 in neuropeptide catabolism. *J. Immunol.* 175, 2237–2243. doi: 10.4049/jimmunol.175.4.2237

Proffitt, K. D., Madan, B., Ke, Z., Pendharkar, V., Ding, L., Lee, M. A., et al. (2013). Pharmacological Inhibition of the Wnt acyltransferase PORCN prevents growth of WNT-driven mammary cancer. *Cancer Res.* 73, 502–507.

Rajendran, L., Knobloch, M., Geiger, K. D., Dienel, S., Nitsch, R., Simons, K., et al. (2007). Increased Abeta production leads to intracellular accumulation of Abeta in flotillin-1-positive endosomes. *Neurodegener. Dis.* 4, 164–170. doi: 10.1159/000101841

Rao, D. M., Shackleford, M. T., Bordeaux, E. K., Sottnik, J. L., Ferguson, R. L., Yamamoto, T. M., et al. (2019). Wnt family member 4 (WNT4) and WNT3A activate cell-autonomous Wnt signaling independent of porcupine O-acyltransferase or Wnt secretion. *J. Biol. Chem.* 294, 19950–19966. doi: 10.1074/jbc.ra119.009615

Raposo, G., and Stoorvogel, W. (2013). Extracellular vesicles: exosomes, microvesicles, and friends. *J. Cell Biol.* 200, 373–383. doi: 10.1083/jcb.201211138

Richards, M. H., Seaton, M. S., Wallace, J., and Al-Harthi, L. (2014). Porcupine is not required for the production of the majority of Wnts from primary human

astrocytes and CD8+ T cells. *PLoS One* 9:e92159. doi: 10.1371/journal.pone.0092159

Shtanko, O., Watanabe, S., Jasenosky, L. D., Watanabe, T., and Kawaoka, Y. (2011). ALIX/AIP1 is required for NP incorporation into mopeia virus Z-induced virus-like particles. *J. Virol.* 85, 3631–3641. doi: 10.1128/jvi.01984-10

Shu, S. L., Yang, Y., Allen, C. L., Hurley, E., Tung, K. H., Minderman, H., et al. (2020). Purity and yield of melanoma exosomes are dependent on isolation method. *J. Extracell. Vesicles* 9:1692401. doi: 10.1080/20013078.2019.1692401

Solis, G. P., Lüchtenborg, A.-M., and Katanaev, V. L. (2013). Wnt secretion and gradient formation. *Int. J. Mol. Sci.* 14, 5130–5145. doi: 10.3390/ijms14035130

Takada, R., Satomi, Y., Kurata, T., Ueno, N., Norioka, S., Kondoh, H., et al. (2006). Monounsaturated fatty acid modification of Wnt protein: its role in Wnt secretion. *Dev. Cell* 11, 791–801. doi: 10.1016/j.devcel.2006.10.003

Takada, S., Fujimori, S., Shinozuka, T., Takada, R., and Mii, Y. (2017). Differences in the secretion and transport of Wnt proteins. *J. Biochem.* 161, 1–7. doi: 10.1093/jb/mvw071

Tang, X., Wu, Y., Belenkaya, T. Y., Huang, Q., Ray, L., Qu, J., et al. (2012). Roles of N-glycosylation and lipidation in Wg secretion and signaling. *Dev. Biol.* 364, 32–41. doi: 10.1016/j.ydbio.2012.01.009

Théry, C., Witwer, K. W., Aikawa, E., Alcaraz, M. J., Anderson, J. D., Andriantsitohaina, R., et al. (2018). Minimal information for studies of extracellular vesicles 2018 (MISEV2018): a position statement of the international society for extracellular vesicles and update of the MISEV2014 guidelines. *J. Extracell. Vesicles* 7:1535750.

Théry, C., Zitvogel, L., and Amigorena, S. (2002). Exosomes: composition, biogenesis and function. *Nat. Rev. Immunol.* 2, 569–579. doi: 10.1038/nri855

Torres, V. I., Godoy, J. A., and Inestrosa, N. C. (2019). Modulating Wnt signaling at the root: porcupine and Wnt acylation. *Pharmacol. Ther.* 198, 34–45. doi: 10.1016/j.pharmthera.2019.02.009

Torres, V. I., Vallejo, D., and Inestrosa, N. C. (2017). Emerging synaptic molecules as candidates in the etiology of neurological disorders. *Neural Plast.* 2017:8081758.

Valadi, H., Ekström, K., Bossios, A., Sjöstrand, M., Lee, J. J., and Lötvall, J. O. (2007). Exosome-mediated transfer of mRNAs and microRNAs is a novel mechanism of genetic exchange between cells. *Nat. Cell Biol.* 9, 654–659. doi: 10.1038/ncb1596

van den Heuvel, M., Harryman-Samos, C., Klingensmith, J., Perrimon, N., and Nusse, R. (1993). Mutations in the segment polarity genes wingless and porcupine impair secretion of the wingless protein. *EMBO J.* 12, 5293–5302. doi: 10.1002/j.1460-2075.1993.tb06225.x

Vlassov, A. V., Magdaleno, S., Setterquist, R., and Conrad, R. (2012). Exosomes: current knowledge of their composition, biological functions, and diagnostic and therapeutic potentials. *Biochim. Biophys. Acta* 1820, 940–948. doi: 10.1016/j.bbagen.2012.03.017

Wang, Y., Balaji, V., Kaniyappan, S., Krüger, L., Irsen, S., Tepper, K., et al. (2017). The release and trans-synaptic transmission of Tau via exosomes. *Mol. Neurodegener.* 12:5.

Yamamoto, H., Awada, C., Hanaki, H., Sakane, H., Tsujimoto, I., Takahashi, Y., et al. (2013). The apical and basolateral secretion of Wnt11 and Wnt3a in polarized epithelial cells is regulated by different mechanisms. *J. Cell Sci.* 126(Pt 13), 2931–2943.

Zecca, M., Basler, K., and Struhl, G. (1996). Direct and long-range action of a wingless morphogen gradient. *Cell* 87, 833–844. doi: 10.1016/s0092-8674(00)81991-1

Zhai, L., Chaturvedi, D., and Cumberledge, S. (2004). *Drosophila* wnt-1 undergoes a hydrophobic modification and is targeted to lipid rafts, a process that requires porcupine. *J. Biol. Chem.* 279, 33220–33227. doi: 10.1074/jbc.m403407200

Zhang, L., and Wrana, J. L. (2014). The emerging role of exosomes in Wnt secretion and transport. *Curr. Opin. Genet. Dev.* 27, 14–19. doi: 10.1016/j.gde.2014.03.006

Conflict of Interest: The authors declare that the research was conducted in the absence of any commercial or financial relationships that could be construed as a potential conflict of interest.

Publisher's Note: All claims expressed in this article are solely those of the authors and do not necessarily represent those of their affiliated organizations, or those of the publisher, the editors and the reviewers. Any product that may be evaluated in this article, or claim that may be made by its manufacturer, is not guaranteed or endorsed by the publisher.

frontiers in Cell and Developmental Biology

ORIGINAL RESEARCH
published: 04 November 2021
doi: 10.3389/fcell.2021.735001

A Comparative Proteomic Analysis of Extracellular Vesicles Associated With Lipotoxicity

*Yasuhiko Nakao[1,2], Masanori Fukushima[1,2], Amy S. Mauer[1], Chieh-Yu Liao[1], Anya Ferris[1,3], Debanjali Dasgupta[1,4], Carrie Jo Heppelmann[5], Patrick M. Vanderboom[5,6], Mayank Saraswat[7,8,9], Akhilesh Pandey[7,8,9,10], K. Sreekumaran Nair[6], Alina M. Allen[1], Kazuhiko Nakao[2] and Harmeet Malhi[1]**

[1]Division of Gastroenterology and Hepatology, Rochester, MN, United States, [2]Department of Gastroenterology and Hepatology, Graduate School of Biomedical Sciences, Nagasaki University, Nagasaki, Japan, [3]California Polytechnic State University, San Luis Obispo, CA, United States, [4]Department of Physiology and Biomedical Engineering, Manipal, India, [5]Mayo Clinic Medical Genome Facility-Proteomics Core, Manipal, India, [6]Mayo Endocrine Research Unit, Manipal, India, [7]Department of Laboratory Medicine and Pathology, Rochester, MN, United States, [8]Institute of Bioinformatics, Bangalore, India, [9]Manipal Academy of Higher Education (MAHE), Manipal, India, [10]Center for Individualized Medicine, Rochester, MN, United States

OPEN ACCESS

Edited by:
Jeffrey David Galley, The Ohio State University, United States

Reviewed by:
Chen Zhao, Fudan University, China
Yi Huan, Fujian Women and Children Hospital, China
Xinlei Li, Nationwide Children's Hospital, United States

***Correspondence:**
Harmeet Malhi
Malhi.harmeet@mayo.edu

Specialty section:
This article was submitted to Molecular and Cellular Pathology, a section of the journal Frontiers in Cell and Developmental Biology

Received: *01 July 2021*
Accepted: *18 October 2021*
Published: *04 November 2021*

Citation:
Nakao Y, Fukushima M, Mauer AS, Liao C-Y Ferris A, Dasgupta D, Heppelmann CJ, Vanderboom PM, Saraswat M, Pandey A, Nair KS, Allen AM, Nakao K and Malhi H (2021) A Comparative Proteomic Analysis of Extracellular Vesicles Associated With Lipotoxicity. Front. Cell Dev. Biol. 9:735001. doi: 10.3389/fcell.2021.735001

Extracellular vesicles (EVs) are emerging mediators of intercellular communication in nonalcoholic steatohepatitis (NASH). Palmitate, a lipotoxic saturated fatty acid, activates hepatocellular endoplasmic reticulum stress, which has been demonstrated to be important in NASH pathogenesis, including in the release of EVs. We have previously demonstrated that the release of palmitate-stimulated EVs is dependent on the *de novo* synthesis of ceramide, which is trafficked by the ceramide transport protein, STARD11. The trafficking of ceramide is a critical step in the release of lipotoxic EVs, as cells deficient in STARD11 do not release palmitate-stimulated EVs. Here, we examined the hypothesis that protein cargoes are trafficked to lipotoxic EVs in a ceramide-dependent manner. We performed quantitative proteomic analysis of palmitate-stimulated EVs in control and STARD11 knockout hepatocyte cell lines. Proteomics was performed on EVs isolated by size exclusion chromatography, ultracentrifugation, and density gradient separation, and EV proteins were measured by mass spectrometry. We also performed human EV proteomics from a control and a NASH plasma sample, for comparative analyses with hepatocyte-derived lipotoxic EVs. Size exclusion chromatography yielded most unique EV proteins. Ceramide-dependent lipotoxic EVs contain damage-associated molecular patterns and adhesion molecules. Haptoglobin, vascular non-inflammatory molecule-1, and insulin-like growth factor-binding protein complex acid labile subunit were commonly detected in NASH and hepatocyte-derived ceramide-dependent EVs. Lipotoxic EV proteomics provides novel candidate proteins to investigate in NASH pathogenesis and as diagnostic biomarkers for hepatocyte-derived EVs in NASH patients.

Keywords: exosome, microvesicle, DAMP, hepatocyte, StAR-related lipid transfer domain 11

INTRODUCTION

Extracellular vesicles (EVs) are emerging mediators of liver injury and inflammation in nonalcoholic steatohepatitis (NASH), a lipotoxic disorder characterized by the accumulation of the toxic saturated fatty acid, palmitate (Hirsova et al., 2016a; Kakazu et al., 2016). EVs are heterogeneous membrane-defined nanoparticles released by most cell types. The quantity and cargo of EVs shift from healthy to disease states and reflects the pathophysiological state of the cell of origin (Goetzl et al., 2016; Sehrawat et al., 2020; Nakao et al., 2021). Furthermore, the mechanisms leading to the formation and release of EVs and of cargo selection in to EVs remain incompletely understood (van Niel et al., 2018). We have previously demonstrated that palmitate-induced activation of the endoplasmic reticulum (ER) stress sensor inositol requiring enzyme 1 alpha (IRE1α) mediates the release of EVs *via* the *de novo* synthesis of ceramide (Fukushima et al., 2018). These lipotoxic EVs are enriched in ceramides and other sphingolipids (Kakazu et al., 2016; Dasgupta et al., 2020). In addition to lipid cargoes, EVs contain protein and nucleic acid cargoes (Povero et al., 2014a). However, whether protein selection or trafficking into lipotoxic EVs is impacted by ceramide trafficking remains unknown.

There are no gold standard methods for EV isolation, and each method isolates EVs with variable purity and yield (Li et al., 2019). EVs have broad biophysical properties and many methods of EV isolation rely on these biophysical properties or on protein antigens for antibody-based EV isolation. For proteomic studies, differential ultracentrifugation (UTC) is one of the most utilized EV isolation techniques (Serrano et al., 2012; Mathieu et al., 2019), though increasingly size exclusion chromatography (SEC) and density gradient (DG) flotation (Kowal et al., 2016) are being employed. Here, we initially compared EV proteomics data obtained from mass spectrometry of EVs isolated by utilizing these three methods. Based on our initial results, we next utilized SEC for comparative proteomics of EVs isolated from palmitate-treated hepatocyte cell lines from cells with intact or deficient ceramide trafficking (Fukushima et al., 2018). In addition, we performed human plasma EV proteomics, where EVs were isolated by SEC or DG from control and NASH plasma samples, for comparison with the proteome of hepatocyte-derived EVs.

Our proteomics data demonstrate that SEC yielded most unique proteins, followed by UTC, and then DG (Keerthikumar et al., 2016; Consortium, 2020). Lipotoxic EVs collected by SEC contained numerous ribosomal proteins. Further analysis demonstrated that ceramide-dependent lipotoxic EVs contained damage-associated molecular patterns (DAMPs) and cell adhesion molecules. Human NASH EVs included immune response processing proteins. Haptoglobin, vanin 1 (VNN1), and insulin-like growth factor-binding protein complex acid labile submit (IGFALS) were commonly detected in NASH EVs and hepatocyte-derived ceramide-dependent EVs.

MATERIALS AND METHODS

Cells. We used previously described mouse hepatocyte cell lines derived from Immortalized Mouse Hepatocytes (IMH) and CRISPR/Cas9-mediated deletion of STARD11 (STARD11-/-) in IMH cells, and empty vector controls [designated throughout this manuscript as wild type (WT)] (Fukushima et al., 2018). Cells were cultured to 90% confluency on 150-mm tissue culture dishes. Cells were washed twice with phosphate-buffered saline (PBS) to eliminate fetal bovine serum (FBS)-derived EVs. Then, cells were treated with either 400 μM palmitate or vehicle in Dulbecco's Modified Eagle Medium (DMEM) supplemented with 5% EV-depleted FBS, 1% bovine serum albumin (BSA), and penicillin and streptomycin for 16 h (Fukushima et al., 2018). EV-depleted FBS was prepared by overnight centrifugation at 100,000 × g at 4°C according to standard protocols (Théry et al., 2006). Conditioned medium from palmitate or vehicle-treated cells was collected before the onset of apoptosis using a validated concentration and duration (Kakazu et al., 2016; Fukushima et al., 2018). Collected cell-conditioned medium was depleted of cells and cellular debris initially by low-speed centrifugation at 2000 × g for 20 min and 10,000 × g for 40 min. Small EVs were next isolated as described below. For each experimental condition, isolated EVs were normalized to cell number and expressed relative to the vehicle-treated condition.

Size exclusion chromatography. The supernatant of the 10,000 × g spin was concentrated by a centrifugal filter device (Centricon Plus-70) at 3,500 × g for 40 min. After the concentration step, the device was inverted and centrifuged at 1,000 × g for 2 min to recover the concentrated supernatant. The concentrated supernatants were next diluted with PBS to a total volume of 2 ml. These were then applied to primed 2-ml size exclusion columns (qEV2, IZON, Medford, MA), followed by elution with PBS (pH 7.4, 0.22 μm filtered). The first void volume (13 ml, fractions 1–6.5) was discarded and fractions 6.5–10.5 were collected and pooled, per the manufacturer's instructions. The EVs in pooled fractions 6.5–10.5 were pelleted by UTC at 100,000 × g for 2 h and resuspended in 100 μL of PBS.

Differential ultracentrifugation. The supernatant of the 10,000 × g spin was followed by UTC at 100,000 × g for 90 min to pellet EVs. The pellets were washed in PBS and centrifuged again 100,000 × g for 2 h and resuspended in 100 μL of PBS.

Differential ultracentrifugation followed by iodixanol density gradient separation. Iodixanol density gradient separation was performed (Fukushima et al., 2018) and collected fractions were combined as follows: fractions 1–2, fractions 3–6, and fractions 7–10, respectively. Each combined fraction was centrifuged at 100,000 × g for 2 h and resuspended in 100 μL of PBS. Five microliters was reserved for nanoparticle tracking analysis (NTA), and the remainder was employed for quantitative proteomic analysis. The density of each fraction was confirmed with a refractometer (**Supplementary Figure S1**). This method was based on the protocol described by Kowal et al. (Kowal et al., 2016).

Plasma EV isolation. Banked EDTA fasting plasma was obtained from adults following written informed consent using materials approved by the Mayo Clinic's Institutional Review Board. We pooled plasma from two males with NASH diagnosed on expert pathologist review of liver biopsy and divided the plasma into 1-ml aliquots each for SEC and DG. The control plasma was from an age- and sex-matched individual with no underlying liver disease. Plasma samples were thawed on ice and divided into two sets of 1 ml each for SEC and DG, respectively. Each plasma aliquot was centrifuged at 3,000 × g for 15 min at room temperature to obtain clarified supernatants. Nine hundred microliters of supernatant was transferred to new tubes and diluted 1:1 with PBS, pH 7.4, and centrifuged at 2,000 × g for 30 min at 4°C. The resulting supernatant was then centrifuged at 12,000 × g for 45 min at 4°C. For SEC, this supernatant was applied to primed 2-ml size exclusion columns as described above. For DG, the supernatant was adjusted to 10 ml with PBS and centrifuged at 110,000 × g for 120 min to pellet EVs, which were applied to the iodixanol density gradient as described above.

Nanoparticle tracking analysis. Size distribution and concentration of isolated EVs was assessed by NTA as previously described by us (Kakazu et al., 2016). Briefly, EVs were diluted in PBS to be in the linear dynamic range of the instrument and each sample was perfused through the chamber at a rate of 25 μL/min while recording the Brownian motion of particles. Particle tracks were analyzed to measure the concentration of the particles (particles/ml) and size (in nanometers).

Quantitative proteomics analysis. This was performed at the Mayo Clinic Proteomics Core Laboratory. For the method finding studies, one biological replicate each was included. Three biological replicates were included for the comparative proteomics in WT and STARD11-/- cell with palmitate or vehicle treatment. For sample preparation, EVs were lysed in 50 mM Tris containing 0.1% SDS. Samples were vortexed and heated to 95°C followed by snap cooling on ice. Tris (2-corboxyethyl)phosphine hydrochloride solution (Sigma) was added to a final concentration of 10 mM and incubated at 65°C for 30 min followed by the addition of iodoacetamide (Sigma) to a final concentration of 20 mM and incubated at room temperature in the dark for 30 min. Digestion of the EV proteins was accomplished by adding 0.6 μg of trypsin (Promega) and incubated at 37°C overnight. Sample clean-up was performed using Detergent Removal Spin Columns (Pierce), according to directions. EV peptide samples were analyzed by nano-flow liquid chromatography electrospray tandem mass spectrometry (nanoLC-ESI-MS/MS) using a Thermo Scientific Q-Exactive Mass Spectrometer (Thermo Fisher Scientific, Bremen, Germany) coupled to a Thermo Ultimate 3,000 RSLCnano HPLC system. Sample digests were loaded onto a 0.33-μL PEP ES-C18 trap, 330-nL Halo 2.7 ES-C18 trap (Optimize Technologies, Oregon City, OR). Chromatography was performed using a 5–45% gradient of solvent B over 90 min where solvent A is (98% water/2% acetonitrile/0.2% formic acid) and solvent B is (80% acetonitrile/10% isopropanol/10% water/0.2% formic acid). Peptides were eluted at a flow rate of 400 nL/min from the trap through a PicoFrit (New Objective, Woburn, MA) 100 μm × 33 cm column hand packed with Agilent Poroshell 120 EC C18 packing (Agilent Technologies, Santa Clara, CA). Q-Exactive mass spectrometer was set to acquire an ms1 survey scan from 350 to 1,600 m/z at resolution 70,000 (at 200 m/z) with an AGC target of 3e6 ions and a maximum ion inject time of 60 ms. Survey scans were followed by HCD MS/MS scans on the top 15 ions at resolution 17,500, AGC target of 2e5 ions, maximum ion inject time of 60 ms, and the isolation window set at 2.5 m/z with a 0.3 m/z offset. Dynamic exclusion placed selected ions on an exclusion list for 40 s.

Method determination: In-house software was used to set up database searches in Mascot (Matrix Sciences) and X! Tandem (https://www.thegpm.org/tandem/). Scaffold (Proteome Software) was used to combine and view these results. Criteria for protein identification required two peptide minimum and a protein 0.5% false discovery rate (FDR). Total spectral count was used as a rough estimation of protein concentration. To compare across groups ($n = 3$) the MaxQuant software (Max Planck Institute of Biochemistry, Martinsried, Germany), version 1.6.0.16, was used to extract, time align, and database search chromatographic extracted peptide peaks generated from mass spectrometry files (first and second MQ reference). Label-free relative quantitation parameters within the MaxQuant software were used to generate normalized protein intensities reported in a protein groups table (third MQ reference). Perseus software (Max Planck Institute of Biochemistry, Martinsried, Germany), version 1.6.2.1, was used to perform differential expression of identified proteins (Perseus reference). Briefly, protein intensities were log2 transformed, missing values were imputed, Student's *t*-tests were performed in which an estimation of difference was calculated, and *p*-values and *q*-values were reported.

Statistical and data analysis. All analyses, except the ones reported above, and graphical preparations were conducted in GraphPad Prism 8 (GraphPad Software Inc., La Jolla, CA). Figures were prepared with R-studio and the package ggplot2, heatmaply, and Rtsne. For data analysis of EV proteomics, ExoCarta (www.ExoCarta.org) (Keerthikumar et al., 2016), MetaboAnalyst (www.metaboanalyst.ca) (Pang et al., 2021), FUNRICHNEW (www.funrich.org) (Benito-Martin and Peinado, 2015), STRING (www.string-db.org) (Szklarczyk et al., 2019), and Ingenuity (QIAGEN Inc., https://www.qiagenbioinformatics.com/products/ingenuitypathway-analysis) Pathway Analysis (Krämer et al., 2013) were used. FDR was calculated by Benjamini–Hochberg procedure.

RESULTS

Comparison of EV isolation methods for proteomics. To investigate the optimal isolation technique for EV proteomics, EVs were isolated from vehicle-treated IMH cells by SEC, UTC, or DG (**Figure 1A**). **Figure 1B** displays the number of identified proteins for each method. Each color bar represents total number

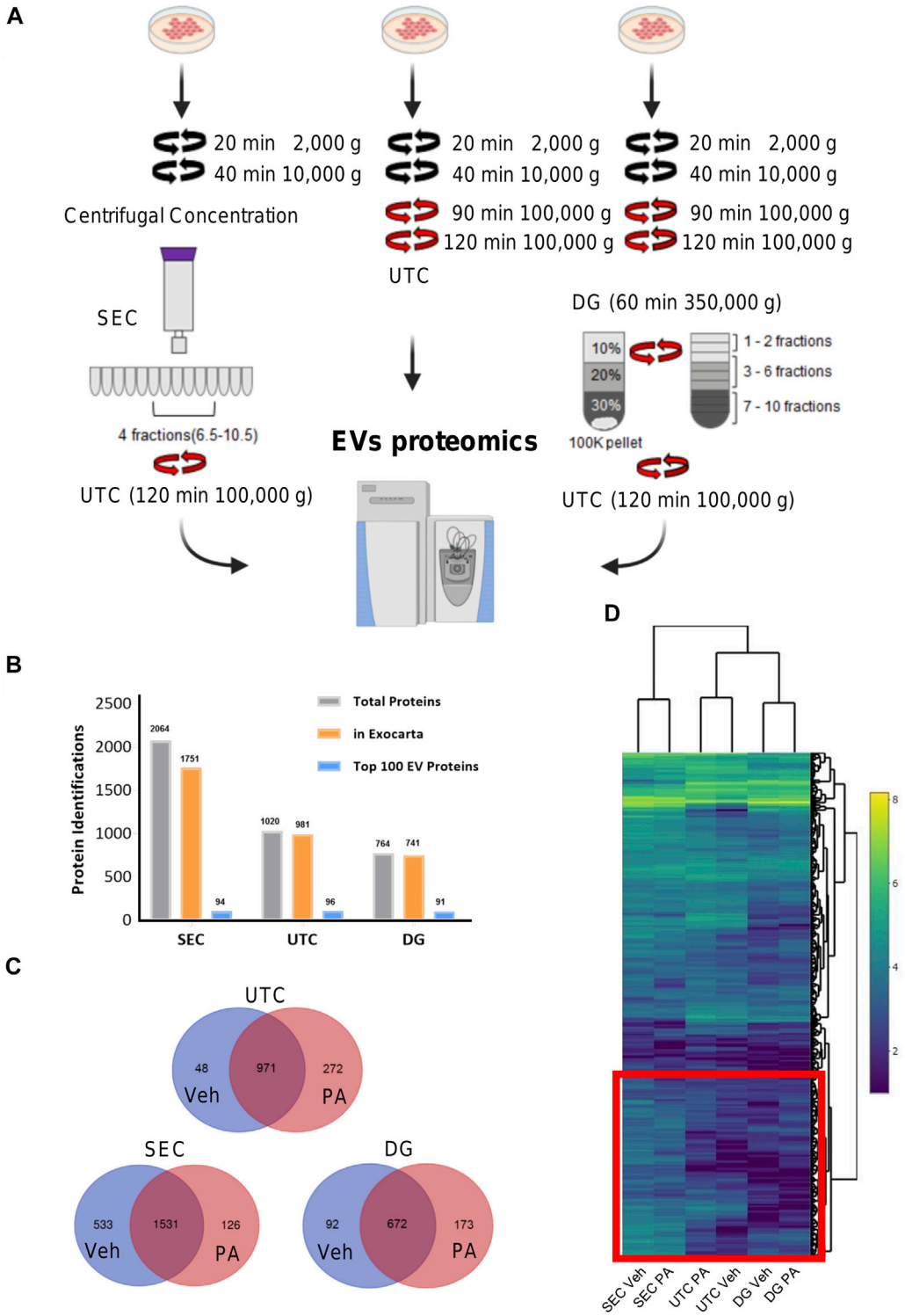

FIGURE 1 | Overview of EV proteomics methods. **(A)** Schema represents three extracellular vesicle (EV) isolation methods for EV proteomics. In size exclusion chromatography (SEC) methods, fractions 6.5 to 10.5 were combined and pelleted by ultracentrifugation (UTC). For the UTC sample, the 100,000 × g fraction was utilized. For Iodixanol, density gradient (DG) fractions 1–2, 3–6, and 7–10 were collected and combined. **(B)** The number of identified proteins for each of the three methods, SEC, UTC, and DG. The gray bars display the total number of identified proteins, the orange bars display the number of the total protein IDs that were found in the ExoCarta database, and the blue bars display the number of proteins from each method that was found in the ExoCarta top 100 EV proteins. **(C)** Venn diagrams depicting the number of unique proteins that were detected in vehicle (Veh) or palmitate (PA) stimulated EVs by each method. **(D)** Heatmap shows common 537 proteins that were detected by each method. Heatmap color represents Log2 protein abundances. The red box encloses the cluster of proteins with higher abundance in EVs isolated by SEC.

TABLE 1 | EV markers identified by SEC, UTC, and DG f3-6.

	SDCBP	ADAM10	PDCD6IP	CD63	CD9	CD81	TSG101	Flot1	Anxa1	Anxa2	Anxa5	Anxa6	Anxa7	Anxa11
SEC	X	X	X	—	X	X	X	X	X	X	X	X	X	X
UTC	X	X	X	X	X	X	X	X	X	X	X	X	X	X
DG f3-6	X	X	X	—	—	X	—	X	X	X	X	X	—	X

of identified proteins, the number of the total protein IDs that were found in the ExoCarta database (Keerthikumar et al., 2016), and the number of proteins from each method that were found in the ExoCarta top 100 EV proteins, respectively (Keerthikumar et al., 2016). This showed that SEC yielded the most proteins and almost as many proteins in the ExoCarta database as UTC. The yield of total proteins and ExoCarta proteins was least in DG. The yield of proteins isolated by UTC was in between SEC and DG. Thus, SEC had the highest sensitivity to detect proteins. To determine the specificity of these methods in enriching EV proteins, we determined the yield of top 100 EV proteins across the three methods. **Table 1** demonstrates a summary of 14 common EV markers that were detected by each method under basal conditions. All 14 were detected by UTC; however, SEC was non-inferior by detection 13 out of 14 common EV markers, and 94 of top 100 ExoCarta proteins in comparison to 96 detected by UTC. Next, we examined the EV proteome from palmitate-treated IMH cells in comparison to the vehicle-treated cells. Like vehicle-treated EVs, palmitate-stimulated EVs yielded the most proteins by SEC, followed by UTC, followed by DG. The Venn diagrams (**Figure 1C**) illustrate the comparison of vehicle- and palmitate-stimulated EV proteins for each of the three isolation methods. The Venn diagrams demonstrate that there was a significant shift in the EV proteome following palmitate treatment. To compare the abundance of proteins across methods in vehicle- and palmitate-stimulated EVs, we excluded all proteins that were not detected across all six conditions. A total of 537 proteins were detected in EVs across all six conditions (**Figure 1D**). In the 537 commonly detected proteins, there was variability across methods and proteins were more abundantly detected by SEC. However, 83 of the top 100 ExoCarta EV proteins that were detected by all methods were of comparable abundance across conditions (**Figure 2A**). **Figures 2B–D** represent comparison of palmitate upregulated proteins detected by each method. The abundance of palmitate-stimulated EV proteins detected by each method, indicated in the figures, was compared with palmitate-stimulated EV proteins enriched in EVs isolated by UTC (*y*-axis, **Figures 2B–D**). Within these plots, the red dots represent EV proteins that are included in the top 100 ExoCarta EV proteins. Comparative analysis of EV proteins enriched in palmitate-stimulated EVs by each method demonstrated higher abundance of EV proteins by UTC than DG (**Figure 2B**), and higher by SEC than DG (**Figure 2C**). When comparing UTC to SEC, most EV protein abundances were comparable except CD81 (**Figure 2D**). **Figure 2E** represents t-distributed stochastic neighbor embedding (tSNE) analysis of all the data including missing values. The number of unique proteins that were only detected by SEC, UTC, and DG were 797, 140, and 30, respectively. Altogether, SEC detected most unique proteins and was comparable to UTC and DG for the detection of top 100 ExoCarta EV proteins. Thus, SEC had the most sensitivity to detect proteins while retaining specificity for known EV proteins. As our objective was to discover unique palmitate-stimulated ceramide-dependent EV proteins, based on this initial method finding analysis, we pursued SEC for further proteomic analysis of ceramide-dependent proteomic changes in EV cargo.

Lipotoxic EV proteins are significantly altered by knockout of StAR-related lipid transfer domain 11 (STARD11). We have previously demonstrated that *de novo* ceramide biosynthesis and ceramide trafficking by the ceramide transport protein STARD11 mediates the release of lipotoxic EVs (Kakazu et al., 2016; Fukushima et al., 2018). To assess cargoes that may be selected in to lipotoxic EVs in a ceramide-dependent manner, we compared the proteome of equal amounts of lipotoxic EV proteins derived from WT or STARD11-/- cells treated with palmitate. EVs were isolated by SEC and characterized by mass spectrometry. Quantification of EVs isolated from STARD11-/- and WT cells by SEC (**Supplementary Figure S2**) was consistent with our previous observations that STARD11 mediates the release of palmitate-stimulated EVs (Fukushima et al., 2018). A Venn diagram of proteins identified in EVs from WT or STARD11-/- cells with or without palmitate treatment (**Supplementary Figure S3**) demonstrated that 1,146 proteins were commonly detected in all four conditions. To try to understand relational differences between the samples, we performed principal component analysis of each condition (**Figure 3A**). We observed that the proteome of WT EVs was different from STARD11-/- EVs both basally and following palmitate treatment. Palmitate treatment led to a shift in the proteome of EVs in both the WT control cell and STARD11-/- cells. A heatmap of the 50 most significantly different proteins from the four conditions (**Figure 3B**) demonstrates that proteins significantly enriched in STARD11-/- EVs were depleted in WT EVs, and *vice versa*, suggesting that ceramide trafficking influences the EV proteome. To understand the role of palmitate and ceramide trafficking in EV abundance of specific cargoes, we compared the magnitude of change and *p*-values. The volcano plot (**Figure 3C**) depicts the most significantly palmitate-regulated EV proteins. Spermatogenesis-associated protein 5 (SPATA5) was the most significantly upregulated protein in palmitate-stimulated EVs. The comparison between palmitate-stimulated EVs from WT versus STARD11-/- cells (**Figure 3D**) demonstrated significant enrichment of histone H3.3 (H3F3A), intercellular adhesion molecule 1 (ICAM1), embigin (Emb), haptoglobin (Hp), immunoglobulin superfamily member 3 (IGSF3) in WT versus STARD11-/- palmitate-stimulated EVs. In contrast, collagen alpha-1 chain (COL1A1), angiopoietin-like

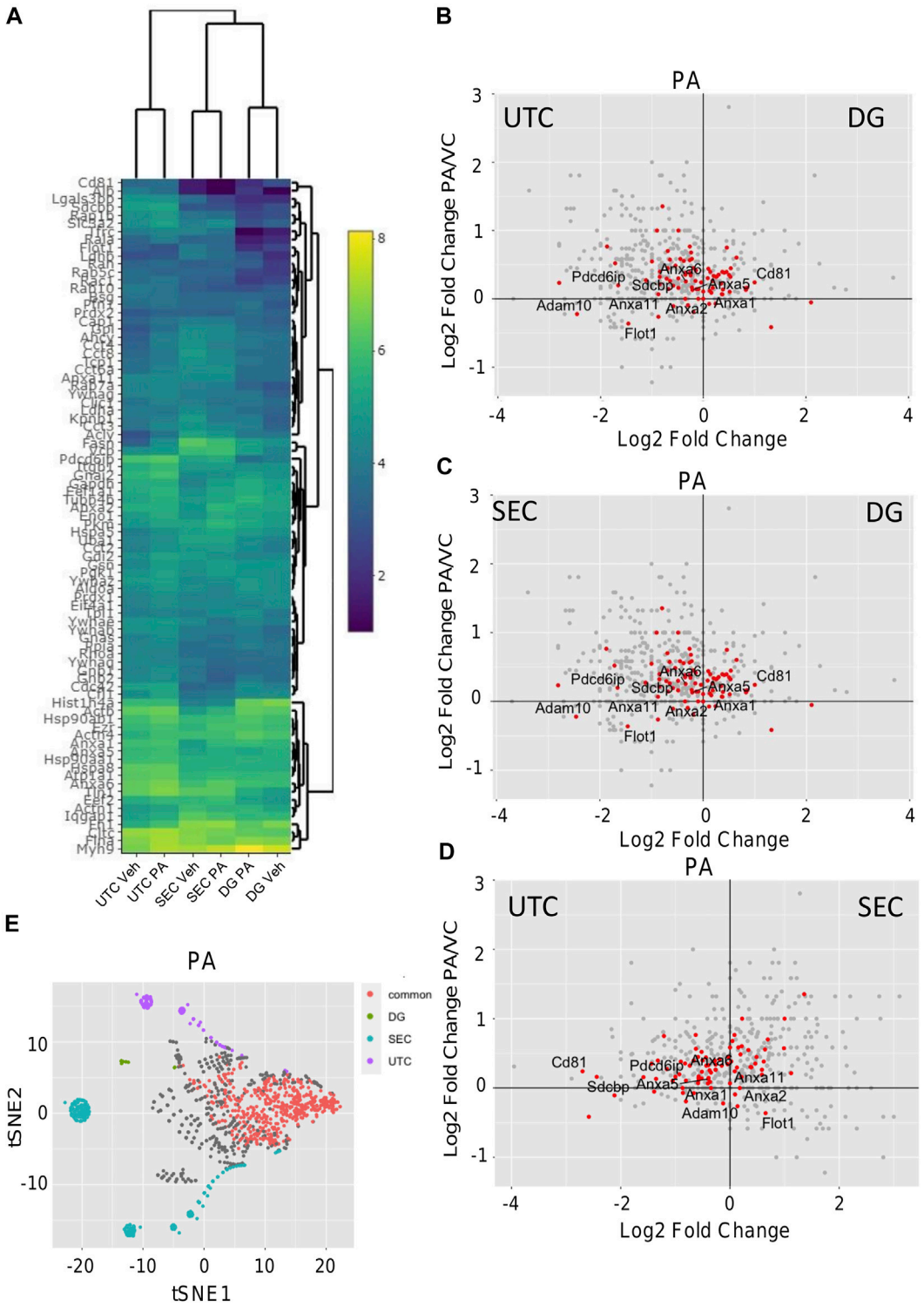

FIGURE 2 | Comparison of EV proteomics. **(A)** Heatmap depicting the abundance 83 common proteins (Log2 protein abundance) of ExoCarta top 100 EV proteins detected by each method. **(B)** Differential expression of proteins by volcano plot where the *x*-axis represents Log2 (DG PA/UTC PA) and the *y*-axis represents Log2 (UTC PA/UTC Veh). **(C)** Differential expression of proteins by volcano plots where the *x*-axis represents Log2 (DG PA/SEC PA) and the y-axis represents Log2 (UTC PA/UTC Veh). **(D)** Differential expression of proteins by volcano plots where the x-axis represents Log2 (SEC PA/UTC PA) and the y-axis represents Log2 (UTC PA/UTC Veh). For **(B–D)**, red dots indicate proteins from the top 100 ExoCarta EV proteins. **(E)** tSNE dimension reduction analysis was performed by Rtsne R package in all the data including missing values from PA stimulated EVs to depict the commonly and uniquely detected proteins by each of the three methods.

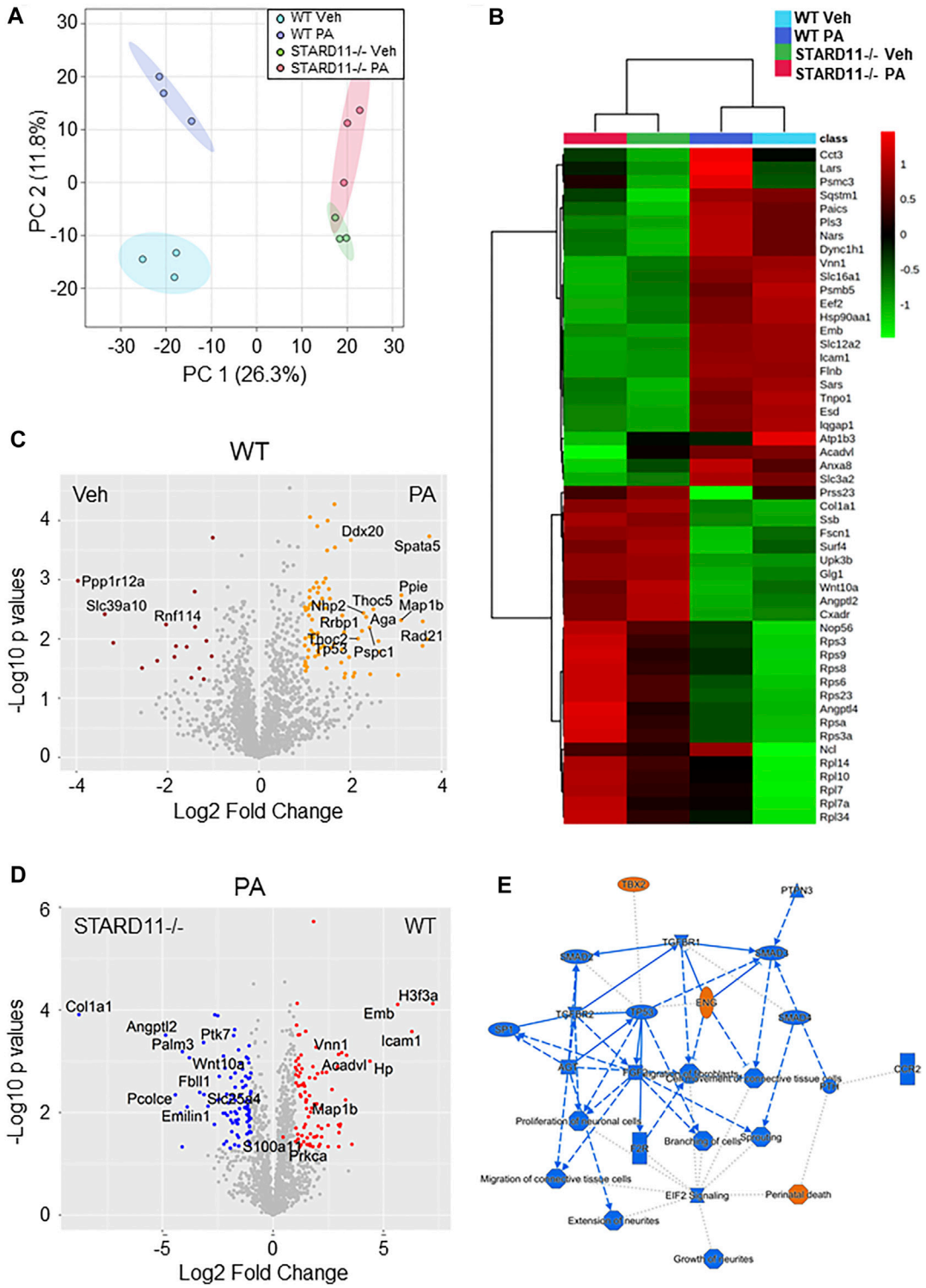

FIGURE 3 | Comparative proteomics of lipotoxic EVs from WT or STARD11-/- cells. **(A)** Principal component analysis of proteins detected in wild-type (WT) or STARD11 knockout (STARD11-/-) extracellular vesicles (EVs) from palmitate (PA)- or vehicle (Veh)-treated cells. **(B)** The heatmap depicts top 50 significant proteins between four different groups. **(C)** Volcano plot shows comparison between WT Veh and WT PA; orange circle represents $p < 0.05$ and Log2 Fold change > 1; red circle represents $p < 0.05$ and Log2 Fold change < −1. **(D)** Volcano plot shows comparison between STARD11-/- PA and WT PA; red circle represents $p < 0.05$ and Log2 Fold change > 1; blue circle represents $p < 0.05$ and Log2 fold change < −1. **(E)** Figure shows ingenuity pathway analysis based on WT PA/STARD11-/- PA data.

TABLE 2 | Top 10 canonical pathways in WT versus STARD11-/- PA EV proteins.

Ingenuity canonical pathways	–log (*p*-value)
EIF2 signaling	12.1
mTOR signaling	5.32
Coronavirus pathogenesis pathway	4.69
Hepatic fibrosis/Hepatic stellate cell activation	4.5
Regulation of eIF4 and p70S6K Signaling	4.28
Tumor microenvironment pathway	4.05
Actin cytoskeleton signaling	3.68
Tight junction signaling	3.56
Mechanisms of viral Exit from host cells	3.41
NRF2-mediated oxidative stress response	3.16

protein 2 (ANGPTL2), paralemmin-3 (PALM3), protein tyrosine kinase 7 (PTK7), and Wnt family member 10A (WNT10A) were among the least abundant proteins in palmitate-stimulated lipotoxic EVs, being depleted in WT and enriched in STARD11-/- EV proteins. Based on these data, we performed pathway analysis by IPA software, to investigate STARD11-dependent lipotoxic EV proteins. Graphical summary of the pathway analysis is provided in **Figure 3E**, and **Table 2** lists the top 10 canonical pathways of the 74 that were upregulated. EIF2 signaling was the top canonical pathway upregulated in WT versus STARD11-/- lipotoxic EVs.

We next parsed our EV proteomics data with STRING to gain a functional assessment of EV cargoes and to understand known and predicted protein–protein interactions. We compared the proteomics of vehicle- and palmitate-stimulated EVs in the control cells. We selected the top 100 expressed proteins and analyzed by STRING software to determine protein–protein interactions and functional enrichment (**Figure 4A**). EV proteins included annexin A1, A2, A5, A6 (ANXA1, ANXA2, ANXA5, and ANXA6), S100 family proteins (A6, A10, and A11), ribosomal proteins, cell adhesion related proteins, stress response proteins (HSP90AA1, HSP90AB1, and GCN1l1), and glycolysis-related proteins. The number of ribosomal proteins were increased in palmitate-stimulated lipotoxic EVs (**Figure 4B**). **Supplementary Figure S4** represents gene ontology (GO) analysis of the most abundant proteins; palmitate-stimulated EVs were enriched in ribosomal functions, RNA binding, protein translation, angiogenesis, and cell division. Next, STRING analysis was performed on the proteomics of STARD11-/- lipotoxic palmitate-stimulated EVs. We observed that ribosomal proteins were also enriched in these EVs (**Figure 5**), similar to WT palmitate-stimulated EVs. The Venn diagram (**Figure 5B**) compared the proteome of the top 100 palmitate-stimulated EV proteins in STARD11-/- versus WT. We detected 23 unique proteins each in STARD11-/- and WT EVs, whereas 77 proteins were conserved, and included numerous ribosomal proteins. In WT palmitate-stimulated EVs, some of the unique proteins included S100A11, EIF4A1, and IQGAP1; a complete list of these 23 proteins is provided in **Table 3**. Among trafficking machinery components, we detected 65 proteins (**Table 4**). Of these 65 proteins, 10 were significantly different, of which 6 were upregulated and 4 were downregulated. The majority of trafficking proteins (55 proteins) were not significantly different between in WT versus STARD11-/- lipotoxic EVs. Whether the 10 differentially regulated proteins may impact cargo selection remains to be tested.

Comparison of Human Plasma EVs Isolation Methods for Proteomics

We isolated EVs from plasma from a healthy control and a pooled NASH sample. Each plasma sample was divided into two 1-ml aliquots and EVs were isolated by SEC or DG (**Figure 6A**). We collected and combined fractions 1–2, 3–6, and 7–10 obtained by DG. EVs were higher in NASH plasma than control by each isolation method (**Supplementary Figure S5A,B**). Proteomic analysis of EV fractions isolated from DG fractions (**Supplementary Figure S5C**) demonstrated that fractions 3–6 had the highest numbers of proteins. Furthermore, comparison of cellular components by GO analysis demonstrated that fractions 3–6 had the highest ratio of exosome proteins and plasma membrane proteins and the lowest ratios of blood microparticle proteins, high-density lipoprotein particle, and very-low-density lipoprotein particle (**Supplementary Figure S5D**), demonstrating that fractions 3–6 had least contribution from platelet-derived microvesicles and lipoprotein particles. A greater number of EV proteins was isolated by SEC than DG (sum of all fractions) in control EV (**Figures 6B,D**). The number of NASH unique proteins isolated by SEC and DG fractions 3–6 were 20 and 39, respectively (**Figures 6C,D**). We performed STRING analysis by using these NASH unique proteins (**Figure 6E**). Included among these proteins were immune system processing proteins such as MHC class 1 proteins and C-reactive protein. We next examined the expression levels of proteins between control and NASH, which were detected in both conditions to determine changes in expression. **Figure 7A** represents more than 1.5-fold increase in EV proteins in NASH isolated by SEC. The highest fold change protein was hyaluronan-binding protein 2 (HABP2). **Figure 7B** represents more than 1.5-fold increased EV proteins in NASH isolated by DG. In the comparison of NASH EV proteins to control EV proteins, the three proteins with greatest differential expression (fold change) were serum amyloid A-1 protein (SAA1, 2.3-fold), immunoglobulin heavy variable 6-1 (IGHV6-1, 2.3-fold), and anoctamin-6 (ANO6, 2.3-fold), though these were not the most abundant. Lastly, we combined these NASH expressed proteins either isolated by SEC or DG and performed STRING analysis (**Figure 7C**). This analysis revealed that these proteins contain adhesion proteins, vesicle-mediated transport proteins, and apolipoproteins.

Biological Function Analysis of Hepatocyte-Derived EVs

Plasma EVs are derived from multiple cellular sources. We employed the more homogeneous hepatocyte-derived EV proteins to determine whether hepatocyte-derived EVs were detected in the more heterogenous plasma EV proteins. In this analysis, we included 357 proteins detected in human NASH plasma EVs (by SEC and DG) and 1,866 proteins detected in

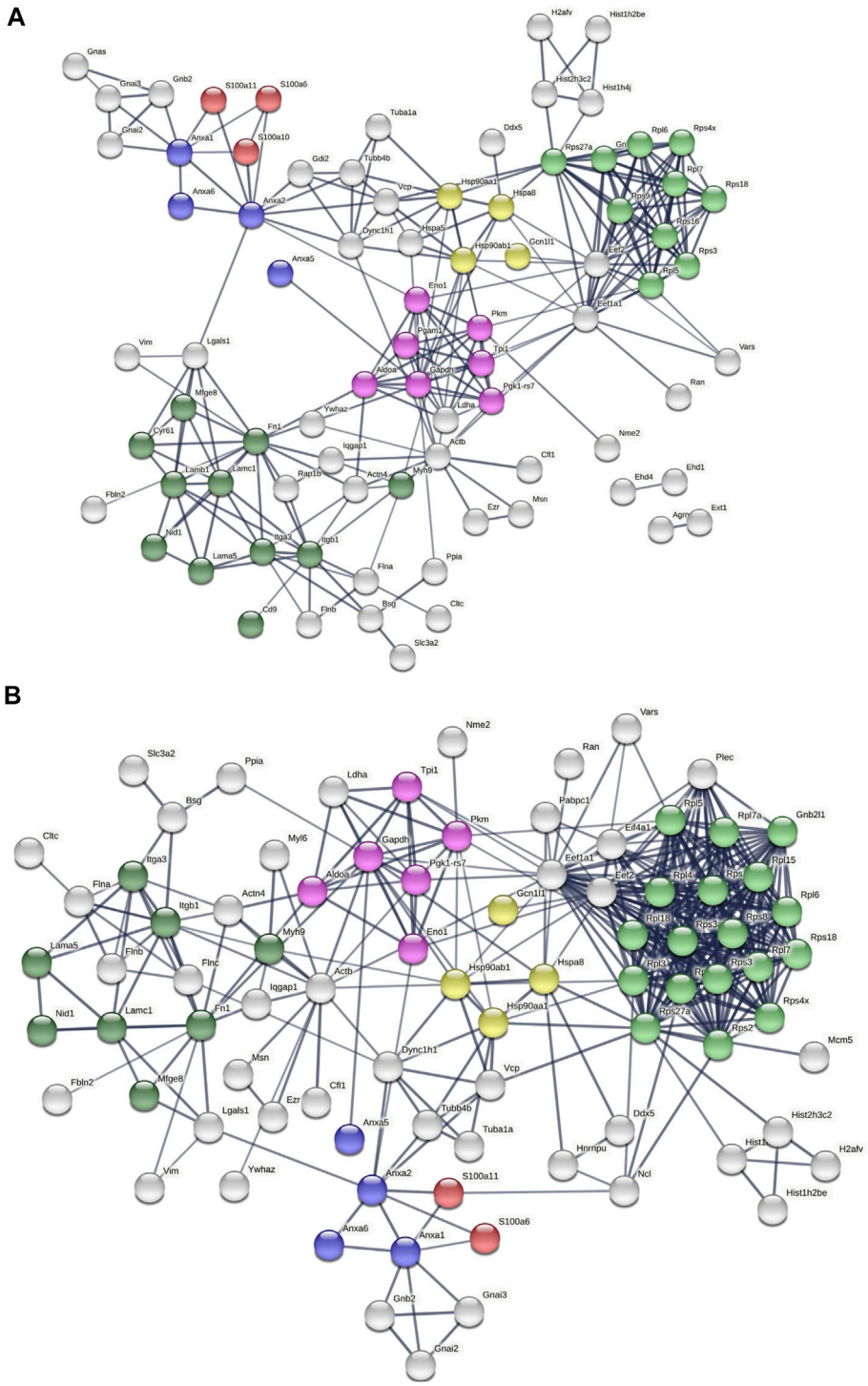

FIGURE 4 | Predicted protein–protein interactions among WT EV proteins. Protein–protein interaction analysis was performed by STRING software **(A)** on WT Veh top 100 expressed proteins, and **(B)** on WT PA top 100 expressed proteins. The edges indicate both functional and physical protein associations; line thickness indicates the strength of data support; we used minimum required interaction score with high confidence (0.700); disconnected nodes in the network were excluded; red color depicts the S100 family proteins; blue color represents the annexin family; green color represents ribosomal proteins; dark green represents cell adhesion proteins; yellow color represents stress response proteins; and pink color represents glycolysis proteins. These proteins were annotated by using UniProt and InterPro.

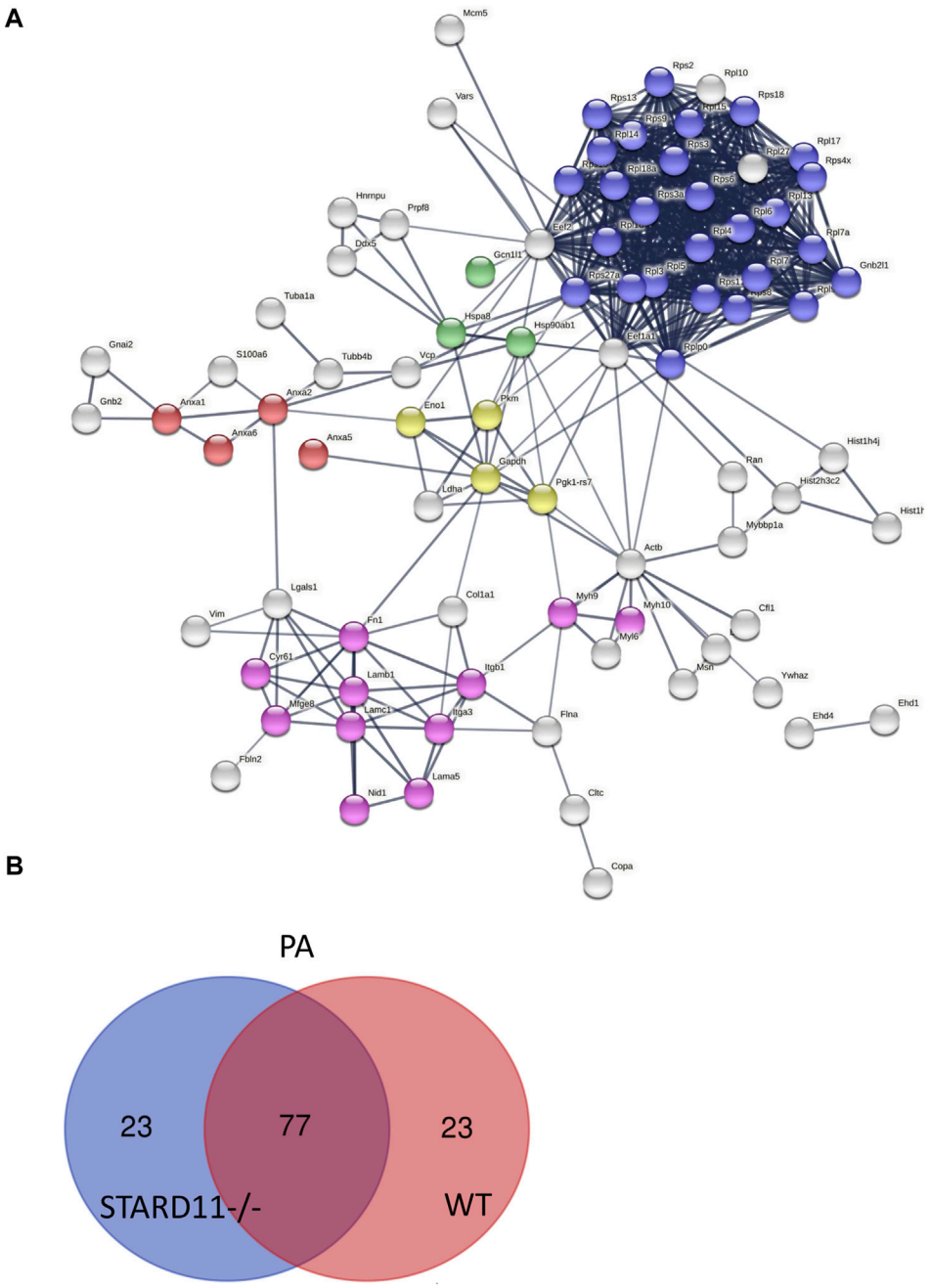

FIGURE 5 | Predicted protein–protein interactions among STARD11-/- EV proteins. **(A)** Protein–protein interaction analysis was performed by STRING software on STARD11-/- PA top 100 expressed proteins; red color shows annexin family proteins; blue color represents ribosomal proteins; green color represents stress response proteins; yellow color represents glycolysis proteins; and pink color represents cell adhesion proteins. **(B)** The Venn diagram represents the number of common and unique proteins between STARD11-/- PA and WT PA EV proteins.

hepatocyte-derived palmitate-stimulated EVs. There were 82 conserved proteins between both conditions (**Figure 8A**). **Figure 8B** demonstrates the STRING analysis of 82 conserved proteins. Included were focal adhesion proteins such as integrin and Rab subfamily of small GTPases (RAB1B, RAB8A, RAB8B, RAB10, and RAB14). Among 82 proteins, coagulation factor XIII A chain (F13A1) was significantly increased (6.1-fold change) by palmitate stimulation. **Figure 8C** depicts EV proteins detected in NASH plasma EVs and ceramide-dependent palmitate-stimulated EVs that were significantly upregulated or downregulated. The three EV proteins that were most enriched in lipotoxic EVs in a STARD11-dependent manner (**Table 5**) and detected in the human NASH plasma sample were haptoglobin, VNN1, and IGFALS.

TABLE 3 | Ceramide-dependent PA-stimulated EV proteins.

Protein IDs			
Ext1	Plec	S100a11	Gmai3
Plxnb2	Ppia	Flnb	Myof
Banf1	Flnc	Hsp90aa1	—
Bsg	Actn4	Aldoa	—
Pabpc1	Shmt2	Iqgap1	—
Nme2	Dync1h1	Ncl	—
Eif4a1	H2afv	Tpi	—

Next, we performed comparison of GO analysis including biological process, molecular function, and cellular component. The numbers of common GO terms annotated as biological process, molecular function, and cellular component were 450, 64, and 86, respectively. Among these common GO terms, we selected top 8 ordered by FDR and depict them as Sankey diagrams in which the arrow width is proportional to the expression level. In biological process analysis, vesicle-mediated transport had the highest FDR ratio between hepatocyte-derived lipotoxic EVs and NASH plasma EVs (**Figure 9A**). Immune system processes, leukocyte-mediated immunity, and immune effector processes were also conserved between the two types of EVs, in keeping with the known proinflammatory role of hepatocyte-derived lipotoxic EVs (Kakazu et al., 2016; Dasgupta et al., 2020). Molecular function analysis demonstrated that hepatocyte-derived EVs were enriched in protein-containing complex binding, protein binding, signaling receptor binding, and integrin binding proteins (**Figure 9B**), all of which are also consistent with the known mechanisms by which EVs activate effector cell responses (Zhou et al., 2020). Lastly, in cellular component analysis, we confirmed that there are EV-related GO terms in both hepatocyte-derived and NASH plasma EVs (**Figure 9C**).

DISCUSSION

EVs are being widely appreciated for their role in cell-to-cell communication and as important mediators in multiple biological functions in NASH pathogenesis, which are mediated by unique EV cargoes. To investigate the proteomic cargoes of EVs, we compared EV isolation methods. Additionally, employing optimized EV proteomics methods, we investigated ceramide trafficking-dependent lipotoxic EV cargoes and compared these EVs with NASH plasma EVs to determine conserved EV-derived signaling pathways. Our principal findings are as follows: 1) SEC yielded the most number of proteins, while preserving the top 100 EV proteins and select EV marker proteins in comparison to UTC and DG; 2) lipotoxic EVs are enriched in many distinct DAMPs and ribosomal proteins; 3) ICAM1 and PRKCA were the most significant ceramide trafficking-dependent lipotoxic EV proteins; and 4) F13A1, haptoglobin, VNN1, and IGFALS were detected in lipotoxic hepatocyte-derived EVs and in NASH plasma EVs, providing candidates for further validation studies.

Efficient isolation of EVs has been an active area of research to understand their biological properties and to explore their potential as disease biomarkers (Melo et al., 2015; Allenson et al., 2017; Palmirotta et al., 2018). Over the past decade, UTC has been the most utilized method for EV isolation (Chhoy et al., 2021). On the other hand, there are a variety of EV isolation methods based on biophysical properties or targeted epitope-based capture (Kowal et al., 2016; Patel et al., 2019). However, the optimal isolation methods for cell culture and plasma EV proteomics remain unclear. Plasma EV isolation is also accompanied with the risks of co-isolating plasma proteins and lipoprotein particles. Thus, any EV isolation method for proteomics analysis must balance yield with purity. Here, we compared SEC, UTC, and DG methods. All the methods were applied to isolate small EVs from the supernatant of 10,000 × g spin to eliminate large EVs. In the comparison of cell culture EV proteomics, SEC yielded the most ExoCarta annotated proteins from both species and abundance aspect. The top 100 ExoCarta EV proteins were almost all identified in EVs isolated by SEC, and SEC identified the most proteins of all three methods. Thus, SEC provided the sensitivity needed for novel cargo discovery while preserving specificity. Therefore, based on yield, abundance, and detection of the top 100 ExoCarta proteins, we selected SEC as the cell culture EV proteomics method for further analyses of ceramide-dependent palmitate-stimulated EV proteome.

Proteomic analysis of lipotoxic EVs detected S100 family proteins and annexin family proteins among the most abundant proteins in lipotoxic EVs. Cellular responses to stress include the release of a group of S100 proteins that function as DAMPs (Xia et al., 2018; Sedaghat and Notopoulos, 2008). Recent studies have demonstrated that S100A11 is an inducible hepatocyte DAMPs (Sobolewski et al., 2020; Zhang et al., 2021). In our data, S100A11 was enriched in EVs as a ceramide trafficking-dependent lipotoxic EV cargo, suggesting that S100A11 may play a role in NASH. Furthermore, it is well known that annexin family proteins are commonly found in EVs (Simpson et al., 2012). It is suggested that the annexin family proteins localize to EVs due to their membrane trafficking function and may play a role in cargo selection into EVs (Popa et al., 2018). As shown in STRING analysis (**Figure 4B**), both S100 and annexin family proteins are known to bind together (Rintala-Dempsey et al., 2008). The interactions of S100–annexin complexes may associate these DAMPs with lipotoxic EVs (Ibrahim et al., 2018).

In the top 100 lipotoxic EV proteins, we detected eukaryotic translation elongation factor 1A-1 (eEF1A-1), which is known to be induced in hepatocytes downstream of lipotoxic ER stress (Stoianov et al., 2015). It is reported that eEF1A1 inhibition reduces lipotoxicity in obese mice with NAFLD (Hetherington et al., 2016; Wilson et al., 2020). The canonical function of eEF1A1 is to recruit aminoacyl-tRNAs to the ribosome during peptide elongation (Mateyak and Kinzy, 2010). In addition to eEF1A1, we detected numerous ribosomal proteins in lipotoxic EVs. The GO biological process analysis suggested that the proteins involved in translation, RNA processing, ribosome biogenesis, and proteolysis processes were enriched in the lipotoxic EVs (**Supplementary Figure S3**). The mechanism for an increase in ribosomal proteins in EVs is likely related to palmitate-induced lipotoxic ER stress. The upregulation of ribosomal proteins under ER stress conditions is known (Mandal

TABLE 4 | Trafficking proteins in palmitate stimulated EVs.

Protein description	Gene	Log2 fold change WTPA and STARD11-/-PA	*p*-value
Metalloreductase STEAP2	Steap2	1.88903333	0.14282126
Ras-related protein Rab-3B	Rab3b	1.40553333	0.01943646
Vesicle transport through interaction with t-SNAREs homolog 1B	Vti1b	1.1873	0.13940431
COP9 signalosome complex subunit 4	Cops4	1.15356667	0.19666602
Unconventional myosin-Va	Myo5a	0.95773333	0.25756553
Ras-related protein Rab-5B	Rab5b	0.94836667	0.01680058
Ras-related protein Rab-27B	Rab27b	0.9091	0.59200059
Clathrin light chain A	Clta	0.84713333	0.02919789
Caveolin-2	Cav2	0.74893333	0.10698931
Lysosome-associated membrane glycoprotein 1	Lamp1	0.7218	0.14618078
Phosphatidylethanolamine-binding protein 1	Pebp1	0.6983	0.00896184
Phosphatidylinositol 4-kinase type 2-alpha	Pi4k2a	0.64753333	0.03888959
Guanine nucleotide-binding protein G(s) subunit alpha isoforms short	Gnas	0.5608	0.01037145
Vesicle-associated membrane protein 8	Vamp8	0.51643333	0.27127569
Clathrin light chain B	Cltb	0.4653	0.10648827
AP-2 complex subunit alpha-2	Ap2a2	0.3966	0.23324825
Clathrin heavy chain 1	Cltc	0.38223333	0.34105627
PDZ domain-containing protein GIPC1	Gipc1	0.38076667	0.39327463
Cell cycle control protein 50A	Tmem30a	0.37986667	0.33252972
Acyl-CoA-binding protein	Dbi	0.36446667	0.07094692
Annexin A5	Anxa5	0.32246667	0.13071344
Syntaxin-2	Stx2	0.3114	0.09850358
Ras-related protein Rab-5C	Rab5c	0.28773333	0.12020886
General vesicular transport factor p115	Uso1	0.28533333	0.41073496
Ras-related protein Rab-8A	Rab8a	0.2654	0.17811217
Endophilin-B1	Sh3glb1	0.23896667	0.64886981
Ras-related protein Rab-6A	Rab6a	0.2291	0.34524828
COP9 signalosome complex subunit 5	Cops5	0.2267	0.19568233
Heat shock cognate 71 kDa protein	Hspa8	0.2044	0.28574623
Ras-related protein Rab-10	Rab10	0.12693333	0.36351494
Ras-related protein Rab-11B	Rab11b	0.12416667	0.32150213
AP-1 complex subunit gamma-1	Ap1g1	0.10696667	0.78671066
Ras-related protein Rab-35	Rab35	0.1055	0.69913638
V-type proton ATPase subunit d 1	Atp6v0d1	0.07626667	0.89081126
Syntaxin-3	Stx3	0.06873333	0.72051544
Peflin	Pef1	0.03376667	0.89760559
Transmembrane emp24 domain-containing protein 10	Tmed10	−0.0147667	0.92350375
Ras-related protein Rab-5A	Rab5a	−0.0152	0.8959618
DnaJ homolog subfamily C member 5	Dnajc5	−0.0513667	0.69111549
Protein SEC13 homolog	Sec13	−0.0656667	0.64568037
Beta-2-syntrophin	Sntb2	−0.132	0.29493827
Calcineurin B homologous protein 1	Chp1	−0.1357667	0.17958119
Dynamin-1-like protein	Dnm1l	−0.1607333	0.63163875
Ras-related protein Rab-8B	Rab8b	−0.2352667	0.4343227
Ras-related protein Rab-14	Rab14	−0.2371667	0.13506351
Protein transport protein Sec23A	Sec23a	−0.2438	0.735827
Protein transport protein Sec31A	Sec31a	−0.2536333	0.10230817
Syntaxin-12	Stx12	−0.2754667	0.13695112
Phosphatidylinositol-binding clathrin assembly protein	Picalm	−0.3006333	0.73843355
SEC23-interacting protein	Sec23ip	−0.3045667	0.32428489
GTP-binding protein SAR1a	Sar1a	−0.3352	0.11837466
Secretory carrier-associated membrane protein 1	Scamp1	−0.3650333	0.54405532
Voltage-dependent anion-selective channel protein 1	Vdac1	−0.4649667	0.00746836
Copper-transporting ATPase 1	Atp7a	−0.5209667	0.19120787
V-type proton ATPase 116 kDa subunit a isoform 1	Atp6v0a1	−0.5223	0.49067594
Voltage-dependent anion-selective channel protein 2	Vdac2	−0.5464667	0.01837449
Programmed cell death protein 6	Pdcd6	−0.5767333	0.07925068
Vesicle-associated membrane protein 7	Vamp7	−0.5904333	0.67137801
Voltage-dependent anion-selective channel protein 3	Vdac3	−0.6144333	0.31277254
Cation-independent mannose-6-phosphate receptor	Igf2r	−0.7044	0.0856667
Protein transport protein Sec23B	Sec23b	−0.787	0.00603393
Myc box-dependent-interacting protein 1	Bin1	−0.8680667	0.25621378
Secretory carrier-associated membrane protein 2	Scamp2	−0.8799333	0.5918047

(Continued on following page)

TABLE 4 | (*Continued*) Trafficking proteins in palmitate stimulated EVs.

Protein description	Gene	Log2 fold change WTPA and STARD11-/-PA	*p*-value
Vesicle-trafficking protein SEC22b	Sec22b	−1.0781667	0.01000553
Biglycan	Bgn	−1.1482	0.30109161

et al., 2016). These data suggest that the proteome of EV released from hepatocytes undergoing lipotoxic ER stress reflects the state of cell of origin. In keeping with our findings, Zhu et al. found the components necessary for translation all existed in macrophage exosomes, including mRNA, tRNA, ribosomes, and tRNA-ligase, and hypothesized that EVs might independently express specific proteins (Zhu et al., 2015). Ribosomal protein (RP) L36A and RPL14 were reported in NAFLD and NASH human liver gene expression data (Wang et al., 2016). It is further reported that loss of small nucleolar RNAs (snoRNAs) encoded in the RPL13A is sufficient to confer resistance to lipotoxic and oxidative stress (Michel et al., 2011). In our dataset, we observed high expression of RPL13A in lipotoxic EVs. EV-mediated snoRNA transfer could enhance metabolic efficiency in recipient cells (Rimer et al., 2018). We also detected nucleophosmin (NPM1), which is involved in several cellular processes, including centrosome duplication, protein chaperoning, and cell proliferation. These RNA binding proteins (RBPs) could serve as key players in this mechanism, by making complexes with RNAs and transporting them into EVs during the biosynthesis of EVs (Statello et al., 2018).

In our ceramide-dependent lipotoxic EV analysis, ICAM1 was highly upregulated. Rat hepatocyte-derived EV proteomics (Conde-Vancells et al., 2008) and NAFLD mouse model EV detected ICAM1 (Povero et al., 2014b). The plasma membrane colocalization and interaction of ICAM1 and ceramide was reported during endocytosis (Serrano et al., 2012), suggesting that ICAM1 and ceramide might be involved in the uptake of lipotoxic EVs by target cells. Another protein enriched in a ceramide-dependent manner on lipotoxic EVs protein is protein kinase C-α, which can be directly activated by ceramide (Müller et al., 1995; Huwiler et al., 1998; Aschrafi et al., 2003), and is induced in the liver in NASH (Wang et al., 2016). These proteins might serve as ceramide-dependent lipotoxic EV markers and suggest that EV cargo is influenced by the signaling pathways known to be upregulated in lipotoxicity.

Next, we compared EV proteomics from human plasma EVs isolated by SEC or DG. We excluded UTC from human plasma EV proteomics to avoid confounding by contaminating lipoprotein particles and protein aggregates. In NASH plasma EVs, both methods yielded several enriched EV proteins. Among these, serum amyloid A1 (SAA1) was twofold higher than control plasma EVs in both methods. SAA1, SAA2, and SAA4 were also enriched in NASH EVs. It is reported that patients with active liver diseases including NASH had higher serum SAA levels than healthy controls (Yuan et al., 2019). SAA proteins can interact with cell surface receptors and integrins, suggesting a mechanism by which these proteins may be a constituent of EV cargo. ICAM2 was also higher in NASH EV protein isolated by DG. It is reported that ICAM2 on human EVs proteomics can differentiate healthy controls from patients with pre-cirrhotic and cirrhotic NASH (Povero et al., 2020). Immune system process proteins such as C-reactive protein (CRP) and MHC class 1 proteins were detected among 53 NASH unique proteins.

Plasma EVs arise from heterogenous cellular sources; therefore, to determine if hepatocyte-derived EVs are indeed a component of plasma EVs, we compared the proteome of lipotoxic hepatocyte-derived EVs and NASH plasma EVs. Among the proteins that were detected in both sample sets, coagulation factor XIII A Chain (F13A1) was upregulated the most in palmitate-stimulated lipotoxic EVs. This protein was also in plasma EVs isolated from a dietary NASH mouse model (Povero et al., 2014a) and its gene expression was reported to correlate with fat content in human NAFLD (Greco et al., 2008). The top three ceramide-dependent lipotoxic EV proteins were haptoglobin, VNN1, and IGFALS. Haptoglobin is an acute phase protein mainly produced by hepatocytes and detected in plasma EVs in a murine NASH model (Giffen et al., 2003; D'souza et al., 2012). Serum fucosylated-haptoglobin level was reported as a potential diagnostic biomarker for NASH (Kamada et al., 2013). Hepatic VNN1 expression and activity were previously shown to be significantly induced by dietary fatty acids (Rakhshandehroo et al., 2010). Hepatocyte-derived lipotoxic EVs enriched in VNN1 are internalized into endothelial cells and hepatic stellate cells in NASH (Povero et al., 2013; Povero et al., 2015). IGFALS is reported to be upregulated in NASH patients (Younossi et al., 2005). This comparative analysis suggests that F13A1, haptoglobin, VNN1, and IGFALS are potential markers to detect hepatocyte-derived lipotoxic EVs in plasma and serve as biomarkers for NASH. However, these observations will need to be further validated.

In the GO analysis of biological function, EV characteristics, immune effector processes, leukocyte-mediated immunity, and immune system processes were commonly represented in hepatocyte EVs and NASH EVs. NASH is characterized by chronic sterile inflammation in which hepatocyte-to-immune cell communication plays a key role (Hirsova et al., 2016b). Thus, the conserved immune system processes are consistent with the known and emerging role of hepatocyte-derived EVs in recruiting proinflammatory monocytes into the liver directly or *via* sinusoidal endothelial cells. Hepatocyte-derived lipotoxic EVs may also activate hepatic stellate cells (Povero et al., 2015). In the context of EV-mediated intercellular communication in NASH, we and others have characterized hepatocyte-EV derived recipient cell responses for individual bio-active cargoes (Hirsova et al., 2016a; Liao et al., 2018; Furuta et al., 2021). It is also important to note that EVs contain complex cargoes with nuclei acids, lipids, and protein ligands. Signaling roles for some of these cargoes in NASH include microRNAs (miR-128-3p),

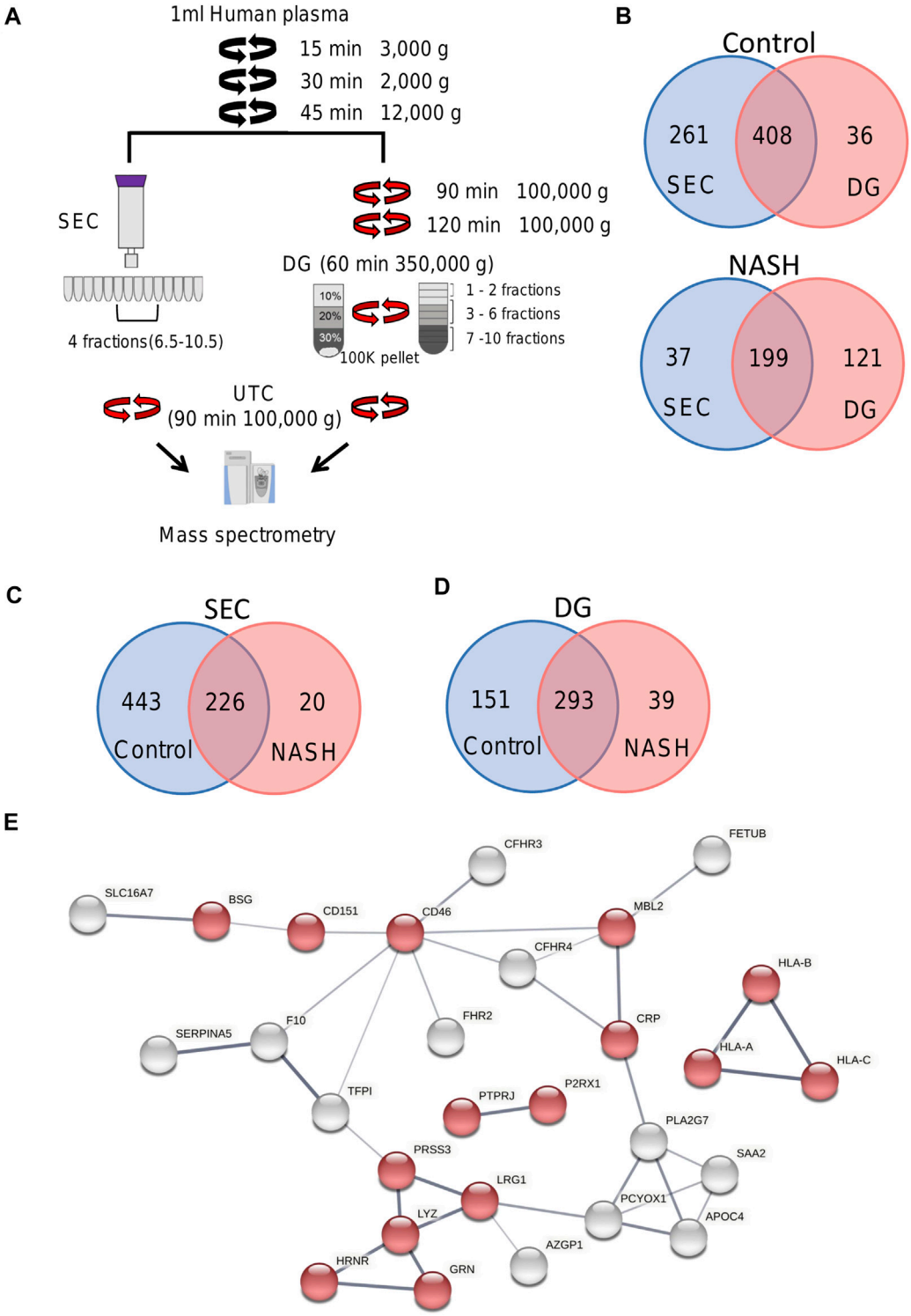

FIGURE 6 | Overview of plasma EV proteomics methods. **(A)** Schema represents two different EV isolation methods. In SEC, fractions 6.5 to 10.5 were combined and pelleted by UTC. For DG fractions 1–2, 3–6, and 7–10 were collected and combined. **(B)** Venn diagram depicting the number of common and unique proteins in control and NASH plasma EVs isolated by SEC compared to DG fractions 3–6. **(C)** Venn diagram depicting the number of common and unique proteins in control plasma EVs isolated by SEC and NASH plasma EVs isolated by SEC. **(D)** Venn diagram depicting the number of common and unique proteins in control plasma EVs isolated by DG fractions 3–6 and NASH plasma EVs isolated by DG fractions 3–6. **(E)** Protein–protein interaction analysis was performed by STRING software on unique NASH EV proteins; the edges indicate both functional and physical protein associations; line thickness indicates the strength of data support; we used minimum required interaction score with medium confidence (0.400); disconnected nodes in the network were excluded; red color represents immune system process. The annotation of these proteins was done by using Gene Ontology.

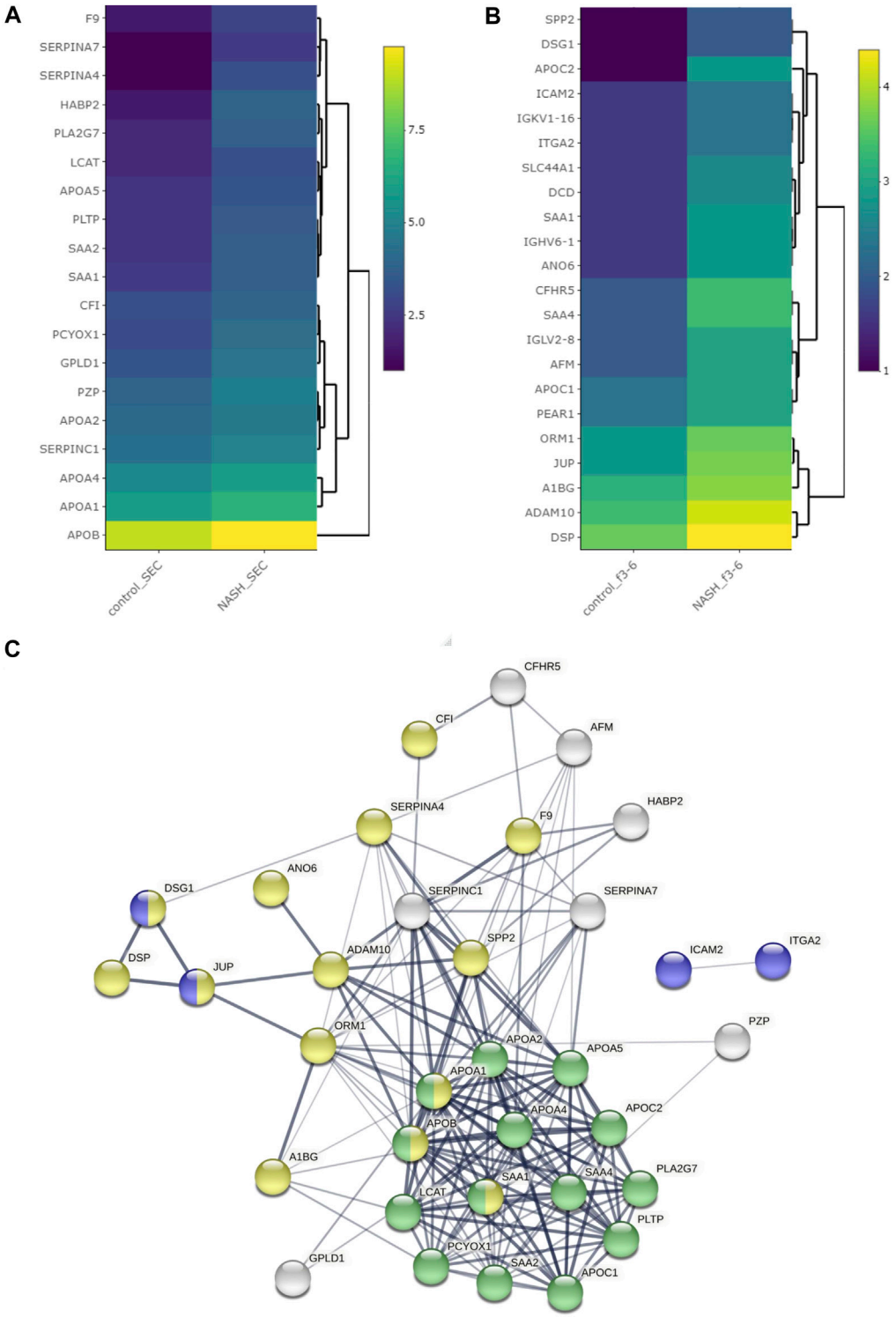

FIGURE 7 | Differentially expressed proteins among plasma EVs. Heatmap representing proteins with greater than 1.5-fold change in NASH plasma EVs, which were isolated **(A)** by SEC and **(B)** by DG. **(C)** Protein–protein interaction analysis was performed by STRING software on significantly enriched proteins in NASH EVs; the edges indicate both functional and physical protein associations; line thickness indicates the strength of data support; we used minimum required interaction score with medium confidence (0.400); disconnected nodes in the network were excluded; blue color represents cell adhesion proteins; green color represents plasma lipoprotein particle protein; yellow color represents vesicle-mediated transport; these proteins annotation was done by using Gene Ontology and UniProt.

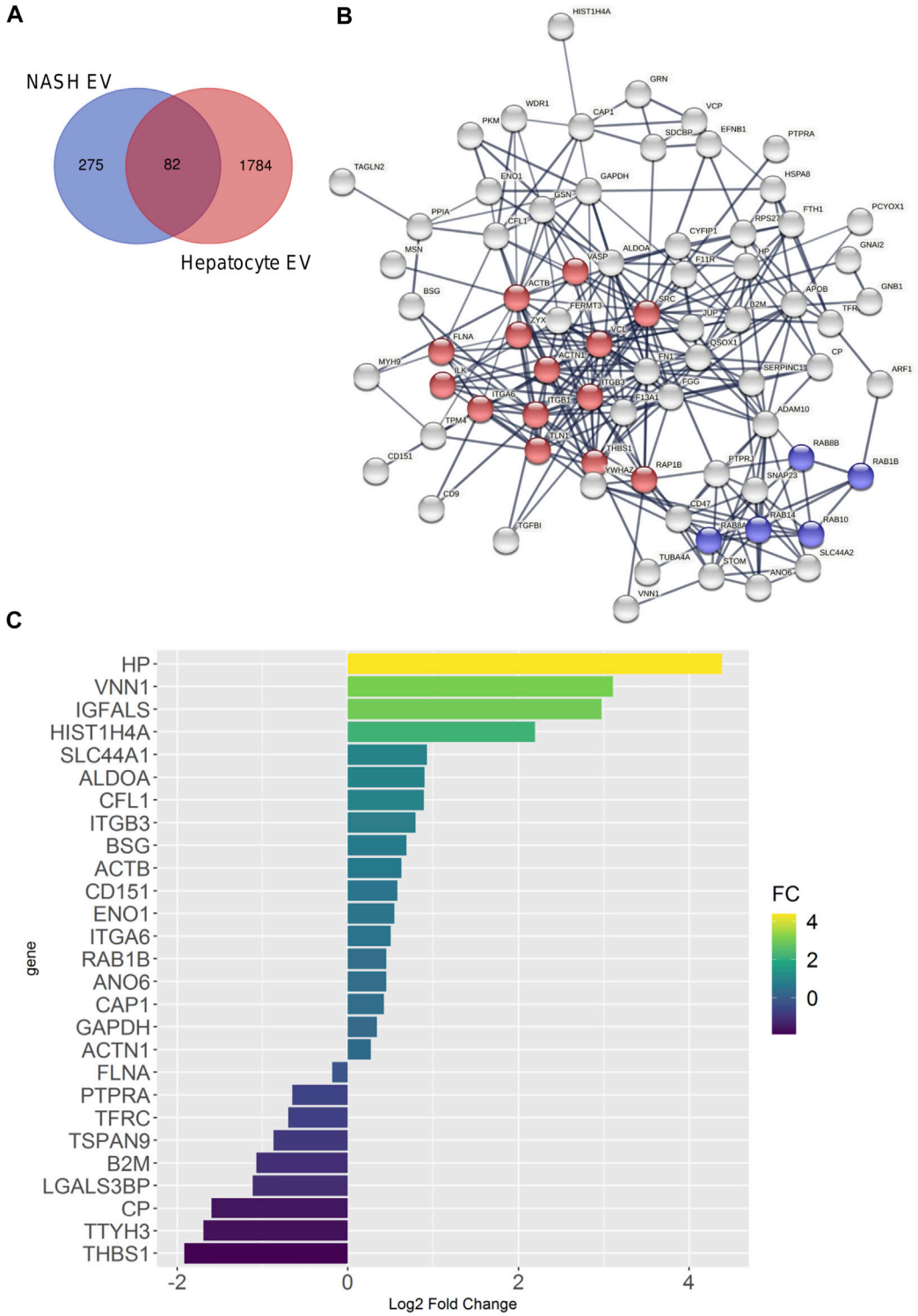

FIGURE 8 | Comparison of palmitate-stimulated EV proteins with NASH plasma EV proteins. **(A)** Venn diagram compared 357 proteins of human NASH plasma EVs and 1,866 proteins of mouse hepatocyte-derived, palmitate-stimulated EVs. **(B)** Protein–protein interaction analysis was performed by STRING software; the edges indicate both functional and physical protein associations; line thickness indicates the strength of data support; we used minimum required interaction score with high confidence (0.700); disconnected nodes in the network were excluded; red color represents focal adhesion proteins; blue color represents RAB subfamily of small GTPases proteins; these proteins annotation was done by using KEGG and SMART. **(C)** Bar graph depicts EV proteins detected in ceramide-dependent palmitate-stimulated lipotoxic EVs and NASH plasma EVs; proteins are shown which had $p < 0.05$; *x*-axis and color represents Log2 fold change.

TABLE 5 | Palmitate-stimulated EV proteins also detected in plasma.

Protein description	Gene name	Log2 FC WTVC and STARD11-/-VC	*p*-value	Log2 FC WTPA and STARD11-/-PA	*p*-value
Haptoglobin	Hp	1.71966667	0.328	4.38716667	0.000993
Pantetheinase	Vnn1	2.7149	0.000382	3.10726667	0.000682
Insulin-like growth factor-binding protein complex acid labile subunit	Igfals	−0.5061667	0.636	2.97173333	0.0464

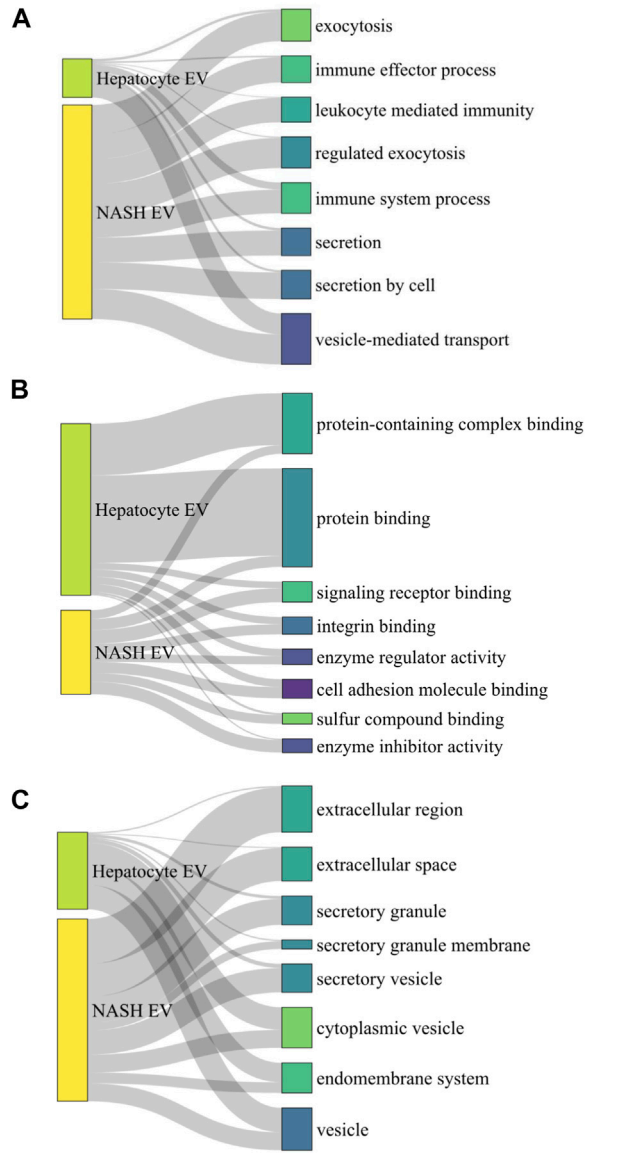

FIGURE 9 | Sankey diagram linking palmitate-stimulated EV proteins with NASH plasma EV proteins. Sankey diagram linking top 8 commonly detected gene ontology (GO) terms from 1,766 hepatocyte-derived palmitate-stimulated EV proteins and 357 human NASH plasma EV proteins, **(A)** by biological process analysis, **(B)** by molecular function analysis, and **(C)** by cellular component analysis. A ribbon's thickness indicates −log10FDR for each cluster of GO terms in each GO analysis.

lipids (sphingosine 1-phosphate), and proteins (CXCL10, Vanin) (Povero et al., 2013; Povero et al., 2015; Ibrahim et al., 2016; Liao et al., 2018). How these complex cargoes interact in recipient cell responses remains to be experimentally tested; for example, a balance of changes in proinflammatory versus anti-inflammatory cargoes per EV or proinflammatory EV concentration versus anti-inflammatory EV concentration may determine recipient cell responses. Our human dataset is a significant limitation due to the small sample size. These findings will need confirmation in larger human plasma EV proteomic datasets. Here, our objective with the human plasma samples was to optimize and disseminate our comparative methods for plasma EV proteomics.

In summary, we have provided a methodological resource for investigators and defined ceramide-dependent proteomic cargo of EVs. Hepatocyte-derived lipotoxic EVs contain DAMPs and cell adhesion molecules such as S100a11 and ICAM1, which might affect immune cell responses, thus promoting liver inflammation in NASH. Limited analysis of human NASH EV proteome included ICAM2, F13A1, haptoglobin, VNN1, and IGFALS, which were also detected in hepatocyte-derived EVs. These findings will need further validation in larger plasma datasets and as technological advances permit the identification of hepatocyte-derived EVs in plasma with minimal processing.

DATA AVAILABILITY STATEMENT

The datasets presented in this study can be found in online repositories. The names of the repository/repositories and accession number(s) can be found below: http://proteomecentral.proteomexchange.org/ PXD028175.

ETHICS STATEMENT

The studies involving deidentified human biospecimens were reviewed and approved by the Mayo Clinic, IRB. The deidentified biospecimens were from patients/participants who had provided their written informed consent.

AUTHOR CONTRIBUTIONS

Study conceptualization was performed by YN, PV, and HM. Data were acquired and interpreted by YN, MF, AM, C-YL, AF,

DD, CH, PV, MS, AP, KN, AA, KN, and HM. The manuscript was prepared, reviewed, and edited by YN and HM. All authors have read and agreed to the content of the work.

FUNDING

This work is supported by NIH grant DK111378 (to HM) and DK115594 (to AA), the Mayo Foundation (to HM), the Clinical Core of the Mayo Clinic Center for Cell Signaling in Gastroenterology (P30DK084567), and Kanae Foundation Foreign Study Grant (to YN). We thank the Mayo Clinic Medical Genome Facility-Proteomics Core (a shared resource of the Mayo Clinic Cancer Center (NCI P30 CA15083)).

ACKNOWLEDGMENTS

We are grateful to Cynthia Nordyke and Charyl Dutton Gibbs of the Mayo Clinic Center for Cell Signaling in Gastroenterology for sample management, and Michael Holmes of the Mayo Clinic Medical Genome Facility-Proteomics Core for assistance with proteomics.

SUPPLEMENTARY MATERIAL

The Supplementary Material for this article can be found online at: https://www.frontiersin.org/articles/10.3389/fcell.2021.735001/full#supplementary-material

REFERENCES

Allenson, K., Castillo, J., San Lucas, F. A., Scelo, G., Kim, D. U., Bernard, V., et al. (2017). High Prevalence of mutantKRAS in Circulating Exosome-Derived DNA from Early-Stage Pancreatic Cancer Patients. *Ann. Oncol.* 28, 741–747. doi:10.1093/annonc/mdx004

Aschrafi, A., Franzen, R., Shabahang, S., Fabbro, D., Pfeilschifter, J., and Huwiler, A. (2003). Ceramide Induces Translocation of Protein Kinase C-α to the Golgi Compartment of Human Embryonic Kidney Cells by Interacting with the C2 Domain. *Biochim. Biophys. Acta (Bba) - Mol. Cel Biol. Lipids* 1634, 30–39. doi:10.1016/j.bbalip.2003.08.004

Benito-Martin, A., and Peinado, H. (2015). FunRich Proteomics Software Analysis, Let the Fun Begin!. *Proteomics* 15, 2555–2556. doi:10.1002/pmic.201500260

Chhoy, P., Brown, C. W., Amante, J. J., and Mercurio, A. M. (2021). Protocol for the Separation of Extracellular Vesicles by Ultracentrifugation from *In Vitro* Cell Culture Models. *STAR Protoc.* 2, 100303. doi:10.1016/j.xpro.2021.100303

Conde-Vancells, J., Rodriguez-Suarez, E., Embade, N., Gil, D., Matthiesen, R., Valle, M., et al. (2008). Characterization and Comprehensive Proteome Profiling of Exosomes Secreted by Hepatocytes. *J. Proteome Res.* 7, 5157–5166. doi:10.1021/pr8004887

Consortium, T. U. (2020). UniProt: the Universal Protein Knowledgebase in 2021. *Nucleic Acids Res.* 49, D480–D489. doi:10.1093/nar/gkaa1100

D'souza, A. M., Beaudry, J. L., Szigiato, A. A., Trumble, S. J., Snook, L. A., Bonen, A., et al. (2012). Consumption of a High-Fat Diet Rapidly Exacerbates the Development of Fatty Liver Disease that Occurs with Chronically Elevated Glucocorticoids. *Am. J. Physiology-Gastrointestinal Liver Physiol.* 302, G850–G863. doi:10.1152/ajpgi.00378.2011

Dasgupta, D., Nakao, Y., Mauer, A. S., Thompson, J. M., Sehrawat, T. S., Liao, C. Y., et al. (2020). IRE1A Stimulates Hepatocyte-Derived Extracellular Vesicles that Promote Inflammation in Mice with Steatohepatitis. *Gastroenterology*.

Fukushima, M., Dasgupta, D., Mauer, A. S., Kakazu, E., Nakao, K., and Malhi, H. (2018). StAR-related Lipid Transfer Domain 11 (STARD11)-Mediated Ceramide Transport Mediates Extracellular Vesicle Biogenesis. *J. Biol. Chem.* 293, 15277–15289. doi:10.1074/jbc.ra118.002587

Furuta, K., Guo, Q., Pavelko, K. D., Lee, J. H., Robertson, K. D., Nakao, Y., et al. (2021). Lipid-induced Endothelial Vascular Cell Adhesion Molecule 1 Promotes Nonalcoholic Steatohepatitis Pathogenesis. *J. Clin. Invest.* 131. doi:10.1172/jci143690

Giffen, P. S., Turton, J., Andrews, C. M., Barrett, P., Clarke, C. J., Fung, K.-W., et al. (2003). Markers of Experimental Acute Inflammation in the Wistar Han Rat with Particular Reference to Haptoglobin and C-Reactive Protein. *Arch. Toxicol.* 77, 392–402. doi:10.1007/s00204-003-0458-7

Goetzl, E. J., Mustapic, M., Kapogiannis, D., Eitan, E., Lobach, I. V., Goetzl, L., et al. (2016). Cargo Proteins of Plasma Astrocyte-derived Exosomes in Alzheimer's Disease. *FASEB j.* 30, 3853–3859. doi:10.1096/fj.201600756r

Greco, D., Kotronen, A., Westerbacka, J., Puig, O., Arkkila, P., Kiviluoto, T., et al. (2008). Gene Expression in Human NAFLD. *Am. J. Physiology-Gastrointestinal Liver Physiol.* 294, G1281–G1287. doi:10.1152/ajpgi.00074.2008

Hetherington, A. M., Sawyez, C. G., Sutherland, B. G., Robson, D. L., Arya, R., Kelly, K., et al. (2016). Treatment with Didemnin B, an Elongation Factor 1A Inhibitor, Improves Hepatic Lipotoxicity in Obese Mice. *Physiol. Rep.* 4, e12963. doi:10.14814/phy2.12963

Hirsova, P., Ibrabim, S. H., Gores, G. J., and Malhi, H. (2016). Lipotoxic Lethal and Sublethal Stress Signaling in Hepatocytes: Relevance to NASH Pathogenesis. *J. Lipid Res.* 57, 1758–1770. doi:10.1194/jlr.r066357

Hirsova, P., Ibrahim, S. H., Krishnan, A., Verma, V. K., Bronk, S. F., Werneburg, N. W., et al. (2016). Lipid-Induced Signaling Causes Release of Inflammatory Extracellular Vesicles from Hepatocytes. *Gastroenterology* 150, 956–967. doi:10.1053/j.gastro.2015.12.037

Huwiler, A., Fabbro, D., and Pfeilschifter, J. (1998). Selective Ceramide Binding to Protein Kinase C-α and -δ Isoenzymes in Renal Mesangial Cells. *Biochemistry* 37, 14556–14562. doi:10.1021/bi981401i

Ibrahim, S. H., Hirsova, P., and Gores, G. J. (2018). Non-alcoholic Steatohepatitis Pathogenesis: Sublethal Hepatocyte Injury as a Driver of Liver Inflammation. *Gut* 67, 963–972. doi:10.1136/gutjnl-2017-315691

Ibrahim, S. H., Hirsova, P., Tomita, K., Bronk, S. F., Werneburg, N. W., Harrison, S. A., et al. (2016). Mixed Lineage Kinase 3 Mediates Release of C-X-C Motif Ligand 10-bearing Chemotactic Extracellular Vesicles from Lipotoxic Hepatocytes. *Hepatology* 63, 731–744. doi:10.1002/hep.28252

Kakazu, E., Mauer, A. S., Yin, M., and Malhi, H. (2016). Hepatocytes Release Ceramide-Enriched Pro-inflammatory Extracellular Vesicles in an IRE1α-dependent Manner. *J. Lipid Res.* 57, 233–245. doi:10.1194/jlr.m063412

Kamada, Y., Akita, M., Takeda, Y., Yamada, S., Fujii, H., Sawai, Y., et al. (2013). Serum Fucosylated Haptoglobin as a Novel Diagnostic Biomarker for Predicting Hepatocyte Ballooning and Nonalcoholic Steatohepatitis. *PloS one* 8, e66328. doi:10.1371/journal.pone.0066328

Keerthikumar, S., Chisanga, D., Ariyaratne, D., Al Saffar, H., Anand, S., Zhao, K., et al. (2016). ExoCarta: A Web-Based Compendium of Exosomal Cargo. *J. Mol. Biol.* 428, 688–692. doi:10.1016/j.jmb.2015.09.019

Kowal, J., Arras, G., Colombo, M., Jouve, M., Morath, J. P., Primdal-Bengtson, B., et al. (2016). Proteomic Comparison Defines Novel Markers to Characterize Heterogeneous Populations of Extracellular Vesicle Subtypes. *Proc. Natl. Acad. Sci. USA* 113, E968–E977. doi:10.1073/pnas.1521230113

Krämer, A., Green, J., Pollard, J., Jr, and Tugendreich, S. (2013). Causal Analysis Approaches in Ingenuity Pathway Analysis. *Bioinformatics* 30, 523–530. doi:10.1093/bioinformatics/btt703

Li, J., He, X., Deng, Y., and Yang, C. (2019). An Update on Isolation Methods for Proteomic Studies of Extracellular Vesicles in Biofluids. *Molecules* 24. doi:10.3390/molecules24193516

Liao, C.-Y., Song, M. J., Gao, Y., Mauer, A. S., Revzin, A., and Malhi, H. (2018). Hepatocyte-Derived Lipotoxic Extracellular Vesicle Sphingosine 1-Phosphate Induces Macrophage Chemotaxis. *Front. Immunol.* 9, 2980. doi:10.3389/fimmu.2018.02980

Mandal, A., Mandal, S., and Park, M. H. (2016). Global Quantitative Proteomics Reveal Up-Regulation of Endoplasmic Reticulum Stress Response Proteins upon Depletion of eIF5A in HeLa Cells. *Sci. Rep.* 6, 25795. doi:10.1038/srep25795

Mateyak, M. K., and Kinzy, T. G. (2010). eEF1A: Thinking outside the Ribosome. *J. Biol. Chem.* 285, 21209–21213. doi:10.1074/jbc.r110.113795

Mathieu, M., Martin-Jaular, L., Lavieu, G., and Théry, C. (2019). Specificities of Secretion and Uptake of Exosomes and Other Extracellular Vesicles for Cell-To-Cell Communication. *Nat. Cel Biol* 21, 9–17. doi:10.1038/s41556-018-0250-9

Melo, S. A., Luecke, L. B., Kahlert, C., Fernandez, A. F., Gammon, S. T., Kaye, J., et al. (2015). Glypican-1 Identifies Cancer Exosomes and Detects Early Pancreatic Cancer. *Nature* 523, 177–182. doi:10.1038/nature14581

Michel, C. I., Holley, C. L., Scruggs, B. S., Sidhu, R., Brookheart, R. T., Listenberger, L. L., et al. (2011). Small Nucleolar RNAs U32a, U33, and U35a Are Critical Mediators of Metabolic Stress. *Cel Metab.* 14, 33–44. doi:10.1016/j.cmet.2011.04.009

Müller, G., Ayoub, M., Storz, P., Rennecke, J., Fabbro, D., and Pfizenmaier, K. (1995). PKC Zeta Is a Molecular Switch in Signal Transduction of TNF-Alpha, Bifunctionally Regulated by Ceramide and Arachidonic Acid. *EMBO J.* 14, 1961–1969. doi:10.1002/j.1460-2075.1995.tb07188.x

Nakao, Y., Amrollahi, P., Parthasarathy, G., Mauer, A. S., Sehrawat, T. S., Vanderboom, P., et al. (2021). Circulating Extracellular Vesicles Are a Biomarker for NAFLD Resolution and Response to Weight Loss Surgery. *Nanomedicine: Nanotechnology, Biol. Med.* 36, 102430. doi:10.1016/j.nano.2021.102430

Palmirotta, R., Lovero, D., Cafforio, P., Felici, C., Mannavola, F., Pellè, E., et al. (2018). Liquid Biopsy of Cancer: a Multimodal Diagnostic Tool in Clinical Oncology. *Ther. Adv. Med. Oncol.* 10, 1758835918794630. doi:10.1177/1758835918794630

Pang, Z., Chong, J., Zhou, G., de Lima Morais, D. A., Chang, L., Barrette, M., et al. (2021). MetaboAnalyst 5.0: Narrowing the gap between Raw Spectra and Functional Insights. *Nucleic Acids Res.* 49 (W1), W388–W396. doi:10.1093/nar/gkab382

Patel, G. K., Khan, M. A., Zubair, H., Srivastava, S. K., Khushman, M. d., Singh, S., et al. (2019). Comparative Analysis of Exosome Isolation Methods Using Culture Supernatant for Optimum Yield, Purity and Downstream Applications. *Sci. Rep.* 9, 5335. doi:10.1038/s41598-019-41800-2

Popa, S. J., Stewart, S. E., and Moreau, K. (2018). Unconventional Secretion of Annexins and Galectins. *Semin. Cel Dev. Biol.* 83, 42–50. doi:10.1016/j.semcdb.2018.02.022

Povero, D., Eguchi, A., Niesman, I. R., Andronikou, N., de Mollerat du Jeu, X., Mulya, A., et al. (2013). Lipid-Induced Toxicity Stimulates Hepatocytes to Release Angiogenic Microparticles that Require Vanin-1 for Uptake by Endothelial Cells. *Sci. Signal.* 6, ra88. doi:10.1126/scisignal.2004512

Povero, D., Eguchi, A., Li, H., Johnson, C. D., Papouchado, B. G., Wree, A., et al. (2014). Circulating Extracellular Vesicles with Specific Proteome and Liver MicroRNAs Are Potential Biomarkers for Liver Injury in Experimental Fatty Liver Disease. *PLoS ONE* 9, e113651. doi:10.1371/journal.pone.0113651

Povero, D., Eguchi, A., Li, H., Johnson, C. D., Papouchado, B. G., Wree, A., et al. (2014). Circulating Extracellular Vesicles with Specific Proteome and Liver microRNAs Are Potential Biomarkers for Liver Injury in Experimental Fatty Liver Disease. *PloS one* 9, e113651. doi:10.1371/journal.pone.0113651

Povero, D., Panera, N., Eguchi, A., Johnson, C. D., Papouchado, B. G., de Araujo Horcel, L., et al. (2015). Lipid-Induced Hepatocyte-Derived Extracellular Vesicles Regulate Hepatic Stellate Cells via MicroRNA Targeting Peroxisome Proliferator-Activated Receptor-γ. *Cell Mol. Gastroenterol. Hepatol.* 1, 646–663. doi:10.1016/j.jcmgh.2015.07.007

Povero, D., Yamashita, H., Ren, W., Subramanian, M. G., Myers, R. P., Eguchi, A., et al. (2020). Characterization and Proteome of Circulating Extracellular Vesicles as Potential Biomarkers for NASH. *Hepatol. Commun.* 4, 1263–1278. doi:10.1002/hep4.1556

Rakhshandehroo, M., Knoch, B., Müller, M., and Kersten, S. (2010). Peroxisome Proliferator-Activated Receptor Alpha Target Genes. *PPAR Res.* 2010. doi:10.1155/2010/612089

Rimer, J. M., Lee, J., Holley, C. L., Crowder, R. J., Chen, D. L., Hanson, P. I., et al. (2018). Long-range Function of Secreted Small Nucleolar RNAs that Direct 2′-O-Methylation. *J. Biol. Chem.* 293, 13284–13296. doi:10.1074/jbc.ra118.003410

Rintala-Dempsey, A. C., Rezvanpour, A., and Shaw, G. S. (2008). S100-annexin Complexes - Structural Insights. *Febs j* 275, 4956–4966. doi:10.1111/j.1742-4658.2008.06654.x

Sedaghat, F., and Notopoulos, A. (2008). S100 Protein Family and its Application in Clinical Practice. *Hippokratia* 12, 198–204.

Sehrawat, T. S., Arab, J. P., Liu, M., Amrollahi, P., Wan, M., Fan, J., et al. (2020). Circulating Extracellular Vesicles Carrying Sphingolipid Cargo for the Diagnosis and Dynamic Risk Profiling of Alcoholic Hepatitis. *Hepatology*. doi:10.1002/hep.31256

Serrano, D., Bhowmick, T., Chadha, R., Garnacho, C., and Muro, S. (2012). Intercellular Adhesion Molecule 1 Engagement Modulates Sphingomyelinase and Ceramide, Supporting Uptake of Drug Carriers by the Vascular Endothelium. *Arterioscler Thromb. Vasc. Biol.* 32, 1178–1185. doi:10.1161/atvbaha.111.244186

Simpson, R. J., Kalra, H., and Mathivanan, S. (2012). ExoCarta as a Resource for Exosomal Research. *J. extracellular vesicles* 1, 18374. doi:10.3402/jev.v1i0.18374

Sobolewski, C., Abegg, D., Berthou, F., Dolicka, D., Calo, N., Sempoux, C., et al. (2020). S100A11/ANXA2 Belongs to a Tumour Suppressor/oncogene Network Deregulated Early with Steatosis and Involved in Inflammation and Hepatocellular Carcinoma Development. *Gut* 69, 1841–1854. doi:10.1136/gutjnl-2019-319019

Statello, L., Maugeri, M., Garre, E., Nawaz, M., Wahlgren, J., Papadimitriou, A., et al. (2018). Identification of RNA-Binding Proteins in Exosomes Capable of Interacting with Different Types of RNA: RBP-Facilitated Transport of RNAs into Exosomes. *PloS one* 13, e0195969. doi:10.1371/journal.pone.0195969

Stoianov, A. M., Robson, D. L., Hetherington, A. M., Sawyez, C. G., and Borradaile, N. M. (2015). Elongation Factor 1A-1 Is a Mediator of Hepatocyte Lipotoxicity Partly through its Canonical Function in Protein Synthesis. *PloS one* 10, e0131269. doi:10.1371/journal.pone.0131269

Szklarczyk, D., Gable, A. L., Lyon, D., Junge, A., Wyder, S., Huerta-Cepas, J., et al. (2019). STRING V11: Protein-Protein Association Networks with Increased Coverage, Supporting Functional Discovery in Genome-wide Experimental Datasets. *Nucleic Acids Res.* 47, D607–d613. doi:10.1093/nar/gky1131

Théry, C., Amigorena, S., Raposo, G., and Clayton, A. (2006). Isolation and Characterization of Exosomes from Cell Culture Supernatants and Biological Fluids. *Curr. Protoc. Cel Biol* Chapter 3, Unit–22. doi:10.1002/0471143030.cb0322s30

van Niel, G., D'Angelo, G., and Raposo, G. (2018). Shedding Light on the Cell Biology of Extracellular Vesicles. *Nat. Rev. Mol. Cel Biol* 19, 213–228. doi:10.1038/nrm.2017.125

Wang, R., Wang, X., and Zhuang, L. (2016). Gene Expression Profiling Reveals Key Genes and Pathways Related to the Development of Non-alcoholic Fatty Liver Disease. *Ann. Hepatol.* 15, 190–199. doi:10.5604/16652681.1193709

Wilson, R. B., Chen, Y. J., Sutherland, B. G., Sawyez, C. G., Zhang, R., Woolnough, T., et al. (2020). The marine Compound and Elongation Factor 1A1 Inhibitor, Didemnin B, Provides Benefit in Western Diet-Induced Non-alcoholic Fatty Liver Disease. *Pharmacol. Res.* 161, 105208. doi:10.1016/j.phrs.2020.105208

Xia, C., Braunstein, Z., Toomey, A. C., Zhong, J., and Rao, X. (2018). S100 Proteins as an Important Regulator of Macrophage Inflammation. *Front. Immunol.* 8, 1908. doi:10.3389/fimmu.2017.01908

Younossi, Z. M., Gorreta, F., Ong, J. P., Schlauch, K., Del Giacco, L., Elariny, H., et al. (2005). Hepatic Gene Expression in Patients with Obesity-Related Non-alcoholic Steatohepatitis. *Liver Int.* 25, 760–771. doi:10.1111/j.1478-3231.2005.01117.x

Yuan, Z.-Y., Zhang, X.-X., Wu, Y.-J., Zeng, Z.-P., She, W.-M., Chen, S.-Y., et al. (2019). Serum Amyloid A Levels in Patients with Liver Diseases. *Wjg* 25, 6440–6450. doi:10.3748/wjg.v25.i43.6440

Zhang, L., Zhang, Z., Li, C., Zhu, T., Gao, J., Zhou, H., et al. (2021). S100A11 Promotes Liver Steatosis via FOXO1-Mediated Autophagy and Lipogenesis. *Cell Mol. Gastroenterol. Hepatol.* 11, 697–724. doi:10.1016/j.jcmgh.2020.10.006

Zhou, X., Xie, F., Wang, L., Zhang, L., Zhang, S., Fang, M., et al. (2020). The Function and Clinical Application of Extracellular Vesicles in Innate Immune Regulation. *Cell Mol Immunol* 17, 323–334. doi:10.1038/s41423-020-0391-1

Zhu, Y., Chen, X., Pan, Q., Wang, Y., Su, S., Jiang, C., et al. (2015). A Comprehensive Proteomics Analysis Reveals a Secretory Path- and Status-dependent Signature of Exosomes Released from Tumor-Associated Macrophages. *J. Proteome Res.* 14, 4319–4331. doi:10.1021/acs.jproteome.5b00770

Conflict of Interest: The authors declare that the research was conducted in the absence of any commercial or financial relationships that could be construed as a potential conflict of interest.

Publisher's Note: All claims expressed in this article are solely those of the authors and do not necessarily represent those of their affiliated organizations, or those of the publisher, the editors and the reviewers. Any product that may be evaluated in this article, or claim that may be made by its manufacturer, is not guaranteed or endorsed by the publisher.

GLOSSARY

ANGPTL2 angiopoietin-like protein 2

ANO6 anoctamin-6

COL1A1 collagen alpha-1 chain

DAMP damage-associated molecular pattern

DG density gradient

Emb embigin

ER endoplasmic reticulum

EV extracellular vesicles

FDR false discovery rate

GO gene ontology

Hp haptoglobin

H3F3A histone H3.3

ICAM1 intercellular adhesion molecule 1

IGFALS insulin-like growth factor-binding protein complex acid labile submit

IGHV6-1 immunoglobulin heavy variable 6-1

IGSF3 immunoglobulin superfamily member 3

IMH immortalized mouse hepatocytes

IRE1α inositol requiring enzyme 1 alpha

MHC major histocompatibility complex

NTA nano-particle tracking analysis

NAFLD non-alcoholic fatty liver disease

NASH non-alcoholic steatohepatitis

PALM3 paralemmin-3

PTK7 protein tyrosine kinase 7

PRKCA protein kinase C alpha type

SEC size exclusion chromatography

SAA1 serum amyloid A-1 protein

STARD11 StAR-related lipid transfer domain 11

tSNE t-distributed stochastic neighbor embedding

UTC ultracentrifugation

VNN1 vanin 1

WNT10A wnt family member 10A

frontiers in Cell and Developmental Biology

ORIGINAL RESEARCH
published: 14 January 2022
doi: 10.3389/fcell.2021.787356

Alcohol Promotes Exosome Biogenesis and Release *via* Modulating Rabs and miR-192 Expression in Human Hepatocytes

Shashi Bala[1†], *Mrigya Babuta*[1†], *Donna Catalano*[2], *Aman Saiju*[1] *and Gyongyi Szabo*[1*]

[1]*Department of Medicine, Beth Israel Deaconess Medical Center, Harvard Medical School, Boston, MA, United States,*
[2]*Department of Medicine, University of Massachusetts Medical School, Worcester, MA, United States*

OPEN ACCESS

Edited by:
Jeffrey David Galley,
The Ohio State University,
United States

Reviewed by:
Prabhu Mathiyalagan,
New York University, United States
Jafar Rezaie,
Urmia University of Medical Sciences, Iran

****Correspondence:***
Gyongyi Szabo
gszabo1@bidmc.harvard.edu

[†]These authors have contributed equally to this work and share first authorship

Specialty section:
This article was submitted to Molecular and Cellular Pathology, a section of the journal Frontiers in Cell and Developmental Biology

Received: *30 September 2021*
Accepted: *20 December 2021*
Published: *14 January 2022*

Citation:
Bala S, Babuta M, Catalano D, Saiju A and Szabo G (2022) Alcohol Promotes Exosome Biogenesis and Release via Modulating Rabs and miR-192 Expression in Human Hepatocytes. Front. Cell Dev. Biol. 9:787356. doi: 10.3389/fcell.2021.787356

Exosomes are membrane vesicles released by various cell types into the extracellular space under different conditions including alcohol exposure. Exosomes are involved in intercellular communication and as mediators of various diseases. Alcohol use causes oxidative stress that promotes exosome secretion. Here, we elucidated the effects of alcohol on exosome biogenesis and secretion using human hepatocytes. We found that alcohol treatment induces the expression of genes involved in various steps of exosome formation. Expression of Rab proteins such as Rab1a, Rab5c, Rab6, Rab10, Rab11, Rab27a and Rab35 were increased at the mRNA level in primary human hepatocytes after alcohol treatment. Rab5, Rab6 and Rab11 showed significant induction in the livers of patients with alcohol-associated liver disease. Further, alcohol treatment also led to the induction of syntenin, vesicle-associated membrane proteins (VAMPs), and syntaxin that all play various roles in exosome biogenesis and secretion. VAMP3, VAMP5, VAPb, and syntaxin16 mRNA transcripts were increased in alcohol treated cells and in the livers of alcohol-associated liver disease (ALD) patients. Induction in these genes was associated with increases in exosome secretion in alcohol treated hepatocytes. We found that hepatocyte enriched miR-192 and miR-122 levels were significantly decreased in alcohol treated hepatocytes whereas their levels were increased in the cell-free supernatant. The primary transcripts of miR-192 and miR-122 were reduced in alcohol treated hepatocytes, suggesting alcohol partially affects these miRNAs at the transcriptional level. We found that miR-192 has putative binding sites for genes involved in exosome secretion. Inhibition of miR-192 in human hepatoma cells caused a significant increase in Rab27a, Rab35, syntaxin7 and syntaxin16 and a concurrent increase in exosome secretion, suggesting miR-192 regulates exosomes release in hepatocytes. Collectively, our results reveal that alcohol modulates Rabs, VAMPs and syntaxins directly and partly *via* miR-192 to induce exosome machinery and release.

Keywords: alcohol, exosomes, rabs, syntenin, syntaxin, VAMPs, miR-192, miR-122

INTRODUCTION

Exosomes are small membrane extracellular vesicles (<100 nm or <200 nm) released by various cell types into the extracellular space under different physiological and pathological conditions (Trams et al., 1981; Bala et al., 2012; Bala et al., 2015; Thery et al., 2018). Exosomes can be found in most biological fluids such as blood, saliva, and urine (Szabo and Momen-Heravi, 2017). Exosomes contain nucleic acids (for e.g., RNA and miRNA), proteins, lipids and other biomolecules that can modulate the function of the recipient cell. By transferring their cargos, exosomes emerged as a new mode of intercellular communication (Valadi et al., 2007; Momen-Heravi et al., 2015a). Exosome formation comprises of three steps: biogenesis, transport, and release. Briefly, exosomes are formed by inward invagination of the endosomal membrane the first step is the formation of intraluminal vesicles (ILVs) in multivesicular body (MVBs; late endosomes). MVBs are then transported to and fused with the plasma membrane resulting in the release of exosomes into the extracellular space (Hessvik and Llorente, 2018). Various components, such as the endosomal sorting complexes required for transport (ESCRT) machinery, are involved in multivesicular endosome formation and syntenin is one of the proteins known to facilitates ILV formation (Baietti et al., 2012). Furthermore, syndecan-syntenin-ALIX are well recognized for their imperative role in exosomes biogenesis (Baietti et al., 2012).

The transport of MVBs to the plasma membrane is governed by various factors including small Rab GTPases. Till now, more than 70 Rab proteins has been identified. Through their association with the endocytic and secretion pathways, Rabs are widely known for their roles in membrane transport and fusion (Blanc and Vidal, 2018). Various Rabs such as Rab5a, Rab7, Rab11, Rab27a/b, and Rab35 are shown to require for exosome release (Savina et al., 2002; Hsu et al., 2010; Ostrowski et al., 2010; Blanc and Vidal, 2018; Hessvik and Llorente, 2018). Among all the Rab proteins, Rab11, Rab27 and Rab35 have been shown to play direct role in exosome biogenesis and secretion (Blanc and Vidal, 2018). Rab11 and Rab35 are reported to be involve in the recycling of membrane components from endosomal compartment to the plasma membrane (Hsu et al., 2010; Ramel et al., 2013). Whereas Rab27 was shown to involve in the transport of late endosomal/lysosome-like compartments to the plasma membrane (Ostrowski et al., 2010). Both isoforms of Rab27, Rab27a and Rab27b are involved in the exosome secretory pathway (Ostrowski et al., 2010).

Soluble N-ethylmaleimide-sensitive factor attachment protein receptors (SNAREs), proteins are involved in the final step of exosome secretion that is the fusion of MVBs to the plasma membrane (Jahn and Scheller, 2006). SNAREs are classified as either t-SNAREs (target membrane) and v-SNAREs (vesicle membrane). The vSNARE protein, VAMP7 was demonstrated to mediate the fusion of secretory lysosomes with the plasma membrane and to regulate of EVs release (Fader et al., 2009). Syntaxins belong to t-SNAREs proteins and play an important role in membrane trafficking and autophagy (Tang, 2019; Mori et al., 2021).

Liver resident cells including parenchyma (hepatocytes) and non-parenchymal cells are involved in the pathogenesis of alcohol-associated liver disease (ALD) (Osna et al., 2017). Alcohol is predominantly metabolized by hepatocytes that make up to 70 percent of the liver mass (Osna et al., 2017). Alcohol induces oxidative stress and previously we demonstrated an increase in exosome secretion in alcoholic hepatitis patients (Momen-Heravi et al., 2015b; Babuta et al., 2019), *in vivo* alcohol mouse models (Momen-Heravi et al., 2015a; Momen-Heravi et al., 2015b; Babuta et al., 2019) and *in vitro* model of alcohol-treated human hepatocytes (Momen-Heravi et al., 2015a). However, the effect of alcohol on genes involved in exosome biogenesis, transport and secretion is not known.

miRs are small noncoding RNAs that regulate gene expression and are involved in various physiological processes (Szabo and Bala, 2013; Babuta and Szabo, 2021). Altered miRNA expression has been found in ALD (Bala and Szabo, 2012; Bala et al., 2016; Satishchandran et al., 2018). Both miR-122 and miR-192 are highly expressed in hepatocytes (Momen-Heravi et al., 2015a) and a decrease in miR-122 levels was found in ALD (Bala et al., 2012) in Non-alcoholic fatty liver disease (NAFLD) (Csak et al., 2015) and a down-regulation in hepatic miR-192 levels was reported in NAFLD (Liu et al., 2017). Since one miRNA can affect many target genes, thereby have a wider effect on multiple cellular pathways, we hypothesized that alcohol induces exosome secretion *via* affecting multiple factors including miRNA. Recently, we established a link between miR-155 and lysosome dysfunction in exosome release in ALD (Babuta et al., 2019). In this study, we demonstrated that alcohol induces the expression of Rabs, VAMPs, and syntaxins in primary human hepatocytes, human hepatoma cell line, Huh7.5 cells, and in ALD patients. Hepatocyte enriched miR-192 and miR-122 were found to be decreased and a significant increase in the number of exosomes was observed in primary human hepatocytes after alcohol treatment. Our mechanistic studies suggest that inhibition of miR-192 caused an increase in Rabs and syntaxins and a concurrent increase in exosome secretion in hepatocytes. Collectively, our work reveals following two important findings: first, alcohol affects multiple genes involved in exosome biosynthesis and release directly and partly *via* miR-192, and second, a novel role of miR-192 in exosome secretion in hepatocytes.

MATERIALS AND METHODS

Primary Human Hepatocytes and Cell Lines

Primary human hepatocytes were obtained from the National Institutes of Health (NIH) liver tissue cell distribution system (LTCDS; Minneapolis, MN, United States; Pittsburgh, PA; Richmond, VA, United States), and were maintained in low-glucose without phenol red low-glucose Dulbecco's modified Eagle medium (DMEM) media supplemented with 1% anti-anti (Gibco, Thermofisher Scientific, MA, United States), 1% Insulin transferrin (Gibco, Thermofisher Scientific, MA, United States) and 2% exosome depleted fetal bovine serum (System Bioscience, United States). For alcohol treatment, cells

were treated with different dosages of alcohol (25 and 50 mM) and incubated in C.B.S. Scientific incubation culture chambers with twice the alcohol concentration in bottom of the chamber to saturate and maintain a stable alcohol concentration (25 mM or 50 mM) in the chamber.

Human hepatoma cell line, Huh7.5 were maintained and cultured in low-glucose DMEM containing 1% pencillin-streptomycin (Gibco, Thermofisher Scientific, MA, United States) and 10% exosome depleted fetal bovine serum (System Bioscience) and supplemented with nonessential amino acids (NEAA) (Gibco, Thermofisher Scientific, MA, United States). Cells were treated with 50 mM alcohol as described above for 6, 18, 36 and 48 h.

Patient Samples

Human liver samples from control subjects, and patients with alcohol-associated liver disease (n = 8–10) were obtained from the National Institutes of Health Liver Tissue Cell Distribution System (Minneapolis, MN). The BIDMC Institutional Review Board for Protection of Human Subjects in Research approved the study. The criteria to define patients with ALD were based on "Recommendation from the NIAAA Alcoholic Hepatitis Consortia" (Crabb et al., 2016).

RNA Extraction

Total RNA was extracted from the primary human hepatocytes or Huh7.5 cells or from the supernatant using Direct-zol RNA MiniPrep kit (Zymo Research, Irvine, CA) as described by the manufacturer. Synthetic Cel-miR-39 was spiked during the extraction of RNA from the supernatant and used as a normalization control as described previously (Momen-Heravi et al., 2015b). RNA was transcribed into cDNA with the iScript cDNA synthesis supermix kit (Bio-Rad Laboratories Inc, CA, United States). Real-time quantitative polymerase chain reaction was performed on CFX96 iCycler (Bio-Rad). For miRNA, TaqMan miRNA assays were used (Ambion, TX, United States) and RNU48 was used to normalize the data. Primary miR-122 and miR-192 levels were measured using TaqMan gene expression assay (Ambion, TX, United States) and GAPDH was used as a normalization control as described by the manufacturer. For mRNA quantification, 18s was used for normalization of cq values among the samples.

NanoSight/Nanoparticle Tracking Analysis (NTA)

The concentration and size distribution of extracellular vesicles (EVs) from the cell culture supernatants were determined using the NanoSight NS300 system (NanoSight, Amesbury, United Kingdom) (Momen-Heravi et al., 2015a). The samples were captured for 30 s in triplicates at room temperature and NTA post-acquisition settings were kept constants for all samples. The NTA software was used to process the captured videos with setting as threshold of five arbitrary unit (AU) and screen gain of 5AU and concentration (particles/milliliter) and size distribution (in nanometers) were calculated from the measured particles. The particles ranging from 40 to 100 nm were defined as exosomes. In previous reports our laboratory demonstrated that this EV size corresponds to exosomes and express exosome markers including CD63 (Momen-Heravi et al., 2015a)

Transfection

For miR-192 inhibition studies, Huh7.5 cells, human hepatocyte cell line, were either transfected with a negative control miRNA or miR-192 inhibitor at 30pM for 24 h (Applied Biosystems, Foster City, CA) using Lipofectamine RNAi max reagent (Thermo Fisher Scientific) as described by the manufacturer. Cells were harvested 48 h after transfection. Cell-free supernatants were used to determine EVs concentration and size distribution using Nanosight.

Statistical Analysis

Statistical significance was determined using either Mann-Whitney test or one-way ANOVA. Each experiment was repeated at least three times to determine the biological significance. Data are shown as mean ± SEM and considered statistically significant at $p < 0.05$. GraphPad Prism software (version 7 or 8; GraphPad Software Inc.) was used for analysis.

RESULTS

Alcohol Increases Rab GTPases in Primary Human Hepatocytes and in ALD Patients

Previously, we showed that alcohol increases exosome release from human hepatocytes (Momen-Heravi et al., 2015a) and exosome numbers were increased in the circulation in alcoholic hepatitis patients (Momen-Heravi et al., 2015b) and in a mouse model of ALD (Momen-Heravi et al., 2015b). However, the mechanism by which alcohol regulates exosome secretion is not known. In this study, we carried out a comprehensive approach to determine the effect of alcohol on genes involved in exosome biogenesis and secretory pathways using human hepatocytes. We found that alcohol increases the transcription of various Rab GTPases involved in exosome biogenesis and secretory pathways. A time dependent increase in Rab1a (18–24 h, **Figure 1A**), Rab5c (6–48 h, **Figure 1B**), Rab6 (6–48h, **Figure 1C**) and Rab10 (6–48 h, **Figure 1D**), which are the regulators of membrane trafficking and exosome formation, were found in primary human hepatocytes after different doses of alcohol treatment (25 and 50 mM). Rab11, Rab27 and Rab35 have been shown to play a significant direct role in exosome biogenesis and secretion (Blanc and Vidal, 2018) and we found significant increases in the mRNA levels of Rab11b (6–48 h, **Figure 1E**), Rab27a (6 h, and 48 h, **Figure 1F**), and Rab35 (6–48 h, **Figure 1G**) after alcohol treatment. Syntenin, a syndecan binding protein, plays diverse roles in exosome biogenesis (Baietti et al., 2012; Kashyap et al., 2021) and our results indicated a significant induction in its mRNA expression after alcohol treatment (6–48 h, **Figure 1H**). The kinetics of Rabs tested and syntenin upregulation were similar between 25 and 50 mM of alcohol treatment and highest induction in most of these genes was observed 48 h after alcohol treatment (**Figures**

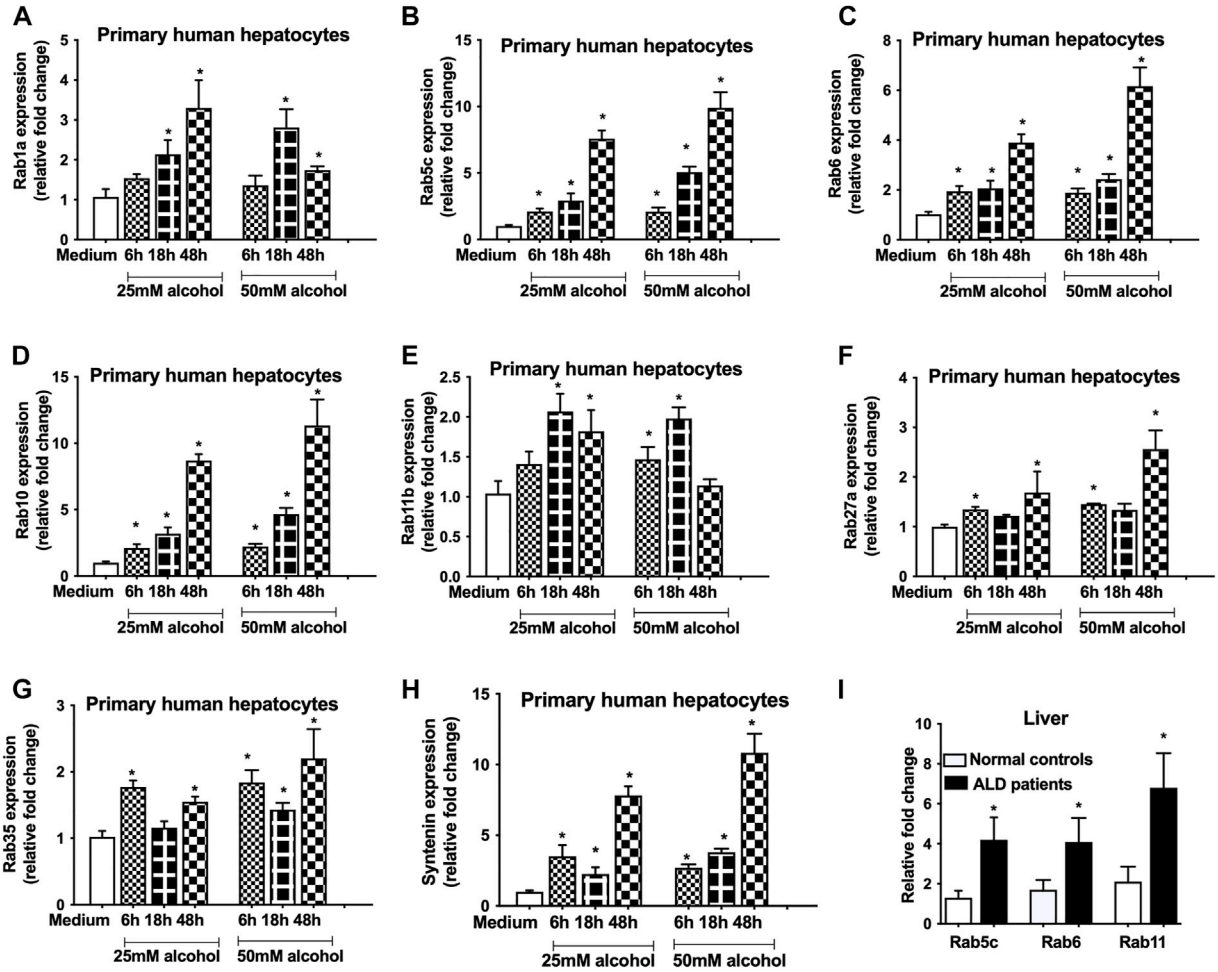

FIGURE 1 | Alcohol induces the expression of Rabs in primary human hepatocytes and in ALD patients.Primary human hepatocytes were cultured and treated with different dosage of alcohol (25 and 50 mM) for indicated times. The expression of Rab1a **(A)**, Rab5c **(B)**, Rab6 **(C)**, Rab10 **(D)**, Rab11b **(E)**, Rab27a **(F)**, Rab35 **(G)** and syntenin **(H)** was determined by qPCR from the total RNA isolated from the cells. Results are representative of three independent experiments. Total RNA was extracted from the livers of normal controls and ALD patients (n = 9) and expression of Rab5c, Rab6 and Rab11 was evaluated by qPCR **(I)**. 18s was used to normalize the cq values. Data represent mean ± SEM. Mann-Whitney test was employed for statistical analysis. *indicates $p < 0.05$ versus control cells **(A-H)** or normal controls **(I)**.

1A–H). Next, we determined the expression of some of these Rabs in patients with ALD and found significant increases in Rab5c, Rab6 and Rab11 in ALD patients compared to controls (**Figure 1I**).

Alcohol Induces the Expression of Soluble N-Ethylmaleimide Sensitive Factor Attachment Protein Receptors Proteins

The vesicle-associated membrane proteins (VAMPs) belong to v-SNARE family protein, and reside in various post-Golgi vesicular compartments, and mediate vesicle fusion with the plasma membrane (Jahn and Scheller, 2006). To determine the effect of alcohol on VAMPs, we checked the levels of VAMP 3, 5 and 7 and found that alcohol significantly increases the VAMP3 (6–48 h, **Figure 2A**), VAMP5 (6–48 h, **Figure 2B**) and VAMP7 (6–48 h, **Figure 2C**) mRNA transcripts. VAPb, a VAMP associated protein (Chen et al., 2010) was also found to be induced after alcohol treatment (18 and 48 h, **Figure 2D**). Syntaxin 16 (STX16), belongs to t-SNARE family protein, is required for the accumulation of recycling endosomes (Amessou et al., 2007), and we found increase in STX16 mRNA transcripts only 48 h after alcohol treatment (**Figure 2E**). Since we found increased expression of Rabs, syntenin and SNAREs, we next determined the EV number and found a time dependent increase in particles ranging from 40 to 100 nm after different doses (25 and 50 mM) of alcohol treatment (6–48 h, **Figure 2F**). Given that size distribution of particles has been defined as exosomes in the 30–150 nm range by some studies (Tschuschke et al., 2020; Babaei and Rezaie, 2021), we also analyzed our data by measuring the particles from 30 to 150 nm. We found no significant differences in quantifying the particles ranging from 40 to 100 nm and 30–150 nm as shown **Figure 2F,G**, respectively. It was observed that maximum induction in VAMPs, VAPb,

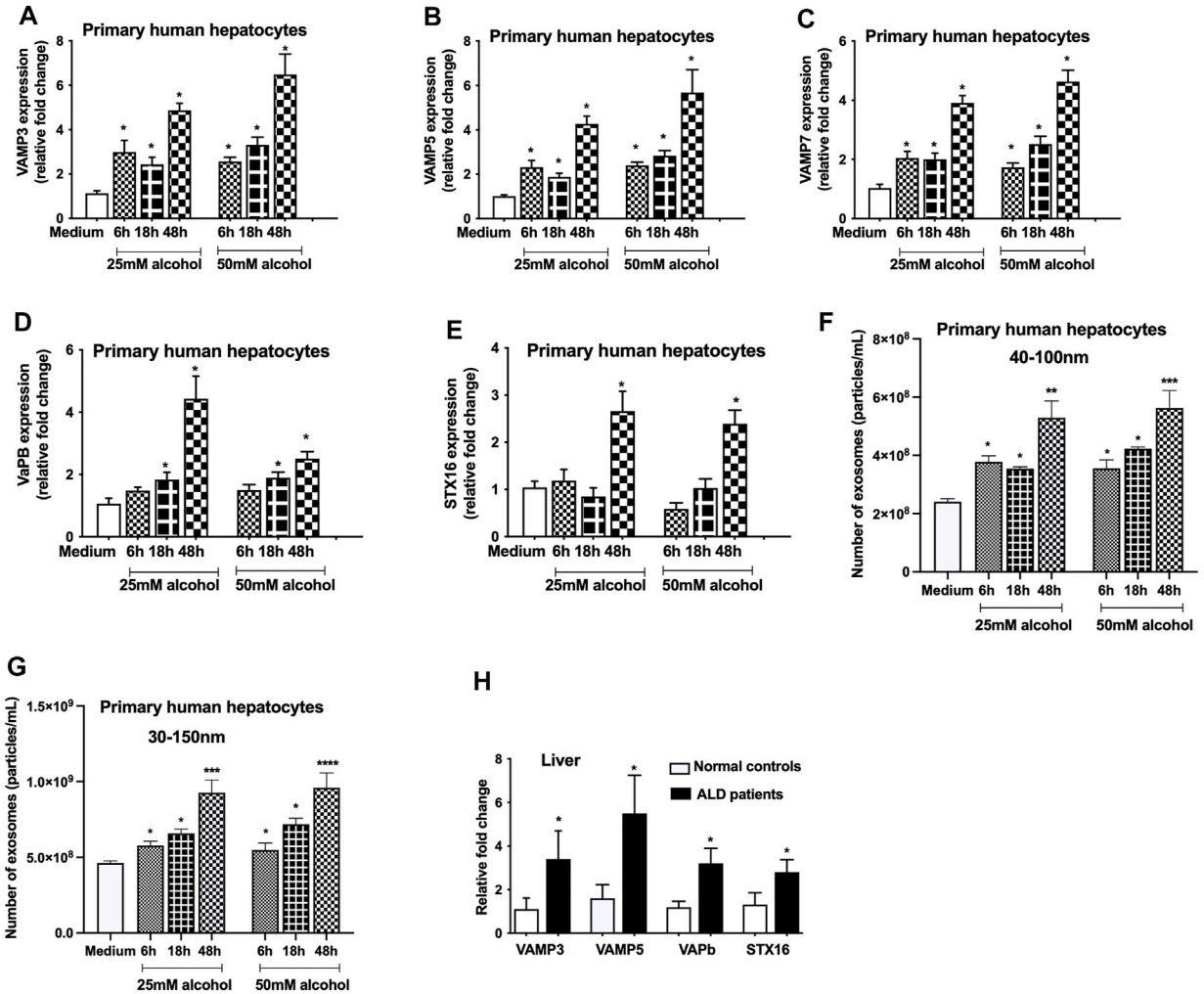

FIGURE 2 | Alcohol increases the expression of VAMPs and syntaxins. Primary human hepatocytes were cultured and treated with different dosage of alcohol (25 and 50 mM) for indicated times and VAMP3 **(A)**, VAMP5 **(B)**, VAMP7 **(C)**, VAPb **(D)**, and STX16 **(E)** expression was assessed by qPCR from the total RNA isolated from the cells. Total number of particles was measured from the cell free supernatant after alcohol treatment (25 and 50 mM) for indicated times using Nanosight **(F and G)**. Data is presented as particles/ml. Number of particles from 40–100 nm and 30–150 nm are represented in F and G, respectively. Total RNA extracted from the livers of normal controls and ALD patients (n = 9) was used to determine the expression of VAMP3, VAMP5, VAPb and STX16 by qPCR **(H)**. 18s was used to normalize the cq values. Data represent mean ± SEM. Mann-Whitney test or one-way ANOVA was used for statistical analysis. *, **, ***,**** indicates $p < 0.05$, $p < 0.005$, $p < 0.0005$, $p < 0.0001$ compared to control cells **(A-G)** or normal controls **(H)**.

STX16 and exosome number occurred 48 h after alcohol treatment (**Figures 2A–G**). Significant increases in VAMP3, VAMP5, VAPb, and STX16 were also observed in ALD patients compared to controls (**Figure 2H**).

Alcohol Regulates miRNAs Expression at the Transcriptional Level

Since miR-122 and miR-192 are highly expressed in hepatocytes (Momen-Heravi et al., 2015a), we evaluated the effect of alcohol on these miRNAs. A significant decrease in miR-192 (6–48 h, **Figure 3A**) and miR-122 (6–48 h, **Figure 3B**) was found in hepatocytes treated with either 25 mM or 50 mM alcohol. To determine the effect of alcohol on the transcriptional levels of these miRNAs, we checked the primary miRNA expression and found a decrease in pri-miR-192 (6 and 18 h, **Figure 3C**) and pri-miR-122 transcripts (6–18 h, **Figure 3D**). Previously, we reported increase in miR-192 and miR-122 levels in the exosomes derived from the serum of alcoholic hepatitis patients (Momen-Heravi et al., 2015b) and in a mouse model of ALD (Bala et al., 2012) therefore, we sought to evaluate their levels in the cell-free supernatant. Our results indicated a significant increase in miR-192 and miR-122 levels in the supernatant of primary hepatocytes 18 h after alcohol treatment (25 and 50 mM) (**Figure 3E**).

miRNA-192 Regulates the Exosome Secretion *via* Targeting Rabs and Syntaxins

Our bioinformatic analysis revealed that Rab27a, Rab35, STX7 and STX16 are predicted targets of miR-192 (www.microrna.org)

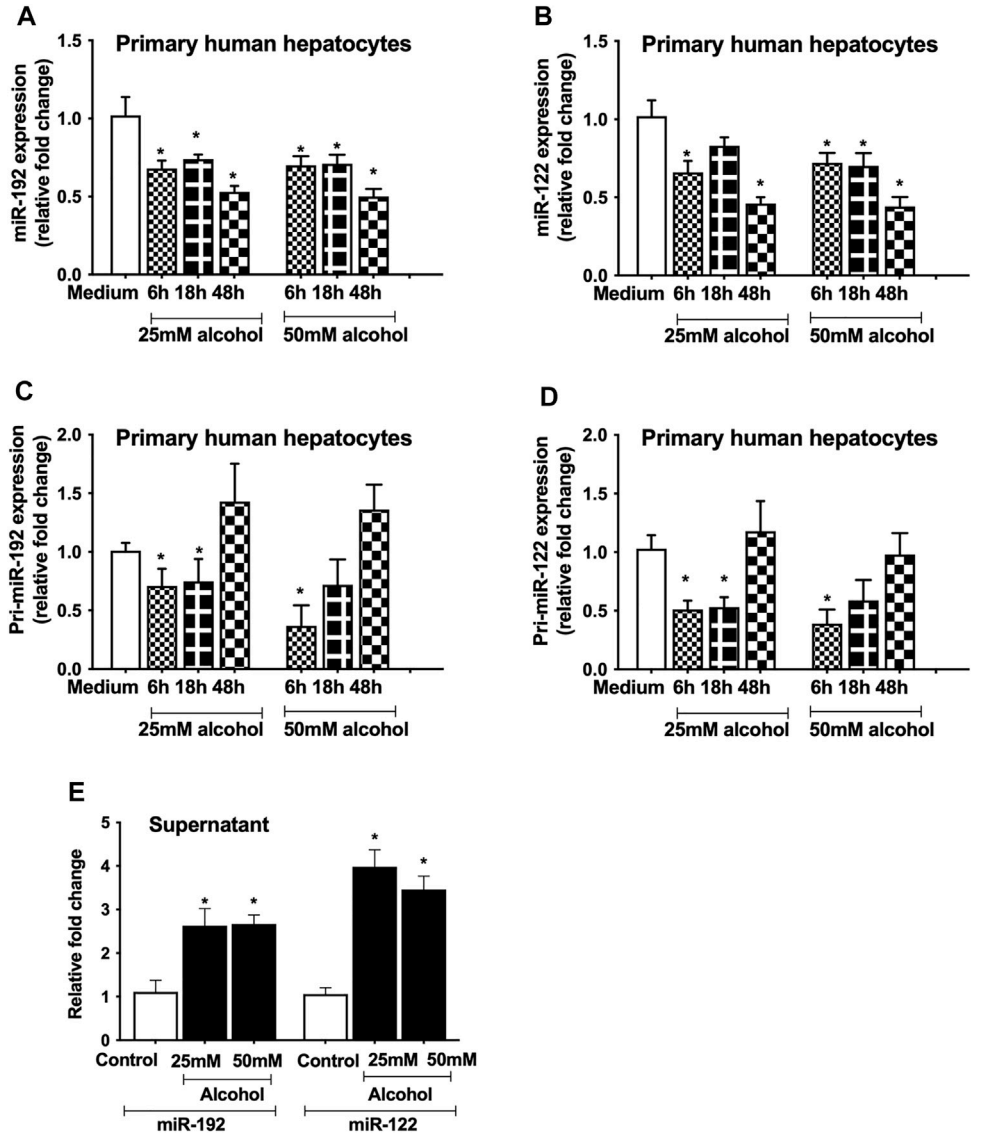

FIGURE 3 | Alcohol regulates miRNA expression at the transcriptional level. Primary human hepatocytes were cultured and treated with different dosage of alcohol (25 and 50 mM) for indicated times. The levels of mature form of miR-192 **(A)** and miR-122 **(B)** were measured by qPCR and RNU48 was used as a normalization control. The primary transcripts of miR-192 **(C)** and miR-122 **(D)** were quantified by qPCR and GAPDH was used as a normalization control. Total RNA was extracted from the cell-free supernatants of primary hepatocytes and miR-192 and miR-122 were evaluated 18 h after alcohol treatment by qPCR and spiked synthetic Cel-miR-39 was used as a normalization control **(E)**. Data represent mean ± SEM. Mann-Whitney test was employed for statistical analysis. *indicates $p < 0.05$ versus control cells.

(**Figure 4A**). Since these genes play critical role in exosome secretion (Hsu et al., 2010; Ostrowski et al., 2010), therefore, to determine the causal effect of alcohol-induced miR-192 downregulation on exosome secretion, we carried out simulation experiments using human hepatoma Huh.7.5 cells. First, we determined the optimal time for the induction of these genes in Huh 7.5 cells and found significant increase in Rab27a (6–36 h, **Figure 4B**), Rab35 (6 and 18 h, **Figure 4C**), STX7 (18 h, **Figure 4D**), and STX16 (6–48 h, **Figure 4E**) mRNA transcripts after alcohol treatment (50 mM). A time dependent increase in exosome (40–100 nm in **Figures 4F**, 30–150 nm in **Figure 2G**) secretion (18–48 h) was found, and a maximum increase in exosomes was observed 48 h after alcohol treatment.

Transfection of a miR-192 inhibitor in hepatocytes caused a significant decrease in miR-192 levels compared to control inhibitor cells (**Figure 4G**). miR-192 inhibition resulted in a significant increase in Rab27a (**Figure 4H**), Rab35 (**Figure 4I**), STX7 (**Figure 4J**), and STX16 (**Figure 4K**). Furthermore, an approximately 1.8-fold induction in exosome secretion was detected in cells transfected with miR-192 inhibitor compared to control inhibitor treated cells (**Figure 4L**).

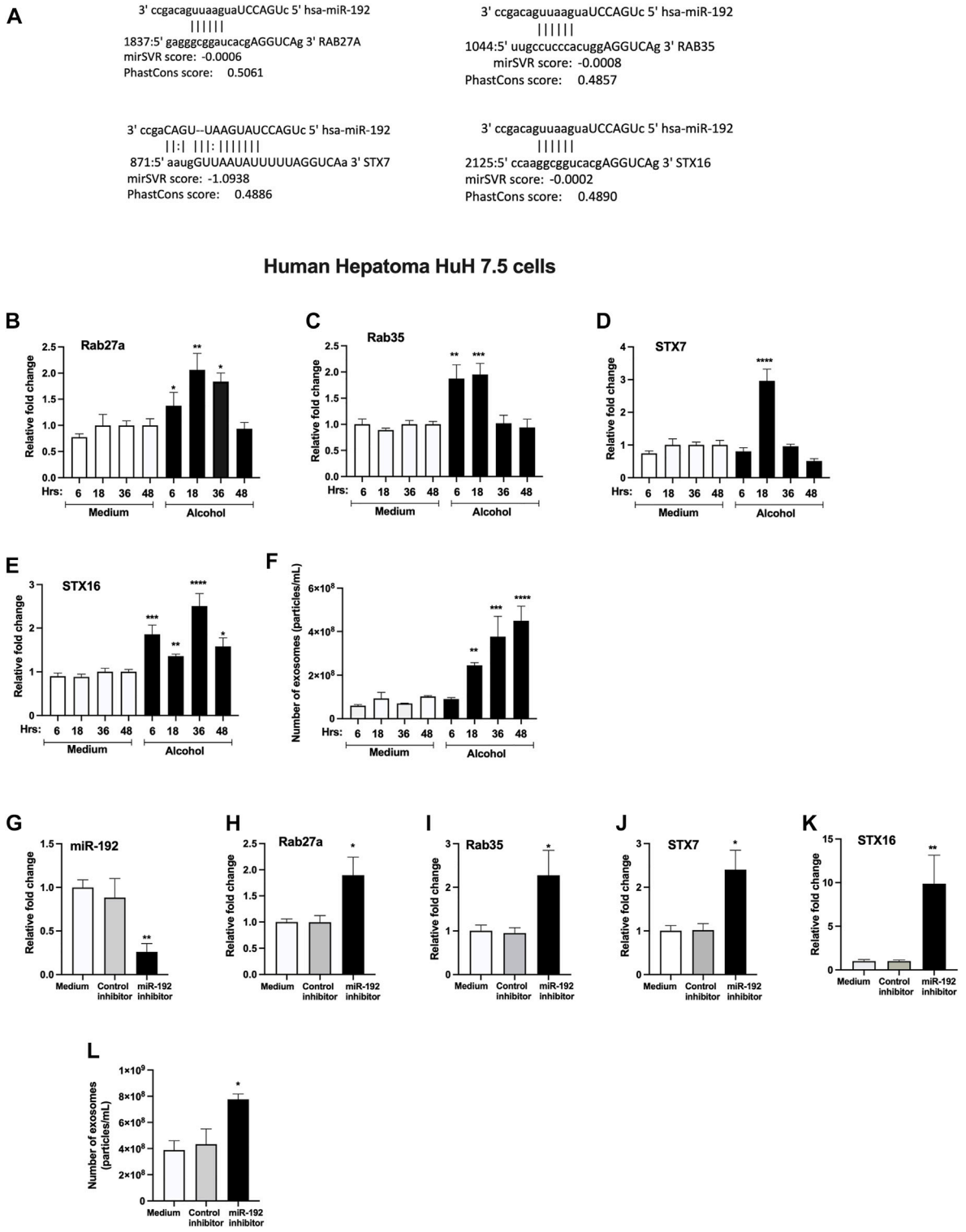

FIGURE 4 | miRNA-192 regulates exosome secretion *via* targeting Rabs and syntaxins.miR-192 putative binding sites at the 3' UTR of Rab27a, Rab35, STX7 and STX16 genes **(A)**. Huh 7.5 cells were treated or not with 50 mM alcohol for indicated times and expression of Rab27a **(B)**, Rab35 **(C)**, STX7 **(D)**, and STX16 **(E)** was quantified from RNA isolated from cells using qPCR. Total number of particles was measured from the cell free supernatant after 50 mM of alcohol treatment for indicated times using Nanosight and presented as particles/ml **(F)**. Huh 7.5 cells were transfected either with negative control-miRNA or miR-192 inhibitor as described in the methods. miR-192 expression was measured from the cells using qPCR and RNU48 was used as a normalization control **(G)**. The expression of Rab27a **(H)**, Rab35 **(I)**, STX7 **(J)**, and STX16 **(K)** was determined using qPCR. Total number of particles was evaluated from the cell free supernatant after miR-192 inhibition using Nanosight and presented as particles/ml **(L)**. 18s was used to normalize the cq values. Data represent mean ± SEM. One-way ANOVA or Mann-Whitney test was used for statistical analysis. *, **, ***, ****indicates $p < 0.05$, $p < 0.005$, $p < 0.0005$, $p < 0.0001$ compared to control cells.

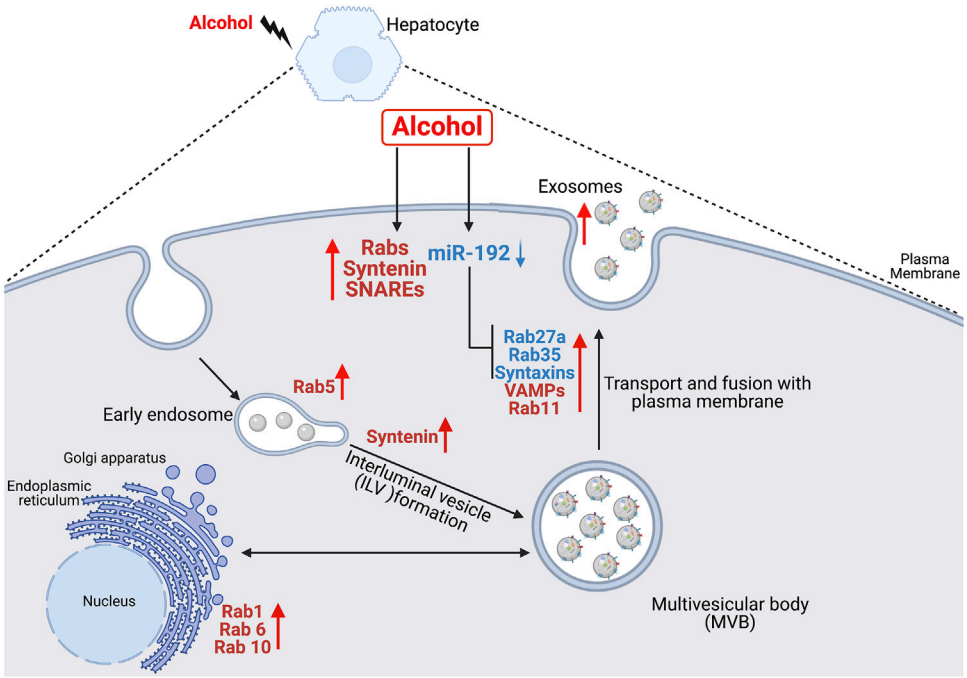

FIGURE 5 | Schematic representation of the effect of alcohol on exosome biogenesis and secretion in human hepatocytes. Alcohol modulates the expression of various Rabs, syntenin, VAMPs and syntaxins directly or partly *via* miR-192 in hepatocytes. Alcohol-induced decrease in miR-192 results in increase in miR-192 target genes (Rab27a, Rab35, syntaxin7 and syntaxin16) and a concurrent induction in exosome secretion.

Discussion

Various studies have shown increased secretion of exosomes during cellular stress (Momen-Heravi et al., 2015a; Momen-Heravi et al., 2015b; Hessvik and Llorente, 2018; Babuta et al., 2019; Babuta and Szabo, 2021). Majority of alcohol is metabolized in hepatocytes and alcohol metabolites induce oxidative stress (Momen-Heravi et al., 2015a). Continuous use of alcohol results in hepatocyte damage and subsequently to alcohol-associated liver disease (ALD) (Momen-Heravi et al., 2015b). Previously, we showed that alcohol increases exosome production in human hepatocytes (Momen-Heravi et al., 2015a), in alcoholic hepatitis patients (Momen-Heravi et al., 2015b) and in mouse models of ALD (Momen-Heravi et al., 2015a; Momen-Heravi et al., 2015b). In this study, we investigated the effect of alcohol on genes involved in the formation of exosomes (biogenesis, transport and fusion to the plasma membrane). Here, we report three major findings, first, alcohol induces the transcription of various Rabs, and v- and t- SNAREs in human hepatocytes and in ALD patients. Second, alcohol downregulates miR-192 and promotes exosome secretion. Third, miR-192 regulates exosome secretion in human hepatocytes *via* targeting Rab27a, Rab35 and syntaxins. To our best knowledge this is the first study demonstrating the effect of alcohol on exosome biogenesis and secretory pathways directly and partly *via* miR-192 and a link between miR-192 and exosome secretion. These findings are illustrated in **Figure 5**.

Syntenin, a syndecan binding protein, plays various roles in exosome biogenesis (Ghossoub et al., 2014; Hessvik and Llorente, 2018; Kashyap et al., 2021). It stimulates exosome production *via* its interaction with syndecan-ALIX-ARF6 complex and other factors (Ghossoub et al., 2014). A recent study signifies that syntenin not only involves in the endosomal budding of cargo (biogenesis) and exosome production, but also regulates the uptake of exosomes (Kashyap et al., 2021). Our results suggest an induction in syntenin in alcohol treated hepatocytes suggesting a potential role of syntenin in exosome production in ALD, this observation deserves further investigation.

Rab GTPases (Rab proteins) are well recognized for their role in vesicular trafficking and exosome formation (Blanc and Vidal, 2018). These proteins regulate a distinct intracellular transport step and are found in exosomes (Blanc and Vidal, 2018). Various Rabs such as Rab11, Rab27 and Rab35 are shown to play essential direct role/s in exosome biogenesis and secretion (Ostrowski et al., 2010; Ramel et al., 2013). Rab11 regulates transferrin receptor secretion *via* the exosome pathway (Ramel et al., 2013) whereas Rab35 promotes exosome release by interacting with its effector protein (Hsu et al., 2010). Rab27 is involved in MVE docking to the plasma membrane (Ostrowski et al., 2010). Both isoforms of Rab27, Rab27a and Rab27b are shown to play a common and different role in exosome secretion by promoting the targeting of MVEs to the cell periphery and docking to the plasma membrane (Ostrowski et al., 2010). We previously showed increase in Rab27b after alcohol treatment (Momen-Heravi et al., 2015a), and in this study, we found Rab27a, and not Rab27b, is a miR-192 predicted target gene. Therefore, we focused on Rab27a.

Other Rabs (Rab1, 5,6 and 10) that we found upregulated after alcohol treatment, have been indicated to play various roles in vesicular transport. Rab1 is known to mediate dynamic membrane trafficking between endoplasmic reticulum and Golgi (Yang et al., 2016) and Rab5 has been proposed to be a master regulator of endosome biogenesis and trafficking (Nagano et al., 2019). Rab6 is a Golgi associated Rab that modulates the constitutive secretory pathway (Patwardhan et al., 2017). Rab10 is present in endoplasmic reticulum and common endosomes, and it was reported to mediate transport from basolateral sorting endosomes to common endosomes (Babbey et al., 2006). Consistent with their role in exosome secretion, we found increase in these Rabs within alcohol treated hepatocytes. Considering the roles of these Rabs in vesicular transport, it is likely that alcohol in general modulates the vesicle trafficking between organelles.

SNARE family proteins play critical roles in all fusion reactions of the secretory pathway and are classified either as vesicular (v-SNARE) and target (t-SNARE) membrane based on their primary subcellular localization (Jahn and Scheller, 2006). VAMPs belong to v-SNARE proteins where as syntaxins belong to t-SNARE proteins, and both are involved in various stages of membrane fusion pathway (Jahn and Scheller, 2006). Our results indicated that alcohol upregulates the expression of VAMP3, VAMP5 and VAMP7 and synatxin16 in hepatocytes and increased levels of these SNAREs were also found in ALD patients. VAMP3, VAMP7 and syntaxin16 were shown to mediate fusion between MVBs with autophagosomes and autolysosome formation (Miller and Shindell, 1998; Tang, 2019), and we recently described a link between miR-155 and lysosome dysfunction and exosome production (Babuta et al., 2019). VAMP7 was also demonstrated to participate in the fusion between MVBs with the plasma membrane to release exosomes (Fader et al., 2009). It is important to note that these proteins (Rabs, syntenin, and SNAREs) are not only involve in the exosome trafficking but also in the transport of other vesicles and in other processes, suggesting that alcohol overall affects the vesicle trafficking and, thereby, has a vast impact on cellular homeostasis.

miR-192 regulates various processes like oxidative stress, cellular proliferation, and inflammatory responses (Fuschi et al., 2017; Ren et al., 2021). miR-192 is the second most expressed miRNA in hepatocytes and is shown to play diverse roles in liver diseases including Non-alcoholic fatty liver disease (NAFLD), drug-induced liver injury and hepatocellular carcinoma (Ren et al., 2021). In a rat model of NAFLD, a decrease in hepatic miR-192 expression has been reported and is shown to involve in the regulation of lipid metabolism and inflammation (Liu et al., 2017). In the present study, we report that alcohol downregulates miR-192 and miR-122 expression in hepatocytes *via* affecting its transcription. Though we found decrease in pri-miRs at 6 and 18 h of alcohol treatment, the mature miRs remained decreased even 48 h after alcohol treatment suggesting alcohol affects other factors that modulate miRs expression at the post-transcriptional level. For instance, mature miR-192 expression is shown to be regulated (inhibited) at the post-transcriptional level by various factors such as p53, TGFβ etc. (Ren et al., 2021) and increase in p53 and TGFβ was reported in alcohol-associated liver disease (Zhou et al., 2019). Since miR-122 locus is under circadian control, it was shown that levels of pri and pre-miR-122 oscillates during the day whereas mature miR-122 remains constant due to its high stability (Gatfield et al., 2009).

While we found decrease in mature miRs in hepatocytes, an induction in these miRs was observed 18 h after alcohol treatment in the cell-free supernatant. Previously, we found that alcohol causes increase in miR-192 and miR-122 levels into exosomes and is an active process (Momen-Heravi et al., 2015a). So, it is likely that majority of miR-192 and miR-122 in the supernatant are associated with exosomes. There are several factors such as RNA binding proteins (Ago2, hnRNPs and others), cellular stress, membrane proteins (such as neural sphingomyelinase 2) and the miRNA induced silencing complex (miRISC)-related pathway that affect the sorting of miRNA/cargoes into exosomes (Zhang et al., 2015; Fabbiano et al., 2020; Groot and Lee, 2020; Babuta and Szabo, 2021). The main components of miRISC include miRNA, miRNA-repressible mRNA, GW182, and Ago2 (Zhang et al., 2015; Babuta and Szabo, 2021), and we previously demonstrated that alcohol induces the expression of GW182 (Bukong et al., 2013). It is possible that alcohol is modulating the expression of these proteins to induce miRs sorting into exosomes. This observation needs to be investigated further.

While we found a similar expression change for both miR-192 and miR-122, miR-192 was selected for mechanistic studies because it exhibits binding sites for several genes in the exosome biogenesis pathway. Our bioinformatic target scan analysis revealed that Rab27a, Rab35, STX7 and STX16 are the predicted miR-192 genes (www.microrna.org) and our mechanistic studies provided the evidence that miR-192 regulates these genes and modulates the exosome secretion in hepatocytes. Various studies have described the enrichment of exosomes with cholesterol, sphingomyelin, and ceramide etc. and suggested that exosome composition resembles that of plasma membrane rafts (Egea-Jimenez and Zimmermann, 2020). Since miR-192 is shown to regulate lipid metabolism (Liu et al., 2017), therefore, it is possible that it has a larger role in exosome secretion. It is highly likely that miR-192 regulates exosome secretion *via* having its effect on multiple genes involved in the biogenesis and secretory pathways and lipid metabolism. Further studies will aid in deciphering the precise role of miR-192 in exosome secretion. Increased miR-192 levels have been reported in biofluids and exosomal miR-192 is suggested as a potential biomarker of the disease progression (Ren et al., 2021). Previously, we demonstrated increase in exosomal miR-192 in alcoholic patients and in a mouse model of ALD (Momen-Heravi et al., 2015b). In the present study, we showed increased levels of miR-192 in the supernatant of alcohol treated hepatocytes. Since miR-192 is enriched in hepatocytes it is likely that hepatocytes are the source of alcohol-induced increase in miR-192 in the exosomes. Hepatocytes are major type of hepatic cells, occupy about 80% of the total liver volume and is shown to communicate with other hepatocytes and other liver cells *via* exosomes (Sung et al., 2018). Exosomes from palmitic acid-treated hepatocytes

resulted in the induction of hepatic stellate cell (HSC) activation and further analysis revealed that exosomal miR-192 caused increase in the expression of profibrotic gene markers in HSC (Lee et al., 2017). We previously showed that exosomes isolated from alcohol treated hepatocyte can reprogram monocytes *via* miR-122, inducing sensitization to LPS and increased levels of pro-inflammatory cytokines (Momen-Heravi et al., 2015a). The stem cell-derived exosomes have been shown to promote angiogenesis both *in vitro* and *in vivo* experimental conditions and demonstrates beneficial effects on ischemic diseases (Babaei and Rezaie, 2021).

In conclusion, our study reveals that alcohol promotes exosome secretion *via* affecting genes involved in exosome biogenesis, transport, and secretion. Further, our results suggest that miR-192 as one of the regulators of exosome secretion in alcohol-induced cellular stress.

DATA AVAILABILITY STATEMENT

The raw data supporting the conclusions of this article will be made available by the authors, without undue reservation.

ETHICS STATEMENT

The studies involving human participants were reviewed and approved by The BIDMC Institutional Review Board for Protection of Human Subjects in Research. Human hepatocytes and human liver samples from control subjects, and patients with alcohol-associated liver disease (n = 8–10) were obtained from the National Institutes of Health Liver Tissue Cell Distribution System (Minneapolis, MN). The patients/participants provided their written informed consent to participate in this study.

AUTHOR CONTRIBUTIONS

SB: Conceptualization, Methodology, Investigation, Validation, Formal Analysis, Visualization, Writing. MB: Conceptualization, Methodology, Investigation, Validation, Formal Analysis, Visualization, Writing. DC: Investigation, Validation, Visualization. AS: Investigation, Validation, Visualization. GS: Conceptualization, Resources, Funding Acquisition, Writing-Review and Editing, Supervision.

FUNDING

Research reported in this publication was supported by National Institute on Alcohol Abuse and Alcoholism of the National Institutes of Health under award number R01AA0207440 to GS.

ACKNOWLEDGMENTS

The authors thank Jeeval Mehta and late Karen Kodys for their assistance.

REFERENCES

Amessou, M., Fradagrada, A., Falguières, T., Lord, J. M., Smith, D. C., Roberts, L. M., et al. (2007). Syntaxin 16 and Syntaxin 5 Are Required for Efficient Retrograde Transport of Several Exogenous and Endogenous Cargo Proteins. *J. Cel Sci* 120 (Pt 8), 1457–1468. doi:10.1242/jcs.03436

Babaei, M., and Rezaie, J. (2021). Application of Stem Cell-Derived Exosomes in Ischemic Diseases: Opportunity and Limitations. *J. Transl Med.* 19 (1), 196. doi:10.1186/s12967-021-02863-w

Babbey, C. M., Ahktar, N., Wang, E., Chen, C. C.-H., Grant, B. D., and Dunn, K. W. (2006). Rab10 Regulates Membrane Transport through Early Endosomes of Polarized Madin-Darby Canine Kidney Cells. *MBoC* 17 (7), 3156–3175. doi:10.1091/mbc.e05-08-0799

Babuta, M., Furi, I., Bala, S., Bukong, T. N., Lowe, P., Catalano, D., et al. (2019). Dysregulated Autophagy and Lysosome Function Are Linked to Exosome Production by Micro-RNA 155 in Alcoholic Liver Disease. *Hepatology* 70 (6), 2123–2141. doi:10.1002/hep.30766

Babuta, M., and Szabo, G. (2021). Extracellular Vesicles in Inflammation: Focus on the microRNA Cargo of EVs in Modulation of Liver Diseases. *J. Leukoc. Biol.* doi:10.1002/JLB.3MIR0321-156R

Baietti, M. F., Zhang, Z., Mortier, E., Melchior, A., Degeest, G., Geeraerts, A., et al. (2012). Syndecan-syntenin-ALIX Regulates the Biogenesis of Exosomes. *Nat. Cel Biol* 14 (7), 677–685. doi:10.1038/ncb2502

Bala, S., Csak, T., Momen-Heravi, F., Lippai, D., Kodys, K., Catalano, D., et al. (2015). Biodistribution and Function of Extracellular miRNA-155 in Mice. *Sci. Rep.* 5, 10721. doi:10.1038/srep10721

Bala, S., Csak, T., Saha, B., Zatsiorsky, J., Kodys, K., Catalano, D., et al. (2016). The Pro-inflammatory Effects of miR-155 Promote Liver Fibrosis and Alcohol-Induced Steatohepatitis. *J. Hepatol.* 64 (6), 1378–1387. doi:10.1016/j.jhep.2016.01.035

Bala, S., Petrasek, J., Mundkur, S., Catalano, D., Levin, I., Ward, J., et al. (2012). Circulating microRNAs in Exosomes Indicate Hepatocyte Injury and Inflammation in Alcoholic, Drug-Induced, and Inflammatory Liver Diseases. *Hepatology* 56 (5), 1946–1957. doi:10.1002/hep.25873

Bala, S., and Szabo, G. (2012). MicroRNA Signature in Alcoholic Liver Disease. *Int. J. Hepatol.* 2012, 1–6. doi:10.1155/2012/498232

Blanc, L., and Vidal, M. (2018). New Insights into the Function of Rab GTPases in the Context of Exosomal Secretion. *Small GTPases* 9 (1-2), 95–106. doi:10.1080/21541248.2016.1264352

Bukong, T. N., Hou, W., Kodys, K., and Szabo, G. (2013). Ethanol Facilitates Hepatitis C Virus Replication via Up-Regulation of GW182 and Heat Shock Protein 90 in Human Hepatoma Cells. *Hepatology* 57 (1), 70–80. doi:10.1002/hep.26010

Chen, H.-J., Anagnostou, G., Chai, A., Withers, J., Morris, A., Adhikaree, J., et al. (2010). Characterization of the Properties of a Novel Mutation in VAPB in Familial Amyotrophic Lateral Sclerosis. *J. Biol. Chem.* 285 (51), 40266–40281. doi:10.1074/jbc.M110.161398

Crabb, D. W., Bataller, R., Chalasani, N. P., Kamath, P. S., Lucey, M., Mathurin, P., et al. (2016). Standard Definitions and Common Data Elements for Clinical Trials in Patients with Alcoholic Hepatitis: Recommendation from the NIAAA Alcoholic Hepatitis Consortia. *Gastroenterology* 150 (4), 785–790. doi:10.1053/j.gastro.2016.02.042

Csak, T., Bala, S., Lippai, D., Satishchandran, A., Catalano, D., Kodys, K., et al. (2015). microRNA-122 Regulates Hypoxia-Inducible Factor-1 and Vimentin in Hepatocytes and Correlates with Fibrosis in Diet-Induced Steatohepatitis. *Liver Int.* 35 (2), 532–541. doi:10.1111/liv.12633

Egea-Jimenez, A. L., and Zimmermann, P. (2019). Lipids in Exosome Biology. *Handb Exp. Pharmacol.* 259, 309–336. doi:10.1007/164_2019_220

Fabbiano, F., Corsi, J., Gurrieri, E., Trevisan, C., Notarangelo, M., and D'Agostino, V. G. (2020). RNA Packaging into Extracellular Vesicles: An Orchestra of

RNA-binding Proteins? *J. Extracellular Vesicles* 10 (2), e12043. doi:10.1002/jev2.12043

Fader, C. M., Sánchez, D. G., Mestre, M. B., and Colombo, M. I. (2009). TI-VAMP/VAMP7 and VAMP3/cellubrevin: Two V-SNARE Proteins Involved in Specific Steps of the Autophagy/multivesicular Body Pathways. *Biochim. Biophys. Acta (Bba) - Mol. Cel Res.* 1793 (12), 1901–1916. doi:10.1016/j.bbamcr.2009.09.011

Fuschi, P., Carrara, M., Voellenkle, C., Garcia-Manteiga, J. M., Righini, P., Maimone, B., et al. (2017). Central Role of the P53 Pathway in the Noncoding-RNA Response to Oxidative Stress. *Aging* 9 (12), 2559–2586. doi:10.18632/aging.101341

Gatfield, D., Le Martelot, G., Vejnar, C. E., Gerlach, D., Schaad, O., Fleury-Olela, F., et al. (2009). Integration of microRNA miR-122 in Hepatic Circadian Gene Expression. *Genes Dev.* 23 (11), 1313–1326. doi:10.1101/gad.1781009

Ghossoub, R., Lembo, F., Rubio, A., Gaillard, C. B., Bouchet, J., Vitale, N., et al. (2014). Syntenin-ALIX Exosome Biogenesis and Budding into Multivesicular Bodies Are Controlled by ARF6 and PLD2. *Nat. Commun.* 5, 3477. doi:10.1038/ncomms4477

Groot, M., and Lee, H. (2020). Sorting Mechanisms for MicroRNAs into Extracellular Vesicles and Their Associated Diseases. *Cells* 9 (4), 1044. doi:10.3390/cells9041044

Hessvik, N. P., and Llorente, A. (2018). Current Knowledge on Exosome Biogenesis and Release. *Cell. Mol. Life Sci.* 75 (2), 193–208. doi:10.1007/s00018-017-2595-9

Hsu, C., Morohashi, Y., Yoshimura, S.-i., Manrique-Hoyos, N., Jung, S., Lauterbach, M. A., et al. (2010). Regulation of Exosome Secretion by Rab35 and its GTPase-Activating Proteins TBC1D10A-C. *J. Cel Biol* 189 (2), 223–232. doi:10.1083/jcb.200911018

Jahn, R., and Scheller, R. H. (2006). SNAREs - Engines for Membrane Fusion. *Nat. Rev. Mol. Cel Biol* 7 (9), 631–643. doi:10.1038/nrm2002

Kashyap, R., Balzano, M., Lechat, B., Lambaerts, K., Egea-Jimenez, A. L., Lembo, F., et al. (2021). Syntenin-knock Out Reduces Exosome Turnover and Viral Transduction. *Sci. Rep.* 11 (1), 4083. doi:10.1038/s41598-021-81697-4

Lee, Y.-S., Kim, S. Y., Ko, E., Lee, J.-H., Yi, H.-S., Yoo, Y. J., et al. (2017). Exosomes Derived from Palmitic Acid-Treated Hepatocytes Induce Fibrotic Activation of Hepatic Stellate Cells. *Sci. Rep.* 7 (1), 3710. doi:10.1038/s41598-017-03389-2

Liu, X.-L., Cao, H.-X., Wang, B.-C., Xin, F.-Z., Zhang, R.-N., Zhou, D., et al. (2017). miR-192-5p Regulates Lipid Synthesis in Non-alcoholic Fatty Liver Disease through SCD-1. *Wjg* 23 (46), 8140–8151. doi:10.3748/wjg.v23.i46.8140

Miller, D., and Shindell, S. (1998). Narrowing the Evidence-Practice gap: Strengthening the Link between Research and Clinical Practice. *Neurology* 51 (4), 1–1234. doi:10.1212/wnl.51.4.1234

Momen-Heravi, F., Bala, S., Kodys, K., and Szabo, G. (2015a). Exosomes Derived from Alcohol-Treated Hepatocytes Horizontally Transfer Liver Specific miRNA-122 and Sensitize Monocytes to LPS. *Sci. Rep.* 5, 9991. doi:10.1038/srep09991

Momen-Heravi, F., Saha, B., Kodys, K., Catalano, D., Satishchandran, A., and Szabo, G. (2015b). Increased Number of Circulating Exosomes and Their microRNA Cargos Are Potential Novel Biomarkers in Alcoholic Hepatitis. *J. Transl Med.* 13, 261. doi:10.1186/s12967-015-0623-9

Mori, Y., Takenaka, K.-i., Fukazawa, Y., and Takamori, S. (2021). The Endosomal Q-SNARE, Syntaxin 7, Defines a Rapidly Replenishing Synaptic Vesicle Recycling Pool in Hippocampal Neurons. *Commun. Biol.* 4 (1), 981. doi:10.1038/s42003-021-02512-4

Nagano, M., Toshima, J. Y., Siekhaus, D. E., and Toshima, J. (2019). Rab5-mediated Endosome Formation Is Regulated at the Trans-golgi Network. *Commun. Biol.* 2, 419. doi:10.1038/s42003-019-0670-5

Osna, N. A., Donohue, T. M., Jr., and Kharbanda, K. K. (2017). Alcoholic Liver Disease: Pathogenesis and Current Management. *Alcohol. Res.* 38 (2), 147–161.

Ostrowski, M., Carmo, N. B., Krumeich, S., Fanget, I., Raposo, G., Savina, A., et al. (2010). Rab27a and Rab27b Control Different Steps of the Exosome Secretion Pathway. *Nat. Cel Biol* 12 (1), 19–30. doi:10.1038/ncb2000

Patwardhan, A., Bardin, S., Miserey-Lenkei, S., Larue, L., Goud, B., Raposo, G., et al. (2017). Routing of the RAB6 Secretory Pathway towards the Lysosome Related Organelle of Melanocytes. *Nat. Commun.* 8, 15835. doi:10.1038/ncomms15835

Ramel, D., Wang, X., Laflamme, C., Montell, D. J., and Emery, G. (2013). Rab11 Regulates Cell-Cell Communication during Collective Cell Movements. *Nat. Cel Biol* 15 (3), 317–324. doi:10.1038/ncb2681

Ren, F.-j., Yao, Y., Cai, X.-y., and Fang, G.-y. (2021). Emerging Role of MiR-192-5p in Human Diseases. *Front. Pharmacol.* 12, 614068. doi:10.3389/fphar.2021.614068

Satishchandran, A., Ambade, A., Rao, S., Hsueh, Y.-C., Iracheta-Vellve, A., Tornai, D., et al. (2018). MicroRNA 122, Regulated by GRLH2, Protects Livers of Mice and Patients from Ethanol-Induced Liver Disease. *Gastroenterology* 154 (1), 238–252. doi:10.1053/j.gastro.2017.09.022

Savina, A., Vidal, M., and Colombo, M. I. (2002). The Exosome Pathway in K562 Cells Is Regulated by Rab11. *J. Cel Sci* 115 (Pt 12), 2505–2515. doi:10.1242/jcs.115.12.2505

Sung, S., Kim, J., and Jung, Y. (2018). Liver-Derived Exosomes and Their Implications in Liver Pathobiology. *Ijms* 19 (12), 3715. doi:10.3390/ijms19123715

Szabo, G., and Bala, S. (2013). MicroRNAs in Liver Disease. *Nat. Rev. Gastroenterol. Hepatol.* 10 (9), 542–552. doi:10.1038/nrgastro.2013.87

Szabo, G., and Momen-Heravi, F. (2017). Extracellular Vesicles in Liver Disease and Potential as Biomarkers and Therapeutic Targets. *Nat. Rev. Gastroenterol. Hepatol.* 14 (8), 455–466. doi:10.1038/nrgastro.2017.71

Tang, B. L. (2019). Syntaxin 16's Newly Deciphered Roles in Autophagy. *Cells* 8 (12), 1655. doi:10.3390/cells8121655

Théry, C., Witwer, K. W., Aikawa, E., Alcaraz, M. J., Anderson, J. D., Andriantsitohaina, R., et al. (2018). Minimal Information for Studies of Extracellular Vesicles 2018 (MISEV2018): a Position Statement of the International Society for Extracellular Vesicles and Update of the MISEV2014 Guidelines. *J. Extracell Vesicles* 7 (1), 1535750. doi:10.1080/20013078.2018.1535750

Trams, E. G., Lauter, C. J., Norman Salem, J., Jr., and Heine, U. (1981). Exfoliation of Membrane Ecto-Enzymes in the Form of Micro-vesicles. *Biochim. Biophys. Acta (Bba) - Biomembranes* 645 (1), 63–70. doi:10.1016/0005-2736(81)90512-5

Tschuschke, M., Kocherova, I., Bryja, A., Mozdziak, P., Angelova Volponi, A., Janowicz, K., et al. (2020). Inclusion Biogenesis, Methods of Isolation and Clinical Application of Human Cellular Exosomes. *Jcm* 9 (2), 436. doi:10.3390/jcm9020436

Valadi, H., Ekström, K., Bossios, A., Sjöstrand, M., Lee, J. J., and Lötvall, J. O. (2007). Exosome-mediated Transfer of mRNAs and microRNAs Is a Novel Mechanism of Genetic Exchange between Cells. *Nat. Cel Biol* 9 (6), 654–659. doi:10.1038/ncb1596

Yang, X.-Z., Li, X.-X., Zhang, Y.-J., Rodriguez-Rodriguez, L., Xiang, M.-Q., Wang, H.-Y., et al. (2016). Rab1 in Cell Signaling, Cancer and Other Diseases. *Oncogene* 35 (44), 5699–5704. doi:10.1038/onc.2016.81

Zhang, J., Li, S., Li, L., Li, M., Guo, C., Yao, J., et al. (2015). Exosome and Exosomal microRNA: Trafficking, Sorting, and Function. *Genomics, Proteomics & Bioinformatics* 13 (1), 17–24. doi:10.1016/j.gpb.2015.02.001

Zhou, H., Zhu, P., Wang, J., Toan, S., and Ren, J. (2019). DNA-PKcs Promotes Alcohol-Related Liver Disease by Activating Drp1-Related Mitochondrial Fission and Repressing FUNDC1-Required Mitophagy. *Sig Transduct Target. Ther.* 4, 56. doi:10.1038/s41392-019-0094-1

Conflict of Interest: GS reports being a paid consult for Allergan, Alnylam, Arrow, Durect Corporation, Generon/Evive, Glympse Bio, Terra Firma, Quest Diagnostics, Pandion Therapeutics, Surrozen, Novartis, Merck, Pfizer and Zomagen. GS has received grants from Gilead, Genfit, Intercept, Novartis, SignaBlok, and Shire; she also holds intellectual property rights with Up to Date.

The remaining authors declare that the research was conducted in the absence of any commercial or financial relationships that could be construed as a potential conflict of interest.

Publisher's Note: All claims expressed in this article are solely those of the authors and do not necessarily represent those of their affiliated organizations, or those of the publisher, the editors and the reviewers. Any product that may be evaluated in this article, or claim that may be made by its manufacturer, is not guaranteed or endorsed by the publisher.

frontiers | Frontiers in Cell and Developmental Biology

METHODS
published: 16 May 2022
doi: 10.3389/fcell.2022.812244

Validation of Effective Extracellular Vesicles Isolation Methods Adapted to Field Studies in Malaria Endemic Regions

*Matteo Zoia[1,2], Bibin Yesodha Subramanian[1], Klara Kristin Eriksson[1], Meera Sruthi Ravi[1], Shekoofeh Yaghmaei[1], Isabelle Fellay[1], Brigitte Scolari[1], Michael Walch[1] and Pierre-Yves Mantel[1]**

[1]Faculty of Science and Medicine, Department of Oncology, Microbiology and Immunology, Anatomy Unit, University of Fribourg, Fribourg, Switzerland, [2]Department for BioMedical Research (DBMR), University of Bern, Bern, Switzerland

Malaria affects the poorer regions of the world and is of tremendous health and economic burden for developing countries. Extracellular vesicles (EVs) are small vesicles released by almost any cells in the human body, including malaria infected red blood cells. Recent evidence shows that EVs might contribute to the pathogenesis of malaria. In addition, EVs hold considerable value in biomarker discovery. However, there are still significant gaps in our understanding of EV biology. So far most of our knowledge about EVs in malaria comes from *in vitro* work. More field studies are required to gain insight into their contribution to the disease and pathogenesis under physiological conditions. However, to perform research on EVs in low-income regions might be challenging due to the lack of appropriate equipment to isolate EVs. Therefore, there is a need to develop and validate EV extraction protocols applicable to poorly equipped laboratories. We established and validated two protocols for EV isolation from cell culture supernatants, rodent and human plasma. We compared polyethylene glycol (PEG) and salting out (SA) with sodium acetate for precipitation of EVs. We then characterized the EVs by Transmission Electron Microscopy (TEM), Western Blot, Size-exclusion chromatography (SEC), bead-based flow cytometry and protein quantification. Both protocols resulted in efficient purification of EVs without the need of expensive material or ultracentrifugation. Furthermore, the procedure is easily scalable to work with large and small sample volumes. Here, we propose that both of our approaches can be used in resource limited countries, therefore further helping to close the gap in knowledge of EVs during malaria.

Keywords: malaria, Plasmodium falciparum, extracellular vesicles, microvesicles, salting-out, polyethylene glycol precipitation

OPEN ACCESS

Edited by:
Jeffrey David Galley, The Ohio State University, United States

Reviewed by:
Dwijendra K. Gupta, Jai Prakash Vishwavidyalaya, India
Muhammad Nawaz, University of Gothenburg, Sweden

****Correspondence:***
Pierre-Yves Mantel
pierre-yves.mantel@unifr.ch

Specialty section:
This article was submitted to Molecular and Cellular Pathology, a section of the journal Frontiers in Cell and Developmental Biology

Received: *09 November 2021*
Accepted: *13 April 2022*
Published: *16 May 2022*

Citation:
Zoia M, Yesodha Subramanian B, Eriksson KK, Ravi MS, Yaghmaei S, Fellay I, Scolari B, Walch M and Mantel P-Y (2022) Validation of Effective Extracellular Vesicles Isolation Methods Adapted to Field Studies in Malaria Endemic Regions. Front. Cell Dev. Biol. 10:812244. doi: 10.3389/fcell.2022.812244

INTRODUCTION

Malaria remains one of the greatest life-threatening diseases worldwide. It is caused by several Plasmodium species of parasites that are introduced into the bloodstream *via* mosquito bites. Mostly at risk are populations in tropical and subtropical areas of over 100 countries (WHO, 2020). The severe disease develops during the blood stage, when the parasite replicates inside red blood cells

(RBCs). Several factors derived from both the parasites and host determine the severity and outcome of the disease (Miller et al., 2002; Schofield and Grau, 2005; Coban et al., 2018). Recently, extracellular vesicles (EVs) have been described to contribute to the pathological processes during malaria infection, and in particular during cerebral malaria and severe anemia (Combes et al., 2005; Coltel et al., 2006). The earliest reports focused on the EVs released by endothelial cells, lymphocytes and platelets (Combes et al., 2004). In fact, endothelial cell derived EVs were elevated in a population of children infected with *P. falciparum*, the highest level was observed at admission in the group of children suffering from cerebral malaria (Combes et al., 2004). In addition to the EVs derived from host, more recent evidence suggests that EVs secreted by Plasmodium infected red blood cells (iRBCs) might contribute to the development of the disease as well (Antwi-Baffour et al., 2020). EVs are an heterogenous collections of vesicles characterized by differences in sizes and biogenesis pathways (Valadi et al., 2007; Babatunde et al., 2018; Théry et al., 2018). EVs are involved in many biological processes, including cellular differentiation and immune regulation. Despite the differences between each biogenesis pathway, a shared characteristic of all EVs released is that their membrane composition reflects their cellular origin. Since EVs contain molecules derived from their mother cells, they constitute a promising source of biomarkers readily available in biofluids.

In malaria, iRBC derived EVs were shown to mediate the transfer of DNA between parasites and to promote the differentiation from the asexual parasites towards gametocytes, to initiate the transmission stage from the human to the mosquito host (Mantel et al., 2013; Regev-Rudzki et al., 2013; Sampaio et al., 2017). Therefore, it seems that the parasites have developed strategies to synchronize and coordinate their behavior during infection. In addition, to their role in parasite-parasite communication, EVs have potent immunoregulatory properties. For instance, EVs can stimulate monocytes and macrophages to secrete proinflammatory cytokines and chemokines (Couper et al., 2010; Sisquella et al., 2017; Mbagwu et al., 2019; Ofir-Birin et al., 2021). EVs secreted by mast cells worsen the development of cerebral malaria in the rodent malaria (Huang et al., 2021). EVs produced during *P. vivax* infections are taken up by human spleen fibroblast, in which they induced the expression of ICAM-1 to potentiate parasite sequestration (Toda et al., 2020). Furthermore EVs might be involved in drug resistance development against some antimalaria drugs (Tandoh et al., 2021). Beside their role in the development of the disease EVs might be used as vaccine to prevent the development of severe malaria (Martin-Jaular et al., 2011) and can be used a drug delivery tools against parasitic disease (Borgheti-Cardoso et al., 2020). It has been reported that during malaria infection by *P. falciparum* or *P. vivax*, the concentration of EVs increases in the blood of malaria patients (Campos et al., 2010; Pankoui Mfonkeu et al., 2010; Antwi-Baffour et al., 2020). Interestingly EVs might be used as biomarkers to detect liver infections in patients infected with *P. vivax* (Gualdrón-López et al., 2018). Although evidence of a prominent role of EVs during malaria is growing, a complete understanding of their physiological function and relevance is still lacking. In fact, most of the knowledge is coming from *in vitro* experiments, more *in vivo* data and field trials are required to fully understand EVs biology and contribution to the pathogenesis of malaria. Despite progresses in EV research, it remains a challenge to purify biologically intact EVs from biofluid samples of limited volumes (Babatunde et al., 2020).

Differential centrifugation remains the gold standard approach to enrich and purify EVs (Momen-Heravi et al., 2013). The separation relies on the differences in the sedimentation speed between EVs and other particles. The first centrifugation steps are meant to remove cellular debris and impurities. Finally, EVs are collected by ultracentrifugation at 100′000 g, followed in some protocols by density gradient, resulting in enhanced sample purity. In fact, iso-osmotic gradients such as sucrose allow to separate vesicles based on their buoyant density, therefore eliminating proteo-lipid complexes (Théry et al., 2006). Size-exclusion chromatography allows to separate molecules varying in their hydrodynamic radius by passing them through a column containing a porous gel. While small molecules are retained in the pores, the larger molecules such as EVs migrate faster through the matrix and are eluted first (Takov et al., 2019). Affinity immunocapturing is an interesting alternative, it is based on the presence of known, specific markers on the surface of the EVs. Therefore, antibodies can be used to target and bind those receptors. Antibodies can be coupled to magnetic beads to allow the EV capture by using a magnet. Therefore, affinity immunocapturing outer perform other methods in terms of specificity as most contaminants are removed (Nakai et al., 2016). However, the relatively low expression of the receptor on the EVs may also reduce the isolation yield.

In addition, several commercial kits are available, however their high cost limits the usage for large volumes of cell culture supernatants or large number of clinical samples, particularly in resource limited regions. Thus, a simple, inexpensive and rapid EV isolation method that can process cell culture media or diverse biofluids is an essential but unmet need in many research and clinical settings.

Recently, simpler and cheaper approaches such as polyethylene glycol (PEG) precipitation and salting out have been described. Here, we analyzed the suitability of those two methods to extract RBC derived EVs derived from *in vitro* and *in vivo* samples. We first demonstrate that PEG or salting out based precipitation can efficiently isolate intact RBC EVs from cell culture media. We then show that we can purify EVs from mouse and human plasma. In conclusion, both approaches efficiently purified EVs. Our platform has a broad application to the processing of EVs in malaria research.

RESULTS

Overall Strategy to Compare Side By Side Extraction of EVs

In order to optimize our RBC EV purification protocol, we compared 2 different approaches based on PEG precipitation and salting-out with a sodium acetate solution. The **Figure 1** illustrates the strategy that we used to compare the efficiency of

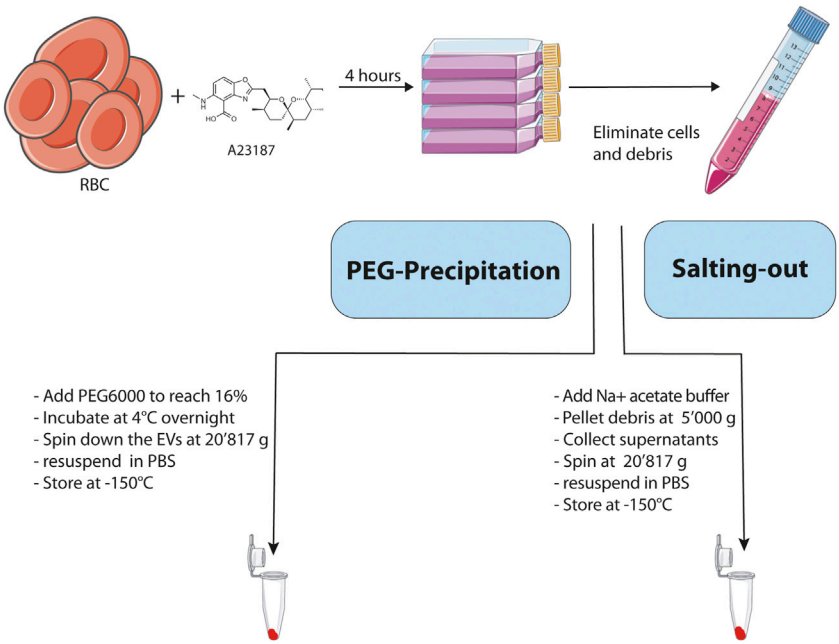

FIGURE 1 | Schematic representation and description of the main steps involved in the 2 methodologies used for the isolation of EVs. Created with BioRender.com.

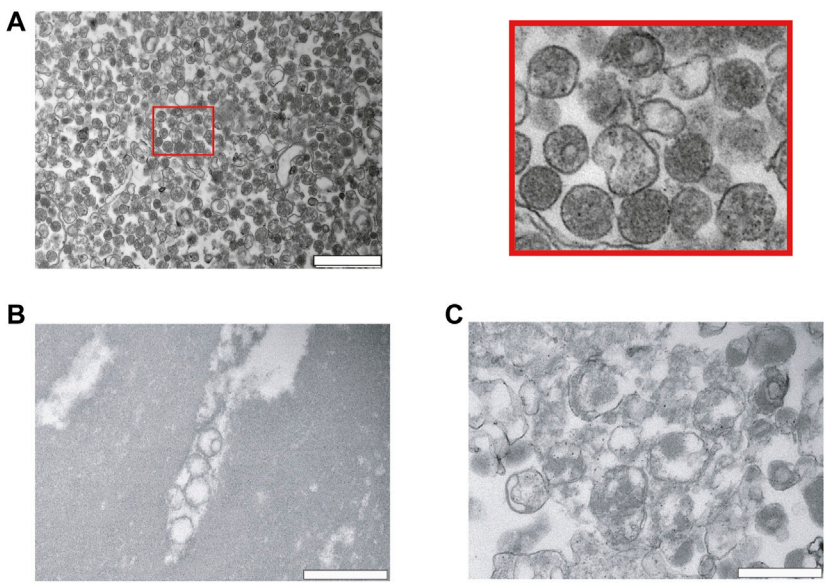

FIGURE 2 | Characterization of red blood cell derived EVs isolated by PEG precipitation. **(A)** Transmission electron microscopy (TEM) visualization of RBC derived EVs isolated from A23487 treated RBCs by PEG precipitation and collected by centrifugation at 20'817 g. Representative TEM image shows individual EVs and a few clumps of varying sizes and intact lipid bilayers. The image on the right is a zoom in of the first panel. The scale bar is 1 μm. **(B)**, **(C)** Analysis of hypo-osmotic lysed RBCs by TEM. The cellular debris were pelleted by centrifugation and the pellet was resuspended in PBS for visualization by TEM. The scale bar is 1 μm.

the two methods for enrichment of EVs derived from RBCs. First, we generated EVs *ex vivo* by incubating during 4 h freshly isolated human RBCs with a calcium ionophore (A23187, 5 μM) in HBSS buffer containing Ca^{2+} and Mg^{2+} at a hematocrit of 25%. The calcium ionophores are known to induce the release of vesicles by RBCs (Allan et al., 1976; Allan et al., 1980). After removing cells and cellular debris by differential centrifugation, the EVs were enriched from the resulting supernatants by using either a PEG solution or salting-out by sodium acetate buffer. Once the EVs were purified, we analyzed their purity and integrity by Transmission Electron Microscopy (TEM), western blot and Size-exclusion Chromatography.

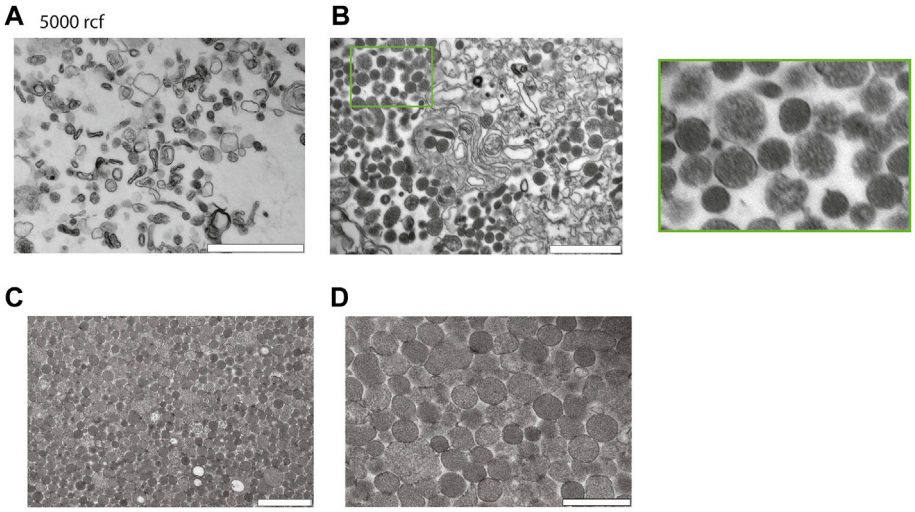

FIGURE 3 | Characterization of red blood cell derived EVs isolated by salting out precipitation. **(A)** Healthy Human RBCs EVs extracted *via* Salting-out precipitation and pelleted at 5′000 g. The images were taken at 24′ × 500 magnification by TEM. Scale bar = 1 µm. **(B)** Healthy Human RBCs EVs extracted via Salting-out precipitation at 20′817 g, imaging has been taken at × 24500 magnification by TEM. Scale bar = 1 µm. **(C)** EVs were precipitated by Salting out and debris were pelleted at 5′000 g, the EVs were then collected by centrifugation at 20′817 g from the resulting supernatant. Scale bar = 1 µm. **(D)** Scale bar = 500 nm.

Polyethylene Glycol Treatment Results in the Enrichment of Cell Culture TEM Imaging of Healthy Human RBC EVs Extracted By PEG Precipitation

To demonstrate that PEG can be used to precipitate RBC EVs, we added PEG solutions to the A23187 induced EVs. First, the cells were pelleted at 500 g, and debris at 10′000 g the resulting supernatants were collected and a 50% PEG solution was added to reach a final concentration of 16% PEG6000. The samples were mixed thoroughly by inversion and incubated at 4°C overnight. On the next day, samples were centrifuged for 1 h at 20′817 g. The resulting pellets were resuspended in PBS and stored at −150°C.

Next, we analyzed our EV preparations by TEM, and found that PEG very efficiently precipitates and enriches for vesicles (**Figure 2A**). The size was relatively homogenous and varied between 100–300 nm. As expected, the vesicles have a rounded shape and are surrounded by a membrane. Most of the vesicles appeared intact and to contain hemoglobin (**Figure 2A**). As a comparison, we investigated lysed RBCs by osmotic pressure using a hypo-osmotic solution of salt. The RBCs lysed and released hemoglobin into the supernatant. The cellular debris were pelleted and analyzed by TEM. On the TEM images, RBC ghosts can be clearly noticed as demonstrated by large patches of membranes without a lumen. Although small vesicles are observed as well, most of them were larger in size, and they are not homogeneous in shape (**Figures 2B,C**).

TEM Imaging of Healthy Human RBC EVs Extracted With Salting Out

Next to investigate the potential of enriching EVs with salting out by sodium acetate. Intact cells and cellular debris were removed by centrifugation at 500 g and 10′000 g, respectively, and supernatants were retrieved. The cleared supernatants were then mixed with 1/10th volume of sodium acetate at a pH -4.5. The suspension immediately becomes turbid and was left on ice for 1 h with a final incubation at 37°C for 5 min. The turbid solution was centrifugated at 5′000 g and we analyzed the pellet after resuspension in PBS by TEM. The TEM revealed that salting out can precipitate vesicles as observed in **Figure 3A**, however after the spin at the 5′000 g, the pellet still contained a large number of cellular debris characterized by larger particles with irregular shapes. Next, to increase the collection of EVs, the precipitate was spun at 20′817 g and the pellet analyzed by TEM. As it can be observed on the **Figure 3B**, we recovered more vesicles, but the pellet still contained debris.

To improve the yield of EV recovery, we collected the supernatant after the spin at 5′000 g, the resulting supernatant was then spun down at 20′817 g and the pellet was analyzed by TEM. Here, the pellet contained vesicles devoid from cellular debris. The TEM revealed that EVs have a size varying from 100–300 nm. In conclusion a spin at 5′000 g is necessary to eliminate most of the debris after the salting out (**Figure 3C,D**).

Salting-Out Efficiently Isolates EVs From *In Vitro* Cultures of *P. Falciparum*-Infected RBC, *P. Yoelii*-Infected Mice Plasma and Healthy Human Plasma

Finally, to demonstrate the usefulness of our methodology with more complex samples, we used supernatants from *P. falciparum* infected RBCs, plasma from *P. yoelii* infected mice and healthy human plasma and purify them by salting out. We opted for salting out, instead of PEG precipitation because the yield is better. First, we collected supernatants from *P. falciparum*

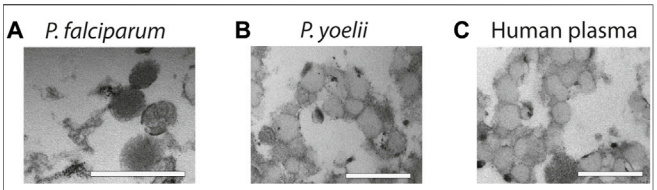

FIGURE 4 | Characterization of EVs from biofluids. **(A)** EVs derived from *in vitro P. falciparum* infected RBC cultures reveal vesicular structures of 100–200 nm. Scale bar = 500 nm. **(B)** EVs isolated from plasma of *P. yoelii* infected Balb/c mice. Scale bar = 500 nm. **(C)** EVs isolated from healthy human plasma. Scale bar = 500 nm. All the EV preparations were analyzed by TEM.

cultures and after elimination of cells and cellular debris by centrifugation, we precipitated EVs by salting out and analyzed the pellet by TEM. The TEM revealed that we were able to purify intact vesicles as it can be observed on **Figure 4A**. Next, we infected BALB/C mice with the *P. yoelii* rodent parasite strain and collected blood, we then isolated EVs from the plasma and again our approach was efficient at extracting EVs as observed on **Figure 4B**. Finally, we extracted EVs from healthy human plasma by using salting out and observed as well the high yield and specific recovery of EVs (**Figure 4C**).

Size-Exclusion Chromatography Revealed a Pure Population of EVs

It is possible that we precipitated proteins and protein-complexes together with our EVs. Therefore, next, we looked at potential contaminations by using FPLCs. The fractions of 1 ml each were collected immediately after loading the column and the void volume is 4 ml. As expected, RBC EVs isolated by PEG or salting out precipitation from A23187 treated EVs, eluted in the fraction 8–11, which corresponds to the EVs profile as determined by our standard curve (**Figure 5A**). Only minor amounts of proteins were detected in the later fractions suggesting that most of our preparations is composed of EVs and does not contain free proteins or protein aggregates that would appear in later fractions. When fractionating unprocessed plasma, we observed a small peak of proteins in fractions 8–10, which corresponds to EVs. However, the plasma is composed mostly of proteins or protein complexes eluting in fractions 18–30. Our Bovine Serum Albumin was eluted in the fractions (12–25), as is shown on the standard curve graph. We performed a sucrose cushion in order to further eliminate protein contamination from our RBC EVs preparation. However, the sucrose cushion resulted in a significant decrease of the yield, without further improving the purity (**Figure 5B**). To demonstrate the presence of EVs in fractions 8–11, we performed a bead-based flow cytometry assay to detect the presence of some classical EV markers (CD9 and CD5L). We confirmed the presence of EVs in the fraction 8–11 in unprocessed plasma (**Figure 5C**) and *P. falciparum* conditioned medium (**Figure 5D**).

Purified Vesicles Express RBC EV Markers

Next, having shown that the EVs have the expected morphology, we looked at the expression of EV markers, we used hemoglobin, CD63, CD5L, TSG101, CD81 and stomatin. Stomatin is an internal membrane protein enriched in the lipid rafts and EVs. First, as a positive control, we prepared ghosts from human RBCs (lysed RBCs) by hypotonic treatment and analyzed protein content by western blot. As expected, the stomatin protein is enriched in our ghost preparations (contain membranes), while it is absent from supernatant (cytosol). Whereas hemoglobin is present in the supernatant and absent from the ghost (**Figure 6A**). Hemoglobin was also detected in RBC EVs and conditioned medium (*Plasmodium falciparum* iRBCs) precipitated by PEG or salting out. Whereas it was absent from plasma derived EVs, as expected. As expected, stomatin was enriched in RBC EVs and in conditioned medium, while it was absent from plasma EVs. The tetraspin proteins (CD81, CD5L and TSG101) were detected in the plasma EVs. Next, we looked at EVs purified by PEG and salting out purification. Stomatin is present in both of our EV preparations. In addition, we could detect Hemoglobin by Coomassie staining of the SDS-PAGE gel, a result consistent with intact vesicles, containing hemoglobin in their lumen (**Figure 6A**). Next, we compared the yield of purification by quantifying the protein content of the EV preparations. In order to compare, we proceeded to the isolation of EVs by PEG precipitation and salting out by starting with the same amount of RBC culture. We found that Salting out is more efficient than PEG in recovering EVs. We recovered on average 0.7 mg/ml versus 0.4 mg/ml of proteins. Therefore, salting out provided a better recovery over PEG (**Figure 6B**). Next to test the role of Calcium in production of EVs *ex vivo* by RBCs, we pre-incubated RBCs with the calcium chelators EDTA or EGTA before stimulating vesiculation with A23187. The addition of calcium chelators diminished significantly the amount of EVs recovered by either PEG precipitation or salting out (**Supplementary Figure S1**). Next, the presence of classical EV markers was determined by bead-based flow cytometry on the purified EVs. The presence of CD9 and CD5L is clearly demonstrated on EVs derived by plasma, whereas the expression of those markers is lower on RBC derived EVs and *P. falciparum* conditioned medium derived EVs (**Figure 6C**).

DISCUSSION

To fully uncover the mysteries hidden behind cellular communication mediated by EVs, efficient protocols for extraction of the vesicles from cell culture supernatants, mouse blood, patient plasma have to be developed and standardize. Here we have compared two different methods to purify RBC derived EVs produced *in vitro*. Finally, we applied these methods to rodent and human plasma samples. In the first method, we used PEG precipitation (Rider et al., 2016) and in the second, salting out with sodium acetate (Brownlee et al., 2014). Both methods resulted in the efficient purification of vesicles of a size between 100–300 nm.

First, we used purified human RBCs and stimulated them with the calcium ionophore A23187, which leads to the massive release of vesicles. The vesiculation was dependent on Calcium, since the

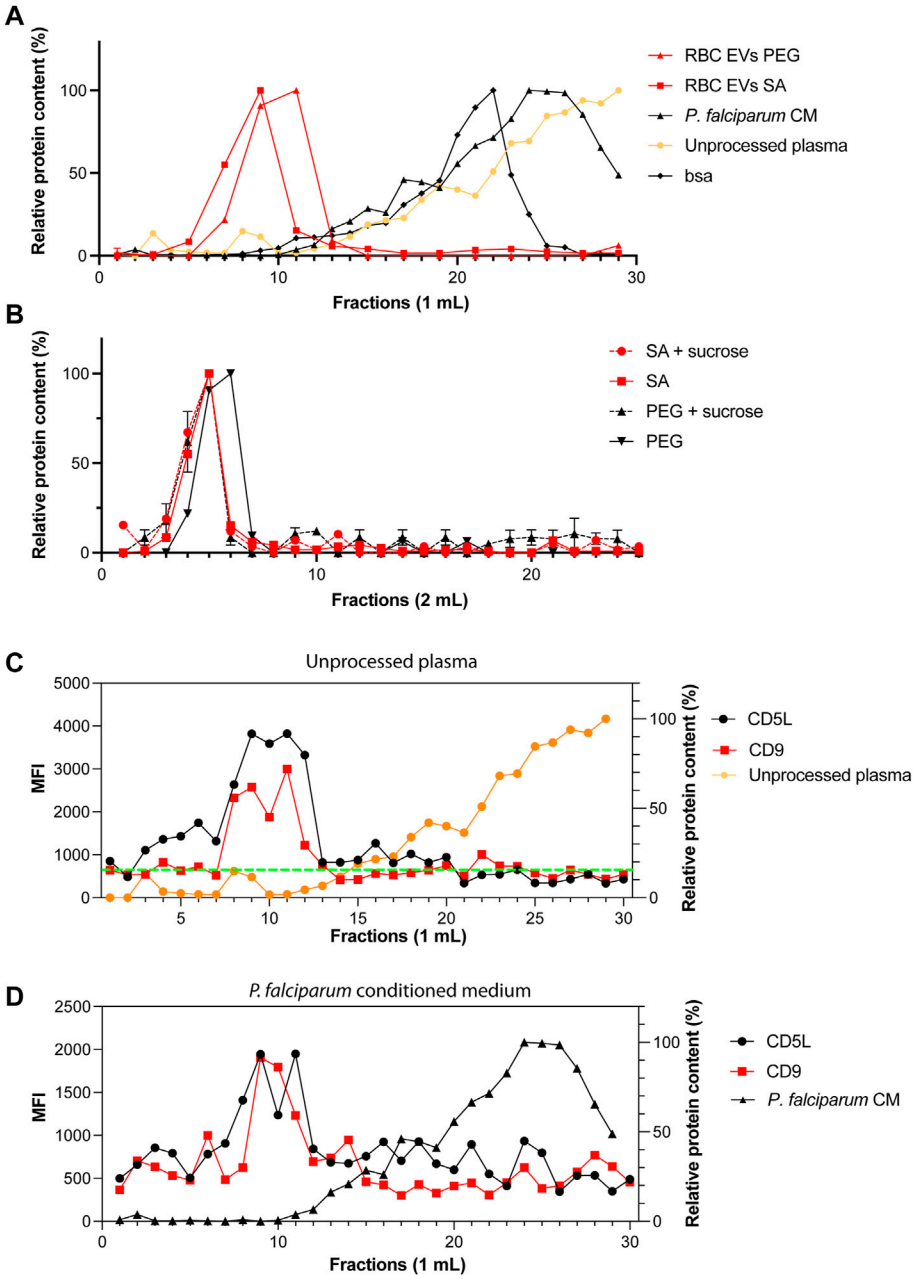

FIGURE 5 | Only one population of EVs are identified by size-exclusion chromatography. **(A)** Standard curves containing the elution profiles of EVs purified by ultracentrifugation, BSA and human serum. Points represent the mean ± s.d. of two independent analyses. **(B)** Elution profile of purified RBC EVs isolated by PEG or salting out precipitation as measured by absorbance at 280 nm. The dashed lines represent EVs further purified by sucrose gradient. Points represent the mean ± s.d. of three experiments. **(C)** MFI values of CD9 and CD5L in SEC fractions. Total of 30 fractions of 1 ml were collected. **(D)** MFI values of CD9 and CD5L in SEC fractions of *P. falciparum* conditioned medium.

Calcium chelator EDTA or EGTA, inhibited the production of EVs.

Several approaches have been described to isolate EVs from different sources including cell culture supernatants or biofluids. Different studies have compared side by side the purification methods, there is no conclusion as to which method is more appropriate. Researchers have to consider yield, purity and cost (Sáenz-Cuesta et al., 2015).

The gold standard method for purification of EVs is differential centrifugation to eliminate cells and cellular debris (Mbagwu et al., 2017). The EVs are then pelleted from the cleared supernatants by ultracentrifugation at 100′000 g or higher speed (Andrea Hernandez-Castaneda et al., 2018). The separation principle of this method is based on the sedimentation speed difference between EVs and other particles. Some protocols add an additional step to eliminate free proteins and other debris

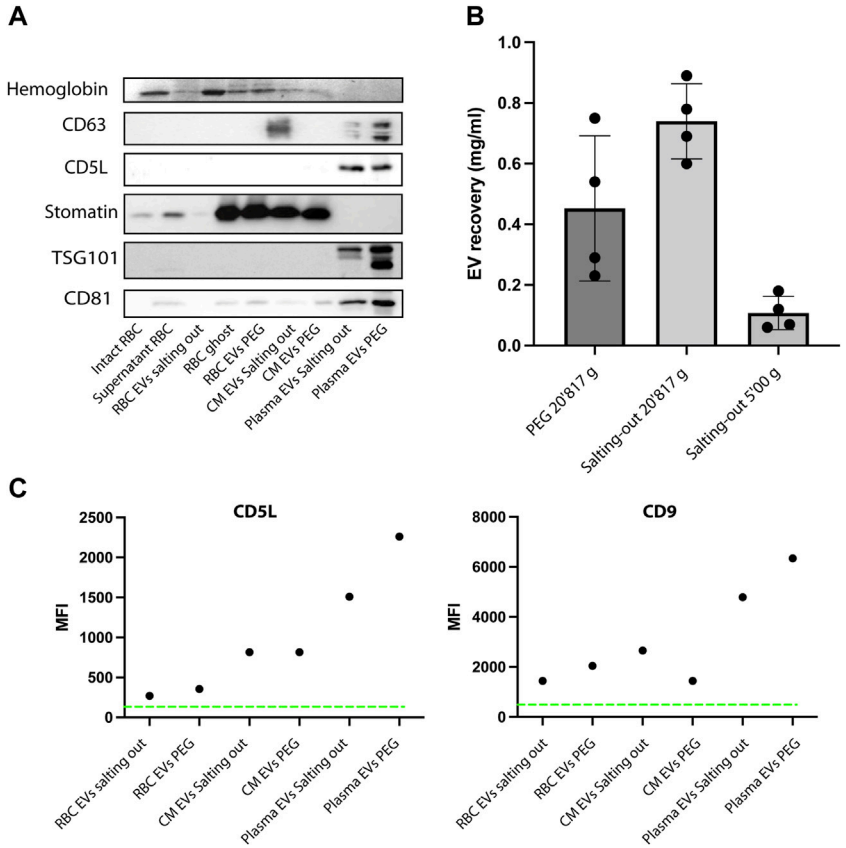

FIGURE 6 | EVs express specific markers. **(A)** Western Blot analysis of RBC EV markers, stomatin, GAPDH and Hemoglobin. In total, 10 µg of protein were loaded on a SDS-PAGE gel. **(B)** A comparison of EV recovery yield between PEG and salting out precipitation as measured by protein content. The mean ± s.d. of four independent analyses is shown. **(C)** Representative experiment of purified EVs from RBCs, plasma and conditioned medium. The presence of EV markers (CD9 and CD5L), was assessed by bead-based flow cytometry assay. The Mean Fluorescence Intensity (MFI) was calculated after measuring 50,000 events (one representative of three experiments).

based on density gradient by using a sucrose cushion or other density based gradient such as iodixanol (Van Deun et al., 2014). Despite being widely used ultracentrifugation has several disadvantages including co-purification of proteins aggregates and other non-EVs particles. Furthermore, ultracentrifugation might favor the aggregation of EVs, and therefore a loss of functionality (Linares et al., 2015). In addition, ultracentrifugation is time-consuming, expensive and requires the access to an ultracentrifuge. Another disadvantage is the poor scalability. In fact, working with large volume of cell culture supernatants or very small volumes from clinical samples makes it difficult to work with and might necessitate different type of ultracentrifuges. Despite those disadvantages, ultracentrifugation remains the most commonly used approach to purify EVs. Both PEG and salting out precipitation of EVs are easily scalable for small volumes such as clinical samples or for rodent experiments. Here, we were also able to precipitate EVs from large cell culture volumes up to 200 ml with minimal costs. Furthermore, there is no special instrumentation required and the time spent to manipulate the samples is relatively moderate. Both of these approaches provide an efficient way to isolate, while preserving the integrity of the vesicles. In fact, as we demonstrated by western blot, our EVs still contain hemoglobin, suggesting that they are intact.

Additional methods exist for the isolation of EVs, such as ultrafiltration (Nordin et al., 2015), fractionation, size-exclusion chromatography (Böing et al., 2014) and affinity interactions (Brennan et al., 2020), as well as microfluidic devices and microchips (Liu et al., 2017) (Shao et al., 2012). All these methods are time consuming and necessitate a specific training. Therefore, these approaches might be difficult to implement in resource limited regions.

Salting out can be performed in a few hours, whereas the PEG precipitation step is performed overnight. Both approaches can be done on small culture volume and therefore are valuable for analyzing patients biofluids that might be limited in quantity. This approach makes it also easier to work with large numbers of samples simultaneously. By adding a centrifugation step at 5′000 g to eliminate debris, we were able to improve the recovery and purity of EVs by salting out without affecting the yield. Although the mechanism responsible for EV precipitation is not fully understood, it has been suggested that the acetate-

mediated removal of the EV hydration layer that promotes hydrophobic interactions result in increasing aggregation and concomitant precipitation.

The precipitated EVs can be washed to remove impurities and are readily "resolubilized" upon resuspension in acetate-free buffer at neutral pH. PEG has been used for many decades for the purification of viruses that have similar properties than EVs.

Both PEG precipitation and salting-out provided a robust highly scalable approach to purify pure EVs from *in vitro* RBC induced EVs. Therefore, these methods can be used for purification of *in vitro* generated EVs. While we used biofluids (plasma) derived from murine and human plasma the results. Although the recovery of EVs was high, the purified samples contained a significant amount of contaminations.

In conclusion, we have tested two approaches that efficiently isolate EVs from cell culture supernatants or from plasma. Both approaches do not require special equipment and therefore can be applied in resource poor regions. There is an urgent need to develop.

MATERIALS AND METHODS

We have submitted all relevant data of our experiments to EV-TRACK knowledgebase (EV-TRACK ID:EV220175).

Cell Culture of Parasites

The *P. falciparum* strain 3D7 was used for this study. Parasites were kept in fresh type 0 + human red blood cells, suspended at 4% hematocrit in HEPES-buffered RPMI 1640 containing 10% (w/v) heat inactivated human serum, 0.5 ml Gentamycin, 2.01 g sodium bicarbonate and 0.05 g Hypoxanthine at pH 6.74. Prior to culture, the complete medium was depleted from EVs and debris by ultracentrifugation at 100′000 g for 1 h. The parasite cultures were maintained in a controlled environment at 37°C in a gassed chamber at 5% CO_2 and 1% O_2.

Size Exclusion Chromatography

Experiments to determine the presence of contaminations in EVs preparations were performed essentially as described (Mantel et al., 2016). Briefly, sephacryl S-500 resin (GE Healthcare) was packed in a chromatography column (0.9 Å~ 30 cm, 19.1 ml bed volume and void volume of 4 ml). Before injection, the column was equilibrated with 25 ml of PBS solution at 0.5 ml/min at room temperature. The column was injected with 0.5 ml of purified EVs and eluted at 4°C for approximately 1 h with PBS solution (pH 7.4) at a flow rate of 0.5 ml/min. A total of 25 fractions of 1 ml each were collected. Fractions were stored at 4°C before use. Protein molecular weight standards included BSA (67 kDa; GE Healthcare), purified EVs by ultracentrifugation and human serum.

Bead-Based Flow Cytometry

Fractions from SEC and EV-enriched fractions from PEG and salting-out were analyzed by flow cytometry to identify the classical EV markers CD5L and CD9. As it has been described previously (Théry et al., 2006; Gualdrón-López et al., 2018). Briefly, 400 µl of each fraction was incubated with 1 µl of aldehyde/sulphate-latex beads (4 µm; 4%, ThermoFisher Scientific) by incubation for 15 min with agitation. Coupled beads were then blocked by incubation overnight with 1 ml of BCB buffer [(PBS 1X/BSA 0.1%/NaN3 0.01% (both from Sigma-Aldrich)] in a rotation device. Beads were centrifuged down at 2,000 × g for 10 min, the supernatant was discarded. The pelleted beads were resuspended in 100 µl of BCB buffer. The bead suspension was incubated with anti-CD5L antibodies (Abcam: ab45408) at 1/100 or anti-CD9 (Santa Cruz Biotechnology: ALB6) or IgG isotype control (To check) for 30 min at 4°C protected from light. After washing, samples were incubated with a rabbit or mouse secondary-antibody conjugated to Alexa 488 (both Diavona) at 1/500 dilution for 30 min at 4°C, protected from light. After two wash steps, beads were resuspended in 200 µl of PBS and 50,000 events were analyzed by flow cytometry using a BD Accuri C6 (BD Biosciences) instrument. Median Fluorescence Intensity (MFI) and count data were obtained using FlowJo v. X Software (TreeStar). As control for specificity, we have incubated SEC fraction 9 and 10 in the presence of a rabbit/mouse isotype IgG antibody and secondary-antibody Alexa (isotype control).

Salting-Out Procedure

RBC conditioned media was cleared from cells and debris by centrifugation. 1/10th volume of Na acetate buffer (1.0 M; pH 4.75) was added to the cleared supernatant solution and incubated at 4°C under rotation. Then the solution was incubated 5 min at 37°C. The turbid suspension was centrifuged for 1 h at 5′000 g and the resulting pellet was washed with a 0.1 M Na acetate buffer solution and the supernatant was then spun at 20′817 g for 10 min. The purified EVs were resuspended in PBS and stored at −150°C.

EVs Isolation By Polyethylene Glycol Precipitation

Vesicle-containing medium from RBC cell culture or plasma were centrifuged at 500 g for 5 min followed by 2′000 g for 30 min at 4°C to remove cells and cellular debris. After centrifugation, a 2 × PEG solution was added to an equal volume of supernatant to reach a16%- PEG concentration. The samples were mixed thoroughly by inversion and incubated at 4°C overnight. On the next day, samples were centrifuged in a tabletop centrifuge at 20′817 g for 1 h at 4°C. conical tubes were then decanted, and allowed to drain for 5 minutes, tapping occasionally to remove excess PEG. The resulting pellet was suspended in 50–500 µl of particle-free PBS (pH 7.4). subsets of samples were then either stored at -150°C or used straight away for experiments.

Transmission Electron Microscopy

A total of 10 µg of EVs purified by Salting out and PEG were fixed in 2% PFA/2.5% GA (EM grade) in 0.1 M Cacodylate Na Buffer, postfixed with an aqueous solution [1% OsO4 and 1.5% $K_4Fe(CN)_6$], and embedded into epon. Ultrathin sections (50 nm)

were contrasted with lead citrate and uranyl acetate and analyzed with a CM 100 (Philips).

Western Blotting

Samples were collected and purified as described in each specific experiment. For SDS–polyacrylamide gel electrophoresis the pellet was washed three times in PBS and taken up in reducing SDS sample buffer (Invitrogen, Carlsbad, CA). Proteins were separated on 4–12% Bis-Tris gels (Invitrogen) and proteins transferred onto Immun-Blot PVDF membranes (Biorad), according to standard protocols. Antibodies used are anti-stomatin (clone M-14; Santa Cruz Biotechnologies), CD63 (clone E-12: Santa Cruz Biotechnology), CD81 (clone 5A6; Santa Cruz Biotechnology), CD9 (ALB6; Santa Cruz Biotechnology), TSG101 (4A10; Novus Biologicals) and CD5L (ab45408, Abcam). Secondary antibodies (IR-Dye-conjugated) were goat anti-rabbit and goat anti-mouse immunoglobulin (LICOR, Lincoln, NE). Immunoreactive bands were detected using the Odyssey imaging system (LICOR).

Red Blood Cells Isolation and Treatment With Calcium Ionophore

Venous blood, collected in acid-citrate-dextrose, was obtained from healthy adult volunteers. The RBCs were washed three times with PBS. And stored at 4°C at a hematocrit of 50%.

Treatment with calcium ionophore. Ca^{2+}ionophore treatment was performed at 37°C by addition of A23187 (Sigma-Aldrich) at a concentration of 5 µM in a HBSS buffer containing Ca2+. Unless otherwise indicated, incubation time of RBCs with ionophore was 4 h.

DATA AVAILABILITY STATEMENT

The raw data supporting the conclusions of this article will be made available by the authors, without undue reservation.

ETHICS STATEMENT

The animal study was reviewed and approved by 2019_36_FR.

AUTHOR CONTRIBUTIONS

P-YM conceived the study. P-YM and MW conceptualized the study by providing the methodology and establishing the major assays. MZ, BYS, KKE, MSR, SY, IF, and BYS conducted the investigation, performed the experiments and analyzed the data. P-YM and MZ wrote the manuscript. P-YM supervised the study.

FUNDING

This work was supported by the Swiss National Science Foundation (SNSF Grant # 31003A_182729 to P-YM) and the Research Pool of the University of Fribourg (to P-YM).

SUPPLEMENTARY MATERIAL

The Supplementary Material for this article can be found online at: https://www.frontiersin.org/articles/10.3389/fcell.2022.812244/full#supplementary-material

REFERENCES

Allan, D., Billah, M. M., Finean, J. B., and Michell, R. H. (1976). Release of Diacylglycerol-Enriched Vesicles from Erythrocytes with Increased Intracellular [Ca2+]. *Nature* 261, 58–60. doi:10.1038/261058a0

Allan, D., Thomas, P., and Limbrick, A. R. (1980). The Isolation and Characterization of 60 Nm Vesicles ('nanovesicles') Produced during Ionophore A23187-Induced Budding of Human Erythrocytes. *Biochem. J.* 188, 881–887. doi:10.1042/bj1880881

Andrea Hernandez-Castaneda, M., Mbagwu, S., Babatunde, K. A., Walch, M., Filgueira, L., and Mantel, P. Y. (2018). Evaluation of Extracellular Vesicle Function during Malaria Infection. *J. Vis. Exp.* 2018, 57067. doi:10.3791/57067

Antwi-Baffour, S., Malibha-Pinchbeck, M., Stratton, D., Jorfi, S., Lange, S., and Inal, J. (2020). Plasma mEV Levels in Ghanain Malaria Patients with Low Parasitaemia Are Higher Than Those of Healthy Controls, Raising the Potential for Parasite Markers in mEVs as Diagnostic Targets. *J. Extracell Vesicles* 9, 1697124. doi:10.1080/20013078.2019.1697124

Babatunde, K. A., Mbagwu, S., Hernández-Castañeda, M. A., Adapa, S. R., Walch, M., Filgueira, L., et al. (2018). Malaria Infected Red Blood Cells Release Small Regulatory RNAs through Extracellular Vesicles. *Sci. Rep.* 8, 884. doi:10.1038/s41598-018-19149-9

Babatunde, K. A., Yesodha Subramanian, B., Ahouidi, A. D., Martinez Murillo, P., Walch, M., and Mantel, P.-Y. (2020). Role of Extracellular Vesicles in Cellular Cross Talk in Malaria. *Front. Immunol.* 11, 22. doi:10.3389/fimmu.2020.00022

Böing, A. N., van der Pol, E., Grootemaat, A. E., Coumans, F. A., Sturk, A., and Nieuwland, R. (2014). Single-step Isolation of Extracellular Vesicles by Size-Exclusion Chromatography. *J. Extracell Vesicles* 3, 23430. doi:10.3402/jev.v3.23430

Borgheti-Cardoso, L. N., Kooijmans, S. A. A., Chamorro, L. G., Biosca, A., Lantero, E., Ramírez, M., et al. (2020). Extracellular Vesicles Derived from Plasmodium-Infected and Non-infected Red Blood Cells as Targeted Drug Delivery Vehicles. *Int. J. Pharmaceutics* 587, 119627. doi:10.1016/j.ijpharm.2020.119627

Brennan, K., Martin, K., FitzGerald, S. P., O'Sullivan, J., Wu, Y., Blanco, A., et al. (2020). A Comparison of Methods for the Isolation and Separation of Extracellular Vesicles from Protein and Lipid Particles in Human Serum. *Sci. Rep.* 10, 1039. doi:10.1038/s41598-020-57497-7

Brownlee, Z., Lynn, K. D., Thorpe, P. E., and Schroit, A. J. (2014). A Novel "Salting-Out" Procedure for the Isolation of Tumor-Derived Exosomes. *J. Immunological Methods* 407, 120–126. doi:10.1016/j.jim.2014.04.003

Campos, F. M., Franklin, B. S., Teixeira-Carvalho, A., Filho, A. L., de Paula, S. C., Fontes, C. J., et al. (2010). Augmented Plasma Microparticles during Acute Plasmodium Vivax Infection. *Malar. J.* 9, 327. doi:10.1186/1475-2875-9-327

Coban, C., Lee, M. S. J., and Ishii, K. J. (2018). Tissue-specific Immunopathology during Malaria Infection. *Nat. Rev. Immunol.* 18, 266–278. doi:10.1038/nri.2017.138

Coltel, N., Combes, V., Wassmer, S. C., Chimini, G., and Grau, G. E. (2006). Cell Vesiculation and Immunopathology: Implications in Cerebral Malaria. *Microbes Infect.* 8, 2305–2316. doi:10.1016/j.micinf.2006.04.006

Combes, V., Taylor, T. E., Juhan-Vague, I., Mège, J. L., Mwenechanya, J., Tembo, M., et al. (2004). Circulating Endothelial Microparticles in Malawian Children with Severe Falciparum Malaria Complicated with Coma. *JAMA* 291, 2542–2544. doi:10.1001/jama.291.21.2542-b

Combes, V., Coltel, N., Alibert, M., van Eck, M., Raymond, C., Juhan-Vague, I., et al. (2005). ABCA1 Gene Deletion Protects against Cerebral Malaria. *Am. J. Pathol.* 166, 295–302. doi:10.1016/s0002-9440(10)62253-5

Couper, K. N., Barnes, T., Hafalla, J. C. R., Combes, V., Ryffel, B., Secher, T., et al. (2010). Parasite-derived Plasma Microparticles Contribute Significantly to Malaria Infection-Induced Inflammation through Potent Macrophage Stimulation. *Plos Pathog.* 6, e1000744. doi:10.1371/journal.ppat.1000744

Gualdrón-López, M., Flannery, E. L., Kangwanrangsan, N., Chuenchob, V., Fernandez-Orth, D., Segui-Barber, J., et al. (2018). Characterization of Plasmodium Vivax Proteins in Plasma-Derived Exosomes from Malaria-Infected Liver-Chimeric Humanized Mice. *Front. Microbiol.* 9, 1271. doi:10.3389/fmicb.2018.01271

Huang, K., Huang, L., Zhang, X., Zhang, M., Wang, Q., Lin, H., et al. (2021). Mast Cells-Derived Exosomes Worsen the Development of Experimental Cerebral Malaria. *Acta Tropica* 224, 106145. doi:10.1016/j.actatropica.2021.106145

Linares, R., Tan, S., Gounou, C., Arraud, N., and Brisson, A. R. (2015). High-speed Centrifugation Induces Aggregation of Extracellular Vesicles. *J. Extracellular Vesicles* 4, 29509. doi:10.3402/jev.v4.29509

Liu, F., Vermesh, O., Mani, V., Ge, T. J., Madsen, S. J., Sabour, A., et al. (2017). The Exosome Total Isolation Chip. *ACS Nano* 11, 10712–10723. doi:10.1021/acsnano.7b04878

Mantel, P.-Y., Hjelmqvist, D., Walch, M., Kharoubi-Hess, S., Nilsson, S., Ravel, D., et al. (2016). Infected Erythrocyte-Derived Extracellular Vesicles Alter Vascular Function via Regulatory Ago2-miRNA Complexes in Malaria. *Nat. Commun.* 7, 12727. doi:10.1038/ncomms12727

Mantel, P.-Y., Hoang, A. N., Goldowitz, I., Potashnikova, D., Hamza, B., Vorobjev, I., et al. (2013). Malaria-infected Erythrocyte-Derived Microvesicles Mediate Cellular Communication within the Parasite Population and with the Host Immune System. *Cell Host & Microbe* 13, 521–534. doi:10.1016/j.chom.2013.04.009

Martin-Jaular, L., Nakayasu, E. S., Ferrer, M., Almeida, I. C., and Del Portillo, H. A. (2011). Exosomes from Plasmodium Yoelii-Infected Reticulocytes Protect Mice from Lethal Infections. *PLoS One* 6, e26588. doi:10.1371/journal.pone.0026588

Mbagwu, S. I., Lannes, N., Walch, M., Filgueira, L., and Mantel, P. Y. (2019). Human Microglia Respond to Malaria-Induced Extracellular Vesicles. *Pathogens* 9, 21. doi:10.3390/pathogens9010021

Mbagwu, S., Walch, M., Filgueira, L., and Mantel, P.-Y. (2017). Production and Characterization of Extracellular Vesicles in Malaria. *Methods Mol. Biol.* 1660, 377–388. doi:10.1007/978-1-4939-7253-1_31

Miller, L. H., Baruch, D. I., Marsh, K., and Doumbo, O. K. (2002). The Pathogenic Basis of Malaria. *Nature* 415, 673–679. doi:10.1038/415673a

Momen-Heravi, F., Balaj, L., Alian, S., Mantel, P.-Y., Halleck, A. E., Trachtenberg, A. J., et al. (2013). Current Methods for the Isolation of Extracellular Vesicles. *Biol. Chem.* 394, 1253–1262. doi:10.1515/hsz-2013-0141

Nakai, W., Yoshida, T., Diez, D., Miyatake, Y., Nishibu, T., Imawaka, N., et al. (2016). A Novel Affinity-Based Method for the Isolation of Highly Purified Extracellular Vesicles. *Sci. Rep.* 6, 33935. doi:10.1038/srep33935

Nordin, J. Z., Lee, Y., Vader, P., Mäger, I., Johansson, H. J., Heusermann, W., et al. (2015). Ultrafiltration with Size-Exclusion Liquid Chromatography for High Yield Isolation of Extracellular Vesicles Preserving Intact Biophysical and Functional Properties. *Nanomedicine: Nanotechnology, Biol. Med.* 11, 879–883. doi:10.1016/j.nano.2015.01.003

Ofir-Birin, Y., Ben Ami Pilo, H., Cruz Camacho, A., Rudik, A., Rivkin, A., Revach, O.-Y., et al. (2021). Malaria Parasites Both Repress Host CXCL10 and Use it as a Cue for Growth Acceleration. *Nat. Commun.* 12, 4851. doi:10.1038/s41467-021-24997-7

Pankoui Mfonkeu, J. B., Gouado, I., Fotso Kuaté, H., Zambou, O., Amvam Zollo, P. H., Grau, G. E. R., et al. (2010). Elevated Cell-specific Microparticles Are a Biological Marker for Cerebral Dysfunctions in Human Severe Malaria. *PLoS One* 5, e13415. doi:10.1371/journal.pone.0013415

Regev-Rudzki, N., Wilson, D. W., Carvalho, T. G., Sisquella, X., Coleman, B. M., Rug, M., et al. (2013). Cell-cell Communication between Malaria-Infected Red Blood Cells via Exosome-like Vesicles. *Cell* 153, 1120–1133. doi:10.1016/j.cell.2013.04.029

Rider, M. A., Hurwitz, S. N., and Meckes, D. G., Jr. (2016). ExtraPEG: A Polyethylene Glycol-Based Method for Enrichment of Extracellular Vesicles. *Sci. Rep.* 6, 23978. doi:10.1038/srep23978

Sáenz-Cuesta, M., Arbelaiz, A., Oregi, A., Irizar, H., Osorio-Querejeta, I., Munoz-Culla, M., et al. (2015). Methods for Extracellular Vesicles Isolation in a Hospital Setting. *Front. Immun.* 6, 50. doi:10.3389/fimmu.2015.00050

Sampaio, N. G., Cheng, L., and Eriksson, E. M. (2017). The Role of Extracellular Vesicles in Malaria Biology and Pathogenesis. *Malar. J.* 16, 245. doi:10.1186/s12936-017-1891-z

Schofield, L., and Grau, G. E. (2005). Immunological Processes in Malaria Pathogenesis. *Nat. Rev. Immunol.* 5, 722–735. doi:10.1038/nri1686

Shao, H., Chung, J., Balaj, L., Charest, A., Bigner, D. D., Carter, B. S., et al. (2012). Protein Typing of Circulating Microvesicles Allows Real-Time Monitoring of Glioblastoma Therapy. *Nat. Med.* 18, 1835–1840. doi:10.1038/nm.2994

Sisquella, X., Ofir-Birin, Y., Pimentel, M. A., Cheng, L., Abou Karam, P., Sampaio, N. G., et al. (2017). Malaria Parasite DNA-Harbouring Vesicles Activate Cytosolic Immune Sensors. *Nat. Commun.* 8, 1985. doi:10.1038/s41467-017-02083-1

Takov, K., Yellon, D. M., and Davidson, S. M. (2019). Comparison of Small Extracellular Vesicles Isolated from Plasma by Ultracentrifugation or Size-Exclusion Chromatography: Yield, Purity and Functional Potential. *J. Extracellular Vesicles* 8, 1560809. doi:10.1080/20013078.2018.1560809

Tandoh, K. Z., Wilson, M. D., Quashie, N. B., and Duah-Quashie, N. O. (2021). Implicating Extracellular Vesicles in Plasmodium Falciparum Artemisinin Resistance Development. *Traffic* 22, 194–200. doi:10.1111/tra.12787

Théry, C., Amigorena, S., Raposo, G., and Clayton, A. (2006). Isolation and Characterization of Exosomes from Cell Culture Supernatants and Biological Fluids. *Curr. Protoc. Cel Biol* Chapter 3, Unit 3.22. doi:10.1002/0471143030.cb0322s30

Théry, C., Witwer, K. W., Aikawa, E., Alcaraz, M. J., Anderson, J. D., Andriantsitohaina, R., et al. (2018). Minimal Information for Studies of Extracellular Vesicles 2018 (MISEV2018): a Position Statement of the International Society for Extracellular Vesicles and Update of the MISEV2014 Guidelines. *J. Extracellular Vesicles* 7, 1535750. doi:10.1080/20013078.2018.1535750

Toda, H., Diaz-Varela, M., Segui-Barber, J., Roobsoong, W., Baro, B., Garcia-Silva, S., et al. (2020). Plasma-derived Extracellular Vesicles from Plasmodium Vivax Patients Signal Spleen Fibroblasts via NF-kB Facilitating Parasite Cytoadherence. *Nat. Commun.* 11, 2761. doi:10.1038/s41467-020-16337-y

Valadi, H., Ekström, K., Bossios, A., Sjöstrand, M., Lee, J. J., and Lötvall, J. O. (2007). Exosome-mediated Transfer of mRNAs and microRNAs Is a Novel Mechanism of Genetic Exchange between Cells. *Nat. Cel Biol* 9, 654–659. doi:10.1038/ncb1596

Van Deun, J., Mestdagh, P., Sormunen, R., Cocquyt, V., Vermaelen, K., Vandesompele, J., et al. (2014). The Impact of Disparate Isolation Methods for Extracellular Vesicles on Downstream RNA Profiling. *J. Extracell Vesicles* 3, 24858. doi:10.3402/jev.v3.24858

WHO (2020). *WHO Malaria Report 2019*. Geneva: WHO

Conflict of Interest: The authors declare that the research was conducted in the absence of any commercial or financial relationships that could be construed as a potential conflict of interest.

Publisher's Note: All claims expressed in this article are solely those of the authors and do not necessarily represent those of their affiliated organizations, or those of the publisher, the editors and the reviewers. Any product that may be evaluated in this article, or claim that may be made by its manufacturer, is not guaranteed or endorsed by the publisher.

Frontiers in
Cell and Developmental Biology

Explores the fundamental biological processes of life, covering intracellular and extracellular dynamics.

The world's most cited developmental biology journal, advancing our understanding of the fundamental processes of life. It explores a wide spectrum of cell and developmental biology, covering intracellular and extracellular dynamics.

Discover the latest Research Topics

See more →

Frontiers

Avenue du Tribunal-Fédéral 34
1005 Lausanne, Switzerland
frontiersin.org

Contact us

+41 (0)21 510 17 00
frontiersin.org/about/contact